

**The Functionalization of Methane and Other Hydrocarbons Mediated by
Organometallic Nitrosyl Complexes of Tungsten**

by

Rhett A. Baillie

B.Sc., The University of British Columbia, 2011

A THESIS SUBMITTED IN PARTIAL FULFILLMENT OF
THE REQUIREMENTS FOR THE DEGREE OF

DOCTOR OF PHILOSOPHY

in

THE FACULTY OF GRADUATE AND POSTDOCTORAL STUDIES

(Chemistry)

THE UNIVERSITY OF BRITISH COLUMBIA

(Vancouver)

April 2016

© Rhett A. Baillie, 2016

Abstract

The novel family of $\text{Cp}^*\text{W}(\text{NO})(\text{H})(\eta^3\text{-allyl})$ complexes has been synthesized and characterized. Upon thermolysis these compounds generate 16e $\text{Cp}^*\text{W}(\text{NO})(\eta^2\text{-alkene})$ intermediate complexes that have been trapped as their corresponding 18e PMe_3 adducts. In neat alkane solutions, these $\text{Cp}^*\text{W}(\text{NO})(\eta^2\text{-alkene})$ compounds effect three successive C-H activations of the alkane to produce a new $\text{Cp}^*\text{W}(\text{NO})(\text{H})(\eta^3\text{-allyl})$ complex in which the allyl ligand is derived from the alkane solvent.

In the presence of CO, the $\text{Cp}^*\text{W}(\text{NO})(\text{H})(\eta^3\text{-allyl})$ complexes effect the regiospecific generation of saturated unsymmetrical ketones from hydrocarbons and CO gas via C-H activation and the formation of two new C-C bonds. For instance, the complex $\text{Cp}^*\text{W}(\text{NO})(\text{H})(\eta^3\text{-CH}_2\text{CHCMe}_2)$ effects the conversion of benzene and mesitylene into the ketones 4-methyl-1-phenylpentan-1-one and 1-(3,5-dimethylphenyl)-5-methylhexan-2-one, respectively. The organometallic product of these reactions is $\text{Cp}^*\text{W}(\text{NO})(\text{CO})_2$ which can be converted into the $\text{Cp}^*\text{W}(\text{NO})(\text{H})(\eta^3\text{-allyl})$ reactant in three steps, thereby completing a complete cycle with respect to tungsten.

The conversion of methane into the β,γ -unsaturated ketone, 5-methylhex-4-en-2-one, is initiated by the complex $\text{Cp}^*\text{W}(\text{NO})(\text{CH}_2\text{CMe}_3)(\eta^3\text{-CH}_2\text{CHCMe}_2)$. In a cyclohexane solution, the complex effects the C-H activation of methane to produce $\text{Cp}^*\text{W}(\text{NO})(\text{CH}_3)(\eta^3\text{-CH}_2\text{CHCMe}_2)$ which has been fully characterized. Under CO pressure, the methyl ligand is converted into an acyl ligand in $\text{Cp}^*\text{W}(\text{NO})(\text{C}(=\text{O})\text{CH}_3)(\eta^3\text{-CH}_2\text{CHCMe}_2)$, and then the acyl and allyl ligands couple to give $\text{Cp}^*\text{W}(\text{NO})(\text{CO})(\eta^2\text{-CH}_2=\text{CHCMe}_2\text{C}(=\text{O})\text{CH}_3)$ which contains an η^2 -bound ketone ligand. Finally, the ketone is released at 170 °C under CO pressure and

$\text{Cp}^*\text{W}(\text{NO})(\text{CO})_2$ is obtained which again can be converted back into the starting organometallic compound. Each of these organometallic complexes has been isolated and fully characterized, thereby allowing the stepwise transformation of methane through C-H activation and C-C bond-forming reactions to be definitively established.

In a similar fashion, the complex $\text{Cp}^*\text{W}(\text{NO})(\text{CH}_2\text{CMe}_3)(\eta^3\text{-CH}_2\text{CHCHPh})$ converts methane and ethane to the corresponding η^2 -bound ketone complexes, $\text{Cp}^*\text{W}(\text{NO})(\text{CO})(\eta^2\text{-PhCH=CHCH}_2\text{C(=O)CH}_3)$ and $\text{Cp}^*\text{W}(\text{NO})(\text{CO})(\eta^2\text{-PhCH=CHCH}_2\text{C(=O)Et})$. The $\text{Cp}^*\text{W}(\text{NO})(\text{CH}_2\text{CMe}_3)(\eta^3\text{-CH}_2\text{CHCHPh})$ complex also effects the terminal C-H activation of other alkanes and heteroatom-containing hydrocarbons. The carbonylation of ligands derived from a long-chain alkane and ether has been performed. In addition, the activation of methane, ethane, and propane has been optimized for the compound $\text{Cp}^*\text{W}(\text{NO})(\text{CH}_2\text{CMe}_3)(\eta^3\text{-CH}_2\text{CHCHMe})$. Finally, the bound ketone ligands of complexes $\text{Cp}^*\text{W}(\text{NO})(\text{CO})(\eta^2\text{-PhCH=CHCH}_2\text{C(=O)(alkyl)})$ have been photolytically released as the cis and trans β,γ -unsaturated ketone products.

Preface

Some of the research presented in this thesis was done in collaboration with other members of the Legzdins research group. Except where noted, the research including the syntheses, reactions, characterization of compounds, and data analyses were carried out by the author (Rhett Baillie). The experimental design was developed by the author. All of the work presented in this thesis was done under the supervision and guidance of Prof. Peter Legzdins.

In Chapter 2 it is noted that the optimization of the syntheses of compounds **2.2** and **2.3**, as well as the reactions of these compounds with trimethylphosphine were carried out by Mr. Aaron Holmes and Dr. Russell Wakeham. Some early work toward the optimized syntheses of **2.2** and **2.3** was carried out by Ms. Monica Shree, Mr. Kevan Dettelbach, and Mr. Tommy Tran.

In Chapter 3, Dr. Aurélien Béthegnies obtained the crystals from which the solid-state structure of **3.1** was obtained. The reactions of **2.2** and **2.3** with benzene and mesitylene under CO pressure were carried out by Mr. Aaron Holmes and Dr. Russell Wakeham using the experimental design determined by the author. Initial reactions of **2.3** under CO pressure were carried out by Mr. Travis Nagle.

In Chapter 5, the reactions of **5.1** with propane and *n*-butane were carried out by Dr. Russell Wakeham. The photolysis reactions were carried out by the author; however, the conditions necessary for selective release of the β,γ -unsaturated ketones were determined by Dr. Russell Wakeham.

All DFT calculations presented in this thesis were performed by Dr. Guillaume Lefèvre. For the solid-state molecular structures determined by single-crystal X-ray diffraction, the data collection and analyses were performed by the author except in the following instances: the

structures of **4.3** and **5.4** were solved by Ms. Catherine Chow, while the structures of compounds **3.1**, **3.4**, **3.5**, **4.2**, **4.4**, **4.6**, and **5.14** were solved by Dr. Brian Patrick. All X-ray data was collected at the UBC X-ray crystallography facility. All mass spectrometric data was collected by Mr. Marshall Lapawa, and elemental analyses were performed by Mr. Derek Smith, both at the UBC microanalytical facility. The specific contributions of coworkers are noted in the discussion of this thesis.

Portions of section 1.2 have been reported as part of a review article in the journal *Coordination Chemistry Reviews* published by Elsevier as: Baillie, R. A.; Legzdins, P. “The Rich and Varied Chemistry of Group 6 Cyclopentadienyl Nitrosyl Complexes.” *Coord. Chem. Rev.* **2016**, *309*, 1-20. Reprinted with permission from *Coordination Chemistry Reviews*. Copyright (2016) Elsevier. The text and Schemes used were written or drawn by the author.

The work presented in Chapter 2 excluding sections 2.2.4 and 2.2.5 has been reported as an article in the journal *Inorganic Chemistry* published by the American Chemical Society as: Baillie, R. A.; Holmes, A. S.; Lefèvre, G. P.; Patrick, B. O.; Shree, M. V.; Wakeham, R. J.; Legzdins, P.; Rosenfeld, D. C. “Synthesis, Characterization, and Some Properties of Cp*W(NO)(H)(η^3 -allyl) Complexes.” *Inorg. Chem.* **2015**, *54*, 5915-5929. Reprinted with permission from *Inorganic Chemistry*. Copyright (2015) American Chemical Society. The article was written in full by the author and research presented was carried out by the author. Contributions by coauthors are noted in the discussion.

The work presented in Chapter 3 has been reported as two articles in the journal *Organometallics* published by the American Chemical Society. The sections 3.1, 3.2.1, 3.2.2, and 3.2.3 have been reported as: Baillie, R. A.; Wakeham, R. J.; Lefèvre, G. P.; Béthegnies, A.; Patrick, B. O.; Legzdins, P.; Rosenfeld, D. C. “Thermal Chemistry of Cp*W(NO)(H)(η^3 -allyl)

Complexes.” *Organometallics* **2015**, *34*, 3428-3441. Reprinted with permission from Organometallics. Copyright (2015) American Chemical Society. The work presented in section 3.2.4 has been published as: Baillie, R. A.; Wakeham, R. J.; Lefèvre, G. P.; Holmes, A. S.; Legzdins, P. “Unsymmetrical Saturated Ketones Resulting from Activations of Hydrocarbon C(sp³)-H and C(sp²)-H Bonds Effected by Cp*W(NO)(H)(η³-allyl) Complexes.” *Organometallics* **2015**, *34*, 4085-4092. Reprinted with permission from Organometallics. Copyright (2015) American Chemical Society. Both of these articles were written in full by the author. Contributions by coauthors are noted in the discussion.

Data from section 4.2.2.4 and Appendix Figures C.3 and C.4 have been reported in an article in the journal Inorganic Chemistry published by the American Chemical Society as: Fabulyak, D.; Baillie, R. A.; Patrick, B. O.; Legzdins, P. Rosenfeld, D. C. “Effects of the η⁵-C₅H₄ⁱPr Ligand on the Properties Exhibited by Its Tungsten Nitrosyl Complexes.” *Inorg. Chem.* **2016**, DOI: 10.1021/acs.inorgchem.5b02738. Adapted with permission from Inorganic Chemistry. Copyright (2016) American Chemical Society.

Work referenced in section 4.2.1 and presented in Appendix C.1 has been reported in an article in the journal Organometallics published by the American Chemical Society as: Lefèvre, G. P.; Baillie, R. A.; Fabulyak, D.; Legzdins, P. “Insights into the Intermolecular C–H activations of Hydrocarbons Initiated by Cp*W(NO)(η³-allyl)(CH₂CMe₃) Complexes.” *Organometallics* **2013**, *32*, 5561-5572. Adapted with permission from Organometallics. Copyright (2013) American Chemical Society. The material adapted from this article was created by the author.

Abstract	ii
Preface	iv
Table of Contents	vii
List of Tables	xvii
List of Figures	xix
List of Schemes	xxv
List of Abbreviations	xxx
Compound numbers of select complexes	xxxvi
Acknowledgements	xxxvii
Dedication	xxxviii
Chapter 1: Introduction	1
1.1 Methane, Natural Gas, and C-H Activation.	2
1.2 Legzdins Group C-H Activation Chemistry	11
1.3 Scope of the Thesis.	15
Chapter 2: Synthesis and Properties of Cp[*]W(NO)(H)(η³-Allyl) Complexes	18
2.1 Introduction	19
2.2 Results and Discussion	20
2.2.1 Synthesis and Characterization of Cp [*] W(NO)(H)(η ³ -CH ₂ CHCMe ₂)	20
2.2.2 Synthesis and Characterization of Additional Cp [*] W(NO)(H)(η ³ -Allyl) Complexes ..	24
2.2.3 Reactions of the Hydride Complexes with PMe ₃	32

2.2.3.1	Reversible Adduct Formation of 2.1 with Trimethylphosphine	34
2.2.3.2	Identification of 16e η^2 -Alkene Intermediate Complexes	39
2.2.3.3	Thermolysis of 2.1 in Neat PMe_3 at 80 °C.....	40
2.2.3.4	Reaction of 2.2 with PMe_3	43
2.2.3.5	Reaction of 2.3 with PMe_3	49
2.2.3.6	Summary of the ^{31}P NMR Chemical Shifts and $^1J_{\text{WP}}$ Coupling Constants for the Various Products Formed from the Reactions of 2.1-2.3 with PMe_3	52
2.2.4	Radical Nature of Tungsten-Hydride Bond	54
2.2.5	Pursuit of Molybdenum Allyl Hydride Complexes	58
2.2.5.1	Preparation of $\text{Cp}^*\text{Mo}(\text{NO})(\eta^3\text{-CH}_2\text{CHCMe}_2)\text{Cl}$	59
2.2.5.2	Synthesis of $\text{Cp}^*\text{Mo}(\text{NO})(\eta^3\text{-CH}_2\text{CHCH}_2)\text{Cl}$	61
2.2.5.3	Reactions of $\text{Cp}^*\text{Mo}(\text{NO})(\eta^3\text{-allyl})\text{Cl}$ Complexes with Hydride Reagents.....	63
2.3	Summary	64
2.4	Experimental Methods	65
2.4.1	General Methods	65
2.4.2	Preparation of $\text{Cp}^*\text{W}(\text{NO})(\text{H})(\eta^3\text{-CH}_2\text{CHCMe}_2)$ (2.1a , 2.1b)	67
2.4.3	Preparation of $\text{Cp}^*\text{W}(\text{NO})(\text{H})(\eta^3\text{-CH}_2\text{CHCHPhMe}_2)$ (2.2)	69
2.4.4	Characterization of $\text{Cp}^*\text{W}(\text{NO})(\text{H})(\eta^3\text{-CH}_2\text{CHCHMe})$ (2.3)	69
2.4.5	Reaction of 2.1 with PMe_3 at 60 °C.....	71
2.4.6	Reaction of 2.1 with PMe_3 at 80 °C.....	73
2.4.7	Reactions of 2.1 with PhSSPh and AIBN by ^1H NMR Spectroscopy	75
2.4.7.1	Reaction of 2.1 with PhSSPh and AIBN	75

2.4.7.2	Monitoring the Reaction of 2.1 with PhSSPh and AIBN at Room Temperature .	77
2.4.7.3	Monitoring the reaction of 2.1 with PhSSPh and AIBN at 50 °C	77
2.4.7.4	Reaction of 2.1 with PhSSPh and a Catalytic Amount of AIBN.....	78
2.4.7.5	Reaction of 2.1 with 1-Iodopentane in the Presence of AIBN	78
2.4.8	Preparation of Cp*Mo(NO)(η^3 -CH ₂ CHCMe ₂)Cl (2.14)	79
2.4.9	Preparation of Cp*Mo(NO)(η^3 -C ₃ H ₅)Cl (2.16)	81
2.4.10	X-ray Crystallography	82
Chapter 3: Reactivity of Cp*W(NO)(H)(η^3-Allyl) Complexes with Hydrocarbons		88
3.1	Introduction.....	89
3.2	Results and Discussion	92
3.2.1	Multiple C-H Activations of Alkanes	92
3.2.1.1	Thermolysis of 2.1 in <i>n</i> -Pentane	92
3.2.1.2	Thermolysis of 2.1 in <i>n</i> -Heptane	97
3.2.1.3	Thermolysis of 2.1 in Cyclohexane	100
3.2.2	Mechanistic Consideration of C-H Activation	101
3.2.2.1	Proposed Mechanism for the Multiple Activation of Alkanes	102
3.2.2.2	Reaction of 2.1 with <i>N</i> -Methylmorpholine.....	105
3.2.3	Reaction of 2.1 with Chloroalkanes.....	111
3.2.4	One-Pot Synthesis of Unsymmetrical Saturated Ketones.....	116
3.2.4.1	Reactions of 2.1-2.3 with benzene under CO pressure.....	117
3.2.4.2	Reactions of 2.1 and 2.3 with Mesitylene Under CO Pressure.....	121
3.2.4.3	Thermolysis of 2.1 in <i>n</i> -Pentane Under CO Pressure	122

3.2.4.4	Mechanistic Considerations for the Regiospecific Generation of Ketones by 2.1	123
3.2.4.5	Thermolysis of 2.2 in Mesitylene Under CO Pressure	127
3.2.4.6	Theoretical Considerations for the Formation of Unsymmetrical Saturated Ketones	131
3.2.4.7	Recyclable Tungsten Cycle for Regiospecific Synthesis of Ketones from Hydrocarbons and CO	132
3.3	Summary	135
3.4	Experimental	136
3.4.1	General Methods	136
3.4.2	Thermolysis of 2.1 in <i>n</i> -Pentane	138
3.4.3	Thermolysis of 2.1 in <i>n</i> -Heptane	140
3.4.4	Thermolysis of 2.1 in Cyclohexane	143
3.4.5	Reaction of 2.1 with <i>N</i> -Methylmorpholine	144
3.4.6	Reaction of 2.1 with 1-Chloropropane	145
3.4.7	Reaction of 2.1 with 1-Chlorobutane	146
3.4.8	Reaction of 2.1 with Benzene and CO; Preparation of 4-Methyl-1-phenylpentan-1-one (3.8)	147
3.4.9	Reaction of 2.1 with Mesitylene and CO; Preparation of 1-(3,5-Dimethylphenyl)-5-methylhexan-2-one (3.11)	148
3.4.10	Preparation of Cp*W(NO)(CO)(η^2 -CH ₂ =CHCHMe ₂) (3.13)	149
3.4.11	Preparation of Unsymmetrical Ketones Under Aerobic Conditions	151
3.4.11.1	Aerobic Preparation of 3.8 from 2.1 and Benzene Under CO Pressure	151

3.4.11.2	Aerobic Preparation of 3.11 from 2.1 and Mesitylene under CO Pressure	151
3.4.12	X-ray Crystallography	152
Chapter 4: The Functionalization of Methane Initiated by Cp*W(NO)(CH₂CMe₃)(η^3-CH₂CHCMe₂)		
155		
4.1	Introduction.....	156
4.2	Results and Discussion	158
4.2.1	Adapted Synthesis of 4.1	158
4.2.2	C-H Activation of Methane	159
4.2.2.1	Optimized Conditions for the C-H Activation of Methane Initiated by 4.1 ...	160
4.2.2.2	Pressure Optimization for the C-H Activation of Methane	164
4.2.2.3	Solvent Optimization for the C-H Activation of Methane.....	165
4.2.2.4	Thermal Optimization of C-H Activation via Kinetic Studies	166
4.2.3	1,1-Insertion of Carbon Monoxide into W-C Bonds	167
4.2.3.1	Functionalization of a Neopentyl Ligand with CO.....	167
4.2.3.2	Carbonylation of the Methyl Ligand.....	170
4.2.4	Additional C-C Bond Formation via Acyl-Allyl Ligand Coupling	175
4.2.4.1	Conversion of 4.2 Under CO Pressure to the η^2 -Bound Ketone Complex	176
4.2.4.2	Conversion of 4.1 Under CO Pressure to the η^2 -Bound Ketone Complex	182
4.2.5	Release of Bound Ketone Ligands.....	185
4.2.5.1	Thermolysis of 4.6 ; Release of 2,2,7-Trimethyloct-6-en-4-one	186
4.2.5.2	Conversion of Methane and CO to β,γ -Unsaturated Ketones from 4.5	188
4.2.6	Complete Cycle for the Direct Conversion of Methane to Unsaturated Ketones...	191
4.3	Summary	194

4.4	Experimental	195
4.4.1	General Methods	195
4.4.2	Adapted Synthesis of $\text{Cp}^*\text{W}(\text{NO})(\text{CH}_2\text{CMe}_3)(\eta^3\text{-CH}_2\text{CHCMe}_2)$ (4.1).....	197
4.4.3	Preparation of $\text{Cp}^*\text{W}(\text{NO})(\text{CH}_3)(\eta^3\text{-CH}_2\text{CHCMe}_2)$ (4.2)	198
4.4.4	Solvent Optimization for the C-H Activation of Methane by 4.1	199
4.4.4.1	Preparation of 4.2 Using C_6F_6 as the Solvent	199
4.4.4.2	Preparation of 4.2 Using a Small Volume of C_6H_{12} as the Solvent.....	200
4.4.4.3	Preparation of 4.2 Using an Increased Volume of C_6H_{12} as the Solvent.....	200
4.4.5	Preparation of $\text{Cp}^*\text{W}(\text{NO})(\text{C}(\text{O})\text{CH}_2\text{CMe}_3)(\eta^3\text{-CH}_2\text{CHCMe}_2)$ (4.3).....	200
4.4.6	Preparation of $\text{Cp}^*\text{W}(\text{NO})(\text{C}(\text{O})\text{CH}_3)(\eta^3\text{-CH}_2\text{CHCMe}_2)$ (4.4)	201
4.4.7	Preparation of $\text{Cp}^*\text{W}(\text{NO})(\text{CO})(\eta^2\text{-CH}_2=\text{CHCMe}_2\text{C}(\text{O})\text{CH}_3)$ (4.5)	203
4.4.8	Preparation of $\text{Cp}^*\text{W}(\text{NO})(\text{CO})(\eta^2\text{-CH}_2=\text{CHCMe}_2\text{C}(\text{O})\text{CH}_2\text{CMe}_3)$ (4.6)	204
4.4.9	Reaction of 4.1 with CO at 170 °C; Preparation of 2,2,7-Trimethyloct-6-en-4-one (4.7)	205
4.4.10	Reaction of 4.2 with CO at 170 °C; Preparation of Ketones 5-Methylhex-4-en-2-one (4.8a), 3,3-Dimethylpent-4-en-2-one (4.8b), and <i>trans</i> -5-Methylhex-3-en-2-one (4.8c)	206
4.4.11	Direct Conversion of Methane to Ketone	208
4.4.12	Identification of $\text{Cp}^*\text{W}(\text{NO})(\text{CO})(\eta^2\text{-C}_6\text{H}_{10})$ Byproduct (4.9)	209
4.4.13	X-ray crystallography	210
 Chapter 5: The Functionalization of Methane, Ethane, and Other Hydrocarbons Initiated		
by $\text{Cp}^*\text{W}(\text{NO})(\text{CH}_2\text{CMe}_3)(\eta^3\text{-Allyl})$ Complexes		213
5.1	Introduction.....	214

5.2	Results and Discussion	216
5.2.1	C-H Activation of Methane by $\text{Cp}^*\text{W}(\text{NO})(\text{CH}_2\text{CMe}_3)(\eta^3\text{-CH}_2\text{CHCHPh})$	216
5.2.1.1	Identification of Isomers through the σ - π Distortion of the Allyl Ligand and ^{13}C NMR Spectroscopy	220
5.2.2	C-H Activation of Ethane by 5.1	222
5.2.3	Single C-H Activation of Propane and <i>n</i> -Butane.....	227
5.2.4	Optimization of the Single C-H Activation of C1-C3 Alkanes by 5.2	232
5.2.4.1	C-H Activation of Methane by 5.2	232
5.2.4.2	Solvent Optimization for the C-H Activation of Methane by 5.2	233
5.2.4.3	C-H activation of Ethane and Propane by 5.2	234
5.2.5	C-H Activation of Heteroatom-Containing Hydrocarbons by 5.1	235
5.2.5.1	Selective C-H Activation of (<i>n</i> -Butyl) ₂ O.....	235
5.2.5.2	Selective Activation 1-Chloropropane.....	240
5.2.5.3	C-H Activation of Tetramethylsilane.....	245
5.2.6	Ethane Functionalization Effected by 5.1	245
5.2.6.1	Functionalization of the Ethyl Ligand by 1,1-CO Insertion	245
5.2.6.2	Sequential C-C Bond Forming Reactions Under CO Pressure.....	249
5.2.7	Methane Functionalization with CO Initiated by 5.1	253
5.2.7.1	Formation of the Bound Ketone Complex from Methane Activation Initiated by 5.1	253
5.2.7.2	Preparation of $\text{Cp}^*\text{W}(\text{NO})(\text{C}(\text{O})\text{CH}_3)(\eta^3\text{-CH}_2\text{CHCHPh})$ (5.17).....	254
5.2.7.3	Formation of $\text{Cp}^*\text{W}(\text{NO})(\text{CO})(\eta^2\text{-PhCH=CHCH}_2\text{C(=O)CH}_2\text{CMe}_3)$ (5.18) ..	256
5.2.8	Acyl Ligands from Long-Chain Hydrocarbons	257

5.2.9	Alkane Functionalization with CO Initiated by 5.2	261
5.2.10	Photolysis of Bound Ketone Complexes	263
5.3	Summary	264
5.4	Experimental	267
5.4.1	General Methods	267
5.4.2	Modified Synthesis of $\text{Cp}^*\text{W}(\text{NO})(\text{CH}_2\text{CMe}_3)(\eta^3\text{-CH}_2\text{CHCHPh})$ (5.1)	269
5.4.3	Preparation of $\text{Cp}^*\text{W}(\text{NO})(\text{CH}_3)(\eta^3\text{-CH}_2\text{CHCHPh})$ (5.3)	270
5.4.4	Preparation of $\text{Cp}^*\text{W}(\text{NO})(\text{CH}_3)(\eta^3\text{-CH}_2\text{CHCHPh})$ (5.4)	272
5.4.5	Optimized C-H Activation of Methane by 5.2	274
5.4.6	Optimization of Methane Activation by 5.2	275
5.4.6.1	C-H Activation of Methane by 5.2 Using C_6F_6 as the Solvent	275
5.4.6.2	C-H Activation of Methane by 5.2 Using 25 mL of C_6H_{12} as the Solvent	276
5.4.7	Preparation of $\text{Cp}^*\text{W}(\text{NO})(\text{C}_6\text{H}_{11})(\eta^3\text{-CH}_2\text{CHCHMe})$ (5.8)	276
5.4.8	Optimized C-H Activation of Ethane by 5.2	277
5.4.9	Optimized C-H Activation of Propane by 5.2	278
5.4.10	Preparation of $\text{Cp}^*\text{W}(\text{NO})((\text{CH}_2)_4\text{O}(\text{CH}_2)_3\text{CH}_3)(\eta^3\text{-CH}_2\text{CHCHPh})$ (5.11)	279
5.4.11	Preparation of $\text{Cp}^*\text{W}(\text{NO})(\text{CH}_2\text{CH}_2\text{CH}_2\text{Cl})(\eta^3\text{-CH}_2\text{CHCHPh})$ (5.12)	281
5.4.12	Preparation of $\text{Cp}^*\text{W}(\text{NO})(\text{CH}_2\text{SiMe}_3)(\eta^3\text{-CH}_2\text{CHCHPh})$ (5.13)	282
5.4.13	Preparation of $\text{Cp}^*\text{W}(\text{NO})(\text{C}(\text{O})\text{CH}_2\text{CH}_3)(\eta^3\text{-CH}_2\text{CHCHPh})$ (5.14)	284
5.4.14	Preparation of $\text{Cp}^*\text{W}(\text{NO})(\text{CO})(\eta^2\text{-PhCH=CHCH}_2\text{C}(\text{O})\text{CH}_2\text{CH}_3)$ (5.15)	285
5.4.15	Preparation of $\text{Cp}^*\text{W}(\text{NO})(\text{CO})(\eta^2\text{-PhCH=CHCH}_2\text{C}(\text{O})\text{CH}_3)$ (5.16)	287
5.4.16	Preparation of $\text{Cp}^*\text{W}(\text{NO})(\text{C}(\text{O})\text{CH}_3)(\eta^3\text{-CH}_2\text{CHCHPh})$ (5.17)	289
5.4.17	Preparation of $\text{Cp}^*\text{W}(\text{NO})(\text{CO})(\eta^2\text{-PhCH=CHCH}_2\text{C}(\text{O})\text{CH}_2\text{CMe}_3)$ (5.18)	290

5.4.18	Preparation of $\text{Cp}^*\text{W}(\text{NO})(\text{C}(\text{O})(\text{CH}_2)_4\text{O}(\text{CH}_2)_3\text{CH}_3)(\eta^3\text{-CH}_2\text{CHCHPh})$ (5.20)	291
5.4.19	Preparation of $\text{Cp}^*\text{W}(\text{NO})(\text{C}(\text{O})(\text{CH}_2)_6\text{CH}_3)(\eta^3\text{-CH}_2\text{CHCHPh})$ (5.21)	292
5.4.20	Preparation of $\text{Cp}^*\text{W}(\text{NO})(\text{CO})(\eta^2\text{-MeCH=CHCH}_2\text{C(=O)CH}_2\text{CMe}_3)$ (5.22)	293
5.4.21	Photolysis of 5.16; Preparation of (<i>E/Z</i>)-5-Phenylpent-4-en-2-one (5.23)	294
5.4.22	Photolysis of 5.18; Preparation of (<i>E/Z</i>)-6,6-Dimethyl-1-phenylhept-1-en-4-one (5.24)	295
5.4.23	X-ray Crystallography	296
Chapter 6: Conclusions and Future Work		301
6.1	Summary and Conclusions	302
6.2	Future Directions	310
6.2.1	Optimization of Alkane Functionalization Initiated by $\text{Cp}^*\text{W}(\text{NO})(\text{CH}_2\text{CMe}_3)(\eta^3\text{-allyl})$ Complexes	310
6.2.1.1	Optimization of the Conversion of Methane and CO into 4.8 Initiated by 4.1	310
6.2.1.2	Optimization of Alkane Functionalization Initiated by 5.1 as well as Investigation of an Expanded Scope of Substrates	311
6.2.1.3	Conversion of Methane to Ketones Initiated by 5.2	312
6.2.2	Further Reactions Initiated by the $\text{Cp}^*\text{W}(\text{NO})(\text{H})(\eta^3\text{-allyl})$ Complexes	313
6.2.2.1	One-Pot Functionalization of Methane Initiated by 2.1	313
6.2.2.2	Reactions with Electrophiles	315
6.2.2.3	Coupling of Alkanes with Aldehydes Initiated by 2.1	316
References		319
Appendices		329

Appendix A Supplementary Materials for Chapter 2	329
Appendix B Supplementary Materials for Chapter 3	331
Appendix C Supplementary Materials for Chapter 4	333
C.1 Attempt to Synthesize the Molybdenum Analogue of 4.1	333
C.2 Additional Figures for Chapter 4	338
Appendix D Supplementary Material for Chapter 5	342
Appendix E Supplementary Material for Chapter 6	345
E.1 Preliminary Reaction: Analysis of the Reaction of 5.7 with CO at 170 °C by ¹ H	
NMR Spectroscopy	345
E.2 Preliminary Reaction: Reaction of 2.1 with Benzaldehyde	346
E.3 Preparation of Cp*W(NO)(CH ₂ -3,5-Me ₂ C ₆ H ₃)(O-CH(CH ₂ CMe ₃)C(Me)HCH=CH ₂)	
(E.1)	347
Appendix F X-ray Crystallography for Appendices	349

List of Tables

Table 2.1. ^1H NMR Chemical Shifts (δ) in ppm of the allyl meso <i>H</i> signals for complexes 2.1-2.3 in C_6D_6 highlighting the relative differences between the endo and exo orientations of the allyl ligands in the isomers.....	31
Table 2.2. Correlation of ^{31}P NMR chemical shifts and $^1J_{\text{WP}}$ coupling frequencies between the various tungsten-phosphine complexes.	53
Table 2.3. X-ray crystallographic data for complexes 2.1 , 2.2a/b , 2.3 , and 2.4	86
Table 2.4. X-ray crystallographic data for complexes 2.7 , 2.8 , 2.14 , and 2.15	87
Table 3.1. WH signals of the isomers of 3.2 as identified by their characteristic ^{183}W satellites. 99	
Table 3.2. Ketones that result from the thermolysis of 2.1-2.3 in benzene under CO pressure .	119
Table 3.3. X-ray crystallographic data for complexes 3.1 , 3.4 , 3.5 , and 3.15	154
Table 4.1. Pressure dependence for the C-H activation of methane.....	165
Table 4.2. The effect of solvent for the yield of 4.2 from the C-H activation of methane	165
Table 4.3. Pseudo first-order rate constants for the thermolysis of 4.1 in C_6D_6	166
Table 4.4. Spectroscopic properties of compounds formed during Steps 1-5 shown in Figure 4.13 tracking the conversion of methane into an unsymmetrical, unsaturated ketone.	195
Table 4.5. X-ray crystallographic data for complexes 4.2-4.6	212
Table 5.1. W-C bond lengths for the alkyl ligand of complexes 5.3-5.6	230
Table 5.2. Effect of solvent on yield of methane activation effected by complex 5.2	234
Table 5.3. Conditions and yields for the C-H activations of methane, ethane, and propane effected by 5.2	235

Table 5.4. Chemical shifts and $^1J_{WC}$ values for the alkene carbon signals for the isomers of 5.15	252
Table 5.5. Chemical shifts of the carbonyl signals in the ^{13}C NMR spectrum of 5.15	252
Table 5.6. ^1H and ^{13}C NMR chemical shifts of the dihapto alkene fragment for the isomers of 5.16	254
Table 5.7. X-ray crystallographic data for complexes 5.3 , 5.4 , and 5.5	299
Table 5.8. X-ray crystallographic data for complexes 5.6 , 5.12 , and 5.14	300
Table 6.1. C=C bond lengths of dihapto alkene ligands for complexes 3.15a , 3.15b , 4.5 , and 4.6	309

List of Figures

Figure 2.1. Solid-state molecular structure of 2.1	23
Figure 2.2. Solution molecular structures of the isomers of 2.2 and 2.3 as determined by ^1H Sel NOE NMR spectroscopy.	25
Figure 2.3. Solid-state molecular structure of 2.2a	27
Figure 2.4. Solid-state molecular structure of 2.2b	28
Figure 2.5. Solid-state molecular structure of 2.3a	30
Figure 2.6. Computed thermal decomposition pathways from 2.3a identify a $16e\ \eta^2$ -alkene intermediate complex as the lowest energy species.....	33
Figure 2.7. Expansion of the $^{31}\text{P}\{^1\text{H}\}$ NMR spectrum (-21.8 to -25.2 ppm) of the mixture of 2.4 and 2.5 in C_6D_6 (162 MHz).....	35
Figure 2.8. Solid-state molecular structure of 2.4	37
Figure 2.9. Expansion of the overlaid ^1H and $^1\text{H}\{^{31}\text{P}\}$ NMR spectra (-0.65 to -1.25 ppm) of 2.4 in C_6D_6 (400 MHz)	39
Figure 2.10. ^1H - ^{31}P and ^{13}C - ^{31}P coupling observed for (a) 2.6b and (b) 2.6c from the ^1H and ^{13}C NMR spectra recorded in C_6D_6 . ^{13}C - ^{31}P coupling is only observed for the C atoms oriented cis to the PMe_3 . The η^2 connectivity of the alkene ligands is established by characteristic ^{183}W satellites.....	42
Figure 2.11. Expansion of the $^{31}\text{P}\{^1\text{H}\}$ NMR spectrum (-9.3 to -17.5 ppm) of 2.6 in C_6D_6 (162 MHz).....	43
Figure 2.12. Solid-state molecular structure of 2.7	45
Figure 2.13. Solid-state molecular structure of 2.8	47

Figure 2.14. (a) Diagram displaying the ^{31}P coupling to the η^2 -alkene ^1H and ^{13}C signals for 2.8 ; (b) Expansion of the overlaid ^1H and $^1\text{H}\{^{31}\text{P}\}$ NMR spectra (2.55 to 2.41 ppm) of 2.8 in C_6D_6 (400 MHz).....	49
Figure 2.15. Expansion of the $^{31}\text{P}\{^1\text{H}\}$ NMR spectrum (-9.6 to -16.7 ppm) of 2.9 in C_6D_6 (162 MHz)	51
Figure 2.16. Computed electronic surface potential of 2.3a	54
Figure 2.17. (a) Colours observed for the reaction of 2.1 with PhSSPh in the presence of AIBN. (b) ^1H NMR spectrum (400 MHz, C_6D_6) for the reaction of 2.1 with PhSSPh in the presence of AIBN at 50 °C for 6 h.....	57
Figure 2.18. . Solid-state molecular structure of 2.15	60
Figure 2.19. Solid-state molecular structure of 2.16 , major component.....	62
Figure 2.20. Solid-state molecular structure of 2.16 , minor component.	63
Figure 3.1. Expansion of the 400 MHz ^1H NMR spectrum (4.66 to 4.24 ppm) of 3.1 in C_6D_6 ...	94
Figure 3.2. Solid-state molecular structure of 3.1a	96
Figure 3.3. Major isomers of 3.2 resulting from the reaction of 2.1 with <i>n</i> -heptane.....	98
Figure 3.4. Expansion of the 400 MHz ^1H NMR spectra (-1.00 to -1.75 ppm) of 3.1 and 3.2 in C_6D_6	100
Figure 3.5. (a) A change in hapticity allowing the position of the allyl ligand substituent(s) to change relative to the other ligands on the metal. (b) A proposed chain-walking mechanism in which the terminal allyl ligand ($\eta^3\text{-CH}_2\text{CHCHEt}$) in 3.1a is converted into the internal allyl ligand ($\eta^3\text{-MeCHCHCHMe}$) in 3.1b	104
Figure 3.6. Trapping of (a) $\text{Cp}^*\text{W}(\text{NO})(\eta^2\text{-MeCH=CHMe})$ and (b) $\text{Cp}^*\text{W}(\text{NO})(\eta^2\text{-CH}_2\text{=CHCH}_2\text{Me})$ with PMe_3 providing evidence for coupling to either terminus of the allyl	

ligand, a feature that is necessary for the mechanism proposed for the transformation of 3.1a to 3.1b shown in Figure 3.5b.	105
Figure 3.7. Solid-state molecular structure of 3.4	108
Figure 3.8. (a) Solution molecular structure of 3.4 as determined by a { ¹ H- ¹ H} NOESY NMR spectrum. (b) The ¹ H NMR spectrum of 3.4 in C ₆ D ₆	109
Figure 3.9. Solid-state molecular structure of 3.5	113
Figure 3.10. Solid-state molecular structure of the second isomer of 3.5	114
Figure 3.11. Solid-state molecular structure of the third isomer of 3.5	115
Figure 3.12. (a) Isomers of 2.3 with the methyl substituent of the allyl ligand proximal to the nitrosyl produce ketone 3.9a . (b) Isomers of 2.3 with the methyl substituent proximal to the hydride ligand produce ketone 3.9b	120
Figure 3.13. Coupling of the hydride to the methylene terminus of the allyl ligand results in the 16e intermediate complex Cp*W(NO)(η ² - <i>trans</i> -β-methylstyrene), which accounts for the formation of 3.10 as the only organic product observed.	121
Figure 3.14. Expansion of the FT-IR spectrum (nujol mull) from 2900 cm ⁻¹ to 1500 cm ⁻¹ for the reaction of 2.1 with benzene under CO pressure.	126
Figure 3.15. Solid-state molecular structure of 3.15a	129
Figure 3.16. Solid-state molecular structure of 3.15b	130
Figure 3.17. Computed Δ <i>G</i> values for the various species involved during the mesitylene reaction involving complex 2.1 shown in Scheme 3.11.	132
Figure 3.18. (a) Synthesis of an unsymmetrical ketone via carbonylative Stille Coupling. (b) Reaction of carboxylic acid derivatives with organometallic reagents to give unsymmetrical ketones and unwanted byproduct.....	135

Figure 4.1. Solid-state molecular structure of 4.2	163
Figure 4.2. Solid-state molecular structure of 4.3	169
Figure 4.3. Solid-state molecular structure of 4.4	172
Figure 4.4. Plot of ^1H NMR spectra from carbonylation of 4.2 taken at 30 min intervals.	174
Figure 4.5. Solid-state molecular structure of 4.5	179
Figure 4.6. Top-down view of solid-state molecular structure of 4.5 showing that the distance between W(1) and O(2) is 5.419 Å.....	180
Figure 4.7. Expansions of the ^1H NMR spectrum (400 MHz, C_6D_6) of 4.5 showing the resonances due to the alkene hydrogens	181
Figure 4.8. Solid-state molecular structure of 4.6	184
Figure 4.9. Expansion of the ^1H NMR spectrum (400 MHz, CDCl_3) of 4.7 from δ 5.45 to 5.18 ppm showing the triplet of septets of the $=\text{CH}$ signals.	187
Figure 4.10. Expansion of the ^1H NMR spectrum (400 MHz, CDCl_3) from δ 6.85 to 5.00 ppm of the mixture of ketones 4.8 displaying the characteristic alkene signals of 4.8a , 4.8b , and 4.8c	189
Figure 4.11. Complete synthetic cycle for the conversion of methane into the ketones 4.8a-c initiated by compound 4.1	192
Figure 5.1. Solid-state molecular structure of 5.3a	219
Figure 5.2. The σ - π distortion of the allyl ligand for isomers of 5.3 with the chemical shifts due to the allyl C atoms from the ^{13}C APT NMR spectrum.....	222
Figure 5.3. The σ - π distortion of the allyl ligand for isomers of 5.4 with the chemical shifts due to the allyl C atoms from the ^{13}C APT NMR spectrum.....	224
Figure 5.4. Solid-state molecular structure of 5.4	225

Figure 5.5. Expansion of the ^1H NMR spectrum (600 MHz, C_6D_6) showing the ethyl CH_3 signal of 5.4 with characteristic satellites due to ^{183}W ($^3J_{\text{HH}} = 7.34$, $^3J_{\text{WH}} = 5.1$ Hz).....	227
Figure 5.6. Solid-state molecular structure of 5.5	229
Figure 5.7. Solid-state molecular structure of 5.6	231
Figure 5.8. ^{13}C APT NMR spectrum of complex 5.11a (100 MHz, C_6D_6)..	237
Figure 5.9. Expansions of the ^{13}C APT NMR spectrum of 5.11 at δ 73.3, 63.1, and 17.9 ppm which display characteristic satellites due to tungsten-183 coupling that indicate the presence of tungsten-carbon bonds.	238
Figure 5.10. Expansion of the ^1H NMR spectrum of 5.11 from δ 3.66 to 3.27 ppm (400 MHz, C_6D_6).....	239
Figure 5.11. Reoriented solid-state molecular structures for the enantiomers of 5.12b	242
Figure 5.12. Solid-state molecular structure of 5.14	248
Figure 5.13. Expansion of the ^1H NMR spectrum of 5.15 from δ 4.05 to 3.50 ppm and δ 2.82 to 2.42 ppm showing the signals due to the alkene protons for each isomer.....	251
Figure 5.14. Expansions of the ^1H NMR spectra from δ 4.20 to 3.80 ppm and δ 3.22 to 2.61 ppm for complex 5.16a and the mixture of 5.16a and 5.18	257
Figure 5.15. Expansions of the $\{^1\text{H}-^{13}\text{C}\}$ HMBC NMR spectra of (a) compound 5.20 and (b) compound 5.21 showing the correlation between the acyl carbon signal and the triplet at the α position to the carbonyl for each complex.....	260
Figure 5.16. IR spectrum (Nujol) of the mixture of isomers of 5.22	262
Figure 6.1. Comparison of the mechanisms for ketone formation initiated by $\text{Cp}^*\text{W}(\text{NO})(\text{H})(\eta^3\text{-allyl})$ (e.g. 2.1) and $\text{Cp}^*\text{W}(\text{NO})(\text{CH}_2\text{CMe}_3)(\eta^3\text{-allyl})$ (e.g. 4.1) complexes.	307

Figure 6.2. Complexes formed at 750 psig CO pressure containing a dihapto bound olefin ligand.

Compounds **4.5**, **5.15**, and **5.16** result from the functionalization of methane and ethane..... 309

Figure 6.3. The proposed conversion of the isomers of **5.7** under CO pressure to afford isomers of *cis/trans*- β,γ -unsaturated and *cis/trans*- α,β -unsaturated ketones that are derived from the initial reaction of **5.2** with methane..... 313

List of Schemes

Scheme 1.1 Early examples of intermolecular C-H activation reported by (a) Bergman and (b) Graham.....	5
Scheme 1.2. The catalytic conversion of methane to methanol and chloromethane by platinum salts	6
Scheme 1.3. Conversion of methane to methyl bisulfate by (bpym)PtCl ₂ in fuming H ₂ SO ₄	7
Scheme 1.4. Hydromethylation of propylene by a scandium sandwich complex	8
Scheme 1.5. The 1,1-insertion of a silver-stabilized across a C-H bond of methane	8
Scheme 1.6. Conversion of methane to a methyl ester using iodate salts	9
Scheme 1.7. Conversion of methane to methyl ester using thallium(III) salts	10
Scheme 1.8. Thermal generation of a 16e η^2 -diene intermediate complex and subsequent single, terminal C-H activation of <i>n</i> -pentane	12
Scheme 1.9. Aryl-hydrogen exchange reactions involving the coupling of the aryl and allyl ligands	13
Scheme 1.10. The reaction of Cp*W(NO)(CH ₂ CMe ₃)(η^3 -CH ₂ CHCHPh) with methylcyclohexane results in the formation of all three types of possible organometallic products stemming from (1) single, terminal C-H activation, (2) R/allyl H exchange, and (3) multiple C-H activations.	14
Scheme 2.1. C-H Activations Effected by Cp*W(NO)(CH ₂ CMe ₃)(η^3 -allyl) Complexes.....	19
Scheme 2.2. Synthesis of Cp*W(NO)(H)(η^3 -CH ₂ CHCMe ₂).....	21
Scheme 2.3. Initially proposed thermal pathway for 2.1	32
Scheme 2.4. Reaction of 2.1 with PMe ₃ at 60 °C	35
Scheme 2.5. Reaction of 2.1 with PMe ₃ at 80 °C	40

Scheme 2.6. Reaction of 2.2 with PMe ₃ at 60 °C	44
Scheme 2.7. Reaction of 2.3 with PMe ₃ at 60 °C	50
Scheme 2.8. Reaction of 2.1 with PhSSPh in the presence of the radical initiator AIBN.....	55
Scheme 2.9. Possible mechanism for the homolytic cleavage of the W-H bond in 2.1 and trapping of the tungsten radical by PhSSPh.....	56
Scheme 2.10. Reaction 2.1 with 1-iodopentane in the presence of a radical initiator	58
Scheme 2.11. Synthesis of Cp*Mo(NO)(η^3 -CH ₂ CHCMe ₂)Cl (2.14).....	59
Scheme 3.1. C-H activations effected by Cp*W(NO)(CH ₂ CMe ₃)(η^3 -allyl) complexes	90
Scheme 3.2. Summary of the 16e η^2 -alkene intermediate complexes generated by the thermolysis of 2.1-2.3 and the trapping of these 16e intermediate complexes by PMe ₃	91
Scheme 3.3. Thermolysis of Cp*W(NO)(H)(η^3 -allyl) complexes in <i>n</i> -pentane.....	93
Scheme 3.4. Thermolysis of complex 2.1 in <i>n</i> -heptane and cyclohexane	97
Scheme 3.5. Proposed mechanism for the conversion of 2.1 into 3.1a	103
Scheme 3.6. Reaction of complex 2.1 with <i>N</i> -methylmorpholine	106
Scheme 3.7. Possible mechanism for the transformation of 2.1 to 3.4	110
Scheme 3.8. Reactions of complex 2.1 with 1-chloropropane and 1-chlorobutane	112
Scheme 3.9. Reaction of 2.1 with benzene under CO pressure	117
Scheme 3.10. General conversion of benzene and CO to ketones effected by 2.1-2.3	118
Scheme 3.11. Reaction of 2.1 with mesitylene under CO pressure	122
Scheme 3.12. Reaction of 2.3 with mesitylene under CO pressure.....	122
Scheme 3.13. Trapping of η^2 -alkene intermediate complex with CO	123
Scheme 3.14. Probable mechanism for the generation of regiospecific ketones by 2.1	124
Scheme 3.15. Trapping of η^2 -alkene intermediate complex from 2.2 with CO	128

Scheme 3.16. Synthetic cycle for forming saturated unsymmetrical ketones	133
Scheme 4.1. The labeling reaction of 4.1 with C ₆ D ₆ provides evidence for two 16e intermediate complexes	156
Scheme 4.2. Thermolysis of 4.1 in neat alkane (e.g. <i>n</i> -pentane) results in multiple C-H activations	157
Scheme 4.3. Adapted synthesis of 4.1	159
Scheme 4.4. C-H activation of methane by complex 4.1	160
Scheme 4.5. Competing solvent activation under methane pressure.....	164
Scheme 4.6. Carbonylation of 4.1	168
Scheme 4.7. Carbonylation of the methyl ligand.....	170
Scheme 4.8. Proposed mechanism for the carbonylation of 4.2	175
Scheme 4.9. C-H activation of methane, followed by subsequent conversion to 4.5 under CO pressure	176
Scheme 4.10. Proposed mechanism for the formation of a η^2 -ketone ligand from a methyl ligand derived from the C-H activation of methane	182
Scheme 4.11. Formation of the η^2 -bound ketone complex 4.6	183
Scheme 4.12. Thermolysis of 4.1 under CO pressure to produce 3.7 and 4.7	186
Scheme 4.13. Thermolysis of 4.2 at 170 °C and 1000 psig CO to afford 3.7 and β,γ -unsaturated ketones 4.8a-c	188
Scheme 4.14. Proposed mechanism to account for the formation of all three ketones 4.8a-c ...	190
Scheme 4.15. Recyclable tungsten center for the conversion of methane to unsaturated ketones	194

Scheme 5.1. The single terminal C-H activation of linear alkanes effected by compounds 5.1 and 5.2	215
Scheme 5.2. C-H activation of methane by 5.1	216
Scheme 5.3. Single C-H activation of ethane by 5.1	223
Scheme 5.4. Optimized C-H activation of methane by 5.2	233
Scheme 5.5. C-H activation of dibutyl ether by 5.1	236
Scheme 5.6. Reaction of 5.1 with 1-chloropropane.....	240
Scheme 5.7. Proposed mechanism for the transformation of 5.12a to 3.5	244
Scheme 5.8. C-H activation of tetramethylsilane by 5.1	245
Scheme 5.9. Carbonylation of 5.4 to produce the acyl allyl complex 5.14	246
Scheme 5.10. C-H activation of ethane and subsequent functionalization with CO initiated by compound 5.1	250
Scheme 5.11. Reaction of 5.3 with CO.....	254
Scheme 5.12. Conversion of 5.13 to 5.17 under CO pressure	255
Scheme 5.13. Conversion of 5.1 to the η^2 -bound ketone complex 5.18 under exposure to CO.	256
Scheme 5.14. Carbonylation of complex 5.11 to produce an acyl ligand derived from the terminal activation of di(<i>n</i> -butyl) ether.....	258
Scheme 5.15. Functionalization of an <i>n</i> -heptyl ligand by 1,1-insertion of CO	258
Scheme 5.16. The thermolysis of 5.2 at 75 °C and 750 psig CO	262
Scheme 5.17. Photolysis of 5.16 to afford β,γ -unsaturated ketones from methane and CO.....	263
Scheme 5.18. Photolysis of 5.18 to afford β,γ -unsaturated ketones	264
Scheme 5.19. The stepwise functionalization of ethane with CO initiated by 5.1	266

Scheme 6.1. The production of (a) an unsymmetrical saturated ketone (3.11) from mesitylene and CO initiated by 2.1 and (b) a β,γ -unsaturated ketone (4.8a) from methane and CO initiated by 4.1	305
Scheme 6.2. Proposed one-pot conversion of methane and CO initiated by compound 2.1 to produce the unsymmetrical saturated ketone 5-methylhexan-2-one	314
Scheme 6.3. Proposed functionalization of alkanes via dehydrogenative coupling to electrophiles initiated by 2.1 . In this proposal, the appropriate selection of X^- could result in an organometallic product that can lose HX and effect the multiple C-H activations of an alkane to reinitiate the cycle.	316
Scheme 6.4. (a) Proposed coupling of alkanes and aldehydes initiated by 2.1 , and (b) preliminary reaction of 2.1 with benzaldehyde	317

List of Abbreviations

°	degree (of angle or temperature)
1D	1-dimensional
2D	2-dimensional
α	alpha, the position once removed from the point of reference
Å	angstrom, 10^{-10} m
Ac	acetyl, $\text{C}(=\text{O})\text{CH}_3$
AIBN	azobisisobutyronitrile \
Anal.	analysis
APT	attached proton test
β	beta, the position twice removed from the point of reference
br	broad (spectral)
Bu	butyl, C_4H_9
^{13}C	carbon-13
$^{13}\text{C}\{^1\text{H}\}$	proton-decoupled carbon-13
ca.	circa (approximately)
Calcd	calculated
cat.	catalyst
cm^{-1}	wavenumber
CO	carbon monoxide; carbonyl ligand
COSY	correlation spectroscopy
Cp	cyclopentadienyl, $\eta^5\text{-C}_5\text{H}_5$

Cp*	pentamethylcyclopentadienyl, $\eta^5\text{-C}_5\text{Me}_5$
deg	degree (angle)
°C	degrees Celcius
Δ	heat, change
δ	delta, chemical shift in ppm; the position four times removed from the point of reference
d	doublet (spectral); day
D	^2H , deuterium
DCM	dichloromethane
dd	doublt of doublets (spectral)
ddd	doublet of doublets of doublets (spectral)
dddd	doublet of doublets of doublets of doublets (spectral)
ddq	doublet of doublets of quartets (spectral)
DFT	density field theory
dt	doublet of triplets
E_a	Arrhenius activation energy
EA	elemental analysis
EI	electron impact
ESI	electrospray ionization
eV	electron volt
ΔH^\ddagger	enthalpy of activation
ΔS^\ddagger	entropy of activation
equiv.	equivalents

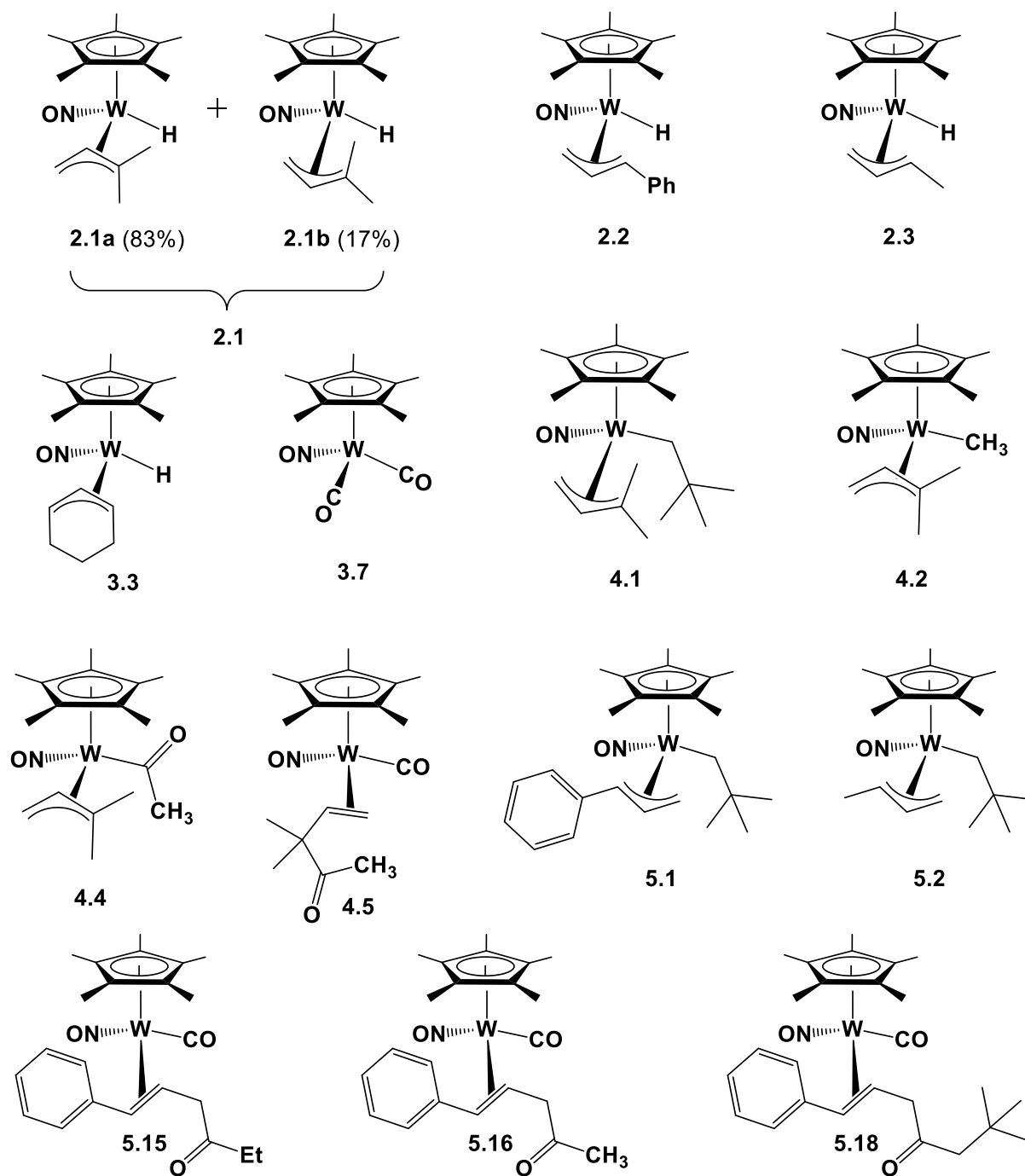
η	eta, used to denote the hapticity
Et	ethyl, CH_2CH_3
γ	gamma, herein the position trice removed from the point of reference
g	gram
^1H	proton, hydrogen
$^1\text{H}\{^{31}\text{P}\}$	phosphorus-decoupled proton
h	hour
HMBC	heteronuclear multiple-bond correlation
HREI	high-resolution electron impact
HSQC	heteronuclear single-quantum correlation
Hz	hertz
IR	infrared
J	joule
J	coupling constant
$^nJ_{\text{AB}}$	n-bond coupling constant between atoms A and B
K	degrees Kelvin
k	kinetic rate constant
kJ	kilojoule
LREI	low-resolution electron impact
m	meta
m	multiplet (spectral)
M^+	molecular ion
Me	methyl, CH_3

Mes	mesityl, 3,5- Me ₂ C ₆ H ₃
mg	milligram
MHz	megahertz
min	minute
mL	milliliter
mmol	millimole
⁹⁸ Mo	molybdenum-98
mp	melting point
MS	mass spectrometry
<i>m/z</i>	mass-to-charge ratio
ⁿ Bu	<i>n</i> -butyl, CH ₂ CH ₂ CH ₂ CH ₃
NMM	<i>N</i> -methyldmorpholine
NMR	nuclear magnetic resonance
NO	nitrosyl
NOESY	nuclear Overhauser effect spectroscopy
ⁿ Pr	<i>n</i> -propyl, CH ₂ CH ₂ CH ₃
ν	nu, stretching frequency
<i>o</i>	ortho
<i>p</i>	para
³¹ P	phosphorus-31
³¹ P{ ¹ H}	proton-decoupled phosphorus-31
π	pi
Ph	phenyl, C ₆ H ₅

ppm	parts per million
Pr	propyl
psig	pounds per square inch gauge
q	quartet (spectral)
qd	quartet of doublets (spectral)
qdd	quartet of doublets of doublets (spectral)
qq	quartet of quartets (spectral)
σ	sigma
s	singlet (spectral); strong (spectral)
Sel NOE	1D selective NOESY
t	triplet (spectral)
td	triplet of doublets (spectral)
TEMPO	2,2,6,6-tetramethylpiperidine 1-oxyl
THF	tetrahydrofuran
tt	triplet of triplets (spectral)
TMS	trimethylsilyl, SiMe ₃
tsep	triplet of septets (spectral)
w	weak (spectral); week
¹⁸² W	tungsten-182
¹⁸³ W	tungsten-183
¹⁸⁴ W	tungsten-184
¹⁸⁶ W	tungsten-186
xs	excess

- ζ zeta, the position five times removed from the point of reference
- used to denote a radical

Compound numbers of select complexes[†]



[†]Compounds that exist as a mixture of two or more isomers are given a number with letter designations for each isomer. For example, compound **2.1** exists as two isomers, **2.1a** and **2.1b**. For convenience, this mixture of isomers is referred to simply as **2.1**. This applies to all such mixtures of isomers presented in this thesis.

Acknowledgements

First I would like to thank Prof. Peter Legzdins for his guidance and supervision. You were always available to talk research or impart life advice. I am grateful to have learned many lessons from you that I will take with me going forward.

Thank you to all of the current and past group member I had the pleasure of working with during the course of this research, in particular those who have collaborated with me on this work. Special thanks to Diana Fabulyak and Taleah Levesque for help with the editing process.

Thank you to all of the collaborators I have had at The Dow Chemical Company over the years. In particular I would like to thank Devon Rosenfeld and Brandon Rodriguez for many insightful discussions, sound advice, and providing me with an industrial perspective toward research.

I would like to thank the Natural Sciences and Engineering Research Council of Canada and the University of British Columbia for the funding they have provided me, and a special thanks to The Dow Chemical Company for generous research funding that made this work possible.

Thanks to the UBC Chemistry department facilities staff who have helped me along the way. To Prof. Laurel Schafer for taking the time to be a reader for this thesis and providing insightful feedback. Special thanks to Dr. Brian Patrick for teaching me everything I know about X-ray Crystallography, and for solving some of the structures presented in this thesis, and to Dr. Maria Ezhova of the NMR facility and Marshall Lapawa for the Microanalysis facility.

Thank you to my family for your support, especially to my father for outstanding encouragement.

Dedication

This thesis is dedicated to my wife, Tara. Without your love, support, and understanding none of this would have been possible.

Chapter 1: Introduction[†]

[†]A version of Section 1.2 has been published. Baillie, R. A.; Legzdins, P. *Coord. Chem. Rev.*

2016, 309, 1-20. Reproduced with permission from Coordination Chemistry Reviews. Copyright (2016) Elsevier.

1.1 Methane, Natural Gas, and C-H Activation.

The conversion of methane into value-added compounds is currently one of the principal chemical issues facing the world. The development of methods to effect the conversion of a relatively unreactive gas into a transportable quantity that is amenable to classical chemical manipulations is a goal at the forefront of organometallic chemical research. Methane is by far the most abundant component of natural gas comprising between 70-90% of most natural gas sources in North America.¹ Natural gas is chiefly used as a chemical feedstock and as a fuel, accounting for approximately a quarter of the world's energy.² Despite its abundance, methane does not contribute to either of these roles.¹⁻³ In recent years there has been a significant shift in natural gas sources away from the established resources such as petroleum to the “unconventional” sources of natural gas, which include shale gas, tight gas, and coal bed methane.⁴ These “unconventional” natural gas reserves contain larger fractions of lighter alkanes such as methane and ethane compared to other conventional sources.^{3, 4} Ethane and heavier light alkanes are typically converted into synthetically useful olefins through steam cracking. The cracking process is extremely energy intensive, and thus expensive, and it leads to mixtures of olefin products; the efficiency of the steam cracking process also leaves room for improvement.⁴ ⁵ To date, the only industrially practiced process for methane conversion is steam reforming to convert methane into synthesis gas (H_2 and CO).⁶ With natural gas becoming an ever more abundant and important resource, the underutilization of methane becomes an issue of increasing urgency. The development of new chemical processes to convert methane into either a C1 feedstock or a transportable fuel source is of paramount importance.

The two largest practical barriers to utilizing methane are its inherent low chemical reactivity and the difficulties in transporting a gas.⁶ Methane is comprised of C-H bonds which are strong and nonpolar, making it chemically challenging to convert the molecule into compounds that are accessible to conventional processes.^{1, 6} Additionally, methane is a volatile and flammable gas which makes transportation uneconomical.¹ The term “stranded” is often used to describe many methane natural gas sources as it is cost prohibitive to transport methane to locations where it could be used as a fuel.^{1, 2} The economic drawbacks of transporting the gas outweigh the benefit of using it as a fuel. It is in fact more cost effective to simply “flare” or burn it off than it is to transport it. It is estimated that 140 billion cubic meters are flared each year worldwide.² The flaring process has environmental ramifications as the burning of methane, itself a potent greenhouse gas molecule, releases carbon dioxide into the atmosphere.⁷ Powerful economic and environmental factors motivate efforts toward the functionalization of methane.

The principal goals of methane functionalization are essentially twofold:

1. Transportation:

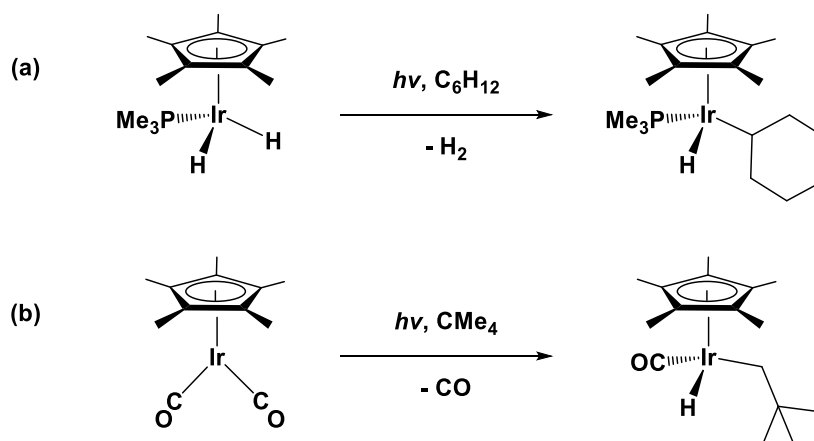
- The conversion of gaseous methane into a transportable liquid/solid so that it can economically be used as a fuel

2. C1 feedstock:

- The installation of functional groups that allow methane to be used as a carbon source for the synthesis of commodity chemicals from polymers to pharmaceuticals

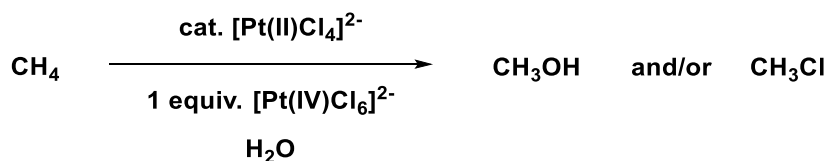
The C-H activation by well-defined transition-metal complexes offers an alternative pathway to transform these alkanes into value-added chemicals. There are many examples of transition-metal mediated C-H activations of alkanes that demonstrate an improved selectivity with a much lower energy cost compared to the conventional cracking processes.⁸ The functionalization of alkanes was first reported in the 1960s and 1970s when C-H bonds of saturated molecules were converted into C-Cl and C-O bonds.⁹ In the early 1980s the research groups of Bergman and Graham both reported the intermolecular C-H activation of saturated alkanes by iridium complexes (Scheme 1.1).^{10, 11} The discovery of these two reactions demonstrated that transition-metal complexes could effect the cleavage of a C-H bond and generate complexes containing well-defined transition metal-carbon bonds. This opened the field of C-H activation chemistry.⁹ More than three decades later there have been many advances in the field of C-H activation.¹² However, the examples of C-H activation and functionalization of methane by molecular complexes or catalysts remain few in number.¹ In addition, the majority of these complexes effect only stoichiometric conversions, and the few examples of catalytically active systems are not considered suitable for industrial-scale conversions.¹³

Scheme 1.1 Early examples of intermolecular C-H activation reported by (a) Bergman¹¹ and (b) Graham¹⁰



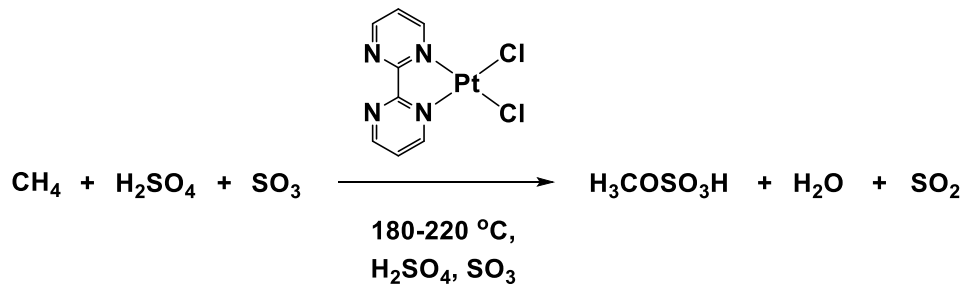
The classic example of transition metal-mediated functionalization of methane comes from Shilov. It involves the conversion of methane by platinum salts to methanol as well as chloromethane. The system uses a Pt(II) salt as the catalyst for the conversion of a C-H bond of methane to a C-O or C-Cl bond (Scheme 1.2). The mechanism of this transformation still remains poorly understood. A major drawback of this system is that it requires a stoichiometric quantity of a Pt(IV) salt to effect the transformation of methane. This renders the process unpractical as a solution to converting stranded methane resources since the cost implications of using equimolar quantities of a noble metal to convert a cheap natural gas molecule are unattractive.^{9, 14}

Scheme 1.2. The catalytic conversion of methane to methanol and chloromethane by platinum salts.^{9, 14}



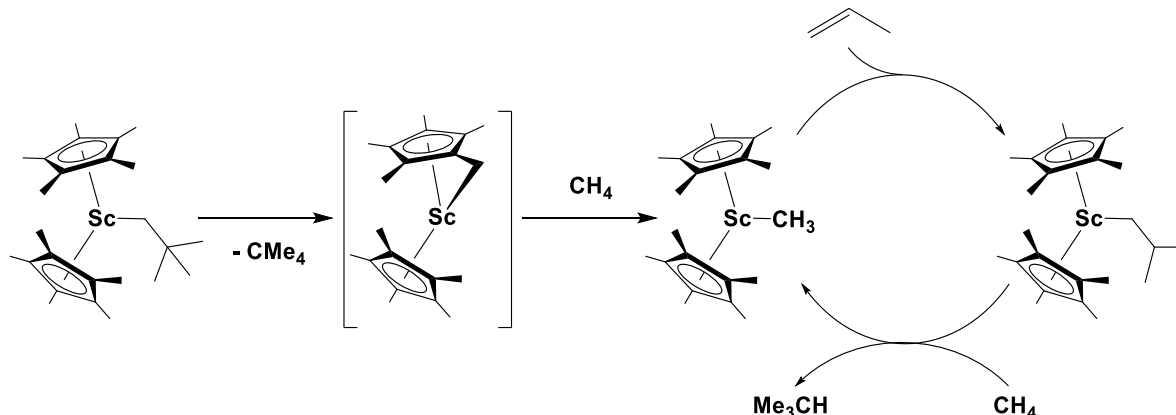
An important example of a homogenous platinum catalyst was reported by Periana in 1998. A Pt(II)/Pt(IV) catalyst system is used to convert methane into methyl bisulfate with an excess of 500 turnovers,¹⁵ one of the better numbers for a homogenous methane catalyst. The conversion of methane to methyl bisulfate occurs in fuming sulfuric acid which provides a significant economic barrier to industrial application. The authors propose that methane is C-H activated by the catalyst to produce (bpym)Pt(II)(CH₃)Cl [bpym = η²-(2,2'-bypyrimidyl)], which they can detect in the H₂SO₄ mixture at room temperature by ¹H NMR spectroscopy. They were unable to detect the platinum-carbon bond-containing intermediate from methane activation during catalysis conditions, but to believe that it is a platinum-catalyzed process.¹⁵ The harsh conditions employed by this system prevent it from being a realistic answer to large-scale functionalization of methane from natural gas resources.¹³ Periana has also reported a Hg(II) system that effects a similar transformation of methane in sulfuric acid.¹⁶

Scheme 1.3. Conversion of methane to methyl bisulfate by (bpym)PtCl₂ in fuming H₂SO₄¹⁵



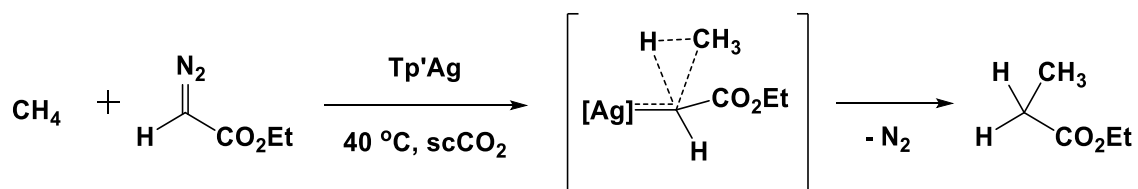
An interesting example of methane functionalization is the hydromethylation of propylene to isobutene reported in 2003 by Tilley. The complex $\text{Cp}^*\text{Sc}(\text{CH}_2\text{CMe}_3)$ loses neopentane to form the tucked-in complex, $\text{Cp}^*\text{Sc}(\eta^1:\eta^5\text{-C}_5\text{Me}_4\text{CH}_2)$, which activates methane via the microscopic reverse.¹⁷ The product from methane activation, $\text{Cp}^*\text{Sc}(\text{CH}_3)$ had been previously reported (synthesized via metathesis rather than through methane activation) and characterized by X-ray diffraction.¹⁸ Following methane activation, exposure of $\text{Cp}^*\text{Sc}(\text{CH}_3)$ to propylene results in the 1,2-addition of the olefin across the Sc-CH_3 bond, an example of σ -bond metathesis. The ligand is then released as isobutene by regenerating the tucked-in complex which then goes on to effect the activation of methane. While catalytic, this scandium system only achieves a maximum turnover number of 4, even when left for weeks to react.¹⁷

Scheme 1.4. Hydromethylation of propylene by a scandium sandwich complex¹⁷



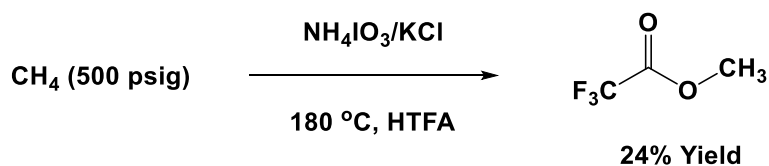
Another type of metal-mediated methane functionalization involves the insertion of carbenes into a C-H bond. An example of this is the addition of methane to a silver-stabilized carbene as reported in 2011 by Pérez and coworkers. In supercritical CO₂, ethyl diazoacetate is added to methane to form ethyl propionate. This process proceeds through a silver-stabilized carbene which adds in a 1,1 fashion across a methane C-H bond (Scheme 1.5).¹⁹ This system can achieve a TON close to that of the platinum catalyst reported by Periana, but it will react with any other C-H bond preferentially to methane, and the formation of olefins from carbene dimerization remains a problem.⁶ Recently, Pérez has reported the functionalization of methane via a copper-stabilized carbene.²⁰

Scheme 1.5. The 1,1-insertion of a silver-stabilized across a C-H bond of methane¹⁹



Recent examples of stoichiometric methane functionalization mediated by main-group elements have been reported by the research groups of Gunnoe and Periana.^{2, 3, 13} The first example, reported by Gunnoe, involves the stoichiometric conversion of methane to a methyl ester using iodate salts. In the presence of a catalytic amount of chloride, methane is partially oxidized by the iodate salt (NH_4IO_3) in a protic solvent such as trifluoroacetic acid (HTFA) to selectively generate the monofunctionalized product (Scheme 1.6). Conversions of methane using this method are reported to be in excess of 20%. The role of the chloride catalyst is not known, but the authors propose that it interacts with the iodate itself, providing an electronic effect to assist in one or both of the C-H bond-activation and the C-O bond-forming steps. Methane chlorination is also observed during this process. This system has also been shown to effect the monofunctionalization of ethane and propane.²

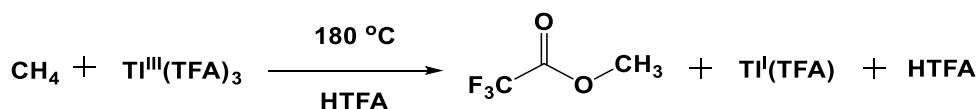
Scheme 1.6. Conversion of methane to a methyl ester using iodate salts²



The stoichiometric conversion of methane to methyl trifluoroacetate using main-group cations has recently been reported by Periana and coworkers. In a trifluoroacetic acid medium, Tl(III) and Pb(IV) cations effect the partial oxidation of methane to the methyl ester and the corresponding Tl(I) or Pb(II) salt (Scheme 1.7). The authors believe that methane C-H bond activation occurs at the cation. In the case of the thallium reaction, they propose that methane C-H activation gives $(\text{TFA})_2\text{Tl}^{\text{III}}\text{CH}_3$, which quickly converts to the methyl ester F_3COOCH_3 and

Tl^I(TFA). A M-CH₃ intermediate complex has not been isolated for either thallium or lead, but the authors report possible detection of (TFA)₂Tl^{III}CH₃ by ¹H NMR spectroscopy, albeit not from the reaction with methane. These cations can effect the same conversions of ethane and propane and can even effect the conversion of all three alkanes simultaneously in a mixture of the gases.³

Scheme 1.7. Conversion of methane to methyl ester using thallium(III) salts³



An alternate path towards methane functionalization involves its transformation into heavier alkanes,²¹ which can then be functionalized through processes such as steam cracking.⁵ For instance, the cross-metathesis of methane and propane to produce ethane is effected by tantalum hydrides supported on silica.²² Another process involving supported tantalum hydrides is the non-oxidative coupling of methane to ethane and dihydrogen.²³ These systems employ supported metal oxides which can effect various transformations of methane into products containing functional sites such as C=C, C-O, and C-Cl bonds.²⁴ Another interesting example of heterogeneous methane functionalization is its direct conversion to methanol by copper and iron zeolites in the presence of peroxide.²⁵

Despite nearly a half century of investigations since Shilov reported the first transition-metal mediated functionalization of methane,¹⁴ there remains no practical system or process that can directly convert methane into value-added products. Chemical investigations into new compounds and systems to effect the activation and functionalization of methane are thus of paramount importance. The reactions of methane effected by well-defined transition-metal

organometallic complexes leading to this goal remain a chief focus of research since homogenous systems offer insights into the probable mechanisms of transformations that can be added to the current knowledge base, thereby progressing towards the development of an industrially viable process for the conversion of methane into value-added chemicals.

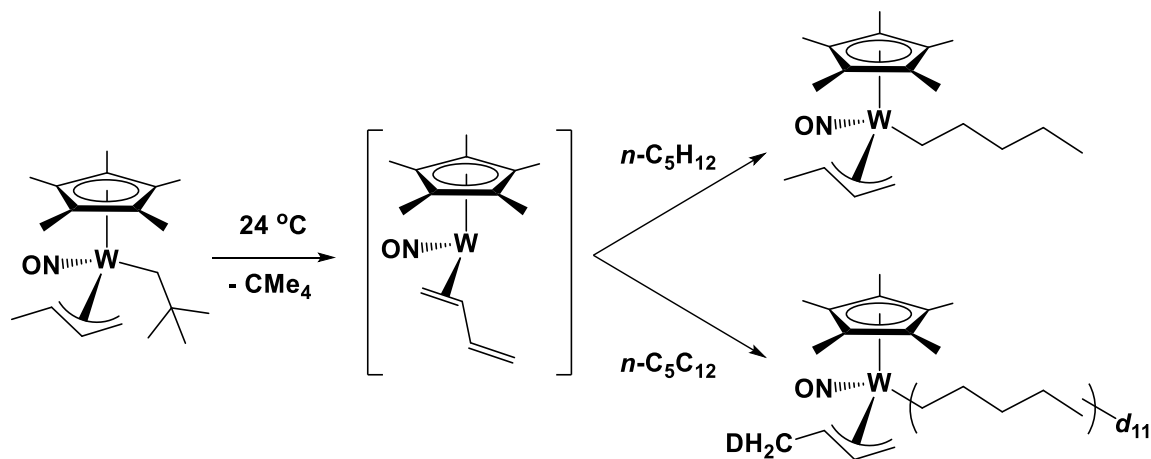
1.2 Legzdins Group C-H Activation Chemistry

Complexes of the general formula $\text{Cp}^*\text{W}(\text{NO})(\text{CH}_2\text{CMe}_3)(\eta^3\text{-allyl})$ have been the focus of study in the Legzdins group in recent years. Members of this family of compounds can effect the single, terminal activation of alkane C-H bonds to form the corresponding $\text{Cp}^*\text{W}(\text{NO})(\text{alkyl})(\eta^3\text{-allyl})$ products. The mechanism of C-H activation involves the intramolecular loss of neopentane (CMe_4) to generate a 16e $\text{Cp}^*\text{W}(\text{NO})(\eta^2\text{-diene})$ and/or $\text{Cp}^*\text{W}(\text{NO})(\eta^2\text{-allene})$ intermediate complex. Through the microscopic reverse of this process, the 16e intermediate species can effect the intermolecular C-H activation of an alkane substrate.²⁶⁻²⁹ In general, the intermediate complexes can react with hydrocarbon substrates, R-H (R = alkyl, aryl), to form three different types of organometallic products resulting from (1) single C-H bond activation, (2) subsequent R/allyl H exchange, or (3) multiple C-H bond activations of the substrate.³⁰ Just which organometallic products ultimately result depends on several factors, including the nature of the allyl ligands, the hydrocarbon substrates themselves, the electron density at the metal centers, the substituents on the cyclopentadienyl ligands, and the experimental conditions employed.^{31, 32}

The first products formed via the thermal pathway are the desired $\text{Cp}^*\text{W}(\text{NO})(\eta^1\text{-R})(\eta^3\text{-allyl})$ complexes that are the result of a single C-H bond activation of R-H. This single C-H

activation step is always selective for a terminal C-H bond, even when the hydrocarbon substrate contains heteroatoms such as oxygen, silicon, chlorine, or bromine.³³ The first example of this type of C-H activation was the C-H bond activation of *n*-pentane effected by $\text{Cp}^*\text{W}(\text{NO})(\text{CH}_2\text{CMe}_3)(\eta^3\text{-CH}_2\text{CHCHMe})$ under ambient conditions (Scheme 1.8). This complex loses neopentane at 24 °C to generate a 16e η^2 -diene intermediate that effects the C-H bond cleavage. Labeling studies using deuterated pentane have established the η^2 -diene complex as the C-H activating species.^{27, 34}

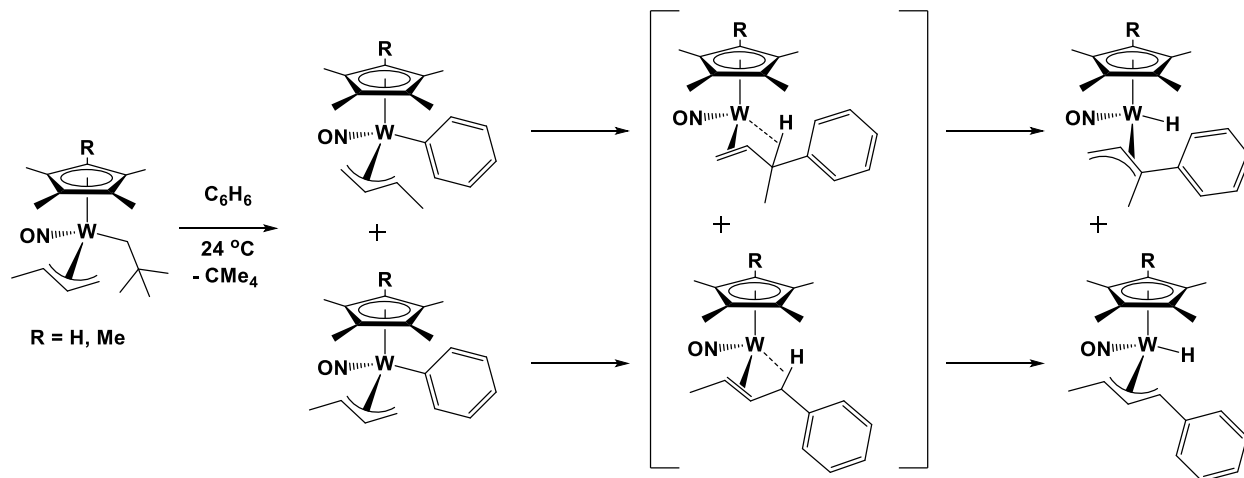
Scheme 1.8. Thermal generation of a 16e η^2 -diene intermediate complex and subsequent single, terminal C-H activation of *n*-pentane



In some cases, the initially formed $\text{Cp}^*\text{W}(\text{NO})(\eta^1\text{-R})(\eta^3\text{-allyl})$ complexes are unstable and undergo an intramolecular R/allyl H exchange. This exchange involves the coupling of the aryl and allyl ligands followed by the intramolecular activation of a C-H bond at the carbon where the coupling occurred (Scheme 1.9). This reactivity typically occurs for the reactions of $\text{Cp}^*\text{W}(\text{NO})(\text{CH}_2\text{CMe}_3)(\eta^3\text{-allyl})$ complexes with aromatic hydrocarbons when $\eta^3\text{-allyl}$ is a

monosubstituted allyl ligand. The identities of the various compounds depicted in Scheme 1.9 were elucidated using the beneficial kinetic effect of a $\eta^5\text{-C}_5\text{Me}_4\text{H}$ ligand in place of Cp^* , a switch that slows down both the C-H activation and coupling steps.³⁵ This information was subsequently used to identify all the various components in the Cp^* system which can contain at least six different complexes (including isomers) at a given time. The 16e η^2 -alkene intermediate complex following the coupling has also been trapped as its PR_3 adducts ($\text{R} = \text{Me}, \text{Ph}$) in a related system.³²

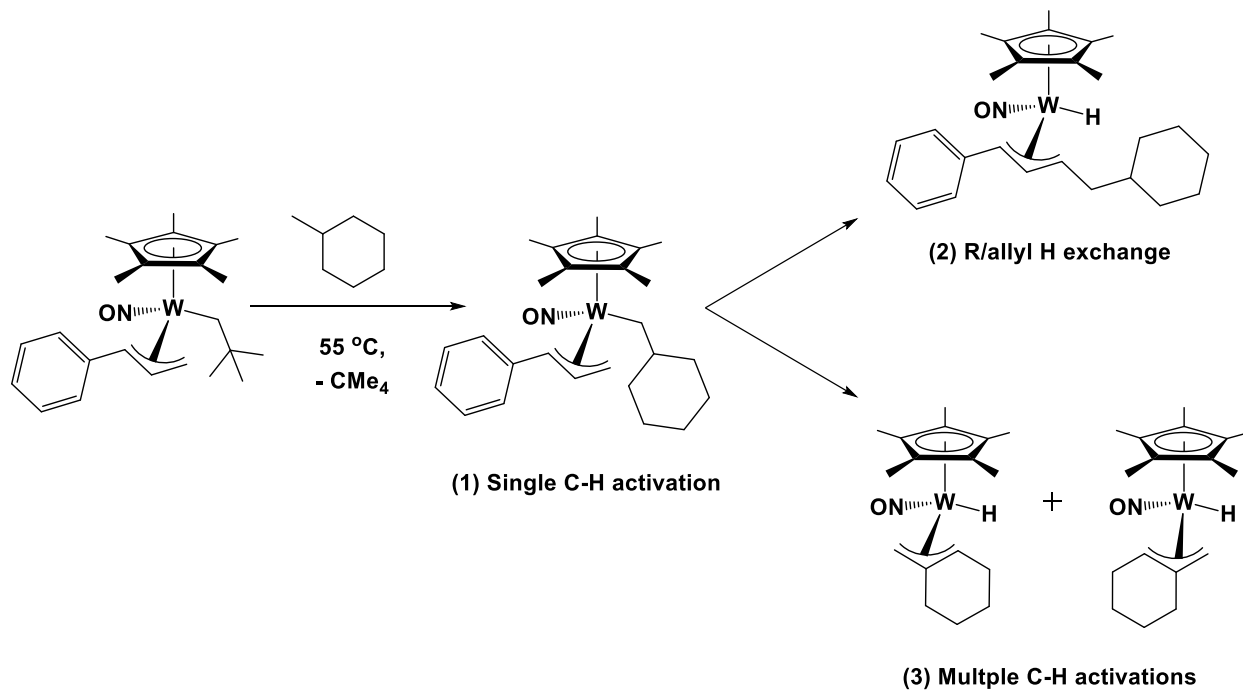
Scheme 1.9. Aryl-hydrogen exchange reactions involving the coupling of the aryl and allyl ligands



A third type of organometallic complex can be formed through three successive C-H activations of the substrate molecule.^{30, 32} This conversion presumably occurs via a β -H elimination of the activated substrate ligand following the initial single C-H activation. The original allyl ligand is then lost, and a third γ -C-H activation gives the new organometallic product, $\text{Cp}^*\text{W}(\text{NO})(\text{H})(\eta^3\text{-allyl})$, in which the allyl ligand is formed from three sequential C-H

activations of the substrate. The organometallic products that result from this mode of activation are again consistent with an initial terminal C-H activation. The reaction of $\text{Cp}^*\text{W}(\text{NO})(\text{CH}_2\text{CMe}_3)(\eta^3\text{-CH}_2\text{CHCHPh})$ with methylcyclohexane is a unique case in which all three possible types of organometallic products are not only formed, but have also been isolated and fully characterized (Scheme 1.10).²⁸

Scheme 1.10. The reaction of $\text{Cp}^*\text{W}(\text{NO})(\text{CH}_2\text{CMe}_3)(\eta^3\text{-CH}_2\text{CHCHPh})$ with methylcyclohexane results in the formation of all three types of possible organometallic products stemming from (1) single, terminal C-H activation, (2) R/allyl H exchange, and (3) multiple C-H activations.



The common theme of the reactions that go beyond the single C-H activation step is the formation of a $\text{Cp}^*\text{W}(\text{NO})(\text{H})(\eta^3\text{-allyl})$ complex. There are many examples of these complexes

being formed via C-H activation(s) initiated by the family of $\text{Cp}^*\text{W}(\text{NO})(\text{CH}_2\text{CMe}_3)(\eta^3\text{-allyl})$ complexes.^{26, 28, 30, 35, 36} The ubiquity of these allyl hydride complexes piques curiosity regarding the properties and chemistry of this new family of compounds. Ultimately, the question arises as to whether these compounds that are derived from alkane activation(s) can themselves be platforms to effect C-H bond activation and perhaps functionalization.

Finally, the promise of transition metal-mediated C-H activations of alkanes and other hydrocarbons is not in the formation of resulting M-alkyl or M-hydrocarbyl complexes, but on the subsequent functionalization and release of the activated ligands as value-added compounds for which classical chemical manipulations are accessible. The reactivity of $\text{Cp}^*\text{W}(\text{NO})(\text{alkyl})(\eta^3\text{-allyl})$ complexes with various reagents has been investigated, and the primary site of reactivity has been demonstrated to be the allyl ligand.^{31, 37-39} The reaction of the $\text{Cp}^*\text{W}(\text{NO})(\text{CH}_2\text{CMe}_3)(\eta^3\text{-allyl})$ complexes with CO to give the corresponding $\text{Cp}^*\text{W}(\text{NO})(\text{C}(=\text{O})\text{CH}_2\text{CMe}_3)(\eta^3\text{-allyl})$ compounds has also been explored previously, but only for the alkyl ligands derived from salt metathesis reactions.^{29, 37} Indeed, the only reported functionalization of an alkyl ligand derived from C-H activation is by the oxidation of $\text{Cp}^*\text{W}(\text{NO})(n\text{-C}_5\text{H}_{11})(\eta^3\text{-CH}_2\text{CHCHMe})$ with molecular iodine, a reaction that liberates 1-iodopentane.³⁴ The functionalization of the alkyl and hydrocarbyl groups derived from single C-H activation is one of the principal aspects that is addressed in this thesis.

1.3 Scope of the Thesis.

In summary, two questions are raised by the C-H activation chemistry produced in the Legzdins group based on the family of $\text{Cp}^*\text{W}(\text{NO})(\text{CH}_2\text{CMe}_3)(\eta^3\text{-allyl})$ complexes. The first

regards the formation of the $\text{Cp}^*\text{W}(\text{NO})(\text{H})(\eta^3\text{-allyl})$ products formed during an array of various C-H activations. Can these $\text{Cp}^*\text{W}(\text{NO})(\text{CH}_2\text{CMe}_3)(\eta^3\text{-allyl})$ be used to effect the C-H activation and functionalization of C-H bonds? The second question involves the products that result from the single C-H activation. Can the functionalization of alkanes and hydrocarbons initiated by the $\text{Cp}^*\text{W}(\text{NO})(\text{CH}_2\text{CMe}_3)(\eta^3\text{-allyl})$ ultimately convert these substrates into value-added compounds containing functional groups. And finally, the general discussion at the beginning of this chapter focuses on the challenge of converting methane to either a transportable fuel or a C1 feedstock. So the question naturally arises: can the $\text{Cp}^*\text{W}(\text{NO})(\text{CH}_2\text{CMe}_3)(\eta^3\text{-allyl})$ compounds be used to effect such transformations of the most abundant and least-utilized alkanes?

Chapter 2 presents the synthesis and characterization of the family of $\text{Cp}^*\text{W}(\text{NO})(\text{H})(\eta^3\text{-allyl})$ complexes. The properties of these complexes are outlined as well as insights into the nature of the W-H bond and the potential thermally-generated intermediates are provided. The reactions of these hydride complexes with trimethylphosphine results in two general types of complexes, depending on the thermal conditions employed. Interesting spectroscopic properties of these compounds are discussed.

Chapter 3 considers the thermal reactivity of the $\text{Cp}^*\text{W}(\text{NO})(\text{H})(\eta^3\text{-allyl})$ complexes with alkanes. These complexes effect three-successive C-H activations of substrates such as *n*-pentane, *n*-heptane, cyclohexane, 1-chloropropane, and 1-chlorobutane. Mechanistic insights for this transformation are presented, and the C-H activation chemistry effected by the allyl hydride complexes is compared to that of the $\text{Cp}^*\text{W}(\text{NO})(\text{CH}_2\text{CMe}_3)(\eta^3\text{-allyl})$ compounds. In addition, it is shown that the $\text{Cp}^*\text{W}(\text{NO})(\text{H})(\eta^3\text{-allyl})$ complexes can effect the one-pot functionalization of hydrocarbons and CO to produce unsymmetrical saturated ketones after which the tungsten reagent can be regenerated.

Chapter 4 focuses on the functionalization of methane initiated by the $\text{Cp}^*\text{W}(\text{NO})(\text{CH}_2\text{CMe}_3)(\eta^3\text{-CH}_2\text{CHCMe}_2)$ complex. This complex initiates the C-H activation of methane and two subsequent C-C bond forming reactions, coupling methane to carbon monoxide and the dimethylallyl ligand. The complexes resulting from each step in this process have been isolated and characterized to provide a complete understanding of this process. Finally, the methane is converted into an unsaturated ketone while the final tungsten product can be reconverted into the starting complex. This unsaturated ketone derived from methane satisfies the conditions for being both a transportable fuel as well as being derived from a C1 feedstock.

Chapter 5 expands the chemistry presented in the previous chapter and extends the reactivity to hydrocarbons larger than methane. The monosubstituted allyl complexes $\text{Cp}^*\text{W}(\text{NO})(\text{CH}_2\text{CMe}_3)(\eta^3\text{-CH}_2\text{CHCHPh})$ and $\text{Cp}^*\text{W}(\text{NO})(\text{CH}_2\text{CMe}_3)(\eta^3\text{-CH}_2\text{CHCHMe})$ are used to initiate these reactions. The functionalization of ethane, as well as methane, is outlined in this chapter. In addition, the ability to activate hydrocarbons containing a heteroatom is demonstrated for the phenylallyl complex as is its ability to functionalize longer chain hydrocarbons with CO. Finally, it is described how the bound ketone ligands resulting from alkane functionalization with CO can be released from the tungsten compounds via photolysis.

Chapter 6 presents an overall summary and conclusions of the research presented in this thesis as well as suggesting potential future research directions for this chemistry.

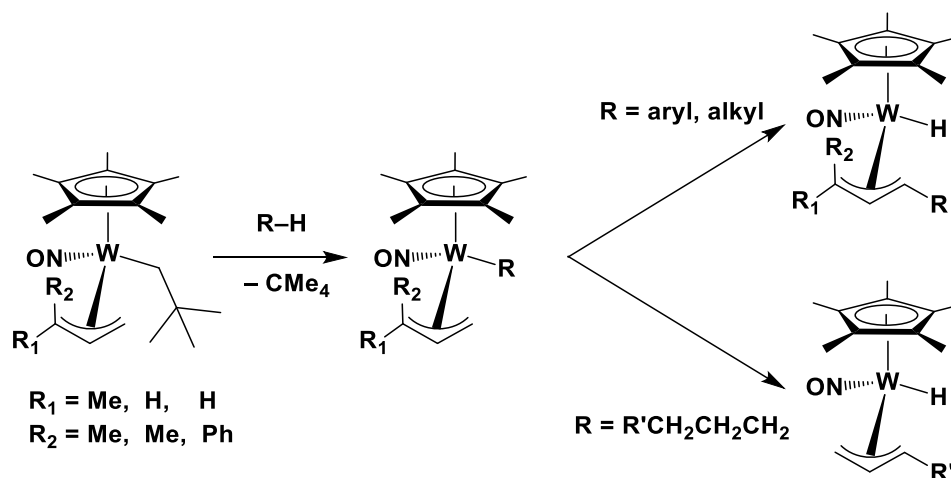
Chapter 2: Synthesis and Properties of $\text{Cp}^*\text{W}(\text{NO})(\text{H})(\eta^3\text{-Allyl})$ Complexes[†]

[†]A version of this chapter has been published. Baillie, R. A.; Holmes, A. S.; Lefèvre, G. P.; Patrick, B. O.; Shree, M. V.; Wakeham, R. J.; Legzdins, P.; Rosenfeld, D. C. *Inorg. Chem.* **2015**, *54*, 5915-5929. Reprinted with permission from Inorganic Chemistry. Copyright (2015) American Chemical Society.

2.1 Introduction

Recent research in the Legzdins group has focused on the investigation of the family of $\text{Cp}^*\text{W}(\text{NO})(\text{CH}_2\text{CMe}_3)(\eta^3\text{-allyl})$ complexes, which initiate various types of hydrocarbon C–H activations.³¹ Gentle thermolyses of these $\text{Cp}^*\text{W}(\text{NO})(\text{CH}_2\text{CMe}_3)(\eta^3\text{-allyl})$ complexes in neat hydrocarbon solutions result in the loss of neopentane from the metal coordination sphere and the transient formation of the 16e $\text{Cp}^*\text{W}(\text{NO})(\eta^2\text{-allene})$ and/or $\text{Cp}^*\text{W}(\text{NO})(\eta^2\text{-diene})$ intermediate species. These transient intermediates can react with hydrocarbon substrates, R–H (R = alkyl, aryl), to form three different types of organometallic products as summarized in Scheme 2.1.³⁰

Scheme 2.1. C–H Activations Effected by $\text{Cp}^*\text{W}(\text{NO})(\text{CH}_2\text{CMe}_3)(\eta^3\text{-allyl})$ Complexes



It is notable that two of the three types of complexes resulting from the C–H activation of various hydrocarbons by $\text{Cp}^*\text{W}(\text{NO})(\text{CH}_2\text{CMe}_3)(\eta^3\text{-allyl})$ complexes are $\text{Cp}^*\text{W}(\text{NO})(\text{H})(\eta^3\text{-allyl})$ compounds which constitute a new family of hydrido nitrosyl complexes, a class of

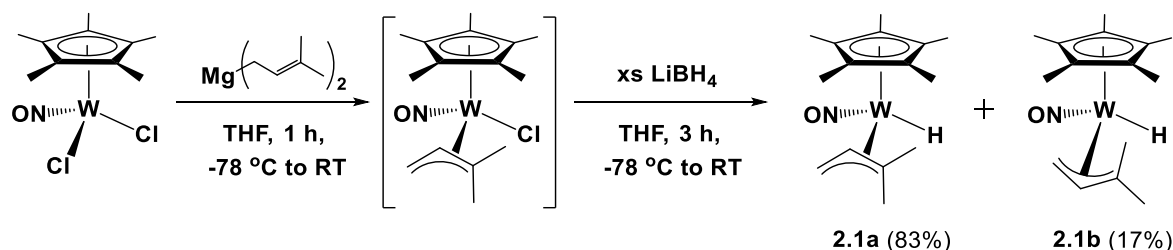
compounds whose chemistry has not been extensively investigated. Consequently, it was decided to investigate this class of complexes by developing the independent synthesis of some of these $\text{Cp}^*\text{W}(\text{NO})(\text{H})(\eta^3\text{-allyl})$ complexes and then establish some of their chemical and physical properties to see how they compared to those exhibited by their $\text{Cp}^*\text{W}(\text{NO})(\text{CH}_2\text{CMe}_3)(\eta^3\text{-allyl})$ precursors.

2.2 Results and Discussion

2.2.1 Synthesis and Characterization of $\text{Cp}^*\text{W}(\text{NO})(\text{H})(\eta^3\text{-CH}_2\text{CHCMe}_2)$

The complex $\text{Cp}^*\text{W}(\text{NO})(\text{H})(\eta^3\text{-CH}_2\text{CHCMe}_2)$ (**2.1**) is synthesized from $\text{Cp}^*\text{W}(\text{NO})\text{Cl}_2$ via two sequential metathesis reactions involving $\text{Mg}(\text{CH}_2\text{CH}=\text{CMe}_2)_2$ and LiBH_4 (Scheme 2.2). The addition of the binary magnesium(II) allyl reagent to $\text{Cp}^*\text{W}(\text{NO})\text{Cl}_2$ is carried out at $-78\text{ }^\circ\text{C}$ and under a N_2 atmosphere. The choice of solvent is critical since under the experimental conditions employed $\text{Cp}^*\text{W}(\text{NO})\text{Cl}_2$ is only sparingly soluble in THF and not at all in Et_2O . After the addition of the allylating reagent is complete, the reaction mixture is allowed to warm to room temperature while being stirred for at least 1 h to produce the intermediate complex, $\text{Cp}^*\text{W}(\text{NO})(\eta^3\text{-CH}_2\text{CHCMe}_2)\text{Cl}$. This 18e intermediate complex can be isolated, but such isolation is not necessary for the synthesis (and can even diminish the overall yield) of **2.1**. The reaction mixture containing $\text{Cp}^*\text{W}(\text{NO})(\eta^3\text{-CH}_2\text{CHCMe}_2)\text{Cl}$ is next cooled in a dry ice/acetone bath, an excess of LiBH_4 is added slowly, and the mixture is allowed to stir for at least 3 h. The addition of the hydride ligand can also be effected with LiAlH_4 , however the use of LiBH_4 improves the yield and reliability of the synthesis of **2.1**.

Scheme 2.2. Synthesis of $\text{Cp}^*\text{W}(\text{NO})(\text{H})(\eta^3\text{-CH}_2\text{CHCMe}_2)$



The purification of **2.1** can be effected on the bench since the complex has a surprising degree of air and moisture stability. The excess LiBH_4 is first neutralized with water in Et_2O , and then the salts are removed by filtration. The mixture is then subjected to column chromatography on a neutral alumina support to obtain analytically pure **2.1**. Finally, the diastereomers **2.1a** and **2.1b** are isolable as a yellow solid in a yield of 45% by removing solvent from the eluate in vacuo. (For ease of discussion, the designation **2.1** refers to the mixture of **2.1a** and **2.1b**; this labeling applies for all such mixtures of isomers that are discussed in this thesis.) The melting point of **2.1** is 123-125 $^\circ\text{C}$ and is reversible; this has been established by dissolving the melt residue in C_6D_6 and analyzing the sample by ^1H NMR spectroscopy. The ^1H NMR spectrum matches the spectrum for the starting hydride complex. Complex **2.1** is air and moisture stable in the solid state for several weeks. In solution (Et_2O or C_6D_6), however, it is slightly less stable, and a small degree of decomposition occurs after several days both in air and under N_2 .

In solution, complex **2.1** exists as two isomers in an 83:17 ratio (Scheme 2.2) that differ with respect to the endo/exo orientation of their allyl ligands. The solution molecular structures have been determined using Sel NOE and NOESY NMR spectroscopy. The selective irradiation of the signals due to the hydride ligands results in NOE enhancement of both allyl *Me* signals for

each isomer [i.e. δ irradi. -0.90 ppm, NOE at 1.90 ppm, 2.29 ppm; δ irradi. -0.59, NOE at 0.87 ppm, 2.45 ppm]. The exo conformation of the allyl ligand of the major isomer is established by the NOESY NMR spectrum which displays cross peaks between the signals due to the C_5Me_5 ligand and the allyl meso H (1.72, 2.68) and the C_5Me_5 ligand and the allyl H that is cis to the meso H (1.72, 2.06). Furthermore, the irradiation of either hydride resonance (δ -0.59, -0.90 ppm) produces NOE enhancement of the other WH, indicating that the two isomers undergo rapid interconversion in solution.

The solid-state molecular structure of **2.1a** has been established by X-ray crystallographic analyses (Figure 2.1). Only a single isomer crystallizes from the mixture of **2.1a** and **2.1b**, and it is major isomer observed in solution. The allyl ligand is in an exo conformation, and its CMe_2 substituent is cis to the smaller hydride ligand instead of the larger nitrosyl ligand, consistent with the NOE and NOESY NMR data. The allyl ligand also exhibits a slight σ - π distortion, a manifestation of the electronic asymmetry extant at the metal center.^{40,41,42} The hydride ligand is found in the electron density map, allowing the determination of the tungsten hydride bond length at 1.62(3) Å. Additionally the nitrosyl ligand is linear with a W(1)-N(1)-O(1) bond angle of 173.62(18)°. The 1H and ^{13}C NMR spectra of **2.1a** in C_6D_6 indicate that its solid-state molecular structure persists in solution. The minor isomer **2.1b** evidently does not cocrystallize with the major isomer during the growth of X-ray quality crystals of **2.1a** from Et_2O at -33 °C. In any event, dissolution of a crystalline sample of **2.1a** in C_6D_6 produces a solution containing both isomers in the same 83:17 equilibrium ratio. All solution reactions of **2.1** have been carried out using this 83:17 mixture of isomers.

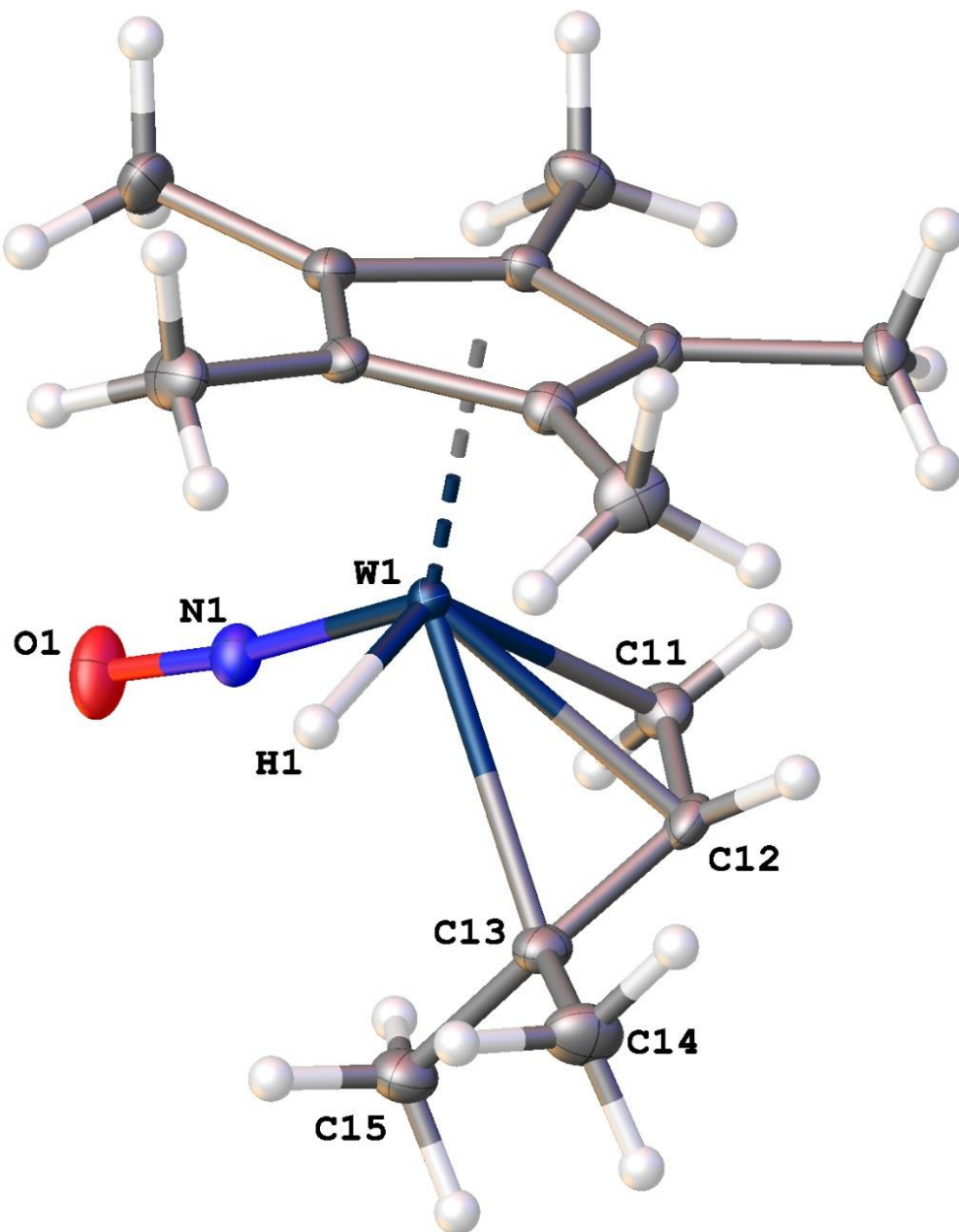


Figure 2.1. Solid-state molecular structure of **2.1** with 50% probability thermal ellipsoids shown.

Selected bond lengths (Å) and angles (deg): W(1)-H(1) = 1.62(3), W(1)-C(11) = 2.271(2), W(1)-C(12) = 2.287(2), W(1)-C(13) = 2.465(2), C(11)-C(12) = 1.419(3), C(12)-C(13) = 1.405(3), W(1)-N(1) = 1.7787(19), N(1)-O(1) = 1.228(2), C(11)-C(12)-C(13) = 124.7(2), C(12)-C(13)-C(14) = 117.5(2), C(12)-C(13)-C(15) = 123.1(2), W(1)-N(1)-O(1) = 173.62(18).

2.2.2 Synthesis and Characterization of Additional Cp*W(NO)(H)(η^3 -Allyl) Complexes

The synthesis of **2.1** is applied as a general synthesis for the family of Cp*W(NO)(H)(η^3 -allyl) complexes, which all proceed from Cp*W(NO)Cl₂ by the sequential installation of the allyl and hydride ligands via salt metatheses. The complexes Cp*W(NO)(H)(η^3 -CH₂CHCHPh) (**2.2**) and Cp*W(NO)(H)(η^3 -CH₂CHCHMe) (**2.3**) have also been prepared using this synthetic methodology. The synthesis of complexes **2.2** and **2.3** which we reported were carried out by Dr. Russell Wakeham and Mr. Aaron Holmes, respectively.⁴³ The characterization of the solid-states by single-crystal X-ray diffraction was performed by the author, as well as the NMR characterization of **2.3**. The purification of each proceeds similarly to that of **2.1**, with the only difference being that complex **2.3** requires an additional recrystallization in hexanes at -15 °C. The isolated yield of complexes **2.2** and **2.3** are 20% and 19%, respectively, which is significantly less than that for **2.1**. Similar to **2.1**, complexes **2.2** and **2.3** exist as a mixture of isomers (vide infra) and display reversible melting points, with **2.2** melting at 75-78 °C and **2.3** melting at 99-100 °C. Interestingly, there is no obvious trend between the hydride complexes regarding the melting point, as **2.2** with the largest allyl substituent has the lowest melting point, and the smallest complex, **2.3**, has the intermediate melting point. Also, like **2.1**, both of these allyl hydride complexes are air and moisture stable as solids and display moderate stability in solution.

Complexes **2.2** and **2.3** each exist as four isomers in solution, all differing by the orientation of the allyl ligand which can have either an endo or exo orientation with the phenyl/methyl groups as shown in Figure 2.2. The allyl ligand orientation and substituent position have been determined using NOE NMR spectroscopy for the isomers of **2.2** and **2.3**. In

both cases, the major isomer of each complex has the allyl in an endo orientation with the substituent proximal to the hydride ligand. For all three $\text{Cp}^*\text{W}(\text{NO})(\text{H})(\eta^3\text{-allyl})$ complexes, overwhelmingly the observed distribution of isomers have the allyl substituent(s) proximal to the hydride ligand, with 100% for **2.1**, 97% for **2.2**, and 81% for **2.3**. This is likely a steric effect as only **2.3**, having a single methyl substituent, has a significant percentage of isomers with the allyl substituent proximal to the nitrosyl ligand. Similarly, for the related $\text{Cp}^*\text{W}(\text{NO})(\text{alkyl})(\eta^3\text{-allyl})$ complexes, having larger alkyl ligands in place of a hydride ligand, the substituents of the allyl ligands are generally found proximal to the nitrosyl ligand,³¹ which is also consistent with a steric effect. In addition to the solution molecular structures, complexes **2.2** and **2.3** have been characterized in the solid state by single-crystal X-ray diffraction.

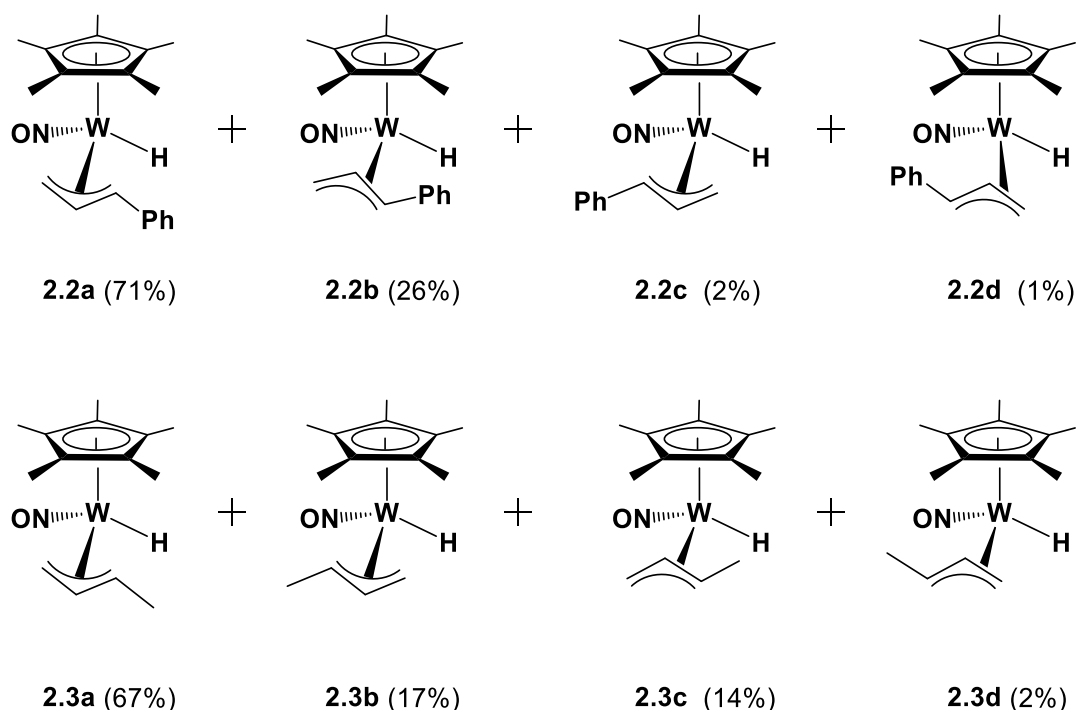


Figure 2.2. Solution molecular structures of the isomers of **2.2** and **2.3** as determined by ^1H Sel NOE NMR spectroscopy.

The crystal structure of **2.2** consists of the packing of two isomers, each displaying a three-legged piano-stool molecular geometry. In the molecular structure of the major isomer **2.2a** (Figure 2.3), the phenylallyl ligand is in an endo conformation while the minor isomer **2.2b** (Figure 2.4) has the ligand in an exo conformation. Both isomers have the phenyl ring of the allyl ligand distal with respect to the nitrosyl ligand. This feature contrasts to that existing in $\text{Cp}^*\text{W}(\text{NO})(\text{CH}_2\text{CMe}_3)(\eta^3\text{-CH}_2\text{CHCHPh})$ which has the phenyl substituent in a proximal configuration with respect to the NO group.⁴⁴ Presumably the lack of steric interference of the hydride ligand in **2.2** allows the distal isomer to be more favourable in the hydride than in the alkyl allyl complex. As with **2.1**, both isomers **2.2a** and **2.2b** display a slight σ - π distortion of the allyl ligand with unequal C-C bond lengths in the allyl ligand. The hydride ligand for **2.2** was found in the electron density map with a W(1)-H(1) bond length of 1.76(4) Å. The nitrosyl ligand is again linear with a W(1)-N(1)-O(1) bond angle of 171.1(3)°.

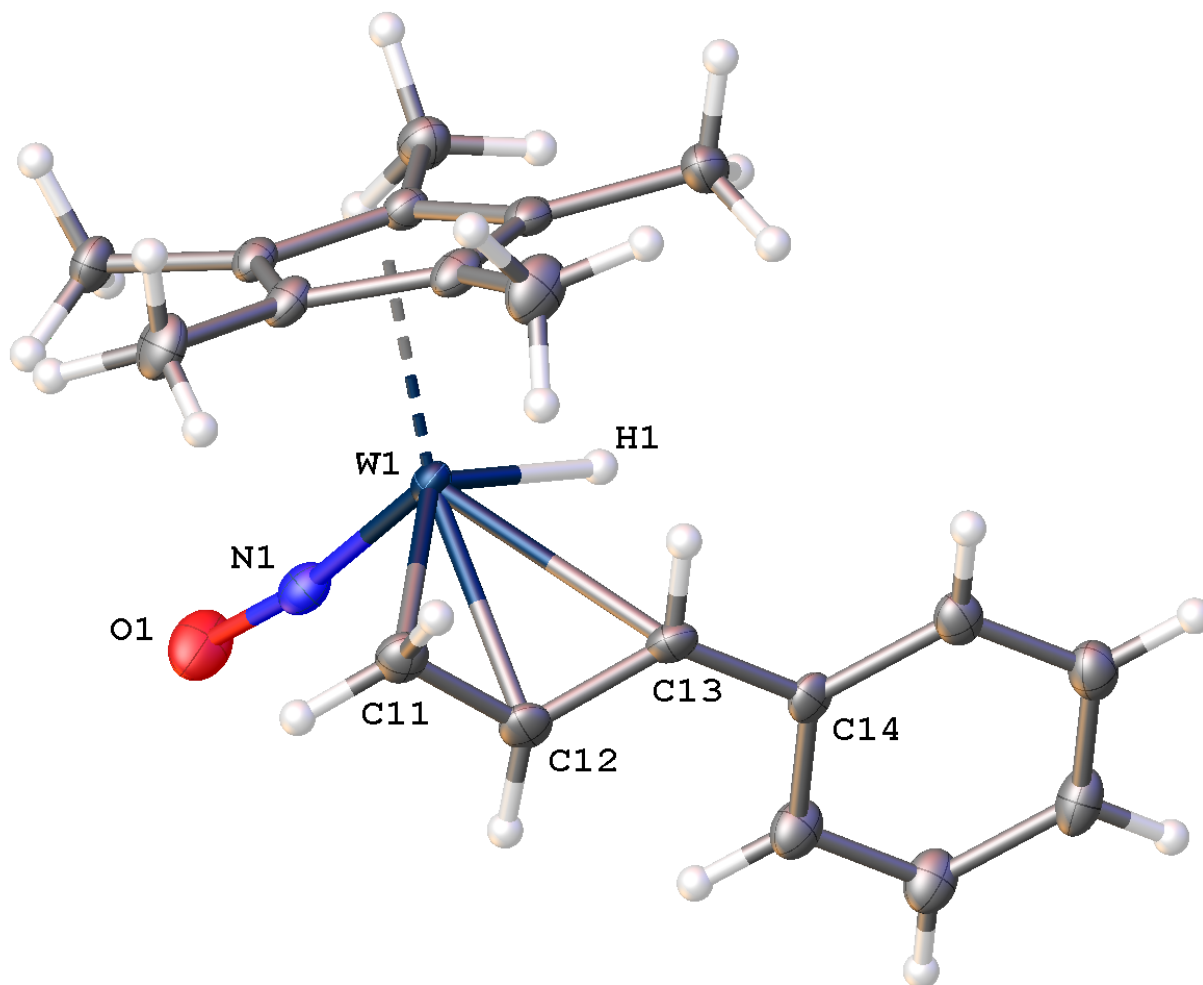


Figure 2.3. Solid-state molecular structure of **2.2a** having the phenylallyl ligand in the endo conformation with 50% probability thermal ellipsoids. Selected bond lengths (Å) and angles (deg): W(1)-H(1) = 1.76(4), W(1)-N(1) = 1.769(3), N(1)-O(1) = 1.235(4), W(1)-C(11) = 2.215(19), W(1)-C(12) = 2.313(6), W(1)-C(13) = 2.472(5), C(11)-C(12) = 1.412(18), C(12)-C(13) = 1.396(8), C(13)-C(14) = 1.483(6), W(1)-N(1)-O(1) = 171.1(3), C(11)-C(12)-C(13) = 120.2(9), C(12)-C(13)-C(14) = 126.0(5).

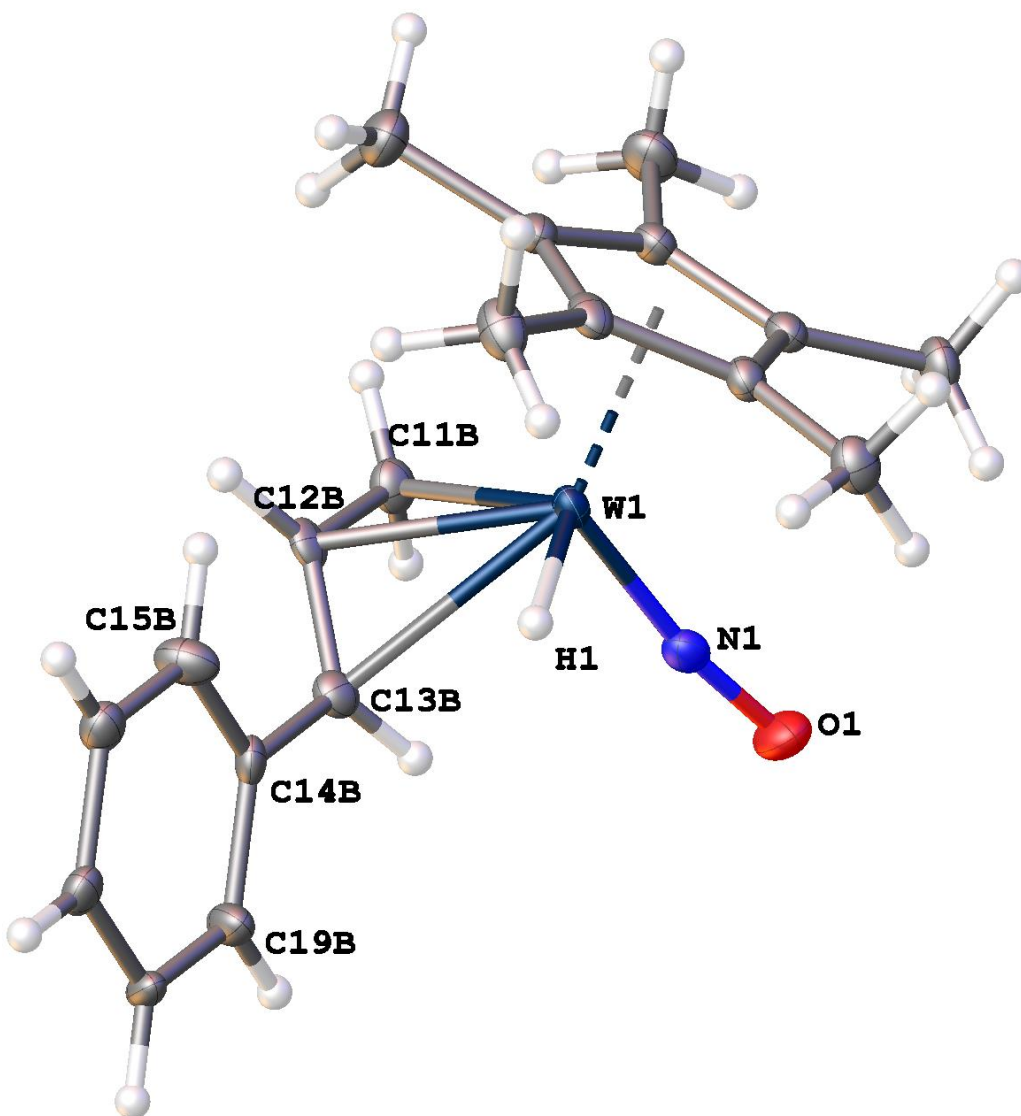


Figure 2.4. Solid-state molecular structure of **2.2b** with the phenylallyl ligand in the exo conformation with 50% probability thermal ellipsoids. Selected bond lengths (Å) and angles (deg): W(1)-H(1) = 1.76(4), W(1)-N(1) = 1.769(3), N(1)-O(1) = 1.235(4), W(1)-C(11b) = 2.31(6), W(1)-C(12b) = 2.302(16), W(1)-C(13b) = 2.526(13), C(11b)-C(12b) = 1.45(5), C(12b)-C(13b) = 1.39(2), C(13b)-C(14b) = 1.461(16), W(1)-N(1)-O(1) = 171.1(3), C(11b)-C(12b)-C(13b) = 121(3), C(12b)-C(13b)-C(14b) = 123.9(14).

X-ray-quality crystals of **2.3** have been obtained via slow evaporation of an Et₂O solution of the compound at room temperature. The crystals contain only a single isomer, namely **2.3a**, which is also the major isomer in solution. The solid-state molecular structure of **2.3a** is shown in Figure 2.5. The allyl ligand is oriented in an endo conformation with the methyl substituent proximal to the hydride ligand. This feature is consistent with the ¹H NMR and Sel NOE NMR data for the major isomer. The allyl ligand exhibits the most pronounced σ - π distortion of all three tungsten hydride complexes with C-C bond lengths of 1.376(5) and 1.423(5) Å. The shorter C(12)-C(13) bond is oriented trans to the nitrosyl ligand, this arrangement is likely a manifestation of the strong π -acid character of the nitrosyl ligand leaving less electron density at the W center to back-donate into the allyl C(12)-C(13) bond. The hydride ligand was again found in the electron density map and the W(1)-H(1) bond length is 1.61(5) Å, which is nearly identical to the W-H bond in **2.1**. The W(1)-N(1)-O(1) bond angle of 169.3(2)° is in agreement with the presence of a linear nitrosyl ligand.

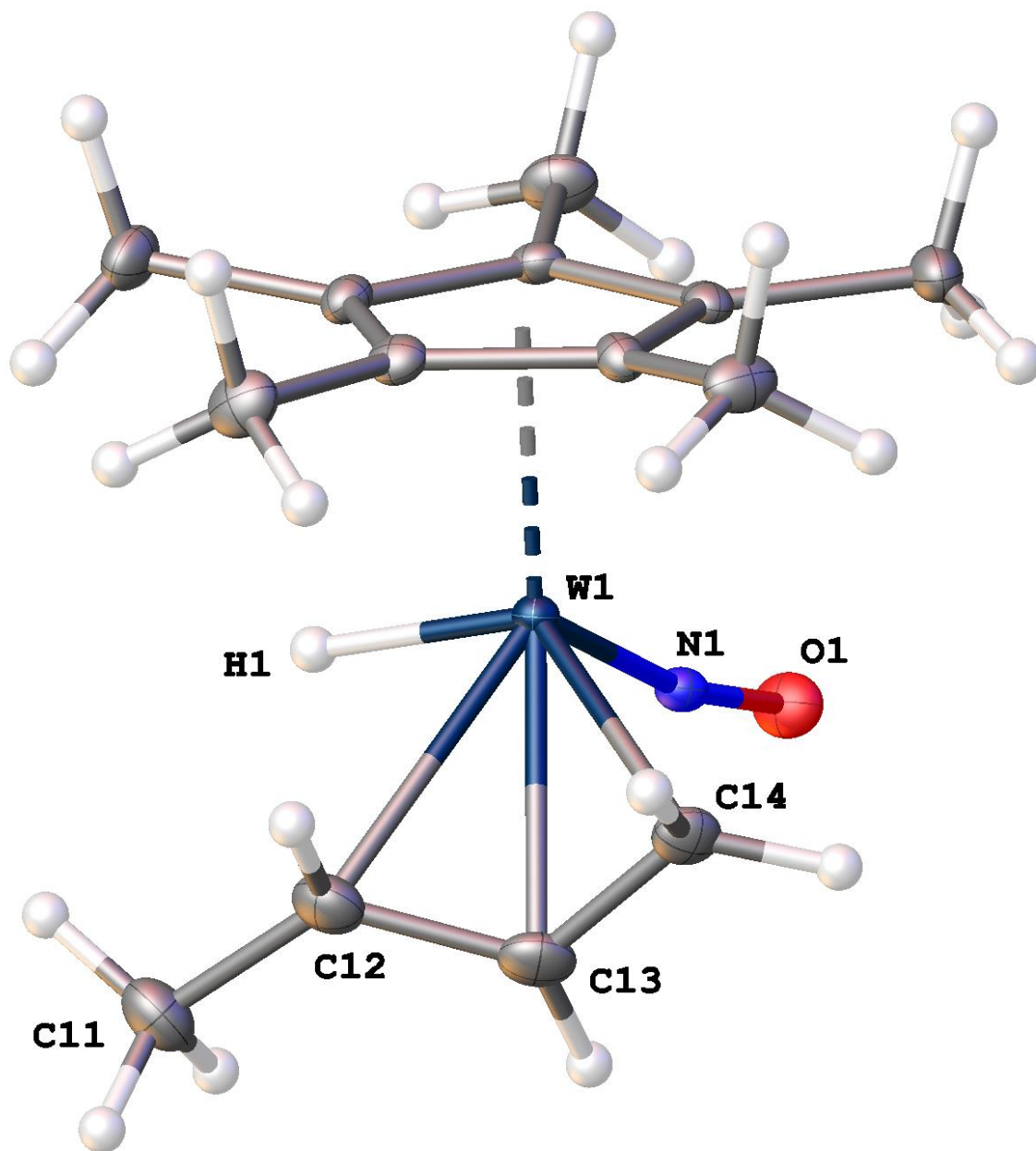


Figure 2.5. Solid-state molecular structure of **2.3a** with 50% probability thermal ellipsoids shown. Selected bond lengths (Å) and angles (deg.): W(1)-H(1) = 1.61(5), W(1)-C(12) = 2.400(4), W(1)-C(13) = 2.324(3), W(1)-C(14) = 2.250(3), C(11)-C(12) = 1.505(5), C(12)-C(13) = 1.376(5), C(13)-C(14) = 1.423(5), W(1)-N(1) = 1.781(3), N(1)-O(1) = 1.224(3), C(11)-C(12)-C(13) = 124.6(3), C(12)-C(13)-C(14) = 119.8(3), W(1)-N(1)-O(1) = 169.3(2).

Interestingly, there is a correlation between the endo/exo orientation of the allyl ligand and the chemical shift of the allyl meso *H* in the ^1H NMR spectra for each complex. For a given complex, the meso *H* signals of the endo isomers have a more downfield chemical shift in the ^1H NMR spectra than do the meso *H* signals of the exo isomers (Table 2.1) presumably because of their differing interactions with the tungsten-Cp* unit. This difference in chemical shifts likely cannot be attributed to simply a difference in the tungsten-hydrogen bond distances for a given complex as these distances for **2.2a** and **2.2b** from the X-ray crystallographic data are nearly identical for the endo and exo isomers [**2.2a** (endo), W(1) to H(12) distance of 2.942 Å; **2.2b** (exo), W(1) to H(12b) distance of 2.926 Å]. Additional evidence to support the chemical shift dependence of a H signal in the ^1H NMR spectrum on the orientation of the ligand in space relative to the tungsten can be seen in the discussion for complex **3.4** (refer to section 3.2.2.2). This observation has been implemented to identify isomers from more complex mixtures of allyl hydride isomers of related complexes.⁴⁵

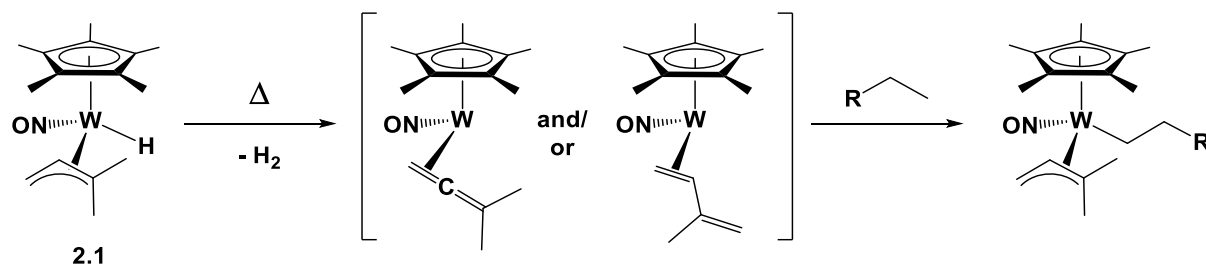
Table 2.1. ^1H NMR Chemical Shifts (δ) in ppm of the allyl meso *H* signals for complexes **2.1-2.3** in C_6D_6 highlighting the relative differences between the endo and exo orientations of the allyl ligands in the isomers.

	Complex 2.1	Complex 2.2	Complex 2.3
<i>Endo</i>	2.1b ; 4.71	2.2a ; 5.36	2.3a ; 4.61
		2.2c ; 5.03	2.3b ; 4.35
<i>Exo</i>	2.1a ; 2.68	2.2b ; 3.76	2.3c ; 2.82
		2.2d ; δ 4.33	2.3d ; δ 2.48

2.2.3 Reactions of the Hydride Complexes with PMe₃

It has been previously established that thermolyses of 18e Cp*W(NO)(CH₂CMe₃)(η^3 -allyl) compounds result in the intramolecular elimination of CMe₄ and the formation of 16e η^2 -diene and/or η^2 -allene intermediate complexes that effect a variety of intermolecular C-H activations of hydrocarbons.³⁰ We therefore anticipated that the thermal decomposition of the related Cp*W(NO)(H)(η^3 -allyl) complexes might involve the analogous intramolecular elimination of H₂ and the formation of the same 16e C-H activating intermediate species (Scheme 2.3).

Scheme 2.3. Initially proposed thermal pathway for 2.1



Instead, the lowest energy thermal pathway of these hydride complexes has been established experimentally and computationally as proceeding through 16e η^2 -alkene intermediate complexes. A computational analysis using **2.3a** as the model complex has been performed by Dr. Guillaume Lefèvre and a summary of the results is shown below in Figure 2.6. The lowest-energy thermal-decomposition pathway identified involves the intramolecular isomerization of **2.3a** to the 16e η^2 -alkene complex, Cp*W(NO)(η^2 -CH₂=CHCH₂Me). The corresponding η^2 -diene and η^2 -allene complexes and their respective transition states are

calculated to be formed via significantly higher-energy pathways and hence are unlikely to be involved in the thermal chemistry exhibited by **2.3a**, and presumably the other $\text{Cp}^*\text{W}(\text{NO})(\text{H})(\eta^3\text{-allyl})$ complexes.

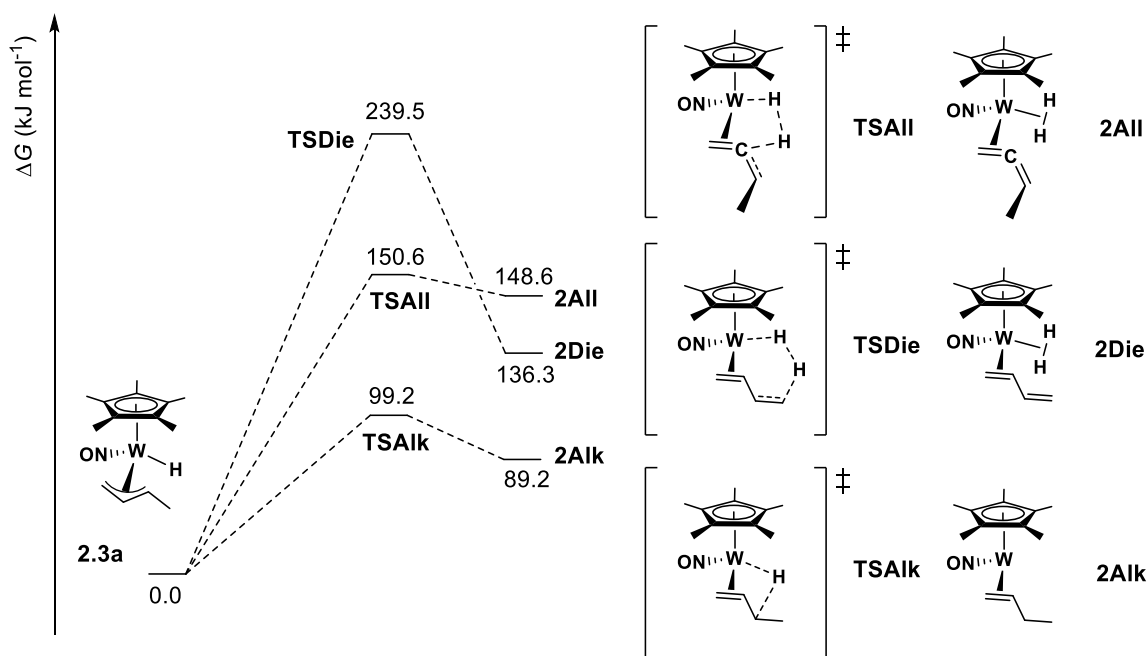


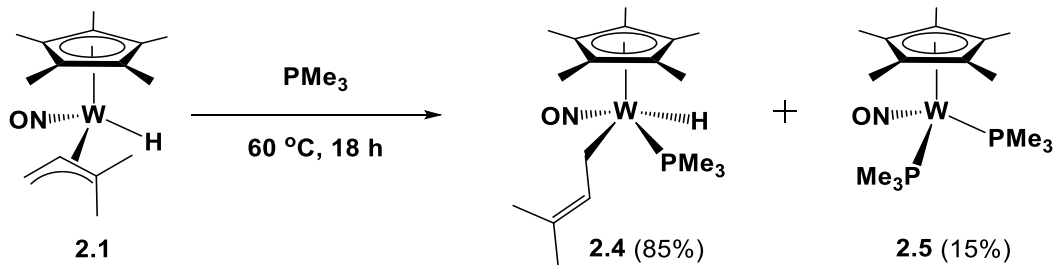
Figure 2.6. Computed thermal decomposition pathways from **2.3a** identify a 16e η^2 -alkene intermediate complex as the lowest energy species.³²

As the first step in experimentally establishing the thermal behavior of the $\text{Cp}^*\text{W}(\text{NO})(\text{H})(\eta^3\text{-allyl})$ complexes, **2.1** has been thermalized in the presence of PMe_3 to trap any coordinatively unsaturated organometallic species that might be formed. This strategy has proven successful in trapping the coordinatively unsaturated reaction intermediates from systems previously studied, including, but not limited to those forming 16e η^2 -allene,^{28, 29, 46} η^2 -diene,³⁴ and alkylidene complexes.⁴⁷

2.2.3.1 Reversible Adduct Formation of **2.1** with Trimethylphosphine

Maintenance of a solution of **2.1** in neat trimethylphosphine at 60 °C for 18 h affords a mixture of two new organometallic complexes, namely Cp*W(NO)(H)(η^1 -CH₂CH=CMe₂)(PMe₃) (**2.4**) and Cp*W(NO)(PMe₃)₂ (**2.5**) in a ratio of 85:15 (Scheme 2.4; complex **2.5** has been mentioned previously, but complete characterization has not been reported.^{48, 49}). Compounds **2.4** and **2.5** are isolated together as an orange powder in good yield by slow recrystallization from pentane at -33 °C. However, various attempts to fully separate the two complexes have been unsuccessful in obtaining either one individually in significant yield. For instance, both complexes decompose on a variety of column supports including basic and neutral alumina and silica, both in air and under an inert atmosphere. Large-scale fractional recrystallization is unsuccessful in separating the two complexes completely. Fortunately, a small sample of **2.4** can be isolated as large yellow crystals by slow evaporation of an Et₂O solution at -33 °C over 1 week, and the complete characterization of **2.4** has been effected with these crystals. Interestingly, the formation of **2.4** is reversible under ambient conditions. Thus, monitoring of a C₆D₆ solution of pure **2.4** by ¹H and ³¹P NMR spectroscopy over several weeks reveals the growth of signals due to **2.1** and free PMe₃ and the consumption of **2.4**. After approximately 2.5 weeks signals due to **2.4** are no longer evident. The reversibility of the formation of **2.4** explains, in part, the difficulty separating the mixture of **2.4** and **2.5** in an appreciable quantity. Consistently, if the thermal reaction of **2.1** is not carried out in neat PMe₃, the conversion of **2.1** to **2.4** never reaches 100 % completion.

Scheme 2.4. Reaction of 2.1 with PMe₃ at 60 °C



Complexes **2.4** and **2.5** each exist as a single isomer in solution. The $^{31}\text{P}\{^1\text{H}\}$ NMR spectrum of the mixture of **2.4** and **2.5** in C_6D_6 is shown in Figure 2.7. The signal due to the phosphorus atom of **2.4** at δ -23.9 ppm is a singlet with tungsten-183 satellites having $^1J_{\text{WP}} = 204.1$ Hz. The resonance due to the two equivalent phosphorus atoms of **5** at δ -22.2 ppm has a much larger $^1J_{\text{PW}}$ coupling of 456.8 Hz.

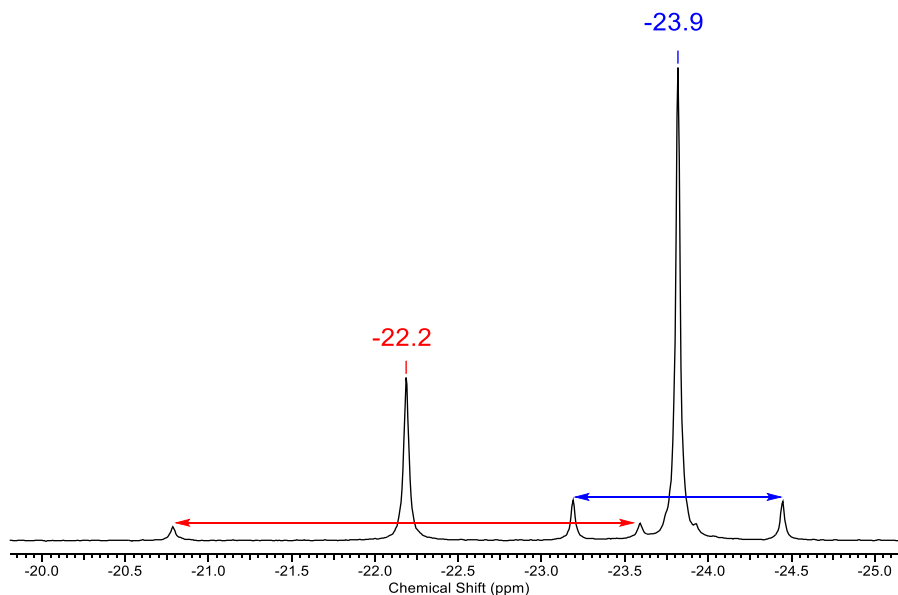


Figure 2.7. Expansion of the $^{31}\text{P}\{^1\text{H}\}$ NMR spectrum (-21.8 to -25.2 ppm) of the mixture of **2.4** and **2.5** in C_6D_6 (162 MHz) displaying the resonances due to the WPMe_3 phosphorus nuclei of **2.4** (δ -23.9, $^1J_{\text{PW}} = 204.1$) and **2.5** (δ -22.2, $^1J_{\text{PW}} = 456.8$).

The nitrosyl-stretching frequency in the infrared spectrum of **2.4** at 1563 cm^{-1} indicates a weaker NO bond and a greater degree of tungsten-nitrosyl backbonding than in the precursor complex **2.1** which has a ν_{NO} of 1601 cm^{-1} . This feature is the result of the strongly Lewis basic PMe_3 ligand donating electron density to the metal center in **2.4**. Consistently, in the case of **2.5** which possesses two PMe_3 ligands, the nitrosyl-stretching frequency is even lower ($\nu_{\text{NO}} = 1552\text{ cm}^{-1}$).

The solid-state molecular structure of **2.4** is shown in Figure 2.8. It is an 18e four-legged piano-stool molecule with only a single isomer containing the PMe_3 ligand trans to the nitrosyl and cis to both the hydride and η^1 -allyl ligands. The trans orientation of the PMe_3 and nitrosyl ligands is likely a manifestation of the strong σ -donor ability of the phosphine ligand and the strong π -acceptor character of the nitrosyl ligand. The hydride ligand has been located in the electron-density map, and the W-H bond length ($1.64(3)\text{ \AA}$) is essentially the same as that found for complex **2.1** ($1.62(3)\text{ \AA}$). The C(11)-C(12) and C(12)-C(13) bond lengths are indicative of single C-C and double C=C bonds with lengths of $1.492(3)\text{ \AA}$ and $1.339(3)\text{ \AA}$, respectively, and the bond angles containing C(12) and C(13) are all consistent with the presence of sp^2 -hybridized C atoms.

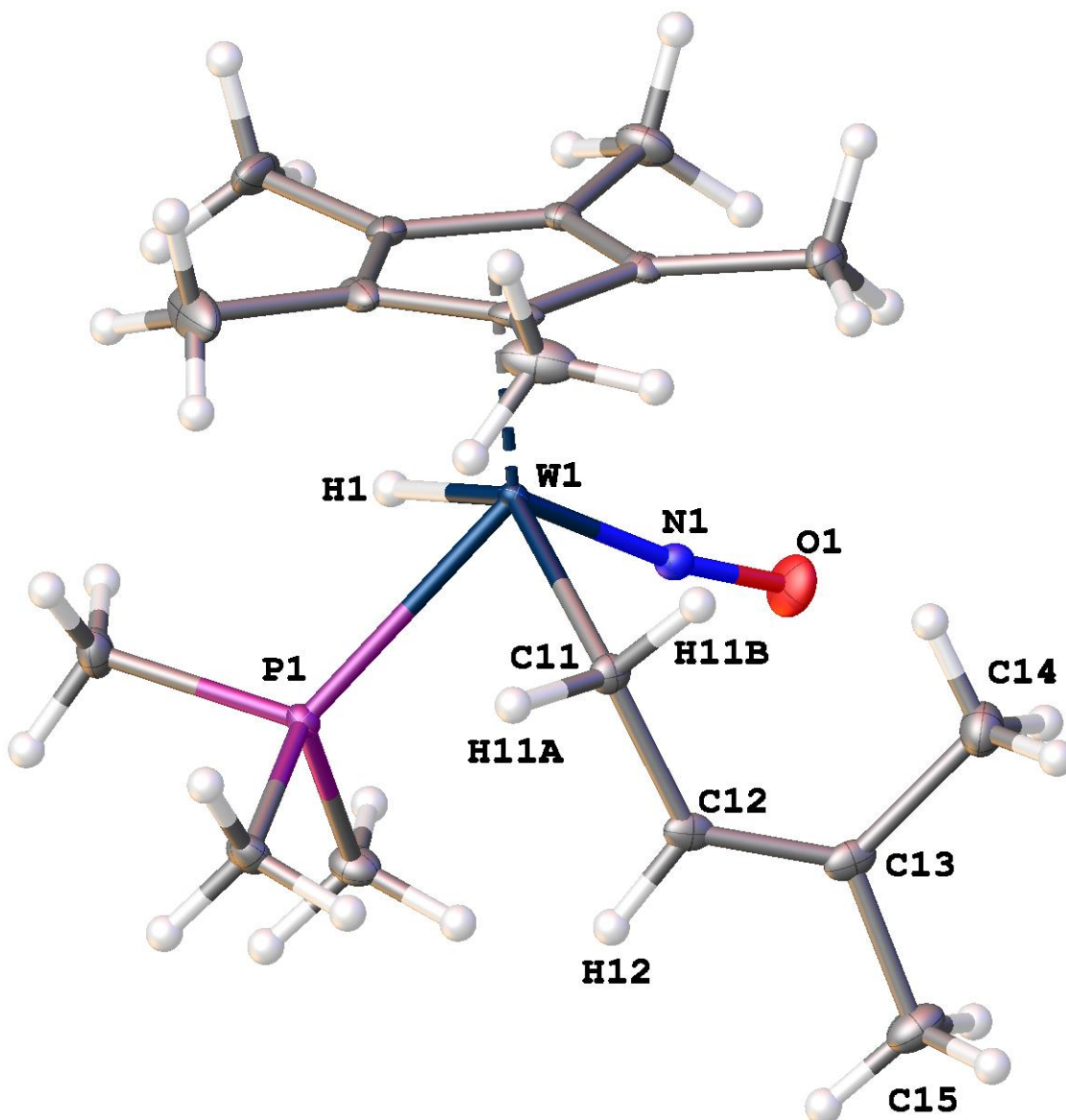


Figure 2.8. Solid-state molecular structure of **2.4** with 50% probability thermal ellipsoids shown.

Selected bond lengths (Å) and angles (deg): W(1)-H(1) = 1.64(3), W(1)-P(1) = 2.4913(9), W(1)-C(11) = 2.259(2), C(11)-C(12) = 1.492(3), C(12)-C(13) = 1.339(3), C(11)-H(11A) = 1.06(3), C(11)-H(11B) = 0.99(3), C(12)-H(12) = 1.00(3), W(1)-N(1) = 1.784(2), N(1)-O(1) = 1.224(2), C(11)-C(12)-C(13) = 127.7(2), C(12)-C(13)-C(14) = 123.7(2), C(12)-C(13)-C(15) = 122.4(2), W(1)-N(1)-O(1) = 171.87(16).

In the ^1H and ^{13}C NMR spectra of **2.4** resonances due to the hydride and η^1 -allyl ligands cis to the phosphine show scalar coupling to the phosphorus atom through the tungsten center. The resonance due to the tungsten hydride in the ^1H NMR spectrum of **2.4** is very distinct and appears as a doublet of triplets with tungsten-183 satellites. The overlaid ^1H and $^1\text{H}\{^{31}\text{P}\}$ NMR spectra of **2.4** are shown in Figure 2.9. The hydride resonance is coupled to the phosphorus atom of the WPMe_3 through the metal center ($^2J_{\text{PH}} = 81.2$ Hz), the tungsten center ($^1J_{\text{WH}} = 61.8$ Hz), and the two methylene protons of the η^1 - $\text{CH}_2\text{CH}=\text{CMe}_2$ ligand ($^3J_{\text{HH}} = 4.1$ Hz) adjacent to the tungsten. The methylene and methine carbon atoms of the η^1 -allyl ligand both show coupling to the PMe_3 phosphorus atom in the ^{13}C NMR spectrum. The resonance at 16.4 ppm due to η^1 - $\text{CH}_2\text{CH}=\text{CMe}_2$, C(11), shows coupling to both the phosphorus ($^2J_{\text{PC}} = 14.2$ Hz) and tungsten ($^1J_{\text{WC}} = 63.5$ Hz) atoms; this feature confirms the point of attachment of the η^1 -allyl ligand to the tungsten and is consistent with the solid-state molecular structure. The signal at 135.6 ppm due to the η^1 - $\text{CH}_2\text{CH}=\text{CMe}_2$ also shows coupling to the phosphorus ($^3J_{\text{PC}} = 8.3$ Hz), albeit with a slightly smaller magnitude, consistent with the larger distance between the atoms. The strong coupling of the phosphorus atom of the PMe_3 ligand with H and C atoms on ligands oriented cis to it is also evident in the NMR spectra of related complexes made from the reaction of complexes **2.1-2.3** with PMe_3 under various conditions (vide infra). This cis-coupling can be used to assign the position of a ligand cis or trans relative to PMe_3 for compounds for which solid-state molecular structures have not been obtained or for whose Sel NOE and/or NOESY spectra are not sufficient to assign isomers such as in the cases of multiple isomers possessing many overlapping signals in their ^1H NMR spectra.

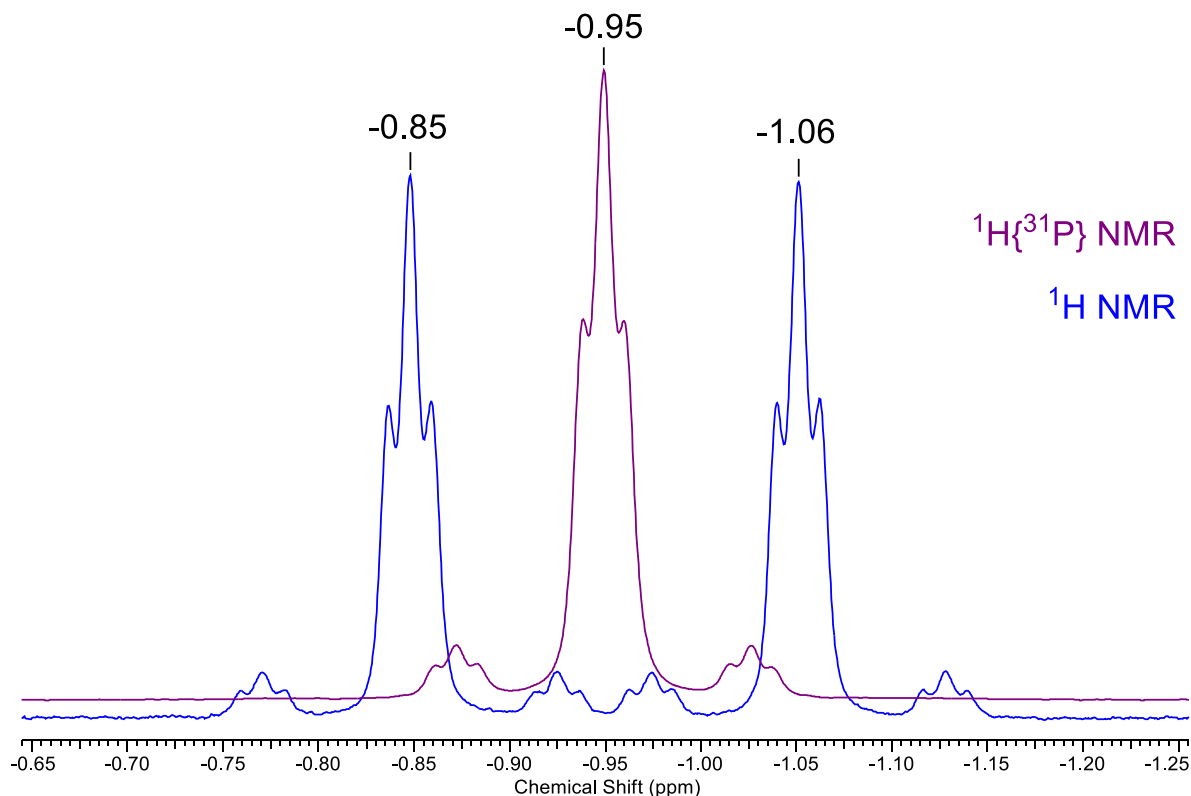


Figure 2.9. Expansion of the overlaid ^1H (blue) and $^1\text{H}\{^{31}\text{P}\}$ (purple) NMR spectra (-0.65 to -1.25 ppm) of **2.4** in C_6D_6 (400 MHz) displaying the resonances due to the WH proton of **2.4** (δ - 0.95, $^3J_{\text{HH}} = 4.3$, $^2J_{\text{PH}} = 81.4$, $^1J_{\text{WH}} = 61.8$).

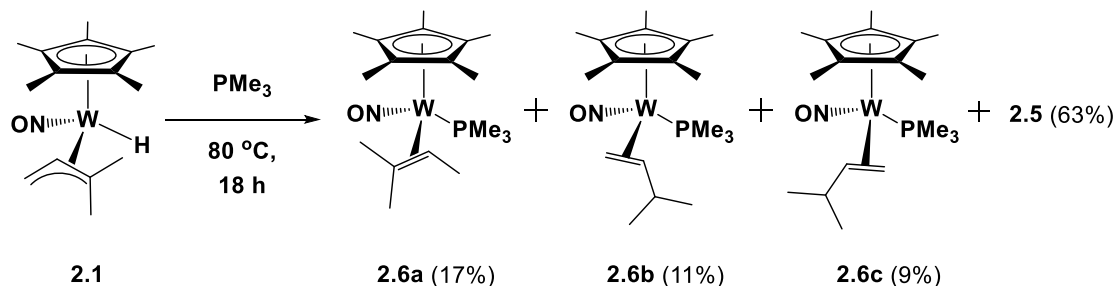
2.2.3.2 Identification of 16e η^2 -Alkene Intermediate Complexes

The reaction of **2.1** with PMe_3 at 60 $^\circ\text{C}$ leads to the reversible formation of the adduct **2.4**, which suggests that 60 $^\circ\text{C}$ is not sufficient to generate a coordinately unsaturated reactive intermediate. Monitoring the reaction of **2.1** with PMe_3 in C_6D_6 by ^1H and ^{31}P NMR spectroscopy at various temperatures identified the formation of new organometallic complexes containing W-P bonds when **2.1** was heated to 80 $^\circ\text{C}$.

2.2.3.3 Thermolysis of 2.1 in Neat PMe₃ at 80 °C

The reaction of **2.1** with neat PMe₃ carried out at a higher temperature (80 °C) results in the formation of **2.5** and the PMe₃-trapped η^2 -alkene complexes, Cp*W(NO)(η^2 -MeCH=CMe₂)(PMe₃) (**2.6a**) and Cp*W(NO)(η^2 -CH₂=CHCHMe₂)(PMe₃) (**2.6b**, **2.6c**) (Scheme 2.5). Complex **2.5** is formed as the major component of the reaction mixture, and the isomers of **2.6** cannot be separated from **2.5** by fractional recrystallization or column chromatography, the latter resulting in decomposition of all of the organometallic products.

Scheme 2.5. Reaction of 2.1 with PMe₃ at 80 °C



The similar and overlapping signals in the ¹H and ¹³C NMR spectra due to the three isomers of **2.6** preclude establishment of the exact orientations of their η^2 -alkene ligands via NOESY NMR spectroscopy. The orientations indicated in Scheme 2.5 are thus based on the ¹H-³¹P and ¹³C-³¹P scalar couplings in the ¹H and ¹³C NMR spectra, respectively. ³¹P coupling to protons and carbons that are oriented cis relative to the PMe₃ group are observed for the isomers of **2.6**. To compare, complex **2.4** displays coupling between the phosphorus of the PMe₃ ligand and the hydride (²J_{PH} = 81.4) and η^1 -allyl ligands, which are both oriented cis to the

phosphine ligand. The methylene ($^2J_{PC} = 14.2$) and methine ($^3J_{PC} = 8.3$) carbons of the η^1 -CH₂CH=CMe₂ ligand both display coupling to the phosphorus, as do the two methylene protons (the multiplets are overlapping at δ 1.52 and 1.55 ppm making identification of the coupling constants impossible, however a comparison of the ^1H and $^1\text{H}\{^{31}\text{P}\}$ NMR spectra of **2.4** qualitatively established an interaction with the phosphorus). Using this information (and additional examples, vide infra) the asymmetric coupling of the phosphorus to predominately one side (cis) of the η^2 -alkene ligands of the isomers of **2.6** has been used to assign the orientation of the alkene ligands of the isomers in solution. Particularly interesting is the ^{31}P coupling observed to the alkene ligands for isomers **2.6b** and **2.6c** (Figure 2.10). In the case of isomer **2.6b** (Figure 2.10a) in which the CHMe₂ substituent of the alkene ligand is oriented cis to the PMe₃ ligand, three-bond coupling is observed to the methine C which is not bound to the tungsten while the alkene methylene directly bound to the W and two bonds distant from the P displays no ^{31}P coupling. In the case of **2.6c** (Figure 2.10b) ^{31}P coupling is only observed to the methylene C oriented cis to PMe₃ ligand.

(a)

2.6b

H coupled to P		C coupled to P	
H ₁	³ J _{PH} = 11.2 Hz	C ₁	None
H ₂	³ J _{PH} = 7.6 Hz	C ₂	² J _{PC} = 12.0 Hz
		C ₃	³ J _{PC} = 4.6 Hz

(b)

2.6c

H coupled to P		C coupled to P	
H ₁	⁴ J _{PH} = 5.5 Hz	C ₁	² J _{PC} = 12.0 Hz
H ₂	None	C ₂	None
		C ₃	None

Figure 2.10. ¹H-³¹P and ¹³C-³¹P coupling observed for (a) **2.6b** and (b) **2.6c** from the ¹H and ¹³C NMR spectra recorded in C₆D₆. ¹³C-³¹P coupling is only observed for the C atoms oriented cis to the PMe₃. The η² connectivity of the alkene ligands is established by characteristic ¹⁸³W satellites.

The ³¹P{¹H} NMR spectrum involving the three isomers of **2.6** is shown in Figure 2.11. The three isomers all possess similar chemical shifts (δ -11.1 to -15.2 ppm) and ¹J_{WP} frequencies (358 to 373 Hz). These values are in the range typical for Cp*W(NO)(η²-R₂C=CR₂)(PMe₃) (R = H, alkyl, aryl) complexes.^{28, 32, 46}

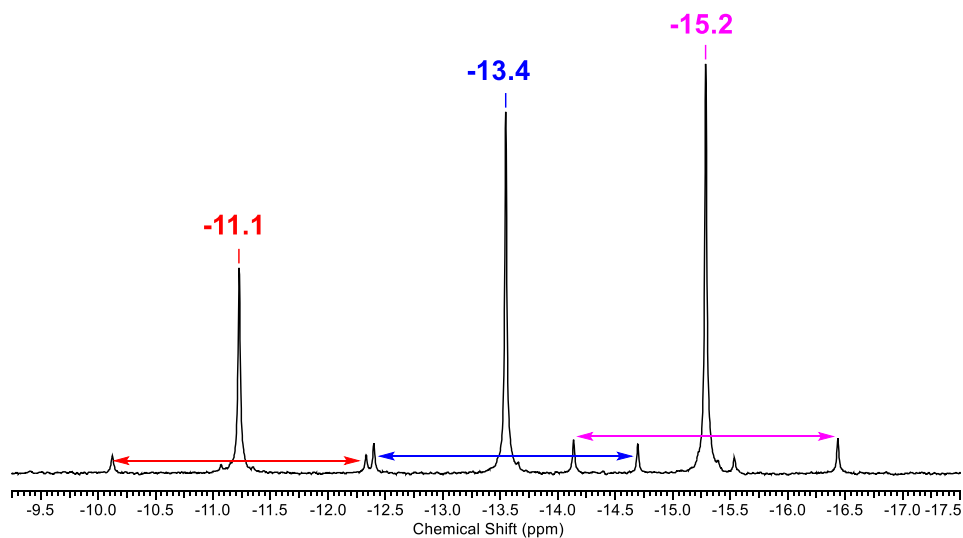
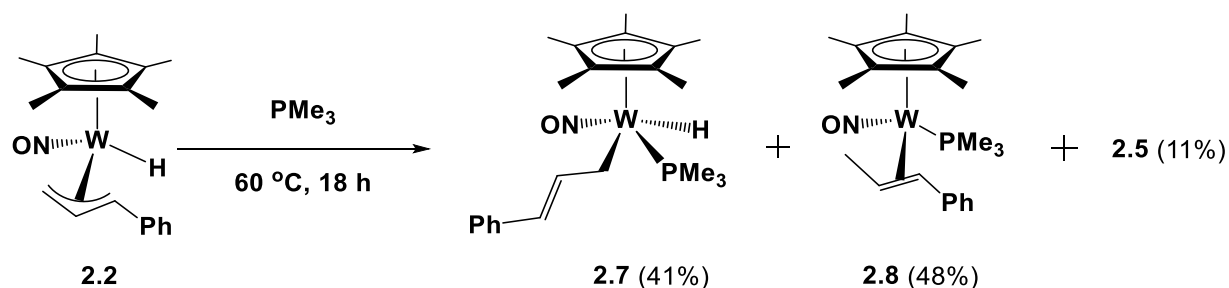


Figure 2.11. Expansion of the $^{31}\text{P}\{^1\text{H}\}$ NMR spectrum (-9.3 to -17.5 ppm) of **2.6** in C_6D_6 (162 MHz) displaying the resonances due to the WPMe_3 phosphorus nuclei of **2.6a** (δ -15.2, $^1J_{\text{PW}} = 373$), **2.6b** (δ -13.4, $^1J_{\text{PW}} = 372$), and **2.6c** (δ -11.1, $^1J_{\text{PW}} = 358$).

2.2.3.4 Reaction of **2.2** with PMe_3

The thermolysis of **2.2** at 60 °C in neat PMe_3 for 18 h was carried out by Dr. Russell Wakeham. The three organometallic complexes $\text{Cp}^*\text{W}(\text{NO})(\text{H})(\eta^1\text{-CH}_2\text{CH=CHPh})(\text{PMe}_3)$ (**2.7**), $\text{Cp}^*\text{W}(\text{NO})(\eta^2\text{-MeCH=CHPh})(\text{PMe}_3)$ (**2.8**), and **2.5** were afforded in a 41:48:11 ratio (Scheme 2.6). This mixture can be fractionally recrystallized from Et_2O at -33 °C to obtain red (**2.5**) and yellow (**2.7**, **2.8**) crystals. Quantitative separation of the mixture has not been achieved due to the instability of the complexes on various chromatographic columns, but a sufficient quantity of crystals could be separated to allow for the full characterization of **2.7** and **2.8**. The solid-state molecular structures for these two new complexes were solved by the author.

Scheme 2.6. Reaction of 2.2 with PMe₃ at 60 °C



Complex **2.7** is analogous to **2.4** (vide supra) in that the PMe₃ coordinates to the tungsten center trans to the nitrosyl ligand and the allyl ligand is shifted to an η^1 coordination mode. The solid-state molecular structure of **2.7** is shown in **Error! Reference source not found.**. There are two asymmetric molecules in the unit cell, both belonging to a single enantiomer of **2.7**.⁵⁰ The hydride ligand could not be located in the electron-density map generated by X-ray diffraction for either asymmetric unit. However, an open coordination site that could accommodate it exists for each molecule trans to the η^1 -allyl ligand and *cis* to the nitrosyl and PMe₃ ligands. This four-legged piano-stool geometry of the molecule closely resembles that of complex **2.4**. Thus, the bond lengths and angles about the C(11)-C(12) and C(33)-C(34) are consistent with C=C double bonds and sp^2 -hybridized C atoms. The characteristic *WH* signal in the ¹H NMR spectrum is also analogous to that of **2.4**, with a chemical shift of δ -0.62 ppm and scalar coupling to the tungsten, and *cis* oriented PMe₃ and η^1 -CH₂CH=CHPh ligands (²*J*_{HP} = 80.6, ¹*J*_{WH} = 30.6, ³*J*_{HH} = 4.3).

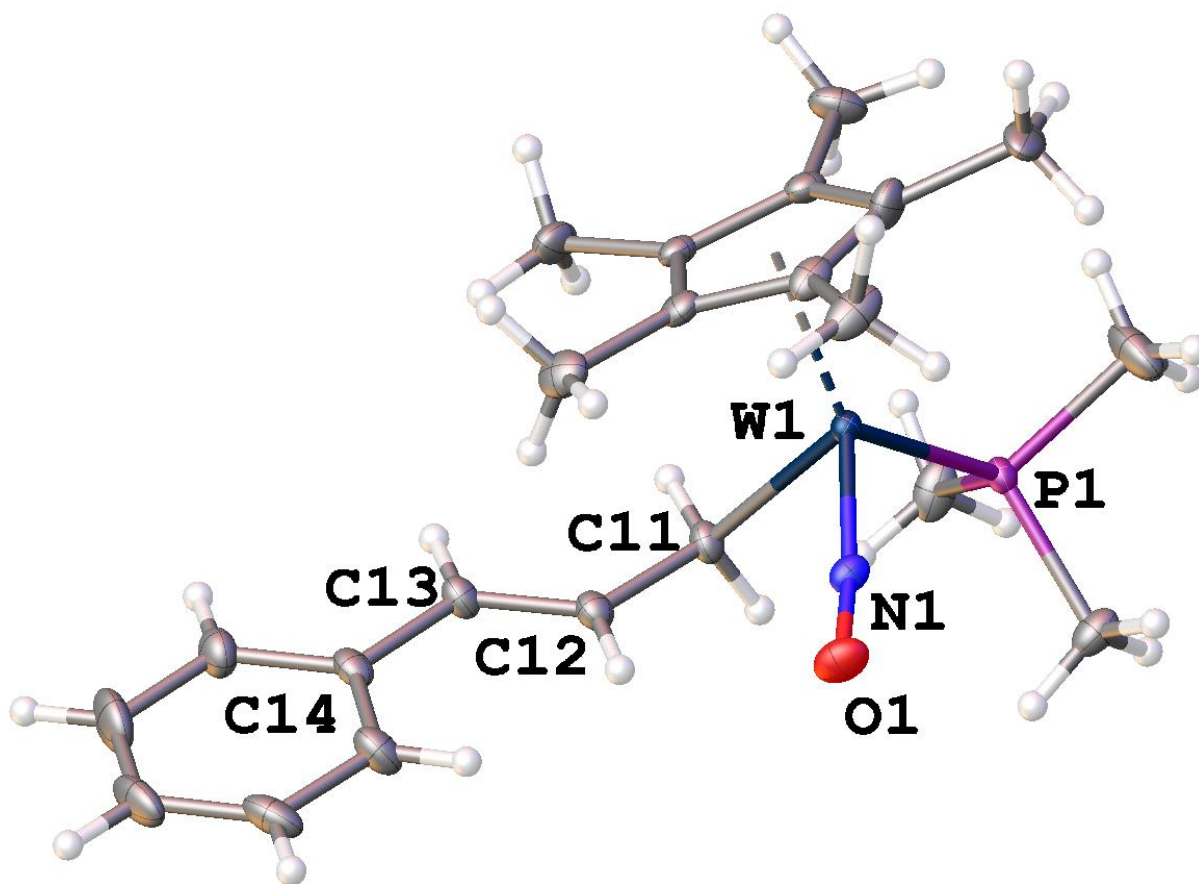


Figure 2.12. Solid-state molecular structure of **2.7** with 50% probability thermal ellipsoids shown. Selected bond lengths (Å) and angles (deg): W(1)-P(1) = 2.4951(10), W(1)-C(11) = 2.284(4), C(11)-C(12) = 1.482(5), C(12)-C(13) = 1.339(5), C(13)-C(14) = 1.466(5), W(1)-N(1) = 1.785(3), N(1)-O(1) = 1.223(4), C(11)-C(12)-C(13) = 127.5(4), C(12)-C(13)-C(14) = 125.5(4), W(1)-N(1)-O(1) = 168.8(3).

The other new compound formed from the reaction of **2.2** with PMe_3 is complex **2.8** which is the result of the coupling of the hydride and allyl ligands to generate a 16e η^2 -alkene complex, $\text{Cp}^*\text{W}(\text{NO})(\eta^2\text{-MeCH=CHPh})$, to which a PMe_3 molecule has coordinated. Large yellow crystals of **2.8** suitable for a single-crystal X-ray diffraction analysis can be grown by

slow evaporation from Et₂O at room temperature. There is only a single isomer of **2.8** both in solution and in the solid state. The η^2 -coordination mode of the *trans*- β -methylstyrene ligand is clearly evident in the solid-state molecular structure shown in Figure 2.13. The C(11)-C(12) bond length of 1.449(4) Å is significantly elongated compared to a typical C=C double bond. Additionally, despite having a C=C bond adjacent to the phenyl ring, the ligand is not planar, but significantly distorted, having a C(12)-C(13)-C(14)-C(19) torsion angle of 34.2(4)°. Both of these features indicate a considerable degree of tungsten to ligand backbonding. This C-C bonding is intermediate between that of an η^2 -alkene complex and a 3-membered metallacyclopropane, with the C-C bond length as well as the bond angles containing C(12) and C(13) being in between typical *sp*²- and *sp*³-hybridized C atoms. The ¹H NMR spectrum of **2.8** is also consistent with a significant tungsten interaction with the bound-olefin ligand, the signals due to the two alkene protons being significantly shifted upfield relative to a free alkene at 2.48 and 2.04 ppm.⁴³

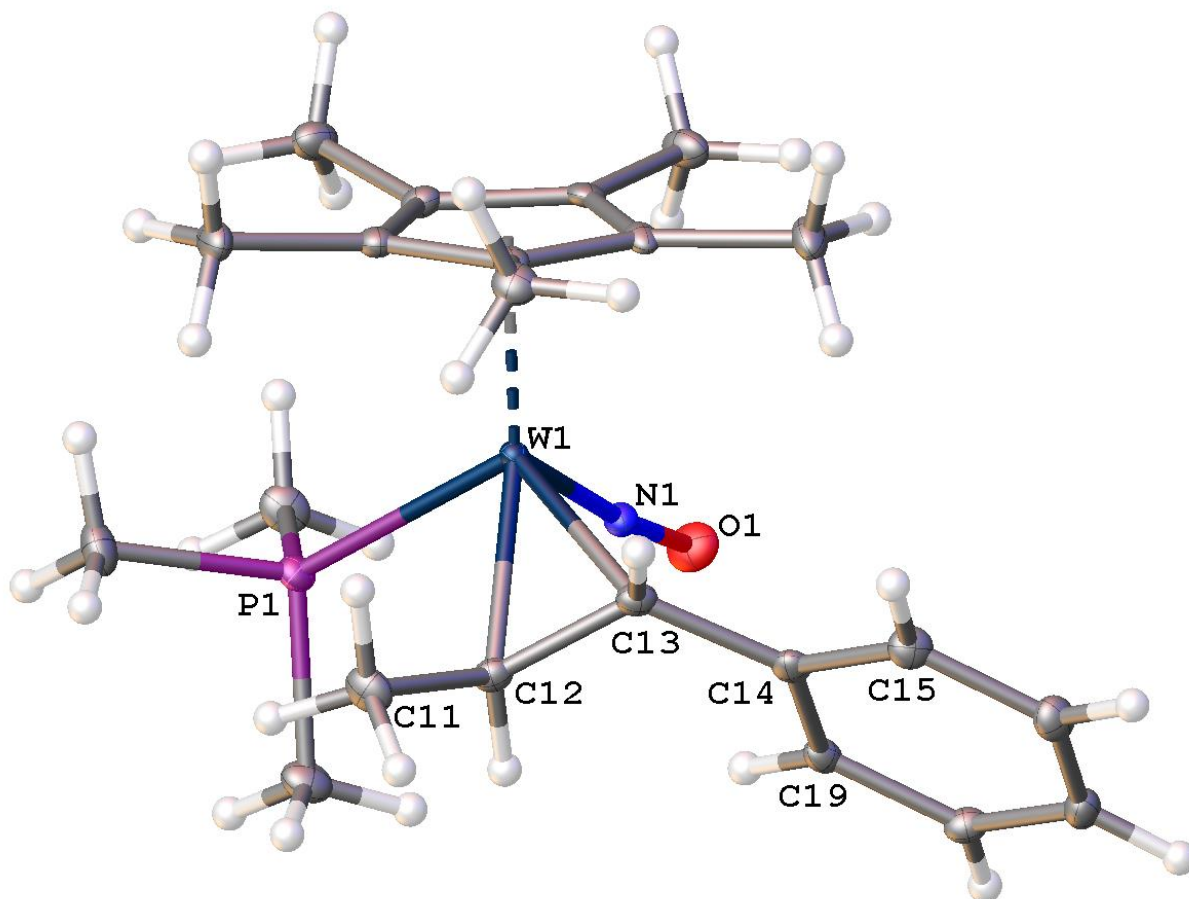


Figure 2.13. Solid-state molecular structure of **2.8** with 50% probability thermal ellipsoids shown. Selected bond lengths (Å) and angles (deg): W(1)-P(1) = 2.4535(10), W(1)-C(12) = 2.232(3), W(1)-C(13) = 2.216(3), C(11)-C(12) = 1.520(4), C(12)-C(13) = 1.449(4), C(13)-C(14) = 1.488(4), C(12)-H(12) = 0.98(4), C(13)-H(13) = 0.93(4), W(1)-N(1) = 1.781(3), N(1)-O(1) = 1.227(4), C(11)-C(12)-C(13) = 118.5(3), C(12)-C(13)-C(14) = 123.4(3), W(1)-N(1)-O(1) = 172.8(2).

The orientation of the methyl substituent cis to the PMe_3 ligand is evident in the solid-state molecular structure and is further confirmed by phosphorus coupling in the ^1H and ^{13}C NMR spectra of **2.8** (Figure 2.14a.). ^1H - ^{31}P coupling can be observed through tungsten and

carbon bonds as shown in Figure 2.14b in which the signal due to MeCHCHPh displays coupling to the adjacent methyl ($^3J_{\text{HH}} = 6.6$ Hz) and methine ($^3J_{\text{HH}} = 8.8$ Hz) protons as well as PMe₃ ($^3J_{\text{PH}} = 11.2$ Hz). The signals due to the alkene methyl and methine protons all display phosphorus-proton coupling; the CH cis to the PMe₃ has a larger $^3J_{\text{PH}}$ than the CH located trans to the PMe₃ ligand (11.2 Hz vs. 2.4 Hz). Likewise, the resonances due to the carbon CH and Me atoms located cis to the PMe₃ ligand are the only C atoms that display any ^{13}C - ^{31}P coupling. The ^1H - ^{31}P and ^{13}C - ^{31}P coupling in the ^1H and ^{13}C NMR spectra, respectively, occurs predominantly with ligands or parts of ligands located cis to the PMe₃ ligand; this cis ^{31}P coupling is also observed for complex **2.4** and the isomers of **2.6** (vide supra). Therefore, the correlation made from the X-ray solid-state molecular structures and NMR spectroscopy is that phosphorus coupling through the tungsten center occurs with ligands cis to the PMe₃. This fact is important for structural assignments of complexes for which single crystals suitable for X-ray diffraction cannot be obtained and complexes having several isomers with many overlapping signals that make solution-structure determinations using Sel NOE and NOESY NMR spectroscopy unreliable. This aspect has also been used for the assignment of the orientation of the η^2 -alkene ligands in the isomers of complexes **2.6** (vide supra) and **2.9** (vide infra).

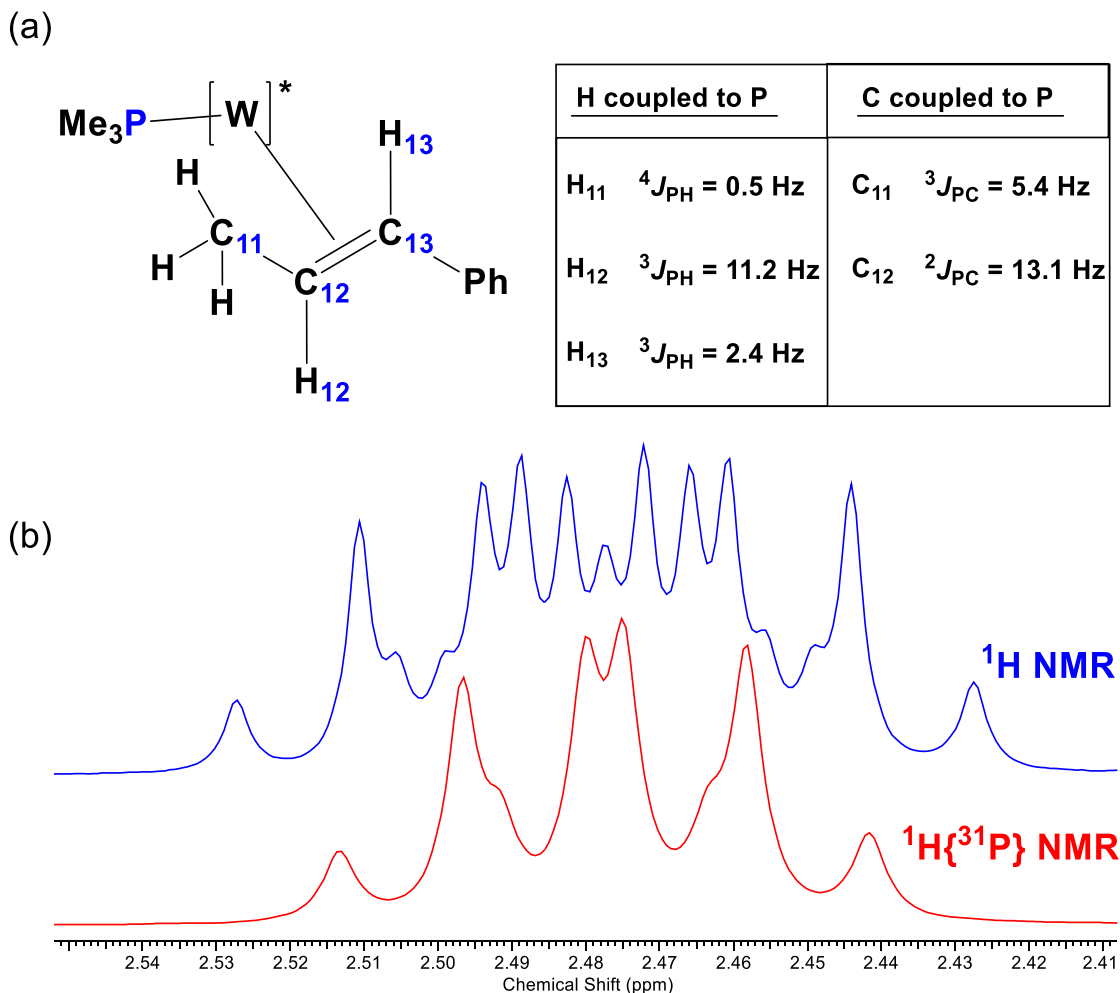


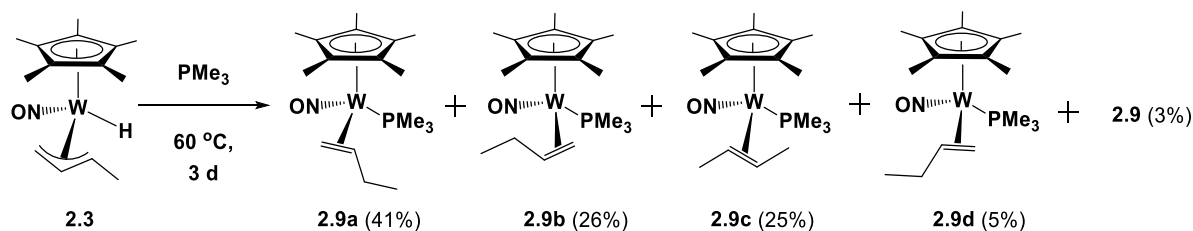
Figure 2.14. (a) Diagram displaying the ³¹P coupling to the η²-alkene ¹H and ¹³C signals for **2.8**; (b) Expansion of the overlaid ¹H (blue) and ¹H{³¹P} (purple) NMR spectra (2.55 to 2.41 ppm) of **2.8** in C₆D₆ (400 MHz) displaying the resonances (ddq) due to the MeCH=CHPh proton (δ -2.48, $^3J_{\text{PH}} = 11.2$, $^3J_{\text{HH}} = 8.8, 6.6$).

2.2.3.5 Reaction of **2.3** with PMe₃

The thermolysis of **2.3** in neat PMe₃ at 60 °C was performed by Mr. Aaron Holmes and produces isomers of the trapped 16e η²-alkene complexes, Cp*W(NO)(η²-

CH₂=CHCH₂Me)(PMe₃) (**2.9a**, **2.9b**, **2.9d**) and Cp*W(NO)(η²-MeCH=CHMe)(PMe₃) (**2.9c**), and complex **2.5** in a 41:26:25:5:3 ratio (Scheme 2.7). While crystals suitable for single-crystal X-ray diffraction analyses have not been obtained, the coordination of the alkene C=C bond to the tungsten center has been established for each isomer via ¹⁸³W satellites on the alkene signals in the ¹³C NMR spectrum. ³¹P-coupling in the ¹H and ¹³C NMR spectra has again been used to assign the orientation of the alkene ligands, with the ¹³C and ¹H atoms whose signals display ³¹P-coupling being *cis* to the PMe₃ ligand. The expansion of the ³¹P{¹H} NMR spectrum displaying the resonances due to PMe₃ ligands for the isomers of **2.9** is shown in Figure 2.15. The chemical shift and ¹J_{WP} values are consistent with the similar η²-alkene adducts **2.6** and **2.7** discussed previously (vide supra).

Scheme 2.7. Reaction of 2.3 with PMe₃ at 60 °C



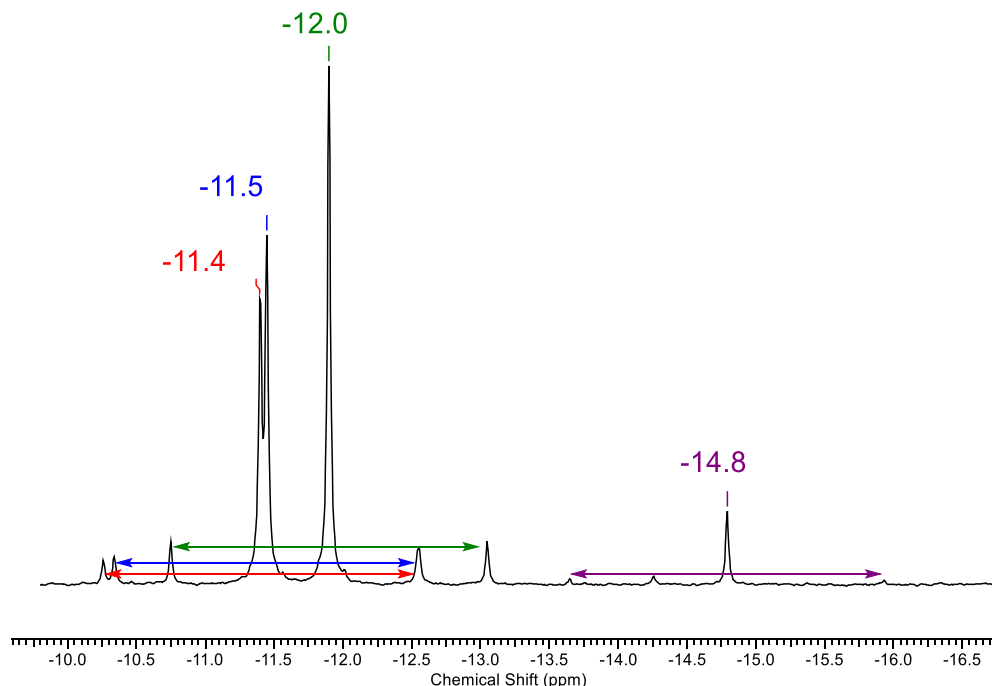


Figure 2.15. Expansion of the $^{31}\text{P}\{^1\text{H}\}$ NMR spectrum (-9.6 to -16.7 ppm) of **2.9** in C_6D_6 (162 MHz) displaying the resonances due to the WPMe_3 phosphorus nuclei of **2.9a** (δ -12.0, $^1J_{\text{PW}} = 372.6$), **2.9b** (δ -11.5, $^1J_{\text{PW}} = 358.7$), **2.9c** (δ -11.4, $^1J_{\text{PW}} = 369.9$), and **2.9d** (δ -14.8 ($^1J_{\text{WP}} = 370.6$)).

Attempts to isolate the $\text{Cp}^*\text{W}(\text{NO})(\text{H})(\eta^1\text{-CH}_2\text{CH=CHMe})(\text{PMe}_3)$ complex (**2.10**) that is analogous to **2.4** and **2.7** in significant quantity from the reaction of **2.3** with PMe_3 have been unsuccessful. It can be detected spectroscopically by its characteristic WH signal in the ^1H NMR spectrum [δ -0.81 (dt, $^3J_{\text{HH}} = 4.6$, $^2J_{\text{PH}} = 80.2$, $^1J_{\text{WH}} = 62.0$, 1H)] and WPMe_3 signal in the $^{31}\text{P}\{^1\text{H}\}$ NMR spectrum [δ -24.0 (s, $^1J_{\text{PW}} = 203.6$)], both of which are similar to the corresponding signals displayed by **2.4** and **2.7** in terms of chemical shifts and coupling constants. The reaction mixture in which **2.10** can be detected contains mainly isomers of **2.9** as well as some unreacted **2.3**. This observation suggests that complex **2.10** is unstable under the

conditions required to form it and is largely converted to **2.9** (either directly or by first reverting to **2.3**) before the starting complex has been completely consumed.

2.2.3.6 Summary of the ^{31}P NMR Chemical Shifts and $^1J_{\text{WP}}$ Coupling Constants for the Various Products Formed from the Reactions of 2.1-2.3 with PMe_3

The allyl hydride complexes **2.1-2.3** all react with PMe_3 to give two different types of organometallic products, either the four-legged piano stool adducts $\text{Cp}^*\text{W}(\text{NO})(\text{H})(\eta^1\text{-allyl})(\text{PMe}_3)$ (**2.4**, **2.7**, **2.10**) or the η^2 -alkene adducts $\text{Cp}^*\text{W}(\text{NO})(\eta^2\text{-alkene})(\text{PMe}_3)$ (**2.6**, **2.8**, **2.9**). In some cases these complexes exist as multiple isomers and in all cases they are difficult to isolate. Conveniently, the different types of products share characteristic chemical shifts and $^1J_{\text{WP}}$ coupling constants which make spectroscopic identification by ^{31}P NMR spectroscopy straightforward. These values are summarized in Table 2.2. The $\text{Cp}^*\text{W}(\text{NO})(\text{H})(\eta^1\text{-allyl})(\text{PMe}_3)$ complexes **2.4**, **2.7**, and **2.10** have chemical shifts between δ -23.8 and -24.0 ppm with $^1J_{\text{WP}}$ values ranging from 203.1 to 204.6 Hz in the ^{31}P NMR spectra. Complex **2.4** is formed reversibly and reverts back to **2.1** and PMe_3 , indicating a weaker W-P bond. Interestingly, the coupling constant of this complex (as well as **2.7** and **2.10**) is much smaller in magnitude than for the η^2 -alkene adducts. The $\text{Cp}^*\text{W}(\text{NO})(\eta^2\text{-alkene})(\text{PMe}_3)$ complexes **2.6**, **2.7**, and **2.9** are identified by characteristic chemical shifts due to the PMe_3 ligand ranging from δ -10.1 to -15.2 ppm with $^1J_{\text{WP}}$ values ranging from 358 to 373 Hz. Similar complexes containing either η^2 -allene or η^2 -alkene ligands display similar properties in their ^{31}P NMR spectra with chemical shifts of the PMe_3 ligands found between δ -9.5 and -17.3 ppm and having $^1J_{\text{WP}}$ coupling constants between 340 and 365 Hz.^{26, 28, 29, 32}

Table 2.2. Correlation of ^{31}P NMR chemical shifts and $^1J_{\text{WP}}$ coupling frequencies between the various tungsten-phosphine complexes.

Entry	Complex	^{31}P NMR δ (ppm)	$^1J_{\text{WP}}$ (Hz)
1	$[\text{W}]^*(\text{PMe}_3)_2$ (2.5)	-22.2	456.8
2	$[\text{W}]^*(\text{H})(\eta^1\text{-CH}_2\text{CH}=\text{CMe}_2)(\text{PMe}_3)$ (2.4)	-23.9	204.1
3	$[\text{W}]^*(\text{H})(\eta^1\text{-CH}_2\text{CH}=\text{CHPh})(\text{PMe}_3)$ (2.7)	-23.8	204.6
4	$[\text{W}]^*(\text{H})(\eta^1\text{-CH}_2\text{CH}=\text{CHMe})(\text{PMe}_3)$ (2.10)	-24.0	203.1
5	$[\text{W}]^*(\eta^2\text{-MeCH}=\text{CMe}_2)(\text{PMe}_3)$ (2.6a)	-15.2	373
6	$[\text{W}]^*(\eta^2\text{-CH}_2=\text{CHCHMe}_2)(\text{PMe}_3)$ (2.6b)	-13.4	372
7	$[\text{W}]^*(\eta^2\text{-CH}_2=\text{CHCHMe}_2)(\text{PMe}_3)$ (2.6c)	-11.1	358
8	$[\text{W}]^*(\eta^2\text{-MeCH}=\text{CHPh})(\text{PMe}_3)$ (2.8)	-10.1	370
9	$[\text{W}]^*(\eta^2\text{-CH}_2=\text{CHCH}_2\text{Me})(\text{PMe}_3)$ (2.9a)	-12.0	373
10	$[\text{W}]^*(\eta^2\text{-CH}_2=\text{CHCH}_2\text{Me})(\text{PMe}_3)$ (2.9b)	-11.5	359
11	$[\text{W}]^*(\eta^2\text{-MeCH}=\text{CHMe})(\text{PMe}_3)$ (2.9c)	-11.4	370
12	$[\text{W}]^*(\eta^2\text{-CH}_2=\text{CHCH}_2\text{Me})(\text{PMe}_3)$ (2.9d)	-14.8	371
13 ²⁶	$[\text{W}]^*(\eta^2\text{-CH}_2=\text{C}=\text{CMe}_2)(\text{PMe}_3)$	-21.4	345
14 ²⁸	Isomers of	(a) -11.8	348
	$[\text{W}]^*(\eta^2\text{-CH}_2=\text{C}=\text{CHPh})(\text{PMe}_3)$	(b) -10.4	340
15 ²⁹	$[\text{W}]^*(\eta^2\text{-CH}_2=\text{C}=\text{CHTMS})(\text{PMe}_3)$	-9.5	348
16 ³²	Isomers of	(a) -17.3	361
	$[\text{W}]^*(\eta^2\text{-CH}_2=\text{CHCMe}_2\text{Ph})(\text{PMe}_3)$	(b) -9.6	356
		(c) -14.4	365

2.2.4 Radical Nature of Tungsten-Hydride Bond

Determining the nature of the tungsten-hydride bond is a critical first step towards understanding the reactivity of these complexes. Dr. Guillaume Lefèvre has been able to model the electronic structure of **2.3a** for which the resulting electronic surface potential map is shown below in Figure 2.16. From this model it is possible to locate the negative charge of **2.3a** largely on the nitrosyl ligand. The hydride ligand itself has a charge close to zero. The lack of significant charge at the W-H linkage helps account for the stability of $\text{Cp}^*\text{W}(\text{NO})(\text{H})(\eta^3\text{-allyl})$ in a weakly acidic media such as water. Additionally, the hydridic/protonic nature of the W-H bond has been investigated by several members of the Legzdins group by exploring the reactivity with acids, bases, and polar bonds. These investigations have led either to no reaction or intractable mixtures, presumably from decomposition of the hydride complexes.

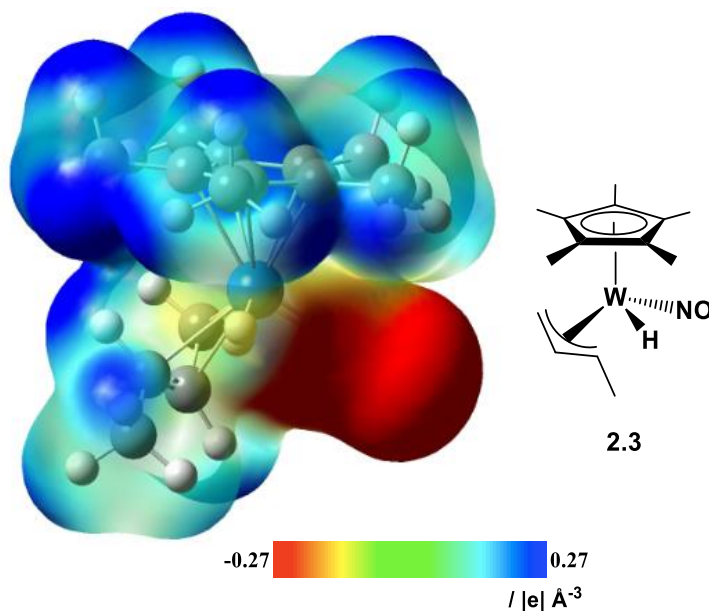
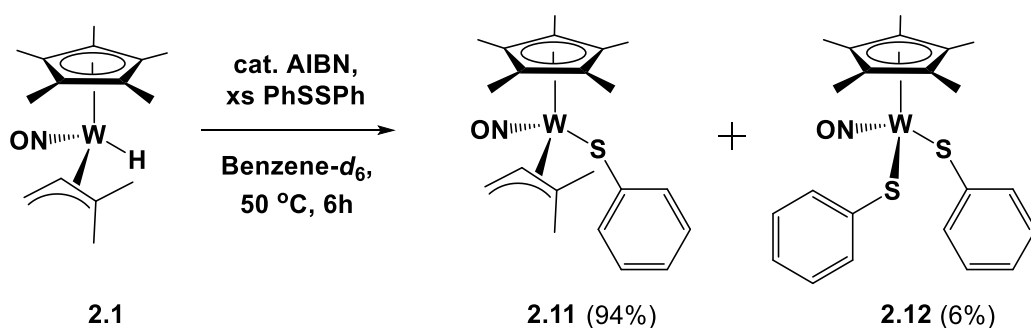


Figure 2.16. Computed electronic surface potential of **2.3a**.

To test the radical nature of the W-H bond experimentally, the reaction of **2.1** in the presence of a radical initiator and radical trapping reagent was carried out.^{51, 52} In the presence of azobisisobutyronitrile (AIBN) and diphenyl disulfide (PhSSPh), complex **2.1** is converted into primarily Cp*W(NO)(SPh)(η^3 -CH₂CHCMe₂) (**2.11**) and small amounts of what appears to be Cp*W(NO)(SPh)₂ (**2.12**) (Scheme 2.8). Monitoring this reaction by ¹H NMR spectroscopy revealed that the consumption of **2.1** is complete within 6 h at 50 °C. The reaction also proceeds under ambient conditions, albeit at a much slower rate.

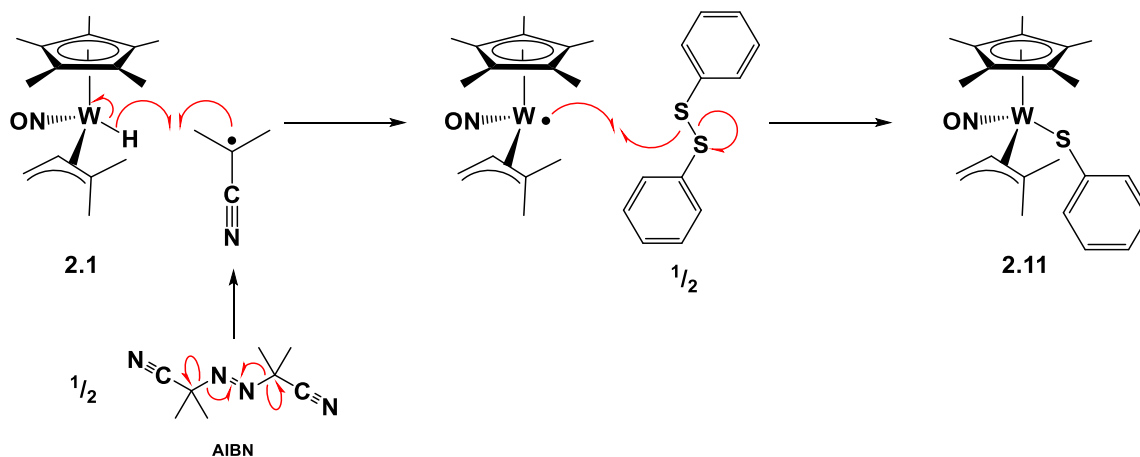
Scheme 2.8. Reaction of 2.1 with PhSSPh in the presence of the radical initiator AIBN



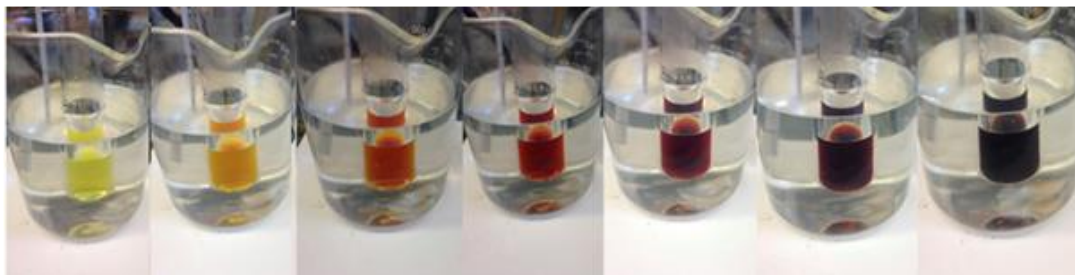
Following the addition of the three components of the reaction there is an immediate colour change observed in which the reaction mixture turns from light yellow to orange within minutes. The colour eventually turns red and continues to darken until a deep burgundy colour is observed (Figure 2.17a). Interestingly, the red/burgundy colour is due to the minor product **2.12** as **2.11** can be isolated as an orange solid. The radical reaction itself is clean with no other apparent W complexes aside from **2.11** or **2.12** generated from the homolytic cleavage of the W-H bond (Figure 2.17b). The reaction has been carried out using both stoichiometric and catalytic (ca. 20%) quantities of AIBN, resulting in the formation of the same products.

A possible mechanism for the formation of **2.11** is shown in Scheme 2.9. The homolytic cleavage of the W-H bond in the presence of the radical initiator AIBN generates the tungsten-centered radical $[\text{Cp}^*\text{W}(\text{NO})(\eta^3\text{-CH}_2\text{CHCMe}_2)]^\bullet$, which can then be trapped by PhSSPh.⁵² To test whether complex **2.1** can undergo homolytic cleavage of its W-H in the absence of a radical initiator, the reaction of **2.1** with TEMPO was carried out. There was absolutely no change to **2.1** in the presence of TEMPO (by ^1H NMR spectroscopy), indicating **2.1** does not generate a radical species in the absence of an initiator.

Scheme 2.9. Possible mechanism for the homolytic cleavage of the W-H bond in 2.1 and trapping of the tungsten radical by PhSSPh



(a)



(b)

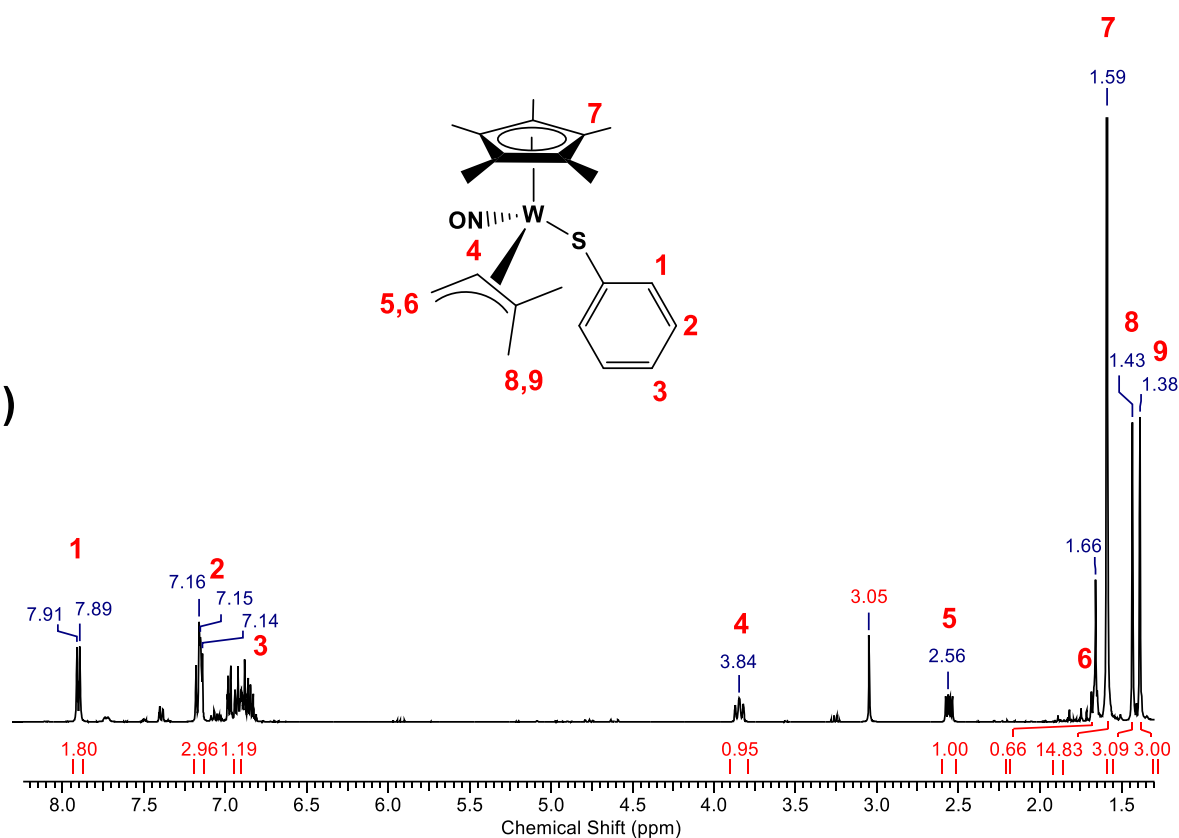
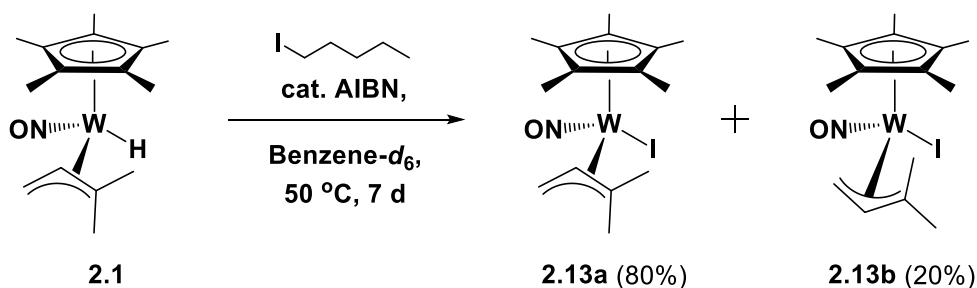


Figure 2.17. (a) Colours observed for the reaction of **2.1** with PhSSPh in the presence of AIBN.

(b) ¹H NMR spectrum (400 MHz, C₆D₆) for the reaction of **2.1** with PhSSPh in the presence of AIBN at 50 °C for 6 h. Assignment of the resonances due to **2.11** is shown. The resonance at δ 1.66 ppm is due to the Cp* of **2.12**. Resonances from δ 7.75 to 6.80 ppm are attributable to **2.12** and excess PhSSPh.

The reaction of **2.1** with 1-iodopentane in the presence of AIBN has been carried out to test if the tungsten-centered radical was capable of cleaving a C-X bond. Heating the mixture at 50 °C for 1 week results in colour changes from yellow to orange to red as well as broad signals in the ^1H NMR spectrum for endo/exo isomers of $\text{Cp}^*\text{W}(\text{NO})(\eta^3\text{-CH}_2\text{CHCMe}_2)(\text{I})$ (**2.13**) (Scheme 2.10). The presence of **2.13** is supported by mass spectrometry with a tungsten isotope pattern observed at $m/z = 545$. The cleavage of the C-I bond by the tungsten-centered radical and formation of a new W-I bond to give **2.13** does not appear to be accompanied by the formation of any new W-C bonds (the expected organometallic product $\text{Cp}^*\text{W}(\text{NO})(n\text{-C}_5\text{H}_{11})(\eta^3\text{-CH}_2\text{CHCMe}_2)$ is inherently unstable and decomposes to an allyl hydride complex,^{30, 32} characteristic W-H signals attributable to this complex are not present in the ^1H NMR spectrum for the reaction in Scheme 2.10).

Scheme 2.10. Reaction 2.1 with 1-iodopentane in the presence of a radical initiator



2.2.5 Pursuit of Molybdenum Allyl Hydride Complexes

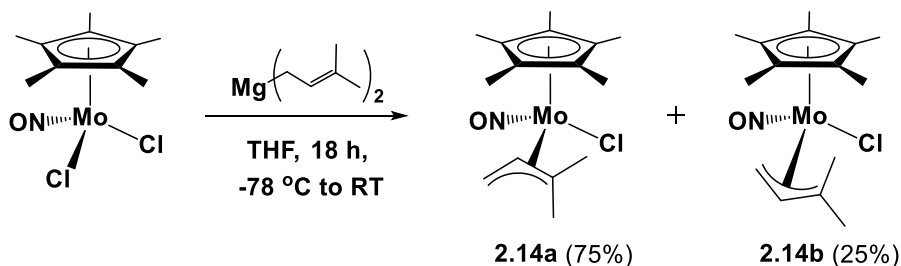
Direct synthesis of the analogous $\text{Cp}^*\text{Mo}(\text{NO})(\text{H})(\eta^3\text{-allyl})$ complexes in a parallel fashion to the synthesis of **2.1** (refer to Scheme 2.2) does not lead to any tractable organometallic

complex. The synthesis and characterization of the synthetic intermediate complexes $\text{Cp}^*\text{Mo}(\text{NO})(\eta^3\text{-allyl})\text{Cl}$ have been investigated to determine if the isolation of these complexes could facilitate the synthesis of the desired molybdenum allyl hydride complexes.

2.2.5.1 Preparation of $\text{Cp}^*\text{Mo}(\text{NO})(\eta^3\text{-CH}_2\text{CHCMe}_2)\text{Cl}$ (**2.14**)

The complex $\text{Cp}^*\text{Mo}(\text{NO})(\eta^3\text{-CH}_2\text{CHCMe}_2)\text{Cl}$ (**2.14**) can be synthesized from $\text{Cp}^*\text{Mo}(\text{NO})\text{Cl}_2$ via a metathesis reaction with $\text{Mg}(\text{CH}_2\text{CH}=\text{CMe}_2)_2$ (Scheme 2.11). The magnesium binary is added slowly at -78°C and the reaction mixture is then stirred at room temperature for 18 h. Complex **2.14** is obtained in high yield (74.2%) as a green-brown solid following an aqueous wash. Only a single water wash is performed to remove the salt byproducts from the metathesis reaction and it must be performed quickly to avoid any decomposition. Complex **2.14** decomposes to $\text{Cp}^*\text{Mo}(\text{O})_2\text{Cl}$ (**2.15**), which has been characterized by single-crystal X-ray diffraction (Figure 2.18) and is identifiable as a singlet at 1.80 ppm in the ^1H NMR spectrum of the mixture when present. The oxidation of **2.14** likely proceeds in a similar manner to the oxidation of $\text{Cp}^*\text{M}(\text{NO})(\text{CH}_2\text{EMe}_3)_2$ ($\text{M} = \text{W}, \text{Mo}$; $\text{E} = \text{C}, \text{Si}$) which produces $\text{Cp}^*\text{M}(\text{O})_2\text{R}$ via oxidatively-induced nitrosyl insertion into a M-C bond followed by loss of RNO_2 .⁵³

Scheme 2.11. Synthesis of $\text{Cp}^*\text{Mo}(\text{NO})(\eta^3\text{-CH}_2\text{CHCMe}_2)\text{Cl}$ (2.14**)**



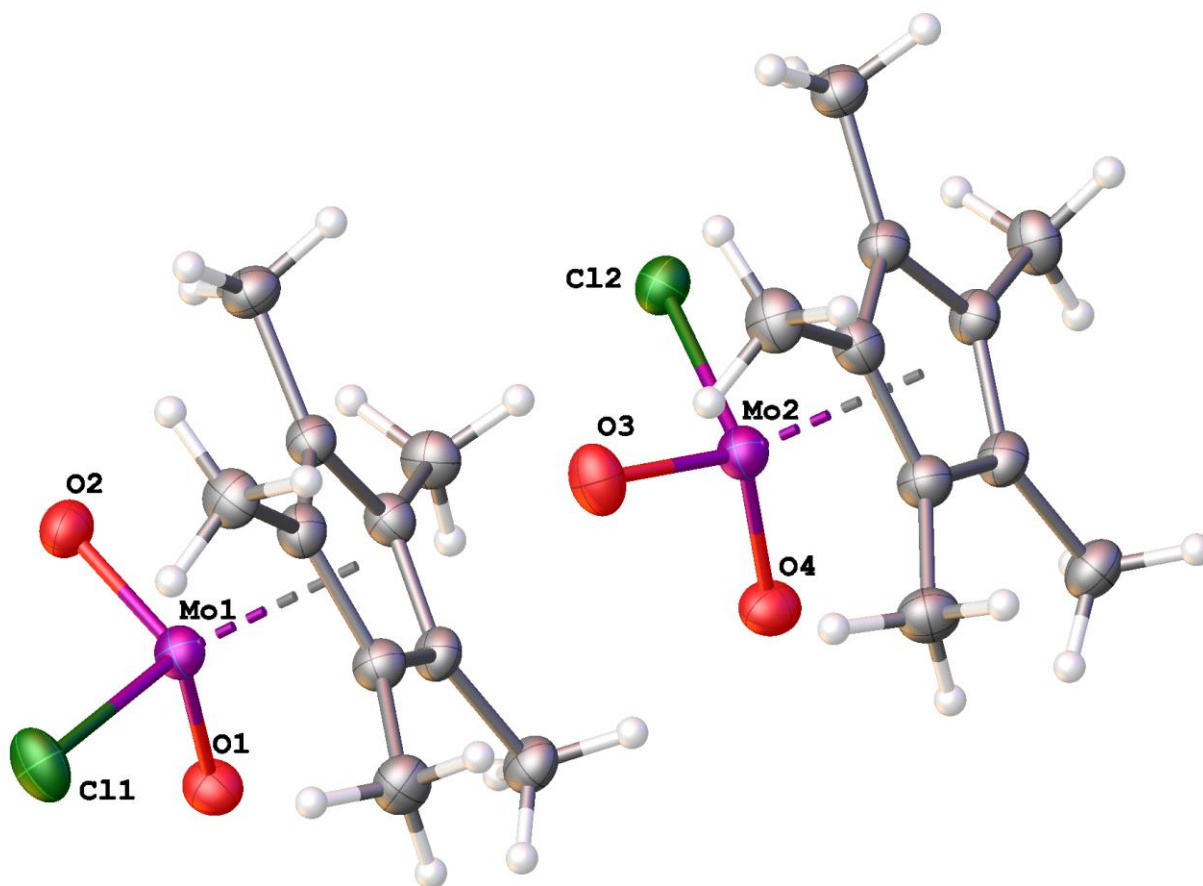


Figure 2.18. . Solid-state molecular structure of **2.15** with 50% probability thermal ellipsoids shown. Selected interatomic distance (Å) and angles (deg.): Mo(1)-Cl(1) = 2.3251(11), Mo(1)-O(1) = 1.711(2), Mo(1)-O(2) = 1.712(2), Mo(2)-Cl(2) = 2.3359(14), Mo(2)-O(3) = 1.714(2), Mo(2)-O(4) = 1.715(2), Cl(1)-Mo(1)-O(1) = 104.10(8), O(1)-Mo(1)-O(2) = 107.68(10), O(2)-Mo(1)-Cl(1) = 105.26(8), Cl(2)-Mo(2)-O(3) = 105.05(8), O(3)-Mo(2)-O(4) = 108.29(11), O(4)-Mo(2)-Cl(2) = 103.52(8).

Complex **2.14** exists in solution as two isomers, in a 3:1 ratio, that differ in the orientation of the allyl ligand. The major isomer (**2.14a**) has the allyl ligand in the exo orientation, while the minor isomer (**2.14b**) has the allyl ligand oriented in the endo orientation.

The exo and endo assignments of the allyl ligand are made using the chemical shift of the meso *H* of the allyl ligand belonging to each isomer. The meso *H* signal belonging to the exo isomer (**2.14a**) at 3.60 ppm is upfield relative to the corresponding signal for the endo isomer (**2.14b**) at 5.06 ppm. The infrared spectrum of **2.14** contains a single nitrosyl-stretching frequency at 1631 cm⁻¹.

2.2.5.2 Synthesis of Cp*Mo(NO)(η^3 -CH₂CHCH₂)Cl

The complex of Cp*Mo(NO)(η^3 -CH₂CHCH₂)Cl (**2.16**) is synthesized from Cp*Mo(NO)Cl₂ and Mg(CH₂CH=CH₂)₂ in an analogous fashion to the preparation of **2.14** and is obtained in 39% yield as a tan-green solid. In solution, **2.16** exists as a single isomer that has the allyl ligand in an endo orientation, with a downfield meso *H* signal in the ¹H NMR spectrum at 5.71 ppm. Yellow crystals suitable for single-crystal X-ray diffraction have been grown by slow evaporation from Et₂O in the air. Two isomers are identified in the solid state which appear to be enantiomers of **2.16**, both having the allyl in the endo orientation (Figure 2.19, Figure 2.20). The three-legged piano stool geometry is confirmed by the X-ray data as well as the presence of linear nitrosyl ligands. The infrared nitrosyl stretching-frequency is 1627 cm⁻¹, which is similar to that for **2.14**, indicating similar electronics at the molybdenum center. Electronic asymmetry is apparent in this complex with signals due to the allyl methylene protons ranging from 0.85 to 4.27 ppm in the ¹H NMR spectrum and signals for the allyl methylene carbons at 50.2 and 97.1 ppm in the ¹³C NMR spectrum.

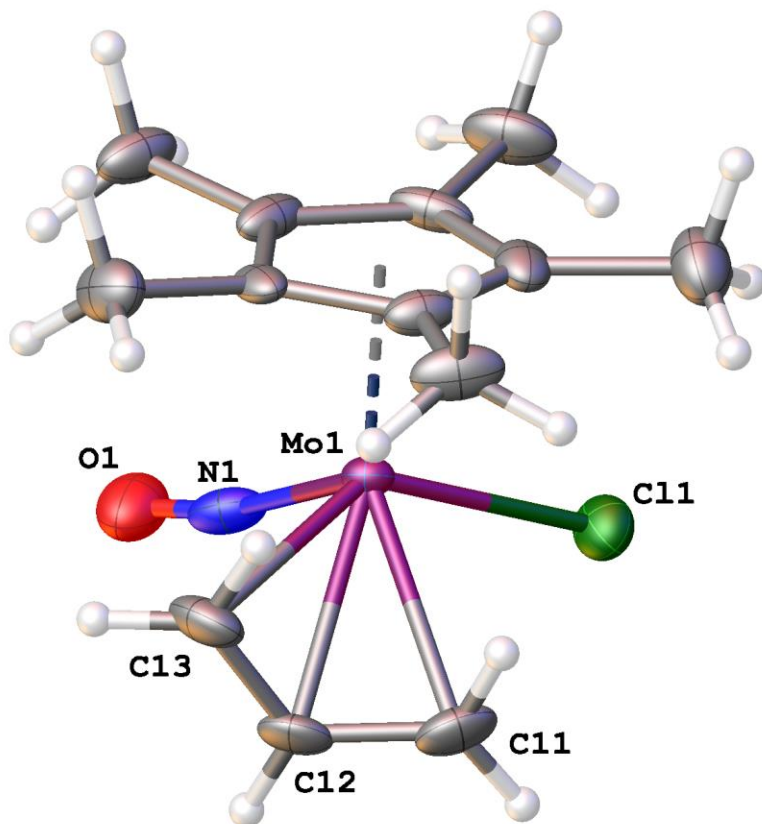


Figure 2.19. Solid-state molecular structure of **2.16** with 50% probability thermal ellipsoids shown. Selected interatomic distance (Å) and angles (deg.) for major component: Mo(1)-C(11) = 2.419(5), Mo(1)-C(12) = 2.353(5), Mo(1)-C(13) = 2.283(6), C(11)-C(12) = 1.367(9), C(12)-C(13) = 1.393(9), Mo(1)-Cl(1) = 2.4237(14), Mo(1)-N(1) = 1.819(6), N(1)-O(1) = 1.138(7), C(11)-C(12)-C(13) = 116.5(7), Mo(1)-N(1)-O(1) = 168.8(4).

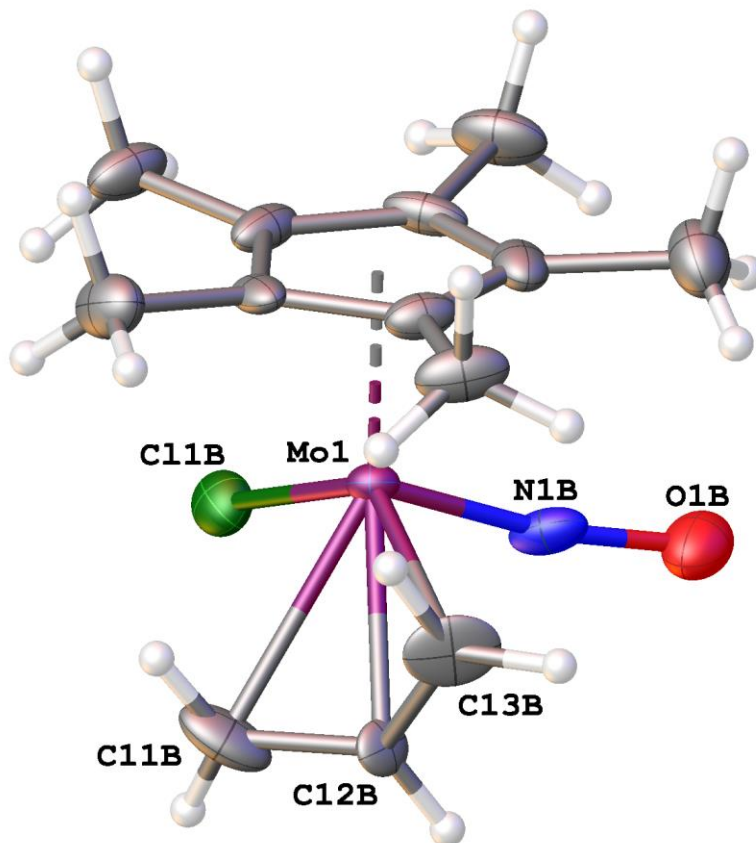


Figure 2.20. Solid-state molecular structure of **2.16** Selected interatomic distance (Å) and angles (deg.) for minor component: Mo(1)-C(11B) = 2.342(9), Mo(1)-C(12B) = 2.33(3), Mo(1)-C(13B) = 2.28(2), C(11B)-C(12B) = 1.39(4), C(12B)-C(13B) = 1.38(4), Mo(1)-Cl(1B) = 2.342(9), Mo(1)-N(1B) = 1.72(2), N(1B)-O(1B) = 1.45(3), C(11B)-C(12B)-C(13B) = 125(3), Mo(1)-N(1B)-O(1B) = 171.1(19).

2.2.5.3 Reactions of Cp*Mo(NO)(η^3 -allyl)Cl Complexes with Hydride Reagents

Attempts to synthesize Cp*Mo(NO)(H)(η^3 -allyl) complexes have been carried out by dissolving either **2.14** or **2.16** in THF and cooling the resulting mixture to -78 °C in a dry ice/acetone bath. Addition of NaAlH₄ to the cold mixtures results in immediate colour change of

the mixtures from green/brown to yellow, a similar colour to the analogous tungsten hydride complexes. The mixtures in all case turn brown within minutes, even when maintained at $-78\text{ }^{\circ}\text{C}$. No tractable organometallic complexes could be isolated or observed from any of the reactions. The colour change to yellow following the addition of the hydride reagent suggests that the metathesis reactions did produce the desired $\text{Cp}^*\text{Mo}(\text{NO})(\text{H})(\eta^3\text{-allyl})$ complexes, but they are unstable and quickly decompose. Further attempts to synthesize the molybdenum hydride complexes have not been investigated.

2.3 Summary

The work presented in this chapter describes the synthesis of a unique class of $\text{Cp}^*\text{W}(\text{NO})(\text{H})(\eta^3\text{-allyl})$ complexes which are surprisingly stable in the presence of air and moisture. Theoretical and experimental studies suggest rather nonpolar W-H bonds which could account for the stability exhibited. The synthesis of the analogous molybdenum allyl hydride complexes have not been successful even though the $\text{Cp}^*\text{Mo}(\text{NO})(\eta^3\text{-allyl})\text{Cl}$ synthetic precursors are easily prepared.

These $\text{Cp}^*\text{W}(\text{NO})(\text{H})(\eta^3\text{-allyl})$ complexes react with PMe_3 to form two different types of 18e compounds of the formulae $\text{Cp}^*\text{W}(\text{NO})(\text{H})(\eta^1\text{-allyl})(\text{PMe}_3)$ or $\text{Cp}^*\text{W}(\text{NO})(\eta^2\text{-alkene})(\text{PMe}_3)$. Characterization of these complexes by ^1H , ^{13}C , and ^{31}P NMR spectroscopies has demonstrated that the strong coupling of the phosphorus atom of the PMe_3 ligand to hydrogen and carbon atoms on ligands oriented cis to it can be used to establish whether a ligand is cis or trans to PMe_3 in the metal's coordination sphere and is particularly useful for compounds whose Sel NOE and/or NOESY spectra do not provide a definitive answer. Furthermore, these

investigations have also demonstrated that the 18e $\text{Cp}^*\text{W}(\text{NO})(\text{H})(\eta^3\text{-allyl})$ compounds can undergo intramolecular isomerizations upon thermolysis to the corresponding 16e $\text{Cp}^*\text{W}(\text{NO})(\eta^2\text{-alkene})$ complexes. The intriguing question that immediately comes to mind is whether these intermediate alkene species can effect the intermolecular activations of hydrocarbon C-H bonds and, if so, how do these activations compare with those documented for the related 16e $\text{Cp}^*\text{W}(\text{NO})(\eta^2\text{-allene})$ and $\text{Cp}^*\text{W}(\text{NO})(\eta^2\text{-diene})$ entities. These studies are the focus of the next chapter in which the thermal chemistry of these allyl hydride complexes is investigated.

2.4 Experimental Methods

2.4.1 General Methods

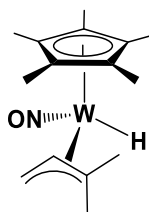
All reactions and subsequent manipulations involving organometallic reagents were performed under anhydrous and anaerobic conditions except where noted. All inert gases were purified by passing them through a column containing MnO and then through a column of activated 4 Å molecular sieves. High vacuum and inert atmosphere techniques were performed either using double-manifold Schlenk lines or in Innovative Technologies LabMaster 100 and MS-130 BG dual-station glove boxes equipped with freezers maintained at $-33\text{ }^{\circ}\text{C}$. Preparative scale reactions were performed with Schlenk or round bottom flasks; reactions were performed in thick-walled glass reaction bombs (larger scale) or J. Young NMR tubes (smaller scale), both of which were sealed by Kontes greaseless stopcocks. Tetrahydrofuran (THF) and diethyl ether (Et_2O) were dried over sodium/benzophenone ketyl and freshly distilled prior to use; solvents

such as hexanes and ethyl acetate were not dried prior to use; all other solvents were dried according to standard procedures.⁵⁴ All binary magnesium reagents used were prepared from the corresponding Grignard reagents.⁵⁵ The complexes $\text{Cp}^*\text{W}(\text{NO})\text{Cl}_2$ and $\text{Cp}^*\text{Mo}(\text{NO})\text{Cl}_2$ were prepared according to the published procedures.⁵⁶ Pentamethylcyclopentadiene was obtained from the Boulder Scientific Company, and LiBH_4 (2.0M in MeTHF) was obtained from Sigma-Aldrich. All other chemicals and reagents were ordered from commercial suppliers and used as received.

Unless otherwise specified, all IR samples were prepared as Nujol mulls sandwiched between ZnCl_2 plates, and their spectra were recorded on a Thermo Nicolet Model 4700 FT-IR spectrometer. All NMR spectra were recorded at room temperature (24.5 °C) on Bruker AV-300, AV-400 (direct and indirect probes), or AV-600 instruments, and all chemical shifts are reported in ppm and coupling constants are reported in Hz. ^1H NMR spectra were referenced to the residual protio isotopomer present in C_6D_6 (7.16 ppm). ^{13}C NMR spectra were referenced to C_6D_6 (128.39 ppm). ^{31}P NMR spectra were externally referenced to 85% H_3PO_4 . For the characterization of most complexes 2D NMR experiments, $\{^1\text{H}-^1\text{H}\}$ COSY, $\{^1\text{H}-^{13}\text{C}\}$ HSQC, and $\{^1\text{H}-^{13}\text{C}\}$ HMBC, were performed to correlate and assign ^1H and ^{13}C NMR signals and establish atom connectivity; ^1H NOE NMR and $\{^1\text{H}-^1\text{H}\}$ NOESY were used for determination of solution structures. Low-resolution mass spectra (EI, 70 eV) were recorded by Mr. Marshall Lapawa of the UBC mass spectrometry facility using a Kratos MS-50 spectrometer, and elemental analyses were performed by Mr. Derek Smith of the UBC microanalytical facility. X-ray crystallographic data collection, solution, and refinement were performed at the UBC X-ray crystallography facility.

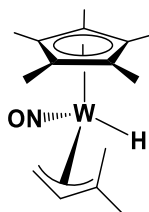
2.4.2 Preparation of Cp*W(NO)(H)(η^3 -CH₂CHCMe₂) (**2.1a**, **2.1b**)

In a glove box, a glass Schlenk flask was charged with Cp*W(NO)Cl₂ (5.14 g, 12.2 mmol), THF (ca. 150 mL), and a magnetic stir bar, and it was then cooled in a dry ice/acetone bath (-78 °C). A second Schlenk flask was charged with Mg(CH₂CH=CMe₂)₂ (1.57 g, 12.3 mmol, 128 g/mol titer) and THF (ca. 100 mL), and then the contents were transferred to the first flask dropwise via cannula. Following this addition, the reaction mixture was allowed to warm to room temperature and was then stirred for 1 h to obtain a yellow-brown mixture. The Schlenk flask was again cooled to -78 °C and 2 equivalents of LiBH₄ (12.0 mL, 24 mmol, 2.0 M in THF) were added slowly via syringe. The contents of the Schlenk flask were warmed to room temperature and stirred for 3 h to obtain a brown mixture. The THF solvent was removed in vacuo, and the resulting residue was dissolved in Et₂O (ca. 100 mL) and washed with H₂O (3 x 50 mL). The Et₂O layer was filtered through a glass frit, the filtrate was collected in a Schlenk flask, and then the solvent volume was reduced in vacuo to obtain a concentrated solution of the crude mixture. Purification was performed by column chromatography using a neutral alumina support. A yellow band was eluted with 0-35% Et₂O in hexanes. The solvent was removed from the eluate under reduced pressure to obtain Cp*W(NO)(H)(η^3 -CH₂CHCMe₂) (**2.1**) as a yellow powder (2.30 g, 45% yield). Pale yellow rod-shaped crystals of **2.1** suitable for a single-crystal X-ray diffraction analysis were grown from Et₂O at -33 °C. Two isomers of the complex, **2.1a** and **2.1b**, were identified in solution by ¹H NMR spectroscopy in an 83:17 ratio, respectively. The solution molecular structure was elucidated by Sel NOE and NOESY NMR spectroscopy. The melting point of **2.1** was recorded as 123-125 °C and is reversible since the presence of **2.1** was confirmed by ¹H NMR spectroscopy following the melt.



2.1a (83%)

Characterization data for **2.1a** (83 %): IR (cm⁻¹) 1601 (s, ν_{NO}). MS (LREI, m/z , probe temperature 120 °C) 419 [M^+ , ^{184}W]. ^1H NMR (600 MHz, C_6D_6) δ -0.90 (s, $^1J_{\text{WH}} = 127.9$, 1H, WH), 1.72 (s, 15H C_5Me_5), 1.90 (s, 3H, allyl Me), 2.06 (m, 1H, allyl CH_2), 2.29 (s, 3H, allyl Me), 2.42 (dd, $^3J_{\text{HH}} = 13.1$, $^2J_{\text{HH}} = 3.2$, 1H, allyl CH_2), 2.68 (dd, $^3J_{\text{HH}} = 13.2$, 7.7, 1H, allyl CH). ^{13}C APT NMR (150 MHz, C_6D_6) δ 11.03 (C_5Me_5), 25.0 (allyl Me), 30.7 (allyl Me), 37.6 (allyl CH_2), 96.0 (allyl CH), 100.3 (allyl CMe_2), 104.4 (C_5Me_5). Sel NOE (400 MHz, C_6D_6) δ irradiat. at -0.90, NOE at 1.72, 1.90, 2.29. mp 123-125 °C (reversible, confirmed by ^1H NMR). Anal. Calcd for $\text{C}_{20}\text{H}_{25}\text{NOW}$: C, 42.98; H, 6.01; N, 3.34. Found: C, 42.85; H, 6.02; N, 3.27.



2.1b (17%)

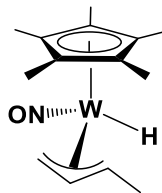
Characterization data for **2.1b** (17 %): ^1H NMR (600 MHz, C_6D_6) δ -0.59 (s, $^1J_{\text{WH}} = 127.4$, 1H, WH), 0.56 (dd, $^3J_{\text{HH}} = 11.7$, $^2J_{\text{HH}} = 3.8$, 1H, allyl CH_2), 0.87 (s, 3H allyl Me), 1.74 (s, 15H C_5Me_5), 2.45 (s, 3H, allyl Me), 2.82 (m, 1H, allyl CH_2), 4.71 (dd, $^3J_{\text{HH}} = 11.7$, 7.3, 1H, allyl CH). ^{13}C APT NMR (150 MHz, C_6D_6) δ 11.00 (C_5Me_5), 21.7 (allyl Me), 31.2 (allyl Me), 40.9 (allyl CH_2), 95.0 (allyl CMe_2), 103.2 (allyl CH), 105.4 (C_5Me_5).

2.4.3 Preparation of Cp*W(NO)(H)(η^3 -CH₂CHCHPhMe₂) (**2.2**)

The synthesis of compound **2.2** is carried out in an analogous fashion for the synthesis of **2.1**. The complete characterization of **2.2** was carried out by Dr. Russell Wakeham and has been reported.⁴³ Complex **2.2** was first prepared from Cp*W(NO)Cl₂ via sequential metathesis reactions using Mg(CH₂CH=CHPh)₂ and NaBH₄, and obtained as a brown residue in extremely low yield (<1%). Crystals suitable for single-crystal X-ray diffraction were obtained via recrystallization in 1:1 Et₂O/pentane at -33 °C overnight.

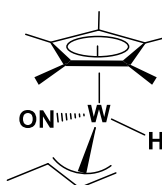
2.4.4 Characterization of Cp*W(NO)(H)(η^3 -CH₂CHCHMe) (**2.3**)

Complex **2.3** was prepared in an analogous manner to the synthesis of **2.1** detailed above. The reported synthesis was carried out Mr. Aaron Holmes.⁴³ Solution- and solid-state structure characterizations were carried out by the author. Crystals suitable for single crystal X-ray diffraction were obtained via slow evaporation from pentane at room temperature and a single isomer (**2.3a**) was identified in the solid-state. In solution, the four isomers of **2.3** were characterized by NMR spectroscopies. The orientation of the allyl ligand of **2.3a** and **2.3b** was determined by Sel NOE NMR spectroscopy while the orientation of the allyl ligand of **2.3c** and **2.3d** was determined by the chemical shifts of the meso *H* and allyl CH₂ and CHMe signals in the ¹H and ¹³C NMR spectra.



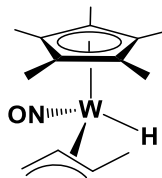
2.3a (67%)

Characterization data for **2.3a** (66.5 %): IR (C_6D_6 , cm^{-1}) 1571 (s, ν_{NO}). MS (LREI, m/z , probe temperature 120 °C) 405 [M^+ , ^{184}W]. ^1H NMR (600 MHz, C_6D_6) δ -1.27 (s, $^1J_{\text{WH}} = 122.2$, 1H, WH), 0.16 (d, $^3J_{\text{HH}} = 10.3$, 1H, allyl CH_2), 1.74 (s, 15H C_5Me_5), 1.83 (m, 1H, allyl CHMe), 2.26 (d, $^3J_{\text{HH}} = 5.8$, 3H, allyl Me), 2.75 (d, $^3J_{\text{HH}} = 7.3$, 1H, allyl CH_2), 4.61 (ddd, $^3J_{\text{HH}} = 13.1$, 10.3, 7.3, 1H, allyl CH). ^{13}C APT NMR (150 MHz, C_6D_6) δ 10.99 (C_5Me_5), 21.8 (allyl Me), 39.2 ($^1J_{\text{WC}} = 30.7$, allyl CH_2), 78.6 (allyl CHMe), 104.6 (allyl CH), 105.0 (C_5Me_5). Sel NOE (600 MHz, C_6D_6) δ irradiat. at -1.27, NOE at 2.26.



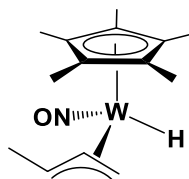
2.3b (17%)

Characterization data for **2.3b** (17.5 %): ^1H NMR (600 MHz, C_6D_6) δ -1.33 (s, $^1J_{\text{WH}} = 122.6$, 1H, WH), 0.59 (d, $^3J_{\text{HH}} = 13.5$, 1H, allyl CH_2), 0.97 (dq, $^3J_{\text{HH}} = 10.0$, 5.8, 1H, allyl CHMe), 1.72 (s, 15H C_5Me_5), 1.95 (d, $^3J_{\text{HH}} = 5.8$, 3H, allyl Me), 4.08 (d, $^3J_{\text{HH}} = 7.3$, 1H, allyl CH_2), 4.35 (ddd, $^3J_{\text{HH}} = 13.5$, 10.0, 7.3, 1H, allyl CH). ^{13}C APT NMR (150 MHz, C_6D_6) δ 11.01 (C_5Me_5), 18.6 (allyl Me), 51.9 (allyl CH_2), 58.8 ($^1J_{\text{WC}} = 23.2$, allyl CHMe), 104.8 (C_5Me_5), 104.9 (allyl CH). Sel NOE (600 MHz, C_6D_6) δ irradiat. at -1.33, NOE at 4.09.



2.3c (14%)

Characterization data for **2.3c** (13.7 %): ^1H NMR (600 MHz, C_6D_6) δ -1.24 (s, $^1J_{\text{WH}} = 124.3$ 1H, WH), 1.71 (s, 15H C_5Me_5), 2.06 (m, 1H, allyl CH_2), 2.14 (m, 3H, allyl Me), 2.28 (obscured, 1H, allyl CH_2), 2.82 (m, 1H, allyl CH), 3.65 (m, 1H, allyl CHMe). ^{13}C APT NMR (150 MHz, C_6D_6) δ 10.8 (C_5Me_5), 20.9 (allyl Me), 39.0 ($^1J_{\text{WC}} = 24.3$, allyl CH_2), 74.9 (allyl CHMe), 99.1 (allyl CH), 104.2 (C_5Me_5).



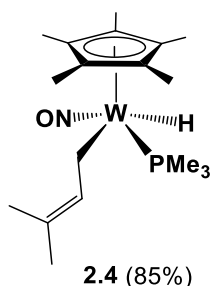
2.3d (2%)

Characterization data for **2.3d** (2.3 %): ^1H NMR (600 MHz, C_6D_6) δ (selected signals) - 0.86 (s, $^1J_{\text{WH}} = 124.8$, 1H, WH), 1.69 (s, 15H C_5Me_5), 2.48 (m, 1H, allyl CH). ^{13}C APT NMR (150 MHz, C_6D_6) δ (selected signals) 10.9 (C_5Me_5), 94.1 (allyl CH), 104.3 (C_5Me_5).

2.4.5 Reaction of **2.1** with PMe_3 at 60 °C

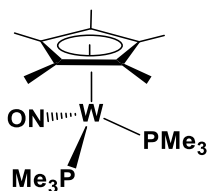
In a glove box, a glass bomb was charged with **2.1** (0.432 g, 1.03 mmol), PMe_3 (ca. 7 mL), and a magnetic stir bar to obtain a golden-coloured solution. The bomb was sealed with a Kontes greaseless stopcock and then placed into an oil bath. The contents of the bomb were heated at 60 °C while being stirred for 18 h, whereupon a red reaction mixture was obtained.

The solvent was removed in vacuo, and an orange solid (0.376 g, combined yield of 74%) was obtained by recrystallization of the residue from pentane at -33 °C for 2 h. This solid contained a mixture of Cp*W(NO)(H)(η^1 -CH₂CH=CMe₂)(PMe₃) (**2.4**) and Cp*W(NO)(PMe₃)₂ (**2.5**) in a 85:15 ratio (by ¹H NMR spectroscopy). Several attempts to separate **2.4** and **2.5** were made. Column chromatography on basic alumina resulted in their partial separation, albeit with the formation of several new products that were recovered with **2.4**. Column chromatography on neutral alumina led to the decomposition of both products, while column chromatography on silica did lead to separation, but only small amounts of the products were recovered. Large yellow crystals of **2.4** that were suitable for X-ray diffraction were grown by dissolving the solid in Et₂O (ca. 1 mL), adding a layer of pentane (ca 1 mL), and letting the mixture sit undisturbed for 1 week at -33 °C.



Characterization data for **2.4** (85 %): IR (cm⁻¹) 1563 (s, ν_{NO}), MS (LREI, m/z , probe temperature 150 °C) 495 [M^+ , ¹⁸⁴W]. ¹H NMR (400 MHz, C₆D₆) δ -0.95 (dt, ³ J_{HH} = 4.3, ² J_{PH} = 81.4, ¹ J_{WH} = 61.8, 1H, WH), 1.11 (d, ² J_{PH} = 8.4, 9H), 1.52 (m, 1H, CH₂CH=CMe₂) 1.55 (m, 1H, CH₂CH=CMe₂), 1.81 (s, 15H, C₅Me₅), 1.98 (s, 3H, CH₂CH=CMe₂), 1.99 (s, 3H, CH₂CH=CMe₂), 6.07 (t, ³ J_{HH} = 7.5, 1H, CH₂CH=CMe₂). ¹³C APT NMR (100 MHz, C₆D₆) δ 10.8 (C₅Me₅), 16.4 (d, ² J_{PC} = 14.2, ¹ J_{WC} = 63.5, CH₂CH=CMe₂), 18.7 (d, ¹ J_{PC} = 30.3, PMe₃), 18.9 (CH₂CH=CMe₂), 26.4 (CH₂CH=CMe₂), 104.9 (C₅Me₅), 122.5 (CH₂CH=CMe₂), 135.6 (d, ³ J_{PC} = 8.3,

CH₂CH=CMe₂). ³¹P NMR (162 MHz, C₆D₆) δ -23.9 (s, ¹J_{PW} = 204.1, WPM₃). Anal. Calcd for C₁₈H₃₄NOPW: C, 43.65; H, 6.92; N, 2.83. Found: C, 43.54; H, 6.88; N, 2.85.



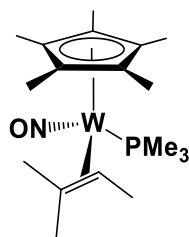
2.5 (15%)

Characterization data for **2.5** (15 %): IR (cm⁻¹) 1552 (s, ν_{NO}). MS (LREI, *m/z*, probe temperature 150 °C) 501 [M⁺, ¹⁸⁴W]. ¹H NMR (400 MHz, C₆D₆) δ 1.35 (d, ²J_{PH} = 6.8, 18H), 1.92 (s, 15H, C₅Me₅). ¹³C APT NMR (100 MHz, C₆D₆) δ 12.5 (C₅Me₅), 24.6 (m, PM₃), 99.4 (C₅Me₅). ³¹P NMR (162 MHz, C₆D₆) δ -22.2 (s, ¹J_{PW} = 456.8, WPM₃).^{48,49}

2.4.6 Reaction of **2.1** with PM₃ at 80 °C

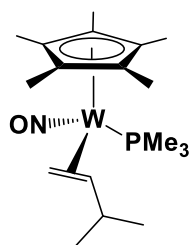
In a glove box, a glass bomb was charged with a sample of **2.1** (0.128 g, 0.305 mmol) and PM₃ (ca. 10 mL), thereby producing a yellow solution. The bomb was sealed with a Kontes greaseless stopcock, and the stirred contents were heated at 80 °C for 18 h to obtain a dark orange mixture. The solvent was removed from the mixture in vacuo, and recrystallization of the residues from Et₂O at 20 °C afforded an orange powder (0.150 g). This powder was analyzed by ¹H and ³¹P NMR spectroscopy and shown to contain **2.5** and the three isomers Cp*W(NO)(η²-MeCH=CMe₂)(PMe₃) (**2.6a**) and Cp*W(NO)(η²-CH₂=CHCHMe₂)(PMe₃) (**2.6b**, **2.6c**). Attempts to separate **2.5** (63%) and **2.6** by fractional recrystallization were unsuccessful, and the complexes decomposed during attempted column chromatographies. The proposed orientation of

the η^2 -alkene ligand for each isomer was assigned using the ^{31}P coupling constants in the ^1H and ^{13}C NMR spectra.



2.6a (17%)

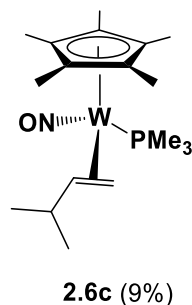
Characterization data for **2.6a** (16.8 %): MS (LREI, m/z , probe temperature 150 °C) 495 [M^+ , ^{184}W]. ^1H NMR (400 MHz, C_6D_6) δ 1.02 (qd, $^3J_{\text{HH}} = 6.3$, $^3J_{\text{PH}} = 2.5$, 1H, $=\text{CHMe}$), 1.28 (d, $^2J_{\text{PH}} = 8.2$, 9H, PMe_3), 1.37 (obscured, 3H, $=\text{CMe}_2$), 1.70 (s, 15H, C_5Me_5), 2.10 (d, $^3J_{\text{HH}} = 6.5$, 3H, $=\text{CHMe}$), 2.12 (s, 3H, $=\text{CMe}_2$). ^{13}C APT NMR (100 MHz, C_6D_6) δ (selected signals) 11.1 (C_5Me_5), 19.2 (d, $^2J_{\text{PC}} = 28.0$, PMe_3), 19.7 (d, $^3J_{\text{PC}} = 1.0$, $=\text{CHMe}$), 29.9 (d, $^3J_{\text{PC}} = 4.6$, $=\text{CMe}_2$), 45.8 ($^1J_{\text{WC}} = 35.8$, $=\text{CHMe}$), 104.1 (C_5Me_5). ^{31}P NMR (162 MHz, C_6D_6) δ -15.2 (s, $^1J_{\text{PW}} = 373$, WPMe_3).



2.6b (11%)

Characterization data for **2.6b** (11.4 %): δ 0.40 (ddd, $^3J_{\text{HH}} = 11.3$, $^3J_{\text{PH}} = 11.2$, $^2J_{\text{HH}} = 4.1$, 1H, $=\text{CH}_2$), 0.73 (dddd, $^3J_{\text{HH}} = 11.4$, $^3J_{\text{HH}} = 11.3$, $^3J_{\text{PH}} = 7.6$, $^3J_{\text{HH}} = 1.7$, 1H, $=\text{CH}$), 0.92 (d, $^3J_{\text{HH}} = 6.4$, 3H, CHMe_2), 1.22 (d, $^2J_{\text{PH}} = 8.3$, 9H, PMe_3), 1.47 (m, 1H, $=\text{CH}_2$), 1.56 (d, $^3J_{\text{HH}} = 6.4$, 3H, CHMe_2), 1.65 (s, 15H, C_5Me_5), 2.54 (m, 1H, CHCMe_2). ^{13}C APT NMR (100 MHz, C_6D_6) δ 10.8

(C_5Me_5), 17.6 (d, $^2J_{PC} = 29.4$, PMe_3), 18.8 ($CHCMe_2$), 18.9 ($=CH_2$), 32.1 ($CHCMe_2$), 32.7 (d, $^3J_{PC} = 4.6$, $CHCMe_2$), 51.2 (d, $^2J_{PC} = 12.0$, $^1J_{WC} = 12.0$, $=CH$), 103.33 (C_5Me_5). ^{31}P NMR (162 MHz, C_6D_6) δ -13.4 (s, $^1J_{PW} = 372$, $WPMe_3$).



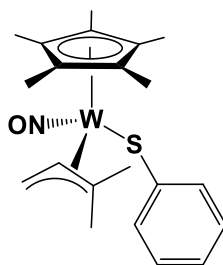
Characterization data for **2.6c** (8.9 %): 1H NMR (400 MHz, C_6D_6) δ -0.06 (ddd, $^3J_{HH} = 9.4$, $^3J_{PH} = 5.5$, $^2J_{HH} = 4.6$, 1H, $=CH_2$), 1.19 (d, $^2J_{PH} = 8.5$, 9H, PMe_3), 1.28 (obscured, 1H, $=CH$), 1.30 (m, 1H, $=CH_2$), 1.42 (d, $^3J_{HH} = 6.1$, 3H, $CHMe_2$), 1.52 (d, $^3J_{HH} = 5.7$, 3H, $CHMe_2$), 1.57 (obscured, 1H, $CHMe_2$), 1.68 (s, 15H, C_5Me_5). ^{13}C APT NMR (100 MHz, C_6D_6) δ (selected signals) 10.9 (C_5Me_5), 16.6 (d, $^2J_{PC} = 31.7$, PMe_3), 31.2 (d, $^2J_{PC} = 12.0$, $^1J_{WC} = 17.5$, $=CH_2$), 39.8 ($CHCMe_2$), 51.8 ($^1J_{WC} = 41.4$, $=CH$), 103.28 (C_5Me_5). ^{31}P NMR (162 MHz, C_6D_6) δ -11.1 (s, $^1J_{PW} = 358$, $WPMe_3$).

2.4.7 Reactions of **2.1** with PhSSPh and AIBN by 1H NMR Spectroscopy

2.4.7.1 Reaction of **2.1** with PhSSPh and AIBN

In a glove box, a glass reaction bomb was charged **2.1** (161 mg, 0.384 mmol), PhSSPh (92 mg, 0.307 mmol), AIBN (67 mg, 0.560 mmol), a magnetic stir bar, and benzene- d_6 (ca. 5 mL) to give a bright yellow mixture. The glass bomb was placed in a 50 °C oil bath and its

contents were stirred for 6 h. The following colour change was observed: yellow, orange, red, deep red. Analysis of the sample by ^1H NMR spectroscopy revealed the presence of two new organometallic complexes, $\text{Cp}^*\text{W}(\text{NO})(\text{SPh})(\eta^3\text{-CH}_2\text{CHCMe}_2)$ (**2.11**) and $\text{Cp}^*\text{W}(\text{NO})(\text{SPh})_2$ (**2.12**) in an approximately 15:1 ratio. The solvent was removed and the crude reaction mixture was dissolved in 3:1 $\text{Et}_2\text{O}/\text{THF}$ and added to the top of a basic alumina column. A red band and an orange band were developed using a 0-100% $\text{Et}_2\text{O}/\text{pentane}$ gradient. The red band was collected lightened in colour upon collection and decomposed. The orange eluate was collected and dried in vacuo to give **2.11** as an orange solid (50 mg, 25 % yield). The complex **2.12** was not recovered following column chromatography, and presumably was the red fraction. A low-resolution EI-MS spectrum of the crude reaction mixture contained a tungsten-isotope pattern at $567\ m/z$, consistent with the formulation of **2.12**.⁵⁷



2.11 (93%)

Characterization data for **2.11**. IR (cm^{-1}) 1563 (s, ν_{NO}). MS (LREI, m/z , probe temperature $150\ ^\circ\text{C}$) 527 [M^+ , ^{184}W]. ^1H NMR (400 MHz, C_6D_6) δ 1.38 (s, 3H, allyl *Me*), 1.43 (s, 3H, allyl *Me*), 1.59 (s, 15H C_5Me_5), 1.66 (dd, $^3J_{\text{HH}} = 8.1$, $^2J_{\text{HH}} = 5.9$, 1H, allyl CH_2), 2.56 (dd, $^3J_{\text{HH}} = 11.0$, $^2J_{\text{HH}} = 5.9$, 1H, allyl CH_2), 3.84 (dd, $^3J_{\text{HH}} = 11.0$, 8.1, 1H, allyl *CH*), 0.94 (tt, $^4J_{\text{HH}} = 1.1$, $^3J_{\text{HH}} = 7.4$, 1H, *p*-aryl *H*), 7.18 (dd, $^3J_{\text{HH}} = 8.1$, 7.4, 2H, *m*-aryl *H*), 7.93 (dd, $^4J_{\text{HH}} = 1.1$, $^3J_{\text{HH}} = 8.1$, 2H, *o*-aryl *H*). ^{13}C NMR (100 MHz, C_6D_6) δ 10.3 (C_5Me_5), 21.0 (allyl *Me*), 29.6 (allyl

Me), 40.3 ($^1J_{WC} = 41.7$, allyl CH₂), 98.5 (allyl CH), 108.2 (C₅Me₅), 124.0 (aryl CH), 128.4 (aryl CH), 133.7 (aryl CH), 146.4 (ipso CH), 151.5 (allyl CMe₂).

2.4.7.2 Monitoring the Reaction of **2.1** with PhSSPh and AIBN at Room Temperature

In a glove box, a J. Young NMR tube was sequentially charged with **2.1** (58 mg, 0.138 mmol), AIBN (21 mg, 0.096 mmol), and PhSSPh (32 mg, 0.19 mmol), all of which were dissolved in C₆D₆ (total ca. 2.5 mL) to give a yellow mixture. The NMR tube was sealed with a Kontes greaseless stopcock. The colour of the reaction mixture began to change from yellow to orange nearly immediately. The ^1H NMR spectrum of the sample was recorded 15 min after addition of the AIBN and signals due **2.11** were present. ^1H NMR spectra were recorded five more times over 1 d.⁵⁸ The colour of the reaction progressed from yellow to orange, dark orange, red, deep red.

2.4.7.3 Monitoring the reaction of **2.1** with PhSSPh and AIBN at 50 °C

In a glove box, a J. Young was charged with **2.1** (53 mg, 0.126 mmol) and benzene-*d*₆ (ca. 1 mL) to give a bright yellow solution. Next AIBN (22 mg, 0.101 mmol), dissolved in benzene-*d*₆ (ca. 0.75 mL), was added to the NMR tube; no colour change was observed. Finally, PhSSPh (32 mg, 0.195 mmol), dissolved in benzene-*d*₆ (ca. 0.75 mL), was added to the NMR tube, which was then sealed with a Kontes greaseless stopcock. Following the addition an immediate colour change from yellow to orange was observed. The sample was heated at 50 °C for 6 h to produce a deep red mixture. Analysis by ^1H NMR spectroscopy revealed the presence

of predominately one new complex, $\text{Cp}^*\text{W}(\text{NO})(\eta^3\text{-CH}_2\text{CHCMe}_2)(\text{SPh})$ (**2.11**). Signals attributed to $\text{Cp}^*\text{W}(\text{NO})(\text{SPh})_2$ (**2.12**) are also observed in the ^1H NMR spectrum.⁵⁹

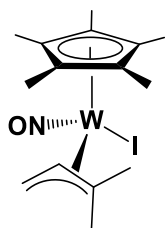
2.4.7.4 Reaction of 2.1 with PhSSPh and a Catalytic Amount of AIBN

In a glove box, a glass bomb was charged sequentially with **2.1** (262 mg, 0.625 mmol), AIBN (29 mg, 0.133 mmol), and PhSSPh (155 mg, 0.920 mmol), all of which was dissolved in C_6D_6 (total ca. 7 mL), to give a yellow solution. The glass bomb was sealed with a Kontes greaseless stopcock and then its contents were heated at 50 °C while being stirred. After 6 h a dark red mixture was obtained. A ^1H NMR spectrum was recorded to reveal the presence of **2.11**.

2.4.7.5 Reaction of 2.1 with 1-Iodopentane in the Presence of AIBN

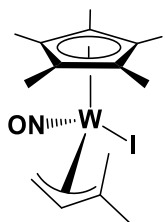
In a glove box, a glass bomb flask was charged with **2.1** (122 mg, 0.291 mmol) and AIBN (49 mg, 0.22 mmol), and C_6D_6 (ca. 10 mL) to give a yellow mixture. To this mixture 1-iodopentane (60 μL , 0.46 mmol) was added and the bomb was sealed with a Kontes greaseless stopcock. The contents of the bomb were heated at 50 °C over 1 week and the colour of the mixture changed from yellow to orange to red. The reaction was monitored by ^1H NMR spectroscopy over 1 week and broad signals corresponding to possible exo/endo isomers of $\text{Cp}^*\text{W}(\text{NO})(\eta^3\text{-CH}_2\text{CHCMe}_2)\text{I}$ (**2.13**) were observed. The solvent was removed in vacuo to give an orange-brown solid (183 mg). The solid was taken up in Et_2O and subjected to aqueous washing and the Et_2O layer was dried in vacuo and an orange solid was obtained in quantitative

yield (159 mg). The isomers were assigned by the relative upfield and downfield chemical shifts of the meso H signals in the ^1H NMR spectrum.



2.13a (80%)

Characterization data for **2.13a** (80%): MS (LREI, m/z , probe temperature 150 °C) 545 $[\text{M}^+, ^{184}\text{W}]$. ^1H NMR (400 MHz, C_6D_6) δ 1.67 (s, 15H C_5Me_5), 1.67 (obscured, 3H, allyl *Me*), 1.93 (br s, 3H, allyl *Me*), 2.56 (overlapping br s, 1H, allyl CH_2), 2.58 (overlapping br s 1H, allyl CH_2), 3.14 (br s, 1H allyl *CH*).



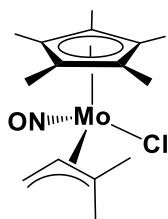
2.13b (20%)

Characterization data for **2.13b** (20%): ^1H NMR (400 MHz, C_6D_6) δ (selected signals) 0.64 (br s, 1H, allyl CH_2), 1.62 (br s, 15H C_5Me_5), 4.71 (br s, 1H allyl *CH*).

2.4.8 Preparation of $\text{Cp}^*\text{Mo}(\text{NO})(\eta^3\text{-CH}_2\text{CHCMe}_2)\text{Cl}$ (**2.14**)

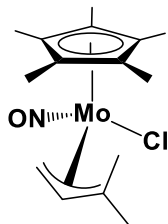
In a glove box a large Schlenk flask was charged with $\text{Cp}^*\text{Mo}(\text{NO})\text{Cl}_2$ (3.346 g, 10.07 mmol) and a magnetic stir bar. THF (ca. 75 mL) was then added via cannula and the flask was placed in a dry ice/acetone bath where its contents were cooled to 78 °C to give a cloudy orange

mixture. A second Schlenk flask was charged in the glove box with $\text{Mg}(\text{CH}_2\text{CH}=\text{CMe}_2)_2$ (1.30 g, 10.16 mmol, 128 g/mol titre) and a magnetic stir bar. The magnesium binary reagent was then dissolved in THF (ca. 50 mL) and the solution was transferred to the first flask via dropwise cannulation. Following the addition, the Schlenk flask was removed from the bath and its contents were allowed to warm to room temperature and then stirred for 18 h to produce a dark yellow-brown mixture. The solvent was removed in vacuo to afford a green-brown solid that was taken up in Et_2O (ca. 125 mL), washed with water (ca. 25 mL), and then filtered through a medium-porous frit. The dark green-brown ether layer was collected and the solvent removed in vacuo to afford $\text{Cp}^*\text{Mo}(\text{NO})(\eta^3\text{-CH}_2\text{CHCMe}_2)\text{Cl}$ (**2.14**) as a green-brown solid (2.732 g, 74.2 % yield). The isomers differ with respect to the exo/endo orientation of the allyl ligand; the meso H signal of **2.14a** has an upfield chemical shift relative to the meso H signal of **2.14b** in the ^1H NMR spectrum.



2.14a (75%)

Characterization data for **2.14a** (75%). IR (cm^{-1}) 1631 (s, ν_{NO}). MS (LREI, m/z , probe temperature 120 °C) 353 [M^+ , ^{98}Mo]. ^1H NMR (400 MHz, C_6D_6) δ 1.56 (s, 15H C_5Me_5), 1.69 (s, 3H, allyl *Me*), 1.76 (s, 3H, allyl *Me*), 1.92 (dd, $^3J_{\text{HH}} = 7.4$, $^2J_{\text{HH}} = 4.1$, 1H, allyl CH_2), 2.76 (dd, $^3J_{\text{HH}} = 12.5$, $^2J_{\text{HH}} = 4.1$, 1H, allyl CH_2), 3.60 (dd, $^3J_{\text{HH}} = 12.5$, 7.4, 1H, allyl *CH*). ^{13}C NMR (100 MHz, C_6D_6) δ 10.5 (C_5Me_5), 21.5 (allyl *Me*), 30.0 (allyl *Me*), 45.2 (allyl CH_2), 99.9 (allyl *CH*), 110.7 (C_5Me_5), 156.2 (allyl CMe_2).



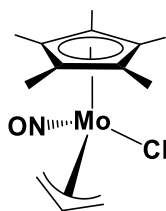
2.14b (25%)

Characterization data for **2.14b** (25%) ^1H NMR (400 MHz, C_6D_6) δ 0.84 (br s, 3H, allyl *Me*), 1.56 (obscured, 15H C_5Me_5), 1.73 (s, 3H, allyl *Me*), 1.72 (obscured, 1H, allyl CH_2), 2.54 (m, 1H, allyl CH_2), 5.06 (m, 1H, allyl CH). ^{13}C NMR (100 MHz, C_6D_6) δ 10.8 (C_5Me_5), 18.8 (allyl *Me*), 29.0 (allyl *Me*), 50.2 (allyl CH_2), 106.3 (allyl CH), 111.6 (C_5Me_5), 146.3 (allyl CMe_2).

2.4.9 Preparation of $\text{Cp}^*\text{Mo}(\text{NO})(\eta^3\text{-C}_3\text{H}_5)\text{Cl}$ (**2.16**)

A Schlenk flask was charged with $\text{Cp}^*\text{Mo}(\text{NO})\text{Cl}_2$ (0.510 g, 1.54 mmol) and THF (ca. 50 mL) and then the flask was placed in a dry ice/acetone bath (-78°C). A second Schlenk flask was charged with $\text{Mg}(\text{CH}_2\text{CH}=\text{CH}_2)_2$ (Titre: 111 g/mol, 0.170 g, 1.53 mmol) and THF (ca. 25 mL). The contents of the second flask were added to the first flask via cannula in a drop wise fashion. The Schlenk was removed from the bath and its contents were stirred while at room temperature for 18 h to produce a dark yellow-brown mixture. The solvent was removed in vacuo and the residue was taken up in Et_2O (ca. 25 mL) and then washed with water (3 x 5 mL) very quickly. The Et_2O layer was passed through a medium porous frit into a round bottom flask. The solvents were removed under reduced pressure to give $\text{Cp}^*\text{Mo}(\text{NO})(\eta^3\text{-C}_3\text{H}_5)\text{Cl}$ (**2.16**) as a tan-green

solid (0.252 g, 39 % yield). Crystals suitable for X-ray diffraction were grown from slow evaporation in Et₂O at room temperature in the air.



2.16

Characterization data for **2.16**: IR (cm⁻¹) 1627 (s, ν_{NO}). MS (LREI, m/z , probe temperature 120 °C) 339 [M^+ , ⁹⁸Mo]. ¹H NMR (400 MHz, C₆D₆) δ 0.85 (m, 1H, allyl CH₂), 1.48 (s, 15H C₅Me₅), 2.17 (m, 1H, allyl CH₂), 3.21 (d, ³ J_{HH} = 14.9, 1H, allyl CH₂), 4.27 (dd, ³ J_{HH} = 7.4, ² J_{HH} = 3.1, 1H, allyl CH₂), 5.71 (dddd, ³ J_{HH} = 17.2, 14.9, 10.2, 7.4, 1H, allyl CH). ¹³C APT NMR (100 MHz, C₆D₆) δ 10.5 (C₅Me₅), 50.2 (allyl CH₂), 97.1 (allyl CH₂), 111.8 (C₅Me₅), 116.6 (allyl CH).

2.4.10 X-ray Crystallography

Data collection was carried out at -173.0 ± 2 °C on a Bruker X8 APEX II diffractometer with graphite-monochromated Mo K α radiation or at -183.0 ± 1 °C on a Bruker APEX DUO diffractometer equipped with a TRIUMPH curved-crystal monochromator using Mo-K α radiation.

Data for **2.1** were collected to a maximum 2θ value of 60.34° in 0.5° oscillations. The structure was solved by direct methods⁶⁰ and expanded using Fourier techniques. All non-hydrogen atoms were refined anisotropically. Hydrogen atoms H1, H11a, H11b, and H12 were

refined isotropically, and all other hydrogen atoms were included in fixed positions. The final cycle of full-matrix least-squares analysis was based on 4505 observed reflections and 186 variable parameters.

Data for **2.2** were collected to a maximum 2θ value of 54.964° in 0.5° oscillations. The structure was solved by direct methods⁶⁰ and expanded using Fourier techniques. The C11–C19 fragment was disordered in two orientations. All non-hydrogen atoms were refined anisotropically, hydrogen atom H1 was refined isotropically, and all other hydrogen atoms were included in fixed positions. The final cycle of full-matrix least-squares analysis was based on 3817 observed reflections and 256 variable parameters.

Data for **2.3** were collected to a maximum 2θ value of 61.1° in 0.5° oscillations. The structure was solved by direct methods⁶⁰ and expanded using Fourier techniques. All non-hydrogen atoms were refined anisotropically. Hydrogen atoms H1, H12, H13, H14a, and H14b were refined isotropically, and all other hydrogen atoms were included in fixed positions. The final cycle of full-matrix least-squares analysis was based on 4354 observed reflections and 179 variable parameters.

Data for **2.4** were collected to a maximum 2θ value of 54.98° in 0.5° oscillations. The structure was solved by direct methods⁶⁰ and expanded using Fourier techniques. All non-hydrogen atoms were refined anisotropically. Hydrogens H1, H11A, H11B, and H12 were refined isotropically. All other hydrogen atoms were included in fixed positions. The final cycle of full-matrix least-squares analysis was based on 4619 observed reflections and 224 variable parameters.

Data for **2.7** were collected to a maximum 2θ value of 60.12° in 0.5° oscillations. The structure was solved by direct methods⁶⁰ and expanded using Fourier techniques. The complex

crystallizes with two crystallographically independent molecules in the asymmetric unit. All non-hydrogen atoms were refined anisotropically. All hydrogen atoms were placed in calculated positions. A residual electron density peak consistent with a W-H linkage was not located; however, there was an open coordination site at both tungsten atoms consistent with the existence of a metal hydrogen linkage. The empirical formula, and any values derived from it, included this hydride, although it did not appear in the model. The final cycle of full-matrix least-squares analysis was based on 13009 observed reflections and 484 variable parameters.

Data for **2.8** were collected to a maximum 2θ value of 54.964° in 0.5° oscillations. The structure was solved by direct methods⁶⁰ and expanded using Fourier techniques. All non-hydrogen atoms were refined anisotropically. Hydrogens H12 and H13 were refined isotropically, and all other hydrogen atoms were included in fixed positions. The final cycle of full-matrix least-squares analysis was based on 4939 observed reflections and 244 variable parameters.

Data for **2.15** collected to a maximum 2θ value of 63.36° in 0.5° oscillations. The structure was solved by direct methods⁶⁰ and expanded using Fourier techniques. All non-hydrogen atoms were refined anisotropically and all hydrogen atoms were included in fixed positions. The final cycle of full-matrix least-squares analysis was based on 7725 observed reflections and 262 variable parameters.

Data for **2.16** were collected to a maximum 2θ value of 60.3° in 0.5° oscillations. The structure was solved by direct methods⁶⁰ and expanded using Fourier techniques. The C11–C13 fragment was disordered in two orientations. All non-hydrogen atoms were refined anisotropically and all other hydrogen atoms were included in fixed positions. The final cycle of

full-matrix least-squares analysis was based on 3980 observed reflections and 198 variable parameters.

For each structure neutral-atom scattering factors were taken from Cromer and Waber.⁶¹ Anomalous dispersion effects were included in F_{calc} ;⁶² the values for $\Delta f'$ and $\Delta f''$ were those of Creagh and McAuley.⁶³ The values for mass attenuation coefficients were those of Creagh and Hubbell.⁶⁴ All calculations were performed using either SHELXL-97⁶⁵ via the WinGX interface⁶⁶ or XL⁶⁷ via the OLEX interface.⁶⁸ X-ray crystallographic data for all eight structures are presented in Table 2.3 and Table 2.4.

Table 2.3. X-ray crystallographic data for complexes **2.1**, **2.2a/b**, **2.3**, and **2.4**.

Compound	2.1	2.2a/2b	2.3	2.4
Empirical formula	C ₁₅ H ₂₅ NOW	C ₁₉ H ₂₅ NOW	C ₁₄ H ₂₃ NOW	C ₁₈ H ₃₄ NOPW
Formula weight	419.21	467.26	405.18	495.29
Crystal size (mm)	0.39 × 0.13 × 0.10	0.23 × 0.09 × 0.07	0.30 × 0.30 × 0.20	0.24 × 0.21 × 0.16
Crystal system	Monoclinic	Orthorhombic	Monoclinic	Monoclinic
Space group	<i>P2₁/n</i>	<i>P2₁2₁2₁</i>	<i>P2₁/c</i>	<i>P2₁/n</i>
Volume (Å ³)	1522.93(6)	1721.0(3)	1426.1(12)	2022.0(16)
a (Å)	8.7924(1)	8.0060(7)	8.539(5)	8.338(5)
b (Å)	14.0726(2)	13.3281(11)	8.321(5)	10.029(5)
c (Å)	13.0010(2)	16.1290(15)	20.138(5)	24.183(5)
α (°)	90	90	90	90
β (°)	108.7881(6)	90	94.691(5)	90.788(5)
γ (°)	90	90	90	90
Z	4	4	4	4
Density, ρ (calculated) (Mg/m ³)	1.828	1.803	1.8871	1.6269
Absorption coefficient, μ (mm ⁻¹)	7.575	6.714	8.085	5.794
F ₀₀₀	816.0	912.0	781.8	982.2
Measured Reflections: Total	26661	9306	17248	19057
Measured Reflections: Unique	4505	3817	4354	4619
Final R Indices	R ₁ = 0.0175, wR ₂ = 0.0402	R ₁ = 0.0132, wR ₂ = 0.0303	R ₁ = 0.0169, wR ₂ = 0.0326	R ₁ = 0.0156, wR ₂ = 0.0345
Goodness-of-fit on F ²	1.050	1.006	1.061	1.167
Largest diff. peak/hole (e ⁻ Å ⁻³)	1.790/-0.560	0.80/-0.59	1.33/-1.07	0.94/-1.14

Table 2.4. X-ray crystallographic data for complexes **2.7**, **2.8**, **2.14**, and **2.15**.

Compound	2.7	2.8	2.14	2.15
Empirical formula	C ₂₂ H ₃₄ NOPW	C ₂₂ H ₃₄ NOPW	C ₁₀ H ₁₅ O ₂ ClMo	C ₁₃ H ₂₀ NOCIMo
Formula weight	543.33	543.33	298.64	337.72
Crystal size (mm)	0.42 × 0.14 × 0.12	0.35 × 0.16 × 0.16	0.16 × 0.06 × 0.06	0.35 × 0.34 × 0.26
Crystal system	Monoclinic	Monoclinic	Triclinic	Orthorhombic
Space group	<i>P</i> 2 ₁ / <i>n</i>	<i>P</i> 2 ₁ / <i>n</i>	<i>P</i> -1	<i>P</i> 2 ₁ 2 ₁ 2 ₁
Volume (Å ³)	4442.2(13)	2163.7(15)	1147.5(9)	1376.77(6)
<i>a</i> (Å)	21.287(4)	9.353(5)	8.562(5)	9.4840(2)
<i>b</i> (Å)	8.0901(14)	14.700(5)	12.213(5)	10.9305(3)
<i>c</i> (Å)	26.846(5)	15.962(5)	12.337(5)	13.2810(3)
α (°)	90	90	116.643(5)	90.00
β (°)	106.087(3)	99.630(5)	93.374(5)	90.00
γ (°)	90	90	92.529(5)	90.00
<i>Z</i>	8	4	2	4
Density, ρ (calculated) (Mg/m ³)	1.6218	1.668	1.7284	1.629
Absorption coefficient, μ (mm ⁻¹)	5.283	5.423	1.348	1.131
<i>F</i> ₀₀₀	2148.4	1080.0	593.9	688.0
Measured Reflections: Total	51304	23145	28173	10978
Measured Reflections: Unique	13009	4939	7725	3980
Final <i>R</i> Indices	<i>R</i> ₁ = 0.0331, <i>wR</i> ₂ = 0.0694	<i>R</i> ₁ = 0.0209, <i>wR</i> ₂ = 0.0484	<i>R</i> ₁ = 0.0391, <i>wR</i> ₂ = 0.0898	<i>R</i> ₁ = 0.0340, <i>wR</i> ₂ = 0.0925
Goodness-of-fit on <i>F</i> ²	1.027	0.911	1.026	1.142
Largest diff. peak/hole (e ⁻ Å ⁻³)	3.70/−3.61	1.12/−0.80	1.71/−1.12	1.12/−1.30

Chapter 3: Reactivity of Cp*W(NO)(H)(η^3 -Allyl)

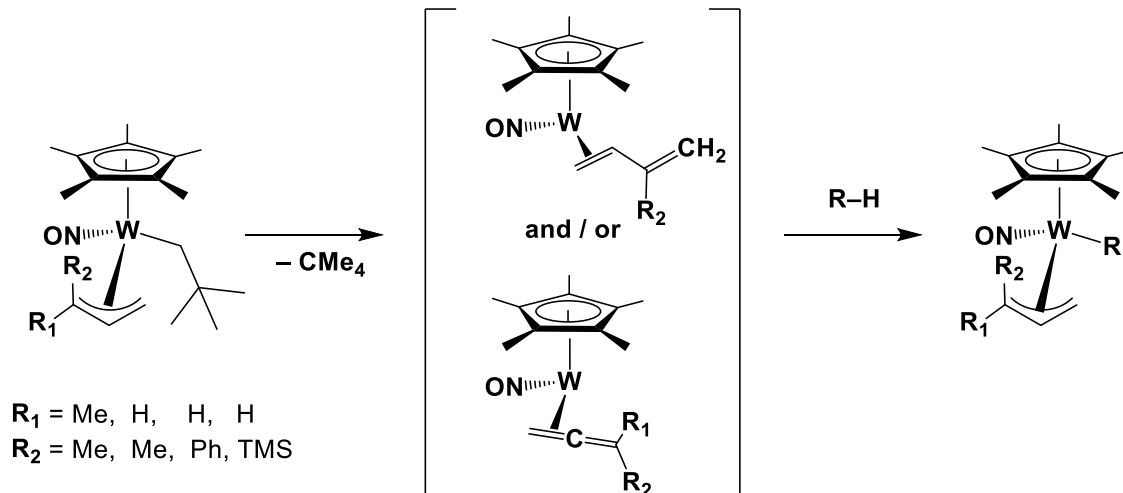
Complexes with Hydrocarbons[†]

[†]The verison of this chapter has been published. Baillie, R. A.; Wakeham, R. J.; Lefèvre, G. P.; Béthegnies, A.; Patrick, B. O.; Legzdins, P.; Rosenfeld, D. C. *Organometallics* **2015**, *34*, 3428-3441, and Baillie, R. A.; Wakeham, R. J.; Lefèvre, G. P.; Holmes, A. S.; Legzdins, P. *Organometallics* **2015**, *34*, 4085-4092. Reproduced with permission from Organometallics. Copyright (2015) American Chemical Society.

3.1 Introduction

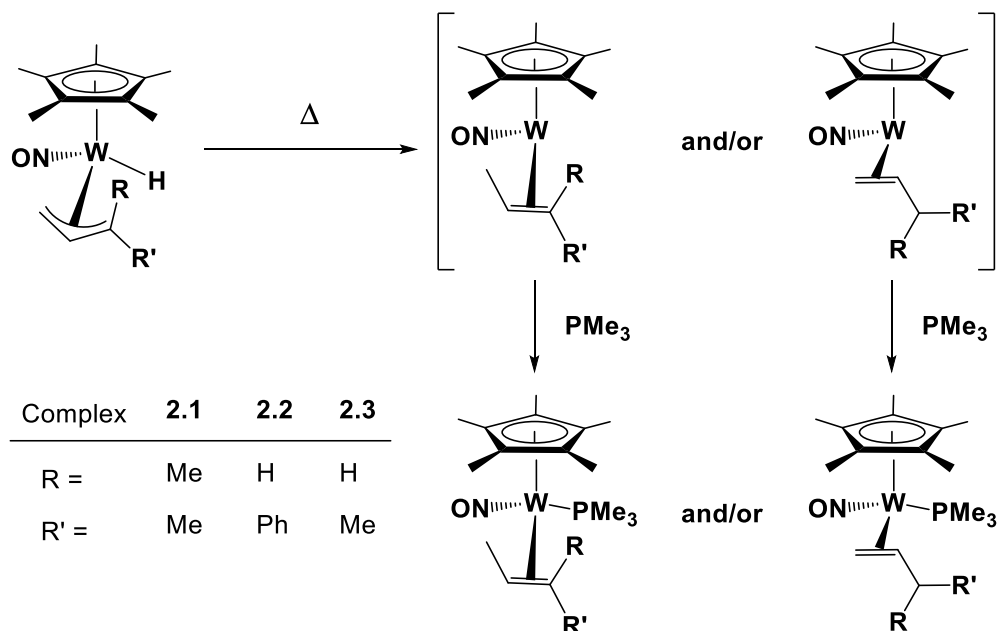
Current research directed at effecting the activation and functionalization of hydrocarbon C–H bonds continues to be motivated by the long-term goal to develop new synthetic pathways to a broad range of industrially important products in an environmentally friendly manner.^{69,70,71,72,73,74,75,76,77} Contributions from the Legzdins group to this chemistry have involved the development of Group 6 organometallic nitrosyl complexes for the initiation and mediation of various hydrocarbon C-H activations.³¹ Specifically, the gentle thermolyses of 18e $\text{Cp}^*\text{W}(\text{NO})(\text{CH}_2\text{CMe}_3)(\eta^3\text{-allyl})$ complexes ($\eta^3\text{-allyl} = \eta^3\text{-CH}_2\text{CHCHMe}$, $\eta^3\text{-CH}_2\text{CHCHSiMe}_3$, $\eta^3\text{-CH}_2\text{CHCHPh}$, or $\eta^3\text{-CH}_2\text{CHCMe}_2$) result in the loss of neopentane and the transient formation of the 16e intermediate species, $\text{Cp}^*\text{W}(\text{NO})(\eta^2\text{-allene})$ and/or $\text{Cp}^*\text{W}(\text{NO})(\eta^2\text{-diene})$. These transient intermediates effect the single, selective terminal activation of alkane C-H bonds intermolecularly via the microscopic reverse of the transformations by which they are generated and form new $\text{Cp}^*\text{W}(\text{NO})(\eta^1\text{-hydrocarbyl})(\eta^3\text{-allyl})$ complexes (Scheme 3.1). Depending on the experimental conditions employed, these latter complexes often persist and can be isolated.

Scheme 3.1. C-H activations effected by $\text{Cp}^*\text{W}(\text{NO})(\text{CH}_2\text{CMe}_3)(\eta^3\text{-allyl})$ complexes



The synthesis of the related family of $\text{Cp}^*\text{W}(\text{NO})(\text{H})(\eta^3\text{-allyl})$ complexes (**2.1-2.3**) and some of their interesting properties has been discussed in the previous chapter. Upon thermolysis, these 18e $\text{Cp}^*\text{W}(\text{NO})(\text{H})(\eta^3\text{-allyl})$ compounds undergo intramolecular isomerizations to the corresponding 16e $\text{Cp}^*\text{W}(\text{NO})(\eta^2\text{-alkene})$ intermediate complexes that can be trapped by PMe_3 as their corresponding 18e adducts, which is summarized below in Scheme 3.2 for convenience.

Scheme 3.2. Summary of the 16e η^2 -alkene intermediate complexes generated by the thermolysis of 2.1-2.3 and the trapping of these 16e intermediate complexes by PMe_3



The 16e η^2 -alkene intermediates generated from **2.1-2.3** are remarkably similar to the 16e η^2 -allene and η^2 -diene intermediates generated from the $\text{Cp}^*\text{W}(\text{NO})(\text{CH}_2\text{CMe}_3)(\eta^3\text{-allyl})$ complexes. The immediate questions that arises are whether these intermediate η^2 -alkene species can also effect the intermolecular activations of hydrocarbon C-H bonds and, if so, how do these activations compare with those documented for the related 16e $\text{Cp}^*\text{W}(\text{NO})(\eta^2\text{-allene})$ and $\text{Cp}^*\text{W}(\text{NO})(\eta^2\text{-diene})$ entities. The focus of this chapter is on the investigations of the thermal chemistry of the $\text{Cp}^*\text{W}(\text{NO})(\text{H})(\eta^3\text{-allyl})$ complexes and their ability to initiate the activation of hydrocarbon C-H bonds.

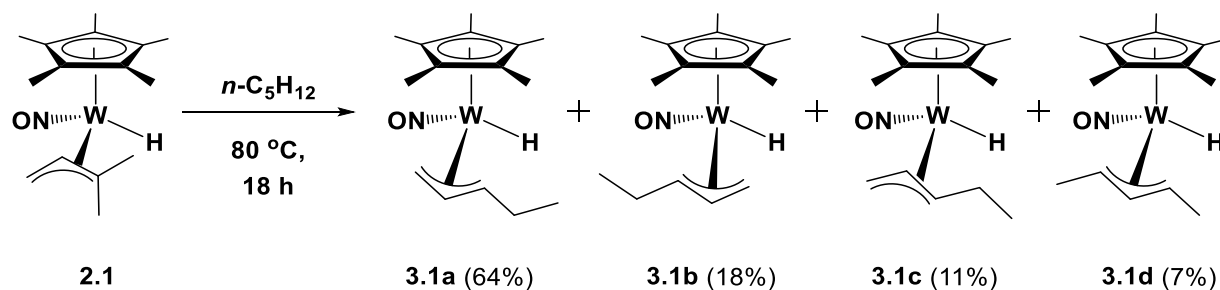
3.2 Results and Discussion

3.2.1 Multiple C-H Activations of Alkanes

3.2.1.1 Thermolysis of **2.1** in *n*-Pentane

Thermolyses of **2.1** in *n*-pentane affords a dark-yellow to brown reaction mixture from an originally yellow solution. The reaction leads to the loss of the original allyl ligand and the formation of the mixture of isomeric products of $\text{Cp}^*\text{W}(\text{NO})(\text{H})(\eta^3\text{-C}_5\text{H}_{11})$ (**3.1**), namely $\text{Cp}^*\text{W}(\text{NO})(\text{H})(\eta^3\text{-CH}_2\text{CHCHEt})$ (**3.1a-c**) and $\text{Cp}^*\text{W}(\text{NO})(\text{H})(\eta^3\text{-MeCHCHCHMe})$ (**3.1d**) (Scheme 3.3). There are at least three isomers of **3.1a** in solution that can be differentiated in the ^1H NMR spectrum as a result of the asymmetry at the tungsten center. The thermolyses of **2.2** and **2.3** with *n*-pentane afford similar mixtures of isomers of **3.1**, albeit in diminished isolated yields.⁴⁵ The fact that all three allyl hydride complexes **2.1-2.3** give the same mixture of isomers of **3.1**, regardless of the original allyl ligand, suggests that the final product is ultimately independent of the original allyl ligand used. Therefore it is fair to assume that the chemistry reported for **2.1** can be generally applied to the family of allyl hydride complexes, differing yields notwithstanding.

Scheme 3.3. Thermolysis of Cp*W(NO)(H)(η^3 -allyl) complexes in *n*-pentane



Complex **3.1** can be purified from each reaction mixture by column chromatography on neutral alumina and is isolable as an analytically pure yellow solid in 53% yield by recrystallization from Et₂O/hexanes. In solution, **3.1** exists as a number of isomers that vary depending on substitution (1-ethylallyl, **3.1a-c**, and 1,3-dimethyl allyl, **3.1d**) and/or orientation of the allyl ligand. The various isomers are identifiable in solution by the multiplicity and chemical shifts of their characteristic meso H signals in the ¹H NMR spectrum of **3.1**, as shown in Figure 3.1. The meso H signals for isomers **3.1a-c** appear as a doublet of doublets of doublets in the ¹H NMR spectrum due to coupling to three non-equivalent allyl H atoms. In contrast, the signal due to the meso H of **3.1d** is a doublet of doublets arising from coupling to only two non-equivalent allyl H atoms. The overall ratio of **3.1a-c** to **3.1d** is 93 to 7, indicating a high selectivity for multiple C-H activations beginning with a terminal C-H activation. The isomer **3.1c** has the allyl ligand in an exo orientation with a relative upfield chemical shift of the meso H signal at 2.84 ppm. The position of the ethyl substituent for the isomers **3.1a-c** has been determined using the chemical shift of the signals due to the terminal carbons of the allyl ligands in the ¹³C APT NMR spectrum. The more downfield (*sp*²-character) carbon atom is located trans to the nitrosyl ligand which allows locating of the substituent either proximal to the hydride or

nitrosyl ligands (For a more detailed discussion using ^{13}C APT NMR spectra to assign the position of a substituent on an allyl ligand refer to the discussion of complex **5.3**). Finally, the upfield hydride resonances of both complexes are readily identifiable by their ^{183}W satellites.

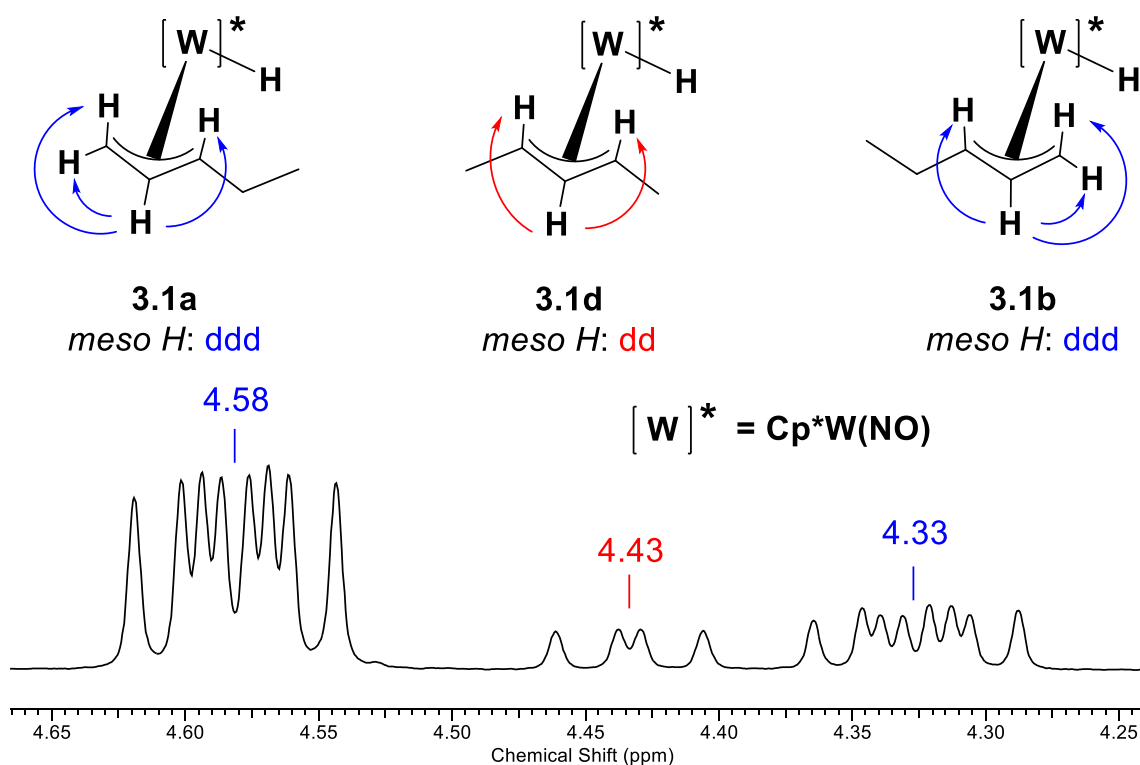


Figure 3.1. Expansion of the 400 MHz ^1H NMR spectrum (4.66 to 4.24 ppm) of **3.1** in C_6D_6 displaying the resonances due to the *endo meso H* protons of **3.1a** (δ 4.58, ddd, $^3J_{\text{HH}} = 13.1$, 10.2), **3.1b** (δ 4.33, ddd, $^3J_{\text{HH}} = 13.4$, 10.0, 7.4) and **3.1d** (δ 4.43, dd, $^3J_{\text{HH}} = 12.7$, 9.4).

The solid-state molecular structure of isomer **3.1a** is shown in Figure 3.2. The crystals were obtained by Dr. Aurélien Béthegnies and solved by Dr. Brian Patrick. This single isomer of **3.1a** crystallizes from the mixture of all the isomers **3.1a-d** in pentane. Complex **3.1a** exists as a three-legged piano stool molecule in the solid state. The nitrosyl ligand is essentially linear with

a W-N-O bond angle of $169.3(3)^\circ$, and the allyl ligand displays the customary σ - π distortion⁴ with C(11)-C(12) and C(12)-C(13) bond lengths of 1.425(5) and 1.390(5) Å, respectively. The hydride ligand is not shown in Figure 3.2 because of refinement instability even though a residual electron density peak corresponding to it was found experimentally.

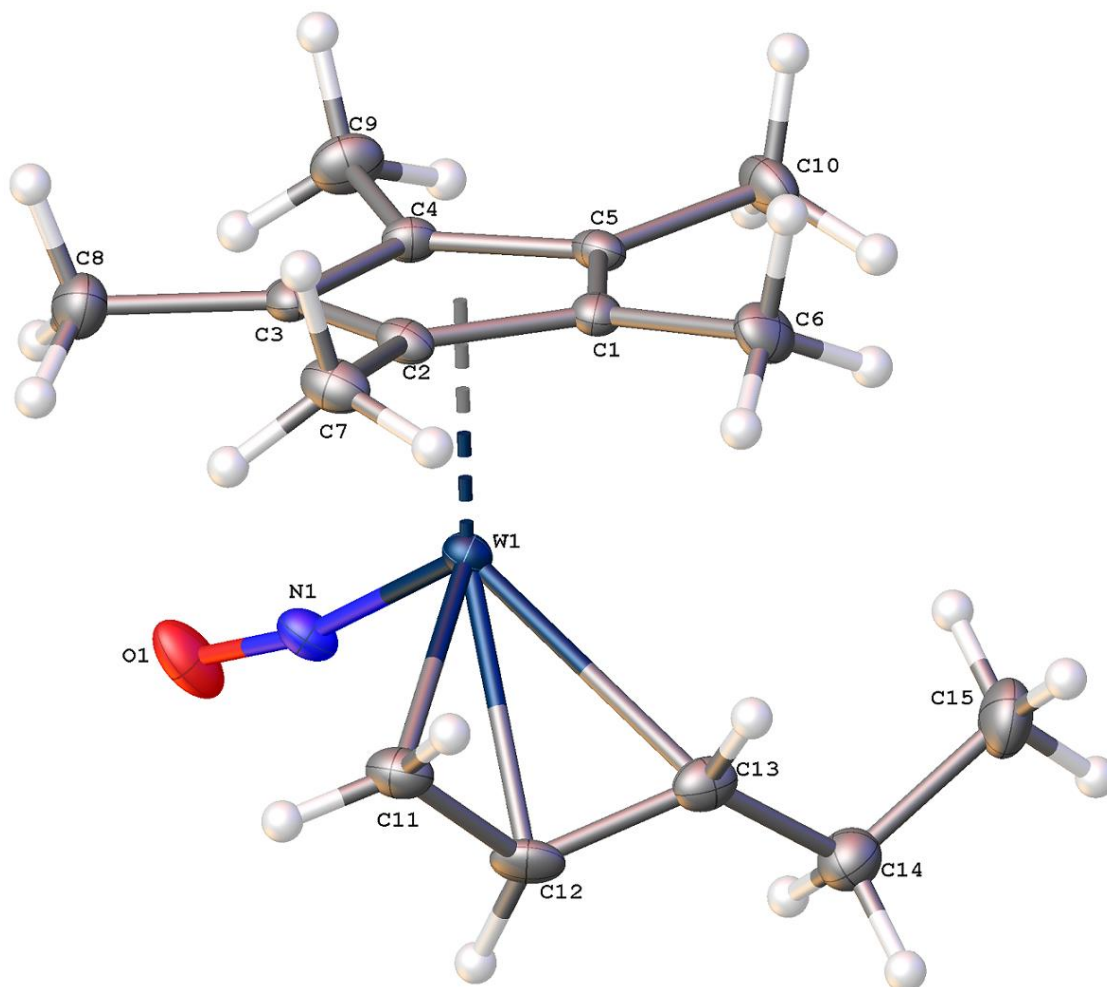
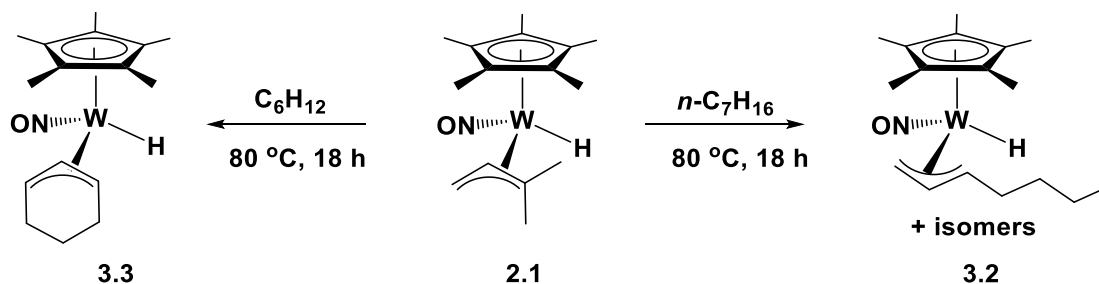


Figure 3.2. Solid-state molecular structure of **3.1a** with 50% probability thermal ellipsoids shown. Selected bond lengths (Å) and angles (deg.): W(1)-C(11) = 2.247(4), W(1)-C(12) = 2.314(3), W(1)-C(13) = 2.402(4), C(11)-C(12) = 1.425(5), C(12)-C(13) = 1.390(5), C(13)-C(14) = 1.498(5), C(14)-C(15) = 1.535(5), W(1)-N(1) = 1.786(3), N(1)-O(1) = 1.216(4), C(11)-C(12)-C(13) = 119.0(3), C(12)-C(13)-C(14) = 124.2(3), C(13)-C(14)-C(15) = 113.7(3), W(1)-N(1)-O(1) = 169.3(3).

3.2.1.2 Thermolysis of 2.1 in *n*-Heptane

The thermolysis of **2.1** in *n*-heptane proceeds analogously to the reaction of **2.1** with *n*-pentane. The products formed are isomers of $\text{Cp}^*\text{W}(\text{NO})(\text{H})(\eta^3\text{-C}_7\text{H}_{13})$ (**3.2**) (Scheme 3.4), resulting from the multiple C-H activations of a substrate molecule while the original 1,1-dimethylallyl ligand is lost. Complex **3.2** can be isolated by column chromatography on basic alumina as a yellow oil in good yield (56%). The complex can be solidified at $-78\text{ }^\circ\text{C}$, but it quickly reverts back to an oil at room temperature. The IR spectrum of **3.2** exhibits a single nitrosyl-stretching frequency at 1594 cm^{-1} , which is essentially identical to that displayed by **3.1** at 1595 cm^{-1} .

Scheme 3.4. Thermolysis of complex 2.1 in *n*-heptane and cyclohexane



Four different isomers of **3.2** have been structurally identified by NMR spectroscopy as shown in Figure 3.3. A total of at least eight isomers are present in solution based on the different upfield hydride resonances having ^{183}W satellites (Table 3.1). Three of the four structurally identified isomers of $\text{Cp}^*\text{W}(\text{NO})(\text{H})(\eta^3\text{-CH}_2\text{CHCHC}_4\text{H}_9)$, namely **3.2a**, **3.2c**, and **3.2d**, have a monosubstituted allyl ligand that results from three successive C-H activations

beginning with a terminal activation. These isomers comprise 64% of the mixture of isomers in solution. A single isomer having a disubstituted allyl ligand, $\text{Cp}^*\text{W}(\text{NO})(\text{H})(\eta^3\text{-MeCHCHCHC}_3\text{H}_7)$ (**3.2b**), is identifiable and comprises 29% of the mixture. At least four more isomers make up the remaining 7% of the mixture, but it has not been possible to determine the exact structures of these isomers. Shown in Figure 3.4 is the overlapping expansion of the ^1H NMR spectra for complexes **3.1** and **3.2** displaying the major W-H signals for each compound. There are approximately twice as many different isomers of **3.2** than of **3.1**, which is not unexpected since the longer carbon chain allows for more possible disubstituted allyl isomers analogous to complex **3.1d**.

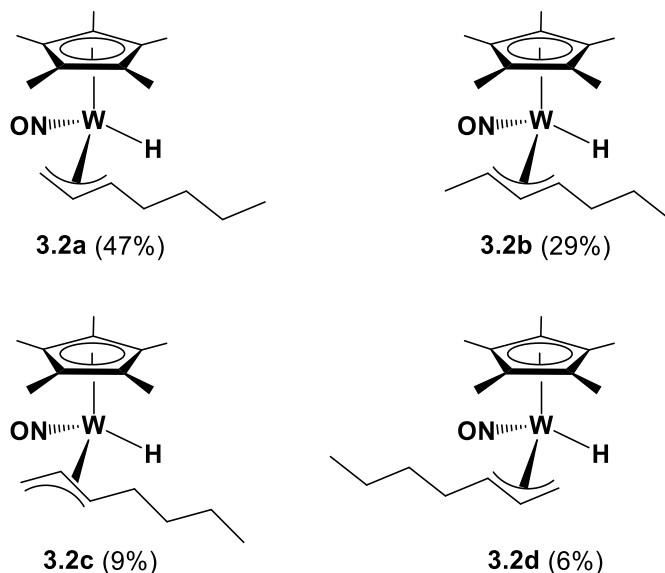


Figure 3.3. Major isomers of **3.2** resulting from the reaction of **2.1** with *n*-heptane.

Table 3.1. WH signals of the isomers of **3.2** as identified by their characteristic ^{183}W satellites.

Isomer	Relative Abundance (%)	^1H NMR δ (ppm)	$^1J_{\text{WH}}$ (Hz)
3.2a	47	-1.30	119.7
3.2b	29	-1.42	123.8
3.2c	9	-1.20	121.3
3.2d	6	-1.34	122.1
3.2e	3	-1.39	122.9
3.2f	3	-0.87	120.9
3.2g	2	-1.53	122.5
3.2.h	1	-0.94	123.6

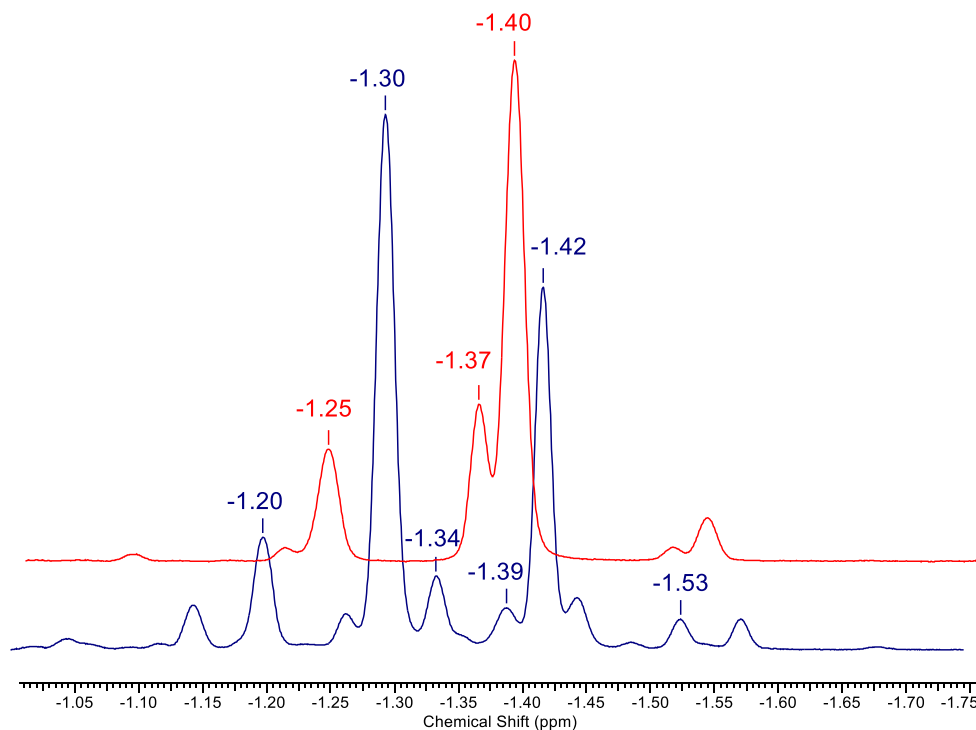


Figure 3.4. Expansion of the 400 MHz ^1H NMR spectra (-1.00 to -1.75 ppm) of **3.1** (red) and **3.2** (blue) in C_6D_6 displaying the resonances due to the W-*H* protons of the isomers of **3.1** and **3.2**.

3.2.1.3 Thermolysis of **2.1** in Cyclohexane

The product distributions from the reaction of **2.1** with *n*-pentane and *n*-heptane suggest that there is a preference for initial terminal C-H activation analogous to that exhibited by the related $\text{Cp}^*\text{W}(\text{NO})(\text{CH}_2\text{CMe}_3)(\eta^3\text{-allyl})$ complexes.³¹ To investigate the preference for primary over secondary initial $\text{C}(\text{sp}^3)\text{-H}$ activations of the $\text{Cp}^*\text{W}(\text{NO})(\text{H})(\eta^3\text{-allyl})$ complexes, the thermal reaction of **2.1** with cyclohexane, a substrate containing only secondary $\text{C}(\text{sp}^3)\text{-H}$ bonds, has been effected. Thermolysis of **2.1** in neat cyclohexane under the same conditions as for the reactions with *n*-pentane and *n*-heptane results in only 30% conversion of **2.1** to

$\text{Cp}^*\text{W}(\text{NO})(\text{H})(\eta^3\text{-C}_6\text{H}_9)$ (**3.3**) (Scheme 3.4), which has been reported previously.²⁶ This result indicates that the C-H activation of primary $\text{C}(\text{sp}^3)\text{-H}$ bonds does indeed occur faster than the activation of secondary $\text{C}(\text{sp}^3)\text{-H}$ bonds. This feature is consistent with a preference for initial terminal C-H activation of the linear alkanes which in turn explains the overall predominance of the terminal allyl isomers (Figure 3.3). Increasing the reaction time of **2.1** with cyclohexane leads to consumption of the starting material; however, **3.3** is not stable under the experimental conditions employed, and only a minimal quantity of product is obtained.

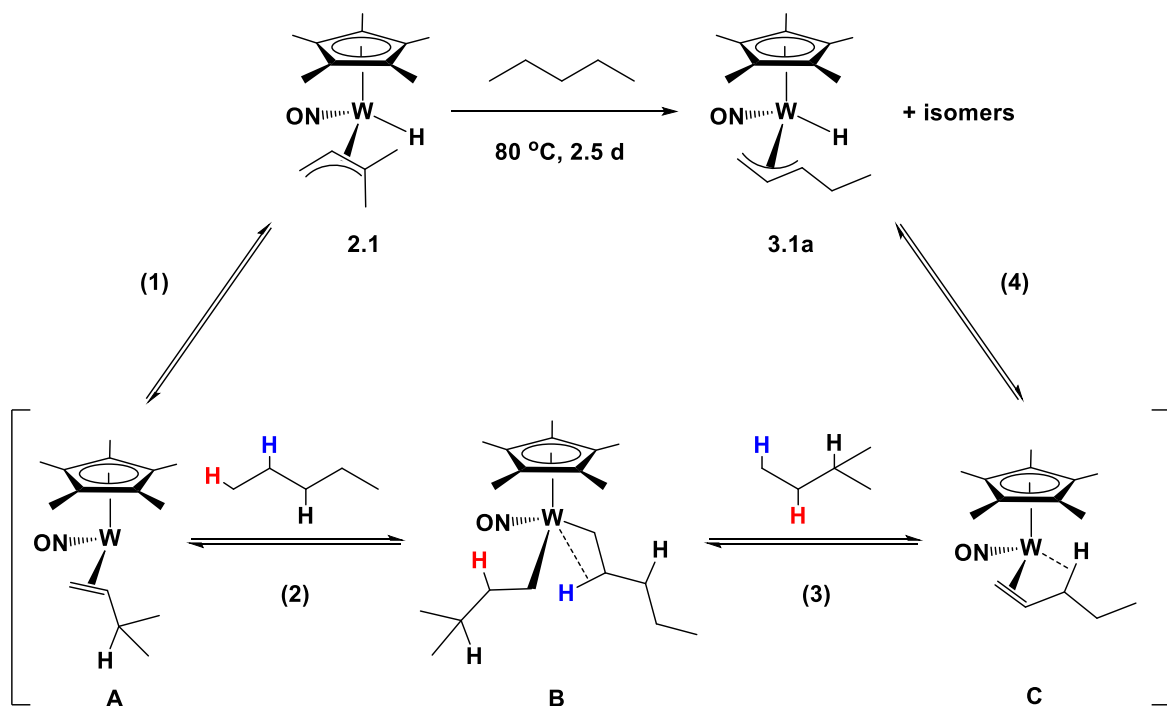
3.2.2 Mechanistic Consideration of C-H Activation

We have previously prepared complex **3.1** by the thermolysis of $\text{Cp}^*\text{W}(\text{NO})(\text{CH}_2\text{CMe}_3)(\eta^3\text{-CH}_2\text{CHCMe}_2)$ in *n*-pentane.³⁰ Interestingly, this alkyl allyl reactant is unique among the family of $\text{Cp}^*\text{W}(\text{NO})(\text{CH}_2\text{CMe}_3)(\eta^3\text{-allyl})$ complexes since it is the only one that does not give the products of the single, terminal C-H activation of linear alkanes. Theoretical calculations concerning the mechanism of this reaction suggest that the single C-H activation of *n*-pentane by $\text{Cp}^*\text{W}(\text{NO})(\text{CH}_2\text{CMe}_3)(\eta^3\text{-CH}_2\text{CHCMe}_2)$ does indeed occur.³² However, the initial product formed, namely $\text{Cp}^*\text{W}(\text{NO})(n\text{-C}_5\text{H}_{11})(\eta^3\text{-CH}_2\text{CHCMe}_2)$, is unstable under the experimental conditions employed and converts to the isomers of **3.1a** and **3.1b** through successive, multiple C-H activations. It is therefore likely that complexes **2.1-2.3** also effect the selective, single terminal C-H activation of linear alkanes, but the resulting products are thermally unstable and undergo two additional successive C-H activations to form the final allyl hydride complexes.

3.2.2.1 Proposed Mechanism for the Multiple Activation of Alkanes

The mechanism proposed for the C-H activation processes involving complex **2.1** is shown in Scheme 3.5, but it can be generalized to apply to complexes **2.2** and **2.3** as well. The principal steps in this mechanism are: (1) The hydride ligand couples to the allyl ligand to generate the 16e intermediate alkene complex, $\text{Cp}^*\text{W}(\text{NO})(\eta^2\text{-CH}_2=\text{CHCHMe}_2)$ (**A**), which has been trapped as its PMe_3 adduct (complex **2.6**); (2) Intermediate **A** effects the single, terminal C-H activation of an *n*-pentane molecule to form the 16e mixed bis(alkyl) complex, $\text{Cp}^*\text{W}(\text{NO})(n\text{-C}_5\text{H}_{11})(\eta^1\text{-CH}_2\text{CH}_2\text{CHMe}_2)$ (**B**), that contains two β C-H agostic interactions and has an open coordination site; (3) Complex **B** then undergoes a β -H abstraction to give a new 16e η^2 -alkene complex, $\text{Cp}^*\text{W}(\text{NO})(\eta^2\text{-CH}_2=\text{CHCH}_2\text{CH}_2\text{Me})$ (**C**), releasing the original $\eta^3\text{-CH}_2\text{CHCMe}_2$ ligand as isopentane. Steps (2) and (3) in this proposed mechanism are the microscopic reverse of each other, and so it is likely that **B** converts to **A** via β -H abstraction and releases *n*-pentane in the process. The conversion of **2.1** into **3.1** must therefore be driven by the large excess of *n*-pentane present relative to the stoichiometric quantity of isopentane released. Finally, in step (4) complex **C** undergoes an additional C-H bond activation to form the final product **3.1a**. The presence of β C-H agostic interactions in related systems have been computationally determined to stabilize many intermediate complexes as well as act as arrested transition states for β -H elimination reactions.^{32, 78-80}

Scheme 3.5. Proposed mechanism for the conversion of 2.1 into 3.1a



The presence in the final reaction mixture of **3.1d**, which contains an internal allyl ligand, is not inconsistent with the initial C-H activation effected by **2.1** being selective for terminal C-H bonds, i.e. showing a preference for primary over secondary C(*sp*³)-H bond activation. A proposed chain-walking type mechanism can account for the presence of isomers such as **3.1d** (and **3.2b**) in which the allyl ligand can readily exchange between η^3 and η^1 coordination modes results in both termini of the allyl ligand being proximal to the hydride ligand (Figure 3.5a). Therefore, coupling of the hydride to either allyl C terminus can occur, resulting in the formation of an internal allyl (η^3 -MeCHCHCHMe) isomer, **3.1d**, from a terminal allyl (η^3 -CH₂CHCHEt) isomer **3.1a** (Figure 3.5b). Additionally, the exchange between η^3 and η^1 coordination modes also explains the presence of isomers (e.g. **3.1c**) with the allyl ligand having an exo orientation.

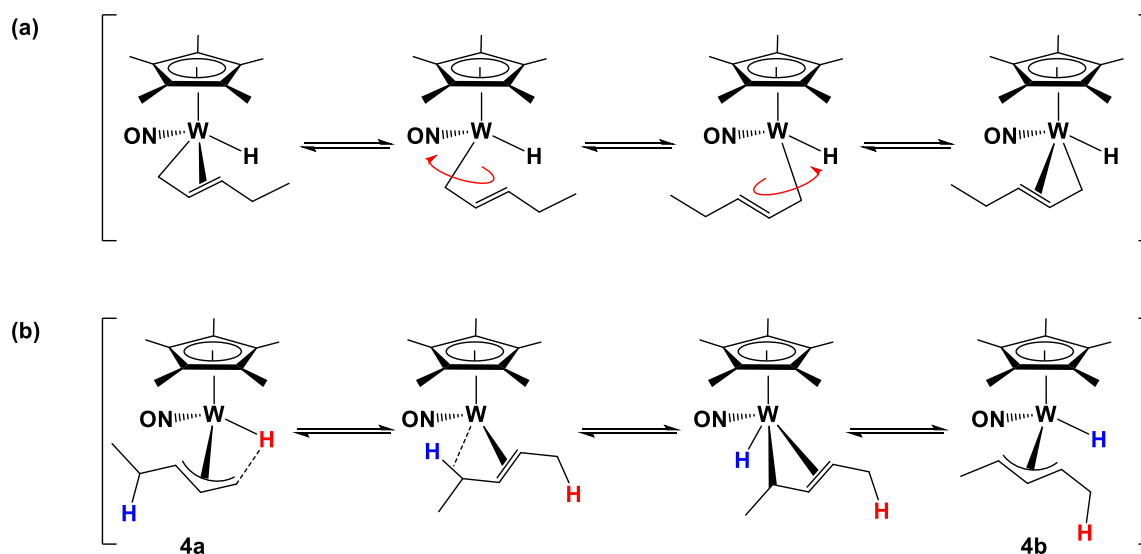


Figure 3.5. (a) A change in hapticity allowing the position of the allyl ligand substituent(s) to change relative to the other ligands on the metal. (b) A proposed chain-walking mechanism in which the terminal allyl ligand (η^3 -CH₂CHCHEt) in **3.1a** is converted into the internal allyl ligand (η^3 -MeCHCHCHMe) in **3.1b**.

Experimental support for the occurrence of this type of chain-walking transformation comes from the previously discussed reaction of complex **2.3** with PMe₃.⁴³ In solution, **2.3** exists as four isomers that differ in whether the allyl ligand is in an *endo* or *exo* conformation and whether the methyl substituent is proximal to the hydride or the nitrosyl ligand. Thermolysis of **2.3** in PMe₃ results in isomers of two products, namely Cp*W(NO)(η^2 -MeCH=CHMe)(PMe₃) (**2.9c**) resulting from coupling of the hydride ligand to the CH₂ terminus of the allyl ligand (Figure 3.6a), and Cp*W(NO)(η^2 -CH₂=CHCH₂Me)(PMe₃) (**2.9a,b,d**), formed from coupling of the hydride ligand to the CHMe terminus of the allyl ligand (Figure 3.6b). Similarly, the thermolysis of **2.1** in the presence of PMe₃ also produces isomers attributable to hydride coupling to both the CH₂ (**2.6a**) and CMe₂ (**2.6b**, **2.6c**) allyl termini.

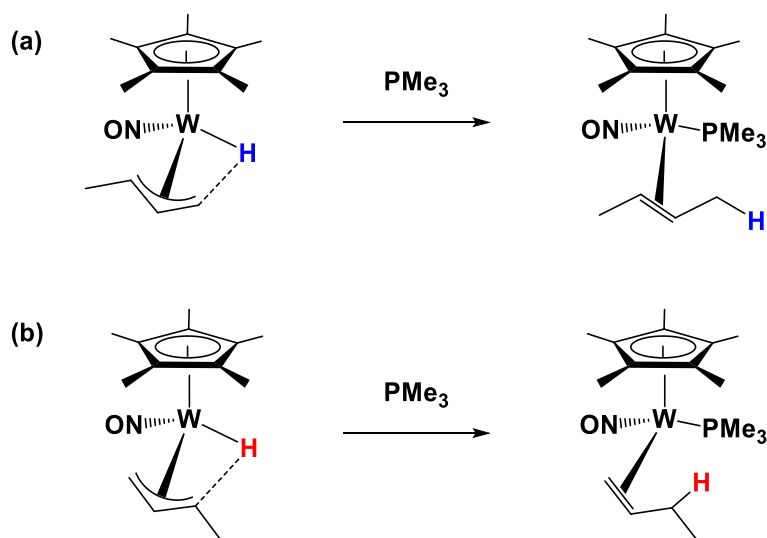
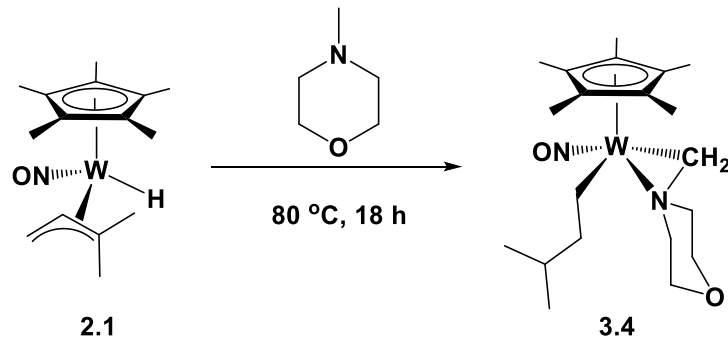


Figure 3.6. Trapping of (a) $\text{Cp}^*\text{W}(\text{NO})(\eta^2\text{-MeCH=CHMe})$ and (b) $\text{Cp}^*\text{W}(\text{NO})(\eta^2\text{-CH}_2\text{=CHCH}_2\text{Me})$ with PMe_3 providing evidence for coupling to either terminus of the allyl ligand, a feature that is necessary for the mechanism proposed for the transformation of **3.1a** to **3.1b** shown in Figure 3.5b.

3.2.2.2 Reaction of 2.1 with *N*-Methylmorpholine

Additional corroboration of the plausible mechanism depicted in Scheme 3.5 would be provided by a demonstration of the existence of the 16e mixed bis(alkyl) intermediate complex, **B**. In principle, such a complex could be trapped as a stable 18e adduct by a Lewis base. We therefore have endeavored to effect such a trapping reaction by using a hydrocarbon substrate having an electron-donor site adjacent to a primary $\text{C}(\text{sp}^3)\text{-H}$ bond. The substrate selected was *N*-methylmorpholine (NMM).

Scheme 3.6. Reaction of complex **2.1** with *N*-methylmorpholine



The thermolysis of **2.1** in NMM at 80 °C for 18 h affords a single organometallic complex, $\text{Cp}^*\text{W}(\text{NO})(\eta^2\text{-CH}_2\text{NC}_4\text{H}_8\text{O})(\eta^1\text{-CH}_2\text{CH}_2\text{CHMe}_2)$ (**3.4**), which is isolable in high yield as yellow crystals by recrystallization from Et_2O /hexanes (Scheme 3.6). Complex **3.4** exists as a single isomer both in solution and in the solid state. Its solid-state molecular structure is shown in Figure 3.7. A methyl $\text{C}(sp^3)\text{-H}$ bond of the NMM molecule has been cleaved by the tungsten center and the nitrogen atom alpha to the methylene formed from the methyl group is coordinated to the tungsten via a dative electron-pair bond. The tungsten, methylene C(16), and N(2) form a three-membered metallacycle having an N-W-C bite angle of $39.38(15)^\circ$. The NMM ring is in a chair conformation, and the *N*-methylene group (C(16)) is axial relative to the ring. The original 1,1-dimethylallyl ligand is now an isopentyl ligand due to hydrogenation involving transfer of the original hydride ligand and the hydrogen from the NMM methyl C-H bond that has been activated. The C(11)-C(12) bond of the isopentyl ligand is parallel to the pentamethylcyclopentadienyl ligand, a feature also evident in the solution structure of **3.4** as determined by $\{^1\text{H}\text{-}^1\text{H}\}$ NOESY NMR spectroscopy (vide infra). The nitrosyl ligand is linear and exhibits a nitrosyl-stretching frequency of 1522 cm^{-1} in the IR spectrum of **3.4** as compared

to 1601 cm⁻¹ for **2.1**. This spectral feature is likely a manifestation of the strong dative bonding from the morpholine-ring nitrogen to the tungsten in **3.4**.

As noted above, complex **3.4** retains its solid-state molecular structure in solution. The solution molecular structure (Figure 3.8a) has been elucidated by NMR spectroscopy, specifically the {¹H-¹H} NOESY NMR spectrum. The ¹H NMR spectrum of **3.4** is shown in Figure 3.8b, and it indicates that the dative coordination of the NMM nitrogen atom to the tungsten is maintained on the NMR timescale. The equivalent NCH₂ and OCH₂ methylene signals in NMM are all nonequivalent in **3.4**, with the signal due to H(8a) being shifted upfield to 0.58 ppm from the other NMM ring proton signals which range from 3.55 to 2.27 ppm. This upfield chemical shift is due to an interaction of the C-H bond with the tungsten center. Hydridic shifts are also observed for the isopentyl alpha proton resonances of H(1a) and H(1b) at 0.71 and 1.10 ppm, respectively, and a very large upfield shift for one of the NCH₂W protons, H(5a), at 0.49 ppm, as compared to 2.01 ppm for H(5b). The upfield chemical shift of resonances for protons pointing up toward the tungsten (and Cp* ligand) is similar to what is observed for the meso H signals of *exo* allyl ligands (as seen for complexes **2.1a**, **2.2b**, **2.2d**, **2.3c**, **2.3d**, **3.1b**, **3.2b**).

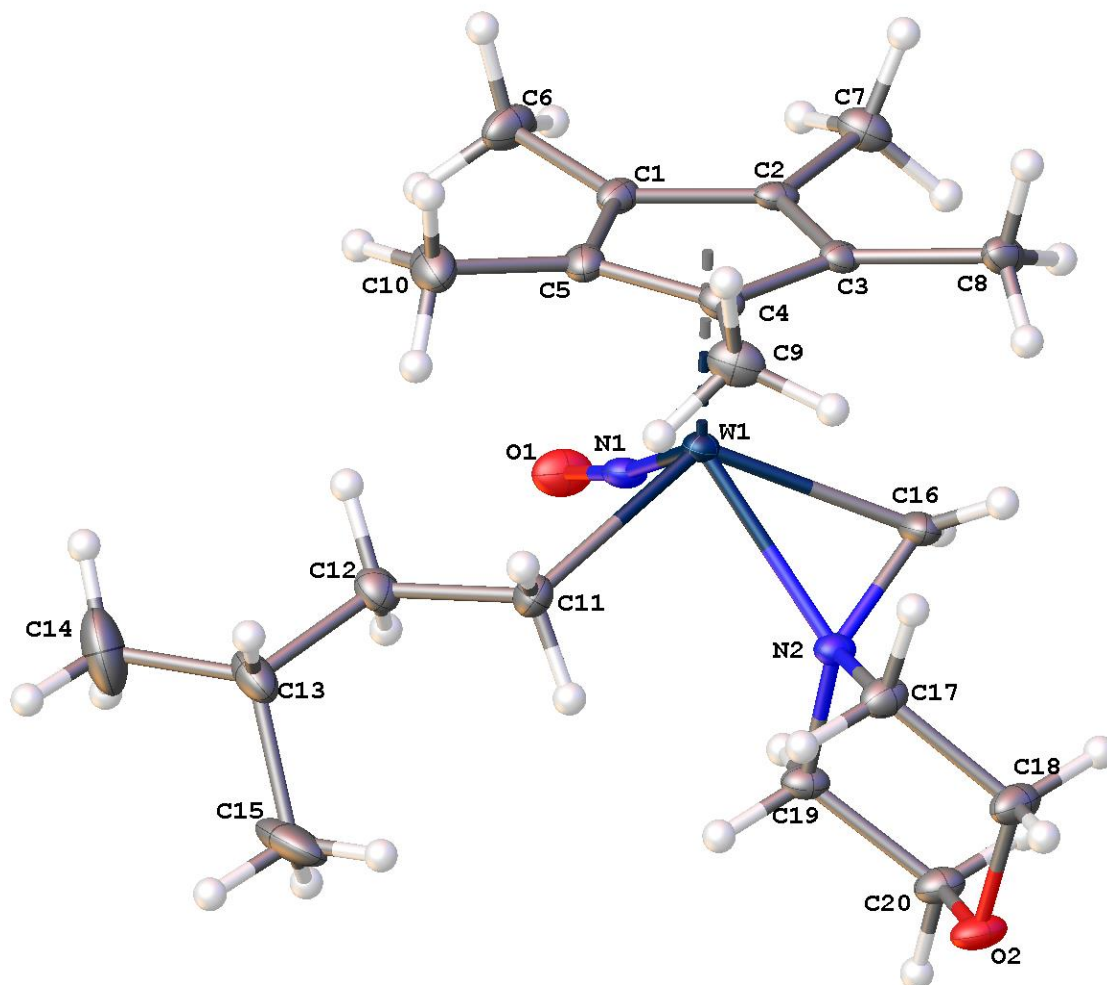


Figure 3.7. Solid-state molecular structure of **3.4** with 50% probability thermal ellipsoids shown.

Selected bond lengths (Å) and angles (deg.): W(1)-N(1) = 1.756(4), N(1)-O(1) = 1.240(5), W(1)-C(11) = 2.222(5), C(11)-C(12) = 1.547(6), C(12)-C(13) = 1.530(7), W(1)-C(16) = 2.137(5), W(1)-N(2) = 2.165(4), C(16)-N(2) = 1.450(6), N(2)-C(17) = 1.476(6), N(2)-C(19) = 1.480(5), C(18)-O(2) = 1.427(5), C(20)-O(2) = 1.429(6), W(1)-N(1)-O(1) = 171.7(3), N(1)-W(1)-C(11) = 93.05(17), C(11)-W(1)-N(2) = 81.37(15), N(2)-W(1)-C(16) = 39.38(15), C(16)-W(1)-N(1) = 96.19(18), W(1)-C(11)-C(12) = 113.4(3), C(11)-C(12)-C(13) = 114.5(4), W(1)-C(16)-N(2) = 71.3(2), W(1)-N(2)-C(16) = 69.3(2)

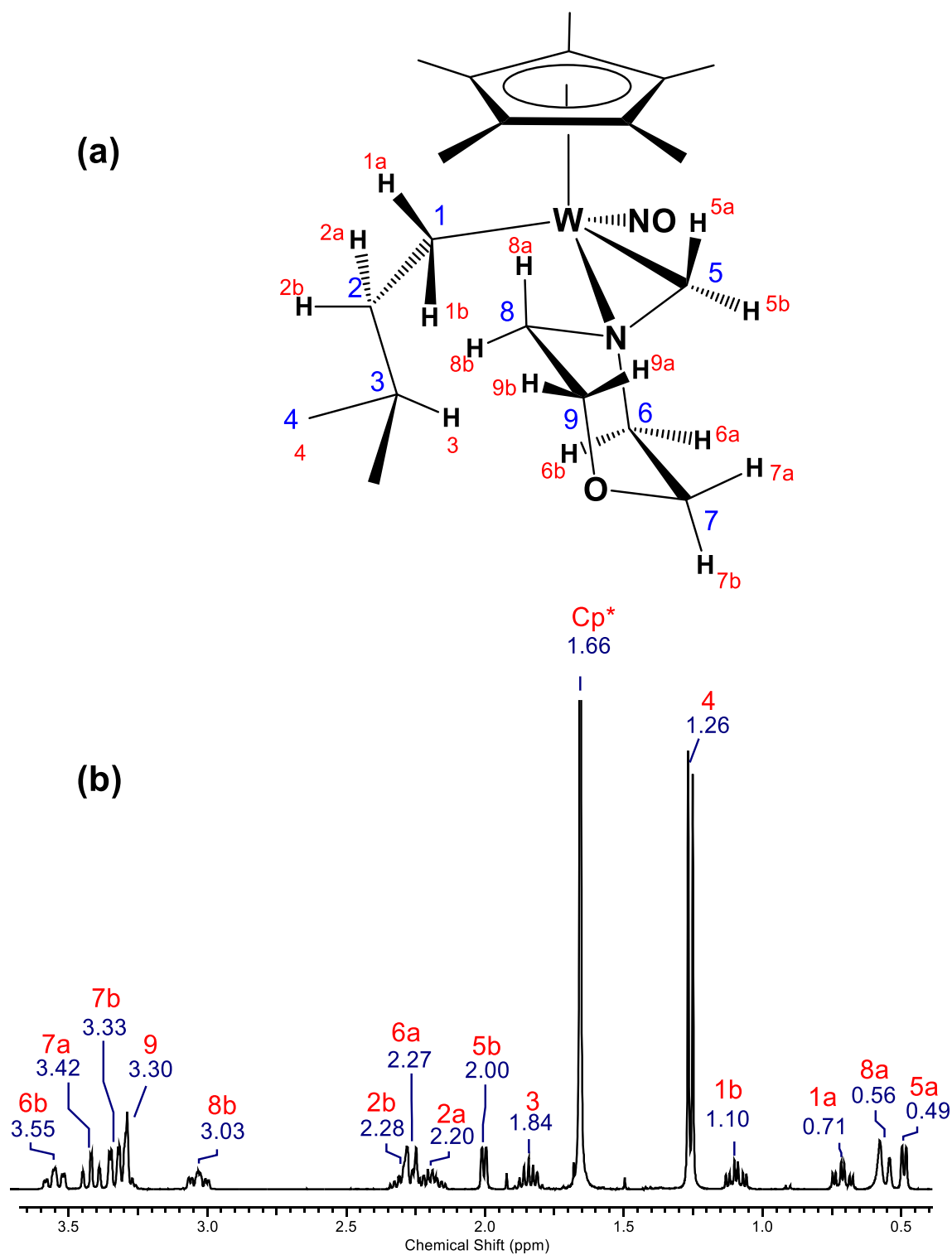
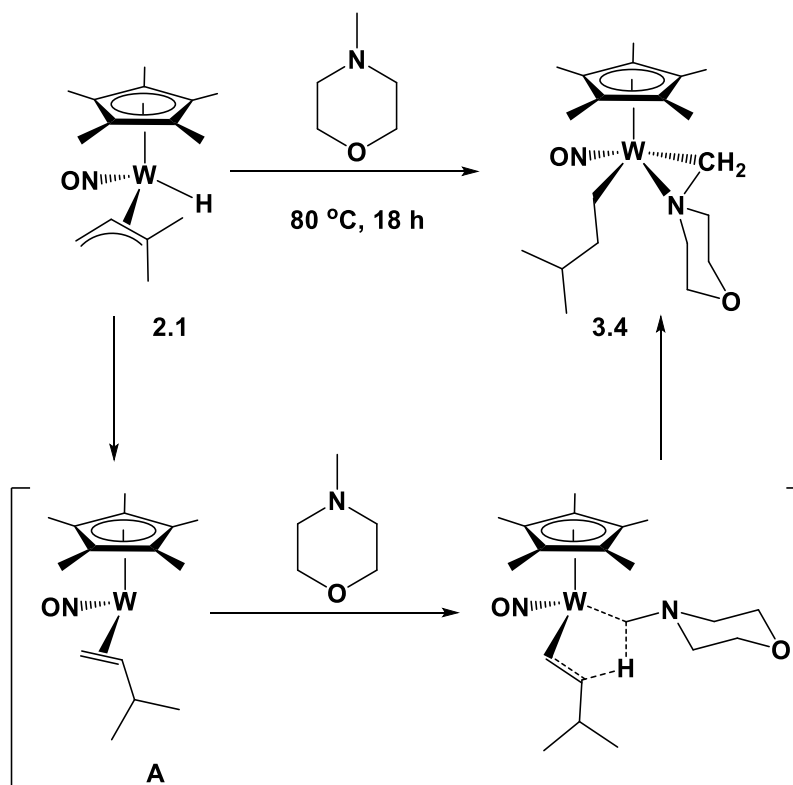


Figure 3.8. (a) Solution molecular structure of **3.4** as determined by a $\{^1\text{H}-^1\text{H}\}$ NOESY NMR spectrum. (b) The ^1H NMR spectrum of **3.4** in C_6D_6 .

Consistent with the mechanism depicted in Scheme 3.5, complex **3.4** is possibly formed in the manner shown in Scheme 3.7. (Alternatively, it is possible that NMM coordinates through the nitrogen atom first, followed by 1,3-addition of the C-H bond to $W(\eta^2\text{-CH}_2=\text{CHCHMe}_2)$. However, there are many examples of stable $\text{Cp}^*\text{W}(\text{NO})(\text{CO})(\eta^2\text{-alkene})$ complexes presented in this thesis, which suggests that coordination of the N atom could result in a stable adduct instead.) Thus, as anticipated, the lone pair of electrons on the N atom alpha to the activated C-H bond serves to stabilize the intermediate mixed dialkyl complex. The reactions of **2.2** and **2.3** with NMM proceed in an analogous fashion, consistent with a common mechanism of multiple C-H activation among the family of $\text{Cp}^*\text{W}(\text{NO})(\text{H})(\eta^3\text{-allyl})$ complexes.⁴⁵

Scheme 3.7. Possible mechanism for the transformation of 2.1 to 3.4

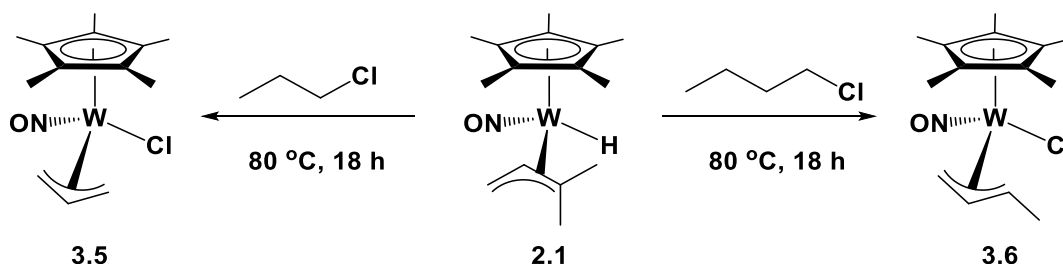


3.2.3 Reaction of **2.1** with Chloroalkanes

The reaction of **2.1** with *N*-methylmorpholine demonstrates that a single C-H activation can be effected in the presence of a heteroatom that is capable of occupying the open coordination site of the 16e bis(alkyl) intermediate (vide supra). Thus the possibility of using a heteroatom as a directing group in order to achieve single C-H activation by a Cp*W(NO)(H)(η^3 -allyl) complex was explored. Since the selective, single C-H activation of haloalkanes and ethers by Cp*W(NO)(CH₂Me₃)(η^3 -CH₂CHCHMe) has been previously demonstrated,³³ similar substrates were selected to investigate directing-group assisted single C-H activation by **2.1**.

As illustrated in Scheme 3.8, thermolysis of **2.1** in 1-chloropropane and 1-chlorobutane for 18 h at 80 °C results in the formation of Cp*W(NO)(η^3 -C₃H₅)Cl (**3.5**) and Cp*W(NO)(η^3 -C₄H₇)Cl (**3.6**), respectively. Consistent with the mechanism shown in Scheme 3.5, both of these complexes probably result from the initial formation of W-CH₂(CH₂)_n(CH₂Cl) (n = 1 or 2) linkages which then undergo subsequent C-H and C-Cl bond activations. Such a monodentate haloalkyl complex, namely Cp*W(NO)(CH₂CH₂CH₂Cl)(η^3 -CH₂CHCHMe), results from the thermolysis of Cp*W(NO)(CH₂Me₃)(η^3 -CH₂CHCHMe) in 1-chlorobutane.³³ Disappointingly, the reaction of **2.1** with di-*n*-butyl ether under analogous experimental conditions affords no tractable organometallic products.

Scheme 3.8. Reactions of complex 2.1 with 1-chloropropane and 1-chlorobutane



Complex **3.5** can be isolated as an analytically pure yellow solid by recrystallization from benzene. It exists as a single isomer in solution with the allyl ligand oriented in an *endo* conformation as evidenced by its *meso H* signal having a diagnostic downfield chemical shift of 5.86 ppm in the ^1H NMR spectrum.^{43, 81} The allyl ligand also displays a σ - π distortion which is evident in the ^{13}C NMR spectrum by the very different chemical shifts of the allyl CH_2 signals. The signal for the more sp^3 -character allyl terminus occurs at 43.7 ppm while the more sp^2 -character terminus resonates at 92.0 ppm. The complex has also been characterized in the solid-state by single crystal X-ray diffraction. There are three isomers of **3.5** in the solid-state resulting from disorder involving the allyl, nitrosyl, and chloro ligands. All three isomers possess the anticipated three-legged piano stool geometry with linear nitrosyl ligands. The first isomer is the same as the solution-state isomer and is shown in Figure 3.9 in which the *endo* conformation and the σ - π distortion of the allyl ligand are clearly evident.

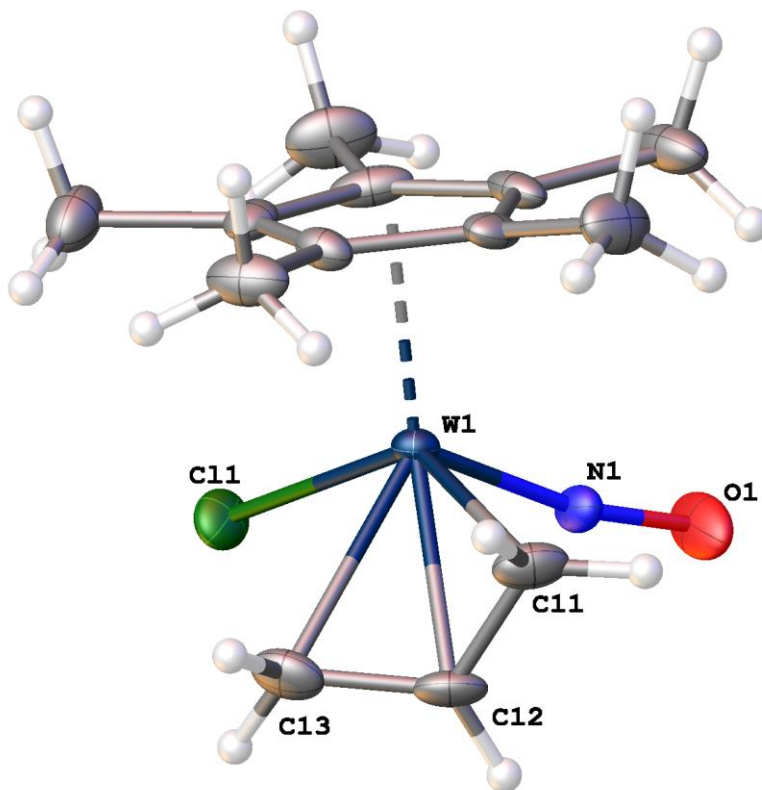


Figure 3.9. Solid-state molecular structure of **3.5** with 50% probability thermal ellipsoids shown.

Selected bond lengths (Å) and angles (deg.): W(1)-N(1) = 1.777(7), N(1)-O(1) 1.229(7), W(1)-Cl(1) = 2.407(2), W(1)-C(11) = 2.264(10), W(1)-C(12) = 2.339(6), W(1)-C(13) = 2.418(7), C(11)-C(12) 1.411(11), C(12)-C(13) = 1.386(12), W(1)-N(1)-O(1) = 168.9(8), C(11)-C(12)-C(13) = 116.7(8).

Two additional isomers of **3.5** have been characterized in the solid state. The second isomer is shown in Figure 3.10, and it is the enantiomer of the first isomer since the allyl ligand is again in the *endo* orientation but the positions of the nitrosyl and chloro ligands are reversed. The third solid-state isomer is shown in Figure 3.11, and it has the σ - π distorted allyl ligand in

the *exo* orientation. The ^1H NMR spectrum of **3.5** exhibits no *meso* H signals that can be attributed to this third isomer.

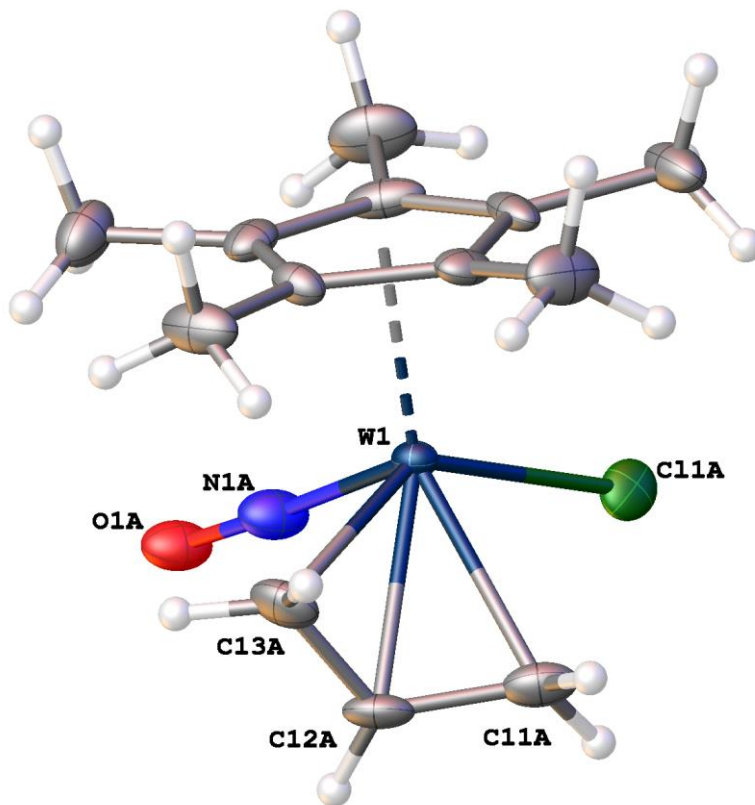


Figure 3.10. Solid-state molecular structure of the second isomer of **3.5** with 50% probability thermal ellipsoids shown. Selected bond lengths (\AA) and angles (deg.): $\text{W}(1)\text{-N}(1\text{A}) = 1.772(13)$, $\text{N}(1\text{A})\text{-O}(1\text{A}) = 1.242(18)$, $\text{W}(1)\text{-Cl}(1\text{A}) = 2.377(14)$, $\text{W}(1)\text{-C}(11\text{A}) = 2.36(3)$, $\text{W}(1)\text{-C}(12\text{A}) = 2.341(12)$, $\text{W}(1)\text{-C}(13\text{A}) = 2.20(4)$, $\text{C}(11\text{A})\text{-C}(12\text{A}) = 1.411(17)$, $\text{C}(12\text{A})\text{-C}(13\text{A}) = 1.387(18)$, $\text{W}(1)\text{-N}(1\text{A})\text{-O}(1\text{A}) = 176(4)$, $\text{C}(11\text{A})\text{-C}(12\text{A})\text{-C}(13\text{A}) = 119(3)$.

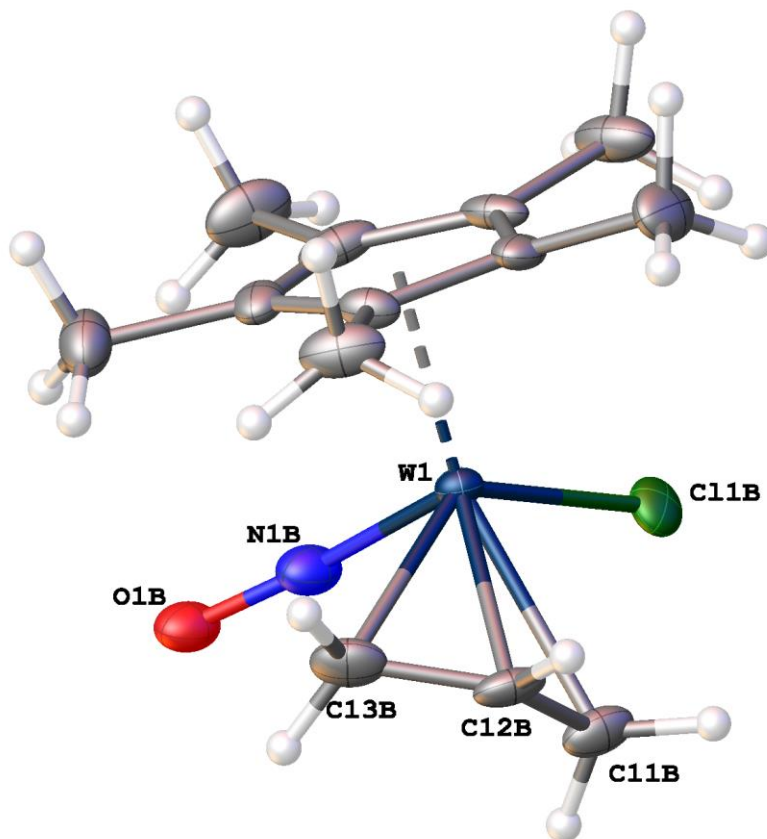


Figure 3.11. Solid-state molecular structure of the third isomer of **3.5** with 50% probability thermal ellipsoids shown. Selected bond lengths (Å) and angles (deg.): W(1)-N(1B) = 1.772(14), N(1B)-O(1B) = 1.25(2), W(1)-Cl(1B) = 2.32(3), W(1)-C(11B) = 2.41(7), W(1)-C(12B) = 2.341(13), W(1)-C(13B) = 2.35(6), C(11B)-C(12B) = 1.39(3), C(12B)-C(13B) = 1.36(3), W(1)-N(1B)-O(1B) = 170(7), C(11B)-C(12B)-C(13B) = 125(4).

The spectroscopic properties of **3.6** are completely consistent with it possessing a piano-stool molecular structure. The allyl ligand has an *exo* orientation as indicated by a downfield resonance for the *meso* *H* in the ^1H NMR spectrum at 5.32 ppm. A very pronounced σ - π distortion of the allyl ligand is evident in the ^{13}C NMR spectrum with the chemical shifts of the

allyl CH_2 and $CHMe$ signals being at 42.6 ppm and 110.7 ppm, respectively. Interestingly, **3.6** is the synthetic precursor to compound **2.3**.⁴³ Complex **3.6** is generated in situ from the reaction of $Cp^*W(NO)(Cl)_2$ with $Mg(CH_2CH=CHMe)_2$; it is not isolated in this reaction since its isolation tends to be problematic. Instead, it is converted directly to **2.3** by treatment with $LiBH_4$.

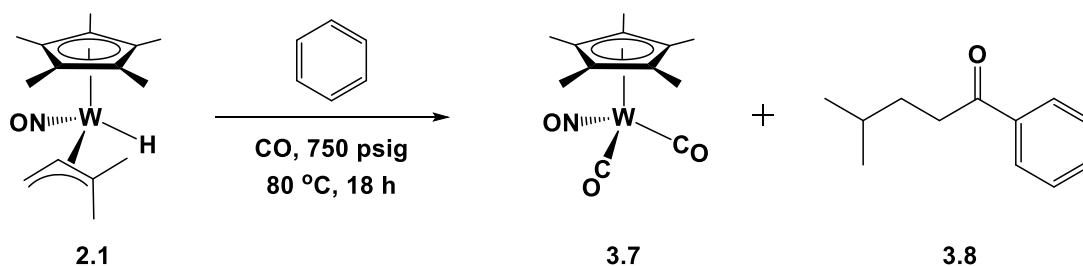
3.2.4 One-Pot Synthesis of Unsymmetrical Saturated Ketones

The reaction of **2.1** with *N*-methylmorpholine suggests that the multiple C-H activation pathway can be prevented in the presence of a Lewis donor. This has led to the hypothesis that effecting the C-H activation of a hydrocarbon under CO pressure could allow for the coordination of CO following the first C-H activation. The use of CO has been proposed with the aim of functionalizing the resulting hydrocarbyl ligand through 1,1-CO insertion into the W-C bond generated following the C-H activation. Benzene and mesitylene are selected as prototypical substrates to determine the ability of **2.1** to activate both $C(sp^2)$ -H and $C(sp^3)$ -H bonds under CO pressure. The expected products from these reactions are $Cp^*(NO)(CH_2CH_2CHMe_2)(\eta^2\text{-acyl})$ complexes, which could be stabilized through a dative interaction from an acyl oxygen lone pair.^{82, 83} Instead, thermolysis of **2.1** in hydrocarbon under CO pressure results in the formation of unsymmetrical, saturated ketones and the well-known organometallic complex $Cp^*W(NO)(CO)_2$ (**3.7**). This work has been subsequently expanded to include the other hydride complexes **2.2** and **2.3** and the reactions of these complexes with benzene and mesitylene under CO pressure were carried out by co-workers Dr. Russell Wakeham and Mr. Aaron Holmes.

3.2.4.1 Reactions of 2.1-2.3 with benzene under CO pressure

Thermolysis of **2.1** in benzene at 80 °C under 750 psig CO pressure for 18 h results in the one-pot formation of the well-known dicarbonyl nitrosyl complex, Cp*W(NO)(CO)₂, (**3.7**),⁵⁶ and the unsymmetrical ketone, 4-Methyl-1-phenylpentan-1-one (**3.8**) (Scheme 3.9), which is obtained in high yield (78%) as the only organic product. This reaction involves one-pot C-H activation of the hydrocarbon followed by 1,1-CO insertion and coupling to the allyl ligand which has been hydrogenated by the hydride ligand and the H atom from the C-H activation. Most notably, this conversion can be effected with undried solvent and without rigorous exclusion of moisture and air since both the organometallic reactant and product are oxidatively and hydrolytically stable.

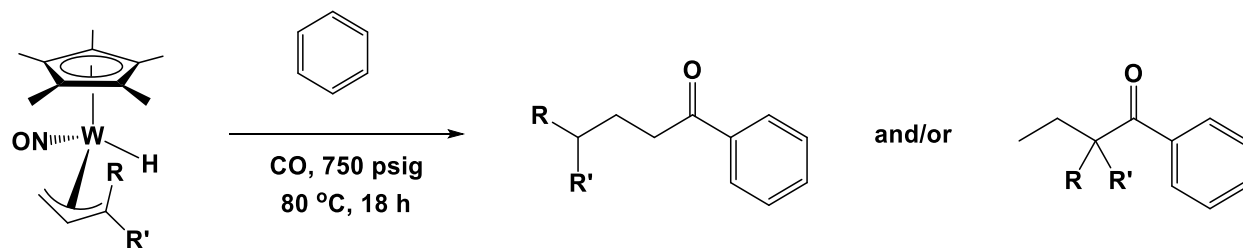
Scheme 3.9. Reaction of 2.1 with benzene under CO pressure



The reaction above in Scheme 3.9 turns out to be generally applicable to the allyl hydride complexes investigated (**2.1-2.3**). Under identical reaction conditions, each of the complexes **2.1-2.3** can effect the conversion of benzene and CO, along with the incorporation of the allyl ligand, to one or more unsymmetrical, saturated ketones (Scheme 3.10). The reaction using **2.3** results in the formation of two ketone products, 2-methyl-1-phenylbutan-1-one (**3.9a**) and 1-phenylpentan-

1-one (**3.9b**), in moderate yield (54%), in addition to **3.7**. Under the same conditions, complex **2.2** produces **3.7** and a single ketone, 1,2-diphenylbutan-1-one (**3.10**), in lower yield (29%). The results are summarized below in Table 3.2.

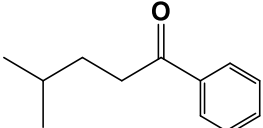
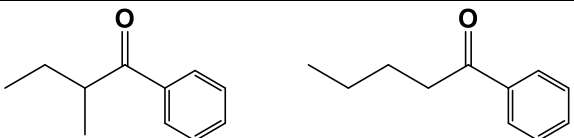
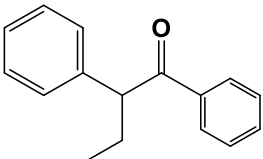
Scheme 3.10. General conversion of benzene and CO to ketones effected by 2.1-2.3



An interesting feature of the reactions presented in Scheme 3.10 is the degree of regioselectivity, particularly for the ketones generated by complexes **2.1** and **2.2**. Thus, the reaction of **2.1** with CO in benzene affords only the single ketone, (**3.8**), (Scheme 3.9), a fact that can be explained by the solution isomers of **2.1**, both of which have the methyl substituents of the allyl ligand proximal to the hydride ligand. The tertiary allyl carbon is the site of the allyl-hydride coupling, a feature that is reflected in the CHMe₂ terminus of the single organic product, **3.8**. In contrast, the same reaction of **2.3** produces two ketones, **3.9a** and **3.9b**, (Table 3.2). Again, the solution isomers of complex **2.3** are consistent with this result since **2.3** exists as four isomers in solution with the methyl substituent of the allyl ligand being proximal to the hydride ligand for two isomers and proximal to the nitrosyl ligand for the other two isomers (refer to Figure 2.2). These Cp*W(NO)(H)(η^3 -allyl) complexes also possess σ - π distorted allyl ligands which result in their having unequal C-C bond lengths. The shorter C-C linkage with the more sp^2 -character C terminus is situated *trans* to the nitrosyl in each complex.⁴³ It is this carbon that

is the site of coupling with the hydride ligand.³⁵ In other words, the substituents on the allyl ligand influence how it is coordinated to the metal center, and the σ - π distortion of the bound allyl ligand determines how it couples with the hydride ligand. These features are illustrated in Figure 3.12 to account for the production of the two ketones **3.9a** and **3.9b**.

Table 3.2. Ketones that result from the thermolysis of 2.1-2.3 in benzene under CO pressure

Complex	Product(s)	Isolated yield
2.1	 3.8	78
2.3	 3.9a 3.9b	54
2.2	 3.10	29

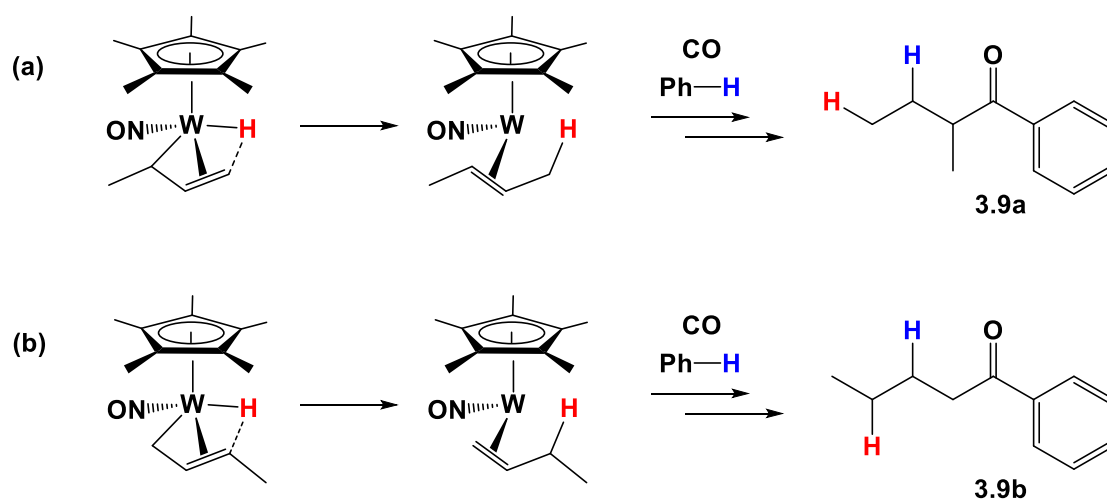


Figure 3.12. (a) Isomers of **2.3** with the methyl substituent of the allyl ligand proximal to the nitrosyl produce ketone **3.9a**. (b) Isomers of **2.3** with the methyl substituent proximal to the hydride ligand produce ketone **3.9b**.

The reaction of **2.2** with CO in benzene produces the single ketone, **3.10** (Scheme 3.10, Table 3.2), that does not follow the isomer trend observed for complexes **2.1** and **2.3**. This difference is probably an electronic effect due to the phenyl substituent on the allyl ligand. The two possible 16e η^2 -alkene intermediate complexes that **2.2** can generate contain either η^2 -MeCH=CHPh or η^2 -CH₂=CHCH₂Ph ligands. The reactive intermediate that contains the conjugated η^2 -*trans*- β -methylstyrene is likely favoured on electronic grounds and is consistent with the formation of ketone **3.10** (Figure 3.13). The yield of ketone from this reaction is markedly lower than for the reactions of **2.1** and **2.3**, which may in part be due to only 3% of **2.2** existing in solution as isomers with the phenyl substituent of the allyl ligand proximal to the hydride ligand.

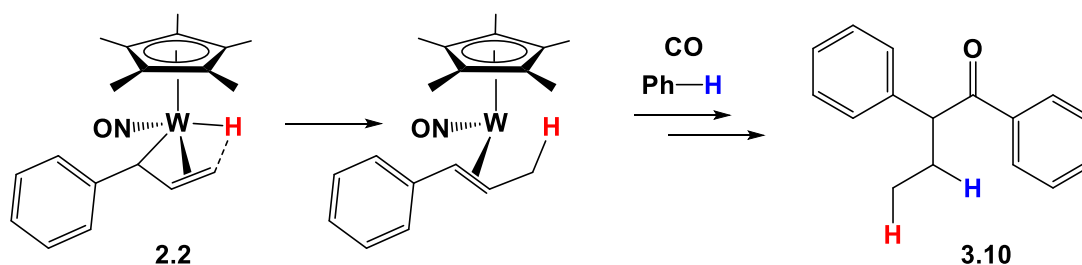
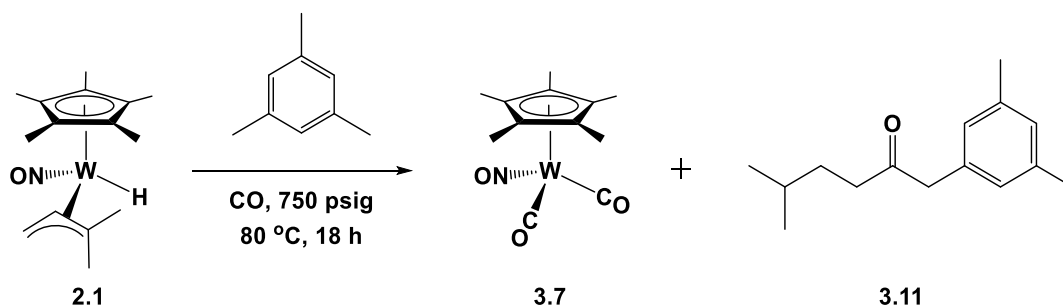


Figure 3.13. Coupling of the hydride to the methylene terminus of the allyl ligand results in the 16e intermediate complex $\text{Cp}^*\text{W}(\text{NO})(\eta^2\text{-trans-}\beta\text{-methylstyrene})$, which accounts for the formation of **3.10** as the only organic product observed.

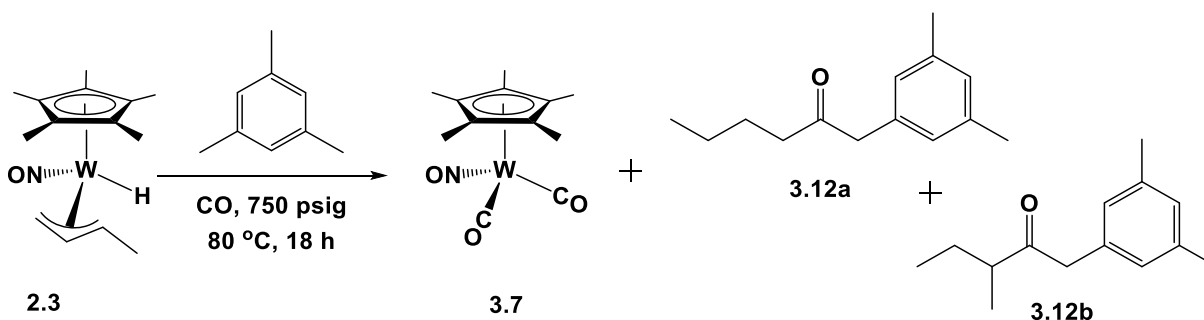
3.2.4.2 Reactions of **2.1** and **2.3** with Mesitylene Under CO Pressure

The reactions of **2.1** and **2.3** with CO in mesitylene parallel the reactions in benzene. Under identical reaction conditions, complex **2.1** gives a single organic product, namely 1-(3,5-dimethylphenyl)-5-methylhexan-2-one (**3.11**), in good yield (78%) (Scheme 3.11). Similarly, complex **2.3** affords the two ketones, 1-(3,5-dimethylphenyl)-3-methylpentan-2-one (**3.12a**) and 1-(3,5-dimethylphenyl)-hexan-2-one (**3.12b**), in moderate yield (50%) (Scheme 3.12). These organic products are analogous to those formed by **2.1** and **2.3** with CO and benzene. The reaction of complex **2.2** with CO in mesitylene does not afford the expected ketone or any organic product. Instead, a single organometallic complex that sheds some light as to the mechanism operative during these conversions is produced (see section 3.2.4.5).

Scheme 3.11. Reaction of 2.1 with mesitylene under CO pressure



Scheme 3.12. Reaction of 2.3 with mesitylene under CO pressure

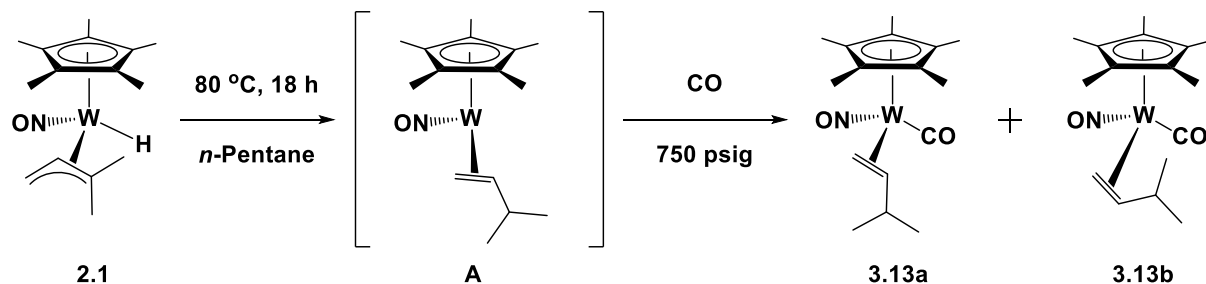


3.2.4.3 Thermolysis of 2.1 in *n*-Pentane Under CO Pressure

The reaction of **2.1** with CO in pentane does not afford a ketone resulting from pentane activation. Instead, the 18e CO adduct of the intermediate **A** can be isolated from the final reaction mixture (Scheme 3.13). Evidently **A** cannot effect the C-H activation of pentane before reacting with CO. The adduct $\text{Cp}^*\text{W}(\text{NO})(\text{CO})(\eta^2\text{-CH}_2\text{=CHCHMe}_2)$ (**3.13**) exists as two isomers in a 52:48 ratio that have been characterized by 1D and 2D NMR spectroscopies, IR spectroscopy, and mass spectrometry. The *dihapto* coordination of the olefin ligand to the tungsten center is established by characteristic ^{183}W satellites evident in the ^{13}C NMR spectrum

[i.e., major isomer **3.13a**: δ 37.3 ppm ($^1J_{\text{WC}} = 11.1$ Hz, CH=CH₂), 59.2 ppm ($^1J_{\text{WC}} = 38.8$ Hz, CH=CH₂); minor isomer **3.13b**: δ 25.8 ppm ($^1J_{\text{WC}} = 36.1$ Hz, CH=CH₂), 65.2 ppm ($^1J_{\text{WC}} = 9.9$ Hz, CH=CH₂)]. As shown in Scheme 3.13, the two isomers probably differ in the orientation of the CHMe₂ substituent on the bound olefin, which is consistent with the two solution isomers of **2.1** that the isomers of **3.13** are generated from. The infrared nitrosyl-stretching frequency for the mixture of isomers of **3.13** is 1614 cm⁻¹ while the carbonyl-stretching-frequency is 1951 cm⁻¹, which is indicative of a terminal CO ligand. The ¹³C NMR spectrum of **3.13** exhibits signals attributable to terminal carbonyls at δ 225.5 and 227.7 ppm for **3.13a** and **3.13b**, respectively.

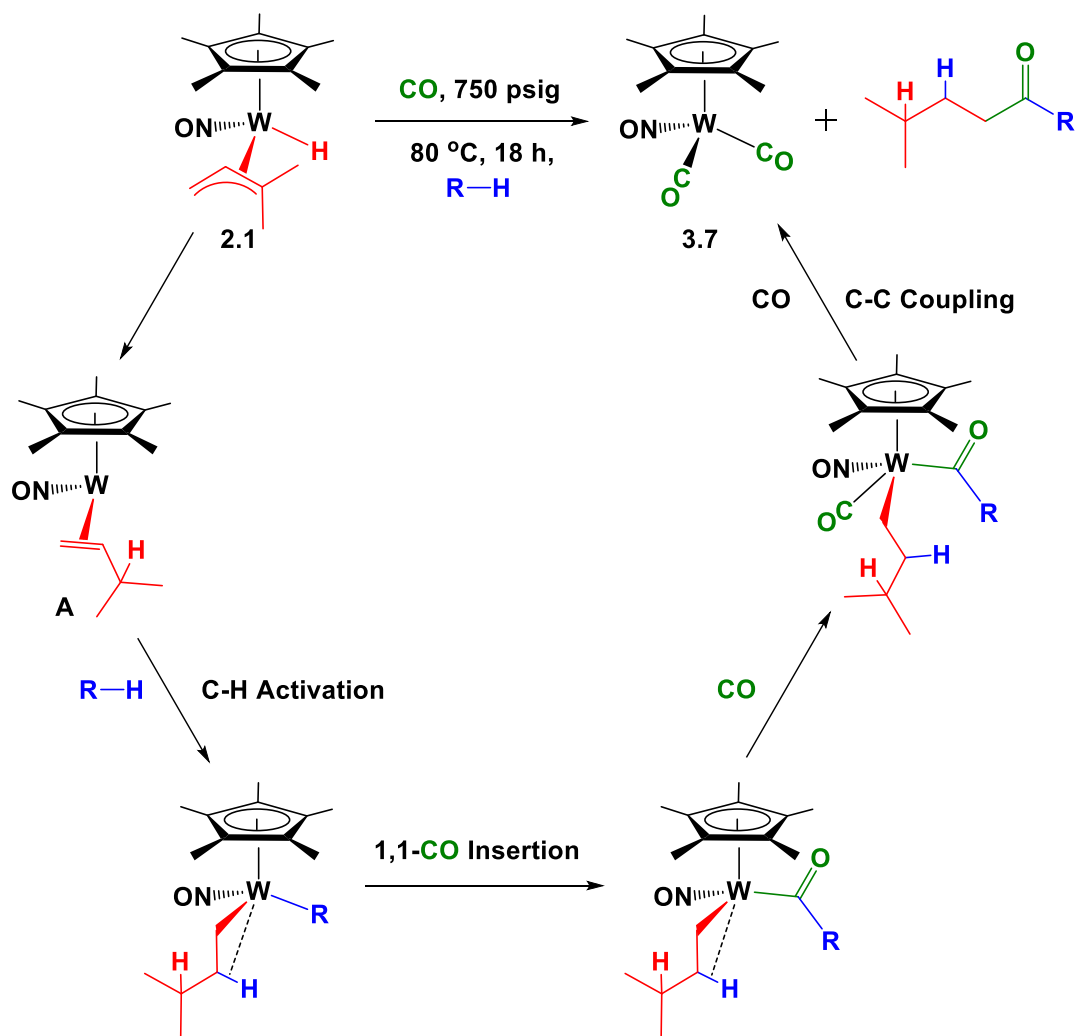
Scheme 3.13. Trapping of η^2 -alkene intermediate complex with CO



3.2.4.4 Mechanistic Considerations for the Regiospecific Generation of Ketones by **2.1**

The probable mechanism of the conversions involving benzene (Scheme 3.9) and mesitylene (Scheme 3.11) is outlined for complex **2.1** in Scheme 3.14 in which the organic reactants are represented by R-H for simplicity.

Scheme 3.14. Probable mechanism for the generation of regiospecific ketones by **2.1**



The key feature of the mechanism outlined in Scheme 3.14 is the formation of the 16e η^2 -alkene complex, $\text{Cp}^*\text{W}(\text{NO})(\eta^2\text{-CH}_2=\text{CHCHMe}_2)$ (**A**), which is generated by coupling of the hydride ligand to the tertiary carbon of the allyl ligand. This regiospecific migration is consistent with the solution molecular structures established for both isomers of **2.1** in which the two methyl substituents of the allyl ligand are proximal to the hydride. The 16e η^2 -alkene intermediate **A** has been trapped as its 18e CO adduct, complex **3.13**. Furthermore, the ketones

such as $\text{CH}_3\text{CH}_2\text{CMe}_2\text{C}(\text{O})\text{R}$ or $\text{Me}_2\text{CHCH}(\text{Me})\text{C}(\text{O})\text{R}$ [$\text{R} = \text{C}_6\text{H}_5$ or $\text{CH}_2(3,5\text{-Me}_2\text{C}_6\text{H}_3)$] resulting from hydride migration to the other allyl carbons have not been detected in the final reaction mixtures.

The C-H activation of hydrocarbon substrate follows the generation of intermediate **A** to give the 16e complex $\text{Cp}^*\text{W}(\text{NO})(\text{R})(\text{CH}_2\text{CH}_2\text{CHMe}_2)$. Formation of the CO adducts of **A** from the thermolysis of **2.1** in *n*-pentane under CO pressure suggests that if CO coordination precedes C-H activation, then the C-H activation does not occur and the reaction ends in the adduct formation. Therefore, for any ketone to be generated the C-H activation of the substrate must occur prior to any coordination of CO to the complex.

The next step of the mechanism involves the coordination and 1,1-insertion of a CO molecule into the W-C bond of the hydrocarbyl ligand to give the formally 16e acyl complex $\text{Cp}^*\text{W}(\text{NO})(\text{C}(\text{O})\text{R})(\text{CH}_2\text{CH}_2\text{CHMe}_2)$. It is worth noting the insertion of CO into the W-C bond of either ligand would result in the observed ketone product. Similar $\text{Cp}^*\text{W}(\text{NO})(\text{acyl})(\text{alkyl})$ complexes have been previously reported and are stabilized via a η^2 -acyl interaction.⁸²

Following the formation of the acyl complex a second CO molecule coordinates to form the 18e complex $\text{Cp}^*\text{W}(\text{NO})(\text{CO})(\text{C}(\text{O})\text{R})(\text{CH}_2\text{CH}_2\text{CHMe}_2)$. Experimental evidence for this proposed intermediate comes from the reaction of **2.1** with benzene at 80 °C for 16 h under 625 psig CO pressure. Analysis of the reaction mixture by IR spectroscopy (Figure 3.14) reveals the presence of **3.7** [IR (cm^{-1}) 1993 (s, ν_{CO}), 1914 (s, ν_{CO}), 1655 (s, ν_{NO})] as well as stretching-frequencies attributable to $\text{Cp}^*\text{W}(\text{NO})(\text{C}(\text{O})\text{C}_6\text{H}_5)(\text{CH}_2\text{CH}_2\text{CHMe}_2)$ (**3.14**) [IR (cm^{-1}) 1962 (s, ν_{CO}), 1694 (s, ν_{CO}), 1617 (s, ν_{NO})].⁵⁶ The carbonyl-stretching frequencies at 1962 and 1694 cm^{-1} are typical for a terminal metal carbonyl and an acyl ligand, respectively.^{37, 82} The nitrosyl-stretching frequency at 1617 cm^{-1} is lower relative to 18e nitrosyl complexes containing two π -

acceptor ligands (such as **3.7**) and higher relative to 18e Cp*W(NO)-containing complexes with no π -acceptor ligands (such as **2.1-2.3** or Cp*W(NO)(CH₂Me₃)(η^3 -allyl) complexes).^{27-29, 43, 44}

The existence of complex **3.14** is also supported by mass spectrometry with tungsten isotope patterns at 553 [M⁺, ¹⁸⁴W] and 525 [M⁺ – CO, ¹⁸⁴W].

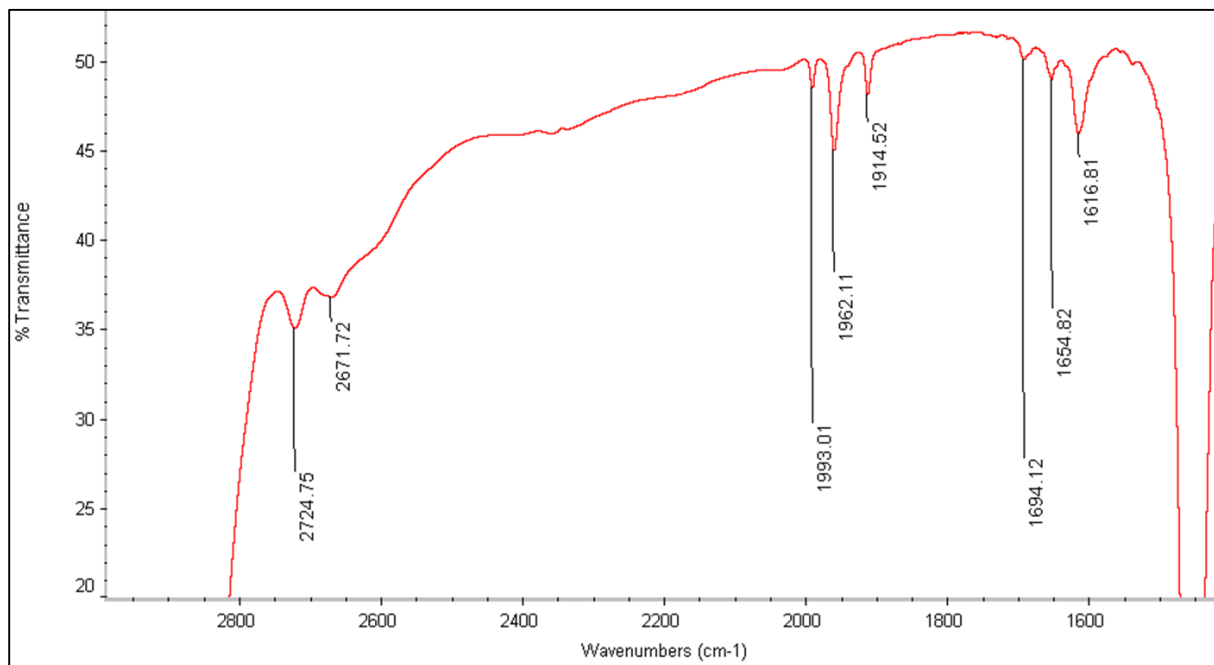


Figure 3.14. Expansion of the FT-IR spectrum (nujol mull) from 2900 cm⁻¹ to 1500 cm⁻¹ for the reaction of **2.1** with benzene under CO pressure.

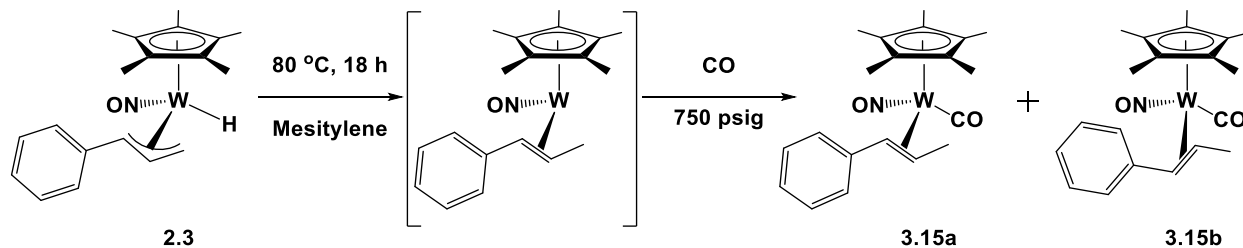
The final step on the proposed mechanism involves the coupling of acyl and alkyl ligands to give the ketone product (**3.8** or **3.11**). The remaining organometallic complex would be the 16e Cp*W(NO)(CO) complex which converts to **3.7** under CO pressure.

3.2.4.5 Thermolysis of **2.2** in Mesitylene Under CO Pressure

In contrast to complexes **2.1** and **2.3**, the reaction of **2.3** with CO in mesitylene does not lead to ketone formation, but rather affords the trapped η^2 -alkene complex, Cp*W(NO)(CO)(η^2 -MeCH=CHPh) (**3.15**) (Scheme 3.15). The reaction of **2.2** with mesitylene under CO pressure was carried out by Dr. Russell Wakeham while the solid-state characterization was performed by the author. As with the formation of **3.13** (vide supra), this outcome again reflects the kinetic discrimination between the two possible reaction pathways available to the η^2 -alkene intermediate complex. Complex **3.15** has been isolated as large orange plate crystals, and it exists as two isomers both in solution (**3.15a**: 63%; **3.15b**: 37%) and in the solid state (**3.15a**: 78%; **3.15b**: 22%) (Figure 3.15 and Figure 3.16). The two isomers differ with respect to the orientation of the η^2 -*trans*- β -methylstyrene ligand. The phenyl substituent of the ligand is proximal to the nitrosyl ligand in both isomers, but the ligand differs in the *exo/endo* orientation of its substituents. The benzylic H is oriented proximal to the C₅Me₅ ligand in the major isomer (Figure 3.15) and distal in the minor isomer (Figure 3.16). This feature is also evident in the solution structures of the isomers since the ¹H NMR spectrum of **3.15** confirms that the signal due to the benzylic H of **3.15a** has a greater upfield shift (δ 2.44 ppm) due to a stronger interaction with the tungsten-Cp* unit than does the signal for the benzylic H of **3.15b** (δ 4.06 ppm). (The relative upfield chemical shift of signals in the ¹H NMR spectrum due to a proton orientated toward the tungsten and Cp* ligand has been established by Sel ¹H NOE NMR for *exo* isomers of the hydride complexes **2.1-2.3** as well as for complex **3.4**.) The strong interaction between the tungsten center and the η^2 -alkene ligands is also evident by the lengthened C=C bonds of 1.428(9) Å and 1.40(3) Å for **3.15a** and **3.15b**, respectively. Consistently, the ¹³C

NMR spectrum of **3.15** contains alkene C signals at δ 50.8 and 55.5 ppm for **3.15a** and δ 43.8 and 59.8 ppm for **3.15b**, significantly more upfield than those for the free alkene. The infrared stretching frequencies of the nitrosyl and carbonyl ligands are 1616 cm^{-1} and 1956 cm^{-1} , and the ^{13}C NMR signals for the carbonyl ligands of the isomers occur at δ 226.1 ppm for **3.15a** and δ 225.2 ppm for **3.15b**. These spectroscopic properties are very similar to those exhibited by the related complexes **3.13a** and **3.13b**. Once formed, the CO adducts **3.13** and **3.15** are thermodynamically stable entities that evidently do not permit re-entry into the synthetic cycle under the experimental conditions employed (refer to Scheme 3.10).

Scheme 3.15. Trapping of η^2 -alkene intermediate complex from 2.2 with CO



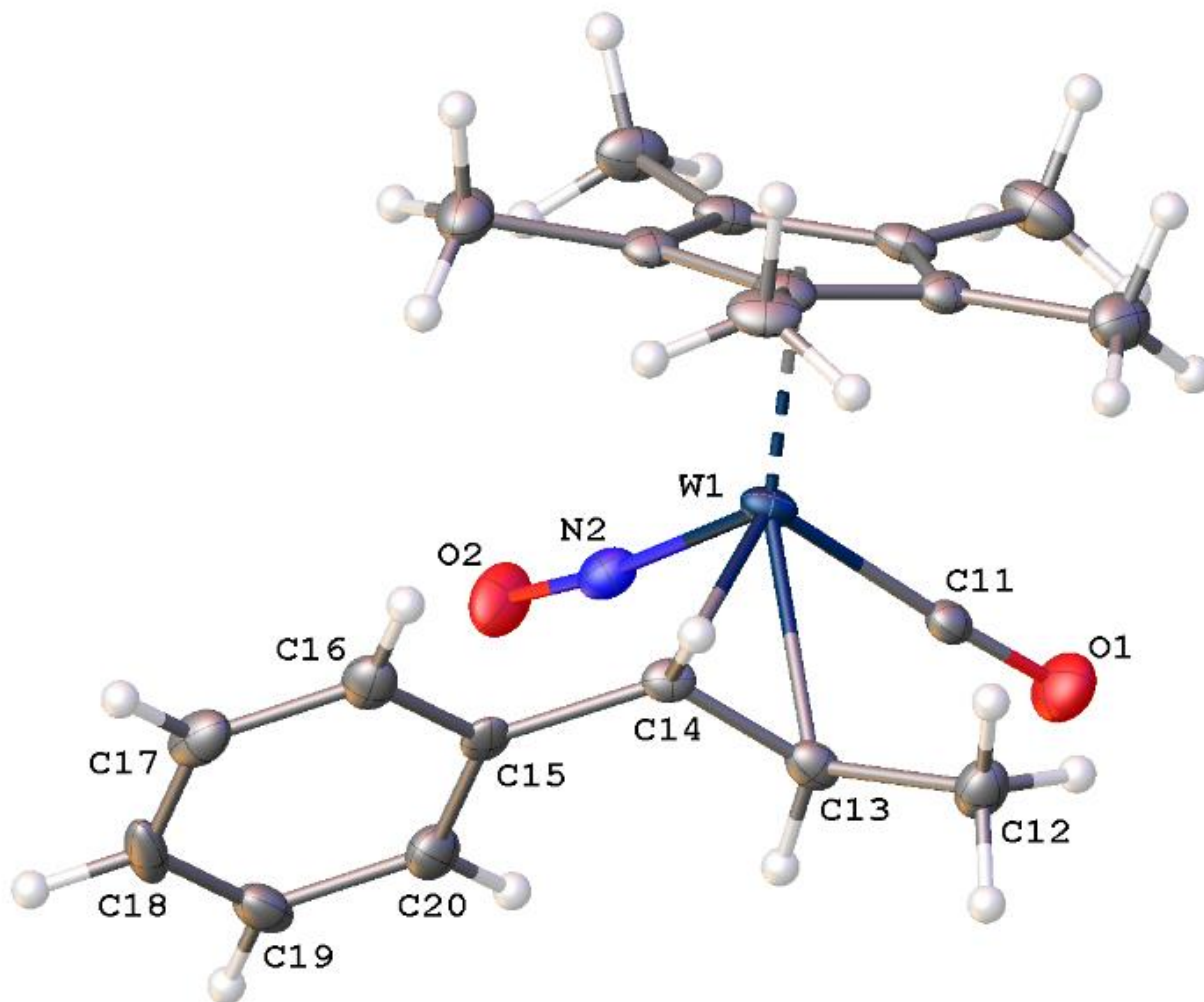


Figure 3.15. Solid-state molecular structure of **3.15a** with 50% probability thermal ellipsoids shown. Selected bond lengths (Å) and angles (deg.): W(1)-N(1) = 1.826(4), N(2)-O(2) = 1.200(5), W(1)-C(11) = 1.925(5), C(11)-O(1) = 1.174(6), W(1)-C(13) = 2.288(6), W(1)-C(14) = 2.254(6), C(12)-C(13) = 1.513(7), C(13)-C(14) = 1.428(9), C(14)-C(15) = 1.498(6), W(1)-N(2)-O(2) = 173.1(4), W(1)-C(11)-O(1) = 177.1(4), C(12)-C(13)-C(14) = 122.3(5), C(13)-C(14)-C(15) = 125.4(5).

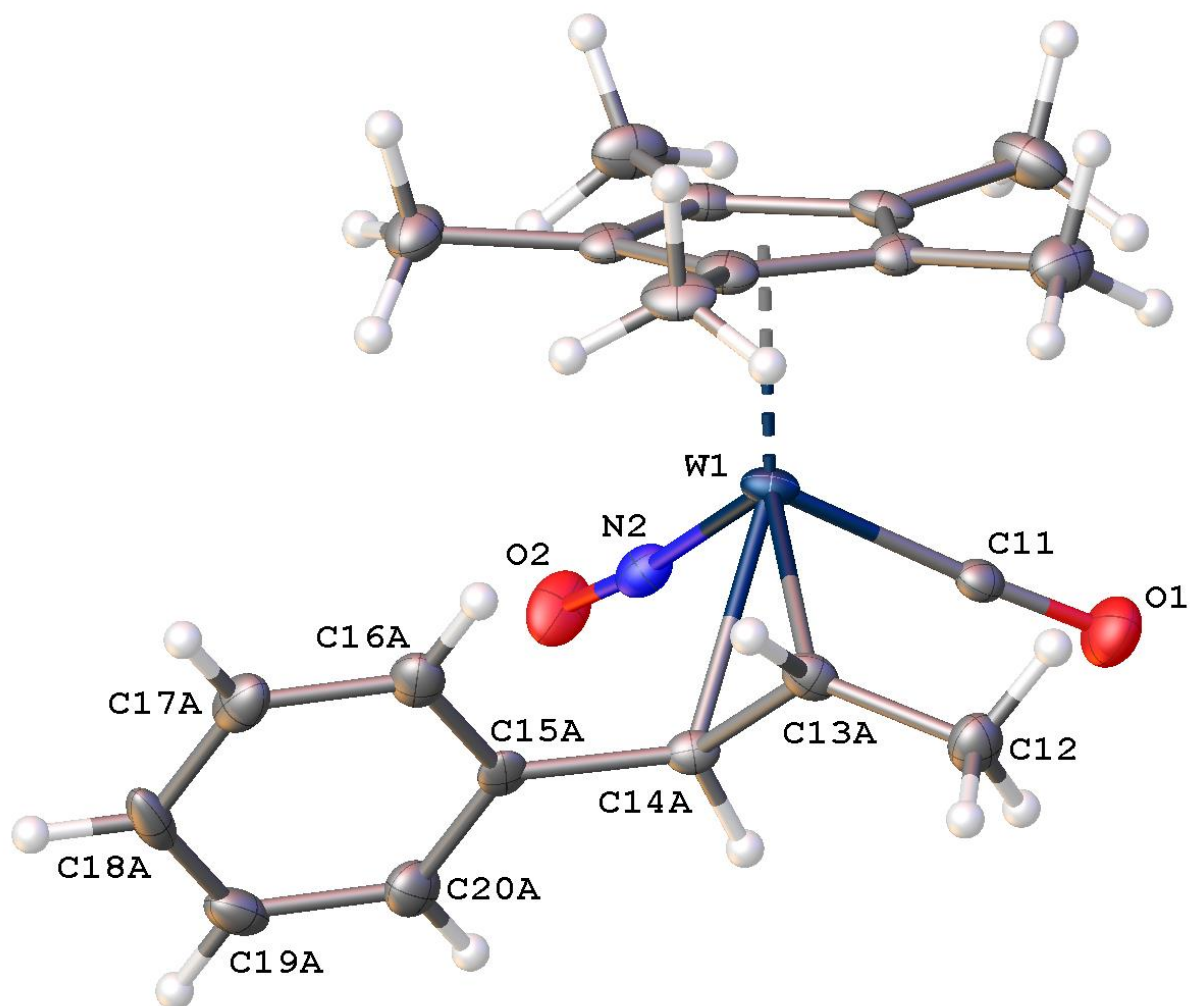


Figure 3.16. Solid-state molecular structure of **3.15b** with 50% probability thermal ellipsoids shown. Selected bond lengths (Å) and angles (deg.): W(1)-C(13A) = 2.27(2), W(1)-C(14A) = 2.30(2), C(12)-C(13A) = 1.42(2), C(13A)-C(14A) = 1.40(3), C(14A)-C(15A) = 1.50(2), C(12)-C(13A)-C(14A) = 126(2), C(13A)-C(14A)-C(15A) = 128(2).

3.2.4.6 Theoretical Considerations for the Formation of Unsymmetrical Saturated Ketones

DFT calculations on the transformation involving mesitylene and complex **2.1** (Scheme 3.11) were carried out by Dr. Guillaume Lefèvre and the results are summarized in Figure 4. The calculations corroborate the mechanistic proposal presented in Scheme 3.14. These calculations indicate that the first step is indeed the formation of the transient reactive 16e η^2 -alkene complex **A** (computed barrier: 75.7 kJ mol⁻¹, **TS1**). Complex **A** can then effect the C-H activation of one of the mesitylene C(sp³)-H bonds which also involves concerted migration of a hydrogen atom onto the ligated C=C double bond to lead to the bis(hydrocarbyl) 16e complex **B** with a barrier of 59.8 kJ mol⁻¹ (**TS2**). Complex **B** is also stabilized by a β -agostic C-H interaction as shown in Scheme 3.14. Coordination of a CO molecule onto the metal center in **B** affords complex **C**, and rapid migration (**TS3**) of the mesityl group onto the W-ligated carbonyl group (computed barrier for the two steps: 15.1 kJ mol⁻¹) results in the formation of complex **D** with a stabilization of 16.7 kJ mol⁻¹ with respect to complex **B**. Exothermic coordination of a CO molecule onto the metal in **D** can then take place, and complex **E** is thus obtained with a stabilization of 28.6 kJ mol⁻¹ with respect to **D**. Complex **E** then undergoes slow reductive coupling (75.9 kJ mol⁻¹, **TS4**) to lead to the η^2 -CO ligated (3-methylbutyl)(mesityl)ketone complex **F**. The large barrier to the conversion of 18e **E** to **F** explains why **3.14**, the analogous complex to **E** from the reaction of **2.1** with benzene under CO pressure, can be observed by IR spectroscopy and mass spectrometry. Further reaction of **F** with CO affords **3.7** and liberates the ketone **3.11** in an overall strongly exothermic process (overall stabilization of 232.9 kJ mol⁻¹ with respect to the reactants). This exothermicity leads to an overall non-reversible process which shifts all the preceding equilibria

towards the formation of **3.11**. In other words, the theoretical calculations confirm that the overall conversion is very thermodynamically favoured and that the rate-limiting steps are the formation of the η^2 -alkene complex (**A**) and the subsequent C-H activation of the hydrocarbon substrate by **A**.

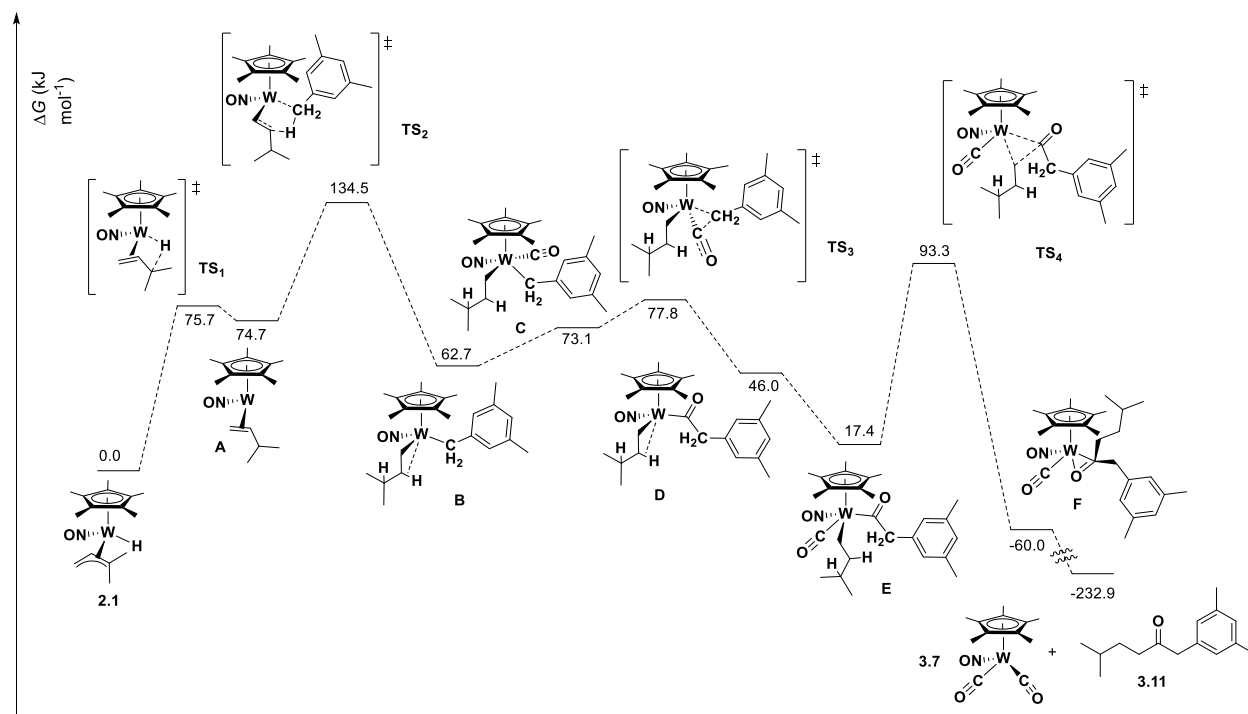


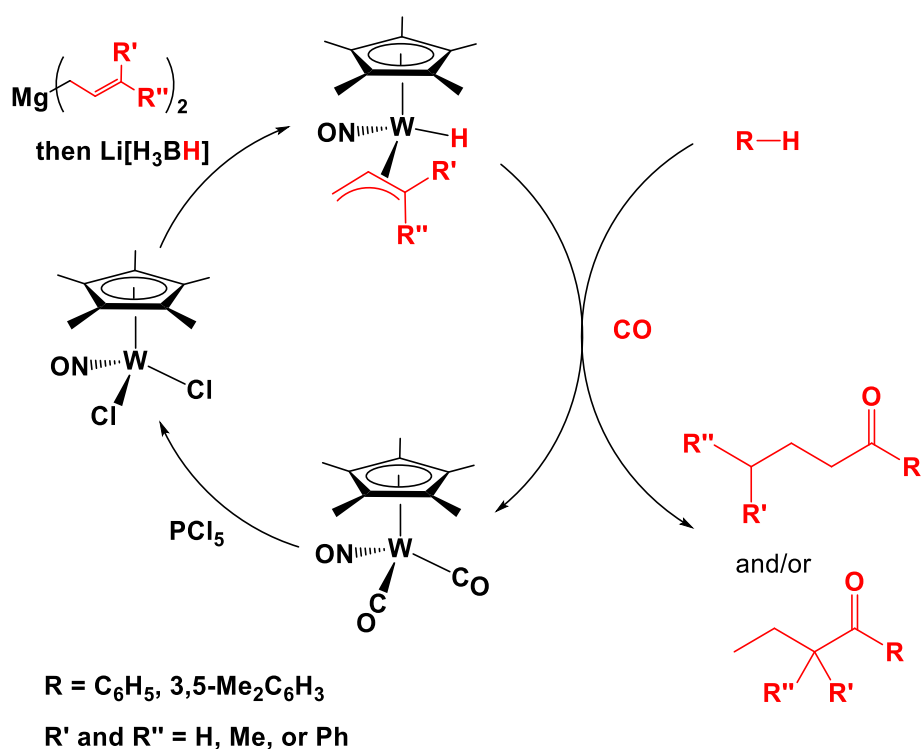
Figure 3.17. Computed ΔG values for the various species involved during the mesitylene reaction involving complex **2.1** shown in Scheme 3.11.

3.2.4.7 Recyclable Tungsten Cycle for Regiospecific Synthesis of Ketones from Hydrocarbons and CO

The reactions of the hydride complexes **2.1-2.3** with the appropriate hydrocarbon under CO pressure result in the formation of various ketones, but all have the same organometallic

product, the well-known complex **3.7**. Treatment of **3.7** with PCl_5 results in the formation of $\text{Cp}^*\text{W}(\text{NO})\text{Cl}_2$, from which the complexes **2.1-2.3** can be synthesized (refer to Scheme 2.2). Thus, the formation of **3.7** allows for the regeneration of the starting hydride complex, resulting in a complete synthetic cycle for the regiospecific synthesis of saturated unsymmetrical ketones from hydrocarbons and CO (Scheme 3.16).

Scheme 3.16. Synthetic cycle for forming saturated unsymmetrical ketones



Additionally, the ketones **3.8** and **3.11** can be synthesized from **2.1**, CO, and benzene or mesitylene without the rigorous exclusion of air and moisture. Benchtop-loading of a pressure vessel with **2.1** and undried benzene or mesitylene followed by thermolysis at 80 °C under 700 psig CO for 2 d affords decent yields of **3.8** (66%) and **3.11** (42%), respectively. These aerobic

ketone syntheses were carried out using optimized conditions which could account for some of the reduction in yield (for instance removal of the mesitylene in vacuo is tricky and product is lost due to bumping).

Complex **2.1** (as well as **2.2** and **2.3**) are used to effect the regiospecific synthesis of unsymmetrical ketones from unactivated hydrocarbon, a greenhouse gas molecule in CO,⁸⁴ and the allyl ligand (ultimately delivered via a magnesium binary reagent). This transformation may be effected without the exclusion of air and using undried solvents while the organometallic product can be reconverted to **2.1**, thereby recycling the tungsten complex.

Unsymmetrical saturated ketones are reagents that play a role in many organic transformations, hence their synthesis has garnered considerable interest.^{85,86,87} A commonly employed method to synthesize unsymmetrical ketones utilizes transition-metal mediated transformations such as carbonylative Stille reactions (Figure 3.18a). These reactions have downsides as requiring costly metals such as palladium or toxic reagents such as organotin compounds.^{88,89,90} Other synthetic options include the reactions of carboxylic acids and their derivatives such as acid chlorides and amides with organometallic reagents; however, these methods can often produce unwanted byproducts (Figure 3.18b).⁹¹ In addition, unsymmetrical unsaturated ketones can be obtained via the cross-coupling between two pre-existing ketones.⁹²

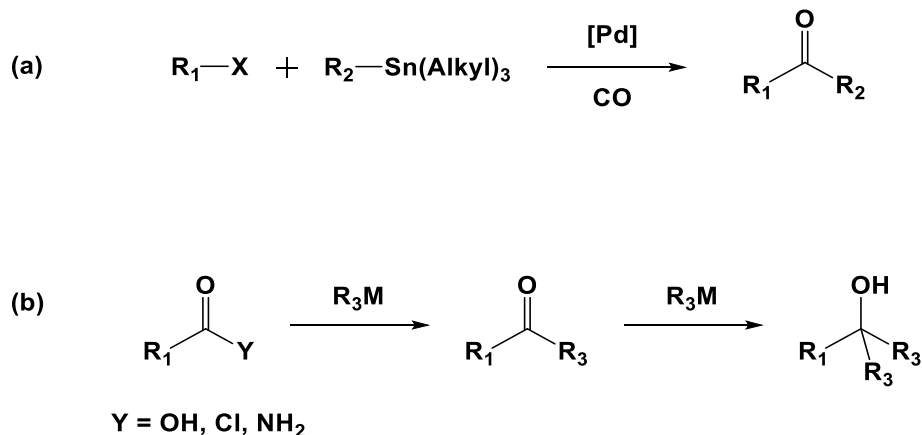


Figure 3.18. (a) Synthesis of an unsymmetrical ketone via carbonylative Stille Coupling. (b) Reaction of carboxylic acid derivatives with organometallic reagents to give unsymmetrical ketones and unwanted byproduct.

3.3 Summary

The work presented in this chapter has demonstrated that, unlike their 18e $\text{Cp}^*\text{W(NO)}(\text{CH}_2\text{CMe}_3)(\eta^3\text{-allyl})$ analogues, the three compounds $\text{Cp}^*\text{W(NO)}(\text{H})(\eta^3\text{-CH}_2\text{CHCMe}_2)$ (**2.1**), $\text{Cp}^*\text{W(NO)}(\text{H})(\eta^3\text{-CH}_2\text{CHCHPh})$ (**2.2**), and $\text{Cp}^*\text{W(NO)}(\text{H})(\eta^3\text{-CH}_2\text{CHCHMe})$ (**2.3**) do not simply effect the single, selective terminal activation of alkane C-H bonds intermolecularly. Rather, they effect two additional successive C-H activations of the hydrocarbon substrates to form new $\text{Cp}^*\text{W(NO)}(\text{H})(\eta^3\text{-allyl})$ complexes in which the allyl ligands result from the alkanes being activated. Consistently, complex **2.1** also effects the multiple C-H activations of 1-chloropropane and 1-chlorobutane and forms the corresponding $\text{Cp}^*\text{W(NO)}(\text{Cl})(\eta^3\text{-allyl})$ complexes. The reaction of **2.1** with *N*-methylmorpholine offers some insights into the operative mechanism for these multiple C-H activations as well as the insight

that the product of the initial single C-H activation can be trapped through coordination of a Lewis base.

Single C-H activation can be obtained in a way through the 1,1-insertion of CO into the W-C bond of the singly-activated hydrocarbyl ligand. In the presence of CO, complexes **2.1-2.3** can effect the regiospecific generation of saturated unsymmetrical ketones from hydrocarbons and CO gas via C-H activation and the formation of two new C-C bonds. The unactivated hydrocarbon substrates benzene and mesitylene are selected to provide examples of the generation of ketones from activation of both C(*sp*²)-H and C(*sp*³)-H bonds. These transformations are not only atom-economical, but also part of a complete synthetic cycle since Cp*W(NO)(CO)₂ (**3.7**) is the final organometallic product formed in all cases, and it can be readily reconverted to the hydrido allyl reactants **2.1-2.3** in three steps via Cp*W(NO)Cl₂. Furthermore, these unsymmetrical ketones incorporate CO, which is an indirect greenhouse gas molecule.⁸⁴ Finally, the organometallic reagents and product are air and moisture stable, making the reactions relatively straightforward to carryout.

3.4 Experimental

3.4.1 General Methods

All reactions and subsequent manipulations involving organometallic reagents were performed under anhydrous and anaerobic conditions except where noted. All inert gases were purified by passing them through a column containing MnO and then through a column of activated 4 Å molecular sieves. High vacuum and inert atmosphere techniques were performed

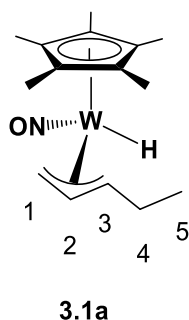
either in Innovative Technologies LabMaster 100 and MS-130 BG dual-station glove boxes equipped with freezers maintained at $-33\text{ }^{\circ}\text{C}$ or using double-manifold Schlenk lines. Preparative scale reactions were carried out using Schlenk or round bottom flasks; reactions were performed in thick-walled glass reaction bombs (larger scale) or J. Young NMR tubes (smaller scale), both of which were sealed by Kontes greaseless stopcocks. Reactions with gases were performed in a Parr 5500 pressure reactor vessel with a capacity of 0.3 L. Carbon monoxide was obtained from Praxair and used as received. Benzene, mesitylene, *n*-pentane, *n*-heptane, cyclohexane, and *N*-methylmorpholine were dried over sodium/benzophenone ketyl and were freshly distilled prior to use. Hexanes and ethyl acetate were not dried prior to use; all other solvents were dried according to standard procedures.⁵⁴

All IR spectra were recorded on a Thermo Nicolet Model 4700 FT-IR spectrometer, and the samples were prepared as Nujol mulls sandwiched between ZnCl_2 plates. All NMR spectra were recorded at room temperature on a Bruker AV-400 (direct and indirect probes) instrument, and all chemical shifts are reported in ppm and coupling constants are reported in Hz. ^1H NMR spectra were referenced to the residual protio isotopomer present in C_6D_6 (7.16 ppm) and CDCl_3 (7.27 ppm). ^{13}C NMR spectra were referenced to C_6D_6 (128.39 ppm) or CDCl_3 (77.0 ppm). Two-dimensional NMR experiments were used for the characterization of most complexes; $\{^1\text{H}-^1\text{H}\}$ COSY, $\{^1\text{H}-^{13}\text{C}\}$ HSQC, and $\{^1\text{H}-^{13}\text{C}\}$ HMBC, were performed to correlate and assign ^1H and ^{13}C NMR signals and establish atom connectivity; $\{^1\text{H}-^1\text{H}\}$ NOESY NMR was used for determination of solution molecular structures. Low-resolution mass spectra (EI, 70 eV) were recorded by Mr. Marshall Lapawa of the UBC mass spectrometry facility using a Kratos MS-50 spectrometer. Elemental analyses were performed by Mr. Derek Smith of the UBC microanalytical facility. X-ray crystallographic data collection, solution, and refinement were

performed at the UBC X-ray crystallography facility; data collection, solution, and refinement of **3.1**, **3.4** and **3.5** were performed by Dr. Brian Patrick.

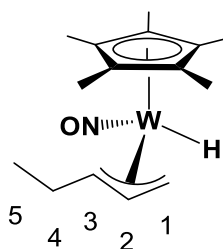
3.4.2 Thermolysis of **2.1** in *n*-Pentane

In a glove box a glass reaction bomb was charged with **2.1** (0.125 g, 0.298 mmol) and *n*-pentane (ca. 15 mL) to produce a yellow mixture. The bomb was sealed with a Kontes greaseless stopcock, and the contents were heated at 80 °C for 18 h. Solvent was removed from the final brown mixture in vacuo to obtain a brown residue. This residue was redissolved in a minimum of pentane, and the resulting solution was transferred to the top of a basic alumina column (0.5 x 4 cm) made up in pentane. Elution of the column using a gradient of 0-25% Et₂O in pentane produced a yellow band that was eluted. The solvent was removed from the yellow eluate in vacuo to obtain isomers of Cp*W(NO)(H)(η^3 -CH₂CHCHEt) (**3.1a-c**) and Cp*W(NO)(H)(η^3 -MeCHCHCHMe) (**3.1d**) as a yellow solid (0.066 g, 53% yield).⁶ The percentages in parentheses listed for each isomer reflect the relative ratio of the given isomer. For a detailed explanation of the isomers assignments refer to section 3.2.1.1.



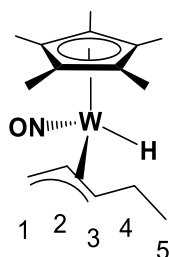
Characterization data for **3.1a** (64%): IR (cm⁻¹) 1595 (s, ν_{NO}). MS (LREI, m/z , probe temperature 150 °C) 419 [M^+ , ¹⁸⁴W]. ¹H NMR (400 MHz, C₆D₆): δ -1.40 (s, ¹ J_{WH} = 118, 1H,

WH), 0.18 (d, $^3J_{\text{HH}} = 10.2$, 1H, C1H₂), 1.10 (t, $^3J_{\text{HH}} = 7.4$, 3H, C5H₃), 1.75 (s, 15H, C₅Me₅), 1.83 (m, 1H, C3H), 2.36 (m, 1H, C4H₂), 2.49 (m, 1H, C4H₂), 2.80 (m, 1H, C1H₂), 4.58 (ddd, $^3J_{\text{HH}} = 13.3$, 10.2, 7.0, 1H, C2H), ^{13}C NMR (100MHz, C₆D₆): δ 11.0 (C₅Me₅), 17.7 (C5H₃), 28.2 (C4H₂), 39.1(C1H₂), 87.9 (C3H), 101.8 (C2H), 104.9 (C₅Me₅).



3.1b

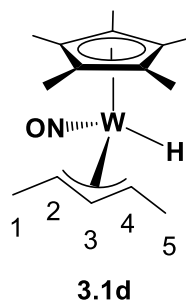
Characterization data for **3.1b** (18%): ^1H NMR (400 MHz, C₆D₆): δ -1.36 (s, $^1J_{\text{WH}} = 121$, 1H, WH), 0.62 (d, $^3J_{\text{HH}} = 13.4$, 1H, C1H₂), 1.05 (m, 1H, C3H), 1.18 (t, $^3J_{\text{HH}} = 7.4$, 3H, C5H₃), 1.73 (s, 15H, C₅Me₅), 2.13 (m, 2H, C4H₂), 4.11 (d, $^3J_{\text{HH}} = 7.2$, 1H, C1H₂), 4.33 (ddd, $^3J_{\text{HH}} = 13.3$, 10.0, 7.2, 1H, C2H), ^{13}C NMR (100MHz, C₆D₆): δ 10.8 (C₅Me₅), 18.9 (C5H₃), 27.6 (C4H₂), 52.4 (C1H₂), 67.5 (C3H), 103.3 (C2H), 104.8 (C₅Me₅).



3.1c

Characterization data for **3.1c** (11%): ^1H NMR (400 MHz, C₆D₆): δ (selected signals) - 1.25 (s, $^1J_{\text{WH}} = 122$, 1H, WH), 1.09 (t, $^3J_{\text{HH}} = 7.4$, 3H, C5H₃), 2.07 (m, 1H, C1H₂), 2.13 (m, 2H, C4H₂), 2.28 (dd, $^3J_{\text{HH}} = 12.7$, $^2J_{\text{HH}} = 1.8$, 1H, C1H₂), 2.84 (ddd, $^3J_{\text{HH}} = 13.6$, 12.7, 7.9, 1H, C2H),

3.68 (dt, $^3J_{\text{HH}} = 13.6, 6.8, 1\text{H}, \text{C3H}$). ^{13}C NMR (100MHz, C_6D_6): δ (selected signals) 19.6 (C5H_3), 28.4 (C4H_2), 38.9 (C1H_2), 84.4 (C3H), 96.8 (C2H), 104.9 (C_5Me_5).

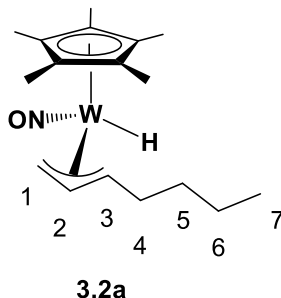


Characterization data for **3.1d** (7%): ^1H NMR (400MHz, C_6D_6): δ -1.40 (s, $^1J_{\text{WH}} 118, 1\text{H}, \text{WH}$), 0.76 (m, 1H, C2H), 1.63 (m, 1H, C2'H), 1.74 (s, 15H, C_5Me_5), 2.02 (d, $^3J_{\text{HH}} = 5.5, 3\text{H}, \text{C1H}_3$), 2.31 (dd, $^3J_{\text{HH}} = 5.9, ^2J_{\text{HH}} = 2.3, 3\text{H}, \text{C1H}_3$), 4.43 (dd, $^3J_{\text{HH}} = 12.9, 9.4, 1\text{H}, \text{C3H}$). ^{13}C NMR (100MHz, C_6D_6): δ 10.8 (C_5Me_5), 18.8 (C1H_3), 22.2 (C5H_3), 52.9 (C2H), 74.6 (C4H), 104.8 (C_5Me_5), 108.0 (C3H).

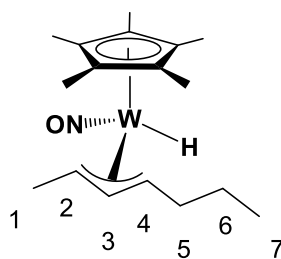
3.4.3 Thermolysis of **2.1** in *n*-Heptane

In a glove box a glass reaction bomb was charged with **2.1** (0.100 g, 0.239 mmol) and *n*-heptane (ca. 10 mL). The reaction bomb was sealed with a Kontes greaseless stopcock and then placed in an ethylene glycol bath at 80 °C. After 18 h a dark brown mixture had formed, and the solvent was removed in vacuo to obtain a dark brown residue. The crude reaction mixture was purified by column chromatography on basic alumina using a gradient of 0-20% EtOAc in hexanes. The $\text{Cp}^*\text{W}(\text{NO})(\text{H})(\eta^3\text{-C}_7\text{H}_{13})$ (**3.2**) product was obtained as a yellow oil (60 mg, 56% yield). At least eight isomers of complex **3.2** in C_6D_6 were identified by their *WH* signals with characteristic ^{183}W satellites in the ^1H NMR spectrum. The exact identity and orientation of the

allyl ligand could only be determined for the four largest isomers **3.2a-d**. The assignment of isomers was made using the multiplicity (dd or ddd) of the meso H signals and their relative chemical shifts in the ^1H NMR spectrum. The effect of the σ - π distortion on the chemical shifts of the allyl C signals was used to determine the orientation of the substituent(s) of the allyl ligand relative to the nitrosyl and hydride ligands.

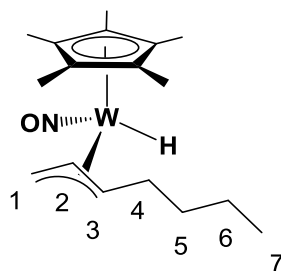


Characterization data for $\text{Cp}^*\text{W}(\text{NO})(\text{H})(\eta^3\text{-CH}_2\text{CHCH}(n\text{-C}_4\text{H}_9))$ (**3.2a**, 47%): IR (cm^{-1}) 1907 (w, ν_{WH}), 1594 (s, ν_{NO}). MS (LREI, m/z , probe temperature 120 $^\circ\text{C}$) 447 [M^+ , ^{184}W]. MS (HREI, m/z , ^{186}W) calcd for $\text{C}_{17}\text{H}_{29}\text{NO}^{186}\text{W}$: 449.17929, found: 449.17920. ^1H NMR (400 MHz, C_6D_6) δ -1.30 (s, $^1J_{\text{WH}} = 119.7$, 1H, WH), 0.20 (d, $^3J_{\text{HH}} = 10.2$, 1H, allyl C1H_2), 0.90 (t, $^3J_{\text{HH}} = 7.3$, 3H, C7H_3), 1.24-1.28 (overlapping m, 1H, C6H_2), 1.31-1.35 (overlapping m, 1H, C6H_2), 1.38-1.45 (overlapping m, 1H, C5H_2), 1.54-1.62 (overlapping m, 1H, C5H_2), 1.77 (s, 15H, C_5Me_5), 1.89 (m, 1H, allyl C3H), 2.39-2.49 (overlapping m, 2H, C4H_2), 2.81 (dt, $^3J_{\text{HH}} = 7.0$, $^2J_{\text{HH}} = 2.7$, 1H, allyl C1H_2), 4.61 (ddd, $^3J_{\text{HH}} = 13.1$, 10.2, 7.0, 1H, allyl C2H). ^{13}C NMR (100 MHz, C_6D_6) δ 10.8 (C_5Me_5), 14.4 (C7H_3), 23.1 (C6H_2), 35.4 (C4H_2), 36.2 (C5H_2), 39.2 (allyl C1H_2), 85.8 (allyl C3H), 102.6 (allyl C2H), 104.9 (C_5Me_5).



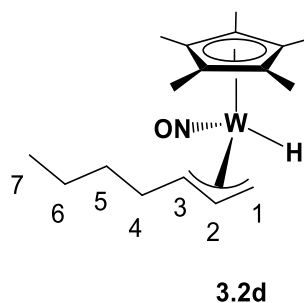
3.2b

Characterization data for $\text{Cp}^*\text{W}(\text{NO})(\text{H})(\eta^3\text{-MeCHCHCH}(n\text{-C}_3\text{H}_7))$ (**3.2b**, 29%): ^1H NMR (400 MHz, C_6D_6) δ -1.42 (s, $^1J_{\text{WH}} = 123.8$, 1H, *WH*), 0.80 (m, 1H, allyl *C2H*), 0.92 (t, $^3J_{\text{HH}} = 7.4$, 3H, *C7H3*), 1.39-1.46 (overlapping m, 1H, *C6H2*), 1.59-1.66 (overlapping m, 1H, *C6H2*), 1.61-1.70 (overlapping m, 1H, allyl *C4H2*), 1.75 (s, 15H, *C5Me5*), 2.03 (d, $^3J_{\text{HH}} = 5.7$, 1H, allyl *C1H3*), 2.40-2.50 (overlapping m, 2H, *C5H2*), 4.44 (dd, $^3J_{\text{HH}} = 12.9$, 9.4, 1H, allyl *C3H*). ^{13}C NMR (100 MHz, C_6D_6) δ 11.0 (*C5Me5*), 14.6 (*C7H3*), 18.9 (*C1H3*), 27.5 (*C6H2*), 38.1 (*C5H2*), 53.1 (allyl *C2H*), 81.6 (allyl *C4H*), 104.1 (*C5Me5*), 106.1 (allyl *C3H*).



3.2c

Characterization data for $\text{Cp}^*\text{W}(\text{NO})(\text{H})(\eta^3\text{-CH}_2\text{CHCH}(n\text{-C}_4\text{H}_9))$ (**3.2c**, 9%): ^1H NMR (400 MHz, C_6D_6) δ (selected signals) -1.20 (s, $^1J_{\text{WH}} = 121.3$, 1H, *WH*), 1.73 (s, 15H, *C5Me5*), 2.88 (ddd, $^3J_{\text{HH}} = 13.3$, 12.9, 7.8, 1H, allyl *C2H*), 3.69 (m, 1H, allyl *C3H*). ^{13}C NMR (100 MHz, C_6D_6) δ (selected signals) 82.0 (allyl *C3H*), 97.6 (allyl *C2H*).

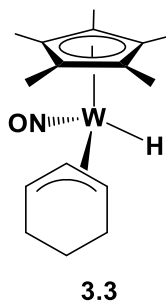


Characterization data for $\text{Cp}^*\text{W}(\text{NO})(\text{H})(\eta^3\text{-CH}_2\text{CHCH}(n\text{-C}_4\text{H}_9))$ (**3.2d**, 6%): ^1H NMR (400 MHz, C_6D_6) δ (selected signals) -1.34 (s, $^1J_{\text{WH}} = 122.1$, 1H, *WH*), 0.64 (d, $^3J_{\text{HH}} = 13.5$, 1H, allyl C1H_2), 1.06-1.10 (overlapping m, 1H, allyl C3H), 1.72 (s, 15H, C_5Me_5), 2.13-2.20 (overlapping m, 2H, C4H_2), 4.12 (m, 1H, allyl C1H_2), 4.35 (ddd, $^3J_{\text{HH}} = 13.5, 10.2, 7.4$, 1H, allyl C2H). ^{13}C NMR (100 MHz, C_6D_6) δ (selected signals) 34.4 (C4H_2), 52.3 (allyl C1H_2), 65.6 (allyl C3H), 104.1 (allyl C2H).

Other diagnostic *WH* singlets with ^{183}W satellites occurred in the ^1H NMR spectrum of **3.2** at -1.53 ($^1J_{\text{WH}} = 122.5$, 2%), -1.39 ($^1J_{\text{WH}} = 122.9$, 3%), -0.94 ($^1J_{\text{WH}} = 123.6$, 1%), and -0.87 ($^1J_{\text{WH}} = 120.9$, 3%).

3.4.4 Thermolysis of **2.1** in Cyclohexane

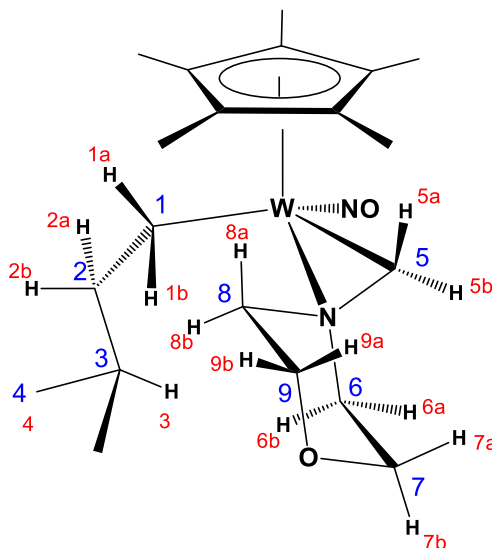
In a glove box, a glass reaction bomb was charged with **2.1** (0.100 g, 0.239 mmol) and cyclohexane (ca. 10 mL) to obtain a yellow solution. The bomb was placed in an ethylene-glycol bath, and its contents were heated at 80 °C for 18 h to produce a brown mixture. Solvent was removed from the final mixture in vacuo to obtain a brown residue. Analysis of the residue by ^1H NMR spectroscopy revealed a 33% conversion of **2.1** to the previously reported complex, $\text{Cp}^*\text{W}(\text{NO})(\text{H})(\eta^3\text{-C}_6\text{H}_{11})$ (**3.3**).²⁶



Characterization data for **3.3**: ^1H NMR (400 MHz, C_6D_6) δ -0.57 (s, $^1J_{\text{WH}} = 132.2$, 1H, WH), 1.16 (m, 1H, cyclohexyl CH_2), 1.42 (m, 1H, cyclohexyl CH_2), 1.70 (s, 15H, C_5Me_5), 2.47 (m, 1H, cyclohexyl CH_2), 2.58 (m, 1H, cyclohexyl CH_2), 2.62 (m, 2H, cyclohexyl CH_2), 2.75 (m, 1H, allyl CH), 3.59 (m, 1H, allyl CH), 5.30 (m, 1H, meso CH).

3.4.5 Reaction of **2.1** with *N*-Methylmorpholine

In a glove box a glass reaction bomb was charged with **2.1** (0.160 g, 0.382 mmol) and dissolved in *N*-methylmorpholine (ca. 10 mL) to produce a bright yellow solution. The stirred contents of the bomb were heated at 80 °C for 18 h whereupon the mixture darkened in color. The solvent was removed in vacuo from the final mixture, and the residue was recrystallized from 1:1 Et_2O /hexanes in air at room temperature to obtain yellow crystals of $\text{Cp}^*\text{W}(\text{NO})(\eta^2\text{-CH}_2\text{NC}_4\text{H}_8\text{O})(\eta^1\text{-CH}_2\text{CH}_2\text{CHMe}_2)$ (**3.4**) (0.135 g, 68% yield).

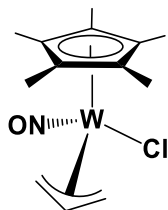


Characterization data for **3.4**: IR (cm^{-1}) 1522 (s, ν_{NO}). MS (LREI, m/z , probe temperature 150 °C) 520 [M^+ , ^{184}W]. MS (HREI, m/z , ^{182}W) calcd for $\text{C}_{20}\text{H}_{36}\text{N}_2\text{O}_2^{182}\text{W}$: 518.22590, found: 518.22613. ^1H NMR (400 MHz, C_6D_6) δ 0.49 (d, $^3J_{\text{HH}} = 5.8$, 1H, H_{5a}), 0.56 (m, 1H, H_{8a}), 0.71 (dt, $^3J_{\text{HH}} = 4.7$, $^2J_{\text{HH}} = 12.3$, $^2J_{\text{WH}} = 3.1$, 1H, $1Ha$), 1.10 (dt, $^3J_{\text{HH}} = 5.1$, $^2J_{\text{HH}} = 12.3$, $^2J_{\text{WH}} = 4.4$, 1H, $1Hb$), 1.26 (d, $^3J_{\text{HH}} = 6.7$, 6H, H_4), 1.66 (s, 15H, C_5Me_5), 1.84 (nonet, $^3J_{\text{HH}} = 6.7$, 1H, H_3), 2.00 (d, $^3J_{\text{HH}} = 5.8$, 1H, H_{5b}), 2.20 (m, 1H, H_{2a}), 2.27 (m, 1H, H_{6a}), 2.28 (m, 1H, H_{2b}), 3.03 (m, 1H, H_{8b}), 3.29 (overlapping m, 1H, $\text{C}9\text{H}_2$), 3.30 (overlapping m, 1H, $\text{C}9\text{H}_2$), 3.33 (overlapping m, 1H, H_{7b}), 3.42 (m, 1H, H_{7a}), 3.55 (m, 1H, H_{6b}). ^{13}C APT NMR (100 MHz, C_6D_6) δ 10.3 (C_5Me_5), 21.5 ($\text{C}1\text{H}_2$), 23.4 ($(\text{C}4\text{H}_3)_2$), 35.3 ($\text{C}3\text{H}$), 44.2 ($\text{WC}5\text{H}_2\text{N}$), 45.8 ($\text{C}2\text{H}_2$), 56.5 ($\text{NC}8\text{H}_2$), 59.7 ($\text{NC}6\text{H}_2$), 65.3 ($\text{C}9\text{H}_2\text{O}$), 67.1 ($\text{C}7\text{H}_2\text{O}$), 106.2 (C_5Me_5).

3.4.6 Reaction of **2.1** with 1-Chloropropane

In a glove box a glass reaction bomb was charged with **2.1** (0.100 g, 0.239 mmol) and 1-chloropropane (ca. 10 mL, anhydrous and degassed with argon) to produce a yellow solution.

The bomb was sealed with a Kontes greaseless stopcock, and the contents of the bomb were heated at 80 °C for 18 h to obtain a dark green mixture. The solvent was removed from the final mixture in vacuo to obtain a brown solid that was washed with pentane to obtain Cp*W(NO)(η^3 -CH₂CHCH₂)Cl (**3.5**) as an orange solid (66 mg, 65% yield). Single crystals of **3.5** suitable for X-ray diffraction were grown by slow evaporation of a C₆D₆ solution under a N₂ atmosphere.



3.5

Characterization data for **3.5**. IR (cm⁻¹) 1605 (s, ν_{NO}). MS (LREI, m/z , probe temperature 150 °C) 425 [M^+ , $^{184}\text{W}^{35}\text{Cl}$]. MS (HREI, m/z , ^{182}W) calcd for C₁₃H₂₀NO³⁵Cl¹⁸²W: 423.07157, found: 423.07135. ¹H NMR (400 MHz, C₆D₆) δ 0.70 (d, $^3J_{\text{HH}} = 7.0$, 1H, allyl CH₂), 1.53 (s, 15H, C₅Me₅), 1.92 (m, 1H, allyl CH₂), 3.08 (d, $^3J_{\text{HH}} = 13.9$, 1H, allyl CH₂), 4.01 (dd, $^3J_{\text{HH}} = 7.2$, $^2J_{\text{HH}} = 3.5$, 1H, allyl CH₂), 5.86 (m, 1H, allyl CH). ¹³C NMR (100 MHz, C₆D₆) δ 10.3 (C₅Me₅), 43.7 (allyl CH₂), 92.0 (allyl CH₂), 109.6 (C₅Me₅), 115.7 (allyl CH). Anal. Calcd for C₁₃H₂₀NO³⁵Cl: C, 36.69; H, 4.74; N, 3.29. Found: C, 36.37; H, 4.75; N, 3.24.

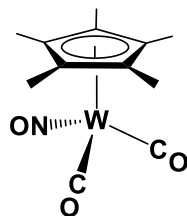
3.4.7 Reaction of **2.1** with 1-Chlorobutane

In a glove box a reaction flask was charged with **2.1** (0.100 g, 0.239 mmol), a magnetic stir bar, and 1-chlorobutane (ca. 8 mL, anhydrous and degassed with argon), and the flask was sealed with a Kontes greaseless stopcock. The reaction flask was removed from the glove box,

and its contents were heated in an ethylene glycol bath at 80 °C for 18 h. The reaction mixture was then allowed to cool to room temperature while being stirred. Removal of excess 1-chlorobutane in vacuo left behind a dark green, oily residue. This oil was washed with pentane to obtain 0.0930 g (89% yield) of $\text{Cp}^*\text{W}(\text{NO})(\eta^3\text{-CH}_2\text{CHCHMe})\text{Cl}$ (**3.6**) as a green solid. Characterization of **3.6** was performed by Dr. Russell Wakeham.⁴⁵

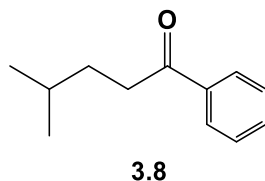
3.4.8 Reaction of **2.1** with Benzene and CO; Preparation of 4-Methyl-1-phenylpentan-1-one (**3.8**)

In a glove box, a Parr 5500 reactor was charged with **2.1** (0.300 g, 0.716 mmol) and dried benzene (ca. 75 mL), producing a yellow solution. The reactor was sealed, removed from the glove box, and then purged three times with carbon monoxide. The reactor was pressurized to 750 psig CO, and its contents were stirred and heated at 80 °C for 18 h to produce an orange solution. The solvent was reduced in volume in vacuo to obtain a concentrated reaction mixture that was then purified by column chromatography on silica, the products being eluted independently using a gradient of 0-5% ethyl acetate in hexanes. The products of the reaction were identified as $\text{Cp}^*\text{W}(\text{NO})(\text{CO})_2$ (**3.7**) (14 mg, 5% yield) and **3.7** (98.2 mg, 78% yield).



3.7

Characterization data for **3.7** which agrees well with that previously reported.⁵⁶ IR (cm⁻¹) 1993 (s, ν_{CO}), 1914 (s, ν_{CO}), 1655 (s, ν_{NO}). ¹H NMR (400 MHz, CDCl₃) δ 2.15 (s, 15H, C₅Me₅). ¹³C NMR (100 MHz, CDCl₃) δ 10.6 (C₅Me₅), 104.7 (C₅Me₅), 222.7 (¹J_{HH} = 203.1, W-CO).

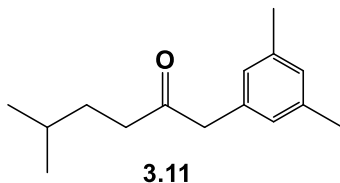


Characterization data for **3.8**, which agrees well with that previously reported.⁹³ IR (cm⁻¹) 1694 (s, ν_{CO}). MS (LREI, m/z , probe temperature 150 °C) 176 [M⁺]. ESI-MS theoretical m/z for [M+H]⁺ = 177.1; found m/z for [M+H]⁺ = 177.2. MS (LREI, m/z , probe temperature 150 °C) 176 [M⁺], 105 [M⁺ - C₅H₁₁], 77 [M⁺ - C(=O)C₅H₁₁]. ¹H NMR (400 MHz, CDCl₃) δ 0.96 (d, ³J_{HH} = 5.8, 6H, Me), 1.619 (m, 2H, CH₂), 1.622 (m, 1H, CH), 2.97 (t, ³J_{HH} = 7.7, 2H, CH₂C(=O)), 7.46 (t, ³J_{HH} = 7.4, 2H, *m*-aryl H), 7.55 (t, ³J_{HH} = 7.4, 1H, *p*-aryl H), 7.97 (d, ³J_{HH} = 7.4, 2H, *o*-aryl H).⁹⁴ ¹³C{¹H} NMR (100 MHz, CDCl₃) δ 22.4, 27.8, 33.2, 36.5, 128.0, 128.5, 132.8, 137.0, 200.6.⁹⁵

3.4.9 Reaction of **2.1** with Mesitylene and CO; Preparation of 1-(3,5-Dimethylphenyl)-5-methylhexan-2-one (**3.11**)

A Parr 5500 reactor was charged with **2.1** (0.300 g, 0.716 mmol) and mesitylene (ca. 20 mL). The reactor was sealed and purged with CO gas and finally pressurized to 750 psig CO. The contents were heated to 80 °C while being stirred for 18 h. The reactor was then cooled, and the gas was carefully vented. The final dark red reaction mixture was collected, and the mesitylene was then removed by flash chromatography on silica using a gradient of 0-5% EtOAc

in hexanes. The resulting crude product was further purified by column chromatography on silica using a gradient of 0-30% EtOAc in hexanes. The organic product **3.11** was obtained in good yield (122 mg, 78%). The organometallic product **3.7**⁵⁶ was also isolated from the reaction mixture (33 mg, 11% yield), but much of it was lost with the mesitylene during the first separation.

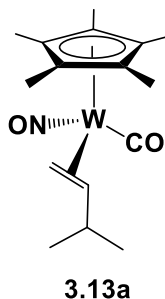


Characterization data for **3.11**: IR (cm⁻¹) 1717 (s, ν_{CO}). MS (LREI, m/z , probe temperature 150 °C) 218 [M⁺]. ¹H NMR (400 MHz, CDCl₃) δ 0.85 (d, ³ J_{HH} = 6.3, 6H, CHMe₂), 1.39-1.54 (m, overlapped, 1H, CHMe₂), 1.39-1.54 (m, overlapped, 2H, CH₂CHMe₂), 2.30 (s, 6H, ArMe₂), 2.44 (t, ³ J_{HH} = 7.3, 2H, (C=O)CH₂CH₂CH), 3.61 (s, 2H, ArCH₂(C=O)CH₂), 6.82 (s, 2H, *o*-aryl *H*), 6.90 (s, 1H, *p*-aryl *H*).⁹⁶ ¹³C NMR (100 MHz, CDCl₃) δ 21.2, 22.3, 27.6, 32.6, 40.0, 50.0, 127.2, 128.6, 134.2, 138.2, 209.1.⁹⁷

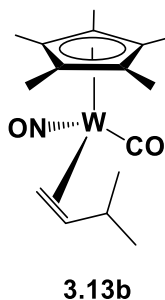
3.4.10 Preparation of Cp*W(NO)(CO)(η^2 -CH₂=CHCHMe₂) (**3.13**).

A Parr 5500 reactor was charged with **2.1** (0.200 g, 0.477 mmol) and *n*-pentane (ca. 100 mL). The reactor was sealed and purged with CO gas and finally pressurized to 750 psig CO. The contents were heated to 80 °C while being stirred for 18 h. The reactor contents were then cooled to room temperature, and the gas was carefully vented. The final orange reaction mixture was collected, and the solvent was removed in vacuo to obtain a dark orange oily residue. The crude product was purified via flash column chromatography on silica eluted with a gradient 0-

100% EtOAc in hexanes. Two isomers of **3.13** were isolated as an orange solid (28 mg, 13% yield). (Note: the percentages in listed in parentheses represent the isomer ratio observed in the ^1H NMR spectrum.)



Characterization data for **3.13a** (52%): IR (cm^{-1}), 1951 (s, ν_{CO}) 1614 (s, ν_{NO}). MS (LREI, m/z , probe temperature 150 $^{\circ}\text{C}$) 447 [M^+ , ^{184}W], 419 [$\text{M}^+ - \text{CO}$, ^{184}W], 417 [$\text{M}^+ - \text{NO}$, ^{184}W]. ^1H NMR (600 MHz, C_6D_6) δ 0.898 (obscured, 1H, $\text{CH}=\text{CH}_2$), 1.24 (d, $^3J_{\text{HH}} = 6.3$, 3H, CHMe_2), 1.29 (d, $^3J_{\text{HH}} = 6.3$, 3H, CHMe_2), 1.60 (s, 15H, C_5Me_5), 1.65 (obscured, 1H, CHMe_2), 1.68 (m, 1H, $\text{CH}=\text{CH}_2$), 2.43 (dd, $^3J_{\text{HH}} = 9.8$, $^2J_{\text{HH}} = 4.4$, 1H, $\text{CH}=\text{CH}_2$). ^{13}C APT NMR (150 MHz, C_6D_6) δ 10.3 (C_5Me_5), 24.4 (CHMe_2), 30.1 (CHMe_2), 37.3 (s, $^1J_{\text{WC}} = 11.1$, $\text{CH}=\text{CH}_2$), 38.6 (CHMe_2), 59.2 (s, $^1J_{\text{WC}} = 38.8$, $\text{CH}=\text{CH}_2$), 104.52 (C_5Me_5), 225.5 (W-CO).



Characterization data for **3.13b** (48%): ^1H NMR (600 MHz, C_6D_6) δ 0.88 (m, 1H, $\text{CH}=\text{CH}_2$), 0.900 (d, $^3J_{\text{HH}} = 6.8$, 3H, CHMe_2), 1.39 (d, $^3J_{\text{HH}} = 6.6$, 3H, CHMe_2), 1.60 (s, 15H, C_5Me_5), 1.969 (m, 1H, $\text{CH}=\text{CH}_2$), 1.973 (m, 1H, $\text{CH}=\text{CH}_2$), 2.90 (m, 1H, CHMe_2). ^{13}C APT

NMR (150 MHz, C₆D₆) δ 10.4 (C₅Me₅), 20.5 (CHMe₂), 25.8 (s, ¹J_{WC} = 36.1, CH=CH₂), 28.9 (CHMe₂), 33.6 (CHMe₂), 65.2 (s, ¹J_{WC} = 9.9, CH=CH₂), 104.54 (C₅Me₅), 227.7 (W-CO).

3.4.11 Preparation of Unsymmetrical Ketones Under Aerobic Conditions

3.4.11.1 Aerobic Preparation of **3.8** from **2.1** and Benzene Under CO Pressure

In the air, a Parr 5500 reactor was charged with **2.1** (0.119 g, 0.284 mmol) and undried benzene (ca. 50 mL). The reactor was sealed and then cycled with CO gas (3 x 500 psig) and then pressurized with 700 psig CO. The contents were heated to 80 °C and then were stirred for 2 d, after which time the gas was carefully vented. An orange solution was collected and then the solvent was removed in vacuo to afford an orange residue. The organic product **3.8** was identified by ¹H and ¹³C NMR spectroscopy, IR spectroscopy, and mass spectrometry. A yield of 33.1 mg (66 % yield) was determined by ¹H NMR spectroscopy.

3.4.11.2 Aerobic Preparation of **3.11** from **2.1** and Mesitylene under CO Pressure

In the air, a Parr 5500 reactor was charged with **2.1** (0.145 g, 0.346 mmol) and undried mesitylene (ca. 50 mL). The reactor was sealed and then cycled with CO gas (3 x 500 psig) and then pressurized with 700 psig CO. The contents were heated to 80 °C and the contents were stirred for 2 d. The contents of the reactor were then cooled and the gas was vented. A dark red-orange mixture was collected and then the solvent was removed in vacuo to afford red residue. The organic product **3.11** was identified by ¹H and ¹³C NMR spectroscopy, IR spectroscopy, and

mass spectrometry. A yield of 32 mg (42 % yield) was obtained by ^1H NMR spectroscopy. The organometallic product was **3.7** and was identified from its ^1H NMR and IR spectra.⁵⁶

3.4.12 X-ray Crystallography

Data collection was carried out at -173.0 ± 2 °C on a Bruker X8 APEX II diffractometer with graphite-monochromated Mo K α radiation or at -183.0 ± 1 °C on a Bruker APEX DUO diffractometer with a TRIUMPH curved-crystal monochromator with Mo-K α radiation.

Data for **3.4** were collected to a maximum 2θ value of 60.3° in 0.5° oscillations with 2.0-second exposures and a crystal-to-detector distance of 59.72 mm. The structure was solved by direct methods.⁹⁸ and expanded using Fourier techniques. All non-hydrogen atoms were refined anisotropically. All hydrogen atoms were placed in calculated positions. The final cycle of full-matrix least-squares analysis was based on 6272 observed reflections and 234 variable parameters.

Data for **3.5** were collected to a maximum 2θ value of 60.1° in 0.5° oscillations using 3.0-second exposures. The crystal-to-detector distance was 39.83 mm. The structure was solved by direct methods⁹⁸ and expanded using Fourier techniques. The material is disordered in three orientations with regard to the coordination sites of the allyl, chloro, and nitrosyl ligands. SADI and EADP restraints were employed to maintain reasonable geometries, and the SOFs of the three fragments were forced to sum to 1.00. The material crystallizes as a racemic twin and was refined as such. All non-hydrogen atoms were refined anisotropically and all hydrogen atoms were placed in calculated positions. The final cycle of full-matrix least-squares analysis was based on 4035 observed reflections and 205 variable parameters.

Data for **3.15** were collected to a maximum 2θ value of 55.078° in 0.5° oscillations with 3.0-second exposures. The structure was solved by direct methods⁹⁸ and expanded using Fourier techniques. The C12–C20 fragment was disordered in two orientations with a 0.782(6) to 0.218(6) occupancy ratio. All non-hydrogen atoms were refined anisotropically, and hydrogen atoms were placed in calculated positions. The final cycle of full-matrix least-squares analysis was based on 4227 observed reflections and 223 variable parameters.

For each structure neutral-atom scattering factors were taken from Cromer and Waber.⁶¹ Anomalous dispersion effects were included in F_{calc} ;⁶² the values for $\Delta f'$ and $\Delta f''$ were those of Creagh and McAuley.⁶³ The values for mass attenuation coefficients are those of Creagh and Hubbell.⁶⁴ All refinements were performed using SHELXL-2014⁹⁹ via the OLEX2 interface.⁶⁸ X-ray crystallographic data for all three structures are presented in Table 3.3.

Table 3.3. X-ray crystallographic data for complexes **3.1**, **3.4**, **3.5**, and **3.15**.

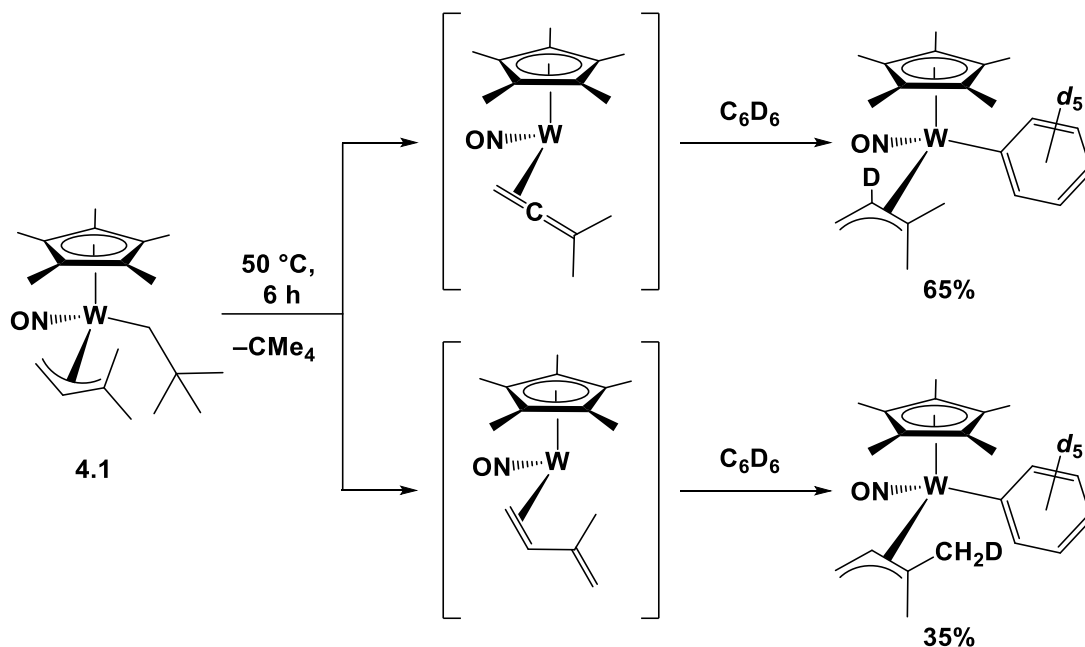
Compound	3.1	3.4	3.5	3.15
Empirical formula	C ₁₅ H ₂₅ NOW	C ₂₀ H ₃₆ N ₂ O ₂ W	C ₁₃ H ₂₀ NOWCl	C ₂₀ H ₂₅ NO ₂ W
Formula weight	419.21	520.36	425.60	495.27
Crystal size (mm)	0.23 × 0.13 × 0.12	0.32 × 0.23 × 0.20	0.16 × 0.15 × 0.15	0.25 × 0.14 × 0.05
Crystal system	Monoclinic	Triclinic	Orthorhombic	Monoclinic
Space group	P2 ₁ /c	P-1	P2 ₁ 2 ₁ 2 ₁	P2 ₁ /c
Volume (Å ³)	1518.1(6)	1066.0(2)	1375.38(7)	1830.5(4)
a (Å)	10.181(2)	7.9811(9)	9.5405(3)	15.1177(19)
b (Å)	8.1358(18)	9.0684(10)	10.9050(3)	7.8813(9)
c (Å)	18.596(4)	15.7146(18)	13.2198(4)	15.4847(19)
α (°)	90	80.986(3)	90	90
β (°)	99.748(5)	78.527(3)	90	97.175(7)
γ (°)	90	74.162(3)	90	90
Z	4	2	4	4
Density, ρ (calculated) (Mg/m ³)	1.834	1.621	2.057	1.797
Absorption coefficient, μ (mm ⁻¹)	7.599	5.433	8.578	6.322
F ₀₀₀	816.0	520.0	817.0	968.0
Measured Reflections: Total	19588	21387	17334	19693
Measured Reflections: Unique	4439	6272	4035	4227
Final R Indices	R ₁ = 0.0248, wR ₂ = 0.0507	R ₁ = 0.0316, wR ₂ = 0.0780	R ₁ = 0.0199, wR ₂ = 0.0411	R ₁ = 0.0312, wR ₂ = 0.0629
Goodness-of-fit on F ²	1.058	1.429	1.122	1.283
Largest diff. peak/hole (e ⁻ Å ⁻³)	2.23/−1.38	3.43/−3.38	1.13/−1.15	2.86/−2.05

**Chapter 4: The Functionalization of Methane Initiated
by $\text{Cp}^*\text{W}(\text{NO})(\text{CH}_2\text{CMe}_3)(\eta^3\text{-CH}_2\text{CHCMe}_2)$**

4.1 Introduction

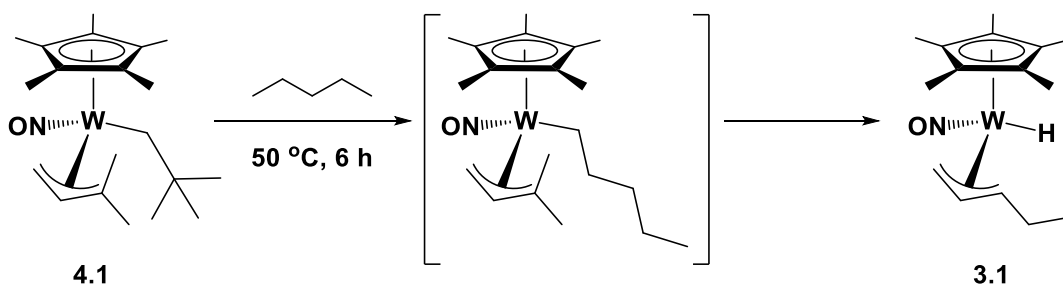
The complex $\text{Cp}^*\text{W}(\text{NO})(\text{CH}_2\text{CMe}_3)(\eta^3\text{-CH}_2\text{CHCMe}_2)$ (**4.1**) was first reported by the Legzdins group in 2002.⁴⁶ Upon thermolysis, it loses neopentane to form two different 16e intermediates (η^2 -allene and η^2 -diene complexes) which can effect C-H activation of aromatic substrates to give $\text{Cp}^*\text{W}(\text{NO})(\text{Ar})(\eta^3\text{-CH}_2\text{CHCMe}_2)$ products (Scheme 4.1).²⁶ The thermolysis of **4.1** with aliphatic alkanes gives mixtures of various $\text{Cp}^*\text{W}(\text{NO})(\text{H})(\eta^3\text{-allyl})$ complexes in which the allyl is derived from multiple C-H activations of the substrate and the original dimethylallyl ligand is lost.^{26, 30}

Scheme 4.1. The labeling reaction of **4.1** with C_6D_6 provides evidence for two 16e intermediate complexes



The family of $\text{Cp}^*\text{W}(\text{NO})(\text{CH}_2\text{CMe}_3)(\eta^3\text{-CH}_2\text{CHCHR})$ ($\text{R} = \text{Me, Ph, or TMS}$) complexes has been shown to effect the single activation of terminal $\text{C}(\text{sp}^3)\text{-H}$ bonds of alkane substrates.³¹ The reactions of these complexes with *n*-pentane give $\text{Cp}^*\text{W}(\text{NO})(n\text{-C}_5\text{H}_{11})(\eta^3\text{-CH}_2\text{CHCHR})$,^{28, 29, 34} whereas the reaction of **4.1** with *n*-pentane results in multiple C-H activations to give isomers of **3.1** regardless of the thermal conditions employed (Scheme 4.2).³⁰ Theoretical investigations suggest that once single C-H activation is effected by **4.1**, β -H elimination occurs with a smaller energy barrier than for the initial C-H activation.³² Indeed, an experimental correlation between the electron-richness of the tungsten center (indicated by the infrared nitrosyl-stretching frequency) and the tendency for multiple C-H activations has been established for these complexes, and a more electron-rich metal center would be more able to effect additional C-H bond activation.³⁰ This explains the observed multiple C-H activations and also implies that **4.1** cannot effect the clean, single C-H activation of alkanes that is seen for related complexes.

Scheme 4.2. Thermolysis of 4.1 in neat alkane (e.g. *n*-pentane) results in multiple C-H activations



Since complex **4.1** effects multiple C-H activations of alkanes, its chemistry has not been expanded over the last decade. However, the simplest and most abundant hydrocarbon, methane, contains only a single carbon atom, which precludes the possibility of multiple C-H activations on adjacent carbons. The focus of this chapter is developing complex **4.1** as a platform for methane activation and subsequent functionalization with the long-term goal of converting methane into value-added chemicals.

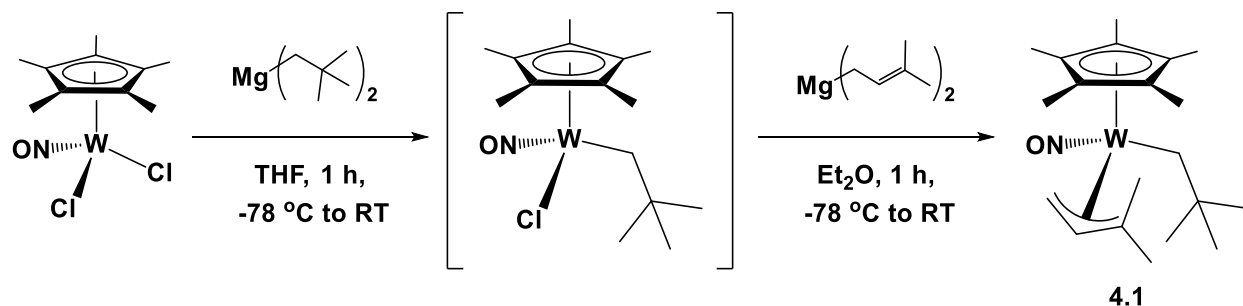
4.2 Results and Discussion

4.2.1 Adapted Synthesis of **4.1**

Complex **4.1** is synthesized via a modified procedure from that reported in the literature and is summarized below in Scheme 4.3.²⁶ Starting from $\text{Cp}^*\text{W}(\text{NO})\text{Cl}_2$, two sequential metathesis reactions are carried out first in THF and then in Et_2O whereby the neopentyl and allyl ligands are delivered by $\text{Mg}(\text{CH}_2\text{CMe}_3)_2$ and $\text{Mg}(\text{CH}_2\text{CH}=\text{CMe}_2)_2$, respectively. THF must be used in the initial step due to the insolubility of $\text{Cp}^*\text{W}(\text{NO})\text{Cl}_2$ in Et_2O , particularly under the cryogenic conditions employed. Switching to Et_2O for the second metathesis is not necessary for the formation of **4.1**, but is essential for a much more facile purification of the product. Purification is effected via filtration of the reaction mixture through basic alumina followed by removal of the solvent in vacuo to give a solid which can be washed with pentane to afford **4.1** as an orange solid in good yield.¹⁰⁰ The primary advantage of this synthesis over the reported procedure is that the 16e intermediate complex, $\text{Cp}^*\text{W}(\text{NO})(\text{CH}_2\text{CMe}_3)\text{Cl}$,¹⁰¹ is generated and

reacted in situ rather than isolated. $\text{Cp}^*\text{W}(\text{NO})(\text{CH}_2\text{CMe}_3)\text{Cl}$ can be difficult to isolate and cannot be stored for long periods of time, unlike both $\text{Cp}^*\text{W}(\text{NO})\text{Cl}_2$ and **4.1**.

Scheme 4.3. Adapted synthesis of 4.1



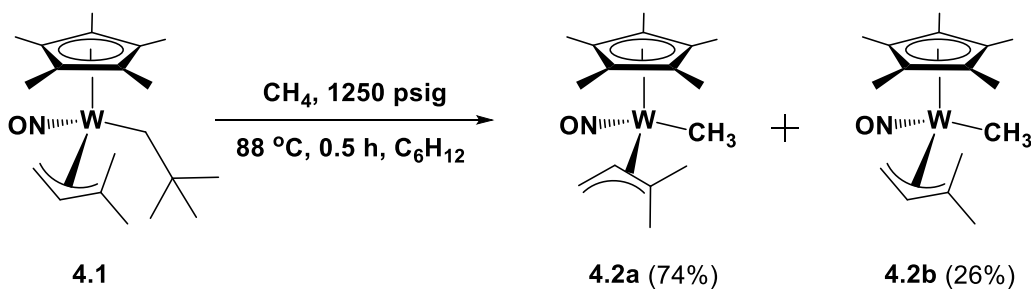
4.2.2 C-H Activation of Methane

The C-H activation chemistry initiated by the family of $\text{Cp}^*\text{W}(\text{NO})(\text{CH}_2\text{CMe}_3)(\eta^3\text{-allyl})$ complexes must be carried out using neat alkane substrate.³¹ This presents a dilemma for the potential activation of gaseous substrates. The products from the reactions of **4.1** with methylcyclohexane²⁶ and pentane³⁰ demonstrate a preference for the activation of primary $\text{C}(\text{sp}^3)\text{-H}$ bonds over secondary ones. This bias towards primary $\text{C}(\text{sp}^3)\text{-H}$ linkages allows for the usage of cyclohexane as a solvent for methane activation chemistry since it contains only secondary $\text{C}(\text{sp}^3)\text{-H}$ bonds, despite the fact that the activation of cyclohexane by **4.1** has been previously reported.⁴⁶

4.2.2.1 Optimized Conditions for the C-H Activation of Methane Initiated by 4.1

Thermolysis of **4.1** in cyclohexane at 88 °C and 1250 psig CH₄ pressure for 0.5 h affords the product of methane C-H activation, Cp*W(NO)(CH₃)(η³-CH₂CHCMe₂) (**4.2**), as the sole organometallic complex (Scheme 4.4). The reaction is conveniently carried out in a Parr 5500 series reactor with a 0.3 L volume vessel, and the reactor is charged under an inert atmosphere. The sealed reactor is purged with methane prior to starting the reaction. The resulting yellow solution of **4.2** can be collected in the air, and purification of the product is performed by column chromatography over basic alumina support. Complex **4.2** is obtained as a yellow solid in good yield (67 %) and is air and moisture stable. The complex has a melting point of 84-87 °C which has been determined to be reversible by an analysis of the melt residue by ¹H NMR spectroscopy. The stability of **4.2** is quite unusual as the vast majority of homogenous complexes resulting from methane C-H activation (i.e. containing the M-CH₃ linkage) are not stable,¹⁰² making isolation and even observation difficult,^{15, 17, 103, 104} if not impossible.^{2, 3, 6, 13, 19, 20, 103} The stability of **4.2** has led to the extensive characterization of this organometallic product from methane activation as well as an exploration of its reactivity.

Scheme 4.4. C-H activation of methane by complex 4.1



In solution, complex **4.2** exists as two isomers in a 3:1 ratio that differ in the endo/exo orientation of the allyl ligand. The major isomer, **4.2a** (74%), has the allyl ligand in the exo orientation with the signal for the allyl meso H having a relative upfield chemical shift at 2.90 ppm in the ^1H NMR spectrum. In contrast, the signal for the allyl meso H of the minor isomer, **4.2b** (26 %), has a downfield chemical shift at δ 4.68 ppm, consistent with the allyl being in an endo orientation. The methyl substituents of the allyl ligand are proximal to the W-CH₃ ligand for both isomers. The existence of **4.2** as a pair of exo/endo isomers is similar to what is seen for the related hydride complex **2.1**. Related dimethylallyl complexes with larger ligands such as neopentyl or phenyl exist as only a single isomer in solution with the allyl ligand in an endo orientation.²⁶ In what appears to be a steric effect, the complexes containing smaller hydride and methyl ligands favour the allyl having an exo orientation.

The signal due to the methyl ligand derived from the C-H activation of methane has an upfield chemical shift of δ 0.25 ppm (δ 0.23 ppm for **4.2b**) in the ^1H NMR spectrum, which is due to its proximity to the tungsten. The methyl ligand signals are broad and overlap, a fact that prevents the observation of satellites due to tungsten-183 coupling. The WCH₃ resonance in the ^{13}C NMR spectrum also has an upfield chemical shift of δ 4.8 ppm.

Crystals suitable for single-crystal X-ray diffraction have been obtained by recrystallization from 2:1 pentane/Et₂O at -33 °C. Only a single isomer is present in the solid-state, which is the major isomer **4.1a**. The allyl ligand is oriented in an exo fashion with the two methyl substituents proximal to the methyl ligand. There is no σ - π distortion of the allyl ligand, which is unusual for Cp*W(NO)(alkyl)(η^3 -allyl) complexes.³¹ This could be due in part to the unequal distances of the W-C bonds of the allyl ligand with the CMe₂ terminus being the furthest from the metal at 2.562(5) Å, which itself is likely a steric effect due to the 1,1-dimethyl

substituents. The nitrosyl ligand is linear with a W-N-O bond angle of $172.9(4)^\circ$. The relatively low nitrosyl-stretching frequency ($\nu_{\text{NO}} = 1591 \text{ cm}^{-1}$) of a linear nitrosyl ligand is typical for many tungsten nitrosyl complexes.³⁹ It is caused by back-bonding from an electron-rich tungsten center; a more accurate interpretation of the bonding would be $\text{W}=\text{N}=\text{O}$; this is consistent with an elongated N-O linkage compared to free NO (1.15 \AA).¹⁰⁵ Finally, the methyl ligand (C16) which was generated from the C-H activation of methane has a W(1)-C(16) bond length of $2.216(5) \text{ \AA}$, which is shorter than the W-C bonds of the allyl ligand.

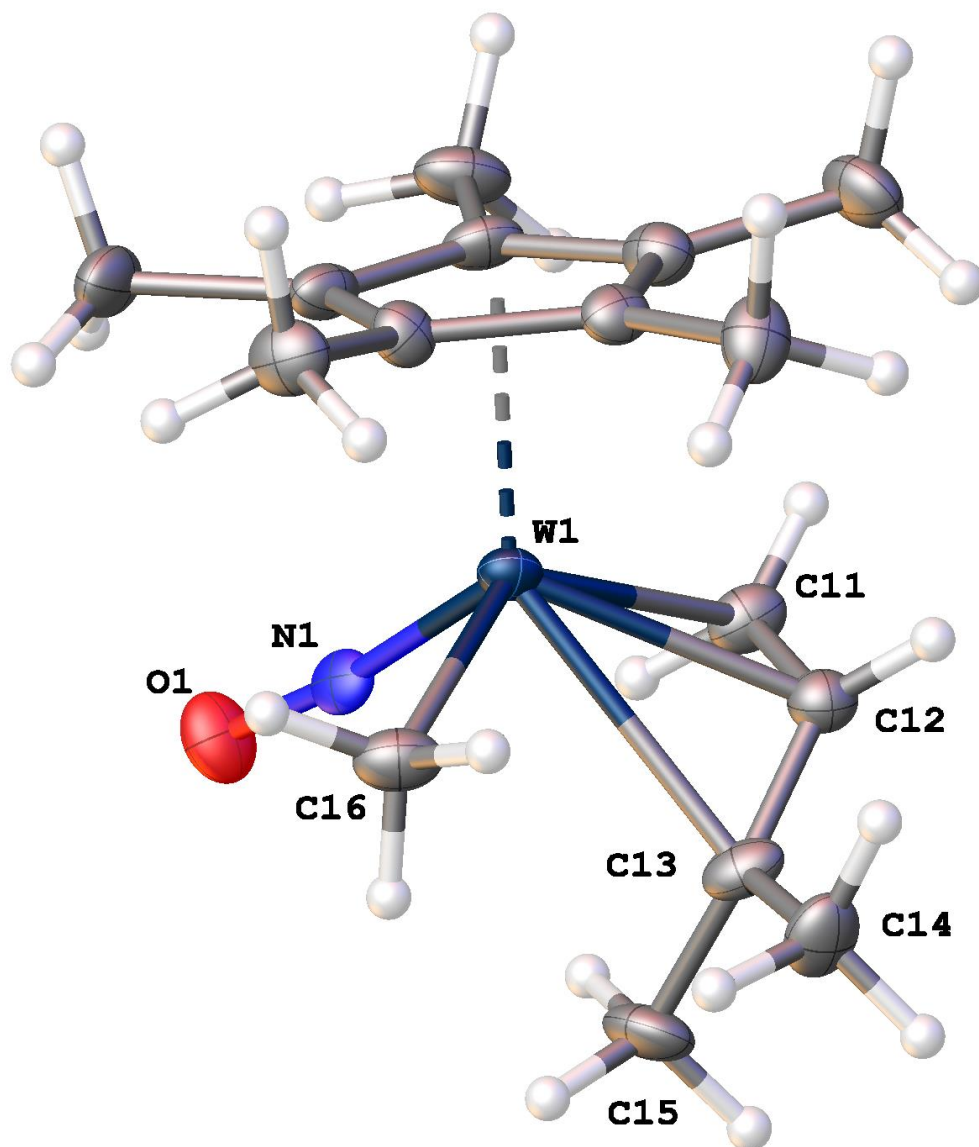


Figure 4.1. Solid-state molecular structure of **4.2** with 50% probability thermal ellipsoids shown.

Selected bond lengths (Å) and angles (deg.): W(1)-C(11) = 2.269(6), W(1)-C(12) = 2.323(5), W(1)-C(13) = 2.562(5), W(1)-C(16) = 2.216(5), W(1)-N(1) = 1.751(5), N(1)-O(1) = 1.242(6), C(11)-C(12) = 1.398(7), C(12)-C(13) = 1.398(7), C(11)-C(12)-C(13) = 122.9(5), C(12)-C(13)-C(14) = 119.0(5), C(12)-C(13)-C(15) = 122.1(5), W(1)-N(1)-O(1) = 172.9(4).

4.2.2.2 Pressure Optimization for the C-H Activation of Methane

Initial investigations of the reaction of **4.1** with methane have been carried out using the previously reported conditions for the C-H activation of benzene by **4.1** which are 50 °C for 6 h.⁴⁶ The thermolysis of **4.1** in cyclohexane while exposed to 500 psig CH₄ yields two organometallic complexes, the desired product of a single C-H activation of methane, **4.2**, and the product from solvent C-H activation, **3.3**, in an 86:14 ratio (Scheme 4.5, Table 4.1 entry 1). This reflects the preference of **4.1** for activating primary C(*sp*³)-H bonds. The presence of **3.3** is hypothesized to be the result of an insufficient concentration of methane in solution. Repeating the reaction under increased methane pressure (1000 psig) results in a product ratio of 95:5 in favour of **4.2** (Table 4.1 entry 2). For reactions carried out at 1150 psig CH₄ no solvent activation is observed (Table 4.1 entry 3). The C-H activation of methane by **4.1** must be carried out at a sufficiently high pressure to avoid the competing solvent C-H activation side reaction.

Scheme 4.5. Competing solvent activation under methane pressure

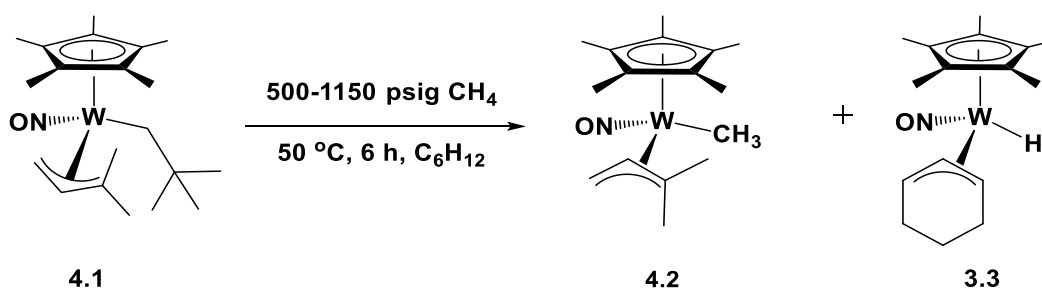


Table 4.1. Pressure dependence for the C-H activation of methane (Scheme 4.5).^[a]

Entry	Methane pressure (psig)	Relative amount of 4.2 (%)	Relative amount of 3.3 (%)
1	500	86	14
2	1000	95	5
3	1150	100	0

^[a] Reactions were carried out at 50 °C for a duration of 6 h.

4.2.2.3 Solvent Optimization for the C-H Activation of Methane

The C-H activation of methane by **4.1** is conveniently performed in cyclohexane under sufficiently high pressure of methane. The C-H activation of methane may be effected using hexafluorobenzene as the solvent as well, albeit with reduction in yield of the product. A comparison between different volumes of cyclohexane has also been examined, demonstrating that a higher yield of **4.2** is obtained when cyclohexane is employed as the solvent and when the reaction mixture is more dilute. These results are summarized below in Table 4.2.

Table 4.2. The effect of solvent for the yield of **4.2** from the C-H activation of methane.^[a]

Entry	Solvent	Volume of solvent	Yield of 4.2
1	C ₆ F ₆	20 mL	40%
2	C ₆ H ₁₂	20 mL	49%
3	C ₆ H ₁₂	125 mL	67%

^[a] In all cases the following conditions were used: 1250 psig CH₄, samples were heated at 50 °C for 6 h.

4.2.2.4 Thermal Optimization of C-H Activation via Kinetic Studies

In an effort to optimize the thermal conditions for the C-H activation of methane by **4.1**, a kinetic analysis of the reaction has been performed. The pseudo first-order rate constant for the thermolysis of **4.1** at 50 °C has been previously reported to be $2.2(1) \times 10^{-4} \text{ s}^{-1}$ ($R^2 = 0.999$), obtained by monitoring the thermolysis of the complex in benzene- d_6 .²⁶ The thermolysis of **4.1** at several higher temperatures in benzene- d_6 has been monitored by ^1H NMR spectroscopy to provide additional rate constants (Table 4.3). These values have been used to obtain Eyring parameters of ΔH^\ddagger and ΔS^\ddagger of 98(3) kJ/mol and 166(11) J/mol K,¹⁰⁶ respectively, and an Arrhenius activation energy (E_a) of 100.9(2.9) kJ/mol.¹⁰⁷ The practical results of these kinetic studies have been to find the appropriate reaction times for higher-temperature C-H activations. The rate constants are all pseudo-first order in consumption of the starting complex **4.1**, by loss of neopentane to generate the reactive 16e η^2 -allene and η^2 -diene intermediates. Therefore, the rate is independent of the nature of the C-H bond being cleaved and applies to the $\text{C}(\text{sp}^3)\text{-H}$ bond activation of methane as it does to the $\text{C}(\text{sp}^2)\text{-H}$ activation of benzene- d_6 .

Table 4.3. Pseudo first-order rate constants for the thermolysis of 4.1 in C_6D_6 .

Entry	T (°C)	$k \text{ (s}^{-1}\text{)}$
1 ^[a]	50	$2.2(1) \times 10^{-4}$
2	65.0	$1.14(2) \times 10^{-3}$
3	75.3	$3.72(12) \times 10^{-3}$
4	85.2	$8.4(8) \times 10^{-3}$

^[a] Rate constant at 50 °C previously reported.²⁶

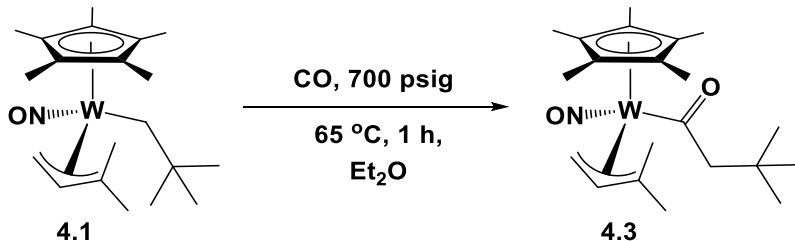
4.2.3 1,1-Insertion of Carbon Monoxide into W-C Bonds

The ability to selectively activate the terminal C-H bond of an alkane is in itself interesting and worthwhile chemistry; however, in order to be useful synthetically the activated hydrocarbyl ligand must be further functionalized and then released. The functionalization of transition-metal carbon σ bonds by insertion of CO is a well-established method for the generation of new C-C bonds.^{82, 83, 108-110} Prior to this work it had been demonstrated that the complexes $\text{Cp}^*\text{W}(\text{NO})(\text{CH}_2\text{CMe}_2)(\eta^3\text{-CH}_2\text{CHCHR})$ ($\text{R} = \text{Ph}$ or Me) can be converted to the corresponding acyl complexes, slowly under CO pressure.³⁷ The functionalization of alkyl and hydrocarbyl ligands derived from intermolecular C-H activations had not been achieved.

4.2.3.1 Functionalization of a Neopentyl Ligand with CO

To begin the investigation of CO-insertion chemistry with $\text{Cp}^*\text{W}(\text{NO})(\text{alkyl})(\eta^3\text{-CH}_2\text{CHCMe}_2)$ complexes, **4.1** has been used as a model reactant. Heating **4.1** at 65 °C under 700 psig of CO in Et_2O for 1 h results in the 1,1-insertion of CO into the tungsten-alkyl bond, giving the product $\text{Cp}^*\text{W}(\text{NO})(\text{C}(\text{O})\text{CH}_2\text{CMe}_3)(\eta^3\text{-CH}_2\text{CHCMe}_2)$ (**4.3**) (Scheme 4.6). Compound **4.3** can be obtained in high yield (93%) as a yellow solid that is pure by elemental analysis without any workup beyond removing the solvent in vacuo. The presence of an acyl ligand from CO insertion is supported by a carbonyl-stretching frequency at 1618 cm^{-1} in the infrared spectrum of **4.3**, which is typical for related acyl complexes.³⁷ In the ^{13}C NMR spectrum of **4.3**, the acyl $\text{C}=\text{O}$ signal occurs at $\delta\ 273.5\text{ ppm}$.

Scheme 4.6. Carbonylation of 4.1



The solid-state molecular structure of **4.3** is shown below in Figure 4.2 and confirms the 1,1-CO insertion into the W-C bond of the neopentyl ligand. The acyl carbonyl has a typical C(16)-O(2) bond length of 1.220(5) Å.³⁷ In addition, the W(1)-C(16)-O(2) and O(2)-C(16)-C(17) bond angles are consistent with an sp²-hybridized C atom. The dimethylallyl ligand is oriented in an endo fashion with the two methyl substituents proximal to the acyl ligand. The nitrosyl ligand is linear with a W-N-O bond angle of 168.3(5)°

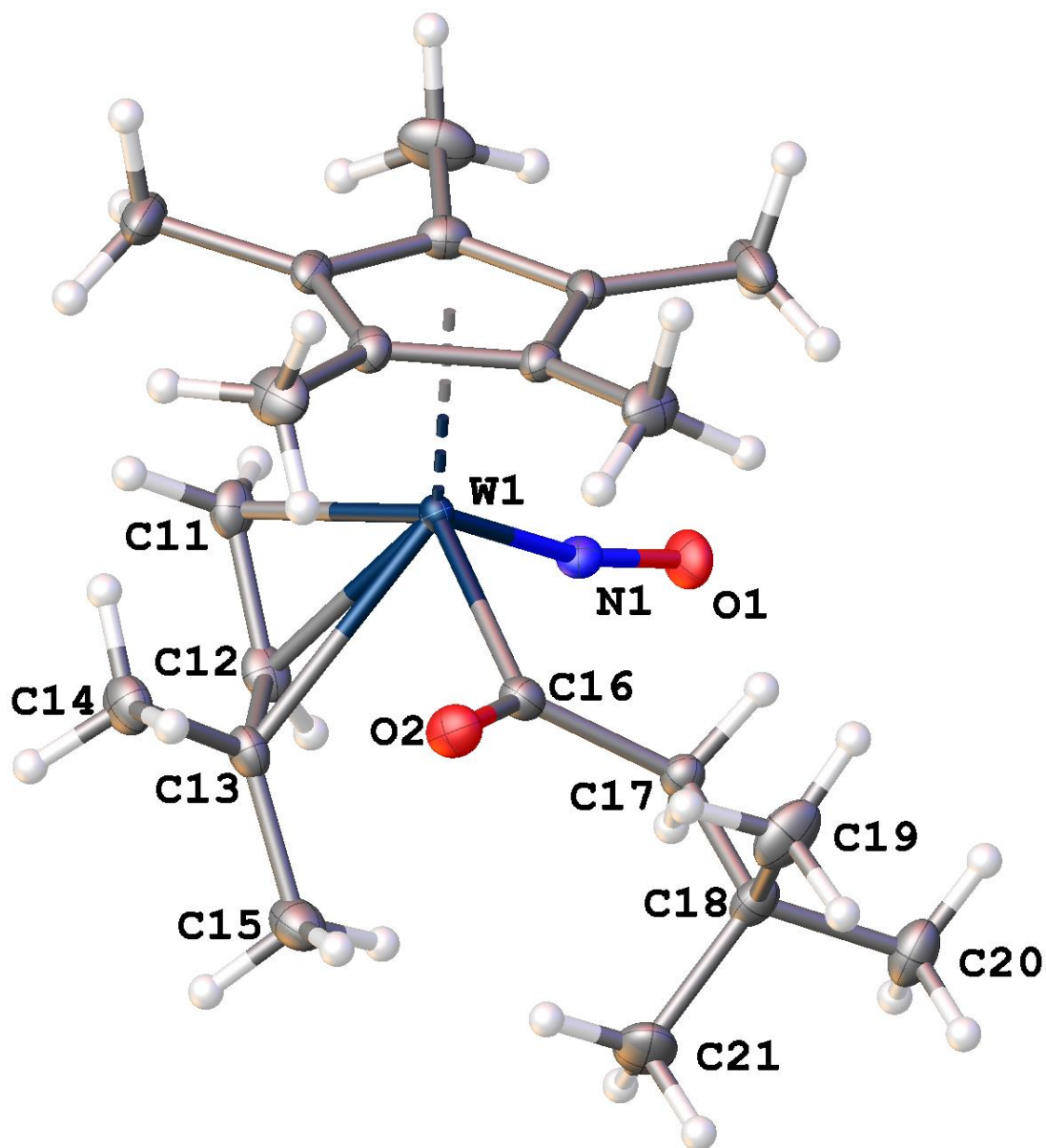


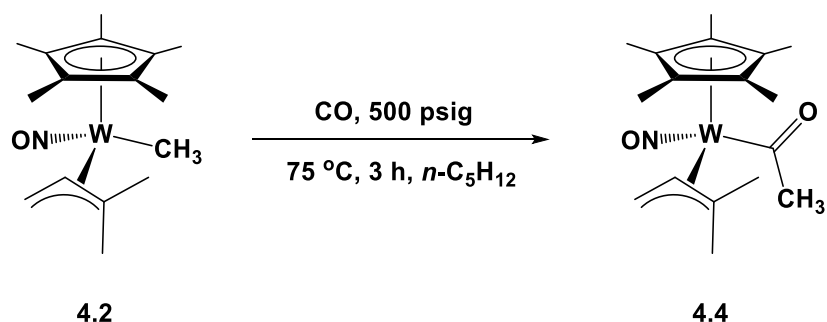
Figure 4.2. Solid-state molecular structure of **4.3** with 50% probability thermal ellipsoids shown.

Selected interatomic distance (Å) and angles (deg.): W(1)-C(11) = 2.240(6), W(1)-C(12) = 2.348(5), W(1)-C(13) = 2.554(5), W(1)-C(16) = 2.226(5), C(16)-O(2) = 1.220(5), C(11)-C(12) = 1.413(7), C(12)-C(13) = 1.393(7), W(1)-N(1) = 1.772(3), N(1)-O(1) = 1.231(4), C(11)-C(12)-C(13) = 122.1(5), C(12)-C(13)-C(14) = 123.5, C(12)-C(13)-C(15) = 117.7(4), W(1)-C(16)-O(2) = 123.5(3), O(2)-C(16)-C(17) = 120.5(4), W(1)-N(1)-O(1) = 168.3(5).

4.2.3.2 Carbonylation of the Methyl Ligand

Exposure of a cyclohexane solution of **4.2** to 500 psig CO pressure and 75 °C for 3 h results in the 1,1-insertion of CO into the W-CH₃ linkage of **4.2** and formation of the yellow acyl complex, Cp*W(NO)(C(=O)CH₃)(η^3 -CH₂CHCMe₂) (**4.4**) in decent yield (Scheme 4.7). The presence of an acyl ligand is confirmed by a carbonyl-stretching frequency at 1614 cm⁻¹. The addition of CO to **4.2** is further supported by mass spectrometry with a tungsten isotope pattern at m/z = 461. In the ¹H NMR spectrum of **4.4** the resonance due to the methyl group of the acyl ligand is a singlet with a chemical shift of δ 2.91 ppm, much downfield relative to the methyl ligand of **4.2** (δ 0.25 ppm). Likewise, the resonance due to the methyl in the ¹³C NMR spectrum at δ 47.8 ppm is shifted downfield compared to the methyl ligand of **4.2** (δ 4.8 ppm). The acyl C has a chemical shift of δ 273.3 ppm in the ¹³C NMR spectrum.

Scheme 4.7. Carbonylation of the methyl ligand



Crystals of **4.4** suitable for X-ray diffraction analysis can be obtained by recrystallization from 2:1 pentane/Et₂O at -33 °C. The solid-state molecular structure of **4.4** (Figure 4.3) contains two molecules in the asymmetric unit. Both structures confirm the 1,1-insertion of CO into the

W-C bond of the methyl ligand, however the W(2) unit is disordered at the tungsten as well as the acyl ligand so parameters discussed are for the W(1) unit. The methyl group C(17) [and C(28)] is derived originally from methane following the C-H activation of the gas molecule by **4.1**. The C(16)-O(3) bond length of 1.204(9) Å is a typical organic carbonyl length similar to that for the acyl ligand seen in compound **4.3**. The W(1)-C(16) bond length of 2.191(8) Å is similar to the W-C bond for the methyl ligand in compound **4.2** (2.216(5) Å), while the C(16)-C(17) length of 1.531(11) Å is indicative of a single C-C bond. Additionally, the bond angles about C(16) are 117.0(6) Å, 118.2(7) Å, and 124.6(6) Å, which agree with a sp²-hybridized acyl C atom. The dimethylallyl ligand has an exo orientation, and the two methyl substituents are proximal to the acyl ligand. A σ-π distortion of the allyl ligand can be seen with unequal C(11)-C(12) and C(12)-C(13) bond lengths of 1.413(11) Å and 1.372(11) Å, with the shorter bond being trans to the nitrosyl ligand.

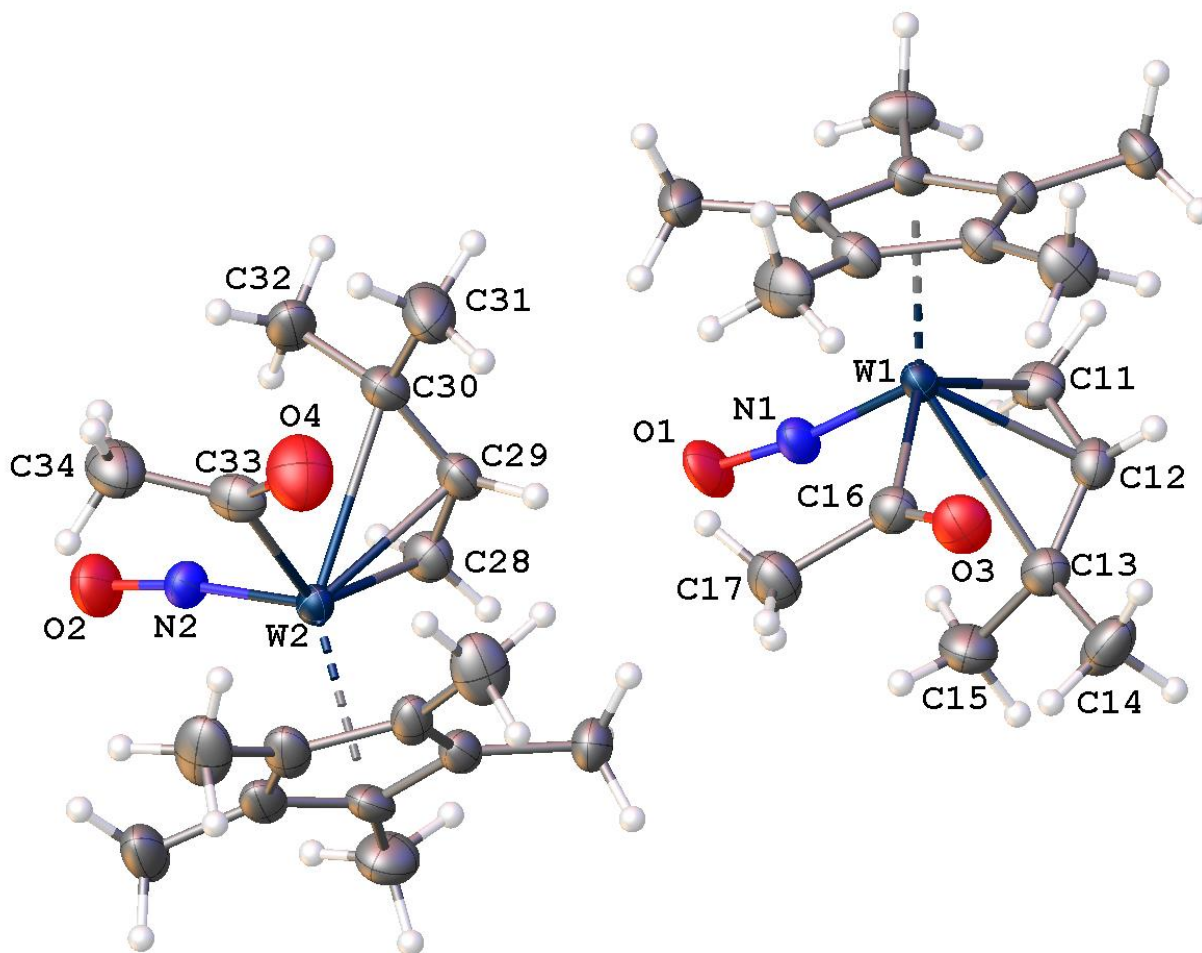


Figure 4.3. Solid-state molecular structure of **4.4** with 50% probability thermal ellipsoids shown.

Selected interatomic distance (Å) and angles (deg.): W(1)-C(16) = 2.191(8), C(16)-O(3) = 1.204(9), C(16)-C(17) = 1.531(11), W(1)-C(11) = 2.237(8), W(1)-C(12) = 2.303(8), W(1)-C(13) = 2.582(8), C(11)-C(12) = 1.413(11), C(12)-C(13) = 1.372(11), W(1)-N(1) = 1.771(6), N(1)-O(1) = 1.222(8), W(1)-C(16)-O(3) = 124.6(6), W(1)-C(16)-C(17) = 117.0(6), O(3)-C(16)-C(17) = 118.2(7), C(11)-C(12)-C(13) = 124.3(8), C(12)-C(13)-C(14) = 119.9(8), C(12)-C(13)-C(15) = 121.9(8), W(1)-N(1)-O(1) = 172.6(6).

In order to determine the optimal conditions for the insertion of CO into the tungsten-methyl bond, the reaction of **4.2** with CO has been monitored by ^1H NMR spectroscopy. The thermolysis of **4.2** at 75 °C under 500 psig CO was monitored by taking samples (ca. 1 mL) from a modified Parr 5500 reactor every 30 minutes. These samples were then analyzed by ^1H NMR spectroscopy, and the spectra obtained are shown in Figure 4.4. The Cp* signal of **4.2** occurs at δ 1.51 ppm in the ^1H NMR spectrum. As the reaction proceeds, a new singlet begins to grow in at δ 1.58 ppm while the signal at δ 1.51 ppm diminishes. The signal due to the methyl of the acyl ligand grows in at δ 2.91 ppm and integrates to 3:15 with the signal at δ 1.58 ppm. Ultimately, the carbonylation of **4.2** is best performed by heating the compound at 75 °C for 3 h under 500 psig CO pressure. Increasing the time of the reaction results in additional organometallic products (vide infra). Monitoring the thermolysis of **4.2** at 75 °C under only 140 psig CO pressure by ^1H NMR spectroscopy shows a reduced rate in the carbonylation of **4.2** to give **4.4**. This demonstrates a dependence on the pressure of CO for the carbonylation reaction. The carbonylation of **4.2** occurs more slowly than that of **4.1** despite the higher temperature required for functionalization of the methyl ligand by CO; this is not surprising as decreased rates of carbonylation with decreasing steric bulk of the ligand have been reported previously.⁸²

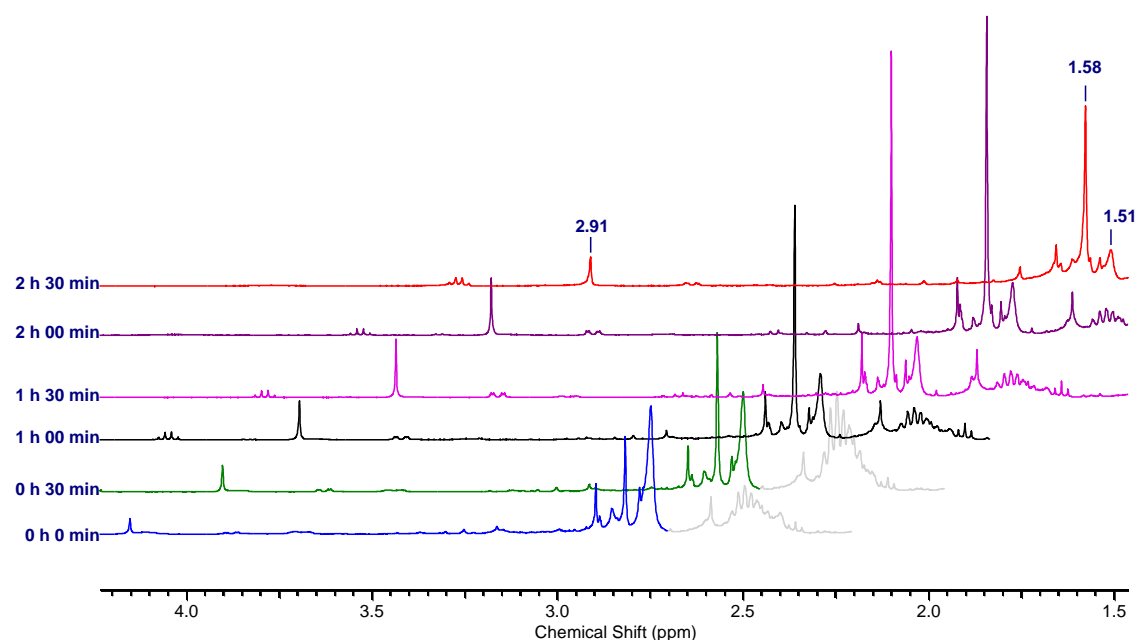
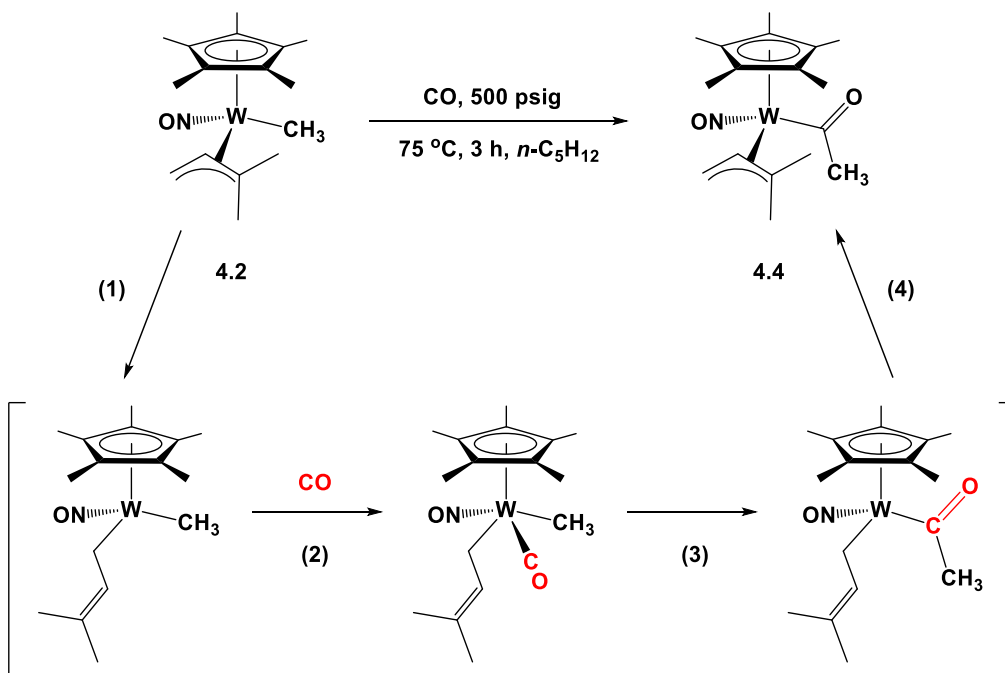


Figure 4.4. Plot of ^1H NMR spectra from carbonylation of **4.2** taken at 30 min intervals. Signal at δ 1.51 ppm belongs to C_5Me_5 ligand of **4.2**, and signals at δ 2.91 and 1.58 ppm belong to the $\text{C}(\text{O})\text{Me}$ and C_5Me_5 of complex **4.5**, respectively.

The mechanism of 1,1-CO insertion into transition metal-carbon σ bonds is well established and involves the migration of the alkyl to the carbonyl ligand.¹¹⁰ For insertion of an external CO molecule into the metal-carbon σ bond there must first be an open coordination site at the metal center.¹⁰⁹ Furthermore, the geometry of the CO and alkyl must be cis otherwise insertion cannot occur.¹¹¹ Compounds **4.1** and **4.2** are 18e, coordinatively saturated complexes that do not have any open coordination site for CO to bind in order to make the corresponding acyl complexes **4.3** and **4.4**. The proposed mechanism for the carbonylation of **4.2** (and **4.1**) is shown in Scheme 4.8. A haptotropic shift of the allyl ligand from η^3 to η^1 (Step 1) produces an open coordination site that allows for formation of the CO adduct, $\text{Cp}^*\text{W}(\text{NO})(\text{CO})(\text{CH}_3)(\eta^1\text{-CH}_2\text{CH}=\text{CMe}_2)$ (Step 2) This is followed by intramolecular nucleophilic attack of the methyl

group on the carbon atom of the newly formed carbonyl ligand to afford the acyl ligand (Step 3). Finally, the allyl ligand reverts to an η^3 coordination to give **4.4** (Step 4).

Scheme 4.8. Proposed mechanism for the carbonylation of 4.2



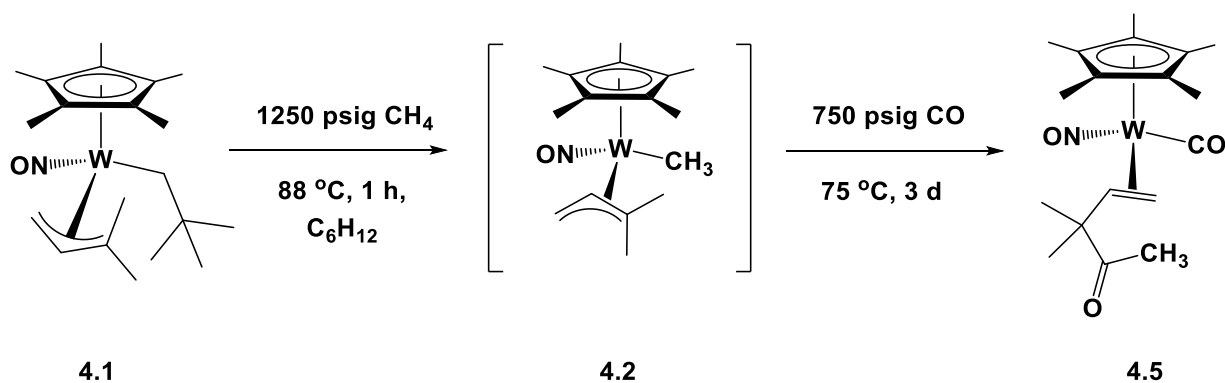
4.2.4 Additional C-C Bond Formation via Acyl-Allyl Ligand Coupling

Monitoring the conversion of **4.2** to **4.4** by ^1H NMR spectroscopy reveals that during the thermolysis at $75\text{ }^\circ\text{C}$ under CO pressure new sets of signals begin to appear in the ^1H NMR spectra recorded beyond 3 h. Additionally, analysis by infrared spectroscopy and mass spectrometry indicates coordination of an additional CO molecule during extended reaction times.

4.2.4.1 Conversion of 4.2 Under CO Pressure to the η^2 -Bound Ketone Complex

Following the formation of **4.2** under the conditions shown in Scheme 4.9, the methane gas is vented and the reactor is repressurized with 750 psig CO. Maintenance of this cyclohexane solution of **4.2** at 750 psig CO pressure and 75 °C for 3 d results in the formation of the η^2 -unsaturated-ketone complex, $\text{Cp}^*\text{W}(\text{NO})(\text{CO})(\eta^2\text{-CH}_2=\text{CH-CMe}_2\text{C(=O)CH}_3)$ (**4.5**). Complex **4.5** can be obtained as an orange solid following column chromatography over silica support. Recrystallization by slow evaporation from DCM/hexanes affords red/orange crystals that are suitable for single-crystal X-ray diffraction analysis. A melting point of **4.5** of 80-83 °C has been determined to be reversible by identifying **4.5** in the ^1H NMR spectrum of the melt.

Scheme 4.9. C-H activation of methane, followed by subsequent conversion to 4.5 under CO pressure



The infrared spectrum of **4.5** is conveniently used to characterize the CO environments of the molecule. A terminal-metal carbonyl-stretching frequency is found at 1965 cm^{-1} while a carbonyl-stretching frequency of 1702 cm^{-1} is in the range of a typical ketone carbonyl. This

would indicate no interaction between the ketone carbonyl and the tungsten center. The nitrosyl-stretching frequency of 1606 cm^{-1} is higher than for compounds **4.1-4.4** which is consistent with the presence of an additional π -acid ligand (the terminal carbonyl ligand). The terminal carbonyl- and nitrosyl-stretching frequencies in the IR spectrum are comparable to those of the structurally similar compounds **3.13** and **3.15**.

The solid-state molecular structure of complex **4.5** is shown in Figure 4.5, and its metrical parameters generally resemble those exhibited by other three-legged “piano stool” molecules containing the $\text{Cp}^*\text{W}(\text{NO})$ fragment (e.g. compounds **4.1-4.4**).³¹ In particular, the bond lengths and bond angles within the bound unsaturated ketone are completely consistent with it being viewed as an η^2 -alkene complex with an elongated C(11)-C(12) bond having a distance of $1.430(3)\text{ \AA}$, indicative of tungsten back-bonding. The coupling of the acyl and allyl ligands to give a new C(13)-C(16) single bond ($1.539(3)\text{ \AA}$) occurs at the CMe_2 terminus of the allyl ligand. The acetyl group derived from methane [C(17)] and carbon monoxide [C(16)-O(2)] is oriented away from the tungsten center; there is clearly no direct interaction between the tungsten center and the ketone oxygen as the distance between W(1) and O(2) is 5.419 \AA (Figure 4.6). Linear nitrosyl and carbonyl ligands are evident with bond angles of $171.39(16)^\circ$ and $178.41(19)^\circ$, respectively.

The dihapto coordination of the bound ketone ligand through the olefin functional site is supported by the ^1H and ^{13}C NMR data. The signals due to the alkene carbon atoms have upfield chemical shifts at $\delta\ 34.1$ ($=\text{CH}_2$) and 55.9 ($=\text{CH}$) ppm, indicating coordination to the tungsten. More importantly, each signal has characteristic tungsten-183 satellites with $^1J_{\text{WC}}$ values of 11.0 and 40.2 Hz , respectively. The methine carbon with the larger magnitude coupling constant to the tungsten is identified as having a shorter W(1)-C(12) bond ($2.245(2)\text{ \AA}$) in the solid-state

molecular structure compare to the longer methylene W(1)-C(11) bond (2.279(2) Å). It is not surprising that the relative strength of the ^{183}W -C coupling is directly related to the strength, and length, of the tungsten-carbon bond. Additionally, the alkene proton signals in the ^1H NMR spectrum all have upfield chemical shifts (Figure 4.7), and the methine signal has satellites characteristic of tungsten-183 coupling ($^2J_{\text{WH}} = 7.3$ Hz).

The methyl group derived from methane activation is identified in the ^1H NMR spectrum as a singlet at δ 2.14 ppm and its carbon resonance in the ^{13}C NMR spectrum is located at δ 25.5 ppm. The ketone carbonyl signal has a chemical shift of δ 212.9 ppm which is in the range of an organic-type carbonyl and supports the lack of a direct interaction between the tungsten and the C=O. The terminal carbonyl ligand has a ^{13}C NMR resonance at δ 224.4 ppm, which is typical for terminal carbonyl ligands on similar tungsten complexes.^{45, 78, 101}

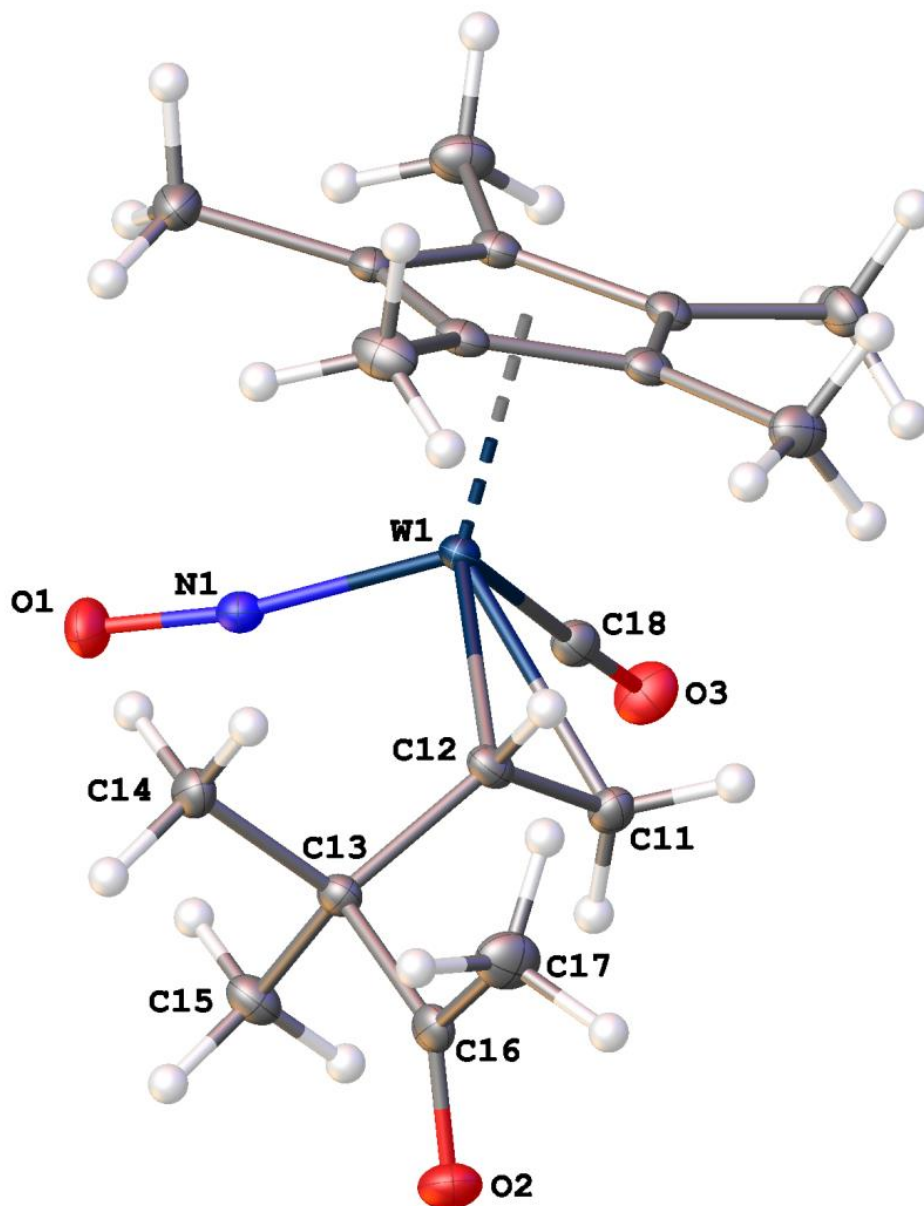


Figure 4.5. Solid-state molecular structure of **4.5** with 50% probability thermal ellipsoids shown.

Selected bond lengths (Å) and angles (deg): W(1)-C(11) = 2.279(2), W(1)-C(12) = 2.245(2), C(11)-C(12) = 1.430(3), C(12)-C(13) = 1.542(3), C(13)-C(16) = 1.539(3), C(16)-C(17) = 1.509(3), C(16)-O(2) = 1.214(3), C(11)-C(12)-C(13) = 122.25(19), C(13)-C(16)-O(2) = 121.5(2), C(17)-C(16)-O(2) = 119.5(2), W(1)-N(1)-O(1) = 171.39(16), W(1)-C(18)-O(3) = 178.41(19).

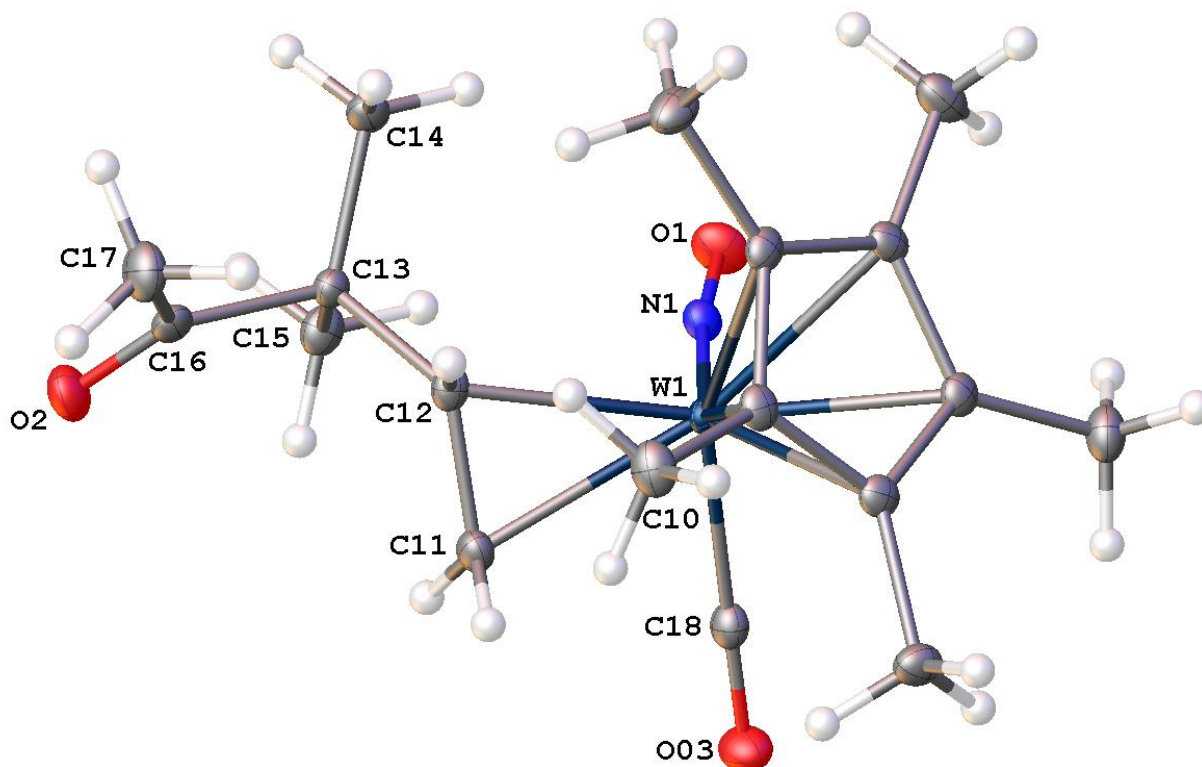


Figure 4.6. Top-down view of solid-state molecular structure of **4.5** showing that the distance between W(1) and O(2) is 5.419 Å

There is no literature precedent for this conversion, but its probable mechanism involves the initial nucleophilic attack of the allyl ligand on the acyl carbon in the tungsten's coordination sphere followed by coordination of CO to fill the open coordination site resulting from the coupling (Scheme 4.10). In the scheme, the σ - π distortion of the allyl ligand (refer to Figure 4.3) is emphasized, with the more sp^2 -character terminus of the allyl ligand oriented cis to the acyl ligand (and trans to the nitrosyl). C-C coupling reactions are favoured for sp^2 -hybridized carbon atoms over sp^3 -hybridized carbons as the increased s -character lowers the activation barrier for the transition state.^{112,113} The more sp^2 -character terminus of σ - π distorted allyl ligands has been reported as the site of C-C coupling to aryl ligands at a tungsten center.^{30-32, 35, 39} Additionally,

the nucleophilicity of the allyl ligand has been established for related complexes.³⁷ Coupling of the acyl and allyl ligands results in the formation of the 16e intermediate complex $\text{Cp}^*\text{W}(\text{NO})(\eta^2\text{-CH}_2=\text{CHCMe}_2\text{C(=O)CH}_3)$. Under CO pressure, this intermediate complex quickly converts to **4.5**.

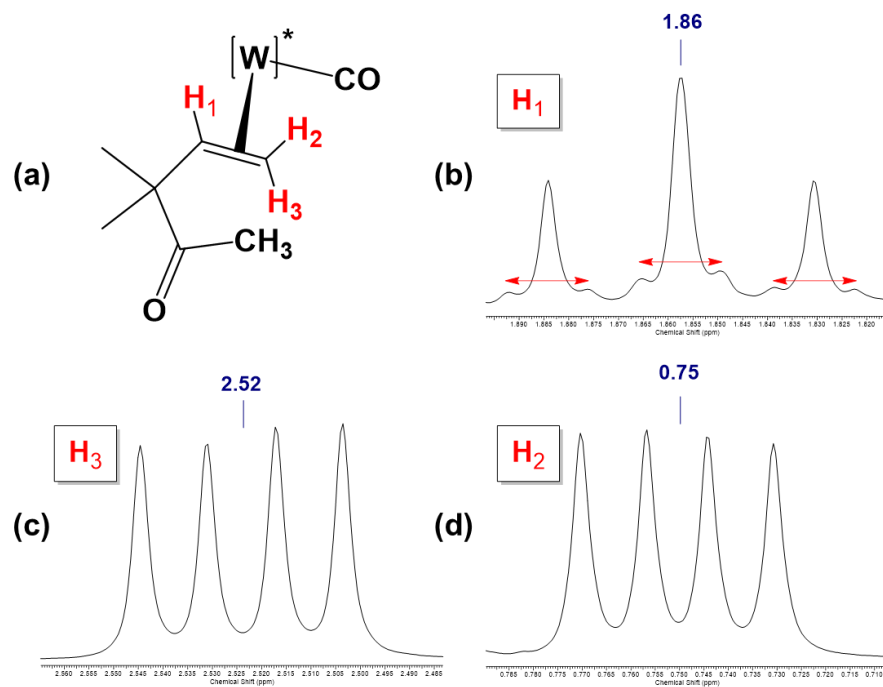
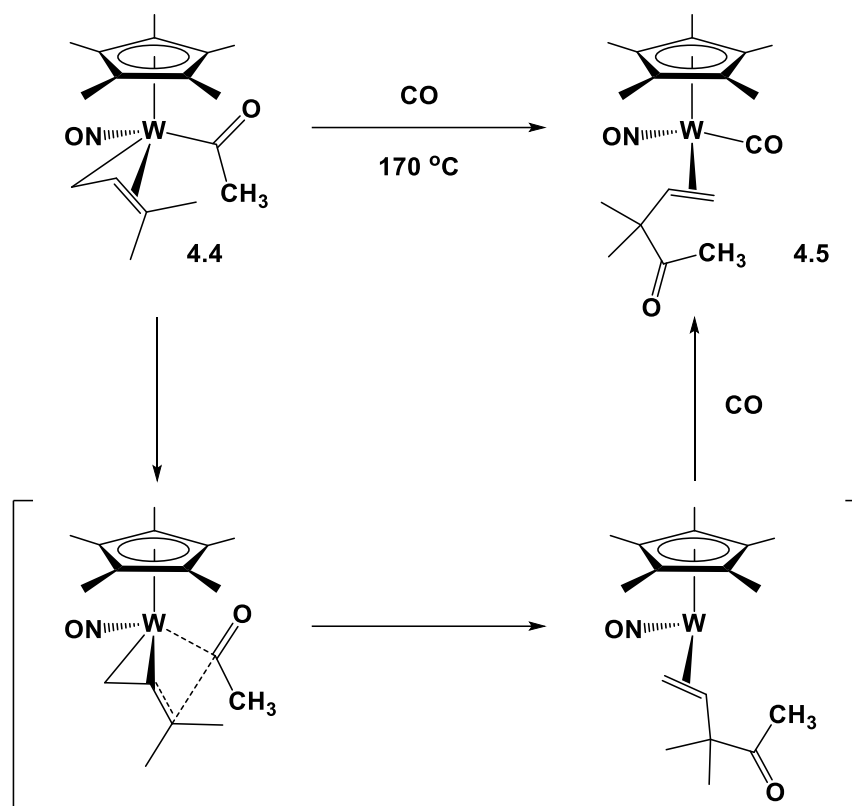


Figure 4.7. Expansions of the ^1H NMR spectrum (400 MHz, C_6D_6) of **4.5** showing the resonances due to the alkene hydrogens. (a) Assignment of protons of **4.5**. (b) Resonance at δ 1.87 ppm (t, $^3J_{\text{HH}} = 10.7$, 1H) due to methine H_1 with characteristic tungsten-183 satellites ($^2J_{\text{WH}} = 7.3$ Hz). (c) Methylene resonance at δ 2.52 ppm (dd, $^3J_{\text{HH}} = 11.0$, $^2J_{\text{HH}} = 5.5$, 1H). (d) Methylene resonance at δ 0.75 ppm (dd, $^3J_{\text{HH}} = 10.5$, $^2J_{\text{HH}} = 5.5$, 1H).

Scheme 4.10. Proposed mechanism for the formation of a η^2 -ketone ligand from a methyl ligand derived from the C-H activation of methane

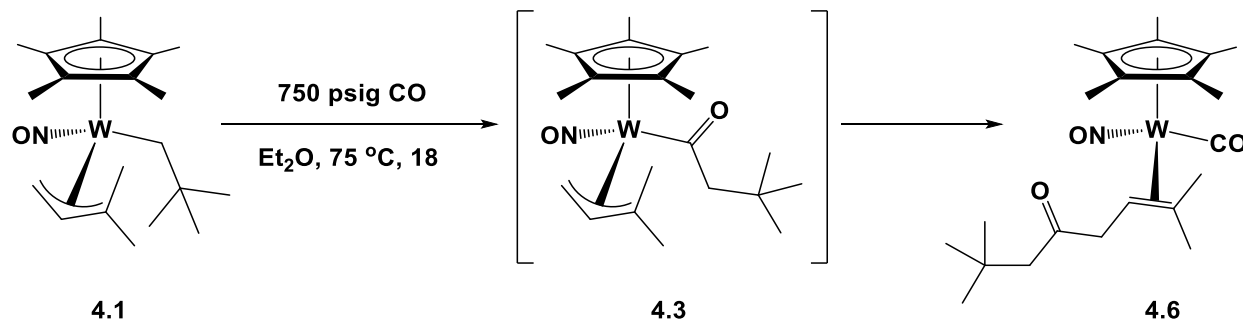


4.2.4.2 Conversion of **4.1** Under CO Pressure to the η^2 -Bound Ketone Complex

Thermolysis of **4.1** at 75 °C for 18 h under CO pressure (750 psig) results in the formation of Cp*W(NO)(CO)(η^2 -Me₂CH₂C(=O)CH₂CMe₃) (**4.6**). Compound **4.6** can be isolated as an orange solid in good yield following column chromatography over silica support. It is air and moisture stable in the solid state and has a reversible melting point of 94-97 °C. Presumably the conversion of **4.1** to **4.6** proceeds through the acyl allyl complex **4.3**, which then undergoes coupling of the acyl and allyl ligands, generating a new C-C bond to form the η^2 bound ketone

complex. As with **4.5**, **4.6** is conveniently characterized by IR spectroscopy exhibiting stretching frequencies for a terminal carbonyl ligand (1944 cm^{-1}), ketone carbonyl (1701 cm^{-1}), and a nitrosyl ligand (1601 cm^{-1}).

Scheme 4.11. Formation of the η^2 -bound ketone complex **4.6**



Single crystals suitable for X-ray diffraction are obtained by recrystallization in DCM/hexane in the air. The solid-state molecular structure (Figure 4.8) confirms the presence of an η^2 -alkene three-legged piano stool compound containing the bound ketone ligand. Most curiously, the acyl ligand appears to have coupled to the methylene terminus of the allyl ligand rather than the CMe_2 terminus, as is observed in complex **4.5**. The η^2 -olefin $\text{C}(14)\text{-C}(15)$ bond length of $1.430(3)\text{ \AA}$ is identical that of **4.5**, indicating a similar degree of tungsten back-bonding. The ketone $\text{C}(17)\text{-O}(3)$ bond has a length of $1.219(3)\text{ \AA}$, similar to that of **4.5** and indicative of a typical ketone carbonyl. The bond angles about $\text{C}(17)$ are consistent with a sp^2 -hybridized carbon. Again, there is no direct interaction between $\text{W}(1)$ and $\text{O}(3)$ which are separated by 5.001 \AA .¹¹⁴

The NMR data is again consistent with the η^2 bound ketone structure. The signals of the two alkene carbon atoms of the η^2 -alkene ligand have upfield chemical shifts of δ 49.4 (=CH) and 65.3 (=CMe₂) ppm in the ¹³C NMR spectrum and each has satellites characteristic of tungsten-183 coupling with ¹J_{WC} values of 41.4 and 7.8 Hz, respectively. The magnitudes of tungsten-carbon coupling are reflective of the strength of the W-C bonding; the longer W(1)-C(14) bond (2.343(2) Å) having the smaller degree of scalar coupling. The signal due to the ketone carbonyl at δ 210.8 ppm is similar to that of **4.5**, as is the resonance for the terminal carbonyl ligand at δ 229.5 ppm, which also has a strong coupling to the tungsten with a ¹J_{WH} = 190.7 Hz. In the ¹H NMR spectrum there is only a single resonance for an alkene signal consistent with acyl coupling to the methylene terminus of the allyl ligand of **4.3**. The upfield chemical shift of the resonance at δ 1.87 (=CH) ppm is indicative of interaction with the tungsten; in addition, this methine signal is a doublet of doublets due to diastereotopic methylene environments adjacent to it (δ 3.07 and 3.15 ppm), which also indicates restricted rotation due to proximity to the tungsten center.

4.2.5 Release of Bound Ketone Ligands

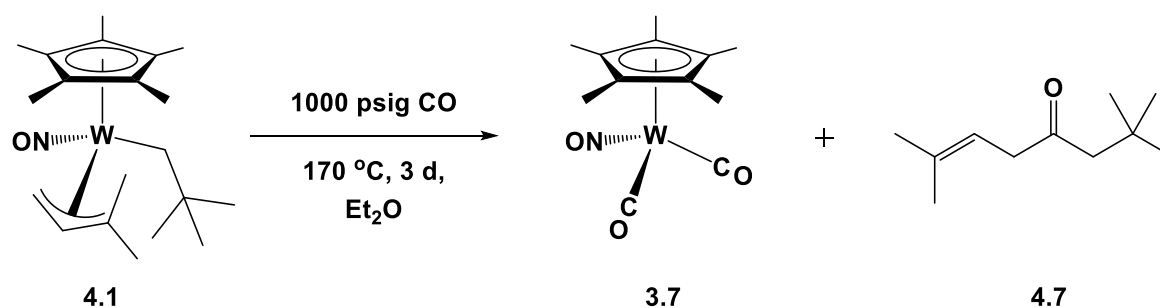
The complexes **4.5** and **4.6** are both exceedingly stable both in solution and as solids. Many efforts to remove the unsaturated ketone ligand from the metal's coordination sphere thermally have been unsuccessful, including heating a solution of either, even in the presence of phosphine, which does not displace the η^2 bound ketone ligand. Heating a sample of **4.6** in a melting tube beyond 160 °C results in the sample boiling and turning brown, suggesting thermal decomposition by 170 °C. However, the reaction outlined in Scheme 4.11 results in the

formation of a small amount of **3.7** and the free ketone ligand alongside formation of **4.6**. This observation suggested that the release of ketone would be possible under elevated temperature and pressure of CO.

4.2.5.1 Thermolysis of **4.6**; Release of 2,2,7-Trimethyloct-6-en-4-one

Heating an Et₂O solution of **4.1** at 170 °C and at 1000 psig CO for 3 d results in the complete conversion of **4.1** to the organometallic product **3.7** and the ketone product 2,2,7-trimethyloct-6-en-4-one (**4.7**) (Scheme 4.12). The two products are obtained as an oily orange solid as separation of the organic and organometallic compounds is difficult by column chromatography since they tend to coelute. Compound **3.7** is easily identified by its strong carbonyl- and nitrosyl-stretching frequencies in the IR spectrum (1991, 1914, 1655 cm⁻¹) and a singlet at δ 2.15 ppm in the ¹H NMR spectrum (CDCl₃) (**Error! Reference source not found.**).

Scheme 4.12. Thermolysis of 4.1 under CO pressure to produce 3.7 and 4.7



The β,γ -unsaturated ketone, **4.7**, has not been previously reported, but has been fully characterized by ¹H and ¹³C NMR spectroscopy. The unsaturated nature of the ketone has been

confirmed using HSQC and HMBC 2D NMR spectroscopy. In addition, an organic ketone carbonyl-stretching frequency in the IR spectrum is observed at 1714 cm^{-1} . Interestingly, the $=CH$ signal is a triplet of septets due to three- and four-bond couplings to the methylene ($^3J_{\text{HH}} = 7.0\text{ Hz}$) and CMe_2 ($^4J_{\text{HH}} = 1.4\text{ Hz}$) protons, respectively (Figure 4.9). A ketone carbonyl-stretching frequency of 1713 cm^{-1} is evident in the IR spectrum.

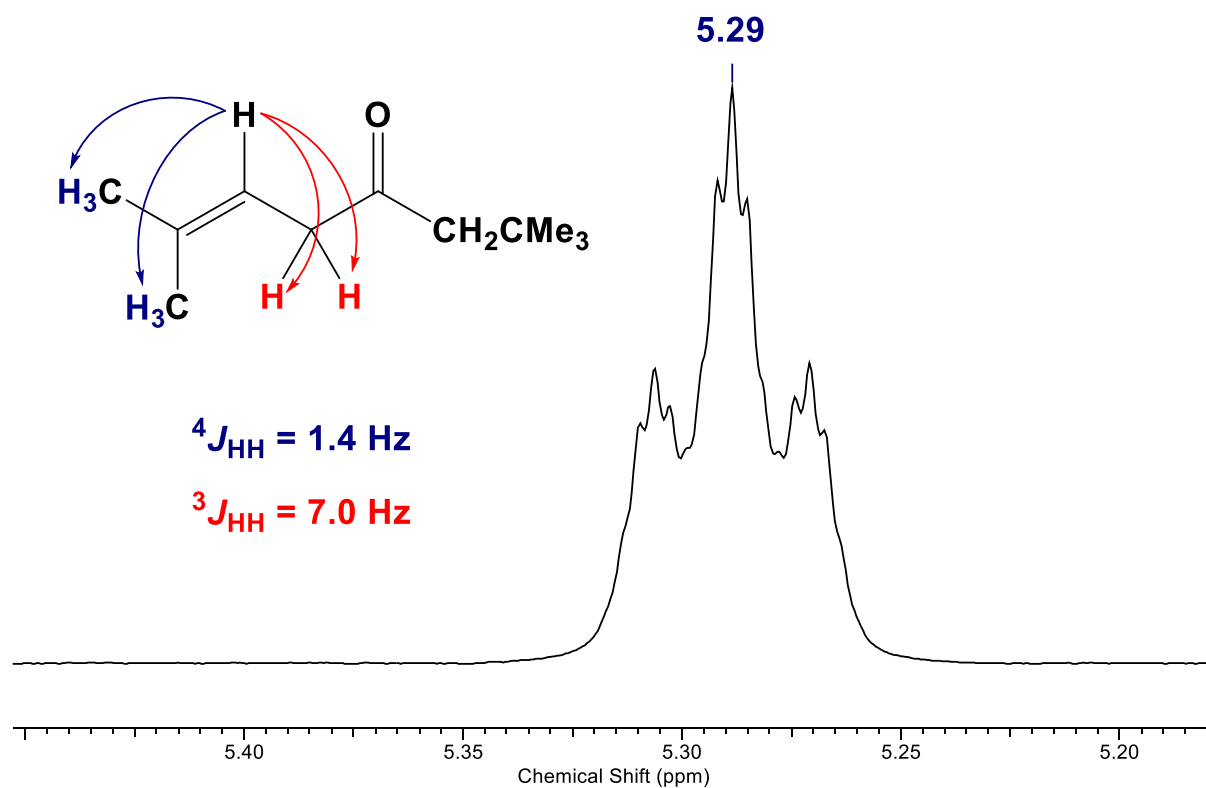
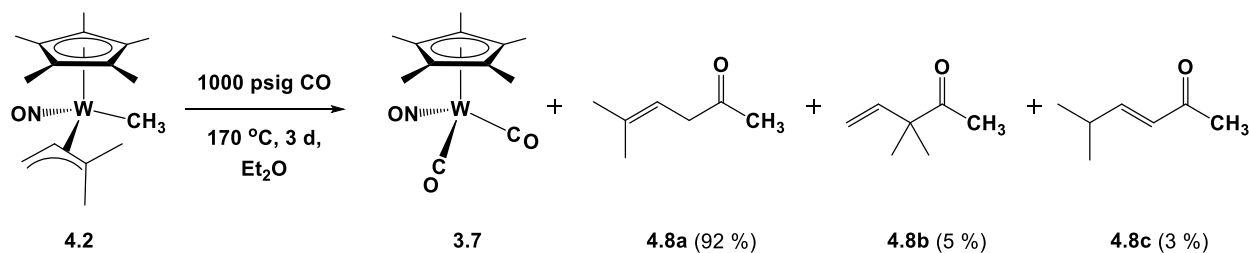


Figure 4.9. Expansion of the ^1H NMR spectrum (400 MHz, CDCl_3) of **4.7** from δ 5.45 to 5.18 ppm showing the triplet of septets of the $=CH$ signals.

4.2.5.2 Conversion of Methane and CO to β,γ -Unsaturated Ketones from 4.5

The thermolysis of **4.2** at 170 °C and 1000 psig CO for 3 days results in the formation of **3.7** and the β,γ -unsaturated ketones 5-methylhex-4-en-2-one (**4.8a**), 3,3-dimethylpent-4-en-2-one (**4.8b**), and *trans*-5-methylhex-3-en-2-one (**4.8c**) (Scheme 4.13) in a 95:5:3 ratio (Figure 4.10). The separation of **3.7** from the mixture of ketones is successful by column chromatography, and it is isolable as an orange solid in decent yield (48%). The three ketones coelute and are isolated as a yellow oil. They are identified and characterized by ^1H and ^{13}C NMR spectroscopy which agrees with the published data for these compounds.¹¹⁵⁻¹¹⁹ As with **4.7**, the $=\text{CH}$ resonance in the ^1H NMR spectrum of compound **4.8a** is characterized as a distinctive triplet of septets (identical to that of **4.7** shown in Figure 4.9) with three- and four-bond coupling to the CH_2 ($^3J_{\text{HH}} = 7.2$ Hz) and CMe_2 ($^4J_{\text{HH}} = 1.4$) protons, respectively. In the IR spectrum the three ketones exhibit a single carbonyl-stretching frequency at 1714 cm^{-1} .

Scheme 4.13. Thermolysis of 4.2 at 170 °C and 1000 psig CO to afford 3.7 and β,γ -unsaturated ketones 4.8a-c



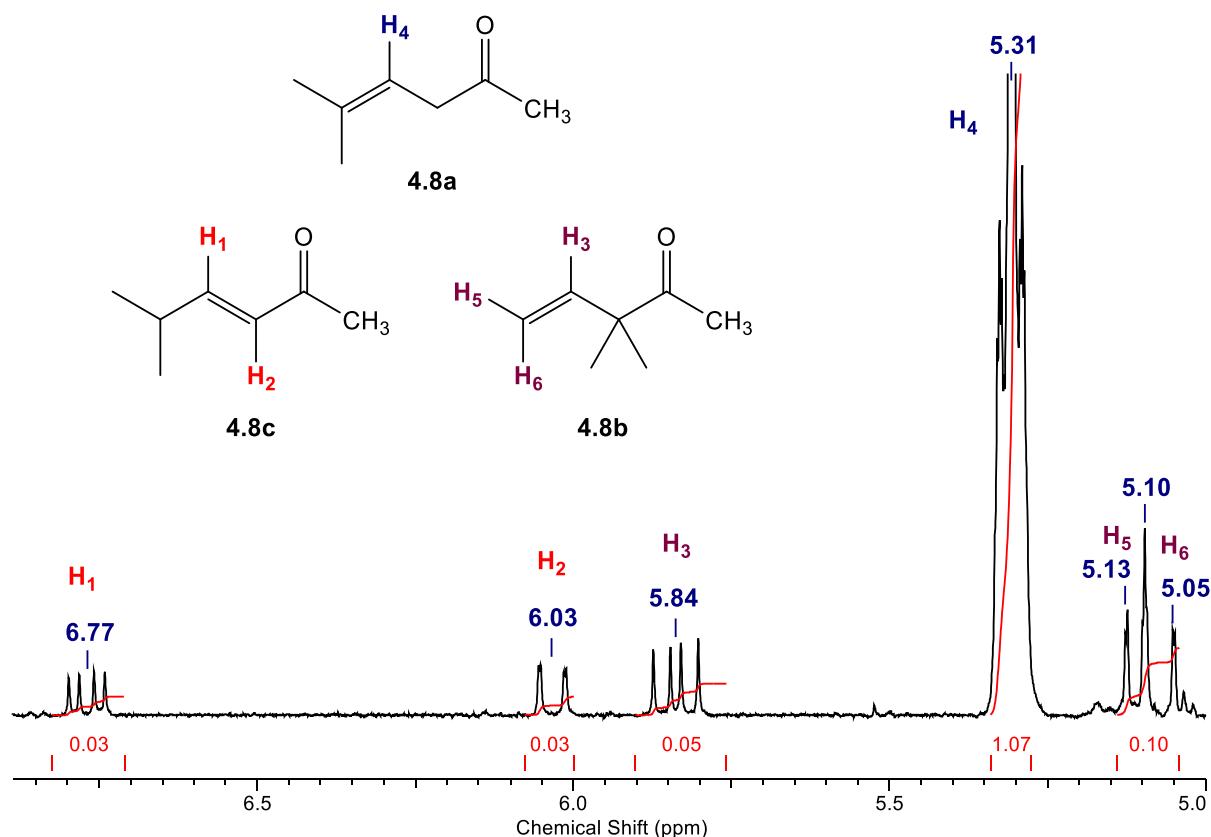
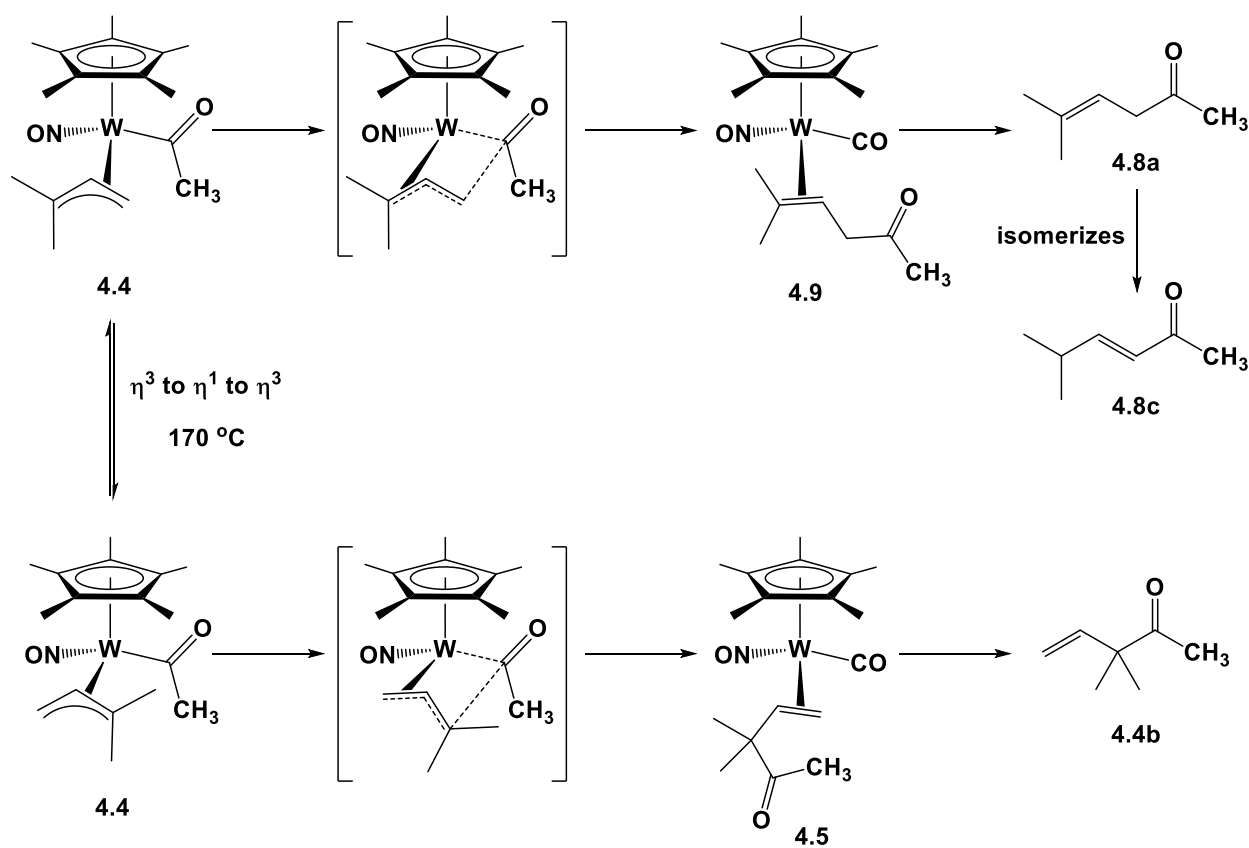


Figure 4.10. Expansion of the ^1H NMR spectrum (400 MHz, CDCl_3) from δ 6.85 to 5.00 ppm of the mixture of ketones **4.8** displaying the characteristic alkene signals of **4.8a** [δ 5.31 (tsep, $^4J_{\text{HH}} = 1.4$, $^3J_{\text{HH}} = 7.2$, 1H, $\text{Me}_2\text{C}=\text{CH}$) ppm], **4.8b** [δ 5.07 (dd, $^3J_{\text{HH}} = 17.6$, $^2J_{\text{HH}} = 1.4$, 1H, $=\text{CH}_2$), 5.11 (dd, $^3J_{\text{HH}} = 11.0$, $^2J_{\text{HH}} = 1.4$, 1H, $=\text{CH}_2$), 5.84 (dd, $^3J_{\text{HH}} = 17.6$, 11.0, 1H, $=\text{CH}$) ppm], and **4.8c** [δ 6.03 (dd, $^4J_{\text{HH}} = 1.4$, $^3J_{\text{HH}} = 16.0$, 1H, $=\text{CHC}(=\text{O})$), 6.77 (dd, $^3J_{\text{HH}} = 16.0$, 6.7, 1H, $\text{Me}_2\text{CHCH}=\text{CH}$) ppm].

Interestingly, the major ketone product is not the ketone released from complex **4.5** (**4.8b**). Instead, the major product is **4.8a**, which is analogous to ketone **4.7** that is released from **4.6**. The coupling of the acyl ligand to the different ends of the allyl ligand must be invoked to account for the different isomers of **4.8** being produced. The proposed mechanism is shown

below in Scheme 4.14 in which the orientation of the allyl ligand changes via a η^3 to η^1 to η^3 haptotropic shift. At 170 °C the favoured orientation of the allyl ligand must be such that the methylene terminus is proximal to the acyl ligand to effect the observed coupling of these two ligands. Under CO pressure the complex $\text{Cp}^*\text{W}(\text{NO})(\text{CO})(\eta^2\text{-Me}_2\text{C=CHCH}_2\text{C(=O)CH}_3)$ (**4.9**) is produced, which ultimately evolves into the products **3.7** and **4.8a**. Ketone **4.8c** is likely produced via the isomerization of the β,γ -unsaturated **4.8a** to the α,β -conjugated ketone **4.8c**.

Scheme 4.14. Proposed mechanism to account for the formation of all three ketones 4.8a-c



The temperature difference during the conversion of **4.4** to **4.5** is the key variable in determining the orientation of the allyl ligand during the coupling. A careful analysis of the

reaction mixtures for the conversion of **4.2** to the η^2 -bound ketone complex at 75 °C and even 120 °C by ^1H NMR spectroscopy reveals small signals only due to ketone **4.8b**, which is released from complex **4.5**. Additionally, heating a sample of pure crystals of **4.5** in a melting tube to 170 °C results in the conversion (ca. 20 %) of some **4.5** to a single ketone product, **4.8b**. This fact supports the hypothesis that temperature during the coupling between the acyl and allyl ligands determines the ketones ultimately released.

4.2.6 Complete Cycle for the Direct Conversion of Methane to Unsaturated Ketones

The final organometallic product, namely $\text{Cp}^*\text{W}(\text{NO})(\text{CO})_2$ (**3.7**) can be readily reconverted to the alkyl allyl reactant **4.1** via $\text{Cp}^*\text{W}(\text{NO})\text{Cl}_2$ which is cleanly obtained by treatment of the dicarbonyl nitrosyl complex with PCl_5 .⁵⁶ Sequential metatheses of $\text{Cp}^*\text{W}(\text{NO})\text{Cl}_2$ with one-half equivalents of the binary magnesium reagents, $\text{Mg}(\text{CH}_2\text{CMe}_3)_2$ and $\text{Mg}(\text{CH}_2\text{CH}=\text{CMe}_2)_2$, then afford the original organometallic nitrosyl complex (refer to Scheme 4.3). This completes a synthetic cycle for the conversion of methane to the ketones **4.8** in which the tungsten complex is recycled (Figure 4.11, *Step 5*).

The direct conversion of methane to ketones has been effected by carrying out the C-H activation of methane by **4.1** to produce **4.2** (*Step 1*, refer to conditions in Scheme 4.4), then carefully exchanging the gas with CO and heating at 75 °C for 3 h to assure formation of **4.4** (*Step 2*). The mixture is then maintained under CO pressure for 3 d at 170 °C which converts **4.4** to **4.5** (and **4.9**, *Step 3*) and ultimately the ketones **4.8a-c** and **3.7** (*Step 4*). Isolation of ketones from the direct, one-pot conversion of methane has been difficult and has resulted in minimal

recovery of isomers of **4.8** (4% yield). Surprisingly, a very good yield of **3.7** has been obtained (72% yield).

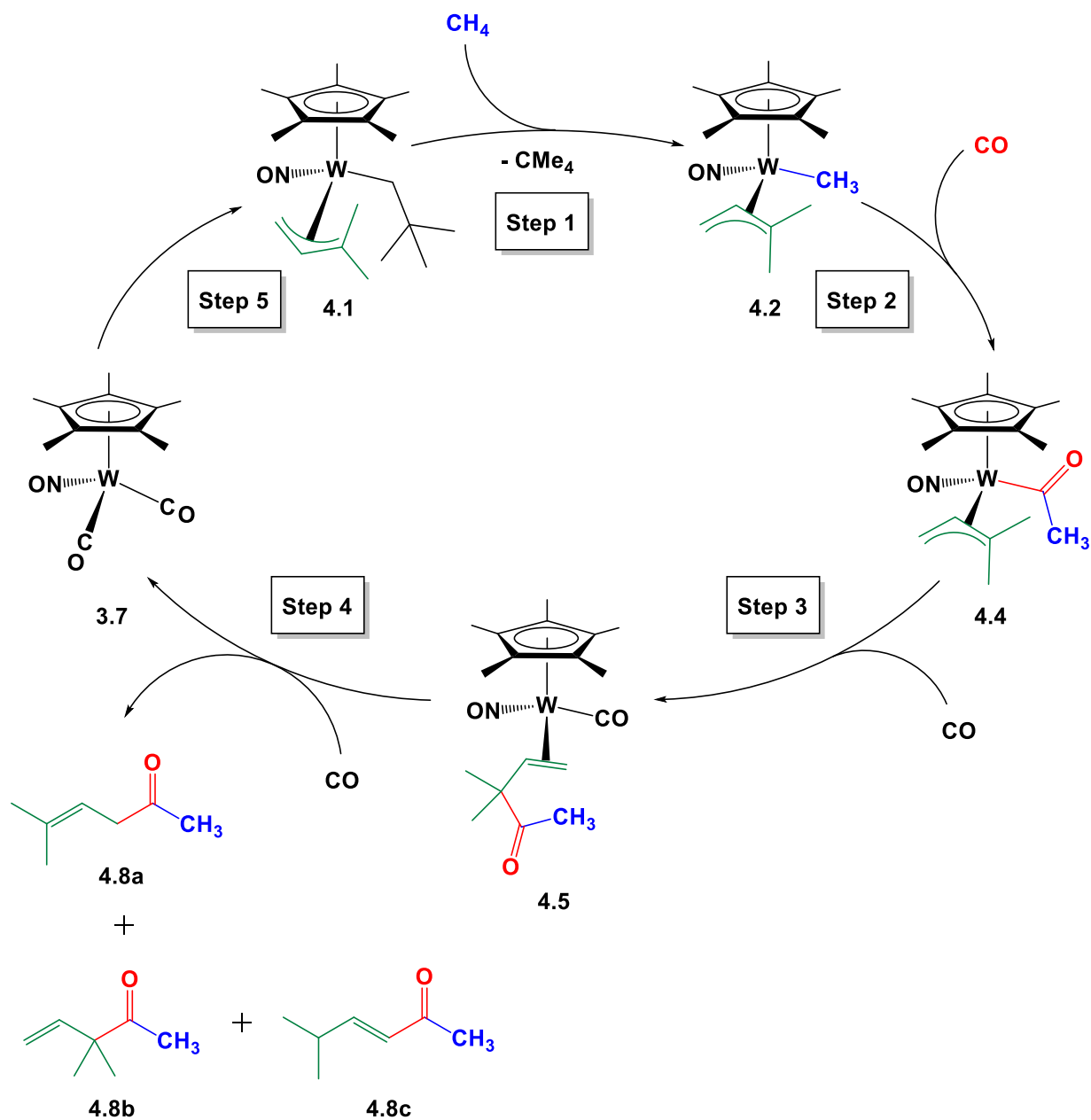


Figure 4.11. Complete synthetic cycle for the conversion of methane into the ketones **4.8a-c** initiated by compound **4.1**.

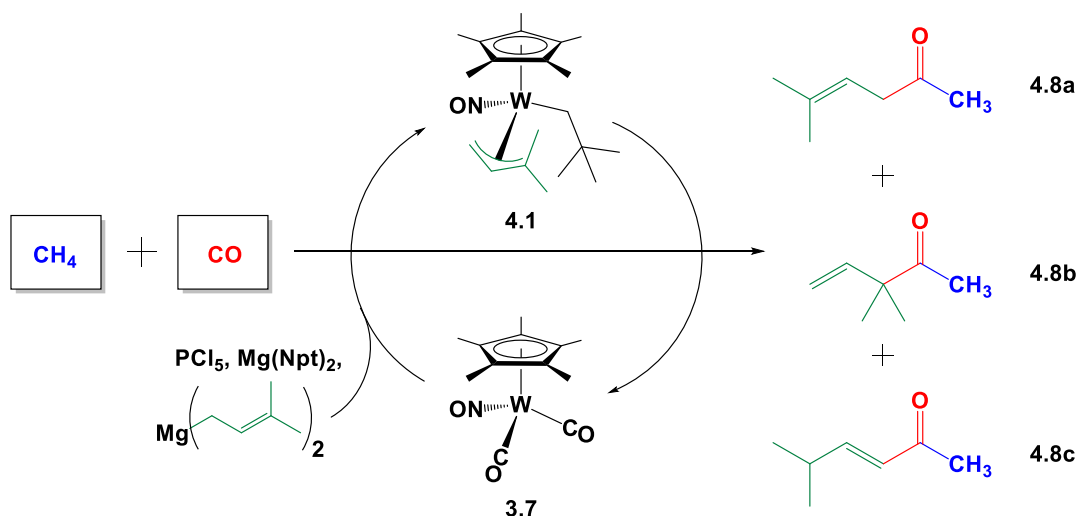
The disparity between the amounts of **3.7** and **4.8** is puzzling and indicates the need for further optimization of the reaction. The isolation of **3.7** suggests that the tungsten complex is not simply decomposing during the combined reaction steps. Pressure optimization steps for the C-H activation of methane showed that **3.3** can be produced as the byproduct from solvent activation. Additionally, the product from the reaction of **3.3** with CO under pressure, Cp*W(NO)(CO)(η^2 -C₆H₁₀) (**4.10**) has been identified from reactions of **4.1** with methane and then CO at 75 °C. This side path could possibly account for the difference in yields between **3.7** and **4.8** as displacement of cyclohexene with CO would account for **3.7** and produce an organic molecule that would be removed in vacuo along with the solvent.

Another possible source of the difference in yields between ketone and **3.7** is that significant quantities of **4.8** are lost while removing solvents. Literature reports of the isolation of one isomer of **4.8** indicate the need to let the solvent evaporate in a fume hood since the volatility of the ketone seems to be problematic.¹¹⁷ A larger isolated yield of the ketone **4.7** compared to **4.8** is obtained by the release from **4.6** and **4.5**, respectively, using the same conditions. In addition the release of **4.8** is carried out in Et₂O, a much more volatile solvent than cyclohexane, which is necessary for the one-pot, direct functionalization of methane. For the one-pot reaction of **4.1** with methane and then CO, an analysis of the reaction mixture by ¹H NMR spectroscopy following the removal of C₆H₁₂ suggest an approximate 2:1 ratio of **3.7** to **4.8**. This supports the hypothesis that the discrepancy in yield may be due to loss of ketone during the work up.

4.3 Summary

The functionalization of methane with CO is initiated by compound **4.1**, converting methane into the unsaturated ketones **4.8a-c**. This transformation involves the C-H activation of methane followed by the formation of two new C-C bonds. In addition, the organometallic complex **3.7** that is obtained from the release of the ketones can be converted back to the starting compound **4.1**, thereby completing a synthetic cycle for the functionalization of methane in which the tungsten complex is recyclable (Scheme 4.15).

Scheme 4.15. Recyclable tungsten center for the conversion of methane to unsaturated ketones



The C-H activation and functionalization of methane involves the formation of various compounds which represent the stepwise transformation of this unreactive gas into an unsaturated ketone. These compounds have all been isolated and characterized, and they contain

distinct spectroscopic properties which allow the transformations occurring during the steps outlined in Figure 4.11 to be conveniently monitored by infrared or NMR spectroscopies (Table 4.4). The end product of these reactions is a methane derivate that is an oil and contains olefin and carbonyl functional sites. This satisfies the criteria of a methane derivative to be suitable both as a fuel (transportable) and as a C1 feedstock (containing conventional functional groups).

Table 4.4. Spectroscopic properties of compounds formed during Steps 1-5 shown in Figure 4.11 tracking the conversion of methane into an unsymmetrical, unsaturated ketone.

Entry	Complex	IR ^[a] (cm ⁻¹)		¹ H NMR ^[b] δ -CH ₃ (ppm)	¹³ C NMR ^[b] δ -CH ₃ (ppm)
		ν NO	ν CO		
1	4.1	1546	–	–	–
2	4.2	1591	–	0.25	4.8
3	4.4	1592	1614	2.91	47.8
4	4.6	1606	1965, 1702	2.14	25.4
5	3.7	1655	1993, 1914	–	–
6	4.8a	–	1712	2.15	29.4

^[a] IR spectra of Nujol mulls. ^[b] NMR spectra of C₆D₆ solutions for entries 1-5, CDCl₃ solution for entry 6.

4.4 Experimental

4.4.1 General Methods

All reactions and subsequent manipulations involving organometallic reagents were performed under anhydrous and anaerobic conditions except where noted. All inert gases were

purified by passing them through a column containing MnO and then through a column of activated 4 Å molecular sieves. High-vacuum and inert atmosphere techniques were performed either using double-manifold Schlenk lines or in Innovative Technologies LabMaster 100 and MS-130 BG dual-station glove boxes equipped with freezers maintained at $-33\text{ }^{\circ}\text{C}$. Preparative scale reactions were performed with Schlenk or round-bottom flasks. Reactions with gases were performed in a Parr 5500 pressure reactor vessel with a capacity of 0.3 L. Reactions with gases that required monitoring were performed using a Parr 5500 pressure reactor that was modified with a sampling arm. Methane and carbon monoxide were obtained from Praxair and used as received. Solvents diethyl ether (Et_2O), and tetrahydrofuran (THF) were dried over sodium/benzophenone ketyl and freshly distilled prior to use; cyclohexane and pentane were dried over calcium hydride, freshly distilled, then dried over molecular sieves prior to use. The binary magnesium reagents used were prepared from the corresponding Grignard reagents⁵⁵ and complex $\text{Cp}^*\text{W}(\text{NO})\text{Cl}_2$ was prepared according to the published procedure.⁵⁶ Pentamethylcyclopentadiene was obtained from the Boulder Scientific Company and other chemicals and reagents were ordered from commercial suppliers and used as received.

All IR samples were prepared as Nujol mulls sandwiched between ZnCl_2 plates, and their spectra were recorded on a Thermo Nicolet Model 4700 FT-IR spectrometer. Except where it has been noted, all NMR spectra were recorded at room temperature on Bruker AV-400 (direct and indirect probes) instruments, and all chemical shifts are reported in ppm and coupling constants are reported in Hz. ^1H NMR spectra were referenced to the residual protio isotopomer present in C_6D_6 (7.16 ppm) or CDCl_3 (7.27 ppm). ^{13}C NMR spectra were referenced to C_6D_6 (128.39 ppm) or CDCl_3 (77.00 ppm). For the characterization of most complexes 2-dimensional NMR experiments, $\{^1\text{H}-^1\text{H}\}$ COSY, $\{^1\text{H}-^{13}\text{C}\}$ HSQC, and $\{^1\text{H}-^{13}\text{C}\}$ HMBC, were performed out to

correlate and assign ^1H and ^{13}C NMR signals and establish atom connectivity. Low- and high-resolution mass spectra (EI, 70 eV) were recorded by Mr. Marshall Lapawa of the UBC mass spectrometry facility using a Kratos MS-50 spectrometer and elemental analyses were performed by Mr. Derek Smith of the UBC microanalytical facility. X-ray crystallographic data collection, solution, and refinement were performed at the UBC X-ray crystallography facility.

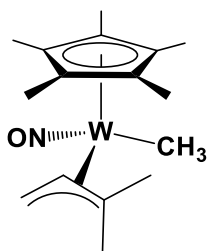
4.4.2 Adapted Synthesis of $\text{Cp}^*\text{W}(\text{NO})(\text{CH}_2\text{CMe}_3)(\eta^3\text{-CH}_2\text{CHCMe}_2)$ (4.1)

In a glove box, $\text{Cp}^*\text{W}(\text{NO})\text{Cl}_2$ (4.2011 g, 10.00 mmol) and $\text{Mg}(\text{CH}_2\text{CMe}_3)_2$ (1.233 g, titre: 126 g/mol, 9.786 mmol) were loaded into two separate Schlenk flasks, and each was charged with a magnetic stir bar and then sealed. On a vacuum line each was charged with Et_2O (ca. 150 mL, 100 mL, respectively), and their contents were cooled in a dry ice/acetone bath (-78°C). The $\text{Mg}(\text{CH}_2\text{CMe}_3)_2/\text{Et}_2\text{O}$ mixture was cannulated into the other flask in a dropwise fashion. This Schlenk flask was then removed from the bath, and its contents were allowed to warm to room temperature while being stirred to afford a dark purple mixture. The solvents were removed under reduced pressure and then transferred with Et_2O (3 x 100 mL) into a third Schlenk flask that had been charged with $\text{Mg}(\text{CH}_2\text{CMe}_3)_2$ (1.466 g, titre: 152 g/mol, 9.645 mmol) and Et_2O (ca. 25 mL) and had already been chilled in a dry ice/acetone bath (-78°C). Following the addition the Schlenk flask was removed from the bath, and its contents were allowed to warm to room temperature while being stirred for about 1 h to give a yellow-brown mixture. The volume of the solvent was reduced in vacuo, and then a concentrated mixture (ca. 150 mL) was directly transferred to the top of a basic alumina column (3 x 12cm). A yellow band was collected with Et_2O to obtain an orange eluate. The solvent was then removed from the

eluate under vacuum to obtain **4.1** as an orange solid (2.418 g, 51% yield) that was then washed with pentane. Characterization of this complex has been reported previously.²⁶

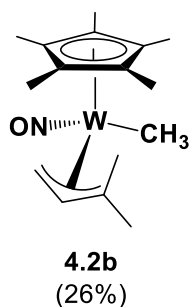
4.4.3 Preparation of $\text{Cp}^*\text{W}(\text{NO})(\text{CH}_3)(\eta^3\text{-CH}_2\text{CHCMe}_2)$ (**4.2**)

In a glove box, a Parr 5500 pressure reactor was charged with **4.1** (0.300 g, 0.613 mmol) and cyclohexane (ca. 75 mL) to give a dark orange mixture. The reactor was sealed and purged three times with 500 psig CH_4 and then pressurized to 1250 psig CH_4 . The contents were heated at 88 °C while being stirred for 0.5 h, after which time the gas was vented and the contents of the reactor were collected as a dark yellow-brown mixture. The solvent was removed in vacuo, and the crude product was purified by column chromatography over basic alumina support. The product was obtained in a yellow eluate using a gradient of 0-30% EtOAc in hexanes. The solvents were removed in vacuo to obtain $\text{Cp}^*\text{W}(\text{NO})(\text{CH}_3)(\eta^3\text{-CH}_2\text{CHCMe}_2)$ (**4.2**) as a yellow powder (184 mg, 69% yield). Yellow crystals suitable for an X-ray diffraction analysis were obtained by recrystallization of this solid from 2:1 pentane/ Et_2O at -33 °C overnight. A melting point of 84-87°C was measured and determined to be reversible by ^1H NMR spectroscopy. The exo/endo orientation of the allyl ligand for each isomer was determined using chemical shift of the meso H signal in the ^1H NMR spectrum.



4.2a
(74%)

Characterization data for **4.2a** (74%): IR (cm⁻¹) 1591 (s, ν_{NO}). MS (LREI, m/z , probe temperature 150 °C) 433 [M^+ , ^{184}W]. ^1H NMR (100 MHz, C_6D_6) δ 0.25 (s, 3H, WCH_3), 1.17 (s, 3H, allyl *Me*), 1.52 (s, 15H, C_5Me_5), 1.58 (s, 3H, allyl *Me*), 1.93 (br s, 1H, allyl CH_2), 2.41 (dd, $^3J_{\text{HH}} = 12.1$, $^2J_{\text{HH}} = 2.7$, 1H, allyl CH_2), 2.90 (dd, $^3J_{\text{HH}} = 12.1$, 8.0, 1H, allyl *CH*). ^{13}C NMR (100 MHz, C_6D_6) δ 4.8 (WCH_3), 10.1 (C_5Me_5), 21.7 (allyl *Me*), 27.4 (allyl *Me*), 36.4 (allyl CH_2), 97.8 (allyl *CH*), 105.6 (C_5Me_5), 120.7 (allyl CMe_2). Anal. Calcd for $\text{C}_{16}\text{H}_{27}\text{NOW}$: C, 44.36; H, 6.28; N, 3.23. Found: C, 44.14; H, 6.22; N, 3.14. Melting point: 84-87 °C.



Characterization data for **4.2b** (26%): ^1H NMR δ 0.23 (overlapping, 3H, WCH_3), 0.49 (br s, 3H, allyl *Me*), 0.72 (br s, 1H allyl CH_2), 1.19 (overlapping, 3H, allyl *Me*), 1.52 (obscured, 15H, C_5Me_5), 2.59 (br s, 1H, allyl CH_2), 4.68 (br s, 1H, meso *H*).

4.4.4 Solvent Optimization for the C-H Activation of Methane by 4.1

4.4.4.1 Preparation of 4.2 Using C_6F_6 as the Solvent

In a glove box a Parr 5500 reactor was charged with **4.1** (0.300 g, 0.613 mmol) and C_6F_6 (ca. 20 mL). The reactor was sealed, purged with CH_4 (3 x 500 psig), and then pressurized to 1250 psig. The contents were heated at 50 °C while being stirred for 6 h. The gas was then

vented, and a yellow mixture was obtained. The solvent was removed in vacuo, and purification was performed by column chromatography over basic alumina support using a gradient of 0-30% EtOAc in hexanes. A yellow eluate was collected, and the solvent was removed in vacuo to afford **4.2** as a yellow solid (130 mg, 49% yield).

4.4.4.2 Preparation of 4.2 Using a Small Volume of C₆H₁₂ as the Solvent

Following the above procedure, a sample of **4.1** (0.300 g, 0.613 mmol) and C₆H₁₂ (ca. 20 mL) were added to a Parr 5500 pressure vessel. The contents were heated at 50 °C for 6 h under 1250 psig CH₄. Following purification by column chromatography, **4.2** was obtained as a yellow solid (106 mg, 40% yield).

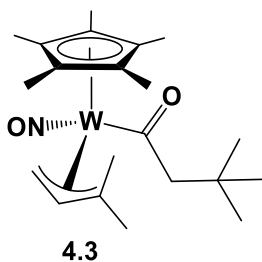
4.4.4.3 Preparation of 4.2 Using an Increased Volume of C₆H₁₂ as the Solvent

Similar to the above procedure, a Parr 5500 pressure vessel was charged with **4.1** (392 mg, 0.801 mmol) and cyclohexane (ca. 125 mL) to give an orange mixture. The reactor contents were pressurized to 1250 psig CH₄ and heated at 50 °C for 6 h. Following purification using column chromatography, **4.2** was obtained as a yellow powder (233 mg, 67% yield).

4.4.5 Preparation of Cp*W(NO)(C(O)CH₂CMe₃)(η^3 -CH₂CHCMe₂) (4.3)

In a glove box, a pressure reactor was charged with **4.1** (251 mg, 0.513 mmol) and a magnetic stir bar. The sample was dissolved in Et₂O (ca. 20 mL) to give a dark orange solution.

Outside the glove box, the reactor was cycled three times with 500 psig of carbon monoxide and then pressurized to 650 psig CO. The contents were stirred and heated to 65 °C for 1 h, and then the reactor was placed in a cold water bath. The gas was vented and a light yellow solution was obtained. The solvent was removed under vacuum to give **4.3** as a yellow solid (246 mg, 93% yield), which was found to be analytically pure. Crystals suitable for single-crystal X-ray diffraction were grown from pentane at -33 °C.

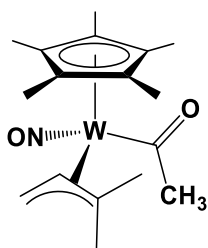


Characterization data for **4.3**: IR (cm⁻¹) 1567 (s, ν_{NO}), 1618 (w, ν_{CO}). MS (LREI, m/z , probe temperature 150 °C) 517 [M^+ , ^{184}W]. ^1H NMR (400 MHz, C_6D_6) δ 1.22 (s, 9H, CMe_3), 1.38 (s, 3H, allyl Me), 1.56 (s, 3H, allyl Me), 1.58 (s, 15H, C_5Me_5), 1.75 (dd, $^3J_{\text{HH}} = 9.4$, $^2J_{\text{HH}} = 2.7$, 1H, allyl CH_2), 2.63 (dd, $^3J_{\text{HH}} = 11.6$, $^2J_{\text{HH}} = 2.7$, 1H, allyl CH_2), 3.14 (d, $^2J_{\text{HH}} = 19.2$, 1H, C(O)CH_2), 3.39 (d, $^2J_{\text{HH}} = 19.2$, 1H, C(O)CH_2), 3.69 (dd, $^3J_{\text{HH}} = 11.6$, 9.4, , 1H, allyl CH). ^{13}C APT NMR (100 MHz, C_6D_6) δ 10.3 (C_5Me_5), 21.2 (allyl Me), 27.8 (allyl Me), 30.4 (CMe_3), 32.1 (CMe_3), 43.8 (allyl CH_2), 75.1 (C(O)CH_2), 102.2 (allyl CH), 107.3 (C_5Me_5), 107.5 (allyl CMe_2), 273.5 (acyl C). Anal. Calcd for $\text{C}_{21}\text{H}_{35}\text{NO}_2\text{W}$: C, 48.75; H, 6.82; N, 2.71. Found: C, 48.65; H, 6.81; N, 2.48.

4.4.6 Preparation of $\text{Cp}^*\text{W}(\text{NO})(\text{C(O)CH}_3)(\eta^3\text{-CH}_2\text{CHCMe}_2)$ (**4.4**)

In a glove box, a Parr 5500 pressure reactor was charged with a sample of **4.2** (95 mg, 0.219 mmol) and Et_2O (ca. 75 mL). The reactor was sealed, removed from the glove box, cycled

three times with 500 psig of CO and then pressurized to 500 psig CO. The contents were mechanically stirred and heated at 75 °C for 3 h, after which time the reactor contents were allowed to cool to room temperature. The gas was then vented, and a yellow solution was obtained. The solvent was removed in vacuo to give a dark yellow oily residue. The yield of complex **4.4** was determined by ^1H NMR spectroscopy (53 mg, 52 % yield). Complex **4.4** is not stable with respect to column chromatography (alumina or silica), and recrystallization is insufficient for maximum recovery. The residue was recrystallized from 2:1 pentane/Et₂O (ca. 2 mL) at -33 °C to produce large orange crystals of **4.4** suitable for X-ray diffraction studies.

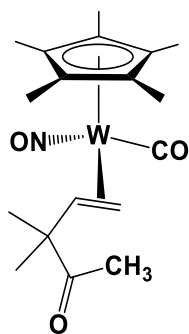


4.4

Characterization data for **4.4**: IR (cm⁻¹) 1592 (s, ν_{NO}), 1614 (w, ν_{CO}). MS (LREI, m/z , probe temperature 150 °C) 461 [M^+ , ^{184}W]. ^1H NMR (600 MHz, C₆D₆) δ 1.35 (s, 3H, allyl *Me*), 1.51 (s, 3H, allyl *Me*), 1.58 (s, 15H, C₅Me₅), 1.71 (m, 1H, allyl CH₂), 2.64 (dd, $^3J_{\text{HH}} = 11.4$, $^2J_{\text{HH}} = 3.1$, 1H, allyl CH₂), 2.91 (s, 3H, C(O)CH₃), 3.76 (br s, 1H, allyl CH). ^{13}C APT NMR (150 MHz, C₆D₆) δ 10.4 (C₅Me₅), 19.5 (allyl *Me*), 28.3 (allyl *Me*), 43.8 (allyl CH₂), 47.8 (C(O)CH₃), 107.5 (C₅Me₅), 109.2 (allyl CMe₂), 116.9 (allyl CH), 273.3 (C(O)CH₃). Anal. Calcd for C₁₇H₂₇NO₂W: C, 44.27; H, 5.90; N, 3.04. Found: C, 44.46; H, 5.95; N, 2.94. Melting point: 93-95 °C.

4.4.7 Preparation of $\text{Cp}^*\text{W}(\text{NO})(\text{CO})(\eta^2\text{-CH}_2=\text{CHCMe}_2\text{C}(\text{O})\text{CH}_3)$ (**4.5**)

In a glove box, a Parr 5500 reactor was charged with complex **4.1** (0.302 g, 0.617 mmol) and C_6H_{12} (ca. 75 mL). The reactor was cycled three times with 500 psig CH_4 and then pressurized to 1250 psig CH_4 . The contents of the reactor were heated at 88 °C while being stirred for 1 h, after which time the contents were cooled and the gas was carefully vented. The reactor was then cycled three times with 500 psig CO and then pressurized to 750 psig CO. The contents of the reactor were heated at 75 °C while being stirred for 3 d. The gas was vented, a yellow-brown mixture was collected, and the solvent was removed in vacuo to afford the concentrated crude product. The crude product was purified via column chromatography over silica using a gradient of 0-100% EtOAc in hexanes. The product was collected as a yellow eluate, and the solvents were removed in vacuo to afford complex **4.5** as an orange oil. Orange crystals suitable for single-crystal X-ray diffraction analysis (70.9 mg, 23% yield) were obtained by recrystallization from 1:1 DCM/hexanes at room temperature. A melting point of 80-83 °C was found to be reversible through identification of **4.5** in the ^1H NMR spectrum of the melt.



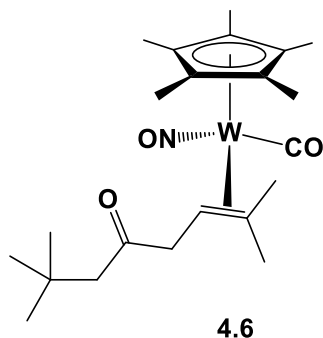
4.5

Characterization data for **4.5**: IR (cm^{-1}) 1606 (s, ν_{NO}), 1702 (w, $\nu_{\text{CO-ketone}}$), 1965 (s, $\nu_{\text{CO-terminal}}$). MS (LREI, m/z , probe temperature 150 °C) 461 [$\text{M}^+ - \text{CO}$, ^{184}W]. MS (HREI, m/z $\text{M}^+ -$

CO, ^{182}W) calcd for $\text{C}_{17}\text{H}_{27}\text{NO}_2^{182}\text{W}$: 459.15240, found: 459.15224. ^1H NMR (400 MHz, C_6D_6) δ 0.75 (dd, $^3J_{\text{HH}} = 10.5$, $^2J_{\text{HH}} = 5.5$, 1H, $=\text{CH}_2$), 0.99 (s, 3H, CMe_2), 1.27 (s, 3H, CMe_2), 1.58 (s, 15H, C_5Me_5), 1.87 (t, $^3J_{\text{HH}} = 10.7$, $^2J_{\text{WH}} = 7.3$, 1H, $=\text{CH}$), 2.14 (s, 3H, $\text{C}(\text{O})\text{Me}$), 2.52 (dd, $^3J_{\text{HH}} = 11.0$, $^2J_{\text{HH}} = 5.5$, 1H, $=\text{CH}_2$). ^{13}C NMR (100 MHz, C_6D_6) δ 10.3 (C_5Me_5), 23.4 (CMe_2), 25.2 (CMe_2), 25.5 ($\text{C}(\text{O})\text{Me}$), 34.1 ($^1J_{\text{WC}} = 11.0$, $=\text{CH}_2$), 53.4 (CMe_2), 55.9 ($^1J_{\text{WC}} = 40.4$, $=\text{CH}$), 105.2 (C_5Me_5), 212.9 ($\text{C}(\text{O})\text{Me}$), 224.4 (W-CO). Anal. Calcd for $\text{C}_{18}\text{H}_{27}\text{NO}_3\text{W}$: C, 44.19; H, 5.56; N, 2.86. Melting point: 80-83 °C.

4.4.8 Preparation of $\text{Cp}^*\text{W}(\text{NO})(\text{CO})(\eta^2\text{-CH}_2=\text{CHCMe}_2\text{C}(\text{O})\text{CH}_2\text{CMe}_3)$ (**4.6**)

In a glove box, a Parr 5500 pressure reactor was charged with **4.1** (2 g, 4 mmol) that was dissolved in Et_2O (ca. 125 mL) to give an orange mixture. The reactor was sealed and purged with CO (3 x 500 psig), then pressurized to 750 psig. The contents of the reactor were heated at 75 °C for 18 h. The gas was then vented, and a dark red mixture was obtained. The solvent was removed under reduced pressure, and the resulting residue was purified by column chromatography over silica support using a gradient of 0-35% EtOAc in hexanes. Two orange bands were collected and then taken to dryness in vacuo. The first band afforded an oily orange solid (0.2444 g) that was a 4:1 mixture (by ^1H NMR spectroscopy) of **3.7** and 2,2,7-trimethyloct-6-en-4-one (vide infra). The band from the second fraction was dried in vacuo to produce $\text{Cp}^*\text{W}(\text{NO})(\text{CO})(\eta^2\text{-CH}_2=\text{CHCMe}_2\text{C}(\text{O})\text{CH}_2\text{CMe}_3)$ (**4.6**) as an orange solid (1.272 g, 58 % yield). Recrystallization from 2:1 DCM/hexanes at room temperature in the air afforded crystals suitable for single crystal X-ray diffraction analysis. A melting point for **4.6** of 94-97 °C was recorded and determined to be reversible by analysis of the melt via ^1H NMR spectroscopy.



Characterization data for **4.6**: IR (cm^{-1}) 1601 (s, ν_{NO}), 1701 (w, $\nu_{\text{CO-ketone}}$), 1944 (s, $\nu_{\text{CO-terminal}}$). MS (LREI, m/z , probe temperature 150 °C) 545 [M^+ , ^{184}W], 517 [$\text{M}^+ - \text{CO}$, ^{184}W]. ^1H NMR (400 MHz, C_6D_6) δ 1.03 (s, 9H, CMe_3), 1.63 (s, 3H, Me), 1.67 (s, 15H, C_5Me_5), 1.87 (dd, $^3J_{\text{HH}} = 8.4, 4.7$, 1H, $=\text{CH}$), 2.07 (s, 2H, $\text{C}(=\text{O})\text{CH}_2\text{CMe}_3$), 2.20 (s, 3H, Me), 3.07 (dd, $^3J_{\text{HH}} = 8.4$, $^2J_{\text{HH}} = 18.6$, 1H, $=\text{CHCH}_2\text{C}(=\text{O})$), 3.15 (dd, $^3J_{\text{HH}} = 4.7$, $^2J_{\text{HH}} = 18.6$, 1H, $=\text{CHCH}_2\text{C}(=\text{O})$). ^{13}C NMR (100 MHz, C_6D_6) δ 10.5 (C_5Me_5), 25.7 ($=\text{CMe}_2$), 30.2 (CMe_3), 30.6 ($=\text{CMe}_2$), 31.2 (CMe_3), 49.4 ($^1J_{\text{WC}} = 41.4$, $=\text{CH}$), 50.4 ($=\text{CHCH}_2\text{C}(=\text{O})$), 54.5 ($\text{C}(=\text{O})\text{CH}_2\text{CMe}_3$), 65.3 ($^1J_{\text{WC}} = 7.8$, $\text{Me}_2\text{C}=\text{C}$), 105.4 (C_5Me_5), 210.8 ($\text{CH}_2\text{C}(=\text{O})\text{CH}_2$), 229.5 ($^1J_{\text{WC}} = 190.7$, W-CO). Anal. Calcd for $\text{C}_{22}\text{H}_{35}\text{NO}_3\text{W}$: C, 48.75; H, 6.82; N, 2.71. Found: C, 48.61; H, 6.47; N, 2.50. Melting point: 94-97 °C.

4.4.9 Reaction of **4.1** with CO at 170 °C; Preparation of 2,2,7-Trimethyloct-6-en-4-one (**4.7**)

In a glove box, a Parr 5500 pressure reactor was charged with **4.1** (0.300 g, 0.613 mmol) that was then dissolved in Et_2O (ca. 100 mL) to give a yellow solution. The reactor was sealed and then cycled with CO (3 x 500 psig) before being pressurized to 1000 psig CO. The contents of the reactor were heated at 170 °C while being stirred. Once cooled, the gas was carefully

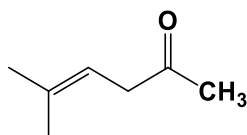
evacuated, and an orange mixture was collected. The solvent was removed to afford a red residue. Purification was performed by column chromatography over silica support using a gradient of 0-35 % EtOAc in hexanes. The products **3.7** and 2,2,7-trimethyloct-6-en-4-one (**4.7**) coeluted as an orange band and were collected as an orange eluate. The solvents were removed under reduced pressure to give a dark orange oily solid that was a mixture of **3.7** (179 mg, 72 % yield) and **4.7** (62 mg, 60 % yield).

Characterization data for **4.7**: IR (cm^{-1}) 1713 (w, ν_{CO}). ESI-MS theoretical m/z for $[\text{M}+\text{H}]^+ = 169.2$; found m/z for $[\text{M}+\text{H}]^+ = 169.3$. ^1H NMR (400 MHz, CDCl_3) δ 1.00 (s, 9H, CMe_3), 1.60 (s, 3H, $=\text{CMe}_2$), 1.73 (s, 3H, $=\text{CMe}_2$), 2.29 (s, 2H, $\text{C}(=\text{O})\text{CH}_2\text{CMe}_3$), 3.06 (d, $^3J_{\text{HH}} = 7.0$, 2H, $=\text{CHCH}_2\text{C}(=\text{O})$), 5.27 (tsep, $^4J_{\text{HH}} = 1.4$, $^3J_{\text{HH}} = 7.0$, 1H, $\text{Me}_2\text{C}=\text{CHCH}_2$).¹²⁰ ^{13}C NMR (100 MHz, CDCl_3) δ 17.9 ($=\text{CMe}_2$), 25.6 ($=\text{CMe}_2$), 29.6 (CMe_3), 30.9 (CMe_3), 44.5 ($=\text{CHCH}_2\text{C}(=\text{O})$), 54.2 ($\text{C}(=\text{O})\text{CH}_2\text{CMe}_3$), 116.0 ($=\text{CH}$), 135.2 ($\text{Me}_2\text{C}=\text{CH}$), 209.0 ($\text{C}(=\text{O})$).¹²¹

4.4.10 Reaction of 4.2 with CO at 170 °C; Preparation of Ketones 5-Methylhex-4-en-2-one (4.8a), 3,3-Dimethylpent-4-en-2-one (4.8b), and *trans*-5-Methylhex-3-en-2-one (4.8c)

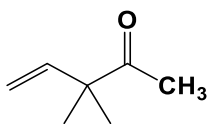
In a glove box, a Parr 5500 series pressure reactor was charged with **4.2** (156 mg, 0.360 mmol) which was dissolved in Et_2O (ca. 100 mL) to give a yellow solution. The reactor was sealed and then purged with CO (3 x 500 psig) before being pressurized to 1000 psig CO. The contents of the reactor were heated at 75 °C while being stirred for 3 h. The temperature was then increased to 170 °C, and the contents of the reactor were stirred at this temperature for 3 d, after which time the contents were allowed to cool and the gas was carefully vented. A light orange mixture was obtained, and then the solvent was removed in vacuo to afford an orange

residue. Purification was performed by column chromatography over silica support using a gradient of 0-15 % EtOAc in hexanes. An orange band was collected as an orange eluate; removal of the solvent afforded **3.7** as an orange solid (70 mg, 48 % yield). A pale yellow eluate was collected immediately after the orange band and the solvent was removed in vacuo to afford a yellow oil that was a mixture of the ketones 5-methylhex-4-en-2-one (**4.8a**), 3,3-dimethylpent-4-en-2-one (**4.8b**), and *trans*-5-methylhex-3-en-2-one (**4.8c**) in a 95:5:3 ratio (10 mg, 25 % yield).



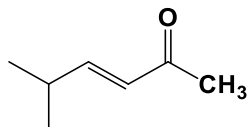
4.8a (92 %)

Characterization data for **4.8a** (92%) which agrees well with that previously reported.^{115,116} IR (cm⁻¹) 1712 (w, ν_{CO}). ¹H NMR (400 MHz, CDCl₃) δ 1.64 (s, 3H, =CMe₂), 1.76 (s, 3H, =CMe₂), 2.15 (s, 3H, C(=O)Me), 3.12 (d, ³J_{HH} = 7.2, 2H, =CHCH₂C(=O)), 5.31 (tsep, ⁴J_{HH} = 1.4, ³J_{HH} = 7.2, 1H, Me₂C=CH).¹²² ¹³C NMR (100 MHz, CDCl₃) δ 18.0 (=CMe₂), 25.7 (=CMe₂), 29.4 (C(=O)CH₃), 43.5 (CH₂C(=O)), 115.9 (=CH), 135.9 (Me₂C=), 207.5 (C(=O)).¹²³



4.8b (5 %)

Characterization data for **4.8b** (5%) which agrees well with that previously reported.^{117,118} ¹H NMR (400 MHz, CDCl₃) δ (selected signals) 5.07 (dd, ³J_{HH} = 17.6, ²J_{HH} = 1.4, 1H, =CH₂), 5.11 (dd, ³J_{HH} = 11.0, ²J_{HH} = 1.4, 1H, =CH₂), 5.84 (dd, ³J_{HH} = 17.6, 11.0, 1H, =CH).



4.8c (3 %)

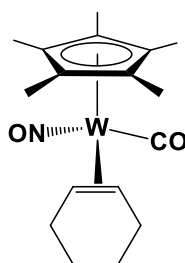
Characterization data for **4.8c** (3%) which agrees well with that previously reported.¹¹⁹ ¹H NMR (400 MHz, CDCl₃) δ 1.09 (d, ³*J*_{HH} = 6.7, 6H, *CMe*₂), 2.26 (s, 3H, C(=O)*Me*), 2.48 (m, 1H, *CHMe*₂), 6.03 (dd, ⁴*J*_{HH} = 1.4, ³*J*_{HH} = 16.0, 1H, =CHC(=O)), 6.77 (dd, ³*J*_{HH} = 16.0, 6.7, 1H, *Me*₂CHCH=).

4.4.11 Direct Conversion of Methane to Ketone

In a glove box, a Parr 5500 series reactor was charged with **4.1** (0.300 g, 0.613 mmol) and C₆H₁₂ (ca.100 mL). The reactor was purged with CH₄ (3 x 500 psig) and then pressurized to 1250 psig CH₄. The contents of the reactor were heated at 88 °C for 0.5 h. The contents of the reactor were allowed to cool, the CH₄ was vented carefully, and the reactor was cycled with CO (3 x 500 psig) before being pressurized with 1000 psig CO. The contents of the reactor were then heated to 75 °C for 3 h before being heated to 170 °C at which temperature the contents were mechanically stirred for 3 d. The contents of the reactor were then cooled, and the CO gas carefully vented. An orange mixture was obtained, and the solvent was carefully removed in vacuo to afford an oily orange solid. Purification of the sample by column chromatography over silica support resulted in the recovery of **3.7** (178 mg, 72% yield) and a mixture of the ketones **4.8a** and **4.8b** (4 mg, 4% yield).

4.4.12 Identification of Cp*W(NO)(CO)(η^2 -C₆H₁₀) Byproduct (4.9)

During a reaction of **4.1** with CH₄ and then CO to produce complex **4.5** (vide supra) the complex Cp*W(NO)(CO)(η^2 -C₆H₁₀) (**4.10**) was recovered during purification of **4.5** by column chromatography over silica support as a yellow eluate that was eluted in 0-1% EtOAc in hexanes. Removal of the solvents in vacuo afforded a yellow oil that was characterized by ¹H and ¹³C NMR spectroscopy and IR spectroscopy.



4.10

Characterization data for **4.10**: IR (cm⁻¹) 1607 (s, ν_{NO}), 1946 (s, $\nu_{\text{CO-terminal}}$). MS (LREI, m/z , probe temperature 150 °C) 459 [M^+ , ¹⁸⁴W], 429 [$\text{M}^+ - \text{NO}$, ¹⁸⁴W]. ¹H NMR (400 MHz, CDCl₃) δ 1.20-1.48 (overlapping m, 4H, CH₂), 1.98 (s, 15H, C₅Me₅), 2.25 (m, 1H, =CH), 2.32 (m, 1H, =CH), 2.46 (m, 1H, =CHCH₂), 2.76 (m, 1H, =CHCH₂), 2.80 (m, 1H, =CHCH₂), 3.10 (m, 1H, =CHCH₂). ¹³C NMR (100 MHz, CDCl₃) δ 10.0 (C₅Me₅), 22.1 (CH₂), 22.4 (CH₂), 27.9 (=CHCH₂), 28.6 (=CHCH₂), 47.2 (¹J_{WC} = 36.5, =CH), 56.6 (¹J_{WC} = 10.1, =CH), 104.4 (C₅Me₅), 228.4 (W-CO).

4.4.13 X-ray crystallography

Data collection was carried out at -183.0 ± 1 °C on a Bruker APEX DUO diffractometer equipped with a TRIUMPH curved-crystal monochromator using Mo-K α radiation or at -173.0 ± 2 °C on a Bruker X8 APEX II diffractometer with graphite-monochromated Mo K α radiation.

Data for **4.2** were collected to a maximum 2θ value of 60.1° in 0.5° oscillations and the crystal-to-detector distance was 39.92 mm. The structure was solved by direct methods¹²⁴ and expanded using Fourier techniques. The complex crystallized as a two-component twin. The twin components were separated using Cell_Now¹²⁵ and TWINABS.¹²⁶ The structure was solved using non-overlapping data from the major twin component (24400 reflections). The final cycle of full-matrix least-squares analysis was based on 11352 observed reflections and 183 variable parameters.

Data for **4.3** were collected to a maximum 2θ value of 60.88° in 0.5° oscillations. The structure was solved by direct methods⁶⁰ and expanded using Fourier techniques. All non-hydrogen atoms were refined anisotropically. All hydrogen atoms were included in fixed positions. The final cycle of full-matrix least-squares analysis was based on 5030 observed reflections and 236 variable parameters.

Data for **4.4** were collected to a maximum 2θ value of 52.928° in 0.5° oscillations. The structure was solved by direct methods⁶⁰ and expanded using Fourier techniques. The structure was a 5-component twin and the twin components were separated using Cell_Now¹²⁵ and TWINABS.¹²⁶ The tungsten atom was disordered for each asymmetric unit. All non-hydrogen atoms were refined anisotropically. All hydrogen atoms were included in fixed positions. The

final cycle of full-matrix least-squares analysis was based on 6990 observed reflections and 428 variable parameters.

Data for **4.5** were collected to a maximum 2θ value of 55.084° in 0.5° oscillations. The structure was solved by direct methods⁶⁰ and expanded using Fourier techniques. All non-hydrogen atoms were refined anisotropically. Hydrogens H11A, H11B, and H12 were refined isotropically. All other hydrogen atoms were included in fixed positions. The final cycle of full-matrix least-squares analysis was based on 4121 observed reflections and 228 variable parameters.

Data for **4.6** were collected to a maximum 2θ value of 60.076° in 0.5° oscillations. The structure was solved by direct methods⁶⁰ and expanded using Fourier techniques. All non-hydrogen atoms were refined anisotropically. Hydrogens H15, H16A, and H16B were refined isotropically. All other hydrogen atoms were included in calculated positions. The final cycle of full-matrix least-squares analysis was based on 6522 observed reflections and 266 variable parameters.

For each structure neutral-atom scattering factors were taken from Cromer and Waber.⁶¹ Anomalous dispersion effects were included in F_{calc} ;⁶² the values for $\Delta f''$ and $\Delta f'''$ were those of Creagh and McAuley.⁶³ The values for mass attenuation coefficients were those of Creagh and Hubbell.⁶⁴ All calculations were performed using either SHELXL-97⁶⁵ via the WinGX interface⁶⁶ or XL⁶⁷ or SHELXL-2014⁹⁹ via the OLEX interface.⁶⁸ X-ray crystallographic data for all five structures are presented in Table 4.5.

Table 4.5. X-ray crystallographic data for complexes **4.2-4.6**.

Compound	4.2	4.3	4.4	4.5	4.6
Empirical formula	C ₁₆ H ₂₇ NO ₂ W	C ₂₁ H ₃₅ NO ₂ W	C ₁₇ H ₂₇ NO ₂ W	C ₁₈ H ₂₇ NO ₃ W	C ₂₂ H ₃₅ NO ₃ W
Formula weight	433.24	517.35	461.24	489.25	545.36
Crystal size (mm)	0.44 × 0.23 × 0.12	0.25 × 0.15 × 0.12	0.18 × 0.12 × 0.11	0.26 × 0.16 × 0.1	0.33 × 0.29 × 0.13
Crystal system	Orthorhombic	Monoclinic	Monoclinic	Triclinic	Monoclinic
Space group	P2 ₁ 2 ₁ 2 ₁	P2 ₁	P2 ₁ /c	P-1	P2 ₁ /n
Volume (Å ³)	1618.33(9)	1058.37(8)	3395.6(7)	901.1(2)	2228.01(16)
a (Å)	8.8311(3)	11.3415(5)	16.0573(19)	7.6755(11)	9.5711(4)
b (Å)	13.2430(4)	8.9764(4)	14.9969(17)	9.6081(14)	9.6143(4)
c (Å)	13.8378(4)	11.5230(5)	15.4854(18)	12.8443(18)	24.3692(9)
α (°)	90	90	90	88.560(3)	90
β (°)	90	115.552(2)	114.412(2)	76.212(2)	96.5040(10)
γ (°)	90	90	90	78.457(2)	90
Z	4	2	8	2	4
Density, ρ (calculated) (Mg/m ³)	1.778	1.623	1.804	1.803	1.626
Absorption coefficient, μ (mm ⁻¹)	7.132	5.470	6.808	6.424	5.205
F ₀₀₀	848.0	516.0	1808.0	480.0	1088.0
Measured Reflections: Total	51796	11193	40967	17030	26734
Measured Reflections: Unique	11352	5030	6990	4121	6522
Final R Indices	R ₁ = 0.0478, wR ₂ = 0.1278	R ₁ = 0.0209, wR ₂ = 0.0585	R ₁ = 0.0375, wR ₂ = 0.0790	R ₁ = 0.0144, wR ₂ = 0.0342	R ₁ = 0.0234, wR ₂ = 0.0422
Goodness-of-fit on F ²	1.079	1.204	1.086	1.061	1.161
Largest diff. peak/hole (e ⁻ Å ⁻³)	2.34/-2.24	1.14/-1.86	2.65/-1.09	1.07/-0.43	2.35/-0.98

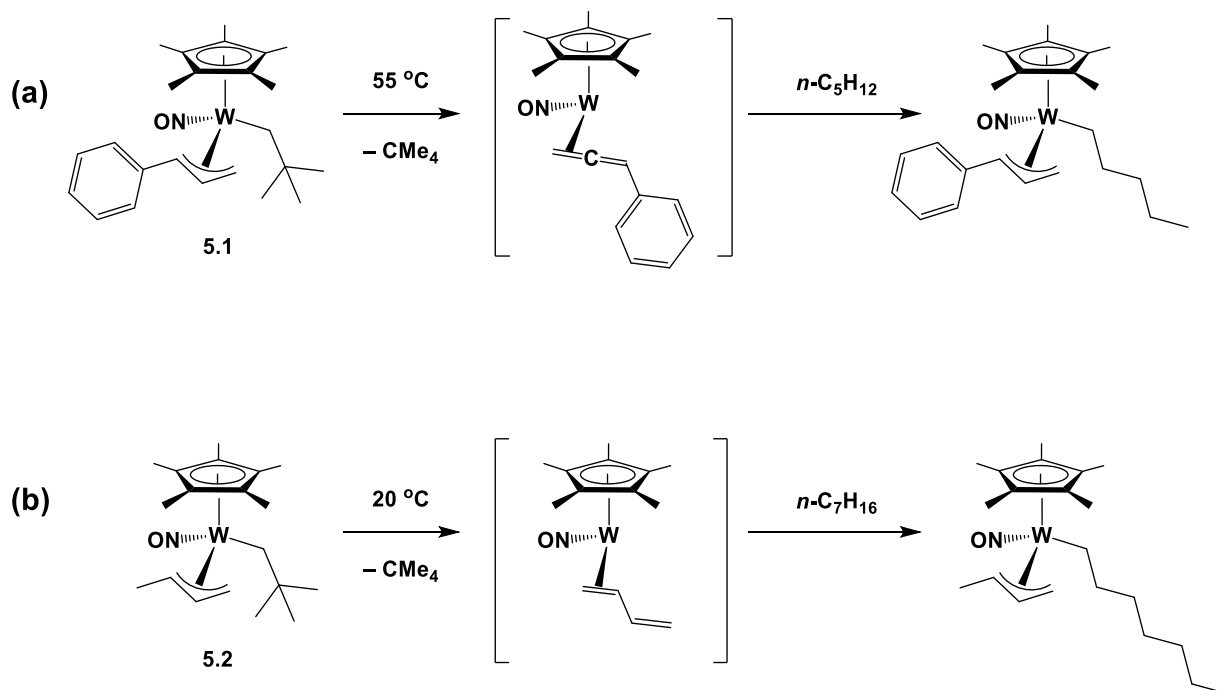
**Chapter 5: The Functionalization of Methane, Ethane,
and Other Hydrocarbons Initiated by
 $\text{Cp}^*\text{W}(\text{NO})(\text{CH}_2\text{CMe}_3)(\eta^3\text{-Allyl})$ Complexes**

5.1 Introduction

The work presented in the previous chapter culminated in the conversion of methane into an unsymmetrical, unsaturated ketone. The transformation involves the coupling of methane to carbon monoxide and the dimethylallyl ligand of complex **5.2**. In theory, effecting this same transformation with different $\text{Cp}^*\text{W}(\text{NO})(\text{CH}_2\text{CMe}_3)(\eta^3\text{-allyl})$ complexes would allow for the incorporation of different functional units into the ketones. Additionally, the ability to effect the functionalization of ethane and larger alkanes and hydrocarbons would increase the scope of the chemistry presented in Chapter 4 and give it a much broader appeal.

The monosubstituted allyl-containing complexes $\text{Cp}^*\text{W}(\text{NO})(\text{CH}_2\text{CMe}_3)(\eta^3\text{-CH}_2\text{CHCHPh})$ (**5.1**) and $\text{Cp}^*\text{W}(\text{NO})(\text{CH}_2\text{CMe}_3)(\eta^3\text{-CH}_2\text{CHCHMe})$ (**5.2**) have been reported to effect the single, C-H activation of linear alkanes. At 55 °C compound **5.1** loses neopentane to generate the 16e intermediate complex $\text{Cp}^*\text{W}(\text{NO})(\eta^2\text{-CH}_2=\text{C}=\text{CHPh})$, which in neat alkane can effect the single, selective terminal C-H bond activation of an alkane molecule (Scheme 5.1a). Likewise, complex **5.2** loses neopentane under ambient temperatures to generate the 16e intermediate complex $\text{Cp}^*\text{W}(\text{NO})(\eta^2\text{-CH}_2=\text{CHCH}=\text{CH}_2)$ that can effect the selective intermolecular C-H activation of a linear alkane (Scheme 5.1b).

Scheme 5.1. The single terminal C-H activation of linear alkanes effected by compounds **5.1 and **5.2****



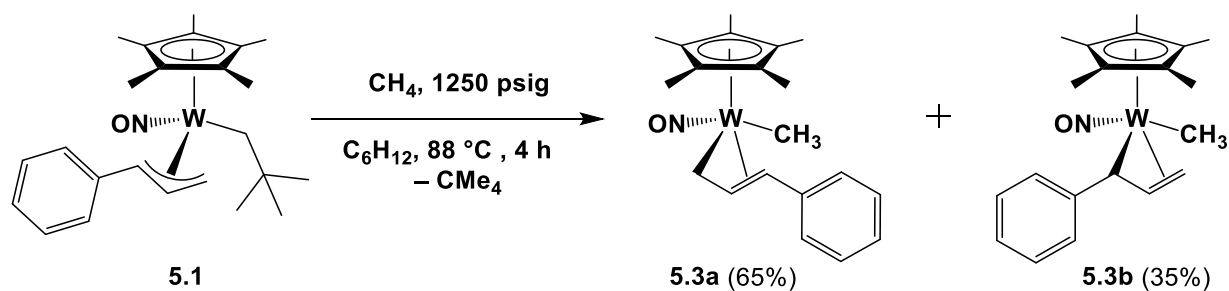
This chapter describes the C-H activation of gaseous alkanes and heteroatom-containing hydrocarbons by the monosubstituted allyl complexes **5.1** and **5.2**. The reactivity of these intermolecular C-H activation products with CO are explored in order to assess the ability of **5.1** and **5.2** to initiate the functionalization of alkanes with CO in a fashion parallel to the conversion of methane to β,γ -unsaturated ketones initiated by compound **4.1** presented in the previous chapter. The functionalization of the *n*-alkyl ligands derived from single, selective alkane activation is the subject of this chapter.

5.2 Results and Discussion

5.2.1 C-H Activation of Methane by $\text{Cp}^*\text{W}(\text{NO})(\text{CH}_2\text{CMe}_3)(\eta^3\text{-CH}_2\text{CHCHPh})$

The reaction of **5.1** with methane is conveniently performed in a Parr 5500 pressure reactor with a 0.3 L volume. The thermolysis of **5.1** at 88 °C for 4 h under 1250 psig CH_4 results in the C-H activation of methane and formation of two isomers of the complex $\text{Cp}^*\text{W}(\text{NO})(\text{CH}_3)(\eta^3\text{-CH}_2\text{CHCHPh})$ (**5.3a,b**) in a 65:35 ratio (Scheme 5.2). As with the reaction of **4.1** with methane, cyclohexane is used as the solvent since it contains only secondary $\text{C}(sp^3)\text{-H}$ bonds and **5.1** has demonstrated a preference for activating primary sp^3 C-H bonds.²⁸ A methane pressure of approximately 500 psig is sufficient in this case to ensure that no solvent activation occurs. Compound **5.3** is purified by column chromatography over basic alumina support and is obtained as a yellow solid that is both air and moisture stable for days. The complex has a melting point of 106-108 °C that has been confirmed to be reversible by ^1H NMR spectroscopy. Complex **5.3** has been characterized by conventional spectroscopic techniques and by single-crystal X-ray diffraction.

Scheme 5.2. C-H activation of methane by **5.1**



In solution **5.3** exists as two isomers which differ in the position of the phenyl substituent of the allyl ligand; in the major isomer (**5.3a**, 65 %) the phenyl substituent is proximal to the methyl ligand while in the minor isomer the phenyl substituent is proximal to the nitrosyl ligand. The orientation of the phenyl substituent has been established by Sel NOE NMR spectroscopy which has also established that the two isomers exchange in solution. The signals for the methyl ligands of the **5.3** isomers in the ^1H NMR spectrum both have upfield chemical shifts of δ -0.18 and 0.45 ppm, and each display satellites due to ^{183}W coupling with $^2J_{\text{HH}}$ values of 5.4 Hz and 6.0 Hz for complexes **5.3a** and **5.3b**, respectively. Likewise, the resonances due to the methyl ligands of **5.3a** and **5.3b** in the ^{13}C NMR spectrum both have upfield chemical shifts of δ 6.7 and -2.7 ppm, with satellites characteristic of tungsten-183 coupling ($^1J_{\text{WC}} = 81.2$ Hz) for the signal belonging to **5.3a**. The IR spectrum of complex **5.3** as a Nujol mull exhibits only a single nitrosyl-stretching frequency at 1583 cm^{-1} . This is consistent with the two isomers differing only in the orientation of the phenyl substituent of the allyl ligand.

Crystals of **5.3** suitable for single-crystal X-ray diffraction are grown from the mixture of isomers, and only the minor isomer **5.3b** is present in the established solid-state molecular structure (Figure 5.1). The exo orientation of the allyl ligand is confirmed with the phenyl substituent proximal to the nitrosyl ligand. A slight σ - π distortion of the allyl ligand is observed with unequal C(11)-C(12) and C(12)-C(13) bond lengths. The shorter, π -character C(11)-C(12) bond ($1.383(10)\text{ \AA}$) is oriented trans to the nitrosyl ligand with the methylene C proximal to the methyl ligand. This agrees with the chemical shifts of the allyl carbon signals in the ^{13}C APT NMR spectrum (vide infra; refer to Figure 5.2) as well as the Sel NOE NMR data. The W(1)-C(20) bond for the methyl ligand derived from the C-H activation of methane has a length of

2.209(7) Å, which is comparable to the W-C bond length of the methyl ligand in complex **4.2** (2.216(5) Å). The nitrosyl ligand is linear with a W-N-O bond angle of 171.4(6)°.

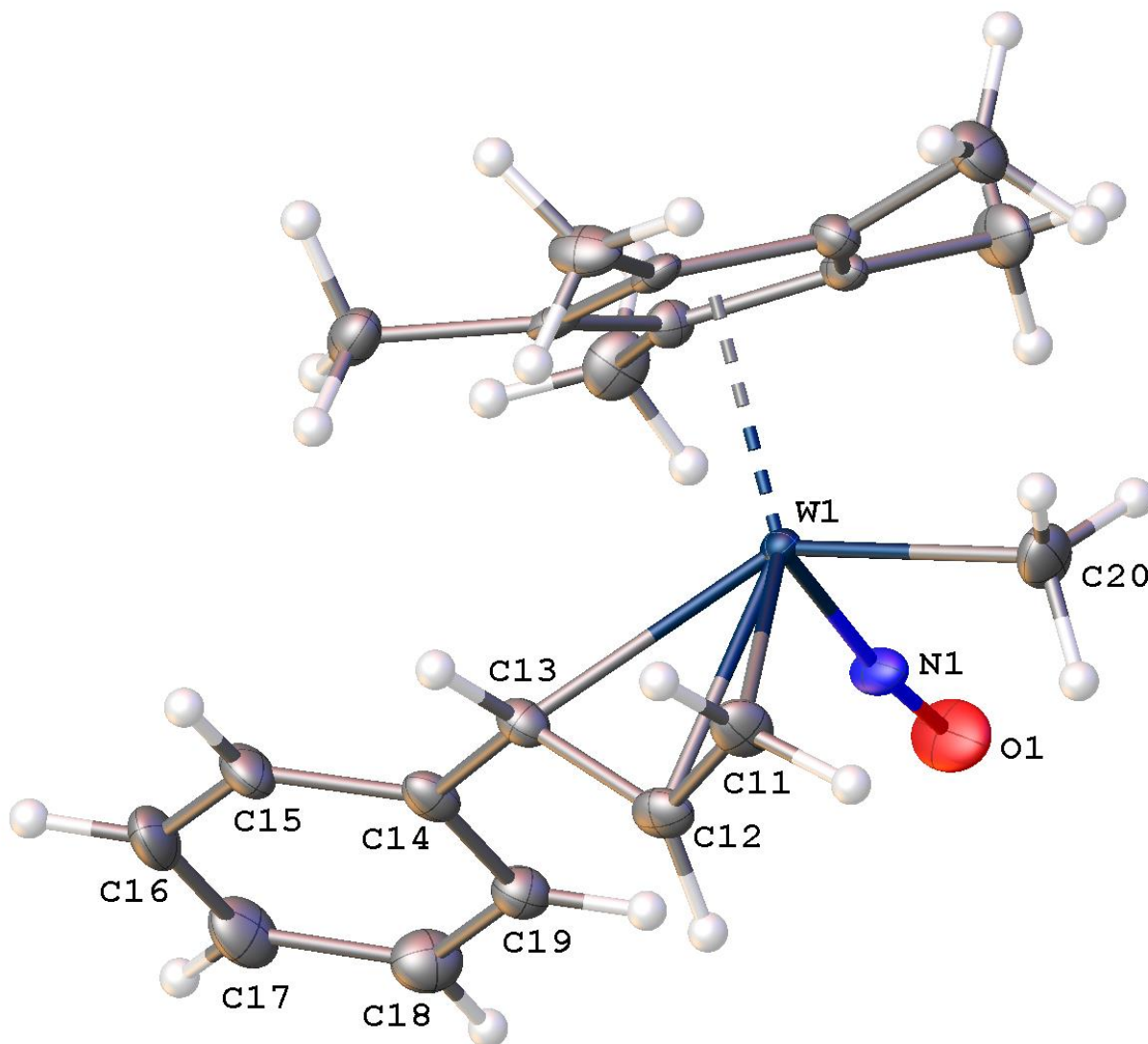


Figure 5.1. Solid-state molecular structure of **5.3a** with 50% probability thermal ellipsoids shown. Selected interatomic distances (Å) and angles (deg.): W(1)-C(20) = 2.209(7), W(1)-C(11) = 2.353(7), W(1)-C(12) = 2.315(7), W(1)-C(13) = 2.323(7), C(11)-C(12) = 1.383(10), C(12)-C(13) = 1.411(10), C(13)-C(14) = 1.484(10), W(1)-N(1) = 1.766(6), N(1)-O(1) = 1.228(8), C(11)-C(12)-C(13) = 117.8(7), C(12)-C(13)-C(14) = 123.2(7), W(1)-N(1)-O(1) = 171.4(6).

The existence of two isomers for a $\text{Cp}^*\text{W}(\text{NO})(\text{alkyl})(\eta^3\text{-CH}_2\text{CHCHPh})$ complex has not been reported previously.²⁸ These complexes all exist as a single isomer in solution, and the phenyl substituent of the allyl ligand is always proximal to the nitrosyl ligand. For complex **5.3**, not only are there two distinct isomers in solution, in the major species **5.3a** the phenyl substituent is proximal to the methyl ligand. A likely explanation for this involves a steric factor, as the methyl group is a much smaller alkyl ligand than the neopentyl in **5.1** (which exists as a single isomer in solution) and alkyl ligands for other reported $\text{Cp}^*\text{W}(\text{NO})(\text{alkyl})(\eta^3\text{-CH}_2\text{CHCHPh})$ complexes.²⁸ Additionally, for the related hydride complex **2.2** (vide supra), the isomer distribution in solution favours the phenyl substituent being proximal to the smaller hydride ligand for 97% of the isomer mixture.⁴³ As the steric bulk of the ligand increases from hydride to methyl to neopentyl, the phenyl substituent of the allyl ligand is increasingly found proximal to the nitrosyl ligand.

5.2.1.1 Identification of Isomers through the σ - π Distortion of the Allyl Ligand and ^{13}C NMR Spectroscopy

The general family of $\text{Cp}^*\text{W}(\text{NO})(\text{alkyl})(\eta^3\text{-allyl})$ complexes displays a characteristic σ - π distortion of the allyl ligand in which the allyl ligand does not have equal carbon-carbon bond lengths, but rather one longer (σ) and one shorter (π). The shorter (π) C-C bond of the allyl is located trans to the nitrosyl ligand (with the σ terminus being proximal to the nitrosyl).³¹ The origin of the σ - π distortion is a result of the electron asymmetry at the metal center which is caused by both the nitrosyl and the cyclopentadienyl ligands.^{31, 127} This effect is observed in the solid-state by X-ray crystallography – by the C-C bond lengths – and in solution by ^{13}C NMR

spectroscopy – the chemical shift values indicating more sp^2 (downfield) or sp^3 (upfield) character of the carbon.^{30, 35}

The isomers of **5.3** present the opportunity for a detailed case study of the σ - π distortion of the allyl ligand and how it can be utilized to identify the orientation of the substituents of the allyl ligand for isomers of a particular $\text{Cp}^*\text{W}(\text{NO})(\text{alkyl})(\eta^3\text{-allyl})$ complex. The orientation of the allyl ligand and positions of the substituents for **5.3a** and **5.3b** have been determined using Sel NOE NMR spectroscopy. The chemical shifts of the signals due to the allyl carbons for each isomer are shown in Figure 5.2. The terminal carbon signal with the more downfield resonance—and having more sp^2 -character—is the one trans to the nitrosyl ligand and proximal to the methyl ligand in each case. Specifically, for the major isomer **5.3a**, the CHPh carbon signal has the more downfield chemical shift (δ 95.6 ppm relative to the methylene C signal at δ 38.1 ppm), which indicates that the phenyl substituent of the allyl ligand is proximal to the allyl methyl ligand. Similarly, for the minor isomer **5.3b** the methylene terminus of the allyl ligand has a signal with the more downfield chemical shift (δ 72.9 ppm compared to δ 63.3 ppm for the CHPh signal), indicating that the phenyl substituent of the allyl ligand is proximal to the nitrosyl ligand for this isomer.

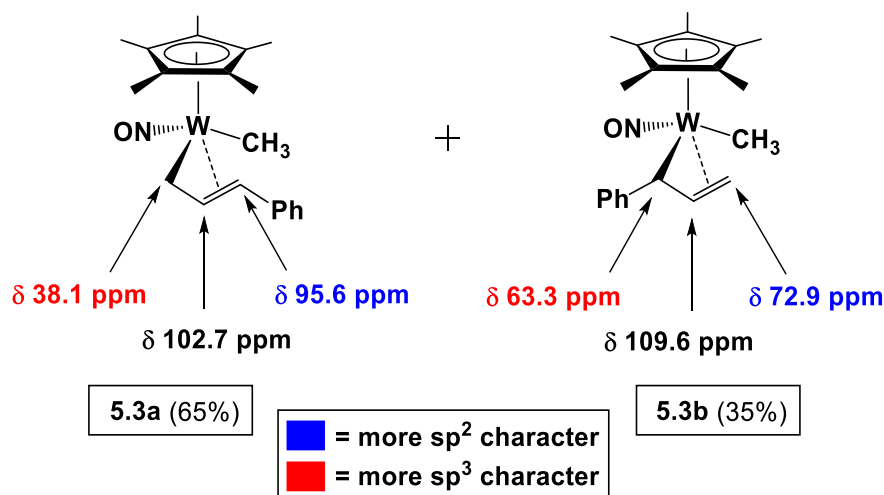


Figure 5.2. The σ - π distortion of the allyl ligand for isomers of **5.3** with the chemical shifts due to the allyl C atoms from the ^{13}C APT NMR spectrum.

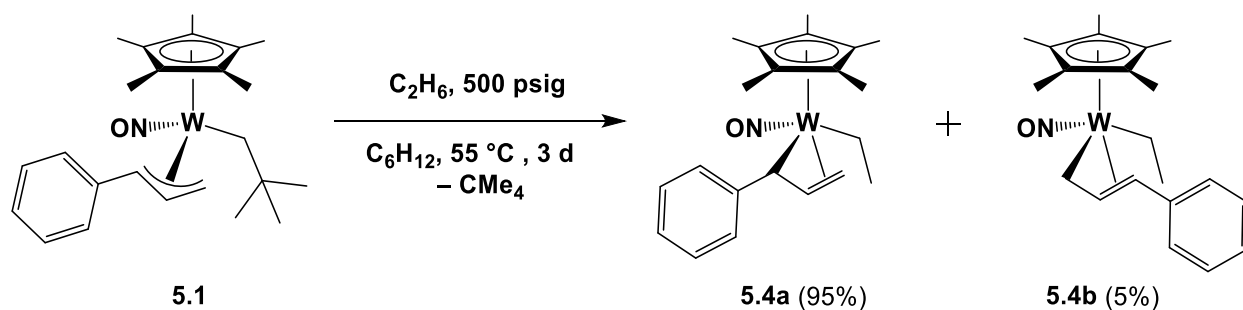
Since the σ - π distortion of the allyl ligand is inherent to the $\text{Cp}^*\text{W}(\text{NO})(\text{R})(\eta^3\text{-allyl})$ ($\text{R} = \text{H, alkyl, aryl}$) complexes,^{31, 43} the use of the chemical shifts of the allyl carbon signals in the ^{13}C NMR spectrum of a mixture of isomers can be used to determine the orientation of the allyl ligand for the various isomers of a complex. The assignment of the isomers based on the ^{13}C NMR data is particularly convenient for the ^{13}C APT NMR spectrum of a given compound as the CH_2 and CHPh carbon signals have opposite phases.

5.2.2 C-H Activation of Ethane by **5.1**

The C-H activation of ethane by complex **5.1** can be effected in a fashion similar to that of methane using cyclohexane as an inert solvent. Exposure of **5.1** to 55 °C and 450 psig ethane for 3 d affords isomers of the compound $\text{Cp}^*\text{W}(\text{NO})(\text{CH}_2\text{CH}_3)(\eta^3\text{-CH}_2\text{CHCHPh})$ (**5.4**) resulting from the single C-H activation of ethane (Scheme 5.3). Complex **5.4** is isolated as a yellow solid

following purification by column chromatography over basic alumina support. As with **5.3**, the compound is air- and moisture-stable for several days. The complex has a reversible melting point of 108-109 °C. The isomers of **5.4** have been characterized by ^1H and ^{13}C NMR spectroscopy, IR spectroscopy, mass spectrometry, and single-crystal X-ray diffraction.

Scheme 5.3. Single C-H activation of ethane by 5.1



In solution complex **5.3** exists as two isomers in a 95:5 ratio. They differ in the position of the phenyl substituent of the allyl which is proximal to the nitrosyl ligand for the major isomer (**5.4a**) and distal to the nitrosyl for the minor isomer (**5.4b**). The orientation of the phenyl substituent of the allyl ligand has been determined by Sel NOE NMR spectroscopy. As with **5.3**, the chemical shifts of the allyl C atoms in the ^{13}C APT NMR spectrum of **5.4** can be used to assign the orientation of the allyl ligand for each isomer (Figure 5.3). The position of the phenyl substituent for the major and minor isomers of **5.4** is reversed from that of **5.3** where the major isomer has the phenyl substituent on the allyl ligand proximal to the methyl ligand. This supports the notion that increasing the steric bulk of the alkyl from a methyl ligand to an ethyl ligand (or larger) favours the phenyl substituent being distal from the alkyl ligand and proximal to the nitrosyl ligand.

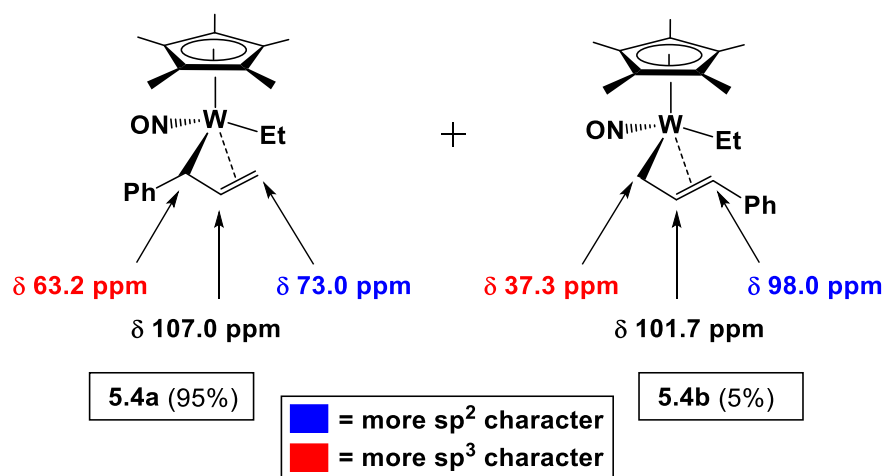


Figure 5.3. The σ - π distortion of the allyl ligand for isomers of **5.4** with the chemical shifts due to the allyl C atoms from the ^{13}C APT NMR spectrum.

Orange crystals of **5.4** suitable for single-crystal X-ray diffraction are grown by recrystallization in a solvent mixture of 1:1 pentane/ Et_2O at $-33\text{ }^\circ\text{C}$. In the solid state complex **5.4** exists as a single isomer, the major isomer **5.4a**; the solid-state molecular structure of **5.4a** is shown in Figure 2.3. The allyl ligand of **5.4a** exhibits a σ - π distortion that agrees with the solution structure based on the ^{13}C APT NMR spectrum (refer to Figure 5.3). The longer (σ character) C(9)-C(7) bond length is $1.435(17)\text{ \AA}$ and the shorter (π character) C(7)-C(8) bond is $1.388(19)\text{ \AA}$. The position of the shorter C(7)-C(8) bond is trans to the nitrosyl ligand, presumably the strong π -acceptor character has a trans-type effect on that C-C linkage of the allyl by diminishing the π -back donation possible from the tungsten. The ethyl ligand is oriented down, away from the Cp^* ligand and has a W(1)-C(16)-C(17) bond angle of $117.5(9)^\circ$. The W(1)-C(16) bond distance is $2.221(13)\text{ \AA}$.

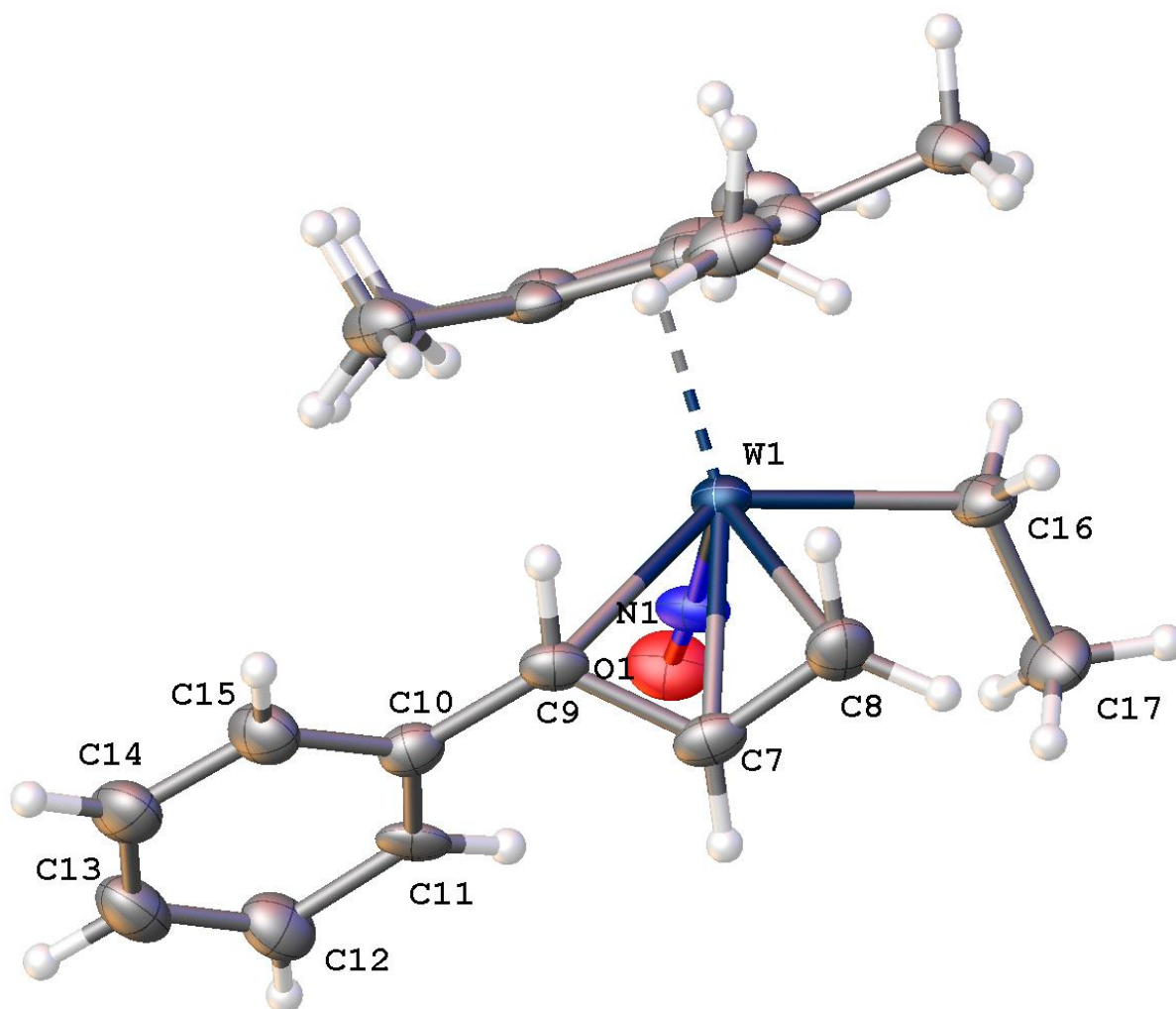


Figure 5.4. Solid-state molecular structure of **5.4** with 50% probability thermal ellipsoids shown.

Selected interatomic distances (Å) and angles (deg.): W(1)-C(7) = 2.348(11), W(1)-C(8) = 2.342(13), W(1)-C(9) = 2.326(12), W(1)-C(16) = 2.221(13), C(7)-C(8) = 1.388(19), C(7)-C(9) = 1.435(17), C(9)-C(10) = 1.474(18), W(1)-N(1) = 1.796(11), N(1)-O(1) = 1.190(14), C(8)-C(7)-C(9) = 117.0(11), C(7)-C(9)-C(10) = 120.9(11), W(1)-C(16)-C(17) = 117.5(9), W(1)-N(1)-O(1) = 172.7(9).

There is evidence for a β -agostic interaction between the tungsten and the terminal ethyl C-H bonds in the ^1H NMR spectrum. As shown in Figure 5.5, the ethyl signal is a triplet ($^3J_{\text{HH}} = 7.34$ Hz) and has an atypically downfield chemical shift for a methyl proton signal at δ 1.78 ppm. Additionally, satellites that are characteristic of the NMR active ^{183}W nucleus are observed in the ^1H NMR spectrum ($^3J_{\text{WH}} = 5.1$ Hz). The small value of the tungsten-proton coupling constant is consistent with a longer-range coupling as tungsten hydrides of similar $\text{Cp}^*\text{W}(\text{NO})(\text{H})(\eta^3\text{-allyl})$ complexes have significantly larger coupling constants, typically 120 Hz in magnitude.³⁰ The β -agostic interaction is an arrested transition state for β -elimination^{79,80, 128, 129} and does not commonly persist in complexes, especially at room temperature.¹³⁰ The fact that **5.4** is formally an 18-electron complex is likely the reason β -elimination is not observed under the conditions used to obtain the complex.

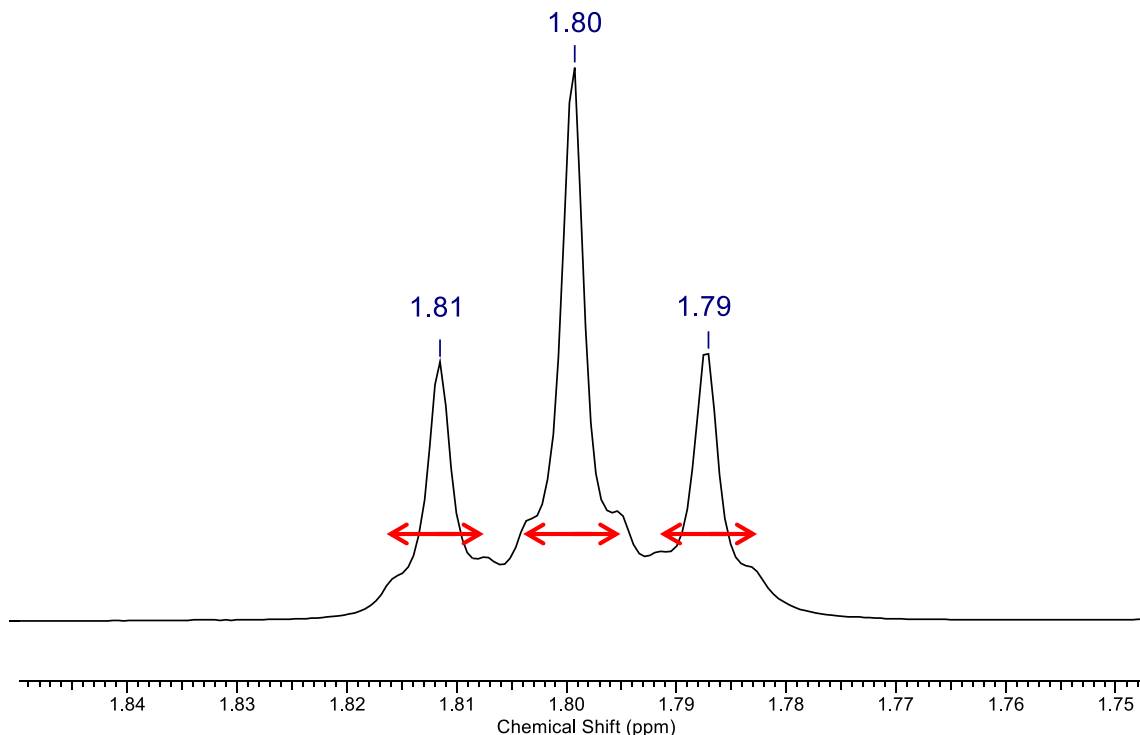


Figure 5.5. Expansion of the ^1H NMR spectrum (600 MHz, C_6D_6) showing the ethyl CH_3 signal of **5.4** with characteristic satellites due to ^{183}W ($^3J_{\text{HH}} = 7.34$, $^3J_{\text{WH}} = 5.1$ Hz).

5.2.3 Single C-H Activation of Propane and *n*-Butane

The C-H activations of propane and *n*-butane gas can be effected by **5.1** using conditions analogous for the activation of ethane using cyclohexane as the solvent to produce to products $\text{Cp}^*\text{W}(\text{NO})(\text{CH}_2\text{CH}_2\text{CH}_3)(\eta^3\text{-CH}_2\text{CHCHPh})$ (**5.5**) and $\text{Cp}^*\text{W}(\text{NO})(\text{CH}_2\text{CH}_2\text{CH}_2\text{CH}_3)(\eta^3\text{-CH}_2\text{CHCHPh})$ (**5.6**), respectively. As with **5.3** and **5.4**, complexes **5.5** and **5.6** both exist as a pair of isomers in solution differing by the orientation of the phenyl substituent of the allyl relative to the nitrosyl and alkyl ligands. The major isomer (>90%) has the phenyl substituent proximal to the nitrosyl and alkyl ligands. Alternatively, the activations of propane and *n*-butane can

be effected in neat hydrocarbons by condensing the appropriate gas in a pressure reactor. The initial reactions and identification of **5.5** and **5.6** were carried out by the author as were the solid-state characterizations by single-crystal X-ray diffraction. The reaction optimization and full characterization of these two complexes were performed by Dr. Russell Wakeham.

The solid-state molecular structure of **5.5** (major isomer) is shown below in Figure 5.6. The compound has a three-legged piano stool geometry with the allyl ligand attached to the tungsten in an endo fashion. The *n*-propyl ligand is oriented down, under the tungsten center, which is similar to the orientation of the ethyl ligand of **5.4**. The β -hydrogens have been located in the electron density map, thus allowing the lengths of the C-H bonds at the β carbon to be determined. The C-H bond lengths are 1.11(6) and 1.02(5) Å, which are longer than typical C-H bonds and agree with those reported for β -agostic metal-alkyl complexes.^{80, 128} The lengthening due to a β -H agostic interaction with the tungsten center is consistent with the evidence discussed for such an interaction in complex **5.4**.

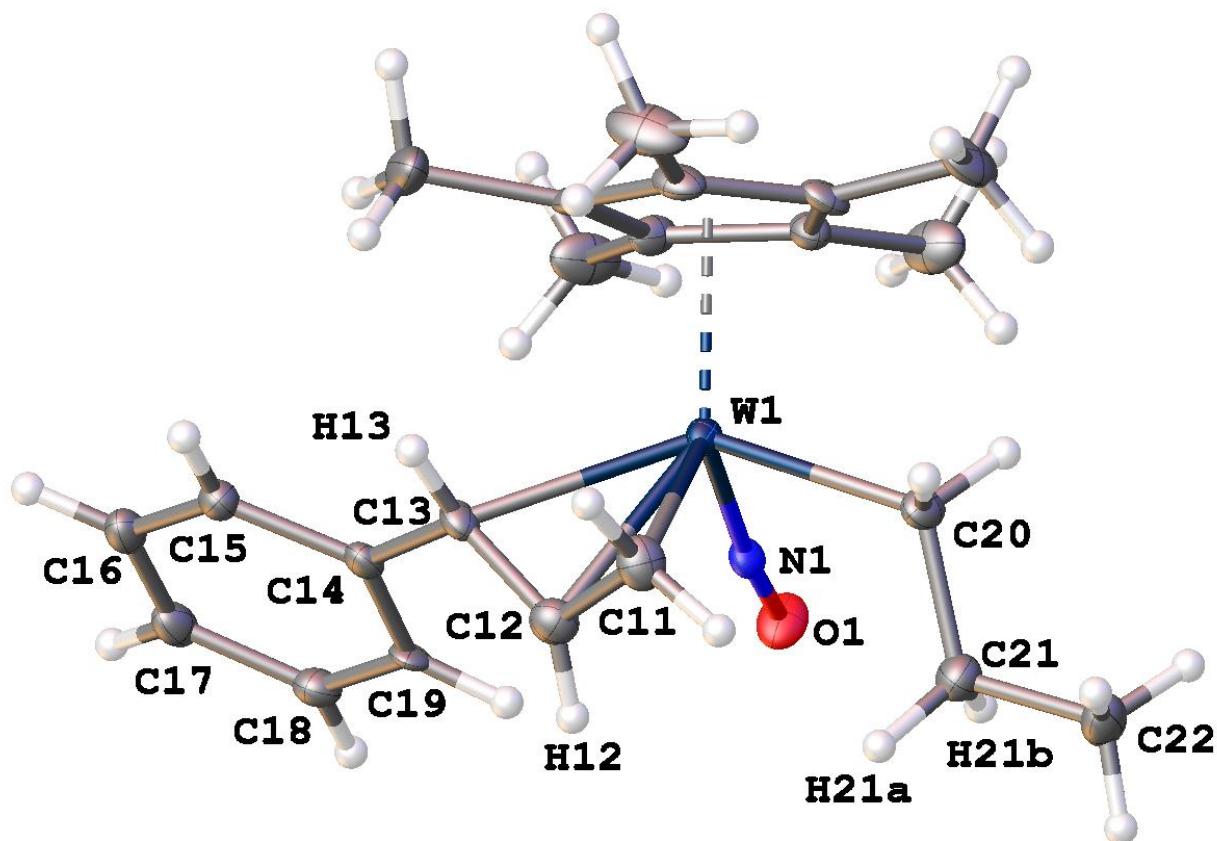


Figure 5.6. Solid-state molecular structure of **5.5** with 50% probability thermal ellipsoids shown.

Selected interatomic distances (Å) and angles (deg.): W(1)-C(11) = 2.341(5), W(1)-C(12) = 2.323(5), W(1)-C(13) = 2.317(4), C(11)-C(12) = 1.390(7), C(12)-C(13) = 1.416(7), C(13)-C(14) = 1.475(6), C(12)-H(12) = 0.92(6), C(13)-H(13) = 0.92(6), W(1)-C(20) = 2.230(5), C(20)-C(21) = 1.539(6), C(21)-H(21a) = 1.11(6), C(21)-H(21b) = 1.02(5), C(21)-C(22) = 1.528(7), W(1)-N(1) = 1.776(4), N(1)-O(1) = 1.227(5), C(11)-C(12)-C(13) = 117.3(4), C(12)-C(13)-C(14) = 125.0(4), W(1)-C(20)-C(21) = 116.2(3), C(20)-C(21)-C(22) = 113.1(4), H(21b)-C(21)-H(21b) = 120(4), W(1)-N(1)-O(1) = 169.6(3).

The solid-state molecular structure of **5.6** (major isomer) is shown in Figure 5.7 and it is analogous to those of **5.3b**, **5.4a** and **5.5**. There is the anticipated σ - π distortion of the allyl ligand, and the phenyl substituent is rotated from the plane of the allyl with a torsional angle (C(12)-C(13)-C(14)-C(19)) of 41.48°. As with the σ - π distortion, this breaking of conjugation is likely a manifestation of the tungsten-to-allyl back-bonding. The *n*-butyl group is oriented down relative to the Cp* ligand as is the case for the ethyl and *n*-propyl ligands in the structures of **5.4** and **5.5**, respectively. While the β -hydrogens could not be located in the electron-density map, the orientation of the *n*-butyl ligand suggests a similar β -agostic interaction to that seen in **5.4** and **5.5**. The W(1)-C(20) bond of the *n*-butyl ligand is 2.253(7) Å and is the longest of the complexes **5.3-5.6**, with the bond length increasing as the size of the ligand increases from methyl to *n*-butyl (Table 5.1). This trend is not surprising and not a feature unique to these complexes.¹⁸

Table 5.1. W-C bond lengths for the alkyl ligand of complexes **5.3-5.6**.

Complex	Ligand	W-C bond length (Å)
5.3	Methyl	2.209(7)
5.4	Ethyl	2.221(13)
5.5	<i>n</i> -Propyl	2.230(5)
5.6	<i>n</i> -Butyl	2.253(7)

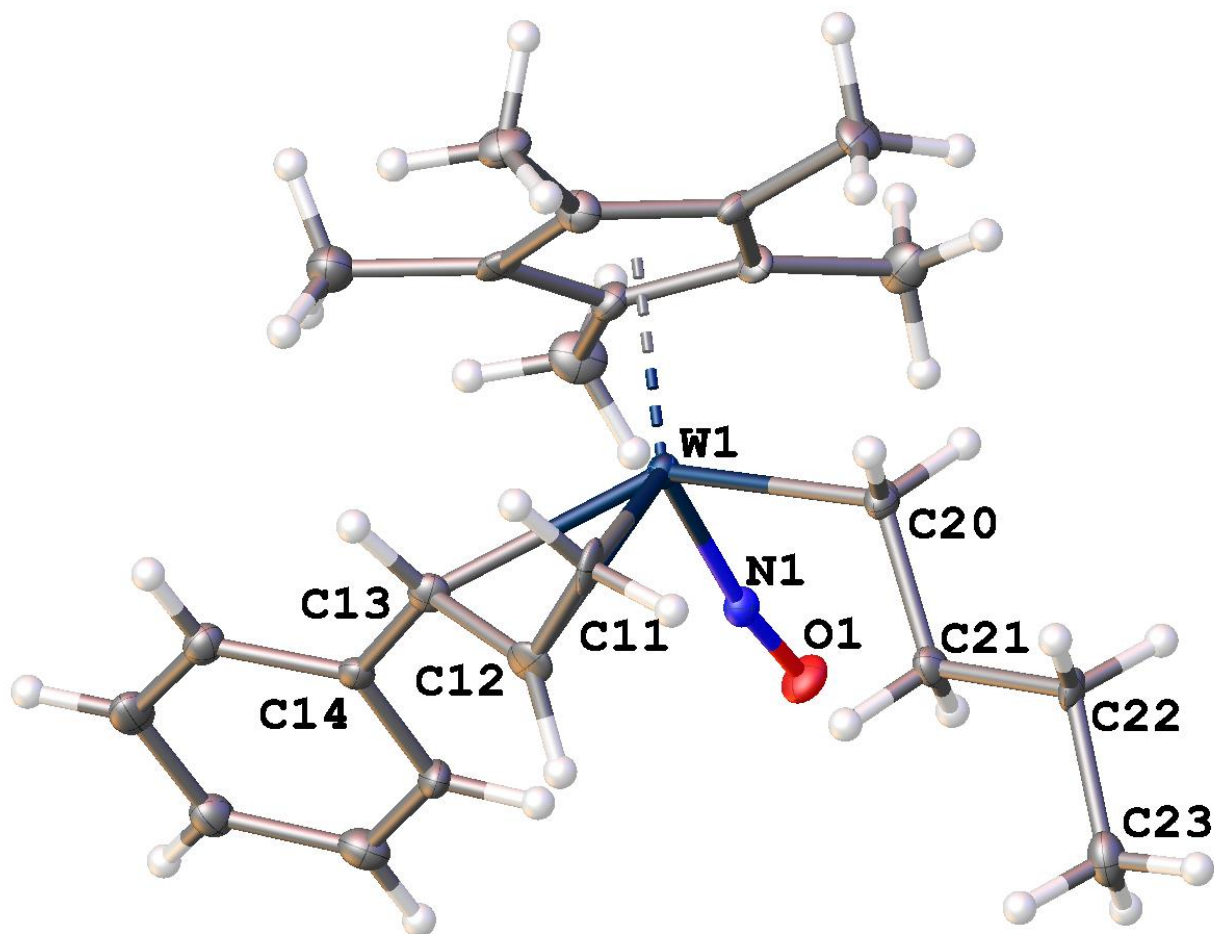


Figure 5.7. Solid-state molecular structure of **5.6** with 50% probability thermal ellipsoids shown.

Selected interatomic distances (Å) and angles (deg.): W(1)-C(11) = 2.347(7), W(1)-C(12) = 2.319(7), W(1)-C(13) = 2.321(7), C(11)-C(12) = 1.399(10), C(12)-C(13) = 1.425(10), C(13)-C(14) = 1.489(9), W(1)-C(20) = 2.253(7), C(20)-C(21) = 1.540(9), W(1)-N(1) = 1.773(6), N(1)-O(1) = 1.230(7), W(1)-C(20)-C(21) = 113.8(4), C(11)-C(12)-C(13) = 116.4(7), C(12)-C(13)-C(14) = 124.7(6), W(1)-N(1)-O(1) = 169.0(5).

5.2.4 Optimization of the Single C-H Activation of C1-C3 Alkanes by **5.2**

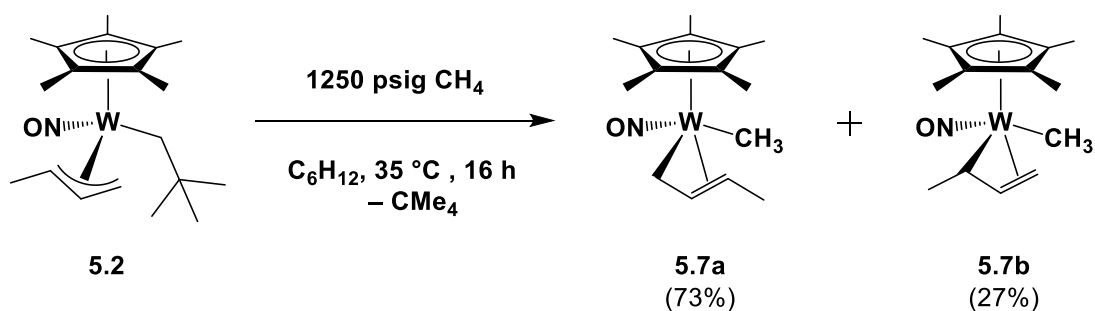
Complex **5.2** can effect the selective terminal C-H activation of linear alkanes²⁷ as well as hydrocarbons containing heteroatom functional groups.³³ The ability to use **5.2** to effect further functionalization of these alkyl and hydrocarbyl ligands presents many possibilities. The functionalization of alkanes (C1-C7) by complex **5.2** has been previously reported.²⁷ However, the attempts of others to reproduce these results for gaseous hydrocarbons have resulted in poor to no yields, suggesting a problem with the reaction conditions or purification of the complexes, or both. Kinetic studies as well as thermodynamic parameters from Eyring and Arrhenius plots for complex **5.2** have been reported,³⁵ which has allowed for selection of optimal pairing of temperature and reaction times for the reaction of **5.2** with alkanes. The most successful combination has been determined to be 35 °C for 16 h. The reactions can be carried out faster at 55 °C, albeit with poorer yields. The optimization of the C-H activation reactions of **5.2** with methane, ethane, and propane is necessary for the investigation of potentially converting these alkanes into unsymmetrical, unsaturated ketones mediated by complex **5.2** analogous to the functionalization of methane by **4.1**.

5.2.4.1 C-H Activation of Methane by **5.2**

Exposure of **5.2** to 1250 psig CH₄ and 35 °C for 15 results in the formation of two isomers of Cp*W(NO)(CH₃)(η^3 -CH₂CHCHMe) (**5.7**) from the C-H activation of methane (Scheme 5.4). The two isomers differ with respect to the orientation of the methyl substituent, which is proximal to the methyl ligand in the major isomer (**5.7a**) and proximal to the nitrosyl

ligand in the minor isomer (**5.7b**). This assignment is made using the effect of the σ - π distortion on the chemical shifts of the allyl carbon signals in the ^{13}C NMR spectrum. For the major isomer, **5.7a**, the more sp^3 -character (σ) allyl CH_2 signal at δ 37.9 ppm places it proximal to the nitrosyl ligand while the more sp^2 -character (π) allyl CHMe signal at δ 90.7 ppm indicates the methyl substituent is trans to the nitrosyl and proximal to the methyl ligand. Interestingly, the major isomer **5.7a** has not been observed previously as the reported preparation of **5.7** identifies a single isomer (**5.7b**, the minor component) as the sole product.²⁷

Scheme 5.4. Optimized C-H activation of methane by **5.2**



5.2.4.2 Solvent Optimization for the C-H Activation of Methane by **5.2**

The investigation of the C-H activation of methane by **5.2** under different solvent conditions is summarized in Table 5.2. Similar to the reaction of **4.1** with methane, the reaction carried out in a larger volume of cyclohexane yields the largest quantity of product. The C-H activation of cyclohexane by **5.2** has been carried out to obtain the complexes $\text{Cp}^*\text{W}(\text{NO})(\text{C}_6\text{H}_{11})(\eta^3\text{-CH}_2\text{CHCHMe})$ (**5.8**) and **3.3** in a 9:1 ratio. However, neither of these complexes are ever observed during the reactions of **5.2** with gaseous hydrocarbon when

cyclohexane is used as the solvent. This would suggest that competing solvent activation does not occur during the reactions of **5.2** with C1-C3 alkanes.

Table 5.2. Effect of solvent on yield of methane activation effected by complex **5.2**.^[a]

Entry	Solvent	Volume of solvent	Yield of 5.7
1	C ₆ F ₆	20 mL	31%
2	C ₆ H ₁₂	20 mL	57%
3	C ₆ H ₁₂	125 mL	75% (94%) ^[a]

^[a] Reactions carried out at 35 °C for 16 h using 0.300 g of **5.2**. ^[b]Yield calculated by ¹C-H activation of

Ethane and Propane by **5.2**

The C-H activations of ethane and propane effected by **5.2** are carried out in a similar manner to the reaction with methane, albeit with different pressures of the two gases. The complexes Cp*W(NO)(CH₂CH₃)(η³-CH₂CHCHMe) (**5.9**) and Cp*W(NO)(CH₂CH₂CH₃)(η³-CH₂CHCHMe) (**5.10**) are obtained from the reactions with ethane and propane, respectively. A comparison of the reactions of **5.2** with the different gases is summarized in Table 5.3. The major isomer of both **5.9** and **5.10** has the methyl substituent of the allyl ligand proximal to the nitrosyl ligand; the influence of alkyl ligand sterics on the orientation of the allyl ligand appears to be a common theme for the monosubstituted allyl alkyl complexes.

Table 5.3. Conditions and yields for the C-H activations of methane, ethane, and propane effected by **5.2**.^[a]

Complex number	R–H,	Pressure	Yield	Relative abundance isomer a	Relative abundance isomer b
5.7	Methane	1250 psig	75	73	27
5.9	Ethane	400 psig	67	85	15
5.10	Propane	100 psig	77	79	21

[a] All reactions carried out at 35 °C for 16 h using 0.300 g of **5.2**.

5.2.5 C-H Activation of Heteroatom-Containing Hydrocarbons by **5.1**

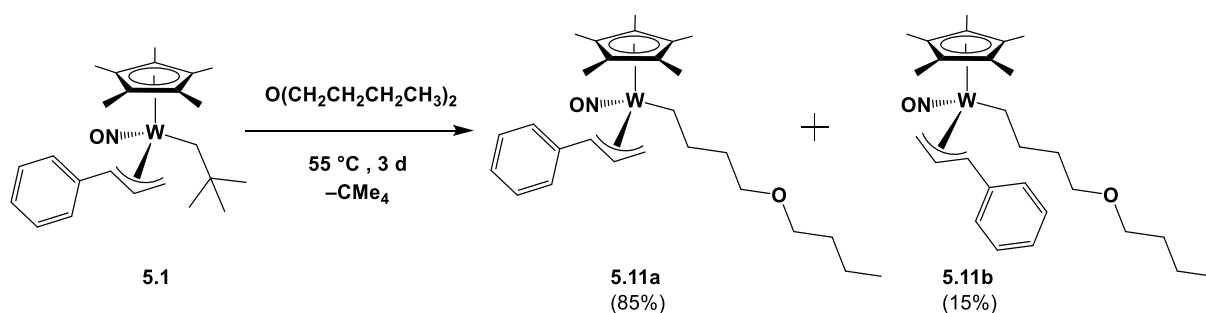
The C-H activation of heteroatom-containing alkanes has been reported previously for complex **5.2** for substrates such as ethers and chloro- and bromoalkanes.³³ The possibility of C-H activation of such substrates by **5.1** was investigated with the long-term goal of effecting functionalization of a heteroatom-containing alkane.

5.2.5.1 Selective C-H Activation of (*n*-Butyl)₂O

Thermolysis of **5.1** in neat di(*n*-butyl) ether at 55 °C for 3 d affords the product Cp*W(NO)((CH₂)₄O(CH₂)₃CH₃)(η³-CH₂CHCHPh) (**5.11**) which is the result of a single activation of a methyl C-H bond (Scheme 5.5). The selectivity of the reaction has been established by the ¹³C APT NMR spectrum (Figure 5.8). There are seven methylene C signals,

including two α to the oxygen, and only one methyl signal due to the ether ligand, thereby showing that a methyl C-H bond has been activated. Non-terminal activation would result in five upward signals (methylene) and three downward signals (2 methyl and 1 methine) in the ^{13}C APT NMR spectrum. There is no evidence for activation of the weaker C-H bonds α to the oxygen, suggesting that the selectivity is determined by steric considerations.

Scheme 5.5. C-H activation of dibutyl ether by 5.1



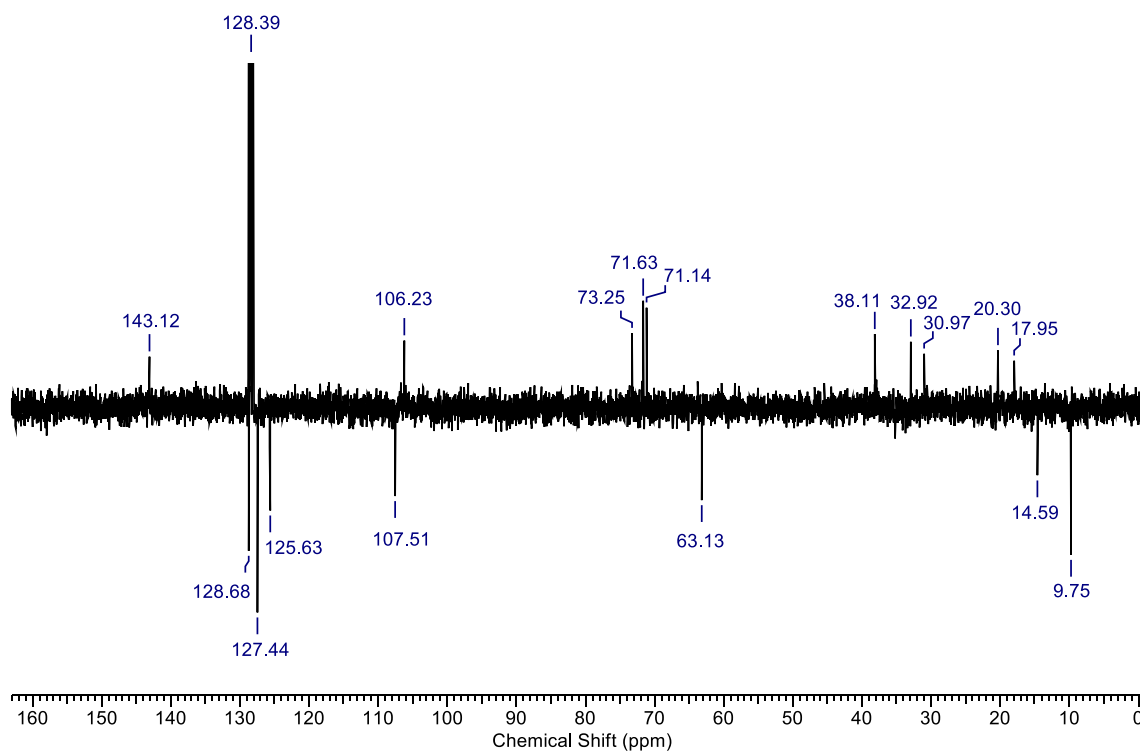


Figure 5.8. ^{13}C APT NMR spectrum of complex **5.11a** (100 MHz, C_6D_6). Seven methylene C signals (pointing upward) from δ 71.63 to 17.95 ppm, including two methylene α to the oxygen (δ 71.63, 71.14 ppm) and a single methyl C signal at δ 14.59 ppm) establish selectivity for terminal C-H activation of dibutyl ether.

Complex **5.11** can be purified by column chromatography over basic alumina support and isolated in 50 % yield as a yellow oily solid. Two isomers are observed in the ^1H NMR spectrum with a relative ratio of 85:15. The isomers differ with respect to the orientation of the allyl substituent, with the phenyl group proximal to the nitrosyl for the major isomer (**5.11a**), and proximal to the ether ligand for the minor isomer (**5.11b**), which has been established by the chemical shifts of the allyl carbons in the ^{13}C APT NMR spectrum. The connectivity of the allyl

and ether ligands to tungsten has been established by characteristic tungsten-183 satellites in the ^{13}C APT NMT spectrum (Figure 5.9).

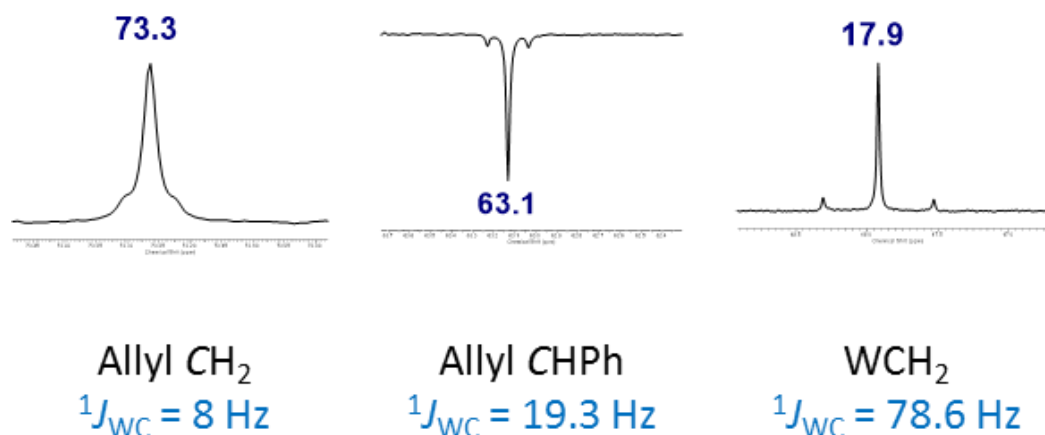


Figure 5.9. Expansions of the ^{13}C APT NMR spectrum of **5.11** at δ 73.3, 63.1, and 17.9 ppm which display characteristic satellites due to tungsten-183 coupling that indicate the presence of tungsten-carbon bonds.

Interactions between the tungsten center and C-H bonds of the ether ligand result in restricted rotation of the four methylene units (between the tungsten and oxygen) for the ether ligand, which is evident in the ^1H NMR spectrum. The signals due to the α - δ (relative to tungsten) methylene protons of the ether ligand are all diastereotopic, showing second-order effects at the α , γ , and δ positions. There is a pronounced split in the chemical shifts of the signals due to the β protons (δ 2.14 and 1.63 ppm), which probably can be attributed to an agostic interaction between the tungsten and the β C-H bond.¹²⁸ Interestingly, the restricted rotation persists all the way to the δ -methylene position, which shows pronounced second-order

effects (Figure 5.10a). In contrast, the other CH_2O signal is observed to be the expected triplet (Figure 5.10b), indicating free rotation for the butyl group attached to the oxygen.

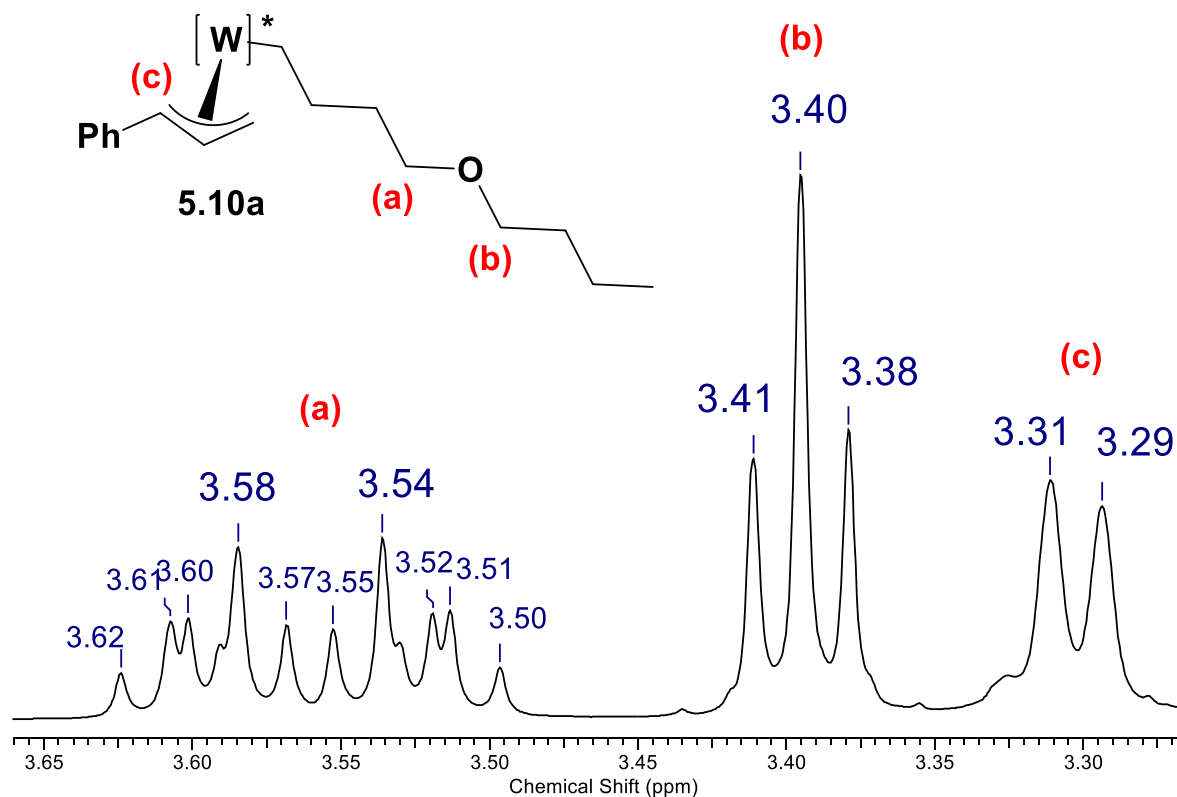
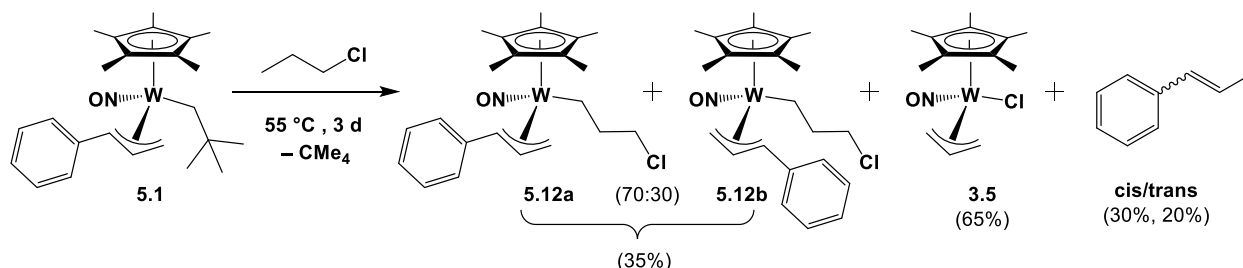


Figure 5.10. Expansion of the ^1H NMR spectrum of **5.11** from δ 3.66 to 3.27 ppm (400 MHz, C_6D_6). (a) Multiplet centered at δ 3.56 ppm corresponding to CH_2O proximal to tungsten shows pronounced second-order effects, indicating possible restricted rotation. (b) Triplet at δ 3.40 ppm corresponding to CH_2O distal to tungsten shows expected first-order effects, indicating free rotation of bonds. (c) Doublet at δ 3.30 corresponds to allyl CH_2 (1H).

5.2.5.2 Selective Activation 1-Chloropropane

To test the capability of **5.1** to effect the single C-H activation of a halocarbon, 1-chloropropane was selected as the substrate. Interestingly, the thermolysis of **5.1** at 55 °C in 1-chloropropane for 3 d affords a dark-green mixture, which is in contrast to the yellow-orange-brown coloured mixtures typically obtained for C-H activation reactions effected by **5.1**. Green colours have been observed for complexes containing W-Cl bonds, such as solutions of $\text{Cp}^*\text{W}(\text{NO})\text{Cl}_2$ ⁵⁶ and $\text{Cp}^*\text{W}(\text{NO})(\eta^3\text{-allyl})\text{Cl}$.^{43, 78} Spectroscopic analysis of the crude reaction mixture reveals the signals for the expected product of C-H activation, $\text{Cp}^*\text{W}(\text{NO})(\text{CH}_2\text{CH}_2\text{CH}_2\text{Cl})(\eta^3\text{-CH}_2\text{CHCHPh})$ (**5.12**), complex **3.5**, as well as *cis*- and *trans*- β -methylstyrene (Scheme 5.6).

Scheme 5.6. Reaction of 5.1 with 1-chloropropane



Complex **5.12** can be purified by column chromatography over basic alumina and is obtained as a yellow solid in low yield (22%). In solution, two isomers are observed in a 70:30 ratio using ^1H NMR spectroscopy. In the ^{13}C APT NMR spectrum, the signals due to the allyl carbons for the major isomer, **5.12a**, reveal the existence of a σ - π distortion consistent with the phenyl substituent of the allyl being oriented proximal to the nitrosyl ligand [δ 63.4 ppm (allyl

CHPh)] and the more sp^2 -character allyl CH_2 [δ 73.4 ppm (allyl CH_2)] trans to the nitrosyl and proximal to the alkyl ligand. The selectivity for activation of a terminal, methyl C-H bond is confirmed by the ^{13}C APT NMR spectrum with three methylene signals for the chloropropyl ligand; non-terminal activation would have been observed as methyl, methylene, and methane signals.

Crystals suitable for single-crystal X-ray diffraction of **5.12** are grown by slow evaporation from a 1:1 mixture of Et_2O /pentane. Only the minor isomer, **5.12b**, has been observed in the solid-state as a pair of enantiomers.¹³¹ For viewing simplicity, the solid-state molecular structure of each enantiomer taken from different angles is shown below in Figure 5.11. The allyl ligand has an endo orientation and the phenyl substituent is oriented proximal to the 3-chloropropyl ligand. The σ - π distortion of the allyl ligand that is characteristic of these complexes is seen with unequal C-C bond lengths. The shorter, more π -character C-C bond [W(1) enantiomer: C(12)-C(13) = 1.360(13); W(2) enantiomer: C(34)-C(35) = 1.374(13)] is trans to the strong π -acid nitrosyl ligand, which has linear conformation ($170.2(7)^\circ$, $170.6(6)^\circ$). The 3-chloropropyl ligand is pointing downward with a W-C-C bond angle of $113.5(5)^\circ/113.0(5)^\circ$ which orients the β C-H bonds toward the tungsten center. This geometry likely allows for a β -agostic interaction¹²⁹ [similar to what is seen for **5.4** (refer to Figure 5.4) in which the β -agostic interaction is established by characteristic ^{183}W satellites in the 1H NMR spectrum (refer to Figure 5.5)]. The split in chemical shifts between the β -hydrogens of **5.11a** (δ 1.70, 2.44 ppm) in the 1H NMR spectrum is similar to that for related complexes.

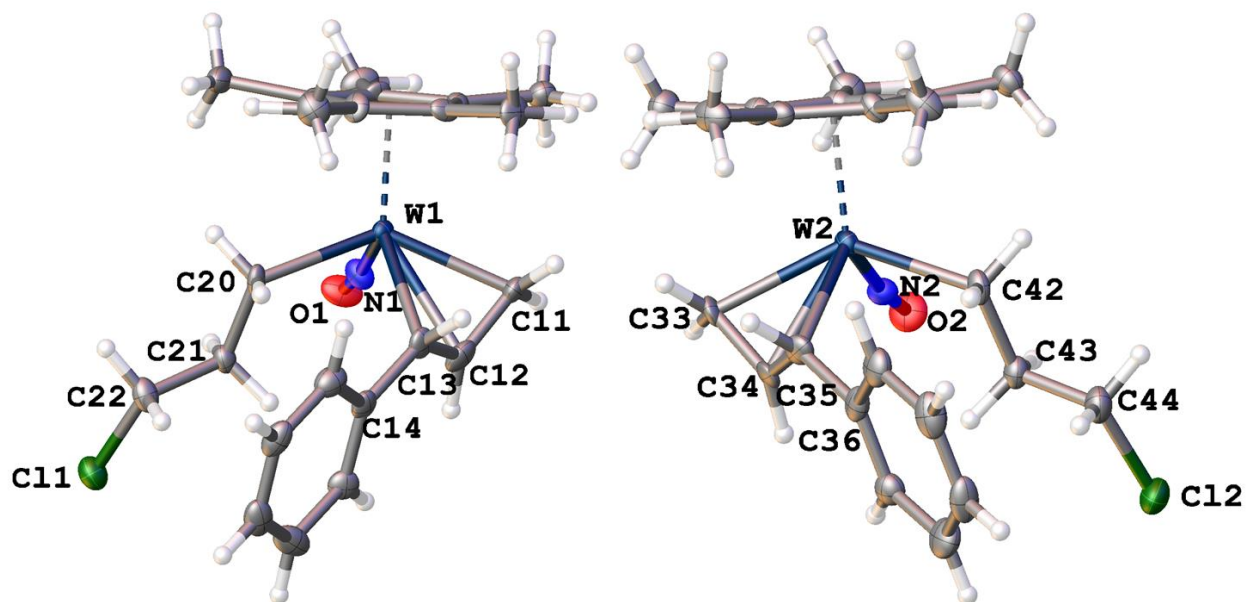
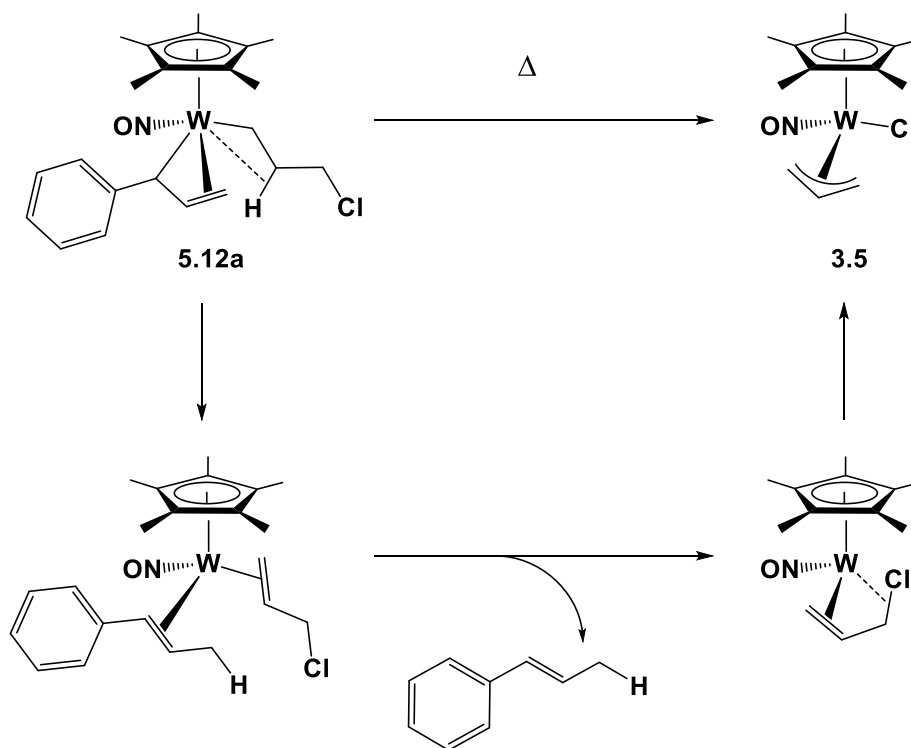


Figure 5.11. Reoriented solid-state molecular structures for the enantiomers of **5.12b** with 50% probability thermal ellipsoids shown. Selected interatomic distances (Å) and angles (deg.): W(1)-C(11)= 2.238(8) , W(1)-C(12) = 2.349(8), W(1)-C(13) = 2.524(8), C(11)-C(12) = 1.435(13), C(12)-C(13) = 1.360(13), C(13)-C(14) = 1.482(12), W(1)-C(20) = 2.227(8), C(20)-C(21) = 1.530(12), C(21)-C(22) = 1.520(11), C(22)-Cl(1) = 1.807(9), W(1)-N(1) = 1.763(7), N(1)-O(1) = 1.232(8), W(2)-C(33) = 2.229(8), W(2)-C(34) = 2.344(7), W(2)-C(35) = 2.518(8), C(33)-C(34) = 1.437(12), C(34)-C(35) = 1.374(13), C(35)-C(36) = 1.477(12), W(2)-C(42) = 2.243(8), C(42)-C(43) = 1.521(12), C(43)-C(44) = 1.520(12), C(44)-Cl(2) = 1.814(10), C(11)-C(12)-C(13) = 119.2(9), C(12)-C(13)-C(14) = 126.0(9), W(1)-C(20)-C(21) = 113.5(5), W(1)-N(1)-O(1) = 170.2(7), C(33)-C(34)-C(35) = 117.6(8), C(34)-C(35)-C(36) = 126.4(9), W(2)-C(42)-C(43) = 113.0(5), W(2)-N(2)-O(2) = 170.6(6).

The low yield of **5.12** and the presence of **3.5** suggest a proclivity for complex **5.12** to undergo β -H elimination more readily than for typical $\text{Cp}^*\text{W}(\text{NO})(n\text{-alkyl})(\eta^3\text{-CH}_2\text{CHCHPh})$

complexes. The probable mechanism for the transformation of **5.12** to **3.5** is outlined below in Scheme 5.7. Complex **5.12** undergoes a β -H abstraction event which transfers the H from the *n*-CH₂CH₂CH₂Cl ligand to the terminus of the phenylallyl ligand to give Cp*W(NO)(η^2 -PhCH=CHMe)(η^2 -CH₂=CHCH₂Cl). The phenylallyl ligand is then lost as *trans*- β -methylstyrene to afford the 16e organometallic complex Cp*W(NO)(η^2 -CH₂=CHCH₂Cl), which then undergoes an intramolecular C-Cl bond cleavage, producing complex **3.10**. Signals for complexes **5.12** and **3.5** are both readily identifiable in the ¹H NMR spectrum of the crude reaction mixture, as are alkene doublet and doublet of quartet signals attributable to *cis*- and *trans*- β -methylstyrene. This is similar to the multiple C-H activation mechanism proposed for complex **2.1**, which also converts 1-chloropropane to **3.5**, with the difference being saturation remaining on the original allyl ligand once it is lost from the organometallic complex.

Scheme 5.7. Proposed mechanism for the transformation of 5.12a to 3.5

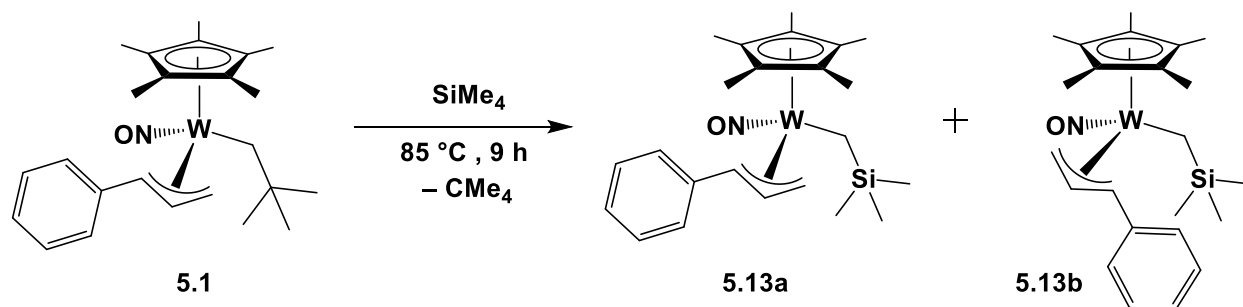


The β -H elimination exemplified by conversion of **5.12** to **3.5** through the loss of *trans*- β -methylstyrene offers insight into the decomposition of Cp*W(NO)(*n*-alkyl)(η^3 -CH₂CHCHPh) complexes. This fact explains why the C-H activation of C2 and larger alkanes must be carried out at 55 °C to avoid decomposition through β -H elimination. This is also consistent with the C-H activation of methane being able to be effected at a higher temperature without decomposition. Additionally, complex **4.1**, which does not give isolable products from the single C-H activation of alkanes, has been shown to readily undergo β -H elimination.^{30, 32}

5.2.5.3 C-H Activation of Tetramethylsilane

The C-H activation of tetramethylsilane by **5.1** is performed at elevated temperature to afford isomers of $\text{Cp}^*\text{W}(\text{NO})(\text{CH}_2\text{SiMe}_3)(\eta^3\text{-CH}_2\text{CHCHPh})$ (**5.13**) (Scheme 5.8). As with the C-H activation of methane, the lack of β -hydrogens in the product makes **5.13** more thermally stable, allowing for a shorter reaction time at a higher temperature. Complex **5.13** is isolated as an analytically pure yellow solid in nearly quantitative yield following removal of the solvent in vacuo. In solution **5.13** exists as two isomers in a 5:1 ratio that differ with respect to the position of the phenyl substituent.

Scheme 5.8. C-H activation of tetramethylsilane by **5.1**



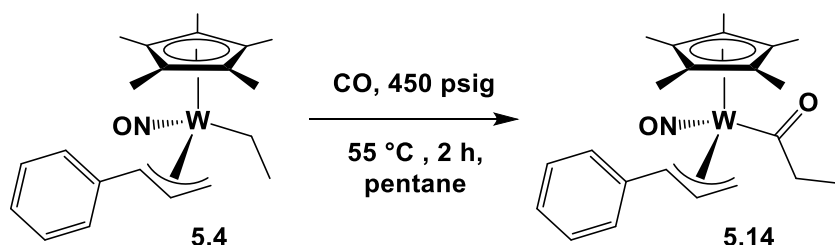
5.2.6 Ethane Functionalization Effected by **5.1**

5.2.6.1 Functionalization of the Ethyl Ligand by 1,1-CO Insertion

The ethyl ligand of complex **5.4** derived from C-H activation of ethane can be selectively functionalized by exposing it to 450 psig CO at 55 °C for 2 h (Scheme 5.9). The acyl complex,

$\text{Cp}^*\text{W}(\text{NO})(\text{C}(=\text{O})\text{CH}_2\text{CH}_3)(\eta^3\text{-CH}_2\text{CHCHPh})$ (**5.14**), is formed cleanly under these conditions and is obtained as a yellow solid in high yield via recrystallization (73% yield). The IR spectrum of **5.14** contains a carbonyl-stretching frequency of 1630 cm^{-1} , which is consistent with an acyl ligand. In the ^{13}C NMR spectrum the acyl carbon is identified by a resonance at $\delta\ 261.0\text{ ppm}$, which is typical of allyl acyl complexes. The chemical shifts of the allyl CH_2 ($\delta\ 65.6\text{ ppm}$), CHPh ($\delta\ 71.2\text{ ppm}$) signals, caused by the σ - π distortion of the ligand, place the phenyl substituent proximal to the nitrosyl ligand. In the ^1H NMR spectrum of **5.14**, the methylene and methylene groups of the acyl ligand are identified as a quartet ($\delta\ 2.99\text{ ppm}$) and triplet ($\delta\ 1.21\text{ ppm}$), respectively. The multiplets are typical for an ethyl group and indicate that there is not restricted rotation, something that is a theme for the $\text{Cp}^*\text{W}(\text{NO})(n\text{-alkyl})(\eta^3\text{-CH}_2\text{CHCHPh})$ complexes.

Scheme 5.9. Carbonylation of 5.4 to produce the acyl allyl complex 5.14



Crystals of **5.14** suitable for analysis by X-ray diffraction have been obtained by recrystallization from Et_2O at $-33\text{ }^\circ\text{C}$. The solid-state molecular structure is shown in Figure 5.12. The 1,1-insertion of CO into the W-C bond of the ethyl ligand is confirmed by the X-ray structure. The C(11)-O(2) bond has a typical length $1.218(6)\text{ \AA}$ and the bond angles about C(11) are consistent with an sp^2 -hybridized carbon. The W(1)-C(11) bond of $2.220(5)\text{ \AA}$ is

approximately the same as the tungsten-carbon bond of the ethyl ligand for the preceding **5.4** (2.221(13) Å). The allyl ligand has an endo conformation relative to the Cp* ligand, and the phenyl substituent is confirmed to be proximal to the nitrosyl ligand. There is a slight σ - π distortion of the allyl ligand with the shorter C(14)-C(15) bond being trans to the nitrosyl ligand. The phenyl substituent is rotated away from the plane of the allyl with a C(15)-C(16)-C(17)-C(18) torsional angle of 36.2(7)°. The nitrosyl retains a linear conformation with a W(1)-N(1)-O(1) bond angle of 171.3(4)°.

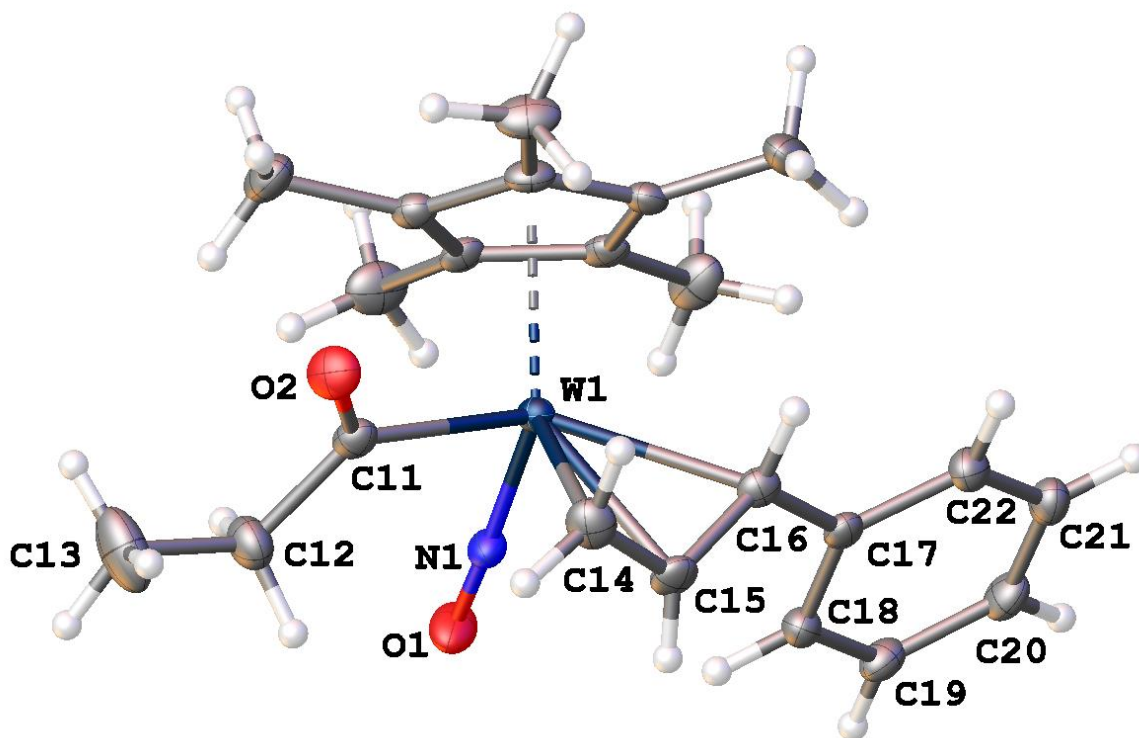


Figure 5.12. Solid-state molecular structure of **5.14** with 50% probability thermal ellipsoids shown. Selected interatomic distance (Å) and angles (deg.): W(1)-C(11) = 2.220(5), C(11)-O(2) = 1.218(6), C(11)-C(12) = 1.536(7), C(12)-C(13) = 1.520(7), W(1)-C(14) = 2.343(5), W(1)-C(15) = 2.328(5), W(1)-C(16) = 2.343(5), C(14)-C(15) = 1.394(7), C(15)-C(16) = 1.407(7), C(16)-C(17) = 1.485(6), W(1)-N(1) = 1.773(4), N(1)-O(1) = 1.223(5), W(1)-C(11)-O(2) = 124.2(4), W(1)-C(11)-C(12) = 116.4(3), O(2)-C(11)-C(12) = 119.4(4), C(14)-C(15)-C(16) = 119.0(5), C(15)-C(16)-C(17) = 123.3(4), W(1)-N(1)-O(1) = 171.3(4).

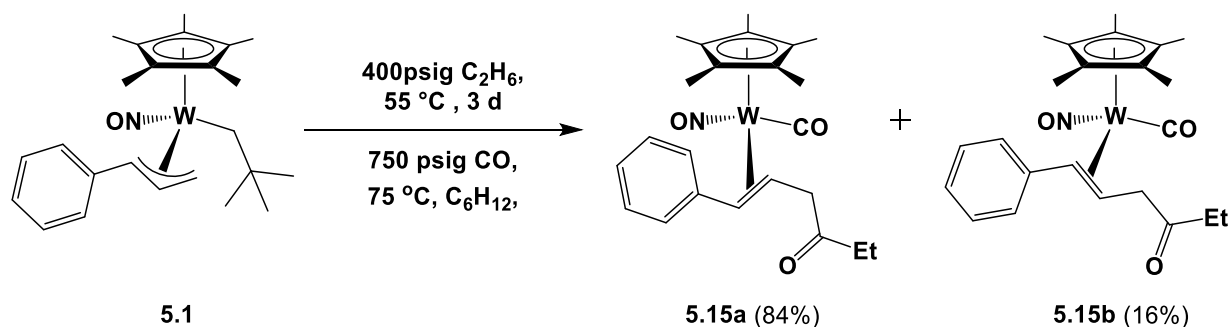
In a similar fashion to the pressure optimization for the conversion of **4.2** to **4.4** with CO, the reaction of **5.4** has been monitored by ^1H NMR spectroscopy by different temperatures using a Parr 5500 reactor vessel that is modified with a sampling arm. These reactions at different temperatures demonstrate the important effect that temperature has on the rate of 1,1-CO

insertion into the W-C bonds of Cp*W(NO)(alkyl)(η^3 -allyl) complexes. The exposure of **5.4** to 450 psig ethane at ambient temperature results in the formation of the acyl complex **5.14** after 4 d. At 450 psig and 75 °C, the acyl complex **5.14** is formed, but begins reacting before **5.4** is consumed. Within 1.5 h at 75 °C compound **5.14** begins to undergo a coupling reaction analogous to that seen for **4.3** and **4.4** (vide supra).

5.2.6.2 Sequential C-C Bond Forming Reactions Under CO Pressure

Sequential exposure of complex **5.1** to 400 psig ethane at 55 °C for 3 d, and then 750 psig CO at 75 °C for 18 h results in the formation of the η^2 -bound ketone complex Cp*W(NO)(CO)(η^2 -PhCH=CHCH₂C(=O)Et) (**5.15**) (Scheme 5.10). The formation of **5.15** from **5.1** represents the one-pot C-H activation of ethane and subsequent functionalization through the formation of two new C-C bonds via insertion of CO and coupling to the phenylallyl ligand. Compound **5.15** is isolated by column chromatography over silica support and obtained as an orange oil in 50% yield. Efforts to obtain crystals suitable for single-crystal X-ray diffraction have been unsuccessful to date. Instead, IR spectroscopy, 1D and 2D NMR spectroscopies, and mass spectrometry have been instrumental in characterizing the compound.

Scheme 5.10. C-H activation of ethane and subsequent functionalization with CO initiated by compound 5.1



The IR spectrum of **5.15** is used for a convenient characterization of the complex. There are two carbonyl-stretching frequencies at 1958 and 1711 cm^{-1} which are indicative of a terminal carbonyl ligand and a ketone carbonyl, respectively. The nitrosyl-stretching frequency of 1608 cm^{-1} is similar to that of the related complexes **4.5** and **4.6**. In solution the compound exists as two isomers that differ in the orientation of the dihapto β,γ -unsaturated ketone ligand. The major isomer **5.15a** (84%) has the benzylic proton pointing away from the metal and the $=\text{CH}$ group oriented up toward the Cp^* ligand. In the ^1H NMR spectrum of **5.15** this is observed as the signal due to the $=\text{CH}$ having a more upfield chemical shift (δ 2.77 ppm) than the PhCH= resonance (δ 3.99 ppm); the signal at δ 2.77 is a doublet of triplets with tungsten-183 satellites ($^1J_{\text{WH}} = 5.5\text{ Hz}$), which identifies it as neighboring the benzylic and methylene groups, as well as proximity to the tungsten (Figure 5.13). For the minor isomer **5.15b** (14%) the chemical shifts for the two alkene proton signals are the opposite, with the more upfield signal due to the PhCH= (δ 2.45 ppm), which is a doublet with tungsten-183 satellites ($^1J_{\text{WH}} = 5.5\text{ Hz}$) indicating coupling only to the other alkene proton and the tungsten (Figure 5.13). The $=\text{CH}$ signal at δ 3.58 ppm couples to both the PhCH and adjacent methylene groups. The orientation of the alkene group of the two

isomers is similar to what is seen for complex **3.15**, the orientation of the isomers having been confirmed in the solid state by X-ray crystallography (refer to Figure 3.15 and Figure 3.16), and for which similar differences in chemical shifts of the bound alkene hydrogen signals are observed.⁴³

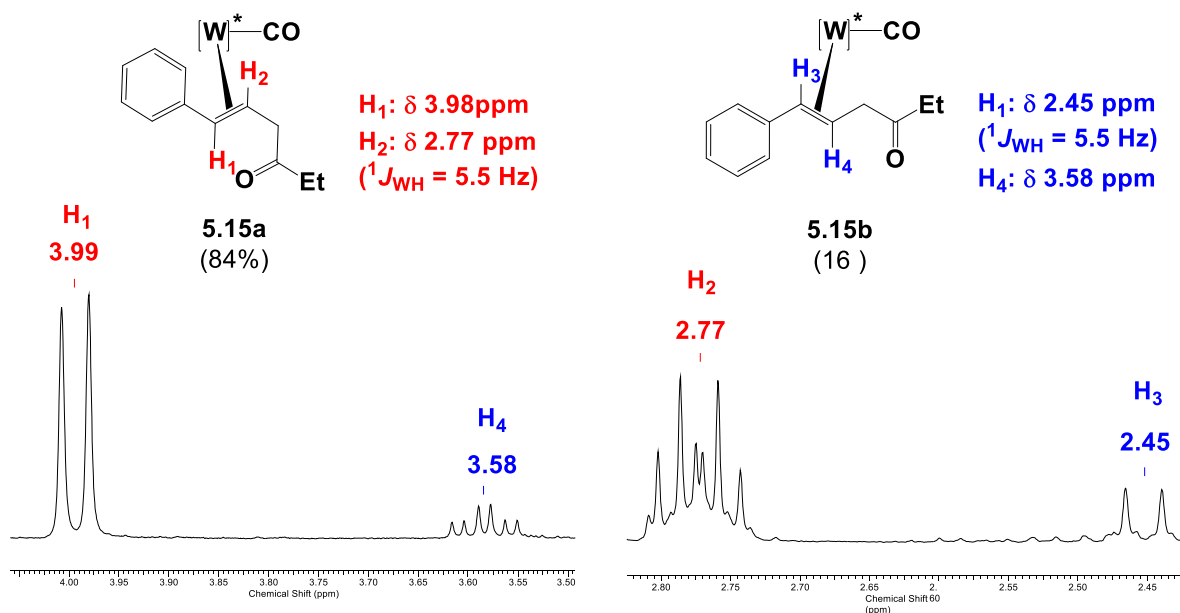


Figure 5.13. Expansion of the ^1H NMR spectrum of **5.15** from δ 4.05 to 3.50 ppm and δ 2.82 to 2.42 ppm showing the signals due to the alkene protons for each isomer.

The ^{13}C NMR spectrum of **5.15** is also instrumental in determining the structure of the isomers. The bonding of the β,γ -unsaturated ketone ligands through the olefin group of each in a dihapto fashion is confirmed by upfield chemical shifts and satellites characteristic of coupling to tungsten-183 (Table 5.4). In addition, each isomer has resonances in the ^{13}C NMR spectrum for a terminal carbonyl ligand and a ketone carbonyl group which are similar to what is seen in the related complexes **4.5** and **4.6** (Table 5.5). For the major isomer, the terminal carbonyl resonance

has characteristic satellites due to coupling to the ^{183}W nucleus with a large $^1J_{\text{WC}}$ magnitude (185.0 Hz) similar to related complexes (e.g. **3.7**, **4.6**).

Table 5.4. Chemical shifts and $^1J_{\text{WC}}$ values for the alkene carbon signals for the isomers of **5.15**.

Isomer	Carbon assignment	^{13}C NMR chemical shift (ppm)	Value of $^1J_{\text{WC}}$ coupling (Hz)
5.15a	PhCH=	δ 57.1	9.2
	=CH	δ 41.8	41.0
5.15b	PhCH=	δ 53.7	34.9
	=CH	δ 48.4	11.0

Table 5.5. Chemical shifts of the carbonyl signals in the ^{13}C NMR spectrum of **5.15**.

Isomer	Carbon assignment	^{13}C NMR chemical shift (ppm)
5.15a	$\text{CH}_2\text{C}(=\text{O})\text{Et}$	211.4
	W-CO	225.0
5.15b	$\text{CH}_2\text{C}(=\text{O})\text{Et}$	210.0
	W-CO	224.1

5.2.7 Methane Functionalization with CO Initiated by **5.1**

5.2.7.1 Formation of the Bound Ketone Complex from Methane Activation Initiated by **5.1**

The sequential exposure of **5.1** to methane (1250 psig, 88 °C, 4 h) and then CO (750 psig, 75 °C, 18 h) results in the formation of $\text{Cp}^*\text{W}(\text{NO})(\text{CO})(\eta^2\text{-PhCH=CHCH}_2\text{C(=O)CH}_3)$ (**5.16**) in decent yield (Scheme 5.11). As with compound **5.15**, IR spectroscopy, 1D and 2D NMR spectroscopies have been instrumental in the characterization of **5.16**.¹³² The IR spectrum of **5.16** has carbonyl- and nitrosyl-stretching frequencies at 1606 (s, ν_{NO}), 1714 (w, $\nu_{\text{CO-ketone}}$), and 1959 (s, $\nu_{\text{CO-terminal}}$) cm^{-1} , which are very similar to that of **5.15**. The carbonyl-stretching frequency for the bound ketone ligand matches that reported for the free ketone.¹³³ Similar to **5.15**, complex **5.16** exists as two isomers in solution that differ with respect to the orientation of the dihapto β,γ -ketone ligand. The chemical shifts of the alkene proton resonances in the ^1H NMR spectrum can be used to assign the orientation of the unsaturated ketone ligand with respect to the tungsten center (Table 5.6). For the major isomer **5.16a**, the more upfield resonance at δ 2.70 ppm is due to the $=\text{CH}$ proton, which is oriented toward the Cp^* ligand; in addition, the resonance also has satellites due to coupling to the ^{183}W nucleus ($^2J_{\text{WH}} = 5.6$ Hz). In the minor isomer **5.16b** the η^2 -alkene is oriented in the opposite direction, the signal due to the PhCH= having the more upfield chemical shift at δ 2.41 ppm. The chemical shifts of the signals due to the alkene carbons (Table 5.6) are nearly identical to those of **5.15** (refer to Table 5.4), supporting strong structural similarities between the two compounds.

Scheme 5.11. Reaction of 5.3 with CO

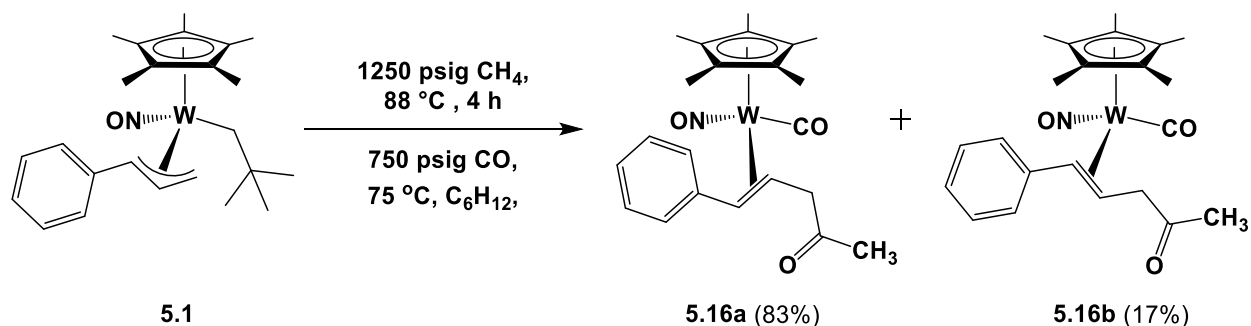


Table 5.6. ¹H and ¹³C NMR chemical shifts of the dihapto alkene fragment for the isomers of 5.16.

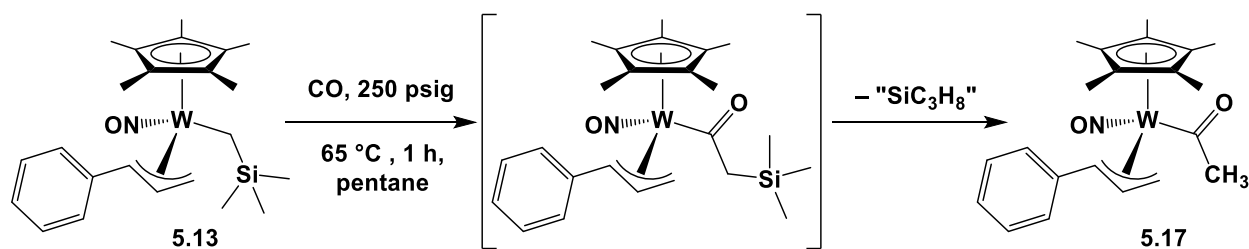
Isomer	Proton/Carbon assignment	¹ H NMR chemical shift (ppm)	¹³ C NMR chemical shift (ppm)
5.16a	PhCH=	δ 3.96	δ 57.2
	=CH	δ 2.70	δ 41.6
5.16b	PhCH=	δ 2.41	δ 53.5
	=CH	δ 3.51	δ 48.2

5.2.7.2 Preparation of Cp*W(NO)(C(O)CH₃)(η³-CH₂CHCHPh) (5.17)

Efforts to effect the clean formation of an acyl complex from **5.3** via the 1,1-insertion of CO have proven to be unsuccessful to date. Instead, the acyl allyl complex Cp*W(NO)(C(=O)CH₃)(η³-CH₂CHCHPh) (**5.17**) has been prepared independently by exposing compound **5.13** to 250 psig CO and 65 °C for 1 h (Scheme 5.12). A similar transformation has been reported for the complex Cp*W(NO)(CH₂SiMe₃)(η³-CH₂CHCHMe). The mechanism of

the transformation is not known, but the paper suggested that the work-up of the expected $\text{Cp}^*\text{W}(\text{NO})(\text{C}(=\text{O})\text{CH}_2\text{SiMe}_3)(\eta^3\text{-CH}_2\text{CHCHMe})$ product may have led to its conversion to $\text{Cp}^*\text{W}(\text{NO})(\text{C}(=\text{O})\text{CH}_3)(\eta^3\text{-CH}_2\text{CHCHMe})$.³⁷ Analysis of the final reaction mixture for the transformation outlined in Scheme 5.12 reveals that **5.17** is already formed. This suggests that the conversion of the CH_2SiMe_3 ligand to $\text{C}(=\text{O})\text{CH}_3$ ligand under exposure to CO is inherent to the reaction and not a result of subsequent manipulations. Regardless, the transformation has been used to obtain and characterize compound **5.17** to assist the monitoring reactions for the transformation of **5.3** to **5.16** (Scheme 5.11). The insertion of CO is slowest for a methyl ligand⁸² so it can be hypothesized that under the conditions necessary to convert **5.3** to **5.17**, the coupling of the $\text{C}(=\text{O})\text{CH}_3$ acyl and the phenylallyl ligands occurs readily, resulting in the consumption of **5.17** as it is formed. The reaction of **5.4** with CO at 75 °C results in a similar transformation where the acyl complex **5.14** begins converting to the η^2 -bound ketone complex before **5.4** is consumed. It is likely the conversion of **5.3** does proceed through the acyl complex **5.17**, but the conversion of **5.17** to **5.16** occurs rapidly and **5.17** is not observed for the transformation.

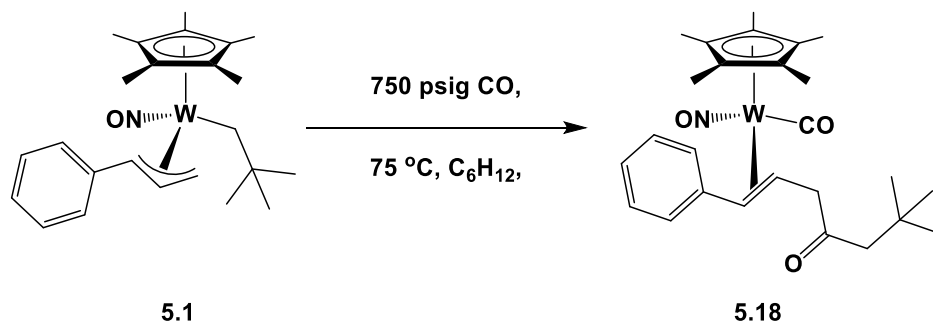
Scheme 5.12. Conversion of 5.13 to 5.17 under CO pressure



5.2.7.3 Formation of $\text{Cp}^*\text{W}(\text{NO})(\text{CO})(\eta^2\text{-PhCH=CHCH}_2\text{C(=O)CH}_2\text{CMe}_3)$ (**5.18**)

When effecting the conversion of methane or ethane to the η^2 -bound ketone complexes **5.15** and **5.16** initiated by **5.1**, a byproduct of the reaction can be obtained when the conversion of **5.1** to **5.3** or **5.4** is not complete. This byproduct is $\text{Cp}^*\text{W}(\text{NO})(\text{CO})(\eta^2\text{-PhCH=CHCH}_2\text{C(=O)CH}_2\text{CMe}_3)$ (**5.18**) from the direction reaction of **5.1** with CO. Spectroscopically compound **5.18** is very similar to **5.16a**, and a comparison of the signals in the ^1H NMR spectra due to the PhCH= , $=\text{CH}$, and $\text{CH}_2\text{C(=O)}$ protons of each complex are shown below in Figure 5.14. The IR spectrum contains carbonyl- and nitrosyl-stretching frequencies similar to those of the isomers of **5.15** and **5.16**.

Scheme 5.13. Conversion of 5.1 to the η^2 -bound ketone complex 5.18 under exposure to CO



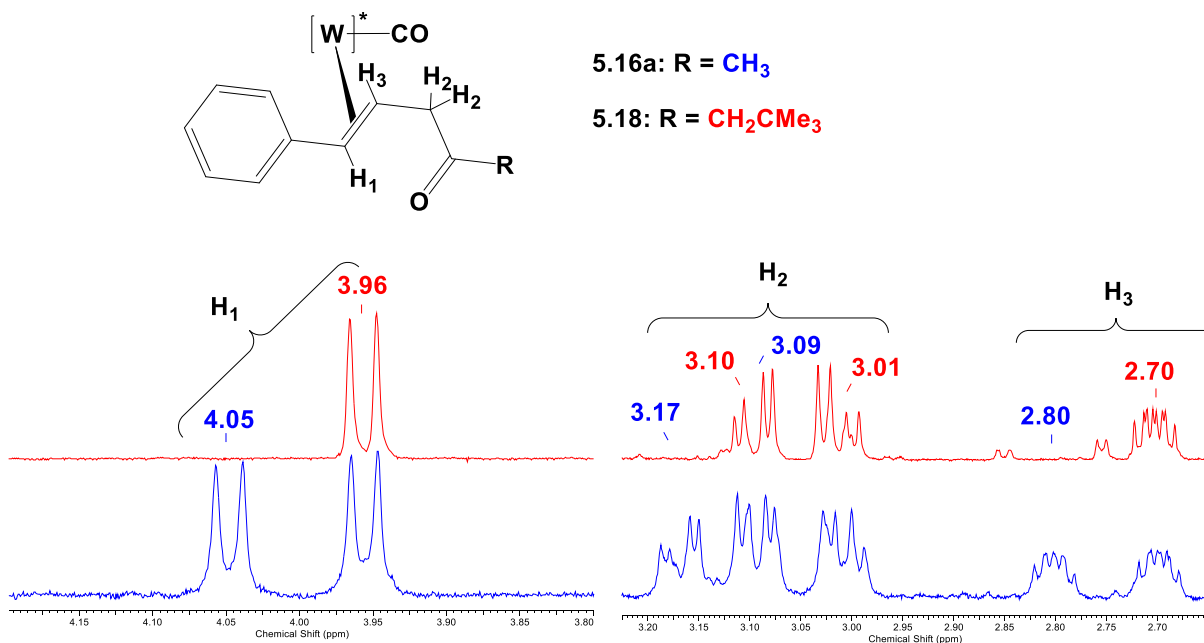


Figure 5.14. Expansions of the ^1H NMR spectra from δ 4.20 to 3.80 ppm and δ 3.22 to 2.61 ppm for complex **5.16a** (red) and the mixture of **5.16a** and **5.18** (blue). The resonances due to the PhCH= , $=\text{CH}$, and $\text{CH}_2\text{C}(=\text{O})$ protons are highlighted.

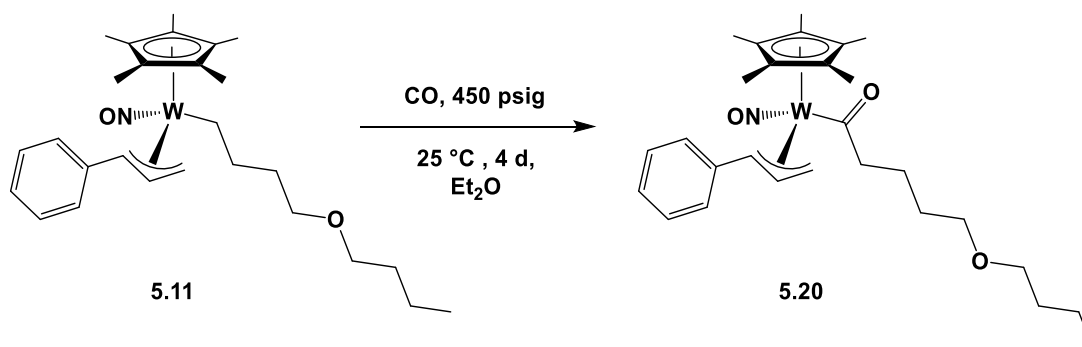
5.2.8 Acyl Ligands from Long-Chain Hydrocarbons

In order to determine if the longer-chain alkanes and heteroatom-containing hydrocarbons can be functionalized with CO, the reactions of **5.11** and $\text{Cp}^*\text{W}(\text{NO})(n\text{-C}_7\text{H}_{15})(\eta^3\text{-CH}_2\text{CHCHPh})$ (**5.19**) with CO have been investigated. Complex **5.19** is obtained from the single, terminal C-H activation of *n*-heptane by **5.1** under conditions analogous for the C-H activation of ethane (refer to Scheme 5.5) and its characterization data have been reported.²⁸

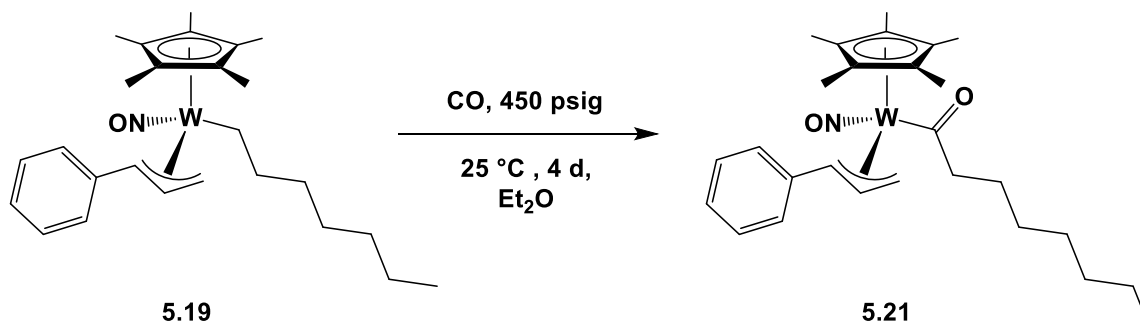
Exposure of an Et_2O solution of either complex **5.11** (Scheme 5.14) or **5.19** (Scheme 5.15) to 450 psig CO at ambient temperature for a period of 4 d results in the 1,1-insertion of CO into the W-C bond of the η^1 -hydrocarbyl/alkyl ligand. The products of each reaction are the acyl

allyl complexes $\text{Cp}^*\text{W}(\text{NO})(\text{C}=\text{O})(\text{CH})_2\text{O}(\text{CH}_2)_3\text{CH}_3)(\eta^3\text{-CH}_2\text{CHCHPh})$ (**5.20**) and $\text{Cp}^*\text{W}(\text{NO})(\text{C}=\text{O})(\text{CH}_2)_6\text{CH}_3)(\eta^3\text{-CH}_2\text{CHCHPh})$ (**5.21**), respectively. They are obtained as yellow oils in both cases. Attempts to obtain crystals suitable for single crystal X-ray diffraction have been unsuccessful to date. Similar complexes with long chain η^1 -hydrocarbyl or η^1 -alkyl ligands are typically isolable as oils and exceedingly difficult to crystallize, due largely to the lengthy hydrocarbon group.^{28, 33} Instead, ^1H and ^{13}C APT as well as 2D NMR spectroscopies such as $\{^1\text{H}/^{13}\text{C}\}$ HMBC and $\{^1\text{H}/^{13}\text{C}\}$ HSQC have been critical to establish the 1,1-insertion of CO into the η^1 -hydrocarbyl/alkyl ligand for each complex.

Scheme 5.14. Carbonylation of complex 5.11 to produce an acyl ligand derived from the terminal activation of di(*n*-butyl) ether



Scheme 5.15. Functionalization of an *n*-heptyl ligand by 1,1-insertion of CO



The acyl ligand of complex **5.20** has a carbon resonance at δ 260.8 ppm in the ^{13}C NMR spectrum. This chemical shift is typical for an acyl group and similar to what is seen in related complexes such as **4.3**, **4.4**, **5.14**, and **5.17**, as well as similar complexes that have been reported.³⁷ In the $\{^1\text{H}/^{13}\text{C}\}$ HMBC spectrum (Figure 5.15a), a cross peak correlates the acyl C(=O) resonance at δ 260.8 ppm with a triplet in the ^1H NMR spectrum at δ 3.08 ppm. This triplet is due to the methylene group α to the C(=O). The multiplicity of the C(=O)CH₂ signal is consistent with coupling to an adjacent methylene group. The full characterization of the acyl ligand by ^1H and ^{13}C NMR spectroscopies has been made using the 2D HMBC and HSQC NMR spectroscopies to confirm the formula of **5.20** shown in Scheme 5.14. Interestingly, complex **5.20** does not display the same degree of restricted rotation seen in the parent complex **5.11**, in which the four methylene groups at the α - δ positions from the tungsten are diastereotopic. As shown in Figure 5.15a, the methylene groups at the α , δ , and ζ positions are characterized as triplets, indicating that there is no restricted rotation of the hydrocarbyl chain of the acyl ligand in complex **5.20**. Additionally, the chemical shifts of the allyl carbons in the ^{13}C APT NMR spectrum of **5.20** caused by the σ - π distortion of the allyl ligand can be used to determine the orientation of the phenyl substituent. The more π -character part of the allyl ligand is trans to the nitrosyl ligand, which is the CH₂ with a signal at δ 71.1 ppm, while the CHPh signal at δ 66.1 ppm indicates more σ -character, which places the phenyl substituent proximal to the nitrosyl ligand.

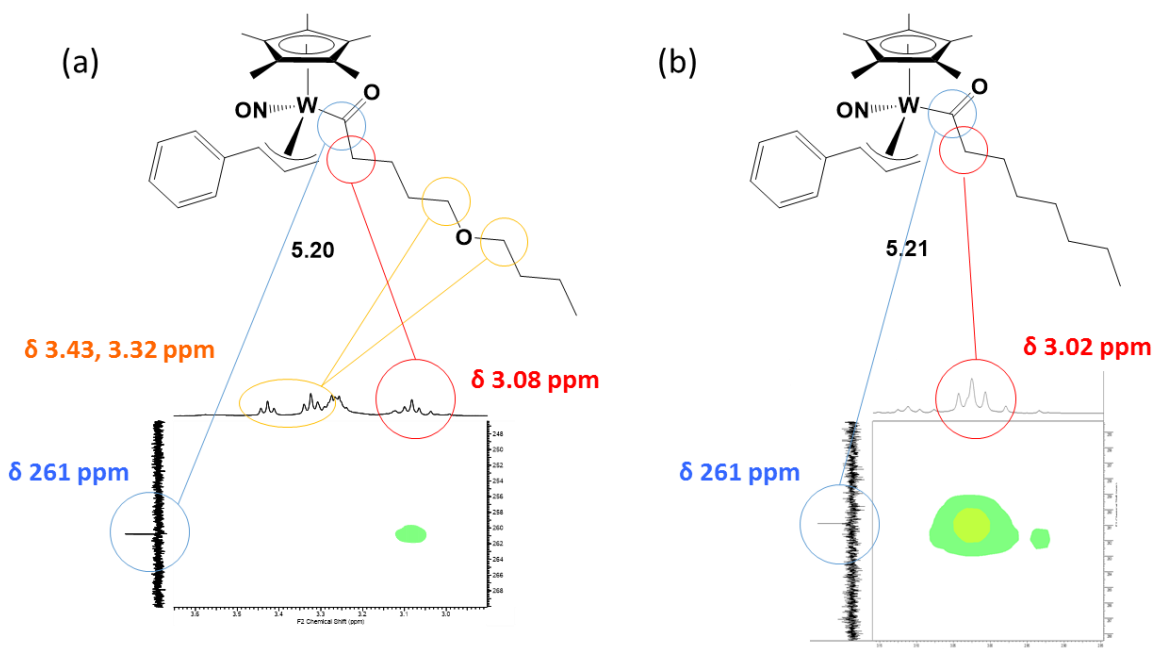


Figure 5.15. Expansions of the $\{^1\text{H}-^{13}\text{C}\}$ HMBC NMR spectra of (a) compound **5.20** and (b) compound **5.21** showing the correlation between the acyl carbon signal and the triplet at the α position to the carbonyl for each complex.

As for **5.20**, the 1,1-CO insertion into the W-C bond of the *n*-heptyl ligand of complex **5.21** is established with the aid of 2D NMR spectroscopy. The acyl carbon has a signal at δ 260.9 ppm in the ^{13}C NMR spectrum which has a cross peak in the $\{^1\text{H}/^{13}\text{C}\}$ HMBC NMR spectrum that correlates to a triplet in the ^1H NMR spectrum at δ 3.02 ppm (Figure 5.15b). The connectivity of the remainder of the *n*-heptyl chain is established by 2D NMR; in addition, the ^{13}C APT NMR spectrum is used to assign six methylene carbons and a single methyl carbon. An acyl ligand is also supported by a carbonyl-stretching frequency in the IR spectrum of 1632 cm^{-1} . The position of the phenyl substituent is proximal to the nitrosyl ligand which is again established using the effect of the σ - π distortion of the allyl ligand on the chemical shifts of the CH_2 (δ 71.3 ppm) and CHPh (δ 66.0 ppm) signals.

5.2.9 Alkane Functionalization with CO Initiated by **5.2**

The facile single C-H activation of methane, ethane, and propane by **5.2** makes the functionalization of the alkanes with CO initiated by **5.2** an attractive possibility. To begin the investigation of the reactions of $\text{Cp}^*\text{W}(\text{NO})(\text{alkyl})(\eta^3\text{-CH}_2\text{CHCHMe})$ complexes with CO, the direct reaction of compound **5.2** with CO was carried out. Exposure of **5.2** to 750 psig CO at 75 °C for 18 h leads to the formation of the corresponding η^2 -bound ketone complex, $\text{Cp}^*\text{W}(\text{NO})(\text{CO})(\eta^2\text{-MeCH=CHCH}_2\text{C(=O)CH}_2\text{CMe}_3)$ (**5.22**) (Scheme 5.16). Compound **5.22** is obtained as a yellow oil in a quantitative conversion. The IR spectrum of the oil is shown in (Figure 5.16). Carbonyl-stretching frequencies consistent with a terminal carbonyl ligand and ketone carbonyl are observed at 1950 and 1712 cm^{-1} , respectively. A nitrosyl-stretching frequency at 1601 cm^{-1} is similar to that for analogous η^2 -bound ketone complexes discussed previously (i.e. **4.5**, **4.6**, **5.15**, **5.16**, and **5.18**). Complexes **5.15**, **5.16**, and **5.18** are also obtained as oils even after column chromatography and attempts at recrystallization. Analysis of the product by 1D and 2D NMR spectroscopies reveals that **5.22** exists as a complex mixture of isomers which are not individually isolable.^{134,135} This observation suggests that even though analogous chemistry can be effected with **5.2**, the plethora of isomers generated by the formation of the bound ketone complex indicates that continuing down this path would result in mixtures containing a multitude of ketone isomers.

Scheme 5.16. The thermolysis of **5.2** at 75 °C and 750 psig CO

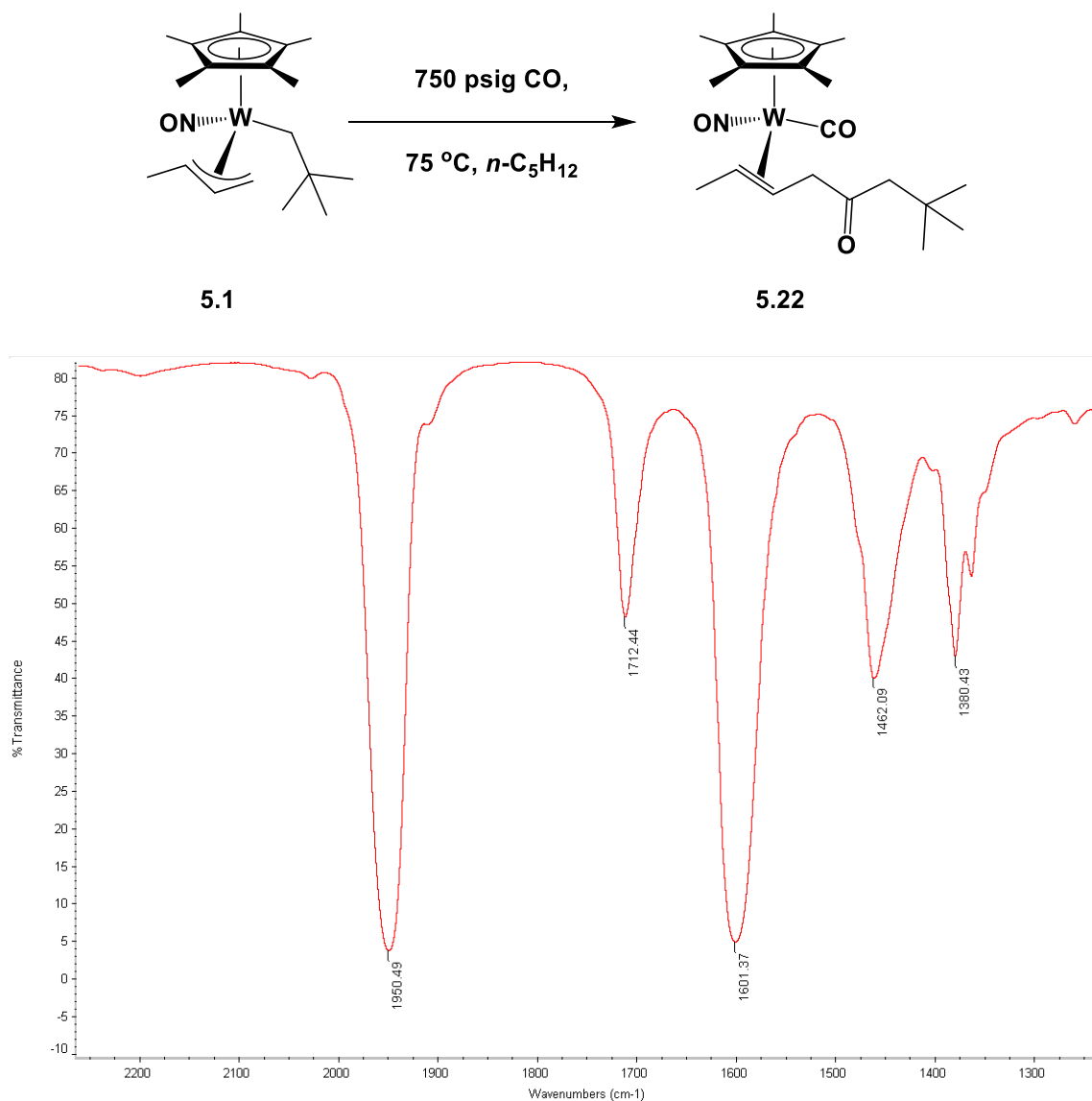
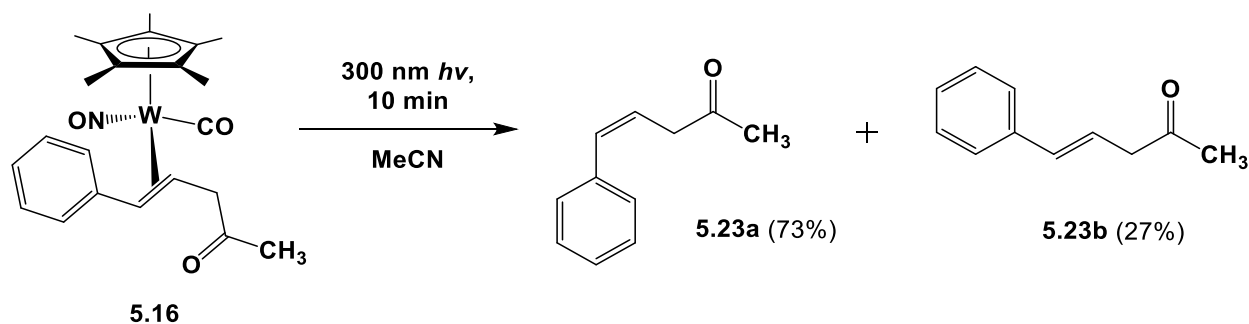


Figure 5.16. IR spectrum (Nujol) of the mixture of isomers of **5.22**. Relevant stretching frequencies are 1601 (s, ν_{NO}), 1712 (w, $\nu_{\text{CO-ketone}}$), and 1950 (s, $\nu_{\text{CO-terminal}}$) cm^{-1} . (The remaining absorptions are due to Nujol.)

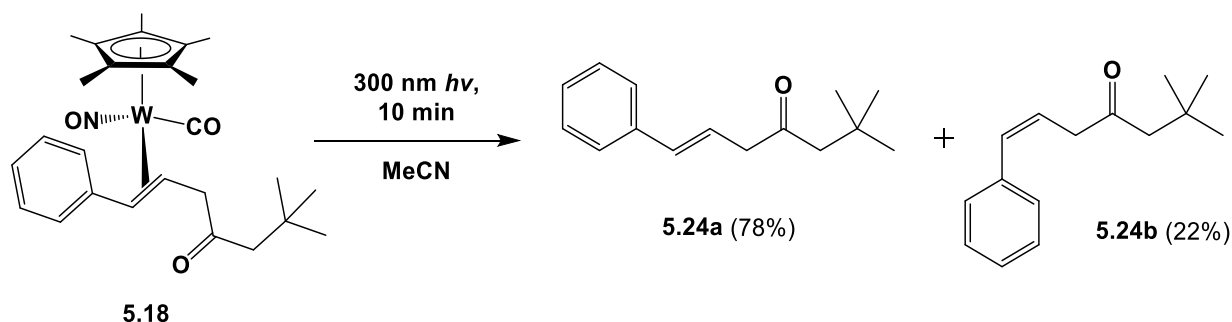
5.2.10 Photolysis of Bound Ketone Complexes

The bound-ketone ligands present in complexes **5.16**, and **5.18** can be liberated by photolysis as the corresponding β,γ -unsaturated ketones. Irradiation of an acetonitrile solution of **5.16** at 300 nm for 10 min results in the release of (Z)-5-phenylpent-4-en-2-one (**5.23a**) and (E)-5-phenylpent-4-en-2-one (**5.23b**) in a 73:27 ratio (Scheme 5.17). The ketones are isolated together as a yellow oil in decent yield (48%). The formation of the isomers of **5.23** represents the conversion of methane and CO into value-added unsaturated ketones. Likewise, the photolysis of an acetonitrile solution of **5.18** results in the formation of the ketones (E)-6,6-dimethyl-1-phenylhept-1-en-4-one (**5.24a**) and (Z)-6,6-dimethyl-1-phenylhept-1-en-4-one (**5.24b**) in a 78:22 ratio in similar yield (59%) (Scheme 5.18). The fate of the tungsten complex in either case is currently not known, but it is likely that any organometallic species obtained via ketone release subsequently decomposes. Attempts to carry out the photolysis in the presence of CO do not result in the formation of the dicarbonyl complex **3.7**.

Scheme 5.17. Photolysis of **5.16** to afford β,γ -unsaturated ketones from methane and CO



Scheme 5.18. Photolysis of 5.18 to afford β,γ -unsaturated ketones



The selection of the wavelength of 300 nm was made by Dr. Russell Wakeham, and it is necessary for the selective release of the β,γ -unsaturated ketone products. Without filtering for the specific wavelength, isomerization of the released ketones occurs and mixtures of *cis/trans*- β,γ -unsaturated ketones and *cis/trans*- α,β -unsaturated ketones are obtained. Working in collaboration with Dr. Wakeham the conversion of **5.5** and **5.6** to the corresponding bound ketone complexes $\text{Cp}^*\text{W}(\text{NO})(\text{CO})(\eta^2\text{-PhCH=CHCH}_2\text{C(=O)}^n\text{Pr})$ and $\text{Cp}^*\text{W}(\text{NO})(\text{CO})(\eta^2\text{-PhCH=CHCH}_2\text{C(=O)}^n\text{Bu})$ has also been effected. The properties of these compounds are similar to those of **5.15**, **5.16**, and **5.18**, and they are both isolable as yellow oils. As expected, the photolysis of these bound-ketone compounds at 300 nm results in the liberation of the *cis/trans*- β,γ -unsaturated ketones derived from propane and *n*-butane activation.

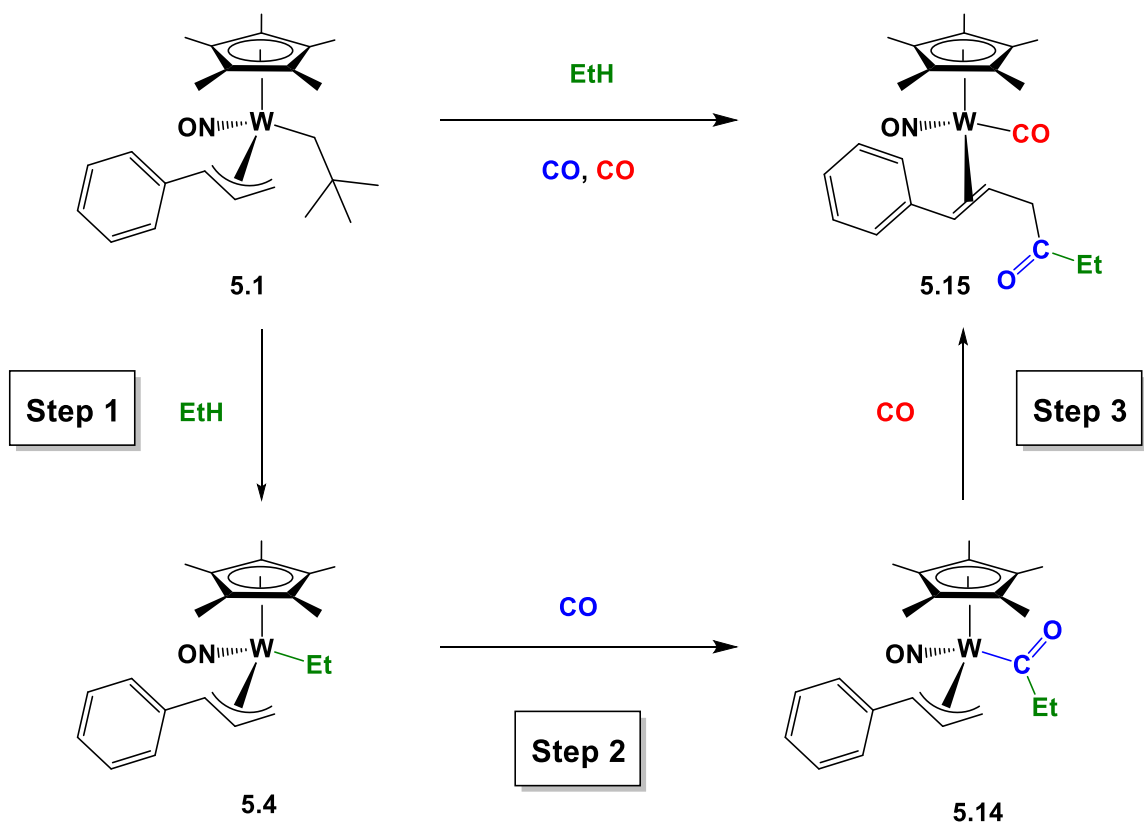
5.3 Summary

Compound **5.1** effects the single, selective C-H activation of the gaseous alkanes methane, ethane, propane, and *n*-butane. The products of these reactions are isolable as air- and moisture-sensitive yellow solids that allow for their complete characterization as well as an

investigation of their chemistry. The selective C-H activation of hydrocarbons containing heteroatoms including O, Cl, and Si has been effected, and the products have been characterized. There is evidence of β -agostic interactions for many of the $\text{Cp}^*\text{W}(\text{NO})(n\text{-alkyl})(\eta^3\text{-CH}_2\text{CHCHPh})$ complexes, despite them being formally 18e compounds. This interaction appears to be an intrinsic property of the complexes and results in decreased thermal stability of $\text{Cp}^*\text{W}(\text{NO})(n\text{-alkyl})(\eta^3\text{-CH}_2\text{CHCHPh})$ complexes containing β -hydrogens. This puts an upper limit on C-H activation temperatures for C2 and larger hydrocarbon substrates. For substrates such as methane and tetramethylsilane, there is no possible β -elimination decomposition pathway, thereby allowing reactions of these substrates to be hastened by employing higher temperatures.

Exposure of the $\text{Cp}^*\text{W}(\text{NO})(n\text{-alkyl})(\eta^3\text{-CH}_2\text{CHCHPh})$ complexes resulting from intermolecular C-H activation to CO either at 75 °C for 2 h or at ambient temperature for 4 d results in the selective 1,1-insertion of CO into the W-alkyl bonds. Exposure of the same $\text{Cp}^*\text{W}(\text{NO})(\text{alkyl})(\eta^3\text{-CH}_2\text{CHCHPh})$ complexes to CO at 75 °C for a longer period of time results in the formation of the bound-ketone compounds, $\text{Cp}^*\text{W}(\text{NO})(\text{CO})(\eta^2\text{-PhCH=CHCH}_2\text{C(=O)(alkyl)})$; these bound-ketone complexes are formed from acyl complexes via the coupling of the acyl and allyl ligands. For the case shown in Scheme 5.19, ethane is functionalized via C-H activation and two subsequent C-C bond forming reactions. Specifically, (1) the C-H activation of ethane by **5.2** gives complex **5.4** containing an ethyl ligand; (2) next, the insertion of CO into the W-ethyl bond forms a new C-C linkage to give an acyl ligand made from CO and ethane in complex **5.14**; (3) finally, the acyl ligand couples to the allyl ligand, generating another new C-C bond and producing complex **5.15**. The conversion of methane and CO to the analogous bound-ketone complex has also been effected.

Scheme 5.19. The stepwise functionalization of ethane with CO initiated by 5.1



This process has been best elucidated for the transformation of ethane first into the ethyl ligand in **5.4**, then into the acyl ligand in **5.14**, and finally into the η^2 -bound β,γ -unsaturated ketone in **5.15**. Ultimately, photolyses of the $\text{Cp}^*\text{W}(\text{NO})(\text{CO})(\eta^2\text{-PhCH=CHCH}_2\text{C(=O)(alkyl)})$ compounds afford isomers of the free β,γ -unsaturated ketones.

The conversion of a long-chain ether and alkane through C-H activation and 1,1-CO insertion to produce the acyl complexes **5.20** and **5.21** has also been performed. This suggests that **5.1** is an appropriate platform for the selective functionalization of a broader scope of alkanes and hydrocarbons. The facile C-H activations of C1-C3 alkanes initiated by **5.2** have been optimized, and preliminary investigations into the reaction of **5.2** with CO have been

performed. However, the bound-ketone complexes generated from **5.2** exist as a plethora of isomers, a fact that ultimately compromises the selectivity of any ketones derived from alkanes activated by this monomethylallyl system.

Finally, α,β -unsaturated ketones can be released by photolysis of the $\text{Cp}^*\text{W}(\text{NO})(\text{CO})(\eta^2\text{-PhCH=CHCH}_2\text{C(=O)(n-alkyl)})$ compounds at a wavelength of 300 nm. Specifically, the photolysis of compound **5.18**, derived from the C-H activation of methane, results in the liberation of (*E/Z*)-5-phenylpent-4-en-2-one (**5.23**). Ketone **5.23** represents the conversion of gaseous methane into a value-added transportable oil that contains carbonyl and olefin functional groups.

5.4 Experimental

5.4.1 General Methods

Unless otherwise noted all reactions involving organometallic reagents were performed under anhydrous and anaerobic conditions. The subsequent manipulations including column chromatography and recrystallization were carried out under aerobic conditions except where otherwise noted. Inert gases were purified by passing them through a column containing MnO and then through a column of activated 4 Å molecular sieves. High vacuum and inert atmosphere techniques were performed either using double-manifold Schlenk lines or in Innovative Technologies LabMaster 100 and MS-130 BG dual-station glove boxes equipped with freezers maintained at $-33\text{ }^{\circ}\text{C}$. Reactions on a preparative scale were performed with Schlenk or round bottom flasks. Reactions with gases were performed in a Parr 5500 pressure reactor vessel with a

capacity of 0.3 L unless otherwise noted. Cyclohexane was dried over calcium hydride, freshly distilled, and then dried over molecular sieves prior to use. Diethyl ether (Et₂O) and tetrahydrofuran (THF) were dried over sodium/benzophenone ketyl and freshly distilled prior to use. The following complexes were prepared according to the published procedures: Cp*W(NO)Cl₂,⁵⁶ Cp*W(NO)(CH₂CMe₃)(η³-CH₂CHCHMe),²⁷ and Cp*W(NO)(*n*-C₇H₁₅)(η³-CH₂CHCHPh).²⁸ Pentamethylcyclopentadiene was obtained from the Boulder Scientific Company. Methane, ethane, propane, butane, and carbon monoxide were obtained from Praxair and used as received. All other chemicals and reagents were ordered from commercial suppliers and used as received.

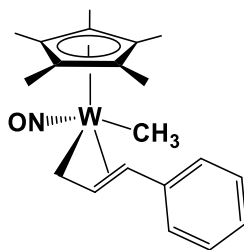
All IR samples were prepared as Nujol mulls sandwiched between ZnCl₂ plates, and their spectra were recorded on a Thermo Nicolet Model 4700 FT-IR spectrometer. Except where it has been noted all NMR spectra were recorded at room temperature on Bruker AV-400 (direct and indirect probes) instruments, and all chemical shifts are reported in ppm and coupling constants are reported in Hz. ¹H NMR spectra were referenced to the residual protio isotopomer present in C₆D₆ (7.16 ppm) or CDCl₃ (7.27 ppm). ¹³C NMR spectra were referenced to C₆D₆ (128.39 ppm) or CDCl₃ (77.00 ppm). For the characterization of most complexes 2-dimensional NMR experiments, {¹H-¹H} COSY, {¹H-¹³C} HSQC, and {¹H-¹³C} HMBC, were performed out to correlate and assign ¹H and ¹³C NMR signals and establish atom connectivity; ¹H NOE NMR and {¹H-¹H} NOESY were used for determination of solution structures. Low- and high-resolution mass spectra (EI, 70 eV) were recorded by Mr. Marshall Lapawa of the UBC mass spectrometry facility using a Kratos MS-50 spectrometer and elemental analyses were performed by Mr. Derek Smith of the UBC microanalytical facility. X-ray crystallographic data collection, solution, and refinement were performed at the UBC X-ray crystallography facility;

5.4.2 Modified Synthesis of $\text{Cp}^*\text{W}(\text{NO})(\text{CH}_2\text{CMe}_3)(\eta^3\text{-CH}_2\text{CHCHPh})$ (**5.1**)

In a glove box, a Schlenk flask was charged with $\text{Cp}^*\text{W}(\text{NO})\text{Cl}_2$ (5.01 g, 11.9 mmol), THF (ca. 150 mL), and a magnetic stir bar, and then sealed with a rubber septum. A second Schlenk flask was charged with $\text{Mg}(\text{CH}_2\text{CMe}_3)_2$ (titer: 159.5 g/mol, 1.87 g, 11.7 mmol), THF (ca. 100 mL), and a magnetic stir bar, and then sealed with a septum. The two Schlenk flasks were transferred to a Schlenk line, placed into a dry ice/acetone bath (-78°C) and the contents of each flask were stirred while being cooled. The contents of the second flask were cannulated dropwise into the first flask to produce a dark purple mixture. The solvent was removed in vacuo while the Schlenk was maintained in a cold water bath to obtain $\text{Cp}^*\text{W}(\text{NO})(\text{CH}_2\text{CMe}_3)\text{Cl}$ as a purple residue. $\text{Cp}^*\text{W}(\text{NO})(\text{CH}_2\text{CMe}_3)\text{Cl}$ was transferred in Et_2O (ca. 400 mL) to a 1 L round bottom flask which was maintained at -78°C in a dry ice/acetone bath. A third Schlenk flask was charged in the glove box with $\text{Mg}(\text{CH}_2\text{CH=CHPh})$ (titer: 224.5 g/mol, 2.68 g, 11.9 mmol), Et_2O (ca. 200 mL), and a magnetic stir bar. The contents of the third flask were transferred slowly via cannula to the round-bottom flask that was maintained at -78°C while being stirred. Following the addition, the round-bottom flask was removed from the bath, and its contents were allowed to warm to room temperature while being stirred for 1 h, thereby producing a brown mixture. The volume of the solvent was reduced in vacuo, and the concentrated mixture was added to the top of a basic alumina column. A yellow band was developed and eluted with 0-5% Et_2O in hexanes to obtain an orange eluate. The solvent was removed from the eluate in vacuo to afford $\text{Cp}^*\text{W}(\text{NO})(\text{CH}_2\text{CMe}_3)(\eta^3\text{-CH}_2\text{CHCHPh})$ (**5.1**) as an orange solid (1.975 g, 31% yield). The characterization of **5.1** was previously reported.⁴⁴

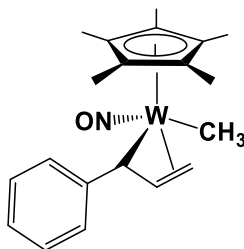
5.4.3 Preparation of $\text{Cp}^*\text{W}(\text{NO})(\text{CH}_3)(\eta^3\text{-CH}_2\text{CHCHPh})$ (**5.3**)

In a glove box, a Parr 5500 pressure reactor was charged with a sample of **5.1** (0.600 g, 1.17 mmol) and cyclohexane (ca. 100 mL) to give a light orange solution. The reactor was sealed and then removed from the glove box. It was then cycled three times with 500 psig CH_4 and then pressurized to 500 psig. The contents were mechanically stirred and heated at 88 °C for 4 h (pressure 575 psig). The gas was then vented from the reactor, and a yellow-brown solution was collected in a 0.5 L round-bottom flask. The solvent was removed in volume in vacuo to give a brown residue which was then dissolved in a minimum volume of Et_2O to give a concentrated solution of the crude product. Purification was performed in the air by column chromatography over activated basic alumina support. A yellow band was eluted using a gradient of 33-66% Et_2O in hexanes. The solvents were removed in vacuo to afford complex **5.3** as a yellow powder (0.282 g, 53% yield). As a solid the complex is air and moisture stable, and in solution the complex decomposes slowly at room temperature over several weeks. Crystals suitable for single-crystal X-ray diffraction were grown by slow evaporation in 1:1 Et_2O /hexanes at room temperature. The solution structures of the isomers were determined by selective ^1H NOE NMR spectroscopy. The complex was found to have a melting point from 106-108 °C that was confirmed to be reversible by ^1H NMR spectroscopy. The orientation of the allyl ligand of each isomer was determined using ^1H NOE NMR spectroscopy as well the chemical shifts of the allyl C and H signals in the ^1H and ^{13}C NMR spectra.



5.3a (65%)

Characterization data for the **5.3a** (65%): IR (cm⁻¹) 1559 (s, ν_{NO}). MS (LREI, m/z , probe temperature 120 °C) 481 [M^+ , ^{184}W]. ^1H NMR (400 MHz, C_6D_6) δ -0.18 (s, $^2J_{\text{WH}} = 5.4$, 3H, WCH_3), 0.65 (dd, $^3J_{\text{HH}} = 9.4$, $^2J_{\text{HH}} = 2.5$, 1H, allyl CH_2), 1.53 (s, 15H, C_5Me_5), 2.63 (dd, $^3J_{\text{HH}} = 7.0$, $^2J_{\text{HH}} = 2.5$, 1H, allyl CH_2), 3.01 (d, $^3J_{\text{HH}} = 13.5$, 1H allyl CHPh), 5.44 (ddd, $^3J_{\text{HH}} = 13.5$, 9.4, 7.0, 1H, allyl CH), 6.81 (d, $^3J_{\text{HH}} = 7.2$, 2H, *o*-aryl H), 7.08 (t, $^3J_{\text{HH}} = 7.4$, 1H, *p*-aryl H), 7.13 (t, $^3J_{\text{HH}} = 7.7$, 2H, *m*-aryl H). ^{13}C APT NMR (100 MHz, C_6D_6) δ 6.7 ($^1J_{\text{WC}} = 81.2$, WCH_3), 10.2 (C_5Me_5), 38.1 ($^1J_{\text{WC}} = 29.4$, allyl CH_2), 95.6 (allyl CHPh), 102.7 (allyl CH), 106.2 (C_5Me_5), 127.2 (*p*-aryl C), 127.6 (*o*-aryl C), 128.6 (*m*-aryl C), 137.6 (ipso C). Sel NOE (400 MHz, C_6D_6) δ irradiat. at -0.18, NOE at 1.53, 3.01, 6.81. Anal. Calcd for $\text{C}_{20}\text{H}_{27}\text{NOW}$: C, 49.91; H, 5.65; N, 2.91. Found: C, 49.97; H, 5.74; N, 2.67.



5.3b (35%)

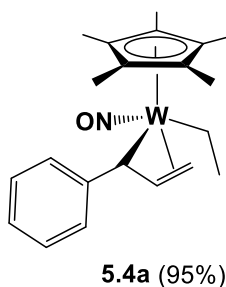
Characterization data for the **5.3b** (35%): ^1H NMR (400 MHz, C_6D_6) δ 0.45 (s, $^2J_{\text{WH}} = 6.0$, 3H, WCH_3), 1.43 (s, 15H, C_5Me_5), 1.64 (m, 1H, allyl CH_2), 2.07 (d, $^3J_{\text{HH}} = 10.0$, 1H allyl CHPh), 2.99 (d, $^3J_{\text{HH}} = 7.0$, 1H allyl CH_2), 5.43 (ddd, $^3J_{\text{HH}} = 13.5$, 10.0, 7.0, 1H, allyl CH), 7.06

(t, $^3J_{\text{HH}} = 7.2$, 1H, *p*-aryl H), 7.30 (t, $^3J_{\text{HH}} = 7.4$, 2H, *m*-aryl H), 7.40 (d, $^3J_{\text{HH}} = 7.4$, 2H, *o*-aryl H). ^{13}C APT NMR (100 MHz, C_6D_6) δ -2.7 (WCH₃), 9.8 (C_5Me_5), 63.3 ($^1J_{\text{WC}} = 19.4$, allyl CHPh), 72.9 ($^1J_{\text{WC}} = 6.6$, allyl CH₂), 106.2 (C_5Me_5), 109.6 (allyl CH), 125.2 (*p*-aryl C), 127.2 (*o*-aryl C), 128.4 (*m*-aryl C), 143.2 (ipso C). Sel NOE (400 MHz, C_6D_6) δ irradiat. at 0.45, NOE at 1.43, 2.99, 5.42.

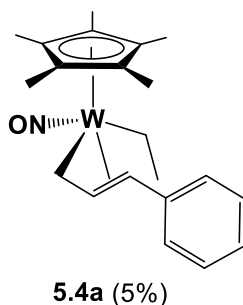
5.4.4 Preparation of $\text{Cp}^*\text{W}(\text{NO})(\text{CH}_3)(\eta^3\text{-CH}_2\text{CHCHPh})$ (**5.4**)

In a glove box, a Parr 5500 pressure reactor was charged with **5.1** (0.391 g, 0.728 mmol) and cyclohexane (ca. 75 mL) to give a light orange solution. The reactor was sealed, then removed from the glove box and cycled three times with 400 psig C_2H_6 (g) before being pressurized to 400 psig. The contents of the reactor were stirred mechanically and heated at 55 °C for 3 d, after which time a yellow solution was obtained. The solvent was removed in vacuo to give a yellow oily residue. The residue was dissolved in a minimum amount of Et_2O to give a concentrated solution of the crude product. Purification of the product was performed using column chromatography on activated basic alumina support (2.5 x 20 cm). A yellow band was eluted with a gradient of 20-50% Et_2O in hexanes, and the solvent was then removed to give **5.4** as a yellow powder (0.308 g, 86 % yield). Yellow crystals suitable for X-ray diffraction were obtained from 1:1 pentane/ Et_2O at -33 °C. The solution structure of the major isomer (**5.4a**) was determined by selective ^1H NOE NMR spectroscopy. The complex was found to have a melting point of 108-109 °C that was confirmed to be reversible by ^1H NMR spectroscopy. The orientation of the allyl ligand of each isomer was determined using the chemical shifts of the

allyl C and H signals in the ^1H and ^{13}C NMR spectra, as well as Sel NOE NMR spectroscopy for isomer **5.4a**.



Characterization data for **5.4a** (95%): IR (cm^{-1}) 1553 (s, ν_{NO}). MS (LREI, m/z , probe temperature 120 $^{\circ}\text{C}$) 495 [M^+ , ^{184}W]. ^1H NMR (400 MHz, C_6D_6) δ 1.11 (q, $^3J_{\text{HH}} = 7.2$, $^2J_{\text{WH}} = 7.1$, 2H, WCH_2CH_3), 1.42 (s, 15H, C_5Me_5), 1.61 (d, $^3J_{\text{HH}} = 13.3$, 1H, allyl CH_2), 1.78 (t, $^3J_{\text{HH}} = 7.2$, $^3J_{\text{WH}} = 5.2$, 3H, WCH_2CH_3), 2.17 (d, $^3J_{\text{HH}} = 9.8$, 1 H, allyl CHPh), 3.24 (d, $^3J_{\text{HH}} = 7.0$, 1H, allyl CH_2), 5.51 (ddd, $^3J_{\text{HH}} = 13.3$, 9.8, 7.0, 1H, allyl CH), 7.05 (t, $^3J_{\text{HH}} = 7.2$, 1H, p -aryl H), 7.28 (t, $^3J_{\text{HH}} = 7.6$, 2H, m -aryl H), 7.36 (d, $^3J_{\text{HH}} = 7.4$, 2H, o -aryl H). ^{13}C APT NMR (100 MHz, C_6D_6) δ 9.7 (C_5Me_5), 10.1 (WCH_2CH_3), 18.3 (WCH_2CH_3), 63.2 ($^1J_{\text{WC}} = 19.6$, allyl CHPh), 73.1 ($^1J_{\text{WC}} = 7.8$, allyl CH_2), 106.2, ($^1J_{\text{WC}} = 4$, C_5Me_5), 107.0 (allyl CH), 125.6 (p -aryl C), 127.4 (o -aryl C), 128.7 (m -aryl C), 143.2 (ipso C). Sel NOE (400 MHz, C_6D_6) δ irradiated at 1.78, NOE at 1.11, 1.42, 3.24, 5.51, 7.36. Anal. Calcd for $\text{C}_{21}\text{H}_{29}\text{NOW}$: C, 50.92; H, 5.90; N, 2.83. Found: C, 51.23; H, 5.89; N, 2.66.



Characterization data for **5.4b** (5%): ^1H NMR (400 MHz, C_6D_6) δ (selected signals) 0.36 (m, 1H, WCH_2CH_3), 0.72 (m, 1H allyl CH_2), 2.62 (m, 1H allyl CH_2), 3.19 (m, 1H, allyl CHPh), 5.39 (br s, 1H, allyl CH), 6.96 (br s, 2H, *o*-aryl H), 7.13 (m, 2H, *m*-aryl H). ^{13}C APT NMR (100 MHz, C_6D_6) δ (selected signals) 10.2 (C_5Me_5), 10.5 (WCH_2CH_3), 16.4 (WCH_2CH_3), 37.5 (allyl CH_2), 98.1 (allyl CHPh), 101.7 (allyl CH), 106.7 (C_5Me_5), 128.3 (*o*-aryl H), 138.9 (ipso C).

5.4.5 Optimized C-H Activation of Methane by **5.2**

In a glove box, a Parr 5500 reactor was charged with **5.2** (0.300 g, 0.631 mmol) and C_6H_{12} (ca. 125 mL) to give a yellow solution. The reactor was sealed, then purged with CH_4 (6 x 500 psig), and then pressurized to 1250 psig CH_4 . The contents of the reactor were heated at 35 $^\circ\text{C}$ for 16 h while being stirred, after which time the gas was vented and a yellow solution was obtained. Solvent was removed in vacuo to afford a yellow solid (crude mass 0.300 g). The yield of the product $\text{Cp}^*\text{W}(\text{NO})(\text{CH}_3)(\eta^3\text{-CH}_2\text{CHCHMe})$ (**5.7**) was determined by ^1H NMR spectroscopy using Cp_2Fe as an internal standard (26.8 mg) to be 0.249 mg (94 % yield). Purification of **5.7** was performed by column chromatography over silica support using a gradient of 0-20% EtOAc in hexanes. A yellow band was collected as a yellow eluate. Removal of the solvents in vacuo afforded **5.7** as a yellow solid (0.199 g, 75 % yield). Two isomers of **5.7** were identified in solution by ^1H NMR spectroscopy. The major isomer, **5.7a**, has not been reported in the literature, while the minor isomer, **5.7b**, was previously reported as being the only product from the reaction of **5.2** with methane.²⁷ The orientation of the allyl ligand of each isomer was determined using the chemical shifts of the allyl C and H signals in the ^1H and ^{13}C NMR spectra.

Characterization data for **5.7a** (73%): ^1H NMR (C_6D_6 , 400 MHz) δ 0.15 (s, $^2J_{\text{HH}} = 5.3$, 3H, WCH_3), 0.34 (m, 1H, allyl CH_2), 1.23 (d, $^3J_{\text{HH}} = 6.0$, 3H, allyl *Me*), 1.52 (s, 15H, C_5Me_5), 1.98 (qdd, $^4J_{\text{HH}} = 0.8$, $^3J_{\text{HH}} = 13.7$, 6.0, 1H, allyl CHMe), 2.49 (dd, $^3J_{\text{HH}} = 7.1$, $^2J_{\text{HH}} = 3.0$, 1H, allyl CH_2), 4.61 (ddd, $^3J_{\text{HH}} = 13.7$, 9.1, 7.1, 1H, meso *H*). ^{13}C NMR (100 MHz, C_6D_6) δ 3.2 (WCH_3), 10.1 (C_5Me_5), 16.0 (allyl *Me*), 37.9 ($^1J_{\text{WC}} = 29.3$, allyl CH_2), 90.7 (allyl CHMe), 105.8 (C_5Me_5), 107.9 (meso *C*).

5.4.6 Optimization of Methane Activation by **5.2**

The effect of solvent and concentration for the C-H activation of methane by **5.2** was carried out by investigating different concentrations of C_6H_{12} and as well as the solvent C_6F_6 .

5.4.6.1 C-H Activation of Methane by **5.2** Using C_6F_6 as the Solvent

In a glove box, a Parr 5500 reactor was charged with **5.2** (0.300 mg) and C_6F_6 (25 g) to give a yellow solution. The reactor was sealed, then purged with CH_4 (3 x 500 psig), and then pressurized to 1250 psig CH_4 . The contents of the reactor were heated at 35 °C for 16 h while being stirred. The gas was then vented, and a light orange mixture was obtained. The solvent was removed in vacuo to afford a yellow residue. The yield of **5.7** in the crude mixture was determined by ^1H NMR spectroscopy using Fc (14.5 mg) as an internal standard to be 155 mg (59 % yield). Purification was carried out using column chromatography over silica support using a gradient of 0-20% EtOAc in hexanes to afford **5.7** as a yellow solid (80.8 mg, 31 % yield).

5.4.6.2 C-H Activation of Methane by **5.2** Using 25 mL of C₆H₁₂ as the Solvent

In a glove box, a Parr 5500 series reactor was charged with **5.2** (0.300 g, 0.631 mmol) and C₆H₁₂ (ca. 25 mL) to afford a yellow solution. The reactor was sealed, purged with CH₄ (3 x 500 psig), pressurized to 1250 psig CH₄, and then its contents were heated at 35 °C for 16 h while being stirred. The gas was then vented, and a dark yellow-brown reaction mixture was obtained. The solvent was removed in vacuo to afford a dark yellow residue (290 mg). The yield of **5.7** was determined by ¹H NMR spectroscopy from the crude reaction mixture using Fc (19.7 mg) as an internal standard to be 176 mg (67 % yield). Purification by column chromatography over silica support using 0-20% gradient of EtOAc in hexanes afforded **5.7** as a yellow solid (0.150 g, 57 % yield).

5.4.7 Preparation of Cp*W(NO)(C₆H₁₁)(η³-CH₂CHCHMe) (**5.8**)

On the bench top a 4-dram vial was charged with Cp*W(NO)(CH₂CMe₃)(η³-CH₂CHCHMe) (0.067 g, 0.14 mmol) and a magnetic stir bar. Undried cyclohexane (ca. 5 mL) was added to the vial to produce a yellow solution, which was then stirred in the air for 18 h to give an orange solution. The solvent was removed under reduced pressure to afford an orange residue. The ¹H NMR spectrum of the residue revealed the presence of **5.8** as the major product as well as complex **3.3** in a 9:1 ratio, respectively.

¹H NMR (400 MHz, C₆D₆) δ 1.31 (m, 1H, allyl CHMe), 1.33-1.98 (m, 8H, cyclohexyl CH₂), 1.47 (m, 1H, allyl CH₂), 1.54 (s, 15H, C₅Me₅), 1.60 (m, 1H, cyclohexyl CH), 1.90 (d, ³J_{HH} = 5.7, 3H, allyl Me), 2.50 (m, 1H, cyclohexyl CH₂), 2.61 (m, 1H, cyclohexyl CH₂), 3.43 (d, ³J_{HH}

= 7.4, 1H, allyl CH₂), 4.89 (ddd, ³J_{HH} = 13.5, 9.0, 7.4, 1H, meso H). ¹³C (100 MHz, C₆D₆): δ 10.1 (C₅Me₅), 17.6 (allyl Me), 28.7 (cyclohexyl CH₂), 32.8 (cyclohexyl CH), 33.3 (cyclohexyl CH₂), 34.1 (cyclohexyl CH₂), 39.2 (cyclohexyl CH₂), 40.4 (cyclohexyl CH₂), 57.0 (allyl CHMe), 71.7 (allyl CH₂), 107.0 (C₅Me₅), 111.6 (meso CH).

5.4.8 Optimized C-H Activation of Ethane by 5.2

In a glove box, a Parr 5500 series reactor was charged with **5.7** (0.300 g, 0.631 mmol) and C₆H₁₂ (ca. 100 mL) to give a yellow solution. The reactor was sealed, then purged with C₂H₆ (3 x 400 psig), and then pressurized to 400 psig C₂H₆ at which pressure the contents of the reactor were heated at 35 °C for 16 h while being stirred. The gas was then vented, and a yellow mixture was collected. The product, Cp*W(NO)(CH₂CH₃)(η³-CH₂CHCHMe) (**5.9**), was then purified via column chromatography over silica support using 0-20% EtOAc in hexanes. A yellow eluate was collected, and the solvent was removed in vacuo to afford **5.9** as a yellow solid (184 mg, 67% yield). Two isomers were identified in solution by NMR spectroscopy in a 85:15 ratio, with only the major isomer, **5.9**, having been previously reported for the reaction of **5.2** with C₂H₆.²⁷

Characterization data for **5.9a** (85 %): MS (LREI, *m/z*, probe temperature 150 °C) 433 [M⁺, ¹⁸⁴W]. ¹H NMR (C₆D₆, 400 MHz) δ 1.06 (qd, ³J_{HH} = 7.4, ²J_{HH} = 10.4, 1H, ethyl CH₂), 1.10 (qd, ³J_{HH} = 9.4, 5.7, 1H, allyl CHMe), 1.19 (qd, ³J_{HH} = 7.2, ²J_{HH} = 10.4, 1H, ethyl CH₂), 1.47 (obscured, 1H, allyl CH₂), 1.49 (s, 15H, C₅Me₅), 1.78 (t, ³J_{HH} = 7.3, ³J_{WH} = 5.1, 3H, ethyl CH₃), 1.94 (d, ³J_{HH} = 5.7, 3H, allyl Me), 3.23 (d, ³J_{HH} = 7.0, 1H, allyl CH₂), 4.91 (ddd, ³J_{HH} = 13.6, 9.4, 7.0, 1H, meso H). ¹³C NMR (100 MHz, C₆D₆) δ 8.4 (¹J_{WC} = 79.7, ethyl CH₂), 9.8 (C₅Me₅), 18.1

(allyl *Me*), 18.5 (ethyl CH_3), 54.7 ($^1J_{\text{WC}} = 21.4$, allyl CHMe), 74.7 ($^1J_{\text{WC}} = 6.7$, allyl CH_2), 105.8 (C_5Me_5), 109.5 (meso *C*).

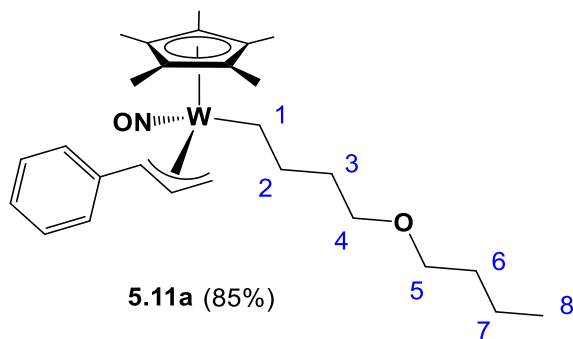
Characterization data for **5.9b** (15 %): ^1H NMR (C_6D_6 , 400 MHz) δ 0.40 (d, $^3J_{\text{HH}} = 7.5$, 1H, allyl CH_2), 0.54 (m, 1H, ethyl CH_2), 1.20 (obscured, 1H, ethyl CH_2), 1.34 (d, $^3J_{\text{HH}} = 5.9$, 3H, allyl *Me*), 1.51 (s, 15H, C_5Me_5), 2.14 (m, 1H, allyl CHMe), 1.81 (obscured, 3H, ethyl CH_3), 2.47 (d, $^3J_{\text{HH}} = 6.5$, 1H, allyl CH_2), 4.64 (m, 1H, meso *H*). ^{13}C NMR (100 MHz, C_6D_6) δ 10.1 (C_5Me_5), 14.3 (ethyl CH_2), 15.3 (allyl *Me*), 18.3 (ethyl CH_3), 36.6 (allyl CH_2), 94.6 (allyl CHMe), 105.9 (C_5Me_5), 106.8 (meso *C*).

5.4.9 Optimized C-H Activation of Propane by 5.2

In a glove box, a Parr 5500 reactor was charged with **5.2** (0.300 g, 0.631 mmol) and C_6H_{12} (ca. 100 mL) to afford a yellow solution. The reactor was sealed and cycled six times with 100 psig C_3H_8 before being pressurized to 100 psig with C_3H_8 . The contents of the reactor were then heated at 35 °C while being stirred for 16 h. The gas was then vented, and a yellow mixture was collected. Purification was carried out by column chromatography over silica support with a 0-20% gradient of EtOAc in hexanes. The product, $\text{Cp}^*\text{W}(\text{NO})(\text{CH}_2\text{CH}_2\text{CH}_3)(\eta^3\text{-CH}_2\text{CHCHMe})$ (**5.10**), was obtained as a yellow solid (0.208 g, 77 % yield). Two isomers of **5.10** were characterized in solution in a 79:21 ratio. Only the major isomer (**5.10a**) has been previously reported for the reaction of **5.2** with propane.²⁷

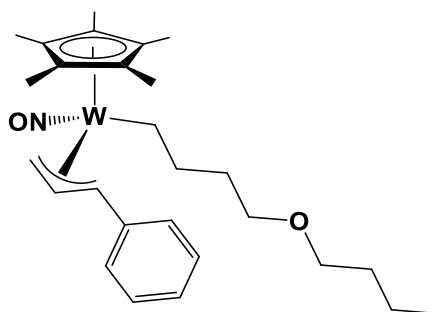
5.4.10 Preparation of Cp*W(NO)((CH₂)₄O(CH₂)₃CH₃)(η^3 -CH₂CHCHPh) (**5.11**)

In a glove box a sample of **5.1** (0.300 g, 0.558 mmol) was dissolved in (*n*-Bu)₂O (ca. 25 mL) to give a light orange solution which was transferred to a reaction bomb and sealed with a Kontes greedless stopcock. The contents were heated at 55 °C for 3 d to give a dark orange solution. The solvent was removed in vacuo to give an orange oily residue. The crude mixture was dissolved in a minimum amount of Et₂O and purified by column chromatography on activated basic alumina (3 x 7 cm). A yellow eluate was collected using a gradient of 0-40% Et₂O in hexanes. The solvents were removed in vacuo to give **5.11** as a yellow oil (0.165 g, 50% yield). Two isomers were identified in solution by NMR spectroscopy in an 85:15 ratio. The orientation of the allyl ligand of each isomer was determined using the chemical shifts of the allyl C and H signals in the ¹H and ¹³C NMR spectra.



Characterization data for **5.11a** (85%): IR (cm⁻¹) 1589 (s, ν_{NO}). MS (LREI, *m/z*, probe temperature 150 °C) 595 [M^+ , ¹⁸⁴W]. ¹H NMR (400 MHz, C₆D₆) δ 0.90 (t, ³*J*_{HH} = 7.4, 3H, C8H₃), 1.01 (dt, ³*J*_{HH} = 3.3, ²*J*_{HH} = 11.7, 1H, C1H₂), 1.11 (dt, ³*J*_{HH} = 5.1, ²*J*_{HH} = 11.7, 1H, C1H₂), 1.42 (obscured, 2H, C7H₂), 1.43 (s, 15H, C₅Me₅), 1.596 (obscured, 2H, C6H₂), 1.599 (obscured, 1H, C2H₂), 1.63 (obscured, 1H, allyl CH₂), 1.87 (m, 1H, C3H₂), 1.97 (m, 1H, C3H₂), 2.14 (obscured, 1H, C2H₂), 2.15 (d, ³*J*_{HH} = 9.8, 1H, allyl CHPh), 3.30 (d, ³*J*_{HH} = 7.2, 1H, allyl CH₂),

3.39 (t, $^3J_{\text{HH}} = 6.5$, 2H, OC5H₂), 3.53 (m, 1H, OC4H₂), 3.59 (m, 1H, OC4H₂), 5.51 (ddd, $^3J_{\text{HH}} = 13.4$, 9.8, 7.2, 1H, allyl CH), 7.042 (t, $^3J_{\text{HH}} = 7.3$, 1H, *p*-aryl *H*), 7.27 (t, $^3J_{\text{HH}} = 7.4$, 2H, *m*-aryl *H*), 7.34 (d, $^3J_{\text{HH}} = 7.7$, 2H, *o*-aryl *H*). ¹³C APT NMR (100 MHz, C₆D₆) δ 9.7 (C₅Me₅), 14.6 (C8H₃), 17.9 ($^1J_{\text{WC}} = 78.6$, C1H₂), 20.3 (C7H₂), 30.9 (C2H₂), 32.9 (C6H₂), 38.1 (C3H₂), 63.1 ($^1J_{\text{WC}} = 19.6$, allyl CHPh), 71.1 (OC5H₂), 71.6 (OC4H₂), 73.2 (allyl CH₂), 106.2, (C₅Me₅), 107.5 (allyl CH), 125.6 (*p*-aryl C), 127.4 (*m*-aryl C), 128.7 (*o*-aryl C), 143.1 (ipso C). HRMS-EI *m/z*: [M⁺, ¹⁸⁴W] Calcd for ¹⁸⁴WC₂₇H₄₁NO₂ 595.26468. [M⁺, ¹⁸²W] Found 595.26501. Calcd for ¹⁸²WC₂₇H₄₁NO₂ 593.26195. Found 593.26206

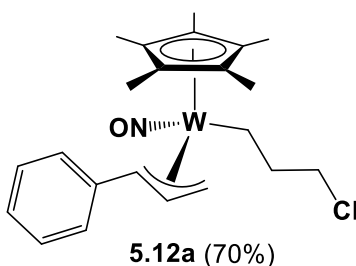


5.11b (15%)

Characterization data for **5.11b** (15%): ¹H NMR (400 MHz, C₆D₆) δ (selected signals) 0.14 (t, $^3J_{\text{HH}} = 11.4$, 1H, WCH₂), 0.68 (br s, 1H, allyl CH₂), 0.88 (obscured, 3H, butyl CH₃), 1.56 (br s, 15H, C₅Me₅), 2.58 (d, $^3J_{\text{HH}} = 6.5$, 1H, allyl CH₂), 3.20 (overlapping, 1H, allyl CHPh), 3.23 (overlapping, 2H, CH₂O), 3.32 (obscured, 2H, CH₂O), 5.37 (br s, 1H, allyl CH), 6.96 (br s, 1H, *p*-aryl *H*), 7.14 (m, 2H, aryl *H*). ¹³C NMR (100 MHz, C₆D₆) δ (selected signals) 10.2 (C₅Me₅), 14.7 (butyl CH₃), 23.5 (WCH₂), 37.2 (allyl CH₂), 71.0 (CH₂O), 71.8 (CH₂O), 98.5 (allyl CHPh), 101.8 (allyl CH), 106.3 (C₅Me₅), 128.8 (aryl CH), 136.9 (ipso C).

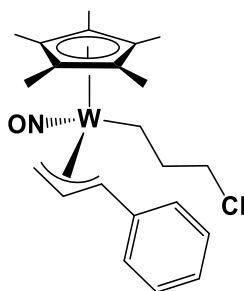
5.4.11 Preparation of $\text{Cp}^*\text{W}(\text{NO})(\text{CH}_2\text{CH}_2\text{CH}_2\text{Cl})(\eta^3\text{-CH}_2\text{CHCHPh})$ (**5.12**)

In a glove box, a glass bomb was charged with **5.1** (0.300 mg, 0.558 mmol) which was then dissolved in 1-chloropropane (ca. 5 mL) to give a dark yellow solution. The bomb was then sealed with a Kontes greaseless stopcock and then placed in a 55 °C ethylene-glycol bath whereupon its contents were heated for 3 d to give a dark green mixture. The solvent was removed in vacuo, and the resulting mixture was analyzed by ^1H NMR spectroscopy. Complexes **3.10** and **5.12** were identified in the ^1H NMR spectrum of the crude mixture, as were signals corresponding to *cis*- and *trans*- β -methylstyrene, in a 65:35:30:20 ratio, respectively. Complex **5.12** was purified by column chromatography over basic alumina using a gradient of 0-30% EtOAc in hexanes to give **5.12** as a yellow solid (67 mg, 22 % yield). Two isomers of **5.12** were observed in solution by NMR spectroscopy. The orientation of the allyl ligand of each isomer was determined using the chemical shifts of the allyl C and H signals in the ^1H and ^{13}C NMR spectra. Crystals suitable for single-crystal X-ray diffraction of the minor isomer, **5.12b**, were grown by slow evaporation from 1:1 Et₂O/pentane at room temperature. The crystals were dissolved in C₆D₆ and both isomers of **5.12** were identified by ^1H NMR spectroscopy.



Characterization data for **5.12a** (70%): IR (cm⁻¹) 1602 (s, ν_{NO}). MS (LREI, m/z , probe temperature 150 °C) 543 [M^+ , ^{184}W]. ^1H NMR (400 MHz, C₆D₆) δ 0.76 (dt, $^3J_{\text{HH}} = 5.1$, $^2J_{\text{HH}} = 11.2$, 1H, WCH_2), 1.05 (dt, $^3J_{\text{HH}} = 5.1$, $^2J_{\text{HH}} = 11.2$, 1H, WCH_2), 1.38 (s, 15H, C_5Me_5), 1.58 (m,

1H, allyl CH₂), 1.70 (m, 1H, WCH₂CH₂), 2.12 (d, ³J_{HH} = 9.9, 1H, allyl CHPh), 2.44 (m, 1H, WCH₂CH₂), 3.12 (d, ³J_{HH} = 7.3, 1H, allyl CH₂), 3.40 (m, 1H, CH₂Cl), 3.53 (ddd, ³J_{HH} = 10.2, 5.9, ³J_{HH} = 7.0, 1H, CH₂Cl), 5.36 (ddd, ³J_{HH} = 13.6, 9.9, 7.3, 1H, allyl CH), 7.07 – 7.31 (m, 5H, aryl H). ¹³C APT NMR (100 MHz, C₆D₆) δ 9.7 (C₅Me₅), 12.9 (WCH₂), 37.6 (CH₂), 51.6 (CH₂Cl), 63.4 (allyl CHPh), 73.4 (allyl CH₂), 106.4 (C₅Me₅), 107.8 (allyl CH), 125.8 (aryl C), 127.4 (aryl C), 128.7 (aryl C), 142.8 (ipso C).



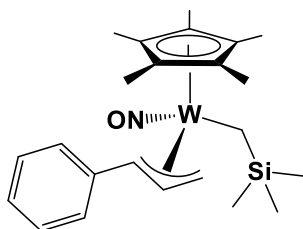
5.12b (30%)

Characterization data for **5.12b** (30%): ¹H NMR (400 MHz, C₆D₆) δ (selected signals) - 0.24 (dt, ²J_{HH} = 2.3, ³J_{HH} = 11.5, 1H, WCH₂), 0.63 (dd, ³J_{HH} = 8.9, ²J_{HH} = 1.9, 1H, allyl CH₂), 1.51 (s, 15H, C₅Me₅), 2.21 (m, 1H, CH₂), 2.47 (obscured, 1H, CH₂), 2.55 (dd, ³J_{HH} = 7.0, ²J_{HH} = 1.9, 1H, allyl CH₂), 2.79 (m, 1H, CH₂Cl), 3.15 (d, ³J_{HH} = 14.9, 1H, allyl CHPh), 5.28 (ddd, ³J_{HH} = 14.9, 8.9, 7.0, 1H, allyl CH) 7.56 (d, ³J_{HH} = 7.4, 1H, *o*-aryl H). ¹³C APT NMR (100 MHz, C₆D₆) δ (selected signals) 10.2 (C₅Me₅), 98.6 (allyl CHPh), 101.9 (allyl CH), 131.1 (*o*-aryl CH).

5.4.12 Preparation of Cp*W(NO)(CH₂SiMe₃)(η³-CH₂CHCHPh) (**5.13**)

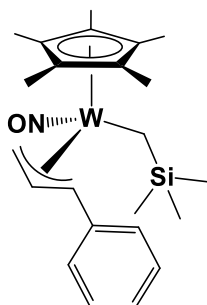
In a glove box, a reaction bomb was charged with **5.1** (81 mg, 0.15 mmol), SiMe₄ (ca. 3 mL), and a magnetic stir bar to give a cloudy orange suspension. The reaction bomb was then

sealed with a Kontes greaseless stopcock and then placed into an oil bath whereupon its contents were heated to 85 °C and stirred for 9 h. The solvent was then removed under reduced pressure. Inside a glove box the contents were transferred to a 4-dram vial with Et₂O (ca. 2 mL). The solvent was removed under reduced pressure to give **5.13** as a yellow solid (80 mg, 96 % yield). Two isomers were identified by ¹H NMR spectroscopy. The orientation of the allyl ligand for **5.13a** was determined using the chemical shifts of the allyl C signals in the ¹³C NMR spectrum.



5.13a (83%)

Characterization data for **5.13a** (83%): IR (cm⁻¹) 1574 (s, ν_{NO}). MS (LREI, *m/z*, probe temperature 120 °C) 553 [M⁺, ¹⁸⁴W]. ¹H NMR (400 MHz, C₆D₆) δ -0.57 (d, ²*J*_{HH} = 11.7, 1H, SiCH₂), -0.04 (d, ²*J*_{HH} = 11.7, 1H, SiCH₂), 0.39 (s, 9H, SiMe₃), 1.41 (s, 15H, C₅Me₅), 1.70 (d, ³*J*_{HH} = 13.2, 1H, allyl CH₂), 2.12 (d, ³*J*_{HH} = 9.4, 1H, allyl CHPh), 3.42 (d, ³*J*_{HH} = 5.9, 1H, allyl CH₂), 5.71 (m, 1H, allyl CH), 7.05 (br t, , ³*J*_{HH} = 7.2, 1H, aryl H), 7.27 (br t, , ³*J*_{HH} = 7.2, 2H, aryl H), 7.40 (br d, , ³*J*_{HH} = 7.2, 2H, aryl H). ¹³C APT NMR (100 MHz, C₆D₆) δ -4.4 (SiCH₂), 4.3 (SiMe₃), 10.0 (C₅Me₅), 62.2 (allyl CHPh), 72.6 (allyl CH₂), 106.8 (C₅Me₅), 111.9 (allyl CH), 125.8 (aryl C), 128.0 (aryl C), 128.7 (aryl C), 140.6 (ipso C). Anal. Calcd for C₂₇H₄₁NO: C, 49.91; H, 6.37; N, 2.53. Found: C, 49.92; H, 6.25; N, 2.45.



5.13b (17%)

Characterization data for **5.13b** (17%): ^1H NMR (400 MHz, C_6D_6) δ (selected signals) - 0.94 (d, $^2J_{\text{HH}} = 9.9$, 1H, SiCH_2), -0.76 (d, $^2J_{\text{HH}} = 9.9$, 1H, SiCH_2), 0.21 (s, 9H, SiMe_3), 1.51 (s, 15H, C_5Me_5), 2.46 (br s, 1H, allyl *H*), 3.64 (br s, 1H, allyl *H*), 5.26 (br s, 1H, allyl *CH*), 6.98 (m, 1H, aryl *H*).

5.4.13 Preparation of $\text{Cp}^*\text{W}(\text{NO})(\text{C}(\text{O})\text{CH}_2\text{CH}_3)(\eta^3\text{-CH}_2\text{CHCHPh})$ (**5.14**)

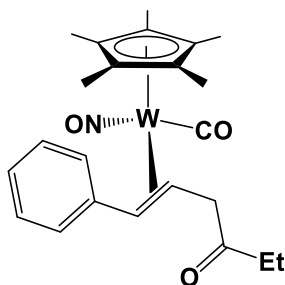
In a glove box, a Parr 5500 pressure reactor was charged with a sample of **5.1** (131 mg, 0.264 mmol) and $n\text{-C}_5\text{H}_{12}$ (ca. 75 mL). The reactor was sealed, removed from the glove box, and then cycled three times with 500 psig of carbon monoxide. The reactor was pressurized with 500 psig of CO, and its contents were stirred mechanically and heated. After 2 h at 55 °C the reactor was cooled in a water bath. The gas was vented, and a light yellow solution was filtered through glass wool and collected in a Schlenk flask. The solvent was removed under vacuum to give a yellow oily residue. In a glove box the residue was dissolved in Et_2O (ca. 2 mL) and filtered through an alumina column (0.5 x 4 cm). Addition of pentane to the yellow filtrate induced solid to precipitate from solution. The precipitate was collected as a yellow solid (101 mg, 73 % yield). Orange crystals of **5.14** suitable for X-ray diffraction were grown from Et_2O at -33 °C.

Characterization data for **5.14**: IR (cm⁻¹) 1599 (s, ν_{NO}), 1630 (w, ν_{CO}). MS (LREI, m/z , probe temperature 120 °C) 523 [M^+ , ^{184}W]. ^1H NMR (400 MHz, C_6D_6) δ 1.21 (t, $^3J_{\text{HH}} = 7.3$, 3 H, $\text{WC(O)CH}_2\text{CH}_3$), 1.54 (s, 15, C_5Me_5), 1.55 (obscured, 1H, allyl CH_2), 2.40 (d, $^3J_{\text{HH}} = 11.0$, 1H, allyl CHPh), 2.99 (q, $^3J_{\text{HH}} = 7.3$, 2 H, $\text{WC(O)CH}_2\text{CH}_3$), 3.22 (dd, $^3J_{\text{HH}} = 7.4$, $^2J_{\text{HH}} = 3.1$, 1H, allyl CH_2), 5.39 (ddd, $^3J_{\text{HH}} = 13.3$, 11.0, 7.4, 1H allyl CH), 7.08 (t, $^3J_{\text{HH}} = 7.4$, 1H, aryl H), 7.25 (t, $^3J_{\text{HH}} = 7.4$, 2H, aryl H), 7.32 (d, $^3J_{\text{HH}} = 7.4$, 2H, aryl H). ^{13}C APT NMR (100 MHz, C_6D_6) δ 10.2 (C_5Me_5), 30.1 ($\text{WC(O)CH}_2\text{CH}_3$), 55.4 ($\text{WC(O)CH}_2\text{CH}_3$), 65.6 (allyl CH_2), 71.2 (allyl CHPh), 108.9, (C_5Me_5), 109.7 (allyl CH), 126.4 (aryl C), 127.7 (aryl C), 129.0 (aryl C), 141.7 (ipso C), 261.0 (acyl C). HRMS-EI m/z : [M^+ , ^{182}W] Calcd for $^{182}\text{WC}_{22}\text{H}_{29}\text{NO}_2$ 521.16805. Found 521.16761. [M^+ , ^{184}W] $^{184}\text{WC}_{22}\text{H}_{29}\text{NO}_2$ 523.17078. Found 523.17042. Anal. Calcd for $\text{C}_{22}\text{H}_{29}\text{NO}_2\text{W}$: C, 50.49; H, 5.59; N, 2.68. Found: C, 50.74; H, 5.69; N, 3.03.

5.4.14 Preparation of $\text{Cp}^*\text{W(NO)(CO)(}\eta^2\text{-PhCH=CHCH}_2\text{C(O)CH}_2\text{CH}_3\text{)}$ (**5.15**)

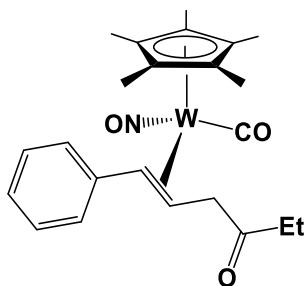
In a glove box, a Parr 5500 reactor was charged with complex **5.1** (0.300 g, 0.558 mmol) and C_6H_{12} (ca. 75 mL). The reactor was sealed, and then purged three times with 400 psig of C_2H_6 , and then pressurized to 400 psig C_2H_6 . The contents of the reactor were heated at 55 °C while being stirred for 3 d. The contents of the reactor were then cooled, and the gas was vented. Then the reactor was purged three times with 500 psig CO before being pressurized to 750 psig CO. The contents of the reactor were heated at 75 °C for 18 h while being stirred. The gas was then vented, and a dark yellow mixture was collected. The solvent was removed in vacuo, and the crude product was purified by column chromatography over silica using a gradient of 0-20% EtOAc over silica. Removal of the solvent from the yellow eluate afforded **5.15** as an orange oil

(153 mg, 50% yield). The orientation of the η^2 -alkene ligand of each isomer was determined using the chemical shifts of the alkene H signals in the ^1H NMR spectrum.



5.15a (84 %)

Characterization data for **5.15a** (84%): IR (cm^{-1}) 1608 (s, ν_{NO}), 1711 (w, $\nu_{\text{CO-ketone}}$), 1958 (s, $\nu_{\text{CO-terminal}}$). MS (LREI, m/z , probe temperature 150 $^{\circ}\text{C}$) 551 [$\text{M}^+ - \text{CO}$, ^{184}W], 523 [$\text{M}^+ - \text{CO}$, ^{184}W]. MS (HREI, m/z , ^{182}W) calcd for $\text{C}_{23}\text{H}_{29}\text{NO}_3$ ^{182}W : 549.16297, found: 549.16337. ^1H NMR (400 MHz, C_6D_6) δ 1.00 (t, $^3J_{\text{HH}} = 7.2$, 3H, $\text{C}(\text{O})\text{CH}_2\text{CH}_3$), 1.56 (s, 15H, C_5Me_5), 2.20 (m, 1H, $\text{C}(\text{O})\text{CH}_2\text{CH}_3$), 2.29 (m, 1H, $\text{C}(\text{O})\text{CH}_2\text{CH}_3$), 2.77 (dt, $^3J_{\text{HH}} = 10.9$, 6.5, $^2J_{\text{WH}} = 5.5$, 1H, PhCH=CH), 3.10 (d, $^3J_{\text{HH}} = 6.3$, 1H, $=\text{CHCH}_2\text{C}(\text{O})$) 3.99 (d, $^3J_{\text{HH}} = 10.9$, 1H, PhCH=CH), 6.89 (t, $^3J_{\text{HH}} = 7.2$, 1H, *p*-aryl *H*), 7.10 (t, $^3J_{\text{HH}} = 7.6$, 2H, *m*-aryl *H*), 7.20 (d, $^3J_{\text{HH}} = 7.6$, 2H, *o*-aryl *H*). ^{13}C NMR (100 MHz, C_6D_6) δ 10.2 (C_5Me_5), 30.1 ($\text{C}(\text{O})\text{CH}_2\text{CH}_3$), 35.7 ($\text{C}(\text{O})\text{CH}_2\text{CH}_3$), 41.8 ($^1J_{\text{WC}} = 41.0$, $=\text{CHCH}_2\text{C}(\text{O})$), 52.3 ($=\text{CHCH}_2\text{C}(\text{O})$), 57.1 ($^1J_{\text{WC}} = 9.2$, PhCH=), 105.9 (C_5Me_5), 125.9 (*p*-aryl *C*), 126.6 (*o*-aryl *C*), 128.2 (*m*-aryl *C*), 143.5 (ipso *C*), 211.4 ($\text{C}(\text{O})\text{CH}_2\text{CH}_3$), 225.0 ($^1J_{\text{WC}} = 185.0$, W-CO).



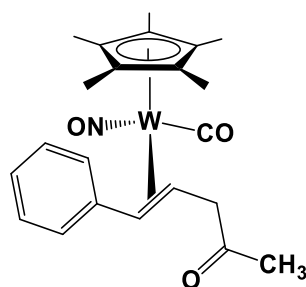
5.15b (16 %)

Characterization data for **5.15b** (16%): ^1H NMR (400 MHz, C_6D_6) δ 0.90 (t, $^3J_{\text{HH}} = 7.2$, 3H, $\text{C}(\text{O})\text{CH}_2\text{CH}_3$), 1.58 (s, 15H, C_5Me_5), 1.59 (obscured, 1H, $=\text{CHCH}_2\text{C}(\text{O})$), 2.28 (m, 2H, $\text{C}(\text{O})\text{CH}_2\text{CH}_3$), 2.45 (d, $^3J_{\text{HH}} = 10.6$, $^2J_{\text{WH}} = 5.5$, 1H, $\text{PhCH}=\text{CH}$), 3.03 (dd, $^3J_{\text{HH}} = 4.9$, $^2J_{\text{HH}} = 14.5$, 1H, $=\text{CHCH}_2\text{C}(\text{O})$) 3.58 (td, $^3J_{\text{HH}} = 10.6$, 4.9, 1H, $\text{PhCH}=\text{CH}$), 6.92 (tt, $^4J_{\text{HH}} = 1.1$, $^3J_{\text{HH}} = 7.3$, 1H, *p*-aryl *H*), 7.00 (dd, $^4J_{\text{HH}} = 1.1$, $^3J_{\text{HH}} = 8.4$, 2H, *o*-aryl *H*), 7.23 (m, 2H, *m*-aryl *H*). ^{13}C NMR (100 MHz, C_6D_6) δ (selected signals) 10.3 (C_5Me_5), 19.2 ($\text{C}(\text{O})\text{CH}_2\text{CH}_3$), 23.4 ($\text{C}(\text{O})\text{CH}_2\text{CH}_3$), 48.4 ($^1J_{\text{WC}} = 11.0$, $=\text{CHCH}_2\text{C}(\text{O})$), 50.5 ($=\text{CHCH}_2\text{C}(\text{O})$), 53.7 ($^1J_{\text{WC}} = 34.9$, $\text{PhCH}=\text{CH}$), 105.8 (C_5Me_5), 125.7 (aryl *C*), 127.3 (aryl *C*), 146.8 (ipso *C*), 210.0 ($\text{C}(\text{O})\text{CH}_2\text{CH}_3$), 224.1 (W-CO).

5.4.15 Preparation of $\text{Cp}^*\text{W}(\text{NO})(\text{CO})(\eta^2\text{-PhCH}=\text{CHCH}_2\text{C}(\text{O})\text{CH}_3)$ (**5.16**)

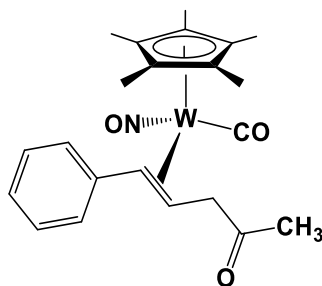
In a glove box, a Parr 5500 reactor was charged with complex **5.1** (1.123 g, 2.090 mmol) and C_6H_{12} (ca. 125 mL). The reactor was sealed, cycled six times with 500 psig of CH_4 , and then pressurized to 1250 psig CH_4 . The contents of the reactor were heated at 88 °C while being mechanically stirred for 4 h. The contents of the reactor were cooled, and the gas was carefully vented. The reactor was purged three times with 500 psig CO and then pressurized to 750 psig CO. The contents of the reactor were heated at 75 °C while being stirred for 18 h. The reactor

was then cooled, the gas vented, and a yellow-brown mixture collected. The solvent was removed in vacuo to give an oil. The desired product was isolated by column chromatography in the air over silica support. Complex **5.16** was eluted in a yellow solution using 0-20% EtOAc in hexanes. The solvents were removed in vacuo to afford complex **5.16** as an orange oil (438.5 mg, 41% yield). The orientation of the η^2 -alkene ligand of each isomer was determined using the chemical shifts of the alkene H signals in the ^1H NMR spectrum.



5.16a (83 %)

Characterization data for **5.16a** (83%): IR (cm^{-1}) 1606 (s, ν_{NO}), 1714 (w, $\nu_{\text{CO-ketone}}$), 1959 (s, $\nu_{\text{CO-terminal}}$). MS (LREI, m/z , probe temperature 150 °C) 537 [M^+ , ^{184}W]. ^1H NMR (600 MHz, C_6D_6) δ 1.55 (s, 15H, C_5Me_5), 1.87 (s, 3H, $\text{C}(\text{O})\text{Me}$), 2.70 (ddd, $^3J_{\text{HH}} = 11.0, 7.0, 5.5$, $^2J_{\text{WH}} = 5.6$, 1H =CH), 3.01 (dd, $^3J_{\text{HH}} = 7.0$, $^2J_{\text{HH}} = 16.8$, 1H, $\text{CH}_2\text{C}(=\text{O})$), 3.10 (dd, $^3J_{\text{HH}} = 5.5$, $^2J_{\text{HH}} = 16.8$, 1H, $\text{CH}_2\text{C}(=\text{O})$), 3.96 (d, $^3J_{\text{HH}} = 11.0$, 1H, PhCH=), 6.87 (t, $^3J_{\text{HH}} = 7.2$, 1H, aryl H), 7.08 (t, $^3J_{\text{HH}} = 7.4$, 2H, aryl H), 7.18 (m, 2H, aryl H). ^{13}C NMR (150 MHz, C_6D_6) δ 10.3 (C_5Me_5), 29.6 ($\text{C}(\text{O})\text{Me}$), 41.6 (=CH), 53.3 ($\text{CH}_2\text{C}(=\text{O})$), 57.2 (PhCH=), 105.82 (C_5Me_5), 125.9 (aryl C), 126.6 (aryl C), 128.6 (aryl C), 143.52 (ipso C), 209.0 ($\text{C}(\text{O})\text{Me}$), 224.9 (WCO).

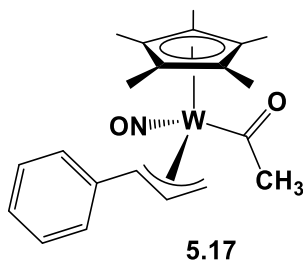


5.16b (17 %)

Characterization data for **5.16b** (17%): ^1H NMR (600 MHz, C_6D_6) δ 1.52 (obscured, 1H, $\text{CH}_2\text{C}(=\text{O})$), 1.56 (s, 15H, C_5Me_5), 1.84 (s, 3H, $\text{C}(\text{O})\text{Me}$), 2.41 (d, $^3J_{\text{HH}} = 10.4$, 1H, PhCH=), 3.01 (obscured, 1H, $\text{CH}_2\text{C}(=\text{O})$), 3.51 (td, $^3J_{\text{HH}} = 10.8$, 5.0, 1H, $=\text{CH}$), 6.93 (t, $^3J_{\text{HH}} = 7.3$, 1H, *p*-aryl *H*), 6.98 (d, $^3J_{\text{HH}} = 7.8$, 2H, *o*-aryl *H*), 7.23 (m, 2H, *m*-aryl *H*). ^{13}C NMR (150 MHz, C_6D_6) δ (selected signals) 28.2 ($\text{C}(\text{O})\text{Me}$), 48.2 ($=\text{CH}$), 51.6 ($\text{CH}_2\text{C}(=\text{O})$), 53.5 (PhCH=), 105.6 (C_5Me_5), 125.7 (aryl C), 146.9 (ipso C), 207.5 ($\text{C}(\text{O})\text{Me}$).

5.4.16 Preparation of $\text{Cp}^*\text{W}(\text{NO})(\text{C}(\text{O})\text{CH}_3)(\eta^3\text{-CH}_2\text{CHCHPh})$ (**5.17**)

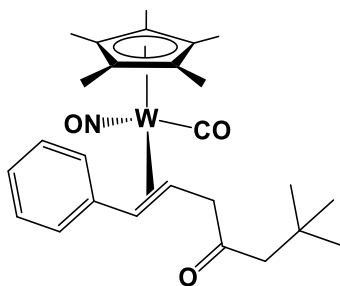
In a glove box, a Parr 5500 reactor was charged with **5.13** (49 mg, 0.089 mmol) and pentane (ca. 75 mL). The reactor was sealed and purged with 500 psig of CO three times. The reactor was then pressurized to 250 psig CO and heated to 55 °C while its contents were stirred for 2 h. The gas was then vented, and a pale yellow solution was collected. The solvent was removed in vacuo to give a yellow oil. The residue was taken up in 3:1 pentane/ Et_2O and transferred to the top of an alumina column (0.5 x 3 cm). A dark yellow band was collected to give a yellow eluate. The solvents were then removed from the eluate in vacuo to afford **5.17** as a yellow oily solid (15 mg, 33 % yield).



Characterization data for **5.17**: IR (cm⁻¹) 1598 (s, ν_{NO}), 1622 (w, ν_{CO}). MS (LREI, *m/z*, probe temperature 150 °C) 553 [*M*⁺, ¹⁸⁴W]. ¹H NMR (400 MHz, C₆D₆) δ 1.54 (s, 15H, C₅Me₅), 1.55 (obscured, 1H, allyl CH₂), 2.38 (d, ³*J*_{HH} = 10.6, 1H, allyl CHPh), 2.73 (s, 3H, C(O)Me), 3.23 (dd, ³*J*_{HH} = 7.0, ²*J*_{HH} = 2.5, 1H, allyl CH₂), 5.35 (ddd, ³*J*_{HH} = 13.3, 10.6, 7.0, 1H allyl CH), 7.05 (t, ³*J*_{HH} = 7.3, 1H, aryl *H*), 7.26 (t, ³*J*_{HH} = 7.5, 2H, aryl *H*), 7.31 (d, ³*J*_{HH} = 7.5, 2H, aryl *H*). ¹³C APT NMR (100 MHz, C₆D₆) δ 10.2 (C₅Me₅), 48.2 (WC(O)Me), 65.8 (allyl CH₂), 70.9 (allyl CHPh), 109.0 (C₅Me₅), 109.6 (allyl CH), 126.5 (aryl C), 127.8 (aryl C), 129.0 (aryl C), 141.7 (ipso C), 264.4 (acyl C).

5.4.17 Preparation of Cp*W(NO)(CO)(η²-PhCH=CHCH₂C(O)CH₂CMe₃) (**5.18**)

During the sequential reactions of **5.1** with CH₄ and then CO to produce complex **5.16** (vide supra) the complex Cp*W(NO)(CO)(η²-PhCH=CHCH₂C(O)CH₂CMe₃) (**5.18**) was recovered during purification of **5.16** by column chromatography over silica support as a yellow eluate that was eluted in 0-25% EtOAc in hexanes. Removal of the solvents in vacuo afforded a yellow oil that was characterized by ¹H and ¹³C NMR spectroscopy, IR spectroscopy and mass spectrometry.

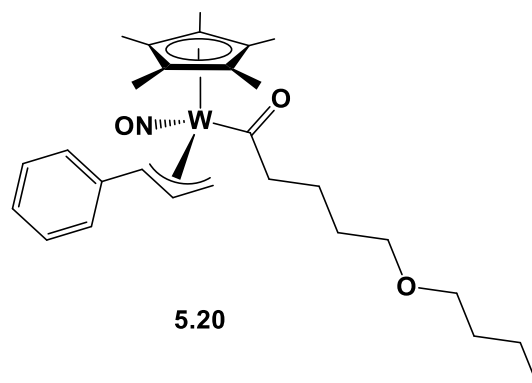


5.18

Characterization data for **5.18**: IR (C_6D_6 , cm^{-1}) 1598 (s, ν_{NO}), 1955 (s, $\nu_{\text{CO-terminal}}$). MS (LREI, m/z , probe temperature 120 °C) 593 [M^+ , ^{184}W]. ^1H NMR (600 MHz, C_6D_6) δ 1.04 (s, 9H, CMe_3), 1.57 (s, 15H, C_5Me_5), 2.21 (s, 2H, $\text{C}(\text{O})\text{CH}_2$), 2.80 (ddd, $^3J_{\text{HH}} = 11.3, 6.8, 5.4$, 1H, $=\text{CH}$), 3.09 (dd, $^3J_{\text{HH}} = 6.8$, $^2J_{\text{HH}} = 17.3$, 1H, $\text{CH}_2\text{C}(=\text{O})$), 3.17 (dd, $^3J_{\text{HH}} = 5.4$, $^2J_{\text{HH}} = 17.3$, 1H, $\text{CH}_2\text{C}(=\text{O})$), 4.05 (d, $^3J_{\text{HH}} = 11.3$, 1H, $\text{PhCH}=\text{}$), 7.03 (t, $^3J_{\text{HH}} = 7.4$, 1H, aryl H), 7.08 (t, $^3J_{\text{HH}} = 7.7$, 2H, aryl H), 7.24 (d, $^3J_{\text{HH}} = 7.7$, 2H, aryl H). ^{13}C APT NMR (150 MHz, C_6D_6) δ 10.2 (C_5Me_5), 30.2 (CMe_3), 30.6 (CMe_3), 41.7 ($=\text{CH}$), 54.6 ($\text{C}(\text{O})\text{CH}_2$), 54.7 ($\text{CH}_2\text{C}(=\text{O})$), 57.1 ($\text{PhCH}=\text{}$), 105.81 (C_5Me_5), 126.8-128.7 (aryl C), 143.46 (ipso C), 210.9 ($\text{C}(\text{O})\text{CH}_2$), 225.2 (WCO).

5.4.18 Preparation of $\text{Cp}^*\text{W}(\text{NO})(\text{C}(\text{O})(\text{CH}_2)_4\text{O}(\text{CH}_2)_3\text{CH}_3)(\eta^3\text{-CH}_2\text{CHCHPh})$ (**5.20**)

In a glove box, a Parr 5500 reactor was charged with **5.11** (30 mg, 0.050 mmol) and Et_2O (ca. 75 mL). The reactor was sealed and purged 3 times with 450 psig CO. Then the reactor was pressurized to 450 psig, and the contents were stirred over 4 d at room temperature. The reactor was vented, and a pale yellow solution was collected. Solvent was removed from the solution under reduced pressure to give **5.20** as a yellow residue (21 mg, 67 % yield).

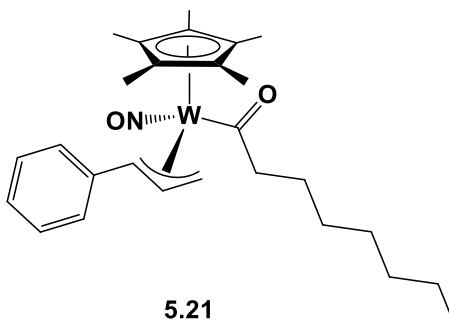


Characterization data for **5.20**: ^1H NMR (400 MHz, C_6D_6) δ 0.88 (t, $^3J_{\text{HH}} = 7.4$, 3H, *n*-butyl CH_3), 1.37 (m, 2H, *n*-butyl CH_2), 1.39 (m, 2H, *n*-butyl CH_2), 1.55 (s, 15H, C_5Me_5), 1.58 (obscured, 1H, allyl CH_2), 1.76 (m, 2H, *n*-butyl CH_2), 1.80 (m, 2H, *n*-butyl CH_2), 2.42 (d, $^3J_{\text{HH}} = 10.6$, 1H, allyl CHPh), 3.08 (t, $^3J_{\text{HH}} = 6.9$, 2H, $\text{C}(\text{O})\text{CH}_2$), 3.27 (m, 1H, allyl CH_2), 3.32 (t, $^3J_{\text{HH}} = 6.6$, 2H, *n*-butyl OCH_2), 3.43 (t, $^3J_{\text{HH}} = 6.2$, 2H, *n*-butyl OCH_2), 5.44 (ddd, $^3J_{\text{HH}} = 13.3$, 10.6, 7.3, 1H, allyl CH), 7.05 (t, $^3J_{\text{HH}} = 7.4$, 1H, aryl H), 7.25 (t, $^3J_{\text{HH}} = 7.4$, 2H, aryl H), 7.33 (d, $^3J_{\text{HH}} = 7.4$, 2H, aryl H). ^{13}C APT NMR (100 MHz, C_6D_6) δ 10.2 (C_5Me_5), 14.6 (*n*-butyl CH_3), 20.2 (*n*-butyl CH_2), 22.7 (*n*-butyl CH_2), 30.6 (*n*-butyl CH_2), 35.5 (*n*-butyl CH_2), 62.3 ($\text{C}(\text{O})\text{CH}_2$), 66.1 (allyl CH_2), 71.1 (*n*-butyl OCH_2), 71.2 (allyl CHPh), 71.7 (*n*-butyl OCH_2), 108.9 (C_5Me_5), 109.6 (allyl CH), 126.4 (aryl C), 127.8 (aryl C), 129.0 (aryl C), 141.7 (ipso C), 260.8 ($\text{C}=\text{O}$).

5.4.19 Preparation of $\text{Cp}^*\text{W}(\text{NO})(\text{C}(\text{O})(\text{CH}_2)_6\text{CH}_3)(\eta^3\text{-CH}_2\text{CHCHPh})$ (**5.21**)

In a glove box, a Parr 5500 reactor was charged with a sample of (**5.19**) and Et_2O (ca. 75 mL). The reactor was sealed and then cycled three times with 500 psig CO before being pressurized to 450 psig CO. The contents of the reactor were stirred over 4 days after which time the gas was vented and a yellow solution was collected. The solvent was removed from the

solution in vacuo to give an oily yellow residue. Recrystallization from pentane overnight at -33 °C afforded **5.21** as an oily yellow solid.



Characterization data for **5.21**: IR (cm⁻¹) 1598 (s, ν_{NO}), 1632 (w, ν_{CO}). MS (LREI, m/z , probe temperature 150 °C) 593 [M^+ , ^{184}W]. ^1H NMR (400 MHz, C_6D_6) δ 0.87 (m, 3H, *n*-heptyl CH_3), 1.19–1.37 (m, 10H, *n*-heptyl CH_2), 1.57 (s, 15H, C_5Me_5), 1.58 (obscured, 1H, allyl CH_2), 2.45 (d, $^3J_{\text{HH}} = 10.6$, 1H, allyl CHPh), 3.02 (t, $^3J_{\text{HH}} = 7.2$, 2 H, WC(O)CH_2), 3.27 (dd, $^3J_{\text{HH}} = 7.0$, $^2J_{\text{HH}} = 2.7$, 1H, allyl CH_2), 5.44 (ddd, $^3J_{\text{HH}} = 13.3$, 10.6, 7.0, 1H allyl CH), 7.04 (t, $^3J_{\text{HH}} = 7.1$, 1H, aryl H), 7.23 (t, $^3J_{\text{HH}} = 7.3$, 2H, aryl H), 7.31 (d, $^3J_{\text{HH}} = 7.3$, 2H, aryl H). ^{13}C APT NMR (100 MHz, C_6D_6) δ 10.3 (C_5Me_5), 14.6 (*n*-heptyl CH_3), 23.7 (*n*-heptyl CH_2), 25.9 (*n*-heptyl CH_2), 29.6 (*n*-heptyl CH_2), 30.4 (*n*-heptyl CH_2), 32.7 (*n*-heptyl CH_2), 62.7 (WC(O)CH_2), 66.0 (allyl CHPh), 71.3 (allyl CH_2), 108.9 (C_5Me_5), 109.6 (allyl CH), 126.4 (aryl C), 127.7 (aryl C), 129.0 (aryl C), 141.7 (ipso C), 260.9 (acyl C). HRMS-EI m/z : [M^+ , ^{184}W] Calcd for $^{184}\text{WC}_{27}\text{H}_{39}\text{NO}_2$ 593.24903. Found 593.24953.

5.4.20 Preparation of $\text{Cp}^*\text{W}(\text{NO})(\text{CO})(\eta^2\text{-MeCH=CHCH}_2\text{C(=O)CH}_2\text{CMe}_3)$ (**5.22**).

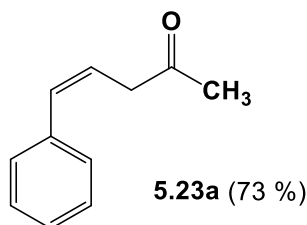
In a glove box, a Parr 5500 pressure reactor was charged with **5.2** (75 mg, 0.16 mmol) and *n*-pentane (ca. 75 mL). The reactor was purged with CO (3 x 500 psig) and then pressurized

to 750 psig CO. The contents of the reactor were heated at 75 °C while being stirred for 18 h. The gas was then vented, and a yellow mixture was obtained. The solvent was removed in vacuo to obtain a mixture of Cp*W(NO)(CO)(η^2 -MeCH=CHCH₂C(O)CH₂CMe₃) (**5.22**) as a yellow oil in quantitative yield (88 mg). The IR spectrum of the oil was consistent with the formation of **5.22**. A ¹H NMR spectrum of the oil was comprised of broad signals, but it was consistent with the formulation of **5.22**. Attempts to purify **5.22** by column chromatography led to some decomposition and a slight separation of isomers. Regrettably, full separation of the isomers was not achieved.

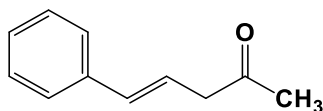
Characterization data for **5.22**: IR (C₆D₆, cm⁻¹) 1601 (s, ν_{NO}), 1712 (w, $\nu_{\text{CO-ketone}}$), 1950 (s, $\nu_{\text{CO-terminal}}$).

5.4.21 Photolysis of **5.16**; Preparation of (*E/Z*)-5-Phenylpent-4-en-2-one (**5.23**)

In a fume hood, a quartz photoreactor was charged with anhydrous MeCN (ca. 200 mL) and then a sample of **5.16** (90 mg, 0.168 mmol) was transferred to the photoreactor using MeCN (4 x 1 mL) to give a pale yellow solution. The reactor was sealed and then purged with Ar for 30 min. The contents of the reactor were then irradiated at 300 nm UV radiation (Hg lamp, filtered through a potassium chromate solution) for 10 min. The solvent was then removed, and the mixture was purified by column chromatography over silica using a gradient of 0-1% EtOAc in hexanes to afford a mixture of (*Z*)-5-phenylpent-4-en-2-one (**5.23a**) and (*E*)-5-phenylpent-4-en-2-one (**5.23b**)¹³³ as a yellow oil (13 mg, 48% yield).



Characterization data for **5.23a** (73%): IR (cm⁻¹) 1714 (w, ν_{CO}). ¹H NMR (400 MHz, C₆D₆) δ 2.19 (s, 3H, C(O)*Me*), 3.45 (dd, ⁴*J*_{HH} = 1.6, ³*J*_{HH} = 7.2, 2H, CH₂C(=O)), 5.92 (dt, ³*J*_{HH} = 11.6, 7.2, 1H, =CH), 6.67 (d, ³*J*_{HH} = 11.6, 1H, PhCH=), 7.15-7.40 (m, 5H, aryl *H*). ¹³C NMR (100 MHz, C₆D₆) δ 29.9 (C(=O)*Me*), 43.2 (CH₂), 123.3 (=CH), 132.2 (PhCH=), 127.1 (aryl *C*), 128.4 (aryl *C*), 128.6 (aryl *C*), 136.8 (ipso *C*), 206.4 (C(=O)*Me*).

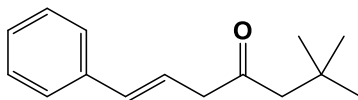


Characterization data for **5.23b** (27%) which agrees well with previously reported.¹³³ ¹H NMR (400 MHz, C₆D₆) δ 2.22 (s, 3H, C(O)*Me*), 3.35 (dd, ⁴*J*_{HH} = 0.9, ³*J*_{HH} = 7.1, 2H, CH₂C(=O)), 6.32 (dt, ³*J*_{HH} = 16.0, 7.1, 1H, =CH), 6.49 (d, ³*J*_{HH} = 16.0, 1H, PhCH=), 7.15-7.40 (m, 5H, aryl *H*). ¹³C NMR (100 MHz, C₆D₆) δ (selected signals) 29.7 (C(=O)*Me*), 47.8 (CH₂), 121.9 (=CH), 133.8 (PhCH=), 126.3 (aryl *C*), 127.6 (aryl *C*), 206.6 (C(=O)*Me*).

5.4.22 Photolysis of **5.18**; Preparation of (*E/Z*)-6,6-Dimethyl-1-phenylhept-1-en-4-one (**5.24**)

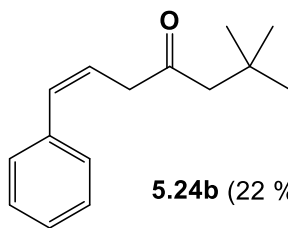
The photolysis of **5.18** (61 mg, 0.168 mmol) at 300 nm was carried out following the previous procedure. The compounds (*E*)-6,6-dimethyl-1-phenylhept-1-en-4-one (**5.24a**) and (*Z*)-

6,6-dimethyl-1-phenylhept-1-en-4-one (**5.24b**) were obtained as a yellow oil (13 mg, 59% yield) following chromatography over silica support using 0-1% EtOAc in hexanes.



5.24a (78 %)

Characterization data for **5.24a** (78%): ^1H NMR (400 MHz, C_6D_6) δ 1.05 (s, 9H, CMe_3), 2.39 (s, 2H, CH_2CMe_3), 3.31 (dd, $^4J_{\text{HH}} = 0.8$, $^3J_{\text{HH}} = 6.9$, 2H, $=\text{CHCH}_2$), 6.31 (dt, $^3J_{\text{HH}} = 15.8$, 6.9, 1H, $=\text{CH}$), 6.46 (d, $^3J_{\text{HH}} = 15.8$, 1H, $\text{PhCH}=\text{}$), 7.21 (m, 1H, *p*-aryl *H*), 7.31 (t, $^3J_{\text{HH}} = 7.6$, 2H, *m*-aryl *H*), 7.38 (d, $^3J_{\text{HH}} = 7.5$, 2H, *o*-aryl *H*).



5.24b (22 %)

Characterization data for **5.24b** (22%): ^1H NMR (400 MHz, C_6D_6) δ 1.01 (s, 9H, CMe_3), 2.34 (s, 2H, CH_2CMe_3), 3.41 (dd, $^4J_{\text{HH}} = 1.7$, $^3J_{\text{HH}} = 7.2$, 2H, $=\text{CHCH}_2$), 5.91 (dt, $^3J_{\text{HH}} = 11.7$, 7.2, 1H, $=\text{CH}$), 6.65 (d, $^3J_{\text{HH}} = 11.7$, 1H, $\text{PhCH}=\text{}$), 7.15-7.40 (m, 5H, aryl *H*).

5.4.23 X-ray Crystallography

Data collection was carried out at -183.0 ± 1 °C on a Bruker APEX DUO diffractometer equipped with a TRIUMPH curved-crystal monochromator using Mo- $\text{K}\alpha$ radiation or at -173.0 ± 2 °C on a Bruker X8 APEX II diffractometer with graphite-monochromated Mo $\text{K}\alpha$ radiation.

Data for **5.3** were collected to a maximum 2θ value of 55.162° in 0.5° oscillations. The structure was solved by direct methods⁶⁰ and expanded using Fourier techniques. All non-hydrogen atoms were refined anisotropically. All hydrogen atoms were included in riding coordinates. The final cycle of full-matrix least-squares analysis was based on 4241 observed reflections and 208 variable parameters.

Data for **5.4** were collected to a maximum 2θ value of 60.74° in 0.5° oscillations. The structure was solved by direct methods⁶⁰ and expanded using Fourier techniques. The complex crystallized as a two-component twin and the twin components were separated using Cell_Now¹²⁵ and TWINABS.¹²⁶ All non-hydrogen atoms were refined anisotropically. All hydrogen atoms were included in calculated positions. The final cycle of full-matrix least-squares analysis was based on 8507 observed reflections and 225 variable parameters.

Data for **5.5** were collected to a maximum 2θ value of 55.06° in 0.5° oscillations. The structure was solved by direct methods⁶⁰ and expanded using Fourier techniques. All non-hydrogen atoms were refined anisotropically. All hydrogen atoms were included in fixed positions. The final cycle of full-matrix least-squares analysis was based on 4542 observed reflections and 241 variable parameters.

Data for **5.6** were collected to a maximum 2θ value of 53.1° in 0.5° oscillations. The structure was solved by direct methods⁶⁰ and expanded using Fourier techniques. All non-hydrogen atoms were refined anisotropically; all hydrogen atoms were included in calculated positions. The final cycle of full-matrix least-squares analysis was based on 4326 observed reflections and 234 variable parameters.

Data for **5.12** were collected to a maximum 2θ value of 55.32° in 0.5° oscillations. The structure was solved by direct methods⁶⁰ and expanded using Fourier techniques. All non-hydrogen atoms were refined anisotropically and all hydrogen atoms were included in calculated positions. The final cycle of full-matrix least-squares analysis was based on 9514 observed reflections and 208 variable parameters.

Data for **5.14** were collected to a maximum 2θ value of 60.06° in 0.5° oscillations. The structure was solved by direct methods¹²⁴ and expanded using Fourier techniques. All non-hydrogen atoms were refined anisotropically. All hydrogen atoms were included in calculated positions. The final cycle of full-matrix least-squares analysis was based on 5903 observed reflections and 257 variable parameters.

For each structure neutral-atom scattering factors were taken from Cromer and Waber.⁶¹ Anomalous dispersion effects were included in F_{calc} ;⁶² the values for $\Delta f'$ and $\Delta f''$ were those of Creagh and McAuley.⁶³ The values for mass attenuation coefficients were those of Creagh and Hubbell.⁶⁴ All calculations were performed using either SHELXL-97⁶⁵ via the WinGX interface⁶⁶ or XL⁶⁷ or SHELXL-2014⁹⁹ via the OLEX interface.⁶⁸ X-ray crystallographic data for all five structures are presented in Table 5.7 and Table 5.8.

Table 5.7. X-ray crystallographic data for complexes **5.3**, **5.4**, and **5.5**.

Compound	5.3	5.4	5.5
Empirical formula	C ₂₀ H ₂₇ NOW	C ₂₁ H ₂₉ NOW	C ₂₂ H ₃₁ NOW
Formula weight	481.27	495.31	509.34
Crystal size (mm)	0.30 × 0.25 × 0.06	0.28 × 0.26 × 0.04	0.28 × 0.21 × 0.09
Crystal system	Orthorhombic	Monoclinic	Monoclinic
Space group	<i>P2₁2₁2₁</i>	<i>P2₁/c</i>	<i>C2/c</i>
Volume (Å ³)	1832.8(4)	1907.3(5)	3982(3)
a (Å)	7.3713(9)	18.350(3)	30.023(5)
b (Å)	14.0596(17)	7.8546(13)	8.402(5)
c (Å)	17.685(2)	14.176(2)	16.013(5)
α (°)	90	90	90
β (°)	90	111.014(7)	99.646(5)
γ (°)	90	90	90
Z	4	4	4
Density, ρ (calculated) (Mg/m ³)	1.744	1.690	1.699
Absorption coefficient, μ (mm ⁻¹)	6.307	6.062	5.810
F ₀₀₀	944.0	936.0	2011.6
Measured Reflections: Total	20382	34807	22490
Measured Reflections: Unique	4241	8507	4542
Final R Indices	R ₁ = 0.0240, wR ₂ = 0.0595	R ₁ = 0.0852, wR ₂ = 0.2755	R ₁ = 0.0285, wR ₂ = 0.0696
Goodness-of-fit on F ²	0.516	1.591	1.274
Largest diff. peak/hole (e ⁻ Å ⁻³)	0.73/-0.88	8.28/-7.70	2.31/-1.83

Table 5.8. X-ray crystallographic data for complexes **5.6**, **5.12**, and **5.14**.

Compound	5.6	5.12	5.14
Empirical formula	C ₂₃ H ₃₃ NO ₂ W	C ₂₂ H ₃₀ NOClW	C ₂₂ H ₂₉ NO ₂ W
Formula weight	523.37	543.77	523.31
Crystal size (mm)	0.16 × 0.07 × 0.05	0.26 × 0.14 × 0.12	0.24 × 0.14 × 0.06
Crystal system	Monoclinic	Orthorhombic	Orthorhombic
Space group	<i>P2₁/c</i>	<i>P2₁2₁2₁</i>	<i>Pbca</i>
Volume (Å ³)	2082.6(9)	4095.1	4049.8(4)
a (Å)	16.592(4)	14.983	7.5576(4)
b (Å)	8.434(2)	15.097	16.6345(9)
c (Å)	16.332(4)	18.104	32.2137(17)
α (°)	90	90	90
β (°)	114.315(4)	90	90
γ (°)	90	90	90
Z	4	4	8
Density, ρ (calculated) (Mg/m ³)	1.6691	1.7149	1.717
Absorption coefficient, μ (mm ⁻¹)	5.558	5.781	5.720
F ₀₀₀	1037.8	2020.8	2064.0
Measured Reflections: Total	16374	64024	66429
Measured Reflections: Unique	4326	9514	5903
Final R Indices	R ₁ = 0.0386, wR ₂ = 0.0852	R ₁ = 0.0490, wR ₂ = 0.1212	R ₁ = 0.0394, wR ₂ = 0.0697
Goodness-of-fit on F ²	1.063	1.032	1.219
Largest diff. peak/hole (e ⁻ Å ⁻³)	2.95/-1.68	5.43/-6.97	2.62/-3.37

Chapter 6: Conclusions and Future Work

6.1 Summary and Conclusions

The $\text{Cp}^*\text{W}(\text{NO})(\text{H})(\eta^3\text{-allyl})$ complexes **2.1-2.3** have been synthesized, and their chemistry has been investigated. Upon thermolysis the hydride couples to the allyl ligand to form a 16e η^2 -alkene intermediate, the PMe_3 adducts of which have been obtained. These 16e η^2 -alkene intermediates effect three successive multiple C-H activations of alkane substrates. The first C-H activation likely generates a 16e bis(alkyl) complex – an analogue of which can be trapped by the reaction of **2.1** with NMM – that then undergoes successive β -H elimination and intramolecular C-H activations forming a new $\text{Cp}^*\text{W}(\text{NO})(\text{H})(\eta^3\text{-allyl})$ complex in which the allyl ligand is derived from the three activations of the substrate. The loss of the original allyl ligand means that the chemistry is independent of the specific allyl ligand.

Under CO pressure, the first C-H activation product can be “trapped” via a 1,1-insertion of CO to transiently form a 16e $\text{Cp}^*\text{W}(\text{NO})(\text{acyl})(\text{alkyl})$ complex. This species does not persist, and the acyl and alkyl ligands couple to generate an unsymmetrical saturated ketone. The organometallic product of the reaction is $\text{Cp}^*\text{W}(\text{NO})(\text{CO})_2$, **3.7**, which can be converted back to the starting hydride compound via successive treatment with PCl_5 , $\text{Mg}(\text{allyl})_2$, and LiBH_4 . The ketones generated are interesting in that they are regiospecifically generated, particularly in the case of those produced by complex **2.1**, and essentially result from the combination of hydrocarbon, CO, and $\text{Mg}(\text{allyl})_2$.

This work is followed by investigations into the functionalization of hydrocarbons initiated by $\text{Cp}^*\text{W}(\text{NO})(\text{CH}_2\text{CMe}_3)(\eta^3\text{-allyl})$ complexes, with a particular emphasis on methane and ethane. Compound **4.1** can effect the C-H activation of methane and the subsequent C-C bond-forming reactions via 1,1-CO insertion and then coupling of acyl and allyl ligands. The

product of this reaction, **4.5**, contains an η^2 -bound β,γ -unsaturated ketone generated from methane via the C-H activation and subsequent C-C bond-forming steps. Heating at 170 °C under CO pressure releases isomers of the unsaturated ketone **4.8** and forms the tungsten dicarbonyl complex **3.7**, which can be converted back to **4.1** via reaction with PCl_5 and two salt metathesis reactions. These reactions complete a synthetic cycle for the transformation of methane and CO into unsaturated ketones after which the original tungsten complex can be regenerated. The organic product is an oil that contains olefin and carbonyl functional groups, a fact that satisfies the criteria for converting methane both into a transportable fuel molecule and using it as a C1 chemical feedstock. In addition, the β,γ -unsaturated ketones themselves are interesting organic molecules which are difficult to synthesize.^{136,137}

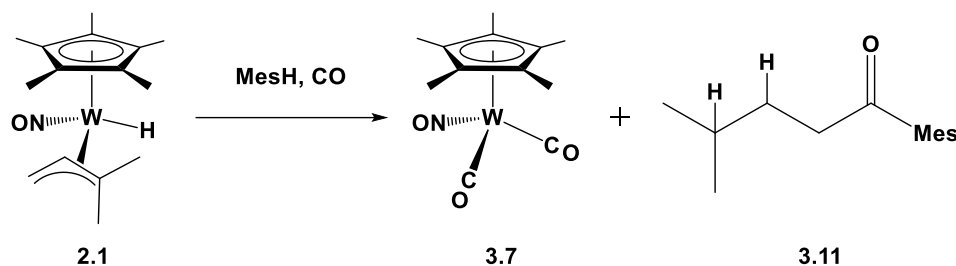
While compound **4.1** can only effect the single activation of methane and not heavier alkanes, the complexes **5.1** and **5.2** can effect the selective C-H activation of both methane and heavier alkanes starting with ethane. Specifically, **5.1** initiates the conversion of both methane and ethane to the corresponding η^2 -bound β,γ -unsaturated ketone complexes **5.15** and **5.16** via the same C-H activation and C-C bond forming steps that are initiated by **4.1**. Photolysis of a η^2 -bound ketone compound results in the release of the cis and trans β,γ -unsaturated ketones. For instance, methane in this case is converted into (*E/Z*)-5-phenylpent-4-en-2-one. Preliminary investigations of this route for longer-chain hydrocarbons show that di(*n*-butyl) ether and *n*-heptane can be converted into acyl ligands following selective, terminal C-H activation and 1,1-CO insertion. Initial investigations into the functionalization initiated by **5.2** suggest similar chemistry to that initiated by **4.1** and **5.1** under CO, albeit with many more isomers being present. This fact results in a loss of the selectivity gained during the C-H activation of gaseous alkanes by **5.2**, which has been optimized during this work. This feature also suggests that the

nature of the allyl ligand helps determine the number of products – organometallic or ketone – that can be generated under CO pressure. This result is similar to that seen for the $\text{Cp}^*\text{W}(\text{NO})(\text{H})(\eta^3\text{-allyl})$ compounds. Thus, **2.1**, containing the 1,1-dimethylallyl ligand regiospecifically generates a single unsymmetrical saturated ketone from the reactions with benzene or mesitylene and CO, while **2.3** containing the 1-methylallyl allyl ligand produces branched and unbranched ketone isomers from the same reactions.

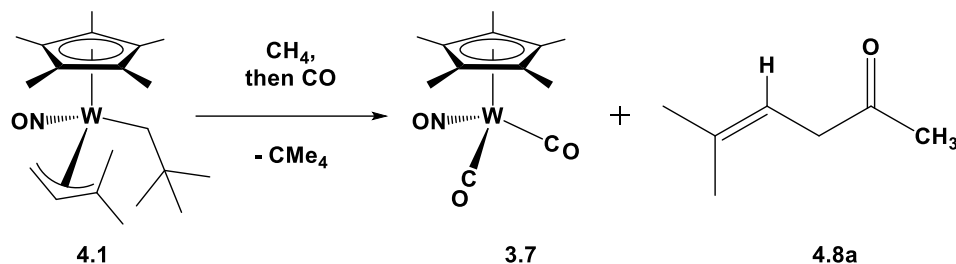
An overarching theme when comparing the two families of $\text{Cp}^*\text{W}(\text{NO})(\text{H})(\eta^3\text{-allyl})$ and $\text{Cp}^*\text{W}(\text{NO})(\text{CH}_2\text{CMe}_3)(\eta^3\text{-allyl})$ complexes is that they both can effect the conversion of an alkane or hydrocarbon under CO pressure into an unsymmetrical ketone. This process for both types of compounds involves C-H activation followed by two subsequent C-C bond-forming reactions. The nature of the unsymmetrical ketone, however, differs between the two classes of compounds, with the $\text{Cp}^*\text{W}(\text{NO})(\text{H})(\eta^3\text{-allyl})$ complexes generating saturated ketones and the $\text{Cp}^*\text{W}(\text{NO})(\text{CH}_2\text{CMe}_3)(\eta^3\text{-allyl})$ complexes producing β,γ -unsaturated ketones (Scheme 6.1).

Scheme 6.1. The production of (a) an unsymmetrical saturated ketone (3.11) from mesitylene and CO initiated by 2.1 and (b) a β,γ -unsaturated ketone (4.8a) from methane and CO initiated by 4.1

(a) unsymmetrical saturated ketones



(b) unsymmetrical β,γ -unsaturated ketones



The key to understanding how the two different families of compounds produce either a saturated or unsaturated product lies in the nature of the 16e intermediate that is responsible for the C-H activation step. In the case of the hydride complexes, the reactive intermediate species is an η^2 -alkene complex. The C-H activation effected by the η^2 -alkene complex results in the conversion of the η^2 -alkene ligand into an η^1 -alkyl ligand and the formation of a 16e bis(alkyl) complex. This transformation is outlined in Figure 6.1a for the specific example of the reaction of **2.1** with mesitylene under CO pressure. Following the formation of the 16e intermediate and subsequent C-H activation of mesitylene, the original dimethylallyl ligand is hydrogenated twice

to afford the η^1 -CH₂CH₂CHMe₂ ligand and the 16e compound Cp*W(NO)(η^1 -CH₂CH₂CHMe₂)(η^1 -CH₂-3,5-Me₂C₆H₃). Next CO insertion into a W-C bond (insertion into either the isopentyl or mesityl ligands will result in the same final product) affords an acyl ligand, and then the acyl and alkyl ligands couple and are released as the unsymmetrical saturated ketone **3.11**.

The unsaturated nature of the ketones produced by the Cp*W(NO)(CH₂CMe₃)(η^3 -allyl) complexes lies in the 16e η^2 -allene and η^2 -diene intermediates that these complexes form. The C-H activation by either intermediate is a microscopic reverse of the neopentane loss that facilitates the formation of these intermediates, and it results in the formation of a new 18e Cp*W(NO)(η^1 -alkyl)(η^3 -allyl) complex. CO insertion affords the 18e acyl compound Cp*W(NO)(η^1 -acyl)(η^3 -allyl). This conversion is followed by the coupling of the acyl and allyl ligands to generate the β,γ -unsaturated ketone which is bound to the tungsten in a dihapto fashion through the olefin site. The ketone is ultimately released at sufficiently high temperatures under CO pressure. A specific example of this transformation is shown in Figure 6.1b for the reaction of **4.1**, first with methane and then CO. As shown in Figure 6.1b **4.1** loses neopentane to form Cp*W(NO)(η^2 -CH₂=C=CMe₂) which activates a C-H bond via the microscopic reverse to form Cp*W(NO)(CH₃)(η^3 -CH₂CHCMe₂) (**4.2**). Exposure to CO pressure forms the acyl compound **4.4**, followed by formation of **4.5**, which results from coupling of the acyl and allyl ligands. Finally the β,γ -unsaturated ketone product is liberated at 170 °C under CO pressure.

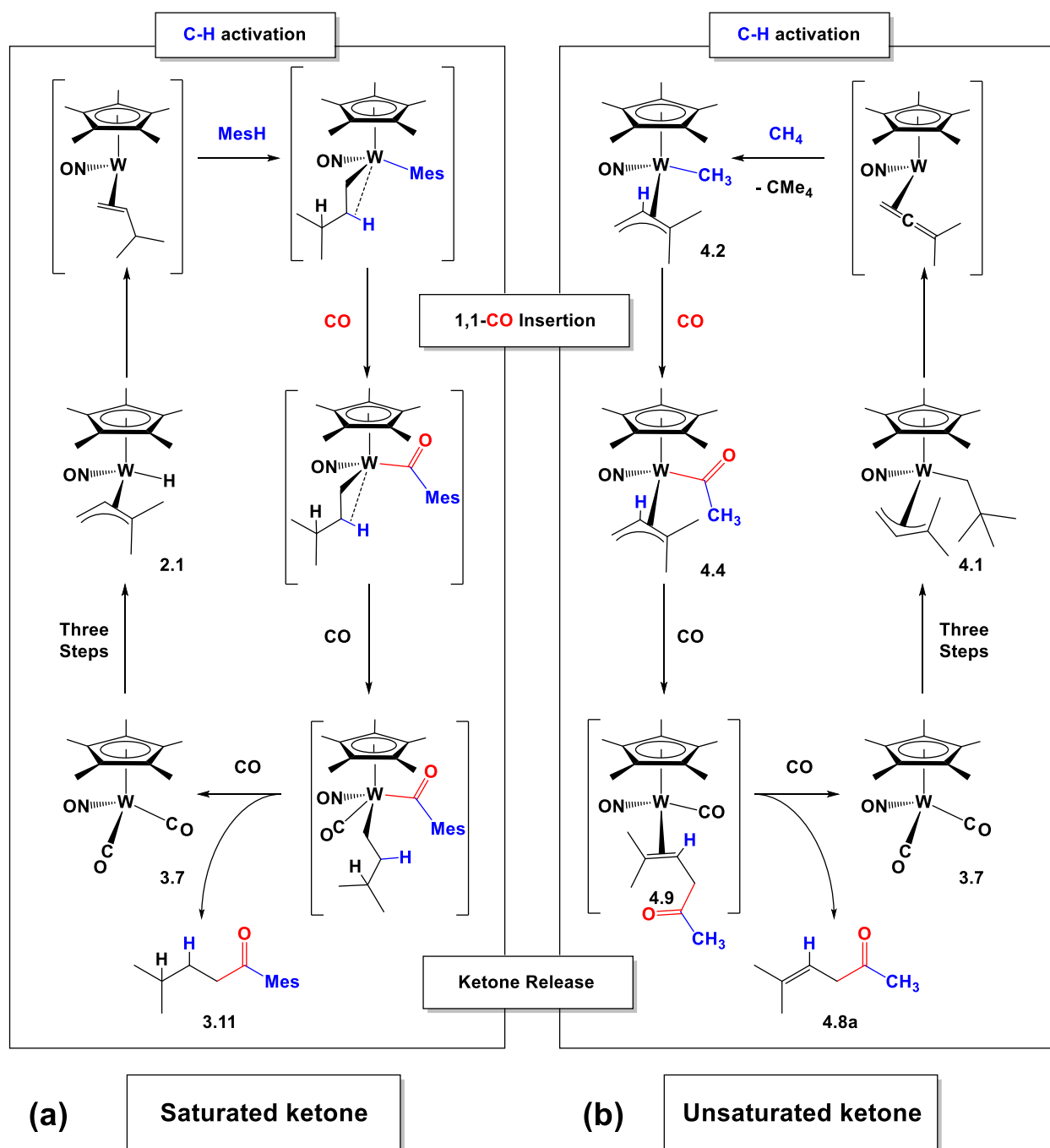


Figure 6.1. Comparison of the mechanisms for ketone formation initiated by Cp*W(NO)(H)(η³-allyl) (e.g. **2.1**) and Cp*W(NO)(CH₂CMe₃)(η³-allyl) (e.g. **4.1**) complexes.

The reactions with alkane and then CO initiated by compounds **4.1** and **5.1** result in the formation of the surprisingly stable η^2 -bound ketone complexes. In fact, the work presented in this thesis describes the formation of a number of similar complexes having the general formula $\text{Cp}^*\text{W}(\text{NO})(\text{CO})(\eta^2\text{-alkene})$ (Figure 6.2). These compounds are all formed at 750 psig CO and the compounds **4.5**, **4.6**, **5.15**, **5.16**, and **5.18** are stable even at 1000 psig CO and 120 °C for several days. The key to the stability is likely in a very strong interaction between the olefin and the tungsten center. The best evidence of this comes from the olefin C=C bond lengths observed in the solid-state molecular structures of **3.15a**, **3.15b**, **4.5**, and **4.6** (Table 6.1). The elongated C=C bonds are all indicative of a significant degree of tungsten back-bonding. The compounds containing a η^2 -unsaturated-ketone ligand have no interaction between the tungsten center and the ketone oxygen. This feature has been established by IR spectroscopy and by X-ray crystallography in the cases of **4.5** and **4.6**, in which the distance between the oxygen and tungsten is found to be in excess of 5 Å in both cases. The thermal release of the β,γ -unsaturated ketones from these compounds requires 170 °C at high pressures of CO. The high degree of stability of these η^2 -alkene complexes has allowed the opportunity to study these compounds that result from the functionalization of methane through a C-H activation and two C-C bond-forming steps. Ultimately the release of these ligands completes the conversion of methane (and other alkanes) into value-added chemicals as well as the closing of a cycle of synthetic reactions in which the tungsten complex can be converted back into the initial reactant, thereby recycling the metal center.

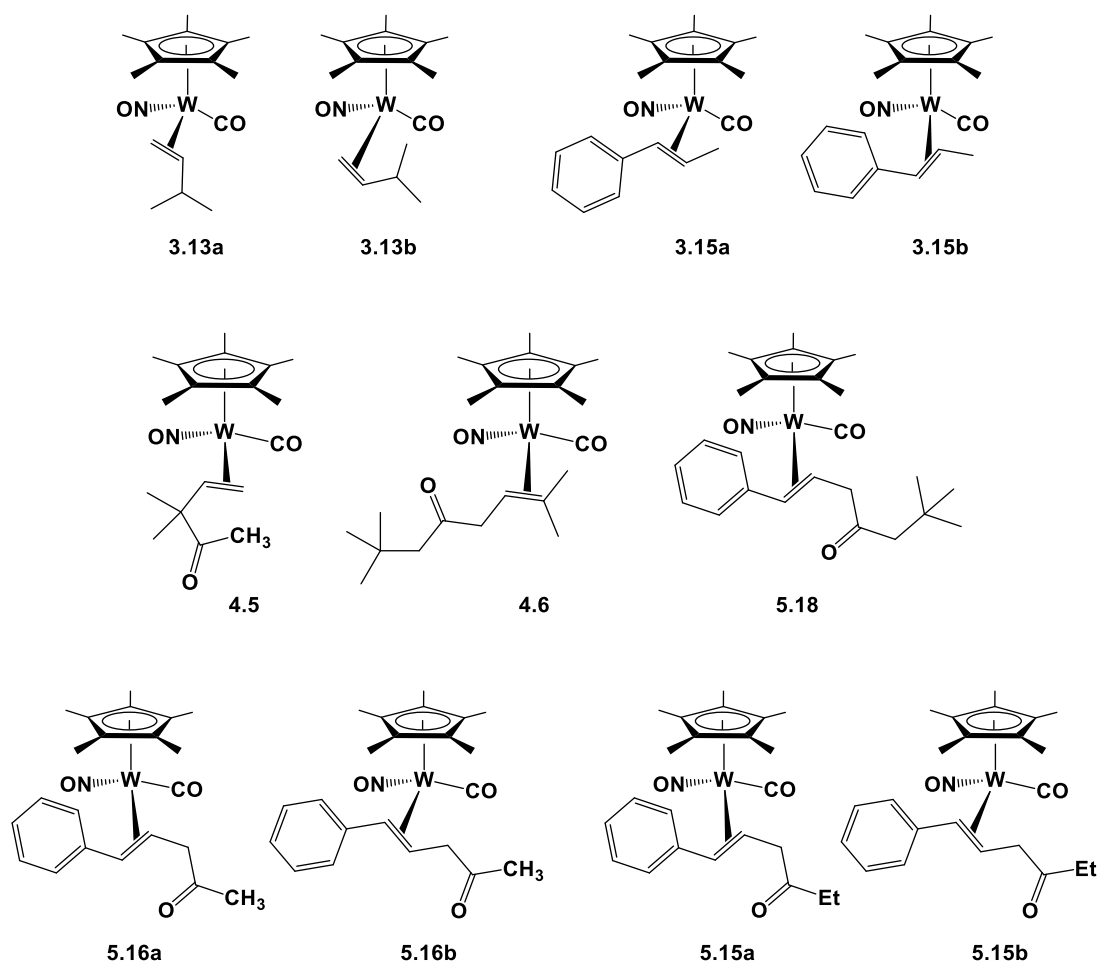


Figure 6.2. Complexes formed at 750 psig CO pressure containing a dihapto bound olefin ligand. Compounds **4.5**, **5.15**, and **5.16** result from the functionalization of methane and ethane.

Table 6.1. C=C bond lengths of dihapto alkene ligands for complexes **3.15a**, **3.15b**, **4.5**, and **4.6**.

Compound	C=C bond length (Å)
3.15a	1.428(9)
3.15b	1.40(3)
4.5	1.430(3)
4.6	1.430(3)

6.2 Future Directions

6.2.1 Optimization of Alkane Functionalization Initiated by $\text{Cp}^*\text{W}(\text{NO})(\text{CH}_2\text{CMe}_3)(\eta^3\text{-allyl})$ Complexes

6.2.1.1 Optimization of the Conversion of Methane and CO into **4.8** Initiated by **4.1**

The work presented in Chapter 4 describes the conversion of methane and CO into the unsaturated ketones **4.8a-c**. The optimization of this process to maximize the yield of ketones needs to be investigated. The cause of the huge discrepancy in yield between the ketone and the dicarbonyl nitrosyl complex **3.7** demands the most attention, particularly for the direct, one-pot process. As mentioned in Chapter 4, the most likely causes of yield reduction are (1) from a competing pathway that originates with the C-H activation of the solvent, or (2) from a loss of ketone during workup. The recovery of a substantial yield of **3.7** would suggest that decomposition of the tungsten complex is not the problem.

Future experiments will examine both the competing reaction with the solvent and the loss of yield due to work-up and product volatility. To assess the role of solvent activation in the yield discrepancy between **4.8** and **3.7**, the sequential reactions could be carried out in C_6F_6 to ensure that cyclohexane activation does not occur. The activation of C-F bonds has not yet been reported for any $\text{Cp}^*\text{W}(\text{NO})(\text{CH}_2\text{CMe}_3)(\eta^3\text{-allyl})$ complex.^{31, 39} The second point to investigate is the issue arising from the volatility of **4.8**. The reaction of **4.2** (or potentially **4.5**) with CO could be carried out in a deuterated solvent (C_6D_6) to allow for a comparison between the relative amounts of **4.8** and **3.7** prior to workup. [This reaction carried out in CDCl_3 results in

decomposition of the complex.] These experiments, and perhaps others, could be used to explore whether the low yield of **4.8** relative to **3.7** is a symptom of workup, solvent activation, or a juxtaposition of the two. In addition, the temperature, pressure, and time of each step in the cycle could also be subjected to optimization studies.

6.2.1.2 Optimization of Alkane Functionalization Initiated by 5.1 as well as Investigation of an Expanded Scope of Substrates

The work presented in Chapter 5 demonstrates that **5.1** can initiate the conversion of methane and ethane to the bound-ketone complexes and that the bound ketone ligands can be released photolytically. Continued investigations into this system are required to determine if the unsaturated ketone ligands can be released thermally under CO pressure, in a manner analogous to the methane cycle initiated by **4.1**. Preliminary investigations into this route show that the dicarbonyl nitrosyl complex **3.7** is formed, suggesting that the ketone is indeed released. The possibility of solvent activation resulting in **4.10**, which then converts to **3.7** through loss of cyclohexene is not likely since **5.1** has not previously shown any reactivity with cyclohexane.²⁸ In addition to investigating the thermal release pathway, the scope of alkanes and hydrocarbons that can be converted needs to be investigated further. While complex **4.1** initiates a complete synthetic cycle for the conversion of methane into unsaturated ketones, compound **5.1** has the potential to extend the same series of reactions to a much larger scope of substrates. The selective, terminal activation and then carbonylation of di(*n*-butyl) ether and *n*-heptane indicate that the scope of functionalization initiated by **5.1** is much wider. Future experiments with **5.1** should focus on determining the conditions necessary for the release of ketones derived from

methane and ethane by thermolysis of the bound ketone complexes **5.15** and **5.16** under CO pressure. Once this has been realized, experiments on expanding the scope of substrates can begin by applying the same conditions for the conversions of the C1 and C2 alkanes to a host of various other alkanes and hydrocarbons.

6.2.1.3 Conversion of Methane to Ketones Initiated by **5.2**

The reaction of **5.2** with CO suggests that the CO insertion and subsequent coupling of the acyl and allyl ligands does occur, but that it results in the formation of many more isomers than is seen for the reactions involving **4.1** and **5.1**. The optimization of the reactions of **5.2** with methane, ethane, and propane shows the potential of this complex from a C-H activation standpoint. However, the reaction of **5.2** with CO suggests that the reactions with CO will have diminishing returns on the selectivity that is afforded by the C-H activations. Nevertheless, one of the primary goals of methane functionalization remains its conversion into a transportable fuel source. Therefore, the presence of numerous product isomers is not necessarily detrimental.

Preliminary investigations into the cycle of reactions initiated by **5.2** for the C-H activation of methane and then subsequent functionalization with CO show the presence of the anticipated dicarbonyl complex **3.7** as well as a multitude of possible ketone isomers. It appears that the coupling of the acyl occurs at either terminus of the allyl ligand, resulting in branched and unbranched dihapto unsaturated ketone ligands (analogous to the reactions of **2.3** with benzene and mesitylene under CO pressure). Figure 6.3 outlines a potential mechanism for the formation of all the potential ketone isomers (cis/trans, branched/unbranched, β,γ -unsaturated/ α,β -unsaturated) from the reaction of **5.2** with methane and then CO. The initial

results suggest as few as four and as many as all seven ketone products are present in the final reaction mixture from the reaction of **5.7** with CO at 170 °C.¹³⁸

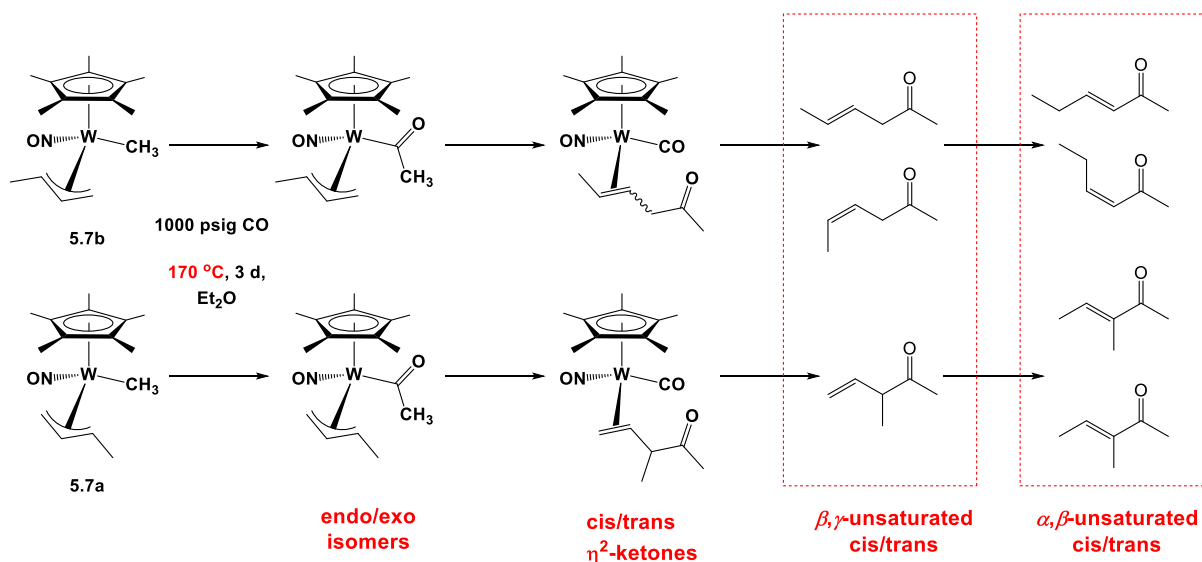


Figure 6.3. The proposed conversion of the isomers of **5.7** under CO pressure to afford isomers of *cis/trans*-β,γ-unsaturated and *cis/trans*-α,β-unsaturated ketones that are derived from the initial reaction of **5.2** with methane.

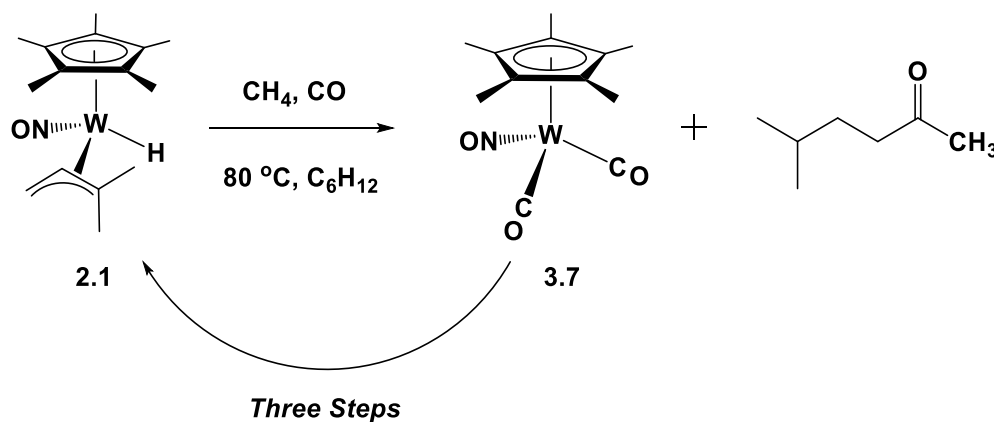
6.2.2 Further Reactions Initiated by the Cp*W(NO)(H)(η³-allyl) Complexes

6.2.2.1 One-Pot Functionalization of Methane Initiated by **2.1**

The thermolysis of a cyclohexane solution of **2.1** under methane pressure has been previously carried out, but no tractable organometallic products could be identified in the final mixture. The anticipated product from the activation of methane by **2.1** is Cp*W(NO)(CH₃)(CH₂CH₂CHMe₂), a 16e complex with an open coordination site and

containing β -hydrogens. Thus, if the activation does occur, the product is not expected to be stable at the 80 °C used to effect C-H activation with **2.1**. It might then be anticipated that the thermolysis of **2.1** under the pressure of both methane and CO simultaneously could result in the formation of an unsymmetrical ketone from methane and CO. The reaction of **2.1** with cyclohexane demonstrates that while cyclohexane is activated, **2.1** reacts more slowly with the alkane comprised only of secondary C(sp^3)-H bonds. Thus, it is reasonable to assume that given the appropriate pressure of methane, compound **2.1** will be selective for methane activation. In addition, the reaction of **2.1** with mesitylene and CO showed that the complex can effect C(sp^3)-H bond activation under CO pressure. The proposed reaction is outlined in Scheme 6.2 with the unsymmetrical saturated ketone Me₂CHCH₂CH₂C(O)CH₃ being the anticipated product based on the regioselectivity seen for the analogous reactions of **2.1** with benzene and mesitylene under CO pressure. The reaction would also require modification of an existing pressure reactor to allow for simultaneous pressurization with two gases.

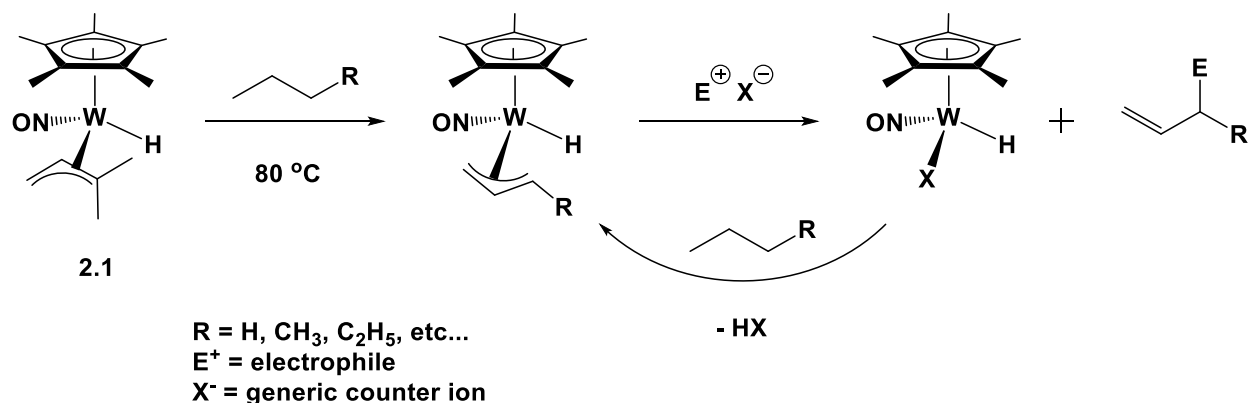
Scheme 6.2. Proposed one-pot conversion of methane and CO initiated by compound 2.1 to produce the unsymmetrical saturated ketone 5-methylhexan-2-one



6.2.2.2 Reactions with Electrophiles

Another potential area of investigations involves the ability of the $\text{Cp}^*\text{W}(\text{NO})(\text{H})(\eta^3\text{-allyl})$ complexes to effect the multiple C-H activations which convert an alkane to allyl and hydride ligands. Previously reported reactions of the related $\text{Cp}^*\text{W}(\text{NO})(\text{alkyl})(\eta^3\text{-allyl})$ complexes demonstrated that the allyl ligands are susceptible to electrophilic attack.³⁷ The proposed study involves reacting a complex containing an allyl ligand obtained from multiple C-H activations with an electrophile to give a compound derived from three C-H activations and coupling to the electrophile (Scheme 6.3). To take this proposal a step further, the exact nature of the electrophile (E^+) and its counter ion would determine the organometallic product of these reactions, designated as $\text{Cp}^*\text{W}(\text{NO})(\text{H})(\text{X})$. Determining the appropriate X that could be lost as HX (or XH_3 to accommodate the first two C-H activations of the next alkane molecule) could result in a potential cycle for the dehydrogenative-coupling of alkanes to electrophiles. The reactions of **2.1** with *n*-pentane and *n*-heptane show that there is a preference, although not exclusive selectivity, for initial terminal activation. Nevertheless, as the size of the alkanes increases, the number of isomers for the $\text{Cp}^*\text{W}(\text{NO})(\text{H})(\eta^3\text{-allyl})$ product increases, which would result in a greater number of products. Propane, the smallest alkane such a system could utilize, would afford the most selectivity to give $\text{CH}_2=\text{CHCH}_2\text{E}$, while the isomers from the *n*-butane reaction would ultimately afford a mixture of $\text{CH}_2=\text{CHC}(\text{E})\text{HCH}_3$ and (*E/Z*)- $\text{CH}_3\text{CH}=\text{CHCH}_2\text{E}$. The product mixtures would again become increasingly complex as the size of the alkane substrate increased. However, the potential to turn alkanes into complex molecules through the installation of alkene and E functional sites remains appealing.

Scheme 6.3. Proposed functionalization of alkanes via dehydrogenative coupling to electrophiles initiated by 2.1. In this proposal, the appropriate selection of X^- could result in an organometallic product that can lose HX and effect the multiple C-H activations of an alkane to reinitiate the cycle.

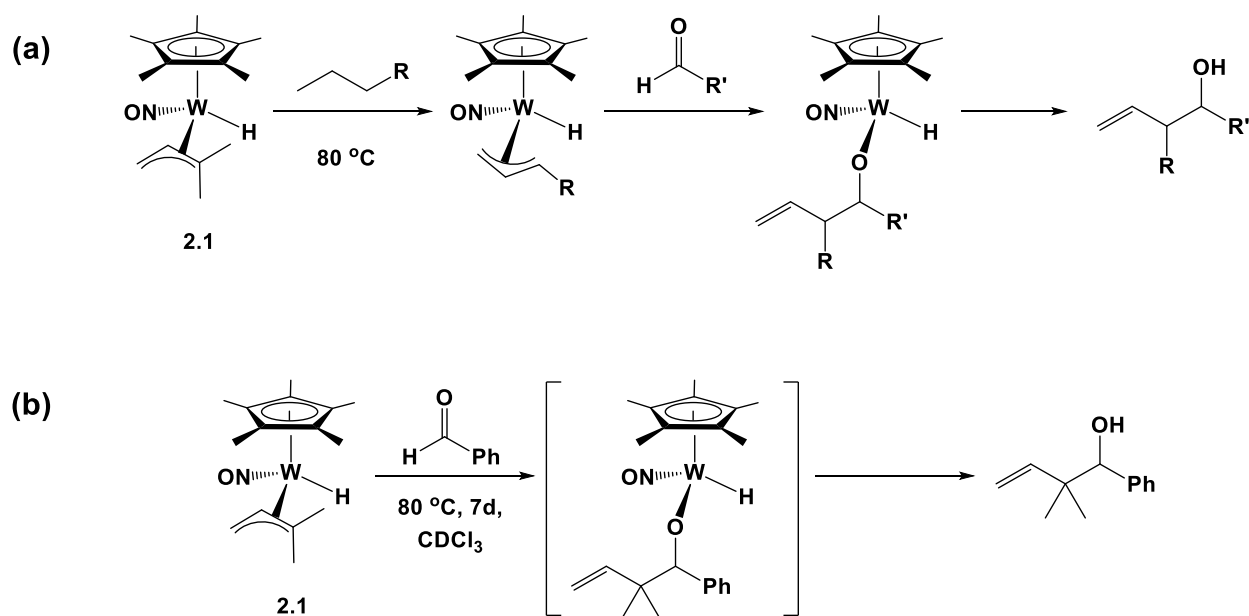


6.2.2.3 Coupling of Alkanes with Aldehydes Initiated by 2.1

Another proposed route taking advantage of the conversion of an alkane molecule to an allyl and a hydride ligand via three successive C-H activations initiated by **2.1** is through the functionalization of an allyl ligand via reaction with an aldehyde. Reactions of $Cp^*W(NO)(alkyl)(\eta^3\text{-allyl})$ and $Cp^*W(NO)(acyl)(\eta^3\text{-allyl})$ complexes with aldehydes result in the 1,2-insertion of the aldehyde carbonyl across a W-C bond of the allyl.^{39, 139-141} These results involved reactions of allyl ligands obtained via metathesis. For the $Cp^*W(NO)(H)(\eta^3\text{-allyl})$ complexes in which the allyl ligand is derived from C-H activations, the products effectively arise from the dehydrogenation and coupling of alkanes to aldehydes. The proposed reaction is outlined in Scheme 6.4a and involves first the thermolysis of **2.1** in neat alkane followed by addition of aldehyde. The 1,2-insertion of the aldehyde carbonyl into a W-C bond of the allyl

results in a 16e $\text{Cp}^*\text{W}(\text{NO})(\text{H})(\text{O-alkyl})$ complex; this mode of reactivity has been previously demonstrated for related complexes.^{140, 141} The 16e alkoxy hydride complexes are generally quite unstable and liberate the alkoxy ligand as the alcohol; the nature of the final organometallic complex is not known.¹³⁹

Scheme 6.4. (a) Proposed coupling of alkanes and aldehydes initiated by 2.1, and (b) preliminary reaction of 2.1 with benzaldehyde



A preliminary reaction of **2.1** with benzaldehyde has been carried out in CDCl_3 and has been monitored by ^1H NMR spectroscopy (Scheme 6.4b). Thermolysis of this mixture at $80\text{ }^\circ\text{C}$ for 7 d produces the compound 2,2-dimethylbut-3-en-1-ol.¹⁴² Some conversion is observed initially at room temperature, but the reaction requires extended heating before all of **2.1** is consumed. Presumably the reaction proceeds via the 1,2-insertion of the aldehyde carbonyl across the W-C bond of the allyl at the CMe_2 terminus to give the 16e intermediate complex

$\text{Cp}^*\text{W}(\text{NO})(\text{H})(\text{OCHPhCMe}_2\text{CH}=\text{CH}_2)$. [This is the mode of reactivity seen for the $\text{Cp}^*\text{W}(\text{NO})(\text{alkyl})(\eta^3\text{-allyl})$ and $\text{Cp}^*\text{W}(\text{NO})(\text{acyl})(\eta^3\text{-allyl})$ complexes with aldehydes]^{139, 141} The alkoxy and hydride ligands then likely reductively eliminate to afford the alcohol. This proof-of-concept reaction demonstrates that the combination of aldehyde with a $\text{Cp}^*\text{W}(\text{NO})(\text{H})(\eta^3\text{-allyl})$ complex can produce an unsaturated alcohol. Therefore, effecting the multiple C-H activations of an alkane by **2.1** followed by reaction with aldehyde should in principle afford an unsaturated alcohol that originated with an alkane. The scope of this carbonylative dehydrogenation reaction can also be investigated by screening a range of alkanes with various aldehydes to afford a variety of different compounds.

References

1. Cavaliere, V. N.; Mindiola, D. J., *Chem. Sci.* **2012**, *3*, 3356-3365.
2. Fortman, G. C.; Boaz, N. C.; Munz, D.; Konnick, M. M.; Periana, R. A.; Groves, J. T.; Gunnoe, T. B., *J. Am. Chem. Soc.* **2014**, *136*, 8393-8401.
3. Hashiguchi, B. G.; Konnick, M. M.; Bischof, S. M.; Gustafson, S. J.; Devarajan, D.; Gunsalus, N.; Ess, D. H.; Periana, R. A., *Science* **2014**, *343*, 1232-1237.
4. McFarland, E., *Science* **2012**, *338*, 340-342.
5. Olah, G. A.; Molnár, Á., Hydrocarbons from Petroleum and Natural Gas. In *Hydrocarbon Chemistry*, John Wiley & Sons, Inc.: 2003; pp 30-84.
6. Caballero, A.; Perez, P. J., *Chem. Soc. Rev.* **2013**, *42*, 8809-8820.
7. Johnson, J., *Chem. Eng. News* **2014**, *92*, 10-15.
8. Labinger, J. A.; Bercaw, J. E., *Nature* **2002**, *417*, 507-514.
9. Bergman, R. G., *Nature* **2007**, *446*, 391-393.
10. Hoyano, J. K.; Graham, W. A. G., *J. Am. Chem. Soc.* **1982**, *104*, 3723-3725.
11. Janowicz, A. H.; Bergman, R. G., *J. Am. Chem. Soc.* **1982**, *104*, 352-354.
12. Hartwig, J. F., *J. Am. Chem. Soc.* **2016**, *138*, 2-24.
13. Konnick, M. M.; Hashiguchi, B. G.; Devarajan, D.; Boaz, N. C.; Gunnoe, T. B.; Groves, J. T.; Gunsalus, N.; Ess, D. H.; Periana, R. A., *Angew. Chem. Int. Ed.* **2014**, *53*, 10490-10494.
14. Shilov, A. E.; Shul'pin, G. B., *Chem. Rev.* **1997**, *97*, 2879-2932.
15. Periana, R. A.; Taube, D. J.; Gamble, S.; Taube, H.; Satoh, T.; Fujii, H., *Science* **1998**, *280*, 560-564.

16. Periana, R. A.; Taube, D. J.; Evitt, E. R.; Löffler, D. G.; Wentrcek, P. R.; Voss, G.; Masuda, T., *Science* **1993**, *259*, 340-343.
17. Sadow, A. D.; Tilley, T. D., *J. Am. Chem. Soc.* **2003**, *125*, 7971-7977.
18. Thompson, M. E.; Baxter, S. M.; Bulls, A. R.; Burger, B. J.; Nolan, M. C.; Santarsiero, B. D.; Schaefer, W. P.; Bercaw, J. E., *J. Am. Chem. Soc.* **1987**, *109*, 203-219.
19. Caballero, A.; Despagne-Ayoub, E.; Mar Díaz-Requejo, M.; Díaz-Rodríguez, A.; González-Núñez, M. E.; Mello, R.; Muñoz, B. K.; Ojo, W.-S.; Asensio, G.; Etienne, M.; Pérez, P. J., *Science* **2011**, *332*, 835-838.
20. Gava, R.; Olmos, A.; Noverges, B.; Varea, T.; Alvarez, E.; Belderrain, T. R.; Caballero, A.; Asensio, G.; Perez, P. J., *ACS Catal.* **2015**, *5*, 3726-3730.
21. Basset, J.-M.; Coperet, C.; Soulivong, D.; Taoufik, M.; Cazat, J. T., *Acc. Chem. Res.* **2010**, *43*, 323-334.
22. Soulivong, D.; Copéret, C.; Thivolle-Cazat, J.; Basset, J.-M.; Maunders, B. M.; Pardy, R. B. A.; Sunley, G. J., *Angew. Chem. Int. Ed.* **2004**, *43*, 5366-5369.
23. Soulivong, D.; Norsic, S.; Taoufik, M.; Coperet, C.; Thivolle-Cazat, J.; Chakka, S.; Basset, J.-M., *J. Am. Chem. Soc.* **2008**, *130*, 5044-5045.
24. Coperet, C., *Chem. Rev.* **2010**, *110*, 656-680.
25. Hammond, C.; Forde, M. M.; Ab Rahim, M. H.; Thetford, A.; He, Q.; Jenkins, R. L.; Dimitratos, N.; Lopez-Sanchez, J. A.; Dummer, N. F.; Murphy, D. M.; Carley, A. F.; Taylor, S. H.; Willock, D. J.; Stangland, E. E.; Kang, J.; Hagen, H.; Kiely, C. J.; Hutchings, G. J., *Angew. Chem. Int. Ed.* **2012**, *51*, 5129-5133.
26. Ng, S. H. K.; Adams, C. S.; Hayton, T. W.; Legzdins, P.; Patrick, B. O., *J. Am. Chem. Soc.* **2003**, *125*, 15210-15223.

27. Tsang, J. Y. K.; Buschhaus, M. S. A.; Graham, P. M.; Semiao, C. J.; Semproni, S. P.; Kim, S. J.; Legzdins, P., *J. Am. Chem. Soc.* **2008**, *130*, 3652-3663.
28. Baillie, R. A.; Man, R. W. Y.; Shree, M. V.; Chow, C.; Thibault, M. E.; McNeil, W. S.; Legzdins, P., *Organometallics* **2011**, *30*, 6201-6217.
29. Chow, C.; Patrick, B. O.; Legzdins, P., *Organometallics* **2012**, *31*, 7453-7466.
30. Baillie, R. A.; Tran, T.; Lalonde, K. M.; Tsang, J. Y. K.; Thibault, M. E.; Patrick, B. O.; Legzdins, P., *Organometallics* **2012**, *31*, 1055-1067.
31. Baillie, R. A.; Legzdins, P., *Acc. Chem. Res.* **2014**, *47*, 330-340.
32. Lefèvre, G. P.; Baillie, R. A.; Fabulyak, D.; Legzdins, P., *Organometallics* **2013**, *32*, 5561-5572.
33. Tran, T.; Chow, C.; Zimmerman, A. C.; Thibault, M. E.; McNeil, W. S.; Legzdins, P., *Organometallics* **2011**, *30*, 738-751.
34. Tsang, J. Y. K.; Buschhaus, M. S. A.; Legzdins, P., *J. Am. Chem. Soc.* **2007**, *129*, 5372-5373.
35. Baillie, R. A.; Tran, T.; Thibault, M. E.; Legzdins, P., *J. Am. Chem. Soc.* **2010**, *132*, 15160-15161.
36. Chow, C.; Patrick, B. O.; Legzdins, P., *Organometallics* **2012**, *31*, 8159-8171.
37. Semproni, S. P.; Graham, P. M.; Buschhaus, M. S. A.; Patrick, B. O.; Legzdins, P., *Organometallics* **2009**, *28*, 4480-4490.
38. Semproni, S. P.; Legzdins, P., *Organometallics* **2009**, *28*, 6139-6141.
39. Baillie, R. A.; Legzdins, P., *Coord. Chem. Rev.* **2016**, *309*, 1-20.
40. Greenhough, T. J.; Legzdins, P.; Martin, D. T.; Trotter, J., *Inorg. Chem.* **1979**, *18*, 3268-3270.

41. Harrison, D. P.; Nichols-Nieler, A. C.; Zottig, V. E.; Strausberg, L.; Salomon, R. J.; Trindle, C. O.; Sabat, M.; Gunnoe, T. B.; Iovan, D. A.; Myers, W. H.; Harman, W. D., *Organometallics* **2011**, *30*, 2587-2597.
42. Villanueva, L. A.; Ward, Y. D.; Lachicotte, R.; Liebeskind, L. S., *Organometallics* **1996**, *15*, 4190-4200.
43. Baillie, R. A.; Holmes, A. S.; Lefèvre, G. P.; Patrick, B. O.; Shree, M. V.; Wakeham, R. J.; Legzdins, P.; Rosenfeld, D. C., *Inorg. Chem.* **2015**, *54*, 5915-5929.
44. Tsang, J. Y. K.; Buschhaus, M. S. A.; Fujita-Takayama, C.; Patrick, B. O.; Legzdins, P., *Organometallics* **2008**, *27*, 1634-1644.
45. Baillie, R. A.; Wakeham, R. J.; Lefèvre, G. P.; Béthegnies, A.; Patrick, B. O.; Legzdins, P.; Rosenfeld, D. C., *Organometallics* **2015**, *34*, 3428-3441.
46. Ng, S. H. K.; Adams, C. S.; Legzdins, P., *J. Am. Chem. Soc.* **2002**, *124*, 9380-9381.
47. Pamplin, C. B.; Legzdins, P., *Acc. Chem. Res.* **2003**, *36*, 223-233.
48. Legzdins, P.; Martin, J. T.; Einstein, F. W. B.; Jones, R. H., *Organometallics* **1987**, *6*, 1826-1827.
49. Lee, K.; Legzdins, P.; Pamplin, C. B.; Patrick, B. O.; Wada, K., *Organometallics* **2005**, *24*, 638-649.
50. See Appendix Figure A.1.
51. Russell, G. A.; Kulkarni, S. V., *J. Org. Chem.* **1993**, *58*, 2678-2685; Booker-Milburn, K. I.; Jones, J. L.; Sibley, G. E. M.; Cox, R.; Meadows, J., *Org. Lett.* **2003**, *5*, 1107-1109.
52. Ju, T. D.; Capps, K. B.; Lang, R. F.; Roper, G. C.; Hoff, C. D., *Inorg. Chem.* **1997**, *36*, 614-621.

53. Graham, P. M.; Buschhaus, M. S. A.; Baillie, R. A.; Semproni, S. P.; Legzdins, P., *Organometallics* **2010**, 29, 5068-5072.
54. Armarego, W. L. F.; Chai, C. L. L., *Purification of Laboratory Chemicals*. 5th ed.; Elsevier: Amsterdam, **2003**.
55. Dryden, N. H.; Legzdins, P.; Rettig, S. J.; Veltheer, J. E., *Organometallics* **1992**, 11, 2583-2590.
56. Dryden, N. H.; Legzdins, P.; Batchelor, R. J.; Einstein, F. W. B., *Organometallics* **1991**, 10, 2077-2081.
57. Jin, G.-X.; Herberhold, M., *Transition Met. Chem.* **2001**, 26, 445-447.
58. See Appendix Figure A.2.
59. See Appendix Figure A.3.
60. SIR-92: Altomare, A.; Cascarano, G.; Giacovazzo, C.; Guagliardi, A., *J. Appl. Crystallogr.* **1993**, 26, 343-350.
61. Cromer, D. T.; Waber, J. T., *International Tables for X-ray Crystallography; The Kynoch Press: Birmingham*. 1974; Vol. IV, Table 2.2 A.
62. Ibers, J. A.; Hamilton, W. C., *Acta Crystallogr.* **1964**, 17, 781-782.
63. Creagh, D. C.; McAuley, W. J., *International Tables for X-ray Crystallography; Kluwer Academic Publishers: Boston*. 1992; Vol. C., Table 4.2.6.8.
64. Creagh, D. C.; Hubbell, J. H., *International Tables for X-ray Crystallography; Kluwer Academic Publishers: Boston*. 1992; Vol. C., Table 4.2.4.3.
65. SHELXL-97: Sheldrick, G. M., *Acta Crystallogr.* **2008**, A64, 112-122.
66. WinGX-V1.70: Farrugia, L., *J. Appl. Crystallogr.* **1999**, 32, 837-838.
67. XL: Sheldrick, G. M., *Acta Crystallogr.* **2008**, A64, 112-122.

68. OLEX2-V1.2.6: Dolomanov, O. V.; Bourhis, L. J.; Gildea, R. J.; Howard, J. A. K.; Puschmann, H., *J. Appl. Crystallogr.* **2009**, *42*, 339-341.
69. Mkhaliid, I. A. I.; Barnard, J. H.; Marder, T. B.; Murphy, J. M.; Hartwig, J. F., *Chem. Rev.* **2010**, *110*, 890-931.
70. Colby, D. A.; Bergman, R. G.; Ellman, J. A., *Chem. Rev.* **2010**, *110*, 624-655.
71. Yamaguchi, J.; Yamaguchi, A. D.; Itami, K., *Angew. Chem. Int. Ed.* **2012**, *51*, 8960-9009.
72. Davies, H. M. L.; Morton, D., *Chem. Soc. Rev.* **2011**, *40*, 1857-1869.
73. Borovik, A. S., *Chem. Soc. Rev.* **2011**, *40*, 1870-1874.
74. Zhou, M.; Crabtree, R. H., *Chem. Soc. Rev.* **2011**, *40*, 1875-1884.
75. Lu, H.; Zhang, X. P., *Chem. Soc. Rev.* **2011**, *40*, 1899-1909.
76. Lewis, J. C.; Coelho, P. S.; Arnold, F. H., *Chem. Soc. Rev.* **2011**, *40* (4), 2003-2021.
77. Webb, J. R.; Bolaño, T.; Gunnoe, T. B., *ChemSusChem* **2011**, *4*, 37-49.
78. Baillie, R. A.; Lefèvre, G. P.; Wakeham, R. J.; Holmes, A. S.; Legzdins, P., *Organometallics* **2015**, *34*, 4085-4092.
79. Hartwig, J. F., In *Organotransition Metal Chemistry: From Bonding to Catalysis*, University Science Books: Sausalito, CA, 2010; pp 71-72.
80. Brookhart, M.; Green, M. L. H.; Parkin, G., *Proc. Natl. Acad. Sci. U. S. A.* **2007**, *104*, 6908-6914.
81. Faller, J. W.; Whitmore, B. C., *Organometallics* **1986**, *5*, 752-755.
82. Dryden, N. H.; Legzdins, P.; Lundmark, P. J.; Riesen, A.; Einstein, F. W. B., *Organometallics* **1993**, *12*, 2085-2093.
83. Durfee, L. D.; Rothwell, I. P., *Chem. Rev.* **1988**, *88*, 1059-1079.

84. Daniel, J. S.; Solomon, S., *Journal of Geophysical Research: Atmospheres* **1998**, *103*, 13249-13260.
85. Cho, C. S., *J. Mol. Catal. A* **2005**, *240*, 55-60.
86. Fujita, K.-i.; Asai, C.; Yamaguchi, T.; Hanasaka, F.; Yamaguchi, R., *Org. Lett.* **2005**, *7*, 4017-4019.
87. Cho, C. S., *Catal. Comm.* **2006**, *7*, 1012-1014.
88. Brunet, J. J.; Chauvin, R., *Chem. Soc. Rev.* **1995**, *24*, 89-95.
89. Tamaru, Y.; Kimura, M., Reactions of Acylpalladium Derivatives with Organometals and Related Carbon Nucleophiles. In *Handbook for Organopalladium Chemistry for Organic Synthesis*, Negishi, E.-I., Ed. Wiley-Interscience: New York, 2002; pp 2425-2454.
90. Hartwig, J. F., In *Organotransition Metal Chemistry: From Bonding to Catalysis*, University Science Books: Sausalito, CA, 2010; pp 877-965.
91. Dieter, R. K., *Tetrahedron* **1999**, *55*, 4177-4236.
92. Arisawa, M.; Kuwajima, M.; Toriyama, F.; Li, G.; Yamaguchi, M., *Org. Lett.* **2012**, *14*, 3804-3807.
93. Ding, B.; Zhang, Z.; Liu, Y.; Sugiya, M.; Imamoto, T.; Zhang, W., *Org. Lett.* **2013**, *15*, 3690-3693.
94. See Appendix Figure B.1.
95. See Appendix Figure B.2.
96. See Appendix Figure B.3.
97. See Appendix Figure B.4.
98. SHELXT: Sheldrick, G. M., *Acta Crystallogr.* **2008**, *A64*, 112-122.
99. SHELXL-2014: Sheldrick, G. M., *Acta Crystallogr.* **2015**, *A71*, 3-8.

100. See Appendix C.1.
101. Debad, J. D.; Legzdins, P.; Batchelor, R. J.; Einstein, F. W. B., *Organometallics* **1993**, *12*, 2094-2102.
102. Flores, J. A.; Cavaliere, V. N.; Buck, D.; Pinter, B.; Chen, G.; Crestani, M. G.; Baik, M.-H.; Mindiola, D. J., *Chem. Sci.* **2011**, *2*, 1457-1462.
103. Sadow, A. D.; Tilley, T. D., *Angew. Chem. Int. Ed.* **2003**, *42*, 803-805.
104. de With, J.; Horton, A. D., *Angew. Chem. Int. Ed.* **1993**, *32*, 903-905.
105. Richter-Addo, G. B.; Legzdins, P., *Metal Nitrosyls*; Oxford University Press: New York, NY. 1992; p 3.
106. See Appendix Figure C.3.
107. See Appendix Figure C.4.
108. Calderazzo, F., *Angew. Chem. Int. Ed.* **1977**, *16*, 299-311.
109. Hartwig, J. F., *Organotransition Metal Chemistry: From Bonding to Catalysis*; University Science Books: Sausalito, CA. 2010; pp 349-364.
110. Kuhlmann, E. J.; Alexander, J. J., *Coord. Chem. Rev.* **1980**, *33*, 195-225.
111. Flood, T. C.; Jensen, J. E.; Statler, J. A., *J. Am. Chem. Soc.* **1981**, *103*, 4410-4414.
112. Low, J. J.; Goddard, W. A., *Journal of the American Chemical Society* **1986**, *108*, 6115-6128.
113. Hartwig, J. F., *Organotransition Metal Chemistry: From Bonding to Catalysis*; University Science Books: Sausalito, CA. 2010; pp 332-334.
114. See Appendix Figure C.5.
115. Moreau, J.-L.; Couffignal, R., *J. Organomet. Chem.* **1985**, *297*, 1-11.
116. Muramatsu, S.; Nakada, Y.; Ide, J., *Agric. Biol. Chem.* **1985**, *49*, 751-760.

117. Masson, S.; Saquet, M.; Thuillier, A., *Tetrahedron* **1977**, 33, 2949-2954.
118. Pirrung, M. C.; Liu, Y.; Deng, L.; Halstead, D. K.; Li, Z.; May, J. F.; Wedel, M.; Austin, D. A.; Webster, N. J. G., *J. Am. Chem. Soc.* **2005**, 127, 4609-4624.
119. Tanaka, K.; Kobayashi, T.; Mori, H.; Katsumura, S., *J. Org. Chem.* **2004**, 69, 5906-5925.
120. See Appendix Figure C.6.
121. See Appendix Figure C.7.
122. See Appendix Figure C.8.
123. See Appendix Figure C.9.
124. SIR-97: Altomare, A.; Burla, M. C.; Camalli, M.; Cascarano, G.; Giacovazzo, C.; Guagliardi, A.; Moliterni, A. G. G.; Polidori, G.; Spagna, R., *J. Appl. Crystallogr.* **1999**, 32, 115-119.
125. Cell_Now; 2008/2; Bruker AXS Inc., M., WI.
126. TWINABS; V2008/4; Bruker AXS Inc., M., Wisconsin, USA (2008).
127. Semproni, S. P.; McNeil, W. S.; Baillie, R. A.; Patrick, B. O.; Campana, C. F.; Legzdins, P., *Organometallics* **2010**, 29, 867-875.
128. Brookhart, M.; Green, M. L. H., *J. Organomet. Chem.* **1983**, 250, 395-408.
129. Hartwig, J. F., In *Organotransition Metal Chemistry: From Bonding to Catalysis*, University Science Books: Sausalito, CA, 2010; pp 398-402.
130. Hartwig, J. F., In *Organotransition Metal Chemistry: From Bonding to Catalysis*, University Science Books: Sausalito, CA, 2010; pp 406-407.
131. See Appendix Figure D.1.
132. See Appendix Figure D.2.
133. Tummatorn, J.; Ruchirawat, S.; Ploypradith, P., *Chem. Eur. J.* **2010**, 16, 1445-1448.

134. See Appendix Figure D.3.
135. See Appendix Figure D.4.
136. Kachinsky, J. L. C.; Salomon, R. G., *J. Org. Chem.* **1986**, *51*, 1393-1401.
137. Aumiller, J. C.; Whittle, J. A., *J. Org. Chem.* **1976**, *41*, 2959-2962.
138. See Appendix E.1.
139. Shree, M. V.; Baillie, R. A., unpublished observations.
140. See Appendix E.3.
141. See Appendix Figure E.1.
142. See Appendix E.2.
143. Bellassoued, M.; Aatar, J.; Bouzid, M.; Damak, M., *Phosphorus Sulfur Silicon Relat. Elem.* **2010**, *185*, 1886-1895.
144. Cadierno, V.; García-Garrido, S. E.; Gimeno, J., *Adv. Synth. Catal.* **2006**, *348*, 101-110.
145. Amemiya, F.; Fuse, K.; Fuchigami, T.; Atobe, M., *Chem. Comm.* **2010**, *46*, 2730-2732.
146. Haddad, T. D.; Hirayama, L. C.; Singaram, B., *J. Org. Chem.* **2010**, *75*, 642-649.
147. Bower, J. F.; Skucas, E.; Patman, R. L.; Krische, M. J., *J. Am. Chem. Soc.* **2007**, *129*, 15134-15135.
148. Skucas, E.; Bower, J. F.; Krische, M. J., *J. Am. Chem. Soc.* **2007**, *129*, 12678-12679.

Appendices

Appendix A Supplementary Materials for Chapter 2

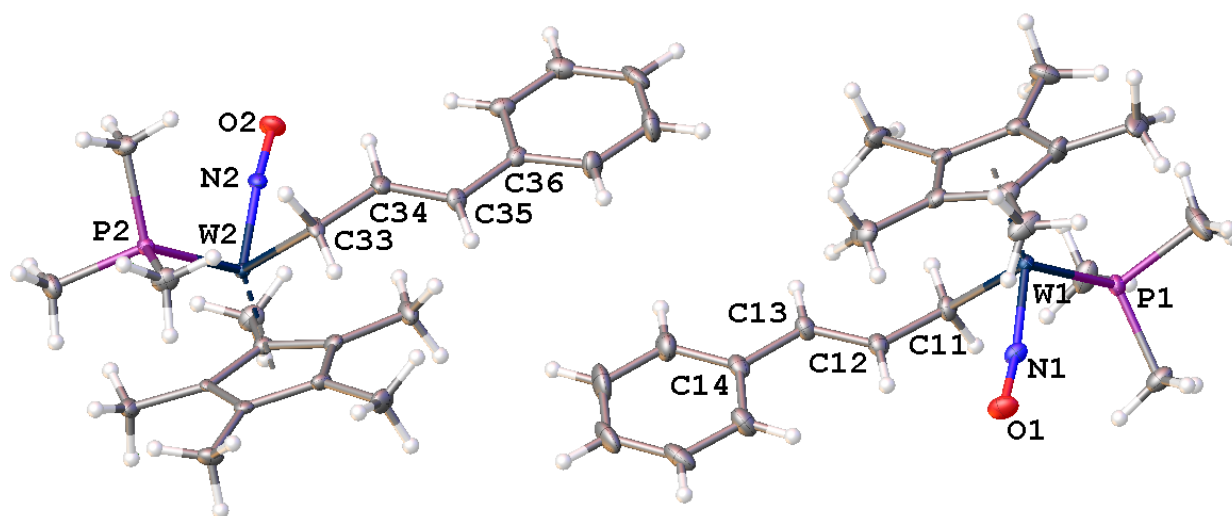


Figure A.1. Solid-state molecular structure of **2.7** showing both molecules in the asymmetric unit with 50% probability thermal ellipsoids shown. Selected bond lengths (Å) and angles (deg):
W(1)-P(1) = 2.4951(10), W(1)-C(11) = 2.284(4), C(11)-C(12) = 1.482(5), C(12)-C(13) = 1.339(5), C(13)-C(14) = 1.466(5), W(1)-N(1) = 1.785(3), N(1)-O(1) = 1.223(4), C(11)-C(12)-C(13) = 127.5(4), C(12)-C(13)-C(14) = 125.5(4), W(1)-N(1)-O(1) = 168.8(3), W(2)-P(2) = 2.4910(10), W(2)-C(33) = 2.302(4), C(33)-C(34) = 1.480(5), C(34)-C(35) = 1.346(5), C(35)-C(36) = 1.468(5), W(2)-N(2) = 1.792(3), N(2)-O(2) = 1.224(4), C(33)-C(34)-C(35) = 129.1(4), C(34)-C(35)-C(36) = 124.5(4), W(2)-N(2)-O(2) = 171.6(3).

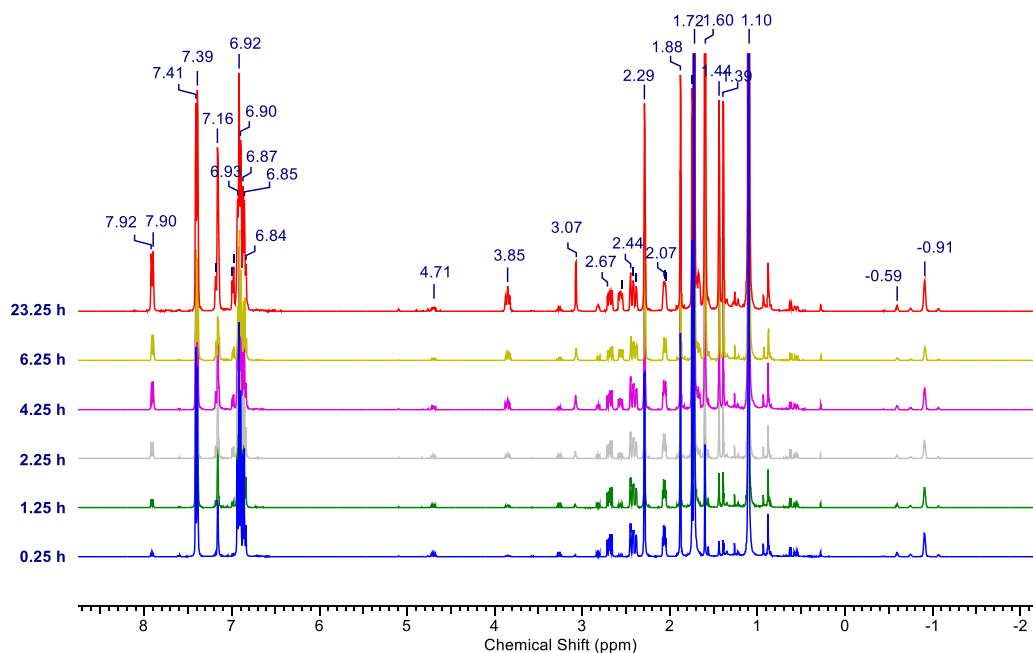


Figure A.2. Monitoring the reaction of **2.1** with PhSSPh in the presence AIBN at room temperature by ^1H NMR spectroscopy (400 MHz, C_6D_6).

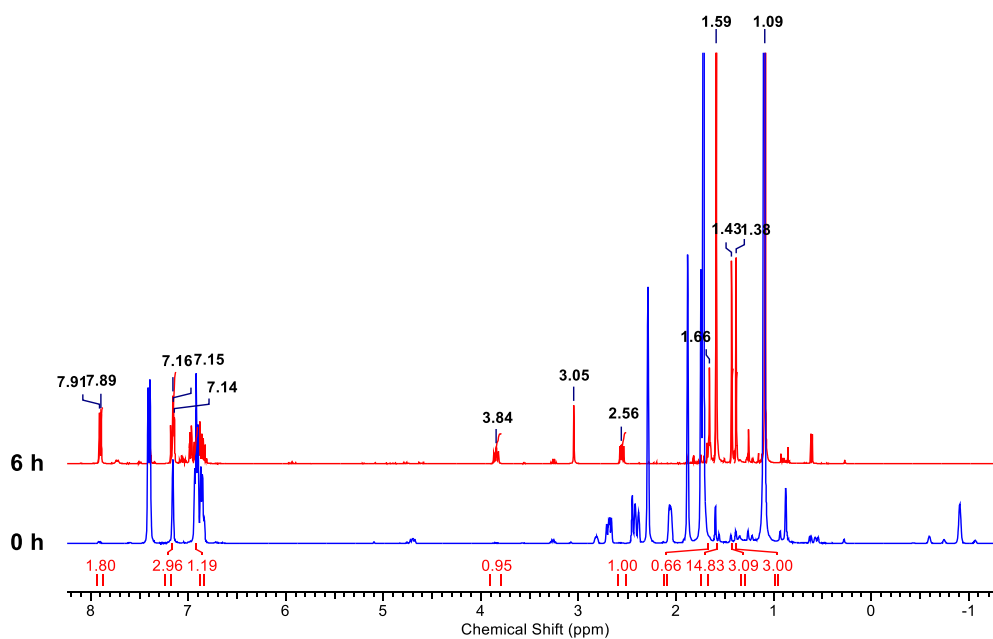


Figure A.3. Conversion of **2.1** (blue spectrum) to **2.11** (red spectrum) at 50 °C as monitored by ^1H NMR spectroscopy (400 MHz, C_6D_6).

Appendix B Supplementary Materials for Chapter 3

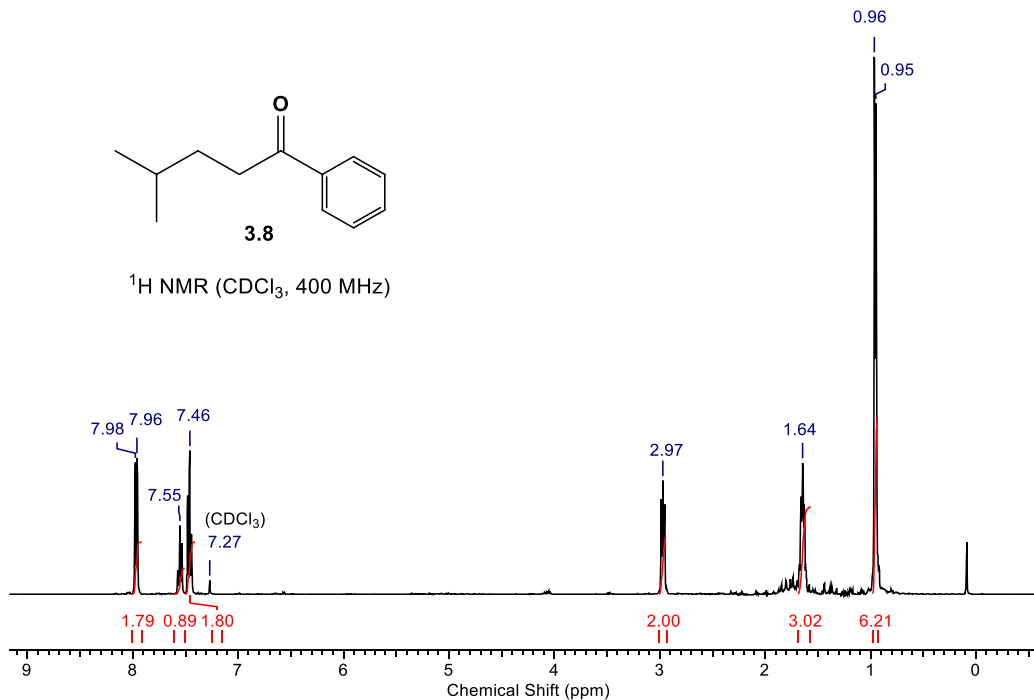


Figure B.1. ^1H NMR spectrum of **3.8** (CDCl_3 , 400 MHz).

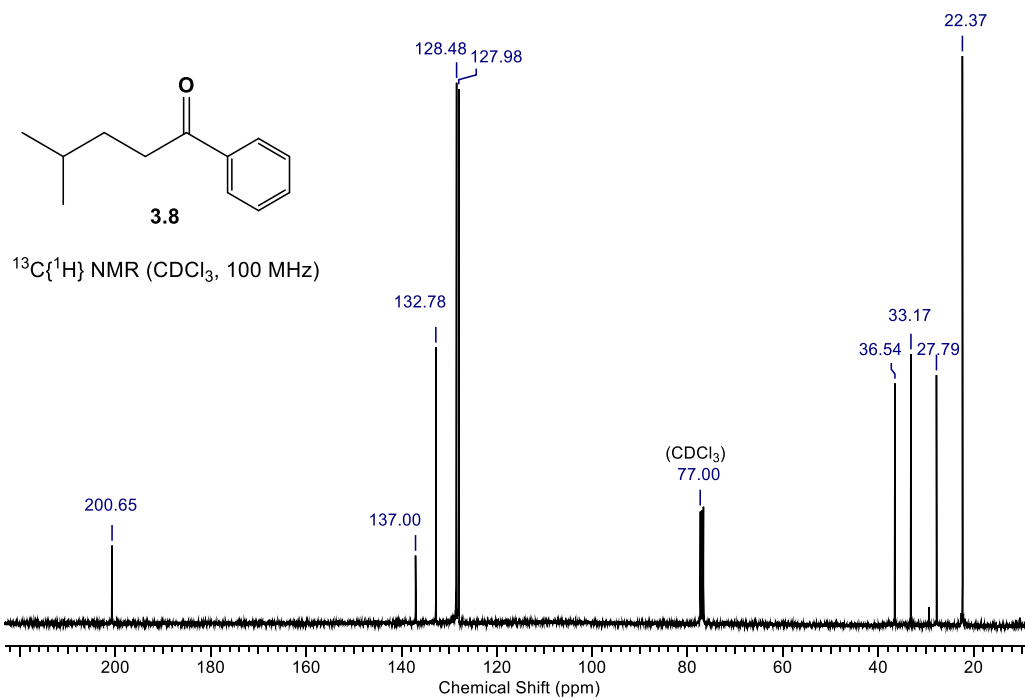


Figure B.2. $^{13}\text{C}\{^1\text{H}\}$ NMR spectrum of **3.8** (CDCl_3 , 100 MHz).

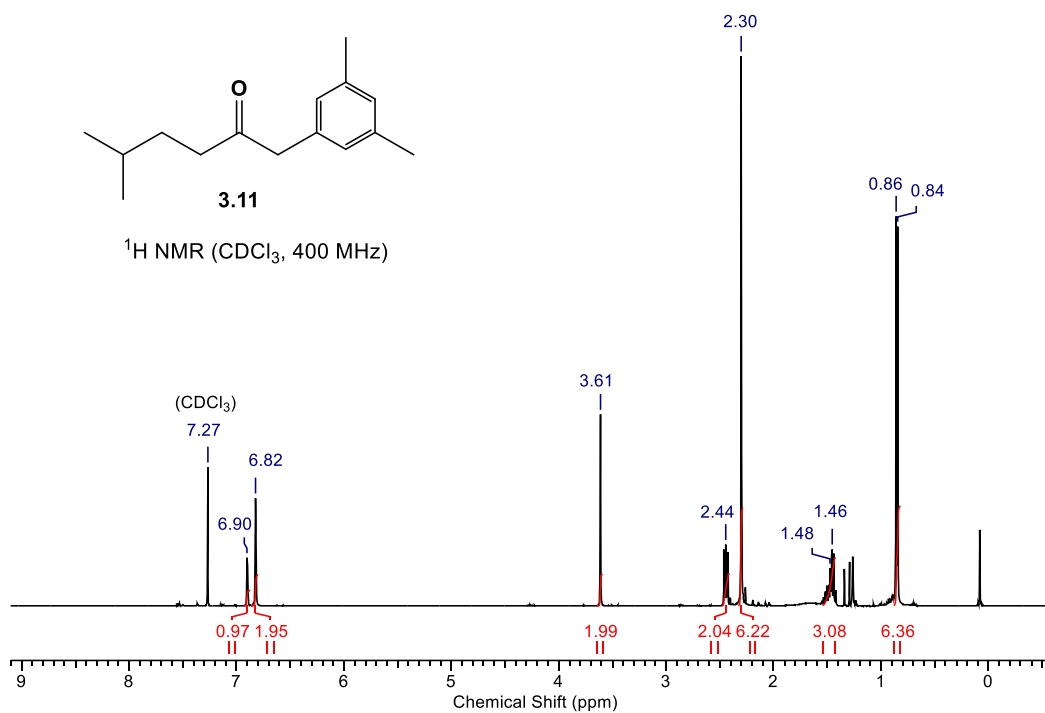


Figure B.3. ^1H NMR spectrum of **3.11** (CDCl_3 , 400 MHz).

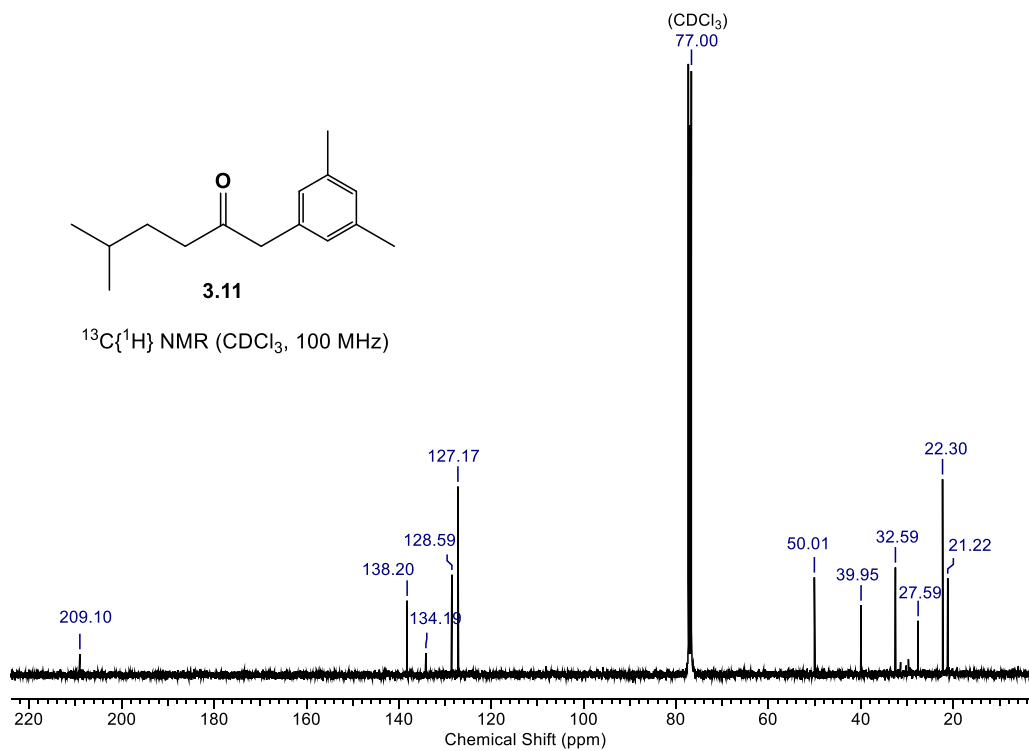


Figure B.4. $^{13}\text{C}\{^1\text{H}\}$ NMR spectrum of **3.11** (CDCl_3 , 100 MHz).

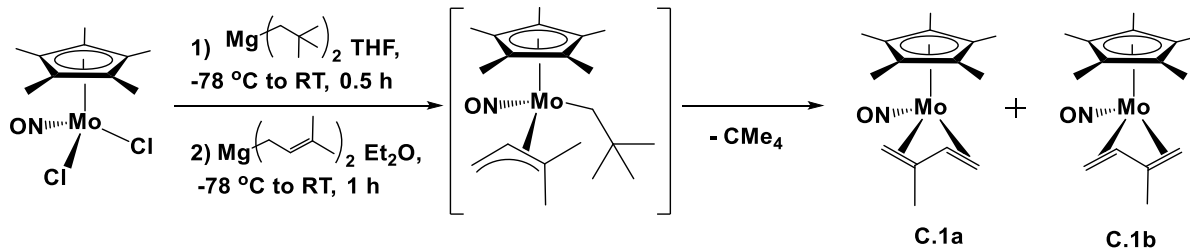
Appendix C Supplementary Materials for Chapter 4

C.1 Attempt to Synthesize the Molybdenum Analogue of **4.1**

The synthesis of the complex $\text{Cp}^*\text{Mo}(\text{NO})(\text{CH}_2\text{CMe}_3)(\eta^3\text{-CH}_2\text{CHCMe}_2)$ (**C.1**) was attempted from $\text{Cp}^*\text{Mo}(\text{NO})\text{Cl}_2$ ⁵⁶ through the sequential metathesis reactions with first $\text{Mg}(\text{CH}_2\text{CMe}_3)_2$ and then $\text{Mg}(\text{CH}_2\text{CH}=\text{CMe}_2)_2$. These reactions were carried out at $-78\text{ }^\circ\text{C}$ and the final mixture was allowed to warm to room temperature, producing a yellow mixture, which was chromatographed on basic alumina to give **C.1** as a yellow-brown solid. The product exists as two isomers in both solution (via ^1H NMR) and in the solid state (via X-ray) diffraction. The two isomers are observed in solid-state due to disorder in the orientation of the η^4 -diene with respect to its coordination to the metal center (Figure C.1, Figure C.2).

This result suggests that the Mo analogue of **4.1** is synthesized, but then quickly evolves neopentane to form the η^2 -diene intermediate complex, which then rapidly converts to the 18e η^4 -diene-containing product (Scheme C.1). A $\text{Cp}^*\text{Mo}(\text{NO})(\eta^2\text{-allene})$ complex has been reported to effect single C-H activation while compounds that form $\text{Cp}^*\text{Mo}(\text{NO})(\eta^4\text{-diene})$ do not show any capability to effect C-H bond activation at all. Unfortunately, it seems that the η^2 -diene intermediate complex has a lower energy than the η^2 -allene intermediate complex, which is the opposite of that of the tungsten analogue **4.1**.

Scheme C.1. Preparation of $\text{Cp}^*\text{Mo}(\text{NO})(\eta^4\text{-CH}_2=\text{C}(\text{Me})\text{CH}=\text{CH}_2)$



Synthesis of $\text{Cp}^*\text{Mo}(\text{NO})(\eta^4\text{-CH}_2=\text{CMe-CH=Me}_2)$ (C.1)

In a glove box, a glass Schlenk flask was charged with $\text{Cp}^*\text{Mo}(\text{NO})\text{Cl}_2$ ⁵⁶ (0.33 g, 0.99 mmol) and a magnetic stir bar. After being connected to a double manifold, the contents of the flask were cooled in a dry ice/acetone bath ($-78\text{ }^\circ\text{C}$) and THF (ca. 25 mL) was added by cannula. A second Schlenk flask was charged in the glove box with $\text{Mg}(\text{CH}_2\text{CMe}_3)_2$ (titre: 145 g/mol, 0.15 g, 1.0 mmol) and a magnetic stir bar. The second flask was charged with THF (ca. 50 mL) and its contents were cannulated into the first Schlenk flask. Following the addition the Schlenk flask was removed from the bath and its contents were allowed to stir at room temperature for 0.5 h to give a dark purple mixture. The solvent was removed in vacuo to afford a dark purple residue. A third Schlenk flask was charged in the glove box with $\text{Mg}(\text{CH}_2\text{CH}=\text{CMe}_2)_2$ (titre: 130 g/mol, 0.12 g, 0.92 mmol) and a magnetic stir bar, Et_2O (ca. 10 mL) was then added by cannula and the Schlenk was cooled to $-78\text{ }^\circ\text{C}$ in a dry ice/acetone bath. The contents of the first flask were transferred to the third flask in Et_2O (ca. 2 x 50 mL) by cannula, and then the third flask was removed from the bath and its contents were allowed to stir at room temperature for 1 h to afford a yellow mixture. The Mixture was then transferred to the top of a basic alumina column (3 x 8 cm). A pale yellow band was collected with Et_2O as a yellow eluate. The solvent was removed under reduced pressure to afford a yellow-brown solid (0.198 g, 65 % yield). Crystals

suitable for single crystal X-ray diffraction were obtained from recrystallization in Et₂O at -33 °C. Compound Cp*Mo(NO)(η^4 -CH₂=CMe-CH=Me₂) (**C.1**) exists as two isomers, **C.1a** and **C.1b**, in a 54:46 ratio determined by ¹H NMR spectroscopy. The isomer **C.1a** has been assigned as the major isomer since it is the major component of the disordered structure obtained by single-crystal X-ray diffraction.

Characterization data for **C.1a** (54 %): IR (cm⁻¹) 1605 (s, ν_{NO}). MS (LREI, m/z , probe temp. 150 °C) 331 [M^+ , ⁹⁸Mo]. MS (HREI, m/z , ⁹²Mo) calcd 325.08477, found 325.08463. Anal. Calcd for C₁₅H₂₃NOMo: C, 54.71; H, 7.04; N, 4.25. Found: C, 53.52; H, 6.91; N, 3.96. ¹H NMR (400 MHz, C₆D₆) δ 0.93 (s, 3H, CMe=CH₂), 1.67 (s, 15H, C₅Me₅), 1.75 (dd, ³ J_{HH} = 13.3, ² J_{HH} = 3.3, 1H, CH=CH₂), 2.52 (d, ² J_{HH} = 1.6, 1H, CMe=CH₂), 3.04 (d, ² J_{HH} = 1.6, 1H, CMe=CH₂), 3.28 (dd, ³ J_{HH} = 13.3, 6.2, 1H, CH=CH₂), 3.41 (dd, ³ J_{HH} = 6.2, ² J_{HH} = 3.3, 1H, CH=CH₂). ¹³C NMR (100 MHz, C₆D₆) δ 11.0 (C₅Me₅), 19.1 (CMe), 59.9 (CH₂), 60.0 (CH₂), 91.4 (CH), 106.3 (C₅Me₅), 106.8 (CMe).

Characterization data for **C.1** (46 %): ¹H NMR (400 MHz, C₆D₆) δ 1.07 (d, ² J_{HH} = 2.7, 1H, CMe=CH₂), 1.36 (dd, ³ J_{HH} = 14.3, 6.7, 1H, CH=CH₂), 1.63 (s, 15H, C₅Me₅), 1.64 (s, 3H, CMe=CH₂), 2.51 (dd, ³ J_{HH} = 6.7, ² J_{HH} = 2.8, 1H, CH=CH₂), 3.17 (dd, ³ J_{HH} = 14.3, ² J_{HH} = 2.8, 1H, CH=CH₂), 3.35 (d, ² J_{HH} = 2.7, 1H, CMe=CH₂). ¹³C NMR (100 MHz, C₆D₆) δ 10.9 (C₅Me₅), 19.4 (CMe), 58.3 (CH₂), 62.7 (CH₂), 88.6 (CH), 106.0 (C₅Me₅), 115.5 (CMe).

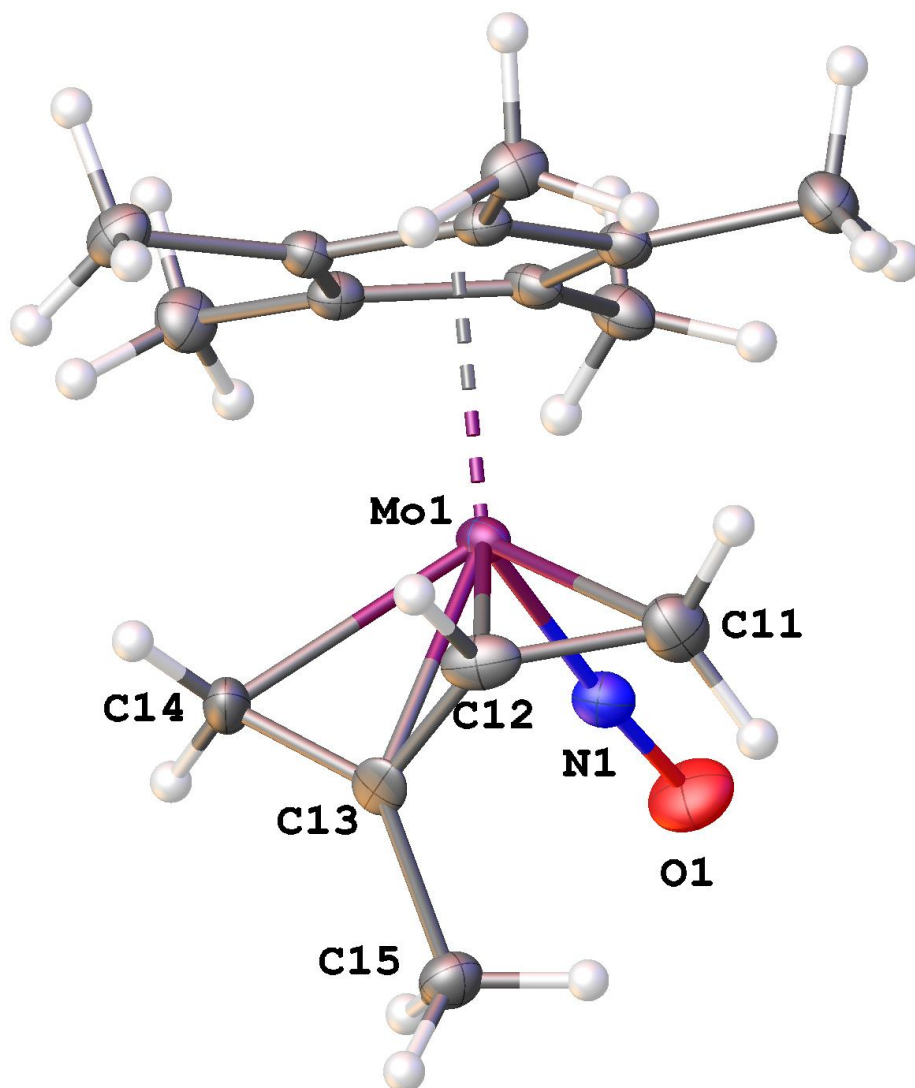


Figure C.1. Solid-state molecular structure of **C.1a** with 50% probability thermal ellipsoids shown. Selected bond lengths (Å) and angles (deg.): Mo(1)-C(11) = 2.379(5), Mo(1)-C(12) = 2.232(7), Mo(1)-C(13) = 2.270(7), Mo(1)-C(14) = 2.250(7), Mo(1)-N(1) = 1.7762(19), N(1)-O(1) = 1.209(2), C(11)-C(12) = 1.430(6), C(12)-C(13) = 1.415(9), C(13)-C(14) = 1.410(7), C(13)-C(15) = 1.520(14), Mo(1)-N(1)-O(1) = 174.38(18), C(11)-C(12)-C(13) = 121.1(6), C(12)-C(13)-C(14) = 115.1(6), C(12)-C(13)-C(15) = 122.6(5).

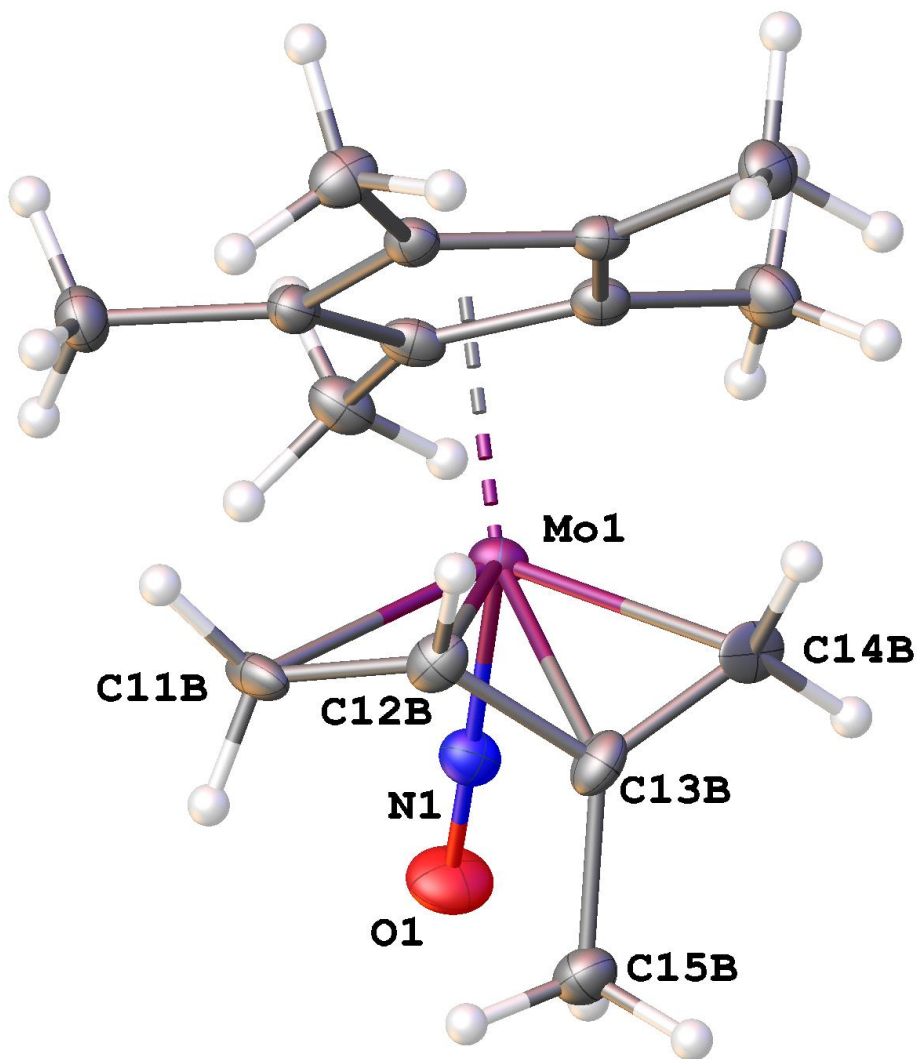


Figure C.2. Solid-state molecular structure of **C.1b** with 50% probability thermal ellipsoids shown. Selected bond lengths (Å) and angles (deg.): Mo(1)-C(11b) = 2.387(8), Mo(1)-C(12b) = 2.214(11), Mo(1)-C(13b) = 2.217(12), Mo(1)-C(14b) = 2.214(8), C(11b)-C(12b) = 1.410(9), C(12b)-C(13b) = 1.442(10), C(13b)-C(14b) = 1.399(13), C(13b)-C(15b) = 1.53(2), C(11b)-C(12b)-C(13b) = 122.0(10), C(12b)-C(13b)-C(14b) = 116.0(10), C(12b)-C(13b)-C(15b) = 119.8(9).

C.2 Additional Figures for Chapter 4

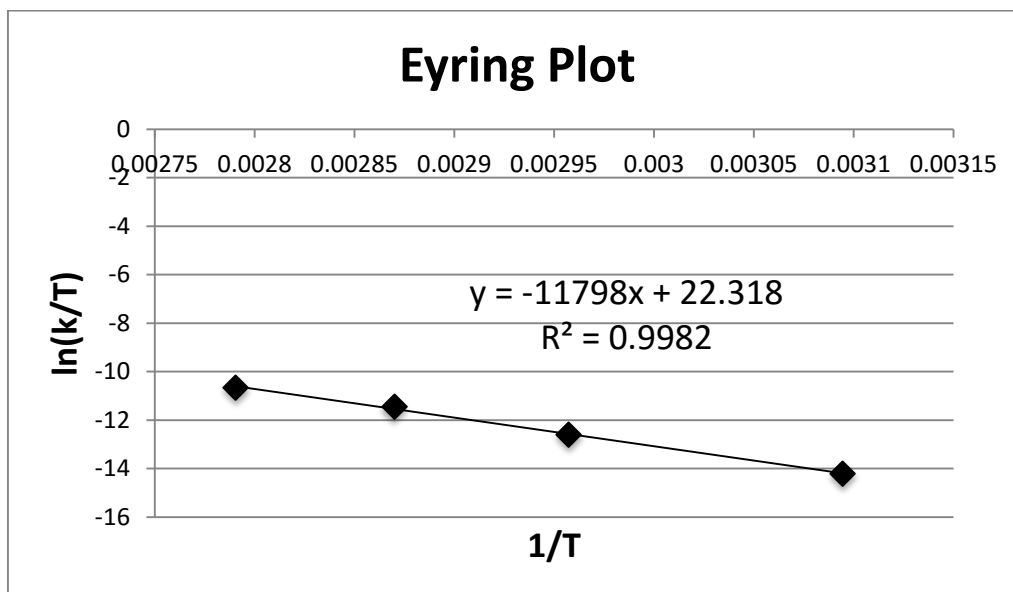


Figure C.3. Eyring plot for the thermolysis of **4.1** in C_6D_6 ; $\Delta H^\ddagger = 98(3)$ kJ/mol, $\Delta S^\ddagger = 166(11)$ J/mol K.

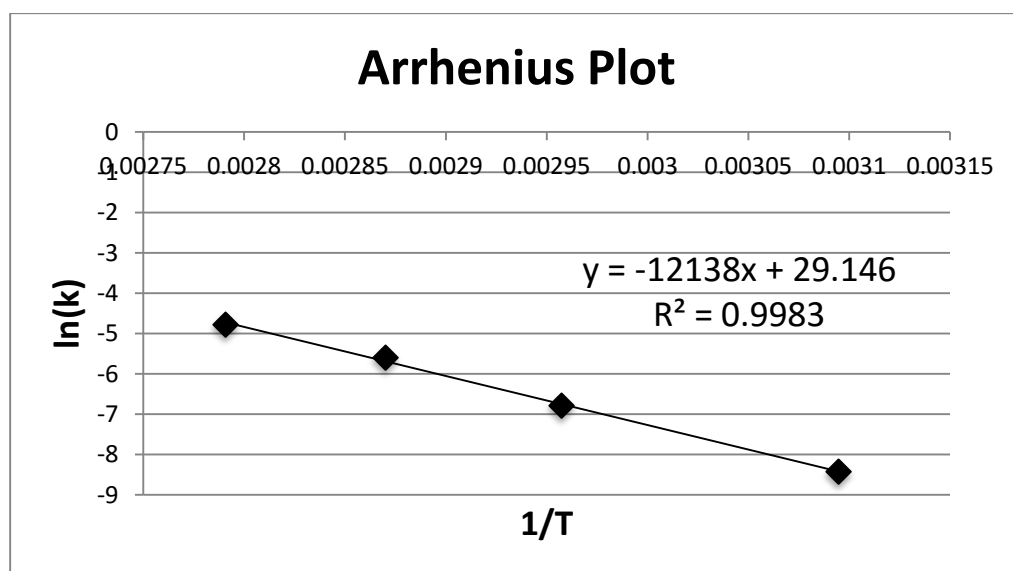


Figure C.4. Arrhenius plot for the thermolysis of **4.1** in C_6D_6 ; $E_a = 101(3)$ kJ/mol.

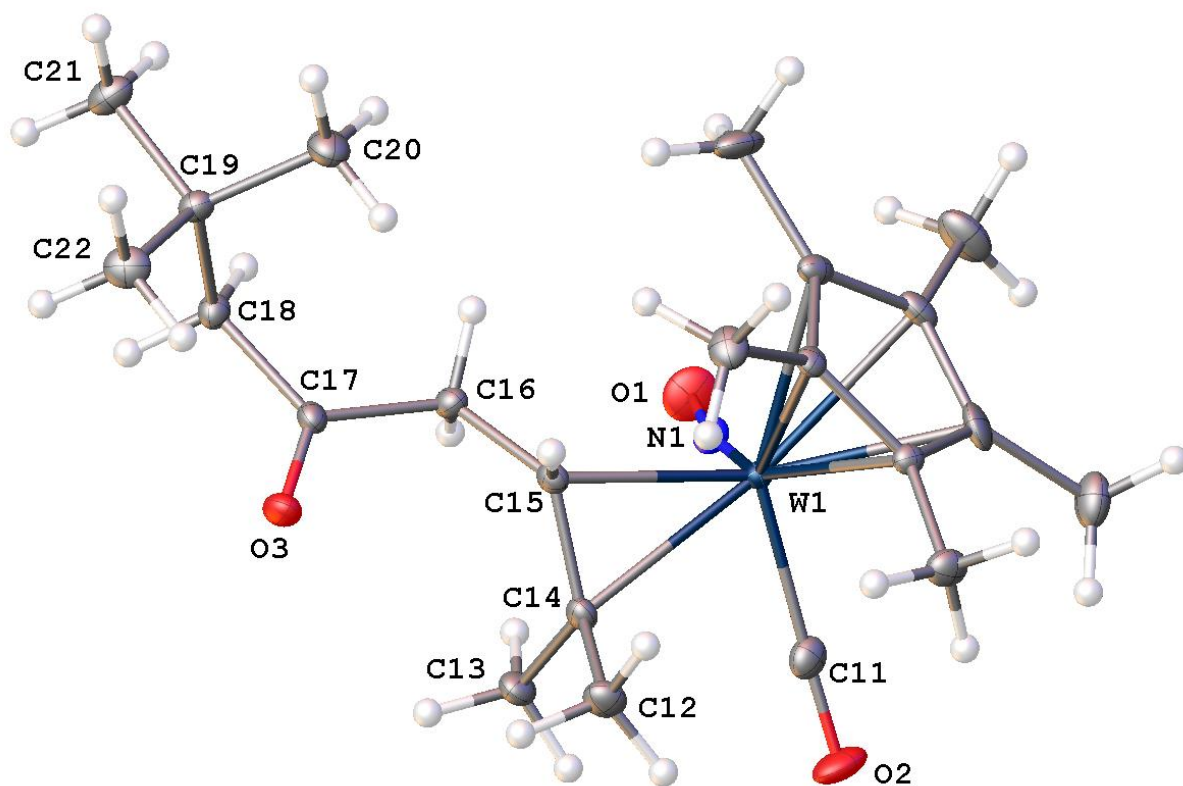


Figure C.5. Top-down view of solid-state molecular structure of **4.6** showing that the distance between W(1) and O(3) which is 5.001 Å.

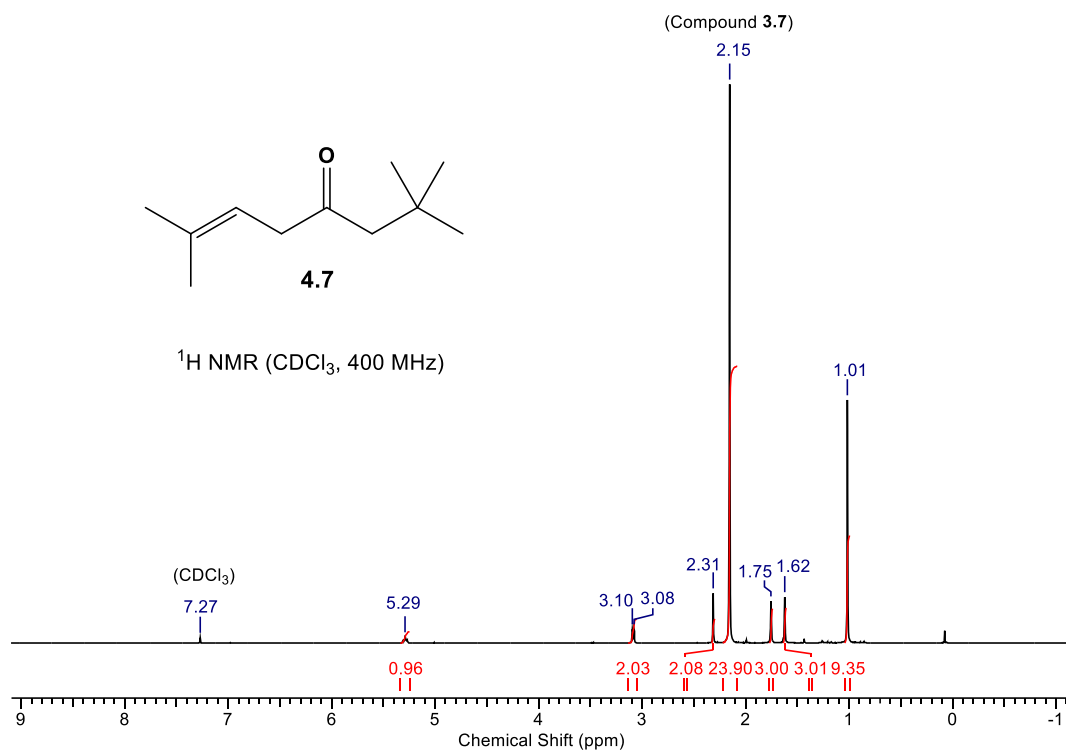


Figure C.6. ^1H NMR spectrum of **4.7** and **3.7** (CDCl_3 , 400 MHz).

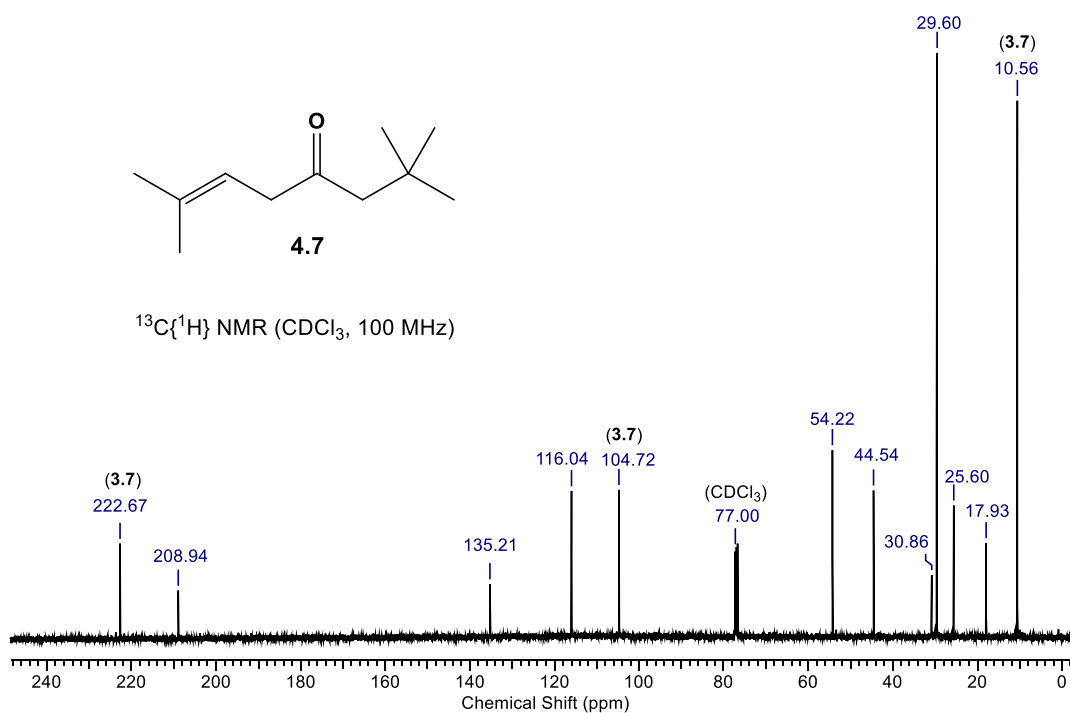


Figure C.7. $^{13}\text{C}\{^1\text{H}\}$ NMR spectrum of **4.7** and **3.7** (CDCl_3 , 400 MHz).

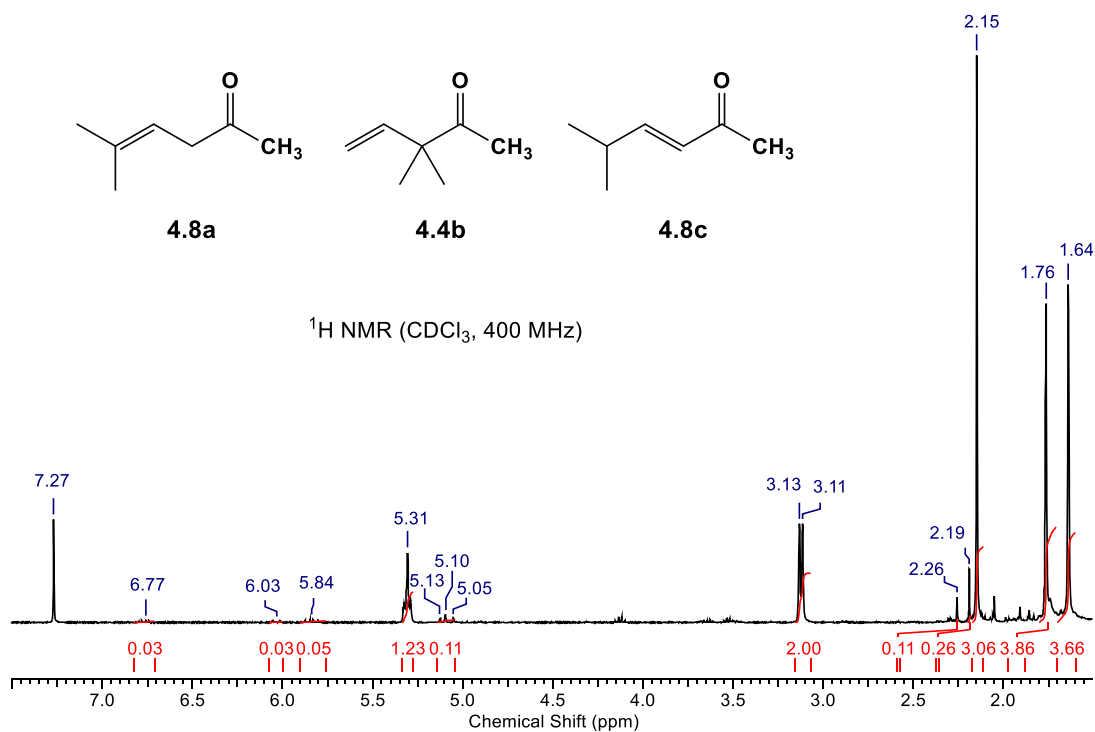


Figure C.8. ^1H NMR spectrum of **4.8a-c** (CDCl_3 , 400 MHz).

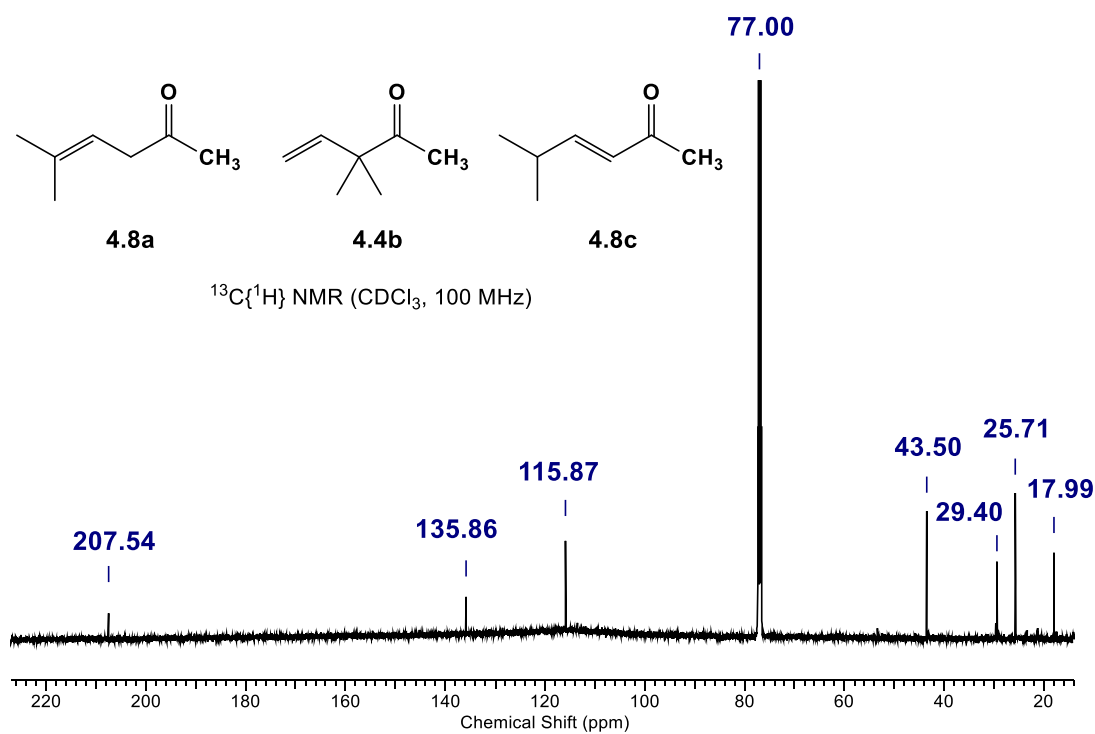


Figure C.9. $^{13}\text{C}\{^1\text{H}\}$ NMR spectrum of **4.8a-c** (CDCl_3 , 400 MHz).

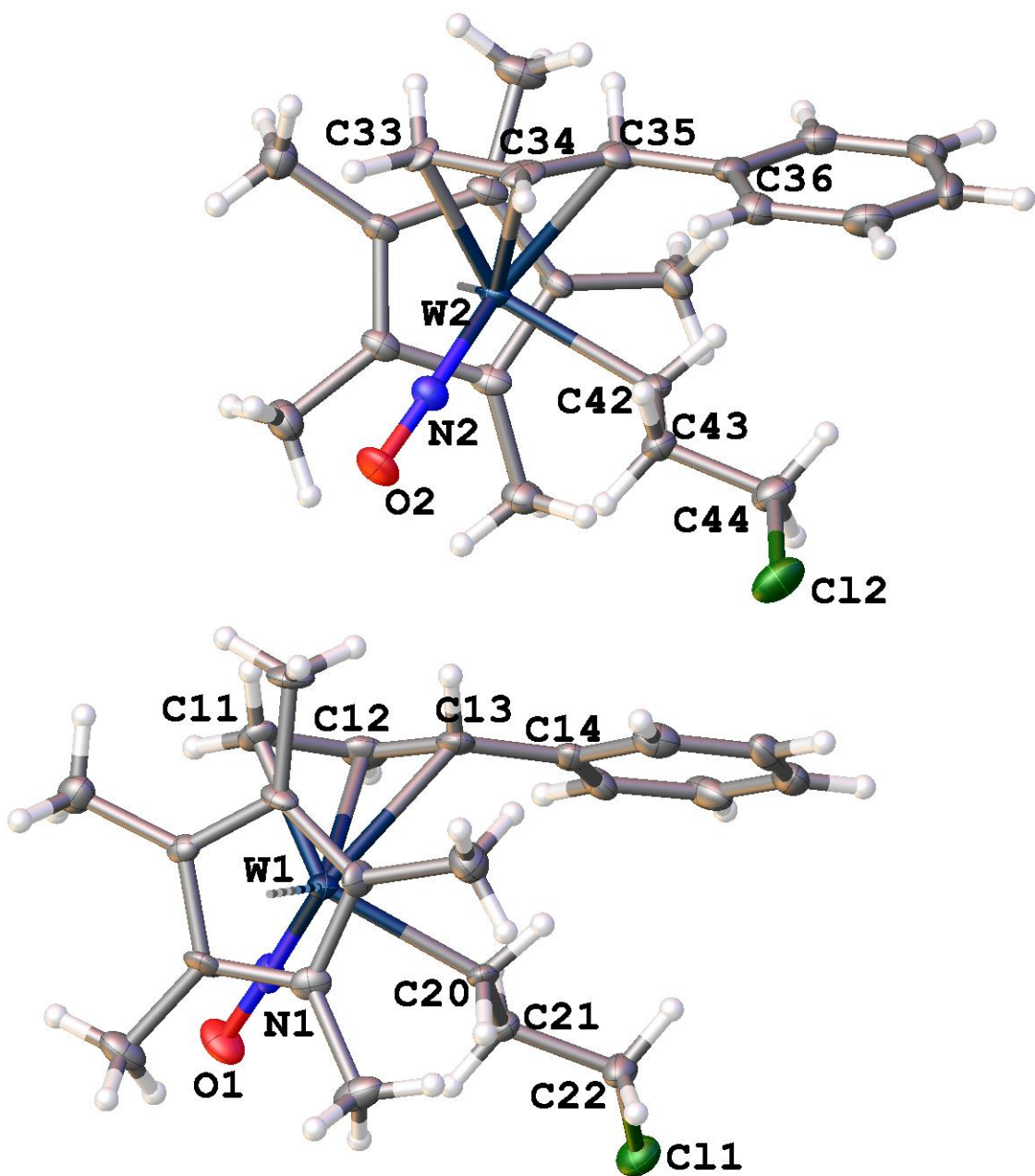


Figure D.1. Solid-state molecular structure of **5.12b** with 50% probability thermal ellipsoids shown.

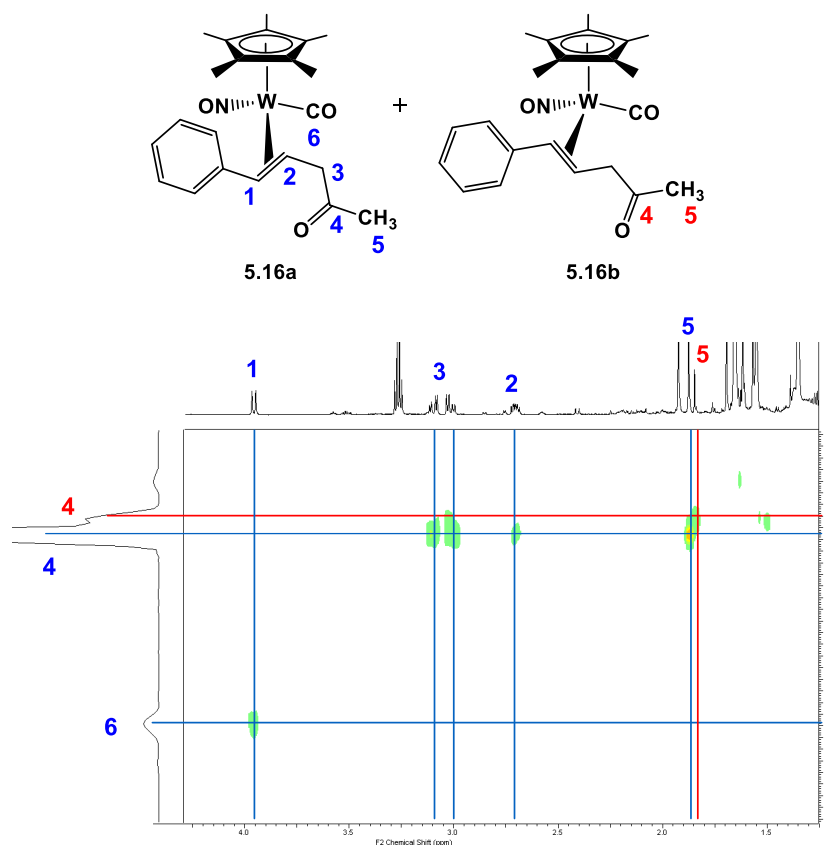


Figure D.2. $\{^1\text{H}/^{13}\text{C}\}$ HMBC NMR spectrum (C_6D_6 , 400 MHz) of **5.16a** (blue) and **5.16b** (red) showing correlations to carbonyl ligand of the bound ketone ligand.

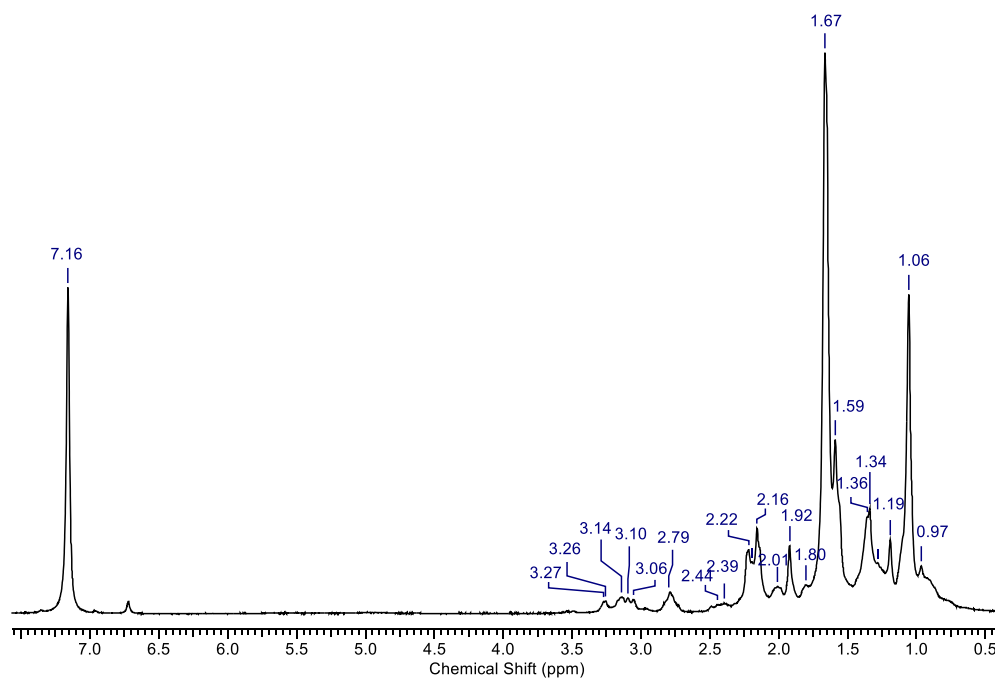


Figure D.3. ^1H NMR spectrum (C_6D_6 , 400 MHz) of the mixture obtained after the thermolysis of **5.2** at 750 psig CO.

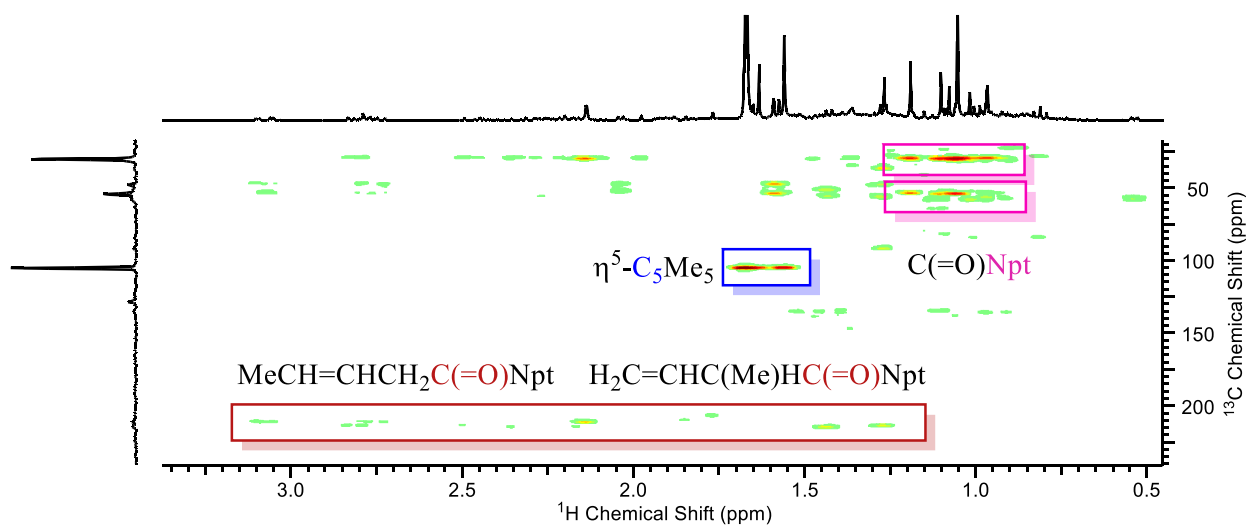


Figure D.4. $\{^1\text{H}/^{13}\text{C}\}$ HMBC NMR (C_6D_6 , 400 MHz) spectrum for the mixture of isomers of **5.22**. Cross peaks corresponding to the CMe_3 , $\eta^5\text{-C}_5\text{Me}_5$, and $\text{C}(=\text{O})\text{CH}_2$ signals are highlighted.

Appendix E Supplementary Material for Chapter 6

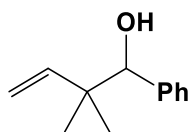
E.1 Preliminary Reaction: Analysis of the Reaction of **5.7** with CO at 170 °C by ¹H NMR Spectroscopy.

In a glove box, a Parr 5500 reactor was charged with a sample of **5.7** (35 mg, 0.083 mmol) and C₆D₆ (ca. 20 mL) and then sealed. The reactor was purged with CO (3 x 500 psig), and then pressurized to 1000 psig CO. The contents of the reactor were heated at 170 °C for 3 d, after which time the contents were allowed to cool to room temperature and then the gas was very carefully vented. The yellow mixture obtained was transferred to a 50-mL round bottom flask and the volume of the solvent was reduced via slow evaporation. The concentrated sample was analyzed by ¹H NMR spectroscopy. Compound **3.7** was identified in the ¹H NMR spectrum, along with multiple isomers of the unsaturated ketone (C₄H₇)C(=O)CH₃. Published data for the ketones reports the ¹H NMR characterization in CDCl₃; the above reaction was attempted in CDCl₃, but the complex decomposed and no products were formed. The identification of the unsaturated ketones offered presently is made based on characteristic multiplets. (*E*)-hex-3-en-2-one, agrees well with reported data¹⁴³ [¹H NMR (C₆D₆, 400 MHz) δ (selected signals) 5.90 (dt, ⁴J_{HH} = 1.8, ³J_{HH} = 16.0, 1H, =CHC(=O)), 6.39 (dt, ³J_{HH} = 16.0, 6.5, 1H, MeCH₂CH=)]; (*Z*)-3-methylpent-3-en-2-one, agrees well with reported data¹⁴⁴ [¹H NMR (C₆D₆, 400 MHz) δ (selected signals) 6.11 (qq, ⁴J_{HH} = 1.4, ³J_{HH} = 6.9, 1H, =CH)]; 3-methylpent-4-en-2-one [¹H NMR (C₆D₆, 400 MHz) δ (selected signals) 4.85-4.91 (m, 1H, =CH₂), 4.95-5.02 (m, 1H, =CH₂), 5.60 (ddd, ³J_{HH} = 17.6, 9.8, 8.0, 1H, =CH)]; (*E*)-hex-4-en-2-one [¹H NMR (C₆D₆, 400 MHz) δ (selected

signals) 2.66 (d, $^3J_{\text{HH}} = 7.0$, 2H, $=\text{CHCH}_2\text{C}(=\text{O})$), 5.25 (dq, $^3J_{\text{HH}} = 15.4$, 6.5, 1H, $\text{MeCH}=\text{}$), 5.45 (dt, $^3J_{\text{HH}} = 15.4$, 7.0, 1H, $=\text{CHCH}_2$)].

E.2 Preliminary Reaction: Reaction of **2.1** with Benzaldehyde

On the bench top, a J. Young. NMR tube was charged with **2.1** (25 mg, 0.060 mmol) dissolved in CDCl_3 (ca. 1 mL). Benzaldehyde was added to this yellow solution (ca. 0.01 mL) and the tube was sealed with a Kontes greaseless stopcock. The sample was heated at 55 °C for 1 w while being monitored by ^1H NMR spectroscopy, after which time signals for the compound **2,2-dimethyl-1-phenylbut-3-en-1-ol** were identified.



Characterization data for **2,2-dimethyl-1-phenylbut-3-en-1-ol**, which agrees well with published data.^{145,146,147,148} ^1H NMR (CDCl_3 , 400 MHz) δ 0.94 (s, 3H, *Me*), 0.99 (s, 3H, *Me*), 4.41 (s, 1H, *CH*), 5.01 (d, $^3J_{\text{HH}} = 17.6$, 1H, $=\text{CH}_2$), 5.07 (d, $^3J_{\text{HH}} = 11.0$, 1H, $=\text{CH}_2$), 5.91 (dd, $^3J_{\text{HH}} = 17.6$, 11.0, 1H, $=\text{CH}$), 7.20-7.40 (m, 5H, aryl *H*). $^{13}\text{C}\{^1\text{H}\}$ (CDCl_3 , 100 MHz) δ 21.2, 24.1, 42.0, 80.4, 113.2, 127.2, 127.6, 128.2, 140.9, 144.9.

E.3 Preparation of $\text{Cp}^*\text{W}(\text{NO})(\text{CH}_2\text{-3,5-Me}_2\text{C}_6\text{H}_3)(\text{O-CH}(\text{CH}_2\text{CMe}_3)\text{C}(\text{Me})\text{HCH=CH}_2)$

(E.1)

The complex $\text{Cp}^*\text{W}(\text{NO})(\text{CH}_2\text{-3,5-Me}_2\text{C}_6\text{H}_3)(\text{O-CH}(\text{CH}_2\text{CMe}_3)\text{C}(\text{Me})\text{HCH=CH}_2)$ was prepared by adding a slight excess of 3,3-dimethylbutanal to a yellow solution C_6D_6 solution of $\text{Cp}^*\text{W}(\text{NO})(\text{CH}_2\text{-3,5-Me}_2\text{C}_6\text{H}_3)(\eta^3\text{-CH}_2\text{CHCHMe})$ in an NMR tube. The color immediately turned dark red and crystals suitable for single-crystal X-ray diffraction precipitated from the mixture at room temperature. The reaction was carried out by Monica Shree and the collection and analysis of the X-ray data was performed by the author. The solid-state molecular structure is shown in Figure E.1. The crystals (and solution) turned from red to yellow within minutes upon exposure to air. Similar complexes have not been isolated from analogues reactions; the stability of this complex is likely increased due to a η^3 -benzyl interaction.

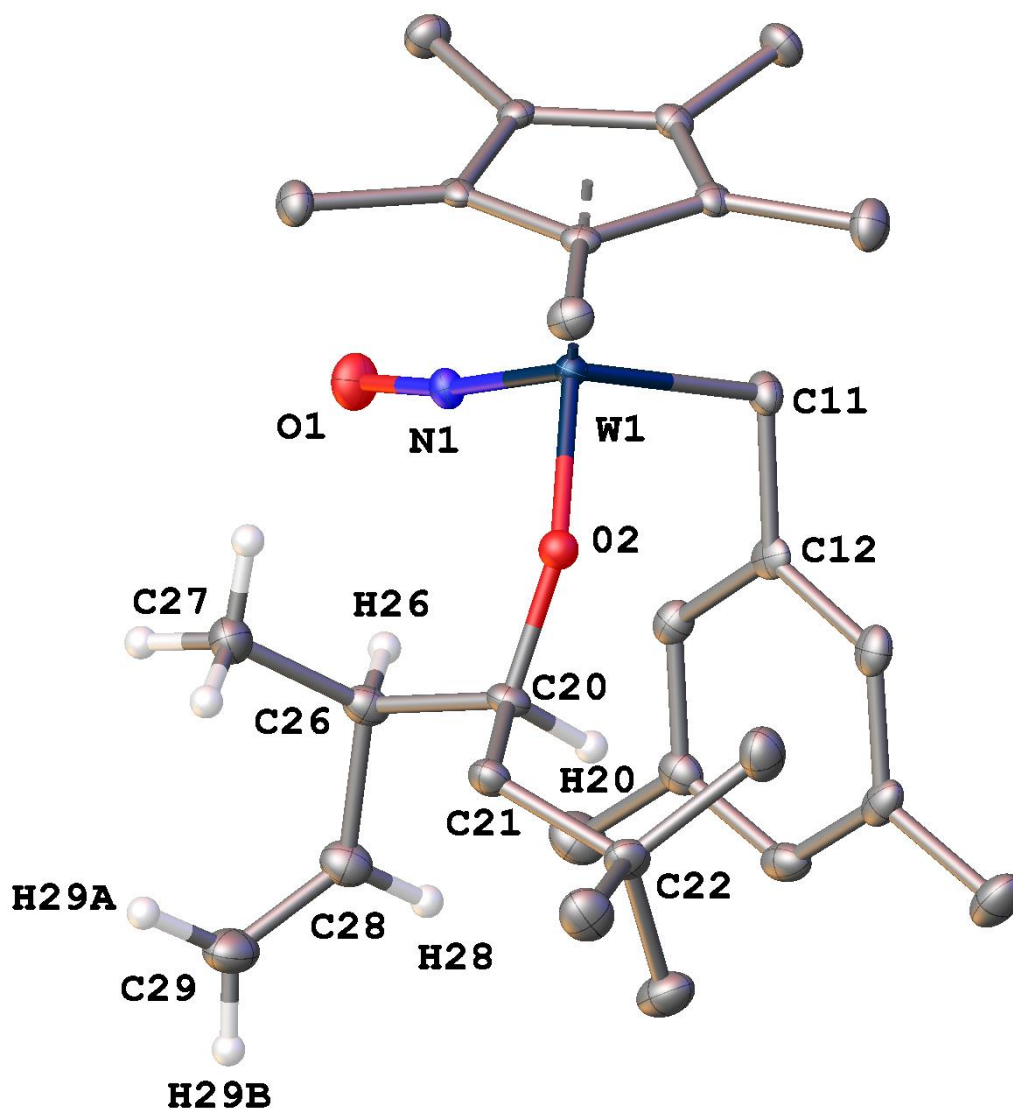


Figure E.1. Solid-state molecular structure of **E.1** with 50% probability thermal ellipsoids shown. Selected bond lengths (Å) and angles (deg.): W(1)-O(2) = 1.889(2), O(2)-C(20) = 1.438(3), C(20)-C(26) = 1.546(4), C(26)-C(28) = 1.508(4), C(28)-C(29) = 1.320(5), W(1)-C(11) = 2.183(3), W(1)-N(1) = 1.763(2), N(1)-O(1) = 1.236(3), W(1)-C(11)-C(12) = 104.18(18), W(1)-O(1)-C(20) = 137.27(18), O(2)-C(20)-C(21) = 108.8(2), C(20)-C(26)-C(28) = 107.9(2), C(26)-C(28)-C(29) = 126.3(3), W(1)-N(1)-O(1) = 171.4(2).

Appendix F X-ray Crystallography for Appendices

Data collection was carried out at -183 ± 2 °C on a Bruker DUO APEX diffractometer, using graphite-monochromated Mo K α radiation.

Data for **C.1a** and **C.1b** were collected to a maximum 2θ value of 55.09° in 0.5° oscillations. The structure was solved by direct methods⁶⁰ and expanded using Fourier techniques. The C11 – C15 fragment was disordered in two orientations in approximately a 76:24 ratio. All non-hydrogen atoms were refined anisotropically, and all other hydrogen atoms were included in calculated positions. The final cycle of full-matrix least-squares analysis was based on 3319 observed reflections and 209 variable parameters.

Data for **E.1** were collected to a maximum 2θ value of 54.99° in 0.5° oscillations. The structure was solved by direct methods⁶⁰ and expanded using Fourier techniques. All non-hydrogen atoms were refined anisotropically. Hydrogens H20, H26, H28, H29a, and H29b were refined anisotropically, and all other hydrogen atoms were included in calculated positions. The final cycle of full-matrix least-squares analysis was based on 6332 observed reflections and 351 variable parameters.

For each structure neutral-atom scattering factors were taken from Cromer and Waber.⁶¹ Anomalous dispersion effects were included in Fc;⁶² the values for $\Delta f'$ and $\Delta f''$ were those of Creagh and McAuley.⁶³ The values for mass attenuation coefficients are those of Creagh and Hubbell.⁶⁴ All calculations were performed using SHELXL-97⁶⁵ via the WinGX interface.⁶⁶ X-ray crystallographic data for both structures are presented in Table F.1.

Table F.1. X-ray crystallographic data for complexes **C.1a/C.1b** and **E.1**.

Compound	C.1a/C.1b	E.1
Empirical formula	C ₁₅ H ₂₃ NOMo	C ₂₉ H ₄₅ NO ₂ W
Formula weight	329.28	623.51
Crystal size (mm)	0.24 × 0.12 × 0.11	0.20 × 0.10 × 0.07
Crystal system	Orthorhombic	Monoclinic
Space group	<i>P2₁2₁2₁</i>	<i>P2₁/c</i>
Volume (Å ³)	1441.7(3)	2759.9(7)
a (Å)	9.6315(12)	18.737(3)
b (Å)	12.1481(14)	9.4060(14)
c (Å)	12.3220(15)	16.501(2)
α (°)	90	90
β (°)	90	108.371(3)
γ (°)	90	90
Z	4	4
Density, ρ (calculated) (Mg/m ³)	1.517	1.501
Absorption coefficient, μ (mm ⁻¹)	0.899	4.210
F ₀₀₀	680.0	1264.0
Measured Reflections: Total	8298	46961
Measured Reflections: Unique	3319	6332
Final R Indices	R ₁ = 0.0221, wR ₂ = 0.0498	R ₁ = 0.0224, wR ₂ = 0.0485
Goodness-of-fit on F ²	1.017	1.037
Largest diff. peak/hole (e ⁻ Å ⁻³)	0.35/-0.50	1.72/-0.88